NORTHWEST GEOLOGY

The Journal of The Tobacco Root Geological Society

Volume 52, July 2023

48th Annual Field Conference

Belt Symposium VI

and Other Papers, Salmon, Idaho

July 27–30, 2023

Published by The Tobacco Root Geological Society, Inc.
P.O. Box 118
Butte, Montana 59703
http://trgs.org

Cover photo: Mesoproterozoic Swauger Formation quartzite with darker, fine-grained beds near Taylor Mountain, Salmon River Mountains, Idaho. Photo by Russ Burmester.

NORTHWEST GEOLOGY

The Journal of The Tobacco Root Geological Society

Volume 52, July 2023

48th Annual Field Conference

Belt Symposium VI
and Other Papers, Salmon, Idaho

July 27–30, 2023

Published by The Tobacco Root Geological Society, Inc.
P.O. Box 118
Butte, Montana 59703

http://trgs.org

Edited by: Alan English

The Tobacco Root Geological Society, Inc.

P.O. Box 118
Butte, Montana 59703

Officers, 2023:

President: Jesse Mosolf, Montana Bureau of Mines and Geology, Butte, MT
Vice-President: Alan English, Montana Bureau of Mines and Geology, Butte, MT
Treasurer: Katie McDonald, Montana Bureau of Mines and Geology, Butte, MT
Secretary/Corresponding Secretary: Sandy Underwood, Bozeman, MT
Webmasters: Jeff Braun, Butte, MT

Board of Directors, 2023:

Ted Antonioli, Geologist, Missoula, MT
Bruce E. Cox, Geologist (semi-retired), Missoula, MT
Larry N. Smith, Dept. of Geological Engineering, Montana Tech, Butte, MT
Mike Stickney, Montana Bureau of Mines and Geology, Butte, MT
John Childs, Childs Geoscience Inc., Bozeman, MT
Emily Geraghty Ward, Geology Dept., University of Colorado, Boulder, CO

2023 Conference Organizers:

Reed Lewis, Idaho Geological Survey
Katie McDonald, Montana Bureau of Mines and Geology
Sandy Underwood, Bozeman, MT

Editors: Alan English, Montana Bureau of Mines and Geology

Layout and Editing: Susan Barth, Montana Bureau of Mines and Geology

Printed by Insty-Prints, Butte, Montana

ISSN: 0096-7769

http://trgs.org

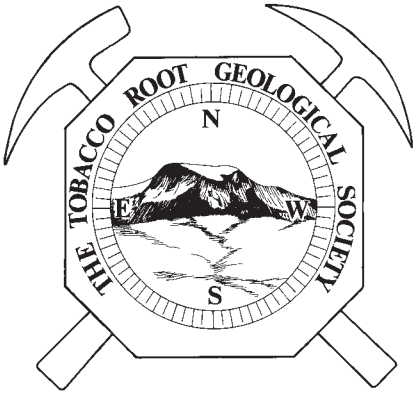

NORTHWEST GEOLOGY

The Journal of The Tobacco Root Geological Society

Volume 52, July 2023

Belt Symposium VI
and Other Papers, Salmon, Idaho

TABLE OF CONTENTS

FIELD GUIDES

TRGS CHARTER MEMBERS

Stanley W. Anderson
Clyde Cody
William S. Cordua
Lanny H. Fisk
Richard I. Gibson†
Thomas Hanley
Stephen W. Henderson
Thomas E. Hendrix
Mac R. Hooton
Inda Immega
Steven W. Koehler
Marian Millen Lankston†
Robert W. Lankston†
J. David Lazor
Joe J. Liteheiser, Jr.
Judson Mead*
Marvin R. Miller
Vicki M. Miller*
Allen H. Nelson
Alfred H. Pekarek
Patricia Price*
Donald L. Rasmussen
Raymond M. Rene

TRGS LIFETIME MEMBERS

John Childs
Rob Foster
Joan (Mrs. Jack) Harrison*
Karen Keefer
Layaka Mann
Chris Pool

† = co-founder

* = deceased

TRGS HAMMER AWARD RECIPIENTS

Awarded for distinguished achievement in the study of the geology of the Northern Rocky Mountains

1993: Ed Ruppel*
1994: Dick Berg
2003: Don Winston*
2004: Dean Kleinkopf*
2009: Betty Skipp
2010: Jim Sears
2011: John Childs
2012: J. Michael O'Neill
2013: Paul Karl Link
2014: Reed Lewis
2015: Jeff Lonn
2016: Bruce Cox
2019: Susan Vuke
2021: Katie McDonald

TRGS HONORARY MEMBERS

1980: Charles J. Vitaliano*
2008: Elizabeth Younggren*
(also honorary Board member)
2010: Dick Berg
2010: Bruce Cox
2010: Dean Kleinkopf*
2010: Dave Lageson
2011: Marie Marshall Garsjo
2011: Paul Link
2011: Rob Thomas
2012: Jeff Lonn
2012: Mitch Reynolds
2013: Reed Lewis
2015: Don Winston*
2020: Ted Antonioli, Larry Smith, Mike Stickney

2023 DEDICATION

DONALD WINSTON II
1931–2022

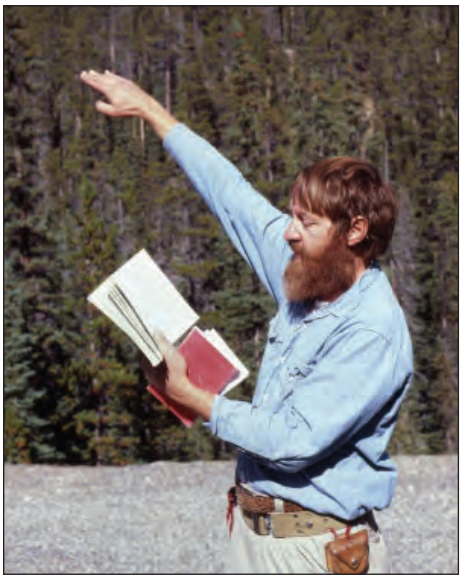

On March 2, 2022, Professor Donald (Don) Winston passed away peacefully at home, just shy of his 91st birthday. Don was a Montana field geologist with a particular passion for the enigmatic Mesoproterozoic Belt Supergroup sedimentary rocks. Don grew up in Minnesota, where he undoubtedly developed a fondness for lakes! He graduated with a geology degree from Williams College in 1953 and went on to earn MS and PhD degrees in geology from the University of Texas at Austin, where he worked with Charlie Bell and Bob Folk. He joined the faculty at the University of Montana in 1961, where he spent his entire career.

Don and his students immediately went about working on the intimidatingly thick and seemingly monotonous pile of Belt rocks. He got after it through endless fieldwork, measuring and correlating stratigraphic sections and building the framework for understanding the environments of deposition. He created a descriptive sediment-type nomenclature, providing a means by which researchers could discuss features like silt-to-clay couplets, microlaminated mud, and crinkle cracks. To help him in the field, Don raised llamas, which he packed into the mountains of western Montana and beyond in search of the next critical measured section. To many, the words Don Winston and Belt Supergroup will forever be linked.

An experiential educator before it was fashionable, Don shared his ideas openly, honestly, and with unparalleled enthusiasm. His energy was legendary and his body impervious to any kind of weather. Countless students on his field trips experienced rocks by van light, the power of ripples to "tell us something," and his backside racing across a coastal mudflat, desert playa, or up a steep mountain. Where Don went, everyone followed, if for no other reason but to see something worth looking at and to hear him exclaim one of his many colorful "Winstonisms." The days ended with Don and his banjo inspiring the crowd around a campfire with song, laughter, and comradery, while mornings brought whiskey and eggs to fuel another day. These experiences reached deep among his students and colleagues.

Don's research contributions were also far-reaching. Decades of graduate students followed his lead through countless feet of Belt rocks, writing it up in theses covered in Don's editorial green ink. Don helped us envision the Belt as a vast lake or sea fed by giant alluvial fans formed when streams were not constrained by land plants or modern soils. His work led him on international quests from Spain to Siberia, trying to match lake deposits to the Belt rocks. Don could be found digging trenches through a playa lake in Mexico, lying on a dune watching sand grains bounce in a windstorm, or chasing a flash flood on a desert fan. His infectious passion inspired other researchers to join him in his quest to understand the Belt rocks, testing his models and refining our understanding. Don consumed it all, responding to debate with a pound of his fist and a growl, exclaiming, "by gawd, now we're really getting somewhere!" He taught others what good science by good people should look like, arguably his greatest contribution to the profession of geology. Montana geology will not be the same without him.

2023 DEDICATION

LARRY JOHNSON
1952–2022

Larry's life's passions were the outdoors and geology. After graduating from Great Falls High School in 1970, he pursued a degree in Geology from the University of Montana and Missoula became his life-long "basecamp." Larry worked a few years in the field for various geologic consultants and then returned to Missoula to complete his Master's degree in Geology; his thesis focused on thrust structures near Bannack, Montana.

The geologic profession took Larry on many adventures and built him an incredible network of friends. Most of his career was devoted to mineral exploration and development projects, principally on gold deposits. He worked placer gold projects in New Zealand and Elk City, Idaho, and numerous lode gold exploration projects in the western U.S. and Alaska, including several years on the McDonald Gold project near Lincoln, Montana (his favorite "digs" were always in Montana). Later in his career, he was employed in mining reclamation projects, always one who wanted to see it done right.

When not working in the outdoors, Larry played in the outdoors – hiking, cross-country skiing or backcountry skiing, and winter camping. Cross-country skiing adventures saw him trekking through New Zealand, Norway, Glacier Park, the Canadian Rockies, or anywhere that offered a challenge or grand vista. His President's Weekend winter camping/skiing tradition with a hardy group of friends lasted from his early college years through 2020.

Larry began his tenure with TRGS as the Society's Secretary in 1997 and served many years as a TRGS director. He co-owned and co-designed the Montana Rocks Geology Van, a vehicle commonly seen at the TRGS annual field conference.

Safe Travels, Friend!

2023 TRIBUTE

REED LEWIS

Many geologists have had the good fortune to unravel geological puzzles throughout Idaho and western Montana with the help of Reed Lewis. Reed has been a cornerstone of Idaho geology during his career as a Research Geologist at the Idaho Geological Survey, serving as a wellspring of information acquired by ground truth reconnaissance of countless square miles of rugged backcountry.

Reed acquired a taste for the rocks at an early age on rock hounding side trips during family vacations. His undergraduate work at the University of Idaho led him to jobs as field assistant to IGS and USGS researchers, and to the special mentorship of Thor Kiilsgaard in central Idaho. Reed earned his B.S. in Geology at the University of Idaho in 1980, a Masters of Science in Geology at the University of Washington in 1984, and his Ph.D. in Geology at Oregon State University in 1990 on Cretaceous and Tertiary plutons in the Soldier Mountains of Idaho.

Despite his predilection for intrusive igneous rocks, work on the Idaho Initiative beginning in 1989 soon introduced him to the ubiquitous, albeit generally highly metamorphosed, Belt Supergroup lithologies in the Elk City area. A few decades later, Reed is still laboring to untangle the complex stratigraphy and structure of the Lemhi Subbasin units of the Belt–Purcell Supergroup in cooperation with the MBMG. He continues his tradition of mentoring young aspiring geologists and collaboration with anyone interested in Idaho rocks statewide. Reed will undoubtedly be noted as one of the most prolific (and accurate) geological mappers in the history of Idaho geological research. No gathering of professional geologists in the region feels quite complete without Reed's friendly guidance and input.

TRGS 2023 SCHOLARSHIP AWARD WINNERS

• Skye Bensel (TRGS), Boise State University:
Examining Seasonal Variations of Subsurface Water Storage in the Critical Zone with Geophysical Imaging

• Zack DeLuca (TRGS), University of Georgia:
Hydrogeomorphic Response to Severe Flooding in Yellowstone National Park

• Samantha Khatri (Skipp), University of Georgia:
The relationship of aggradation rate and fluvial architecture: A test in the Maastrichtian Hell Creek Formation of Montana and South Dakota

• Ariana Miranda (Skipp), Temple University:
Paleosols of Florissant Fossils Beds National Monument, central Colorado

• Oliva Moehl (Belt Association), Dartmouth College:
Are the Appekunny and Greyson Fms. Correlated? A study using litho- and magnetostratigraphy

• Cade Orchard (TRGS), University of Georgia:
Nonmarine stratigraphy and community response to transgression: A test in the Cloverly Formation of Wyoming

• Mollie Pope (Sibanye-Stillwater), University of Wyoming:
Apatite as an indicator of water content in magmatic source regions

• Brett Steck (Kleinkopf), University of Montana:
Microseismic mapping of the aftershock sequences following the magnitude 5.8 Lincoln, MT earthquake

• Adam Trzinski (Harrison), University of Wyoming:
Exhumation history of the Granite Mountains, Wyoming—Insights from the Battle Springs Formation

• Jack Willard (TRGS), Utah State University:
Testing Patterns of Uplift from the Yellowstone Hotspot Along the Gallatin River, SW Montana

Thank You!

In 2021, TRGS awarded 10 scholarships to students from 7 different universities. The scholarships are funded by individual and corporate donations and proceeds from annual memberships and field conferences. We thank scholarship donors, especially our long-term donor Rob Foster and Sibanye Stillwater, who generous donations have and will continue to fund scholarships for many years.

Platinum Level

we are one Sibanye Stillwater

Rob Foster

Gold Level

Bruce Cox

Paul Link

Silver Level

Robert Branstrator
John Childs
Kirk Deal
Alan English
Jim Evans
Susanne Janecke
Dave Johnson
Katie McDonald
Dave Stewart
Mike Stickney
Sandy Underwood

Copper Level

Alan Stine

PAPERS

MOLAR-TOOTH STRUCTURE DERANGEMENT SYNDROME—A CURE

Brian R. Pratt

Department of Geological Sciences, University of Saskatchewan, Saskatoon, SK S7N 5E2, Canada

SUMMARY

Molar-tooth structure is a common feature in carbonate rocks mainly, but not exclusively, of Proterozoic age. It consists mostly of upright to tilted, vertically and often horizontally crumpled, veins composed typically of calcite microspar. It lacked a satisfactory explanation for over 130 years since it was first observed. Detailed petrography and the sedimentological context of molar-tooth structure then showed that it is a seismically induced soft-sediment deformation feature, whereby equant, fine silt-sized calcite mud was segregated from the muddy matrix during a dewatering event and injected into vein-shaped features. In some cases, silt was also injected, and in intervals where the veins cross silt and fine sand layers, some of the siliciclastic grains were incorporated. Cementation by grain growth was rapid, and subsequent ground motion led to brittle failure of the veins. Strong currents occasionally exhumed them, producing intraclastic rudstone. The veins were never gas- or water-filled voids that subsequently became occluded by calcite cement. The puzzle of molar-tooth structure was solved 25 years ago, and in part it is the carbonate analog of "syneresis" cracks that are also injection features, that is, small-scale dikes, or dikelets, emanating from sand and silt interbeds in mudstone.

INTRODUCTION

The great variety of sediments and sedimentary rocks spanning earth history has led to a wide range of features that are not explained by conventional physical processes like currents and suspension fallout. Synsedimentary deformation structures are one such category. This includes a peculiar feature in limestone that was first described by Bauerman (1884), but actually observed by him a quarter of a century earlier, which he compared to the molar tooth of elephants:

> "At the second crossing of the Kootanie, some beds of hard, green sandstone are seen. They appear to be perfectly homogeneous on a fresh surface, but show small irregular false-bedding in green and white quartzose sediment, with included fragments of slate, on a weathered face. There are associated with these beds some laminated white and black shales with small concretionary points of carbonate of lime, which pass into an impure limestone, in which the carbonate of lime is intermingled with argillaceous patches in folds resembling the markings in the molar tooth of an elephant." (Bauerman, 1884, p. 26).

This comparison led to the term "molar-tooth structure" (Daly, 1912, p. 74). Molar-tooth structure then slumbered for almost a century.

Molar-tooth structure turns out to have key geological implications (Pratt, 1998b, 2001, 2011), and yet it did not land an entry in the monumental *Encyclopedia of Sediments and Sedimentary Rocks* (Middleton, 1993). The purpose of this paper is to review the attributes of molar-tooth structure and the petrographic evidence for its mechanism of formation. The description here is based on occurrence in the Belt Supergroup (= Purcell Supergroup in Canada), specifically in the Helena Formation (= Siyeh Formation in Canada) in northwestern Montana and southwestern Alberta, the Chamberlain Formation of the Helena Embayment, exposed in the Little Belt Mountains, central Montana, and the older Waterton Formation of southwestern Alberta.

DESCRIPTION

Molar-tooth structure is present in many Proterozoic limestones worldwide that were deposited in relatively shallow depths within the photic zone (Pratt, 2001). Its relative abundance is variable stratigraphically, however. In the Helena Formation it is nearly ubiquitous (Pratt, 1998b), whereas in the Waterton Formation it has been observed only in a single interval, less than 1 m thick (Pratt and Rule, 2021). It varies widely in shape (Pratt, 1998b, 1999, 2011, 2017), the most common being crumpled, vertical to tilted veins (figs. 1A–1E). Irregularly wavy, tabular sheets and spheroids are less common (fig. 1F). On bedding planes, molar-tooth veins appear variably linear to crudely reticulate, and may be locally discontinuous or branching (figs. 2A–2E). In Glacier National Park, the orientation of linear molar-tooth structure in one studied interval in the middle of the Helena Formation is broadly in a north-northwest–south-southeast direction, at right angles to the tectonically active basin center (Pratt, 1998b).

The density of molar-tooth structure in individual beds is variable, from somewhat separated to closely spaced veins (figs. 3A, 3B). Two and locally three cross-cutting generations may be present, and record increasing stiffness of the matrix lime mud (Pratt, 1998b, 1999). Brecciation is common (figs. 3B, 3C), especially in rheologically inhomogeneous lime mud, due to early cementation of nodules and lenses (fig. 3C).

Molar-tooth structure is composed typically of a mosaic of equant calcite microspar averaging about 12 μm across, although in some cases the fill is micrite. It does not exhibit

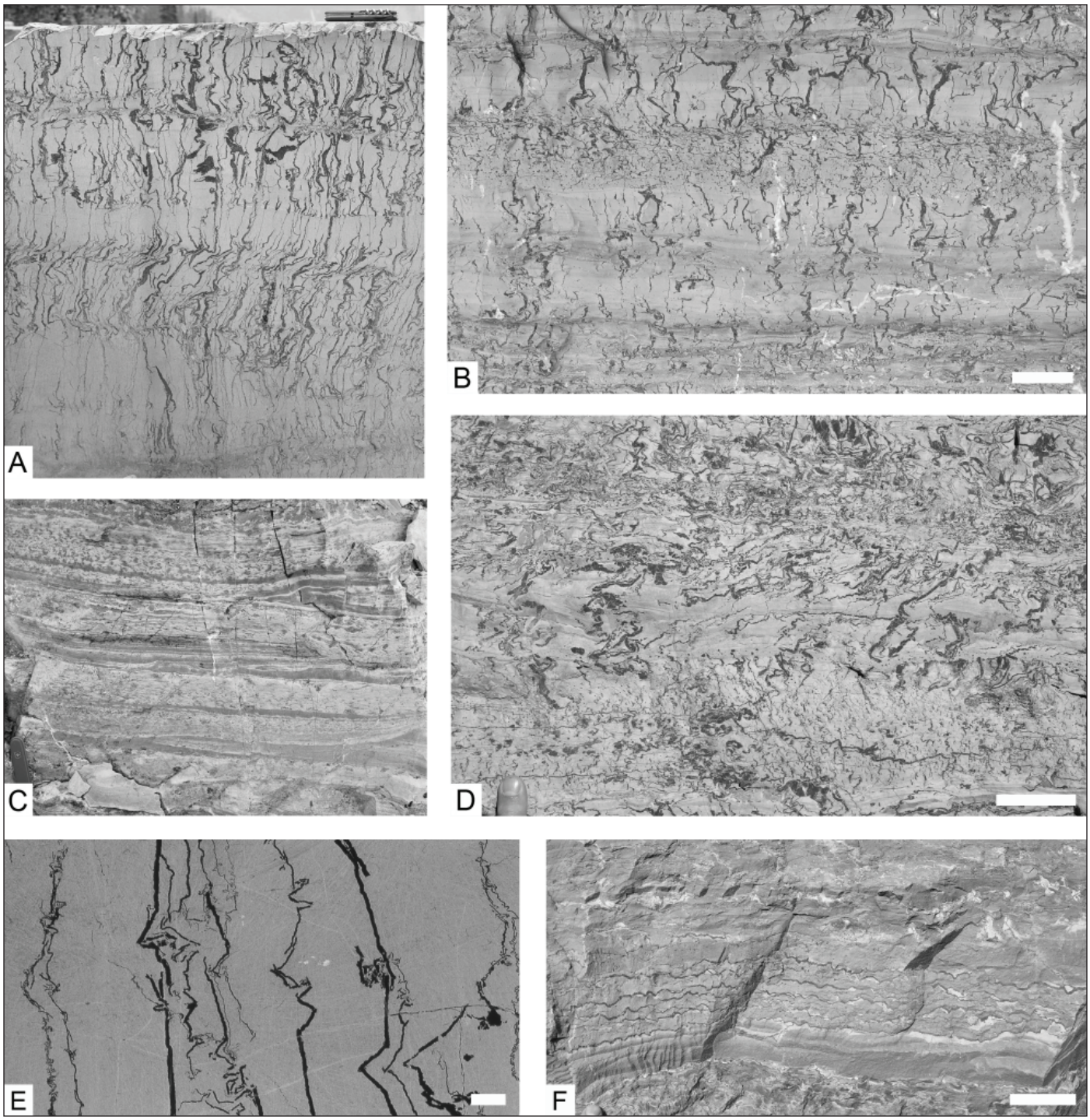

Figure 1. Molar-tooth structure in vertical view. (A, B, D, F) Helena Formation; (C) Waterton Formation; (E) Chamberlain Formation. A and E are sawn surfaces, E is etched with 10% HCl; B–D and F are outcrop surfaces. (A) Upright crumpled veins in thin-bedded dolomitic lime mudstone. Pocket knife is 9 cm long. (B) Stratigraphically variable amounts of crumpled veins in interbedded dolomitic lime mudstone. Scale bar is 10 cm. (C) Thin dolomudstone beds with scoured bases containing short folded veins. Pocket knife is 9 cm long and 2 m wide. (D) Upright to tilted crumpled veins in dolomitic lime mudstone. Scale bar is 5 cm. (E) Upright veins showing variable amounts of folding and breakage in dolomitic lime mudstone. Scale bar is 1 cm. (F) Horizontal veins with a crudely wavy shape in dolomitic lime mudstone. Scale bar is 5 cm.

the basic fabrics of void-filling calcite cements, such as centripetally increasing crystal size or wall-normal elongate crystals. Locally there is some variation in crystal size, internal clay laminae, and evidence of internal cracking, indicative of subsequent deformation before final cementation of the host bed.

In calcareous black shale of the Chamberlain Formation, some molar-tooth structure is preserved in the process of formation, in that dispersed equant, fine calcite silt is concentrated into rows of grains which in turn merge into thicker "wisps" and then into molar-tooth veins (fig. 4A). In these veins, the individual equant grains are still visible because they escaped cementation by grain growth. They

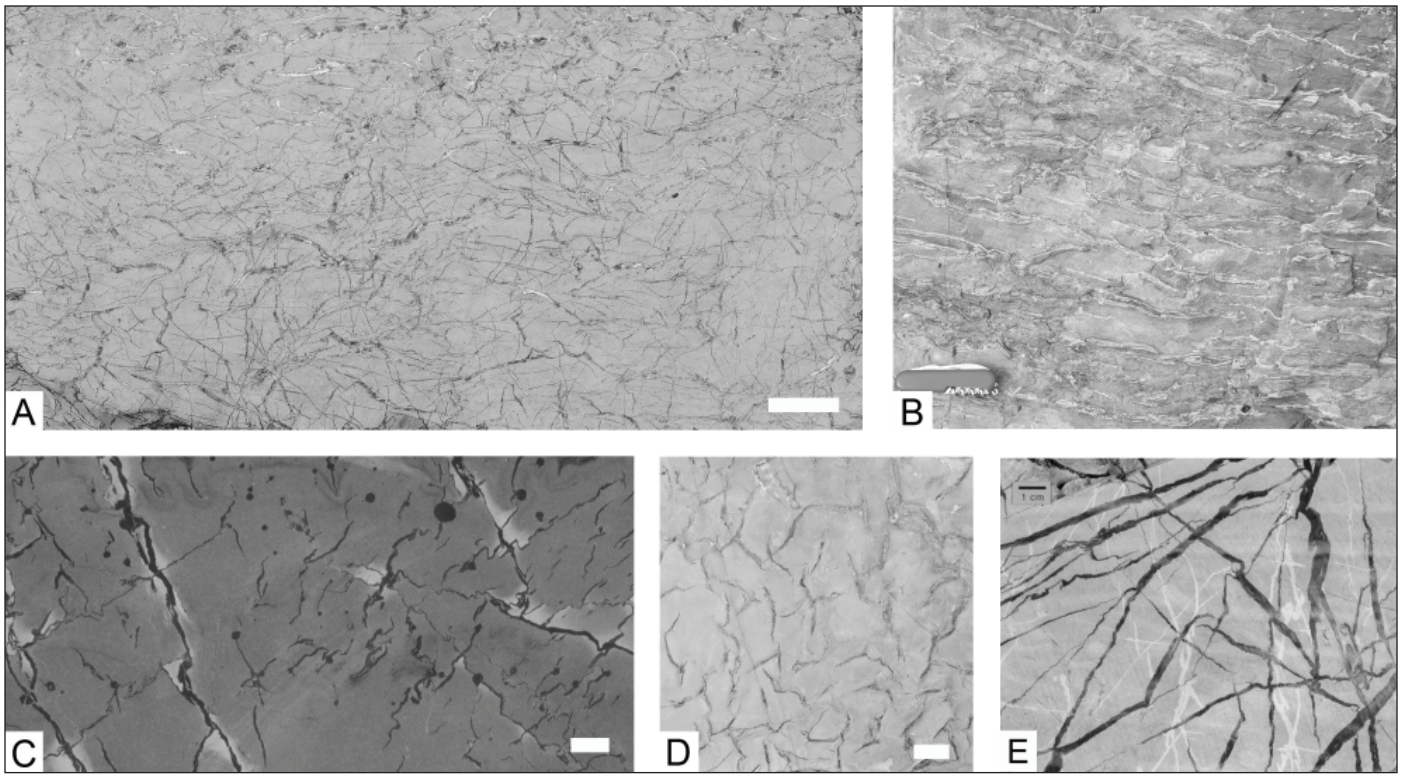

Figure 2. Molar-tooth structure in plan view, i.e. perpendicular to bedding in dolomitic lime mudstone. (A–D) Helena Formation; (E) Chamberlain Formation. A, B, and D are outcrop surfaces; C and E are sawn surfaces, C is etched. (A) Irregularly reticulate with curving veins and variable vein width. Scale bar is 10 cm. (B) Subparallel veins. Pocket knife is 9 cm long. (C) Partly reticulate, zigzagging veins with scattered spheroids. Scale bar is 1 cm. (D) Branching, laterally discontinuous veins. Scale bar is 2 cm. (E) Irregularly reticulate pattern of mainly straight veins. Scale in upper left corner.

are also embedded in early diagenetic quartz crystals (Pratt, 2011). Quartz silt floats in the microspar in some cases (fig. 4B). Where molar-tooth structure crosses a lamina or thin bed of siltstone or fine-grained sandstone in the Helena Formation, it typically incorporates variable amounts of siliciclastic particles (fig. 3D; Pratt, 1998b, 1999). Where molar-tooth structure intersects overlying oolite, in some cases the microspar has displaced the coarser grains, as well as filling adjacent interparticle pores (figs. 4C, 4D).

Backscattered scanning electron microscopy of calcite microspar in Archean molar-tooth structure showed rhombic cores (Bishop and Sumner, 2006), whereas reconnaissance analysis of the Helena Formation showed only very faint, possibly rhombic cores. Cathodoluminescence of other examples revealed rhombic, rounded, and elliptical cores (Kriscautzky and others, 2022). In the Chamberlain Formation, where not cemented into mosaics, individual grains are equant; many appear to be faceted, and some are rhombic. These grains are still apparent because they lack cement overgrowths.

Molar-tooth structure-bearing intervals of the Helena Formation exhibit common thin beds and gutter casts containing fragments of veins and commonly admixed ooids and medium- and coarse-grained quartz and feldspar sand (figs. 5A, 5B). These intraclasts of molar-tooth structure demonstrate that the veins became cemented just under the sediment surface. Sandstone-filled gutter casts are also present in some intervals (fig. 5C). Both kinds of features may be ascribed to erosion and offshore transport by tsunami backwash, which is consistent with a basin that experienced active normal faulting (Pratt, 1998b, 2001).

The Belt Supergroup exhibits common soft-sediment deformation features that can be confidently ascribed to synsedimentary earthquakes (Pratt, 1998a,b, 2001, 2017; Pratt and Ponce, 2019; Pratt and Rule, 2021). The wide variety of features was governed by specific sediment rheology, and in molar-tooth structure-bearing units these include, aside from the folding of the veins, convolute bedding (fig. 5D), ball-and-pillow structures (figs. 3D, 6A, 6B), boudinage (fig. 6A), contorted lamination (fig. 6C), microfaults (fig. 3D), shear veins (figs. 3D, 6D), and breccias (fig. 6E).

ORIGIN

Pflug (1968), on the basis of putative cyanobacterial and algal fossils, interpreted molar-tooth structure as organic. Smith (1968) and O'Connor (1972) also favored an organic origin, with the latter classifying it as a "cryptalgal" (i.e., microbial) feature related to stromatolites. Others thought that molar-tooth structure consisted originally of voids, and various mechanisms were suggested to produce them, such as desiccation (Knoll, 1984), subaqueous syneresis (Horodyski, 1976), seismically induced fracturing (Fairchild and others, 1997), and gas buildup due to decaying organic matter (Horodyski, 1976; Furniss and others,

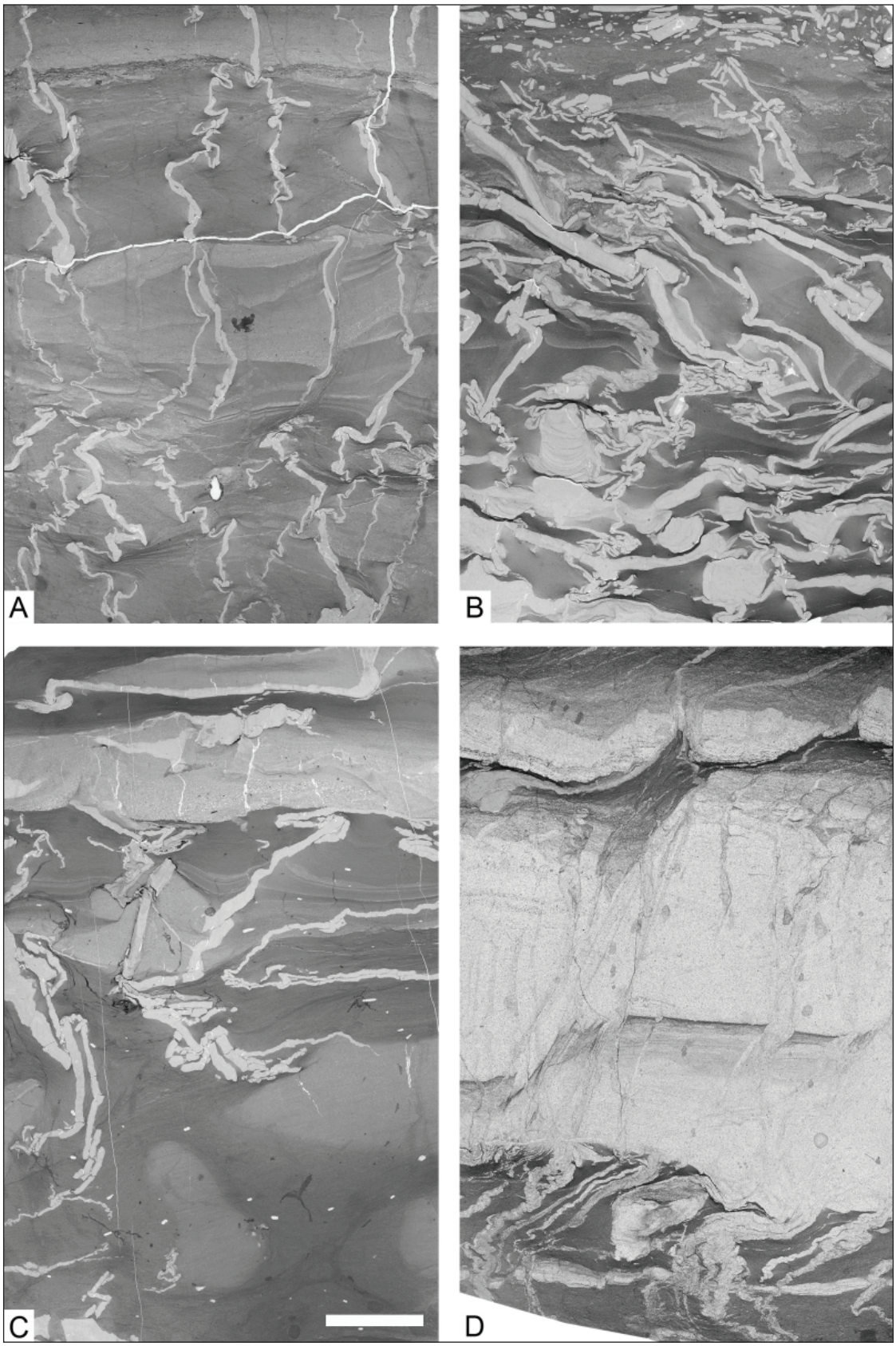

Figure 3. Molar-tooth structure and associated sand-filled dikelets in vertical view. Optical scans of thin sections. Helena Formation. Scale bar for all is 5 mm. (A) Laminated argillaceous, dolomitic lime mudstone and normally graded lime mudstone, with vertically oriented, crumpled veins. Lower part has conspicuously compacted argillaceous sediment. (B) Upright to tilted veins showing variable degree of crumpling, disruption, and brecciation, along with spheroidal "pods" of calcite microspar. In lower left a spheroid shows small-scale ball-and-pillow deformation. (C) Argillaceous dolomitic mudstone (darker colored) and nodules and lenses of lime mudstone (lighter colored) with variably crumpled and brecciated veins. (D) Thin bed of fine-grained sandstone cut by shear veins. Under- and overlying argillaceous dolomitic lime mudstone layers are crosscut by calcitic veins, sand-filled veins ("syneresis" cracks or dikelets), and veins containing microspar and sand.

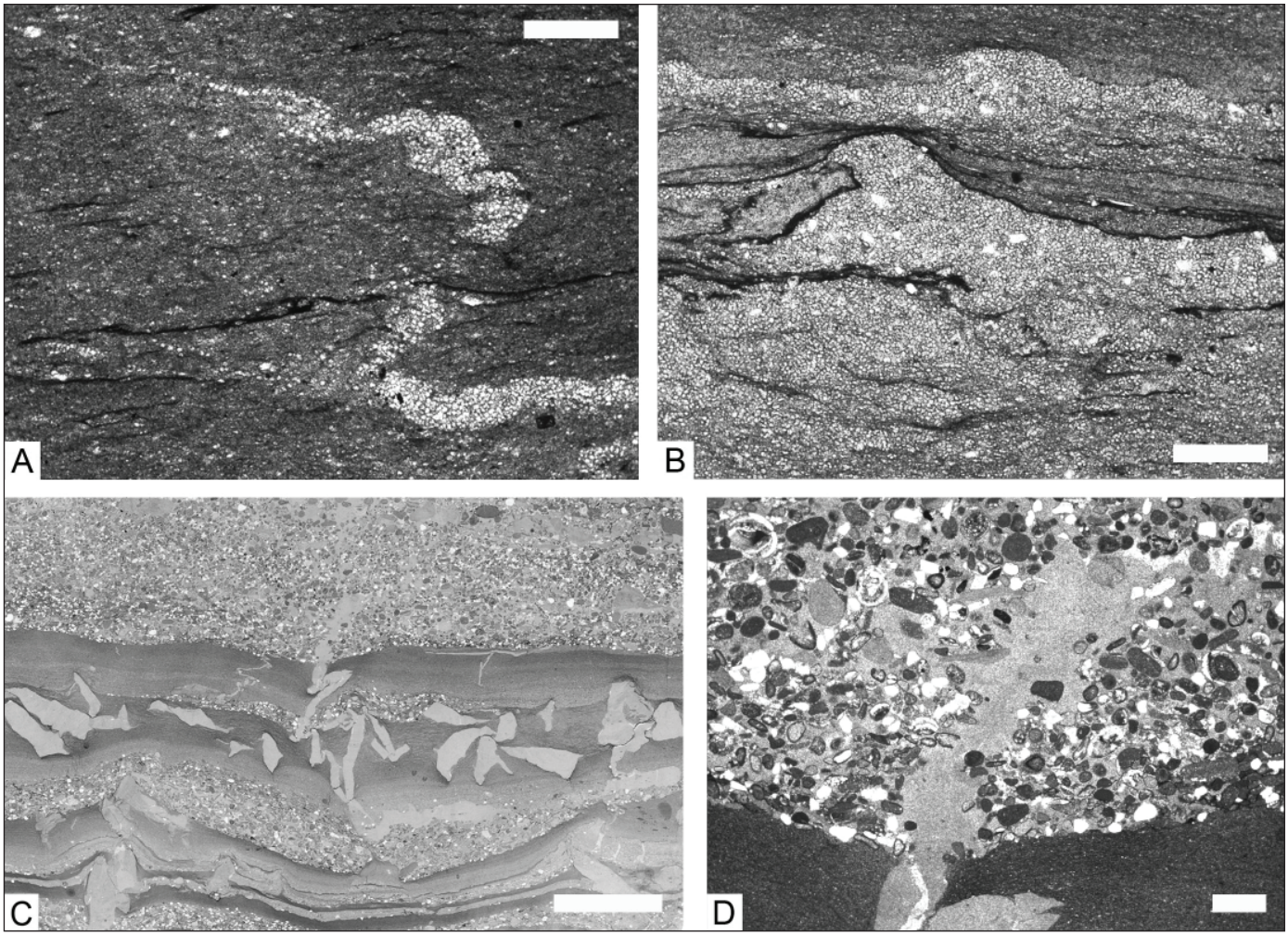

Figure 4. Evidence for lime mud injection. (A, B) Chamberlain Formation; (C, D) Helena Formation. A, B, and D are photomicrographs (plane-polarized light) of vertically oriented thin sections; C is an optical scan of vertically oriented thin section. (A) Folded dikelet, consisting of equant, fine silt-sized calcite grains, tapering into the black shale matrix and becoming a train of individual grains; the same grains are also variably dispersed in the matrix. Scale bar is 200 μm. (B) Horizontal veins containing floating angular quartz silt (white particles). Scale bar is 200 μm. (C) Interlaminated ooidal grainstone and argillaceous lime mudstone with molar-tooth structure veins and vein fragments. Vein in uppermost mudstone lamina passes into microspar that displaces sand and ooids and fills laterally adjacent interparticle porosity (upper-center). Scale bar is 5 mm. (D) Thin-section photomicrograph (plane-polarized light) of part of A, showing injected microspar that displaces siliciclastic sand, ooids, and small micrite intraclasts. Scale bar is 1 mm.

1998, Winston and others, 1999). Furniss and others (1998) created voids experimentally by fermenting sugar in unset plaster mixed with clay. Formation by methane produced in the sediment is the mechanism favored in some recent studies and reviews (Kuang, 2014; Shen and others, 2016; Smith, 2016; Kriscautzky and others, 2022; Tang and others, 2023). However, despite assertions to the contrary (Shen and others, 2016; Tang and others, 2023), there is a notable absence of a distinct C-isotopic signal reflecting sulphate reduction or methanogenesis (Frank and Lyons, 1998; Pratt, 1998b; Hodgskiss and others, 2018; Lyons and others, 2023). There has also not been an appreciation of the amount of organic matter that needs to be degraded in order to create the volume of void space by displacing—seemingly abruptly—muddy sediment under shallow burial, be it by generation of methane or carbon dioxide. Whereas intervals of the Chamberlain Formation contain carbonaceous seams (figs. 4A, 4B, 6C), organic carbon is absent in the Helena Formation.

It has been suggested that wave pumping created voids (Bishop and others, 2006; Hodgskiss and others, 2018). However, molar-tooth structure typically crosscuts laminated lime mudstone of low-energy aspect that shows no evidence of strong wave action from above that would be needed to shift buried mud back and forth and up and down in order to deform it. Some examples of molar-tooth structure taper upwards as well as downwards, suggesting that high energy from post-depositional wave action cannot be invoked. Hodgskiss and others (2018) suggested in addition that conversion of smectite to illite aided in forming voids. However, this is not a reaction that occurs in near-surface sediment where molar-tooth structure formed. Although a role for clays in terms of clay card-house collapse and dewatering was envisioned by Pratt (1998b) as important for molar-tooth structure formation because the Helena Formation is argillaceous, later study of other units in different basins showed that molar-tooth structure also developed

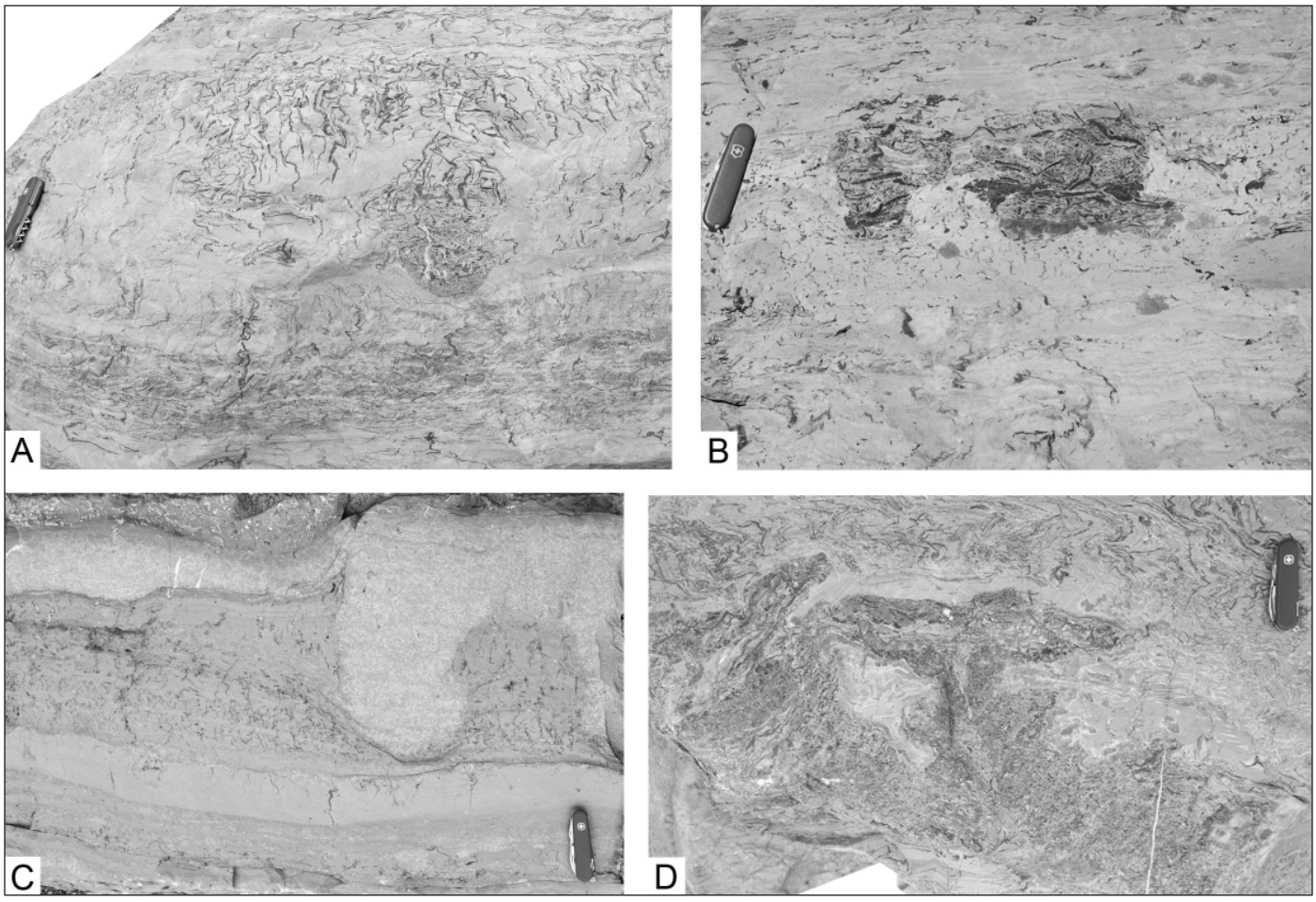

Figure 5. Gutter casts on outcrop surfaces of Helena Formation. Pocket knife is 9 cm long. (A) Lime mudstone with molar-tooth structure, punctuated by gutter cast containing vein fragments and probably ooids. (B) Lime mudstone containing sparse molar-tooth structure, punctuated by gutter cast containing vein fragments and exhibiting a bilobate base. (C) Lime mudstone containing sparse then denser molar-tooth structure, overlain by a thin bed of fine-grained sandstone in places filling deep gutters. (D), Large gutter filled with vein fragments and ooids that was subsequently deformed into a convolute bed by a syndepositional earthquake.

in pure lime muds, thereby negating a key role for clays (Pratt, 2011).

Molar-tooth structure was never a void space during its formation. The material that filled the veins was granular lime mud mobilized and ejected from the lime mud matrix during a liquefaction and dewatering event. The presence of floating and admixed quartz silt is further proof that molar-tooth structure, like 'syneresis' cracks, are sedimentary dikelets. Microspar displacing sand and ooids and filling interparticle pores provides further evidence for injection of fine calcite silt. The veins were typically intensely folded during formation; if they were gas-filled, parts of them would have collapsed. The process that formed the veins was often repeated a second and sometimes a third time, leading to superimposed veins and brittle failure of cemented veins. The dynamic and cyclic nature of this mechanism points to earthquake shock, that is, cyclic ground motion due to shaking of the seafloor.

IMPLICATIONS

Compilations of molar-tooth structure occurrences appear to indicate that it is restricted to Precambrian carbonate rocks (Horodyski, 1976; James and others, 1998; Pratt, 1998b; Kuang, 2014; Smith, 2016; Kriscautzky and others, 2022). This in turn led to various notions that geochemical processes and their secular trends were implicated. For example, Shen and others (2016) suggested that molar-tooth structure was formed by methane degassing, and the water column was sulphidic, whereas Tang and others (2023) claimed that it points to a protracted oxygenation phase. Lyons and others (2023) stated that molar-tooth structure indicates high levels of carbonate saturation, due to high atmospheric pCO_2. Hodgskiss and others (2018) suggested that declining pCO_2 led to diminished dissolved inorganic carbon in the oceans. The decline into the Neoproterozoic was ascribed to changes in the chemistry of seawater, especially a decrease in $CaCO_3$ saturation caused by a drop in pCO_2 (Shields, 2002). The advent of bioturbation has been assumed to have been a key evolutionary phenomenon that prevented molar-tooth structure development in Phanerozoic carbonate muds because it altered the rheology of the sediment (e.g., Pratt, 1998b; Mei and Tucker, 2011).

In reality, features closely matching Proterozoic molar-tooth structure are present in younger carbonate rocks,

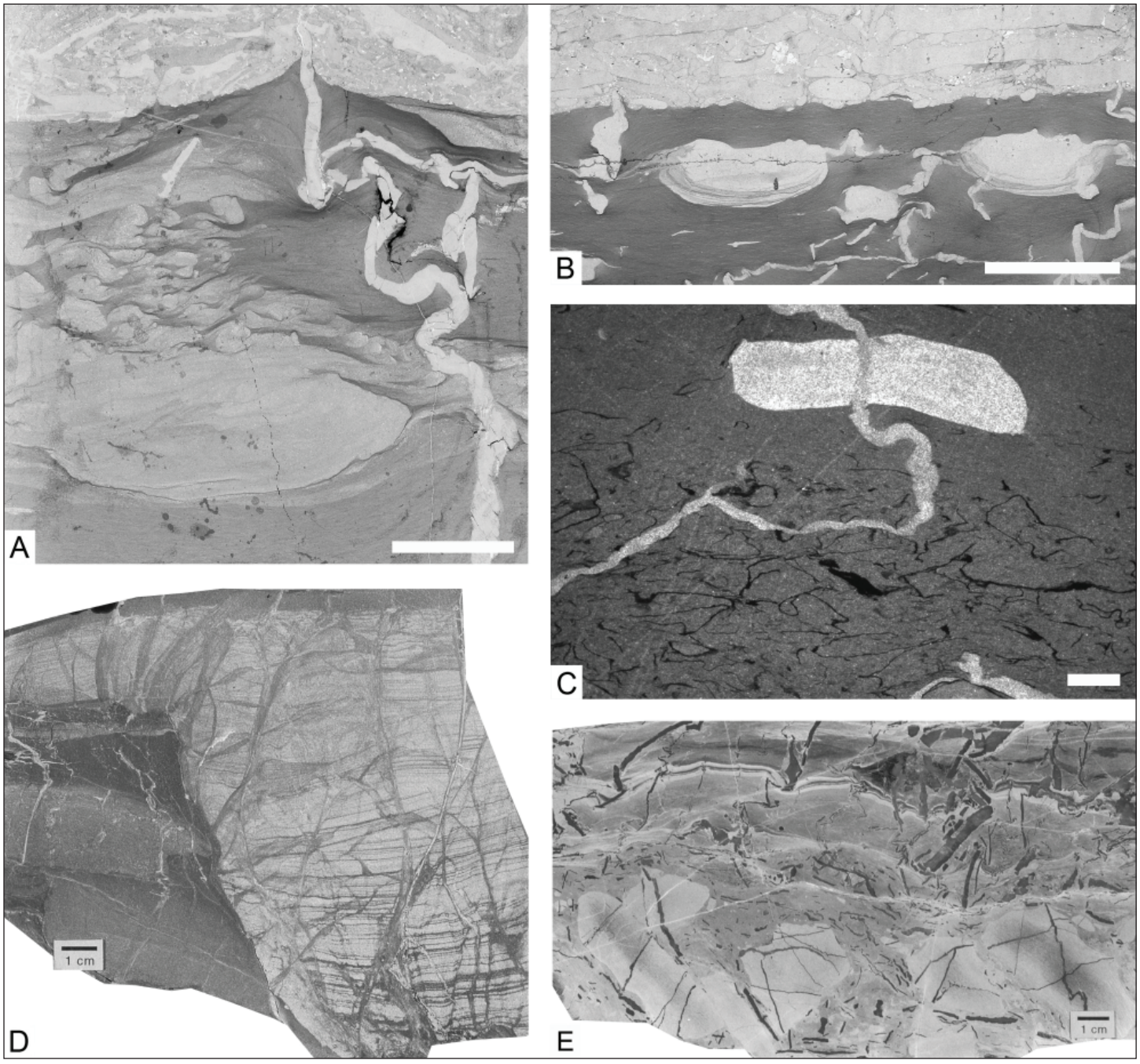

Figure 6. Syndepositional earthquake-induced deformation of beds hosting molar-tooth structure. (A, B, D) Helena Formation; (C, E): Chamberlain Formation. A and B are optical scans of thin sections; C is a thin-section photomicrograph (plane-polarized light); D and E are sawn and etched surfaces. (A) Argillaceous lime mudstone with small ball-and-pillow structure and sheared and boudinaged domains above, with crumpled molar-tooth structure at right. Molar-tooth vein is brecciated and a scouring event left it poking up into intraclastic rudstone consisting of molar-tooth fragments. Scale bar is 10 mm. (B) Molar-tooth structure consisting of spheroids and veins, overlain by intraclastic rudstone consisting of molar-tooth fragments. The two spheroids comprise slightly flattened ball-and-pillow structures with clay laminae at their bottoms. Scale bar is 10 cm. (C) Calcareous black shale with contorted carbonaceous seams, crosscut by molar-tooth vein. Scale bar is 1 mm. (D) Silty, argillaceous lime mudstone downcut by gutter cast composed of cross-laminated, silty, fine-grained sandstone. The lime mudstone is crosscut by molar-tooth veins at left, whereas the sandstone is crosscut by silt- and sand-filled vein arrays that also penetrate the lime mudstone and merge with molar-tooth veins in which microsparry calcite and silt are admixed. (E) Lime mudstone bed containing dispersed fragments of molar-tooth veins and angular blocks of lime mudstone containing undeformed veins, overlain by folded laminae and thin beds containing veins and brecciated veins.

albeit rarely (Pratt, 2011). These include early Paleozoic examples of short, vertically oriented, folded, calcite-filled veins (fig. 7A), vertically and horizontally crumpled dikelets in dolomudstone (fig. 7B; Pratt, 1982), and crumpled dikelets in lacustrine carbonates belonging to the Eocene Green River Formation of Wyoming and Utah (fig. 7C; Törő and Pratt, 2015a,b). By comparison, although an exact counterpart has not been reported from Proterozoic strata, some argillaceous limestone beds in the Green River Formation of Colorado contain dikelets composed mostly of well-sorted, coarse angular quartz silt (fig. 7D; Törő and Pratt, 2015b). This silt appears to have been expelled from the argillaceous lime mud matrix while the dispersed, finer silt remained, unlike "syneresis" cracks that are filled with sediment injected into mud from silt or sand interbeds (Pratt, 1998a; Pratt and Ponce, 2019). Synsedimentary earthquake-induced deformation is common in this succession.

What molar-tooth structure indicates is that: (1) in many Precambrian basins, lime mud consisted of equant, fine silt-sized grains, unlike, for example, the needle-shaped aragonite mud of Florida Bay, and therefore was susceptible to losing its shear strength and being mobilized during cyclic ground motion; (2) lime mud precipitation was probably triggered by microbial activity in the water column, similar to hardwater lakes; (3) the overlying seawater was oxygenated; (4) the atmosphere was probably oxidative; (5) the lack of clay in many host units indicates that clay card-house collapse was not necessary for molar-tooth structure formation after all; (6) the lime mud in the veins lithified rapidly by grain growth just beneath the sediment–water interface, indicating supersaturated seawater; (7) formation, and subsequent deformation if present, are a proxy seismometer for the basin; (8) erosional features, especially gutter casts containing allochthonous, shallow water particles, may have been generated by tsunami back-

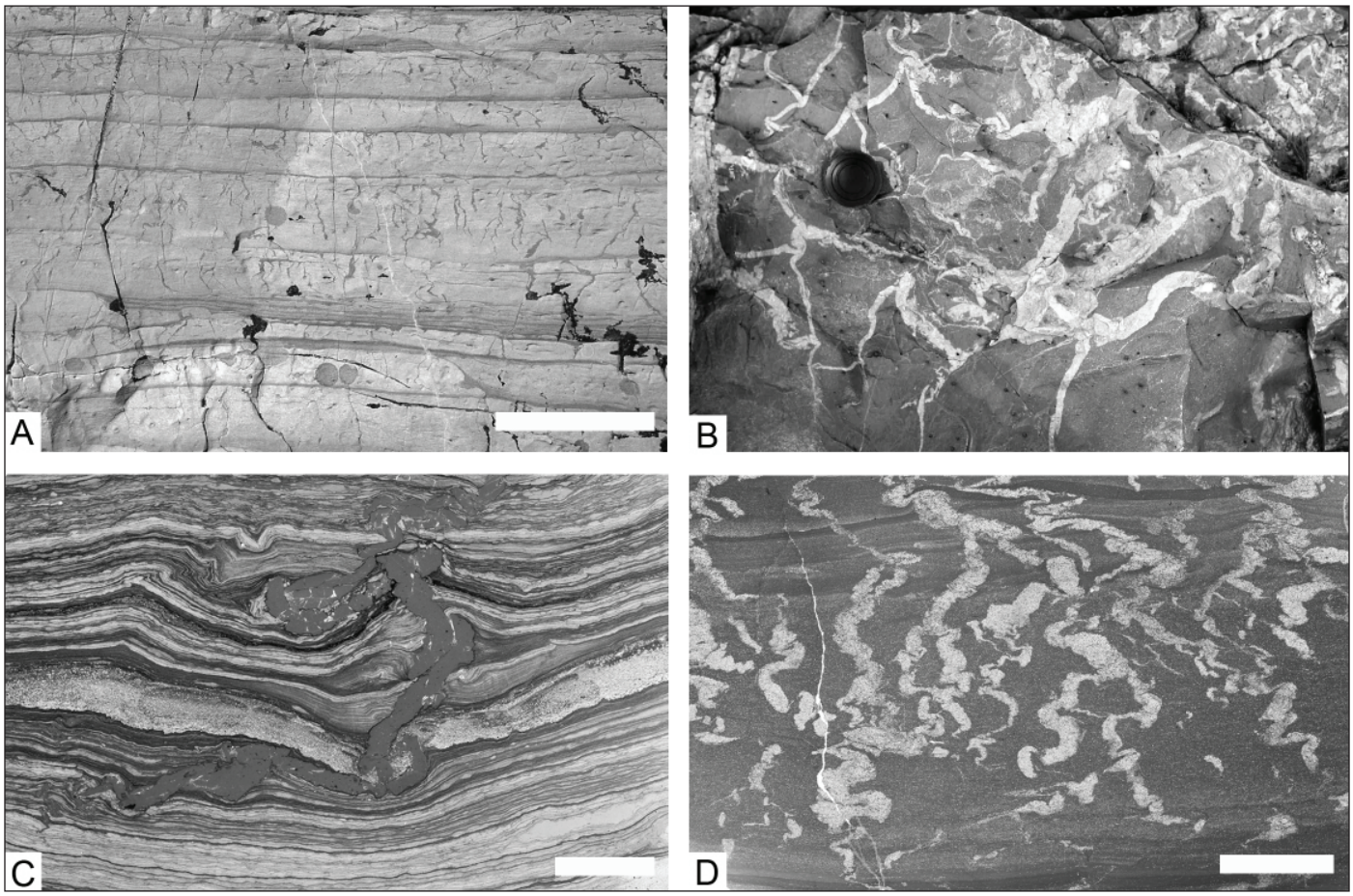

Figure 7. Phanerozoic molar-tooth structure and silty dikelets. (A, B) Shallow-marine carbonates; (B, C) lacustrine carbonates. A and B are outcrop surfaces; C and D are optical scans of thin sections. (A) View perpendicular to bedding of thin-bedded lime mudstone cross-cut by arrays of blocky calcite-filled dikelets corresponding to molar-tooth structure. Scale bar is 10 cm. Lyell Formation (upper Cambrian), southern Rocky Mountains, Alberta. (B) Bedding plane view of dolomudstone containing an irregular network of light-colored dolomudstone dikelets corresponding to molar-tooth structure. Aguathuna Formation, St. George Group (Lower Ordovician), southwestern Newfoundland (Pratt, 1982, fig. 5A). Lens cap is 5.4 cm in diameter. (C) Laminated microsparry calcite and a silty lamina (just below center line) exhibiting soft-sediment deformation (boudinage and microfolds) and cross-cut by disrupted, indistinctly peloidal, micrite-filled dikelet corresponding to molar-tooth structure. Green River Formation (Eocene), Fossil Basin, southwestern Wyoming. Scale bar is 10 mm (Törő and Pratt, 2015a, fig. 12D). (D) Argillaceous silty lime mudstone crosscut by silt-filled dikelets. Here, the dikelets are not composed of calcite grains expelled from the matrix but angular coarse silt, plus some lime mud, expelled from the matrix. Green River Formation (Eocene), Piceance Creek Basin, northwestern Colorado (Törő and Pratt, 2015b, fig. 14F). Scale bar is 10 mm.

wash rather than storm activity; and (9) while Phanerozoic carbonate sediments were largely different, those counterparts that have been observed indicate that the combination of lime mud size and shape and matrix composition duplicated the rheological attributes of Precambrian examples.

The puzzle of molar-tooth structure was solved a quarter of a century ago using petrographic observations and their sedimentological context. There is no need to still regard it as "controversial" and "enigmatic."

ACKNOWLEDGMENTS

I first observed molar-tooth structure in 1976 and became fascinated by it through the 1980s. I am grateful to E.C. Turner for field assistance in the early 1990s and for sharing my Eureka! moment, the staff at Glacier and Waterton Lakes national parks for issuing research and collection permits, D.G.F. Long for collaborative work on molar-tooth structure-bearing Paleoproterozoic limestones of northeastern British Columbia, R.H. Rainbird for introducing me to the Neoproterozoic stratigraphy of Victoria Island, Northwest Territories, and J. Bertrand-Sarfati and A. Moussine-Pouchkine for organizing a rewarding field trip to the Neoproterozoic of Mauritania in 1987. I thank the Natural Sciences and Engineering Research Council of Canada for ongoing funding.

REFERENCES

Bauerman, H., 1884, Report on the geology of the country near the forty-ninth parallel of north latitude west of the Rocky Mountains: From observations made in 1859–1861: Geological and Natural History Survey of Canada, Dawson, Montreal, 42 p. [reprinted as Report on the geology of the country near the forty-ninth parallel of north latitude west of the Rocky Mountains: Geological and Natural History Survey and Museum of Canada, Reports and Maps of Investigations and Surveys 1882–83–84, Report of Progress 1882–83–84, part B, p. 1–42, Dawson, Montreal, 1885.]

Bishop, J.W., and Sumner, D.Y., 2006, Molar tooth structures of the Neoarchean Monteville Formation, Transvaal Supergroup, South Africa. I: Constraints on microcrystalline CaCO3 precipitation: Sedimentology, v. 53, p. 1049–1058.

Bishop, J.W., Sumner, D.Y., and Huerta, N.J., 2006, Molar tooth structures of the Neoarchean Monteville Formation, Transvaal Supergroup, South Africa. II: A wave-induced fluid flow model: Sedimentology, v. 53, p. 1069–1082.

Daly, R.A., 1912, Geology of the North American cordillera at the forty-ninth parallel: Canada Department of Mines, Geological Survey Memoir 38, 546 p.

Fairchild, I.J., Einsele, G., and Song, T., 1997, Possible seismic origin of molar tooth structures in Neoproterozoic carbonate ramp deposits, north China: Sedimentology, v. 44, p. 611–636.

Frank, T.D., and Lyons, T.W., 1998, "Molar-tooth" structures: A geochemical perspective on a Proterozoic enigma: Geology, v. 26, p. 683–686.

Furniss, G., Rittel, J.F., and Winston, D., 1998, Gas bubble and expansion crack origin of "molar-tooth" calcite structures in the middle Proterozoic Belt Supergroup, western Montana: Journal of Sedimentary Research, v. 68, p. 104–114.

Hodgskiss, M.S.W., Kunzmann, M., Poirier, A., and Halverson, G.P., 2018, The role of microbial iron reduction in the formation of Proterozoic molar tooth structures: Earth and Planetary Science Letters, v. 482, p. 1–11.

Horodyski, R.J., 1976, Stromatolites of the upper Siyeh Limestone (Middle Proterozoic), Belt Supergroup, Glacier National Park, Montana: Precambrian Research, v. 3, p. 517–536.

James, N.P., Narbonne, G.M., and Sherman, A.G., 1998, Molar-tooth carbonates: Shallow subtidal facies of the mid- to late Proterozoic: Journal of Sedimentary Research, v. 68, p. 716–722.

Knoll, A.H., 1984, Microbiotas of the Late Precambrian Hunnberg Formation, Nordaustlandet, Svalbard: Journal of Paleontology, v. 58, p. 131–162.

Kriscautzky, A., Kah, L.C., and Bartley, J.K., 2022, Molar-tooth structure as a window into the deposition and diagenesis of Precambrian carbonate: Annual Review of Earth and Planetary Sciences, v. 50, p. 205–230.

Kuang, H.-W., 2014, Review of molar tooth structure research: Journal of Palaeogeography, v. 3, p. 359–383.

Lyons, T.W., Tu, C., and Hancock, L., 2023, Giving some tooth to Precambrian carbonates and the tales they tell about ancient oceans: JGR Biogeosciences, v. 128, article e2023JG007491.

Mei, M., and Tucker, M.W., 2011, Molar tooth structure: A contribution from the Mesoproterozoic Gaoyuzhuang Formation, Tianjin City, North China: Acta Geologica Sinica, v. 85, p. 1084–1099.

Middleton, G.V., ed., 1993, Encyclopedia of Sediments and Sedimentary Rocks: Kluwer, Dordrecht, 821 p.

O'Connor, M.P., 1972, Classification and environmental interpretation of the cryptalgal organosedimentary "molar-tooth" structure from late Precambrian Belt-Purcell Supergroup: Journal of Geology, v. 80, p. 592–610.

Pflug, H.D., 1968, Gesteinsbildende Organismen aus den Molar Tooth Limestone der Beltserie (Präkambrium): Palaeontographica Abt. B, v. 121, p. 134–141.

Pratt, B.R., 1982, Limestone response to stress: Pressure solution and dolomitization—Discussion and examples of compaction in carbonate sediments: Journal of Sedimentary Petrology, v. 52, p. 323–328.

Pratt, B.R., 1998a, Syneresis cracks: Subaqueous shrinkage in argillaceous sediments caused by earthquake-induced dewatering: Sedimentary Geology, v. 117, p. 1–10.

Pratt, B.R., 1998b, Molar-tooth structure in Proterozoic carbonate rocks: Origin from synsedimentary earthquakes, and implications for the nature and evolution of basins and marine sediment: Geological Society of America Bulletin, v. 110, p. 1028–1045.

Pratt, B.R., 1999, Gas bubble and expansion crack origin of "molar-tooth" calcite structures in the middle Proterozoic Belt Supergroup, western Montana—Discussion: Journal of Sedimentary Research, v. 68, p. 1136–1140.

Pratt, B.R., 2001, Oceanography, bathymetry and syndepositional tectonics of a Precambrian intracratonic basin: Integrating sediments, storms, earthquakes and tsunamis in the Belt Supergroup (Helena Formation, c. 1.45 Ga), western North America: Sedimentary Geology, v. 141–142, p. 371–394.

Pratt, B.R., 2011, Molar-tooth structure, *in* Reitner, J., and Thiel, V. eds., Encyclopedia of Geobiology: Springer, Dordrecht, p. 662–666.

Pratt, B.R., 2017, The Mesoproterozoic Belt Supergroup in Glacier and Waterton Lakes national parks, northwestern Montana and southwestern Alberta: Sedimentary facies and syndepositional deformation, *in* Hsieh, J.C.C., ed., Geologic Field Trips of the Canadian Rockies: 2017 Meeting of the GSA Rocky Mountain Section: Geological Society of America Field Guide 48, p. 123–135.

Pratt, B.R., and Ponce, J.J., 2019, Sedimentation, earthquakes, and tsunamis in a shallow, muddy epeiric sea: Grinnell Formation (Belt Supergroup, ca 1.45 Ga), western North America: Geological Society of America Bulletin, v. 131, p. 1411–1439.

Pratt, B.R., and Rule, R.G., 2021, A Mesoproterozoic carbonate platform (lower Belt Supergroup of western North America): Sediments, facies, tides, tsunamis and earthquakes in a tectonically active intracratonic basin: Earth-Science Reviews, v. 217, article 103626.

Shen, B., Dong, L., Xiao, S., Lang, X., Huang, K., Peng, Y., Zhou, C., Ke, S., and Liu, P., 2016, Molar tooth carbonates and benthic methane fluxes in Proterozoic oceans: Nature Communications, v. 7, article 10317.

Shields, G.A., 2002, 'Molar-tooth microspar': A chemical explanation for its disappearance ~750 Ma: Terra Nova, v. 14, p. 108–113.

Smith, A.G., 1968, The origin and deformation of some "molar-tooth" structures in the Precambrian Belt-Purcell Supergroup: Journal of Geology, v. 76, p. 426–443.

Smith, A.G., 2016, A review of molar-tooth structures with some speculations on their origin, *in* MacLean, J.S., and Sears, J.W., eds., Belt Basin: Window to Mesoproterozoic Earth: Geological Society of America Special Paper 522, p. 71–99.

Tang, D., Fang, H., Shi, X., Liang, L., Zhou, L., Xie, B., Huang, K., Zhou, X., Wu, M., and Riding, R., 2023, Mesoproterozoic molar tooth structure related to increased marine oxygenation: JGR Biogeosciences, v. 128, article e2022JG007077.

Törő, B., and Pratt, B.R., 2015a, Eocene paleoseismic record of the Green River Formation, Fossil Basin, Wyoming, U.S.A.: Implications of synsedimentary deformation structures in lacustrine carbonate mudstones: Journal of Sedimentary Research, v. 85, p. 855–884.

Törő, B., and Pratt, B.R., 2015b, Characteristics and implications of sedimentary deformation features in Eocene lacustrine and fluvial strata in the Uinta Basin, Utah and Colorado, *in* Birgenheier, L., Ressetar, R., and Vanden Berg, M., eds., The Uinta Basin and Uinta Mountains: Utah Geological Association Publication 44, p. 371–422.

Winston, D., Rittel, J.F., amd Furniss, G., 1999, Gas bubble and expansion crack origin of "molar-tooth" calcite structures in the middle Proterozoic Belt Supergroup, western Montana—Reply: Journal of Sedimentary Research, v. 68, p. 1140–1145.

LEMHI SUBBASIN STRATIGRAPHY AND STRUCTURE: AN UPDATE

Russell F. Burmester,[1] Reed S. Lewis,[1] Jeffrey D. Lonn,[2] and Mark D. McFaddan[3]

[1]Idaho Geological Survey, Moscow, Idaho
[2]Montana Bureau of Mines and Geology, Butte, Montana
[3]North Idaho College and Idaho Geological Survey (retired), Naples, Idaho

ABSTRACT

The Apple Creek Formation above the Swauger and Lawson Creek Formations comprises the upper part of the Lemhi subbasin strata of the Mesoproterozoic Belt Supergroup in the vicinity of Salmon, Idaho. Lithologic variation of sediment types and features within the Apple Creek Formation reflects the migration, change, or end of depositional environments. Some of this variation may record the effects of syndepositional tectonism, such as the initiation and activity of growth faults. A hindrance to environmental reconstructions is that the strata are exposed on several thrust plates whose original locations are poorly constrained. The Poison Creek thrust plate carries laterally varied Apple Creek units that are not known on the North Fork plate and are much different from those on the Jackson Plate. The Poison Creek fault is yet untraceable through the Mesoproterozoic igneous complex, which intruded rocks now on both the Poison Creek and North Fork plates. To the north–northwest, lack of the distinctive quartzite of the Swauger Formation and increased metamorphism and deformation preclude recognition of those plates. However, the North Fork thrust may have continued northward to east of Elk City, where the Green Mountain fault separates metamorphosed Lemhi subbasin strata and Mesoproterozoic augen gneiss from quartzite and carbonate rocks likely part of the main Belt Basin. If so, strata northeast of the North Fork and Trail Gulch–Freeman thrusts may correlate with strata of the main Belt Basin.

INTRODUCTION

Mesoproterozoic strata near Salmon, Idaho are part of a southern, relatively young portion of the Belt Basin termed the Lemhi subbasin (fig. 1). Intrusion of mafic magmas into wet sediment low in the Prichard Formation of the main Belt Basin was 1469 ± 2.5 Ma (Rogers and others, 2016), but the lowest unit in the Lemhi subbasin, Big Creek Formation (Lonn, 2017), contains zircons with a young age peak of 1424 Ma (see Lonn and others, The Mesoproterozoic Belt– Lemhi connection, this volume). The stratigraphy of the Lemhi subbasin is complicated by thrust faults that divide it into distinct thrust plates (fig. 2) containing different parts of the stratigraphic record. Even individual thrust plates have lateral variations within stratigraphic units that make characterizing the subbasin's history difficult. Here we'll review the current map units of the subbasin and their variation, then the structural progression, in an attempt to constrain correlations of subbasin units with those of the main Belt Basin.

STRATIGRAPHY

Lemhi Subbasin

Sediments in the Lemhi subbasin were early dropouts of water-transported fine sand and mud being conveyed northward (in present coordinates) from the postulated Big White Arc (Link and others, 2016) to be deposited as the Missoula Group in the main Belt Basin. They became what we now call the Lemhi Group and overlying Swauger, Lawson Creek, and Apple Creek Formations. Figure 3 shows a roughly west to east sampling of stratigraphic sections, the locations of which are shown on the generalized geologic map (fig. 2). The most complete section (PC3) is in the Lemhi Range where Tysdal (1996a) subdivided the Apple Creek phyllite of Anderson (1961) into the fine and coarse siltite and diamictite informal units of Ruppel's (1975) Apple Creek Formation. The fine siltite (Yaf; fig. 4) is mostly very fine, thin- to medium-bedded quartzite; the coarse siltite (Yac; fig. 5) is mostly siltite and argillite couplets with some fine quartzite beds. The diamictite unit (Yad, fig. 6) is a concentration of zones, layers, or lenses of matrix-supported breccia or conglomerate (Tietbohl, 1986). We called those units informal members of the Apple Creek Formation (Burmester and others, 2016) and added as the Lem Peak member the basal fine-grained quartzite (Yalp; fig. 7) that Tysdal (1996a,b) had mapped as the Big Creek Formation. The banded siltite (Yab; fig. 8) was recognized north of Lem Peak against the Poison Creek fault (fig. 2) but not as part of the Apple Creek Formation (Tysdal and Moye, 1996) until later (Tysdal, 2002, 2003). The fine siltite and diamictite members (Yafd) have been mapped west of the Salmon River (Evans, 1998; Tysdal, 2000, 2003; see the Salmon to Challis field trip, this volume), but no member below the coarse siltite has been recognized more than a few kilometers farther west. However, higher members, Lake Mountain (Yalm; fig. 9) and overlying Trapper Gulch (Yatg; fig. 10), have been mapped above the banded siltite west of the river to beyond the Blackbird mine (fig. 2).

Lower Apple Creek Formation Strata

The lowest members of the Apple Creek Formation have not been found on the Iron Lake plate, which carries the type sections of the Yellowjacket Formation and Hoodoo Quartzite (figs. 2, 3). There the Hoodoo Quartzite, in

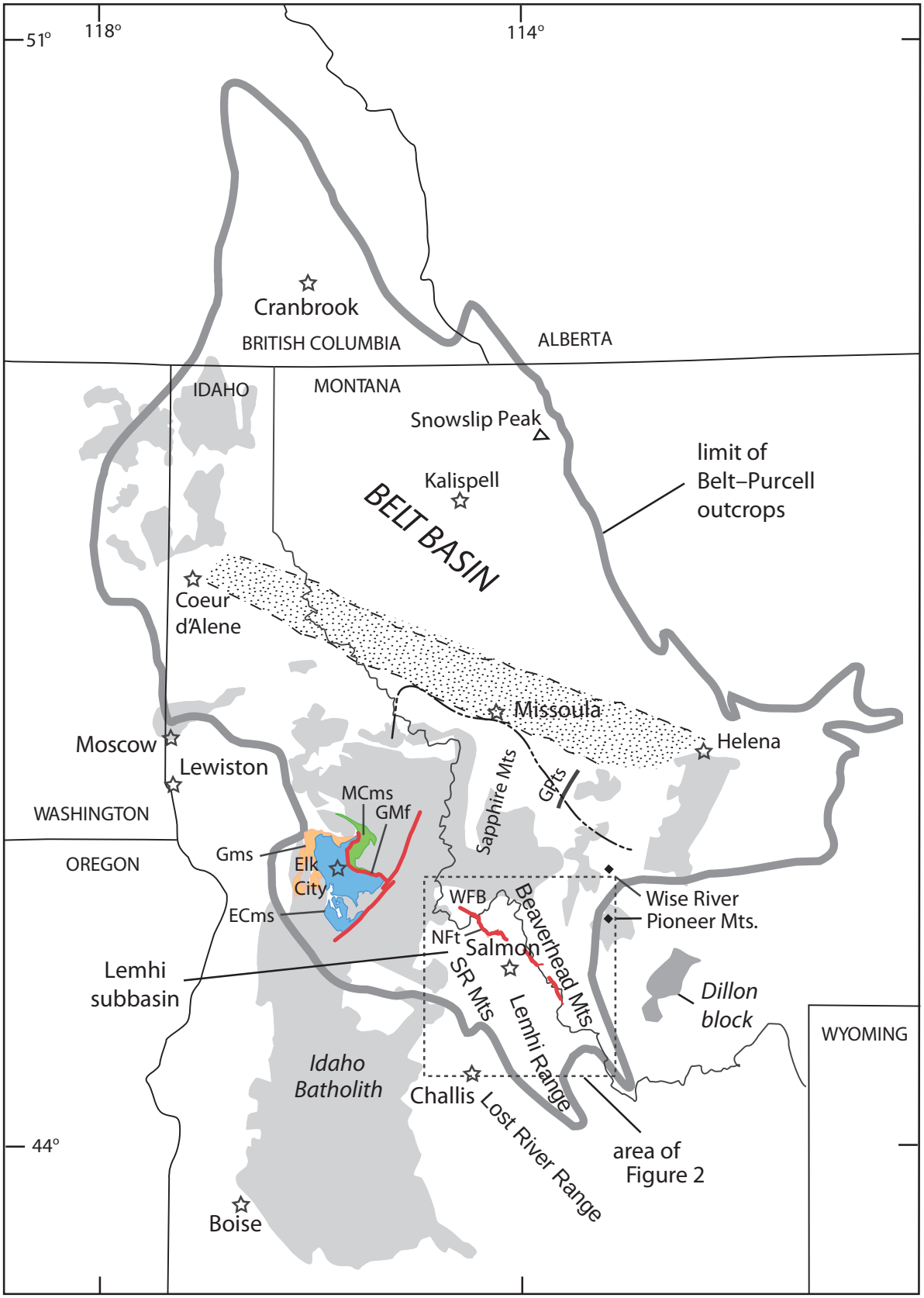

Figure 1. Location map showing areal limit of present outcrops of Belt–Purcell Supergroup strata. Speckled pattern approximates the Lewis and Clark fault zone. Lighter shaded areas are Cretaceous through Eocene plutonic rocks; darker shaded Dillon block is Archean basement. ECms, Elk City metamorphic sequence; Gmf, Green Mountain fault; Gms, Golden metamorphic sequence; GPts, Georgetown–Phillipsburg thrust system; MCms, Meadow Creek metamorphic sequence; NFt, North Fork thrust; SR Mts, Salmon River Mountains; WFB, West Fork Bitterroot River. Missoula Group type sections for lower formations are near Snowslip Peak, for upper ones east of Missoula. Dashed line is fuzzy boundary between strata of the main Belt Basin to the north and of the Lemhi subbasin to the south. Modified from Burmester and others (2015).

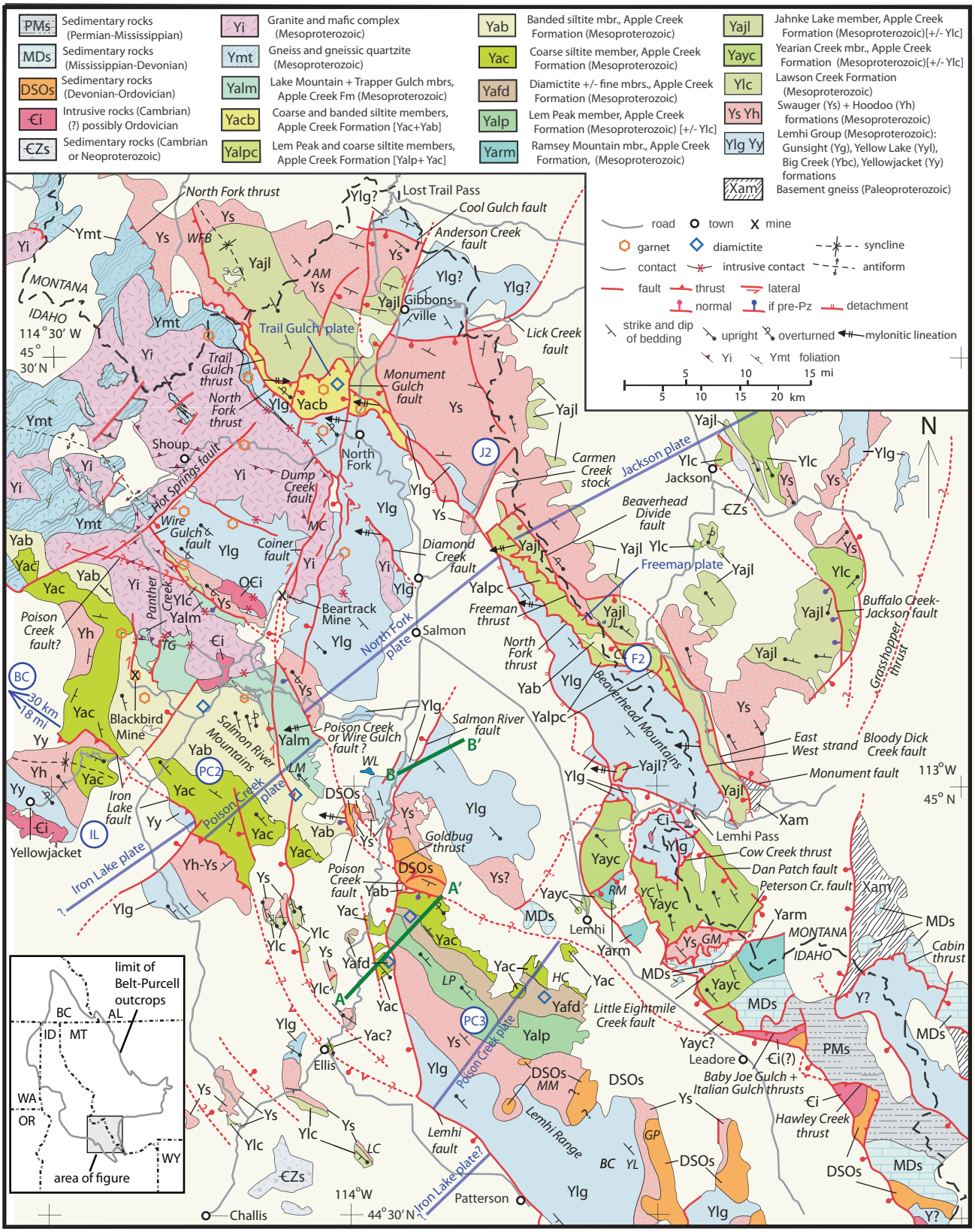

Figure 2. Pre-Mesozoic bedrock geology around Salmon, Idaho. The coarsest clastic unit (Ys = Yh) separates lower formations of the Lemhi Group (in blue) from higher Lawson Creek and Apple Creek Formations (greens and yellows). Units are combined where scale or previous mapping makes separating them impractical. Codes in circles are locations of stratigraphic columns in figure columns; span of thrust plates are blue lines; approximate location of cross sections in figure 16 are dark green lines. Geographic locations are in italics; those for type or reference sections have units in parentheses: AM, Allan Mountain; BC, Big Creek (Ybc); CL, Cowbone Lake; GM, Goat Mountain; GP, Gunsight Peak (Yg); HC, Hayden Creek (Yafd (Yaf+Yad), Yac); JL, Jahnke Lake (Yajl); LC, Lawson Creek (Ylc); LM, Lake Mountain (Yalm); LP, Lem Peak (Yalp); MC, Moose Creek; MM, Mogg Mountain (Ys); RM, Ramsey Mountain (Yarm); TG, Trapper Gulch (Yatg); WFB, West Fork Bitterroot River; WL, Williams Lake; YC, Yearian Creek (Yayc); YL, Yellow Lake (Yyl). Modified after Burmester and others (2020) to include insights from fieldwork in 2020 through 2022.

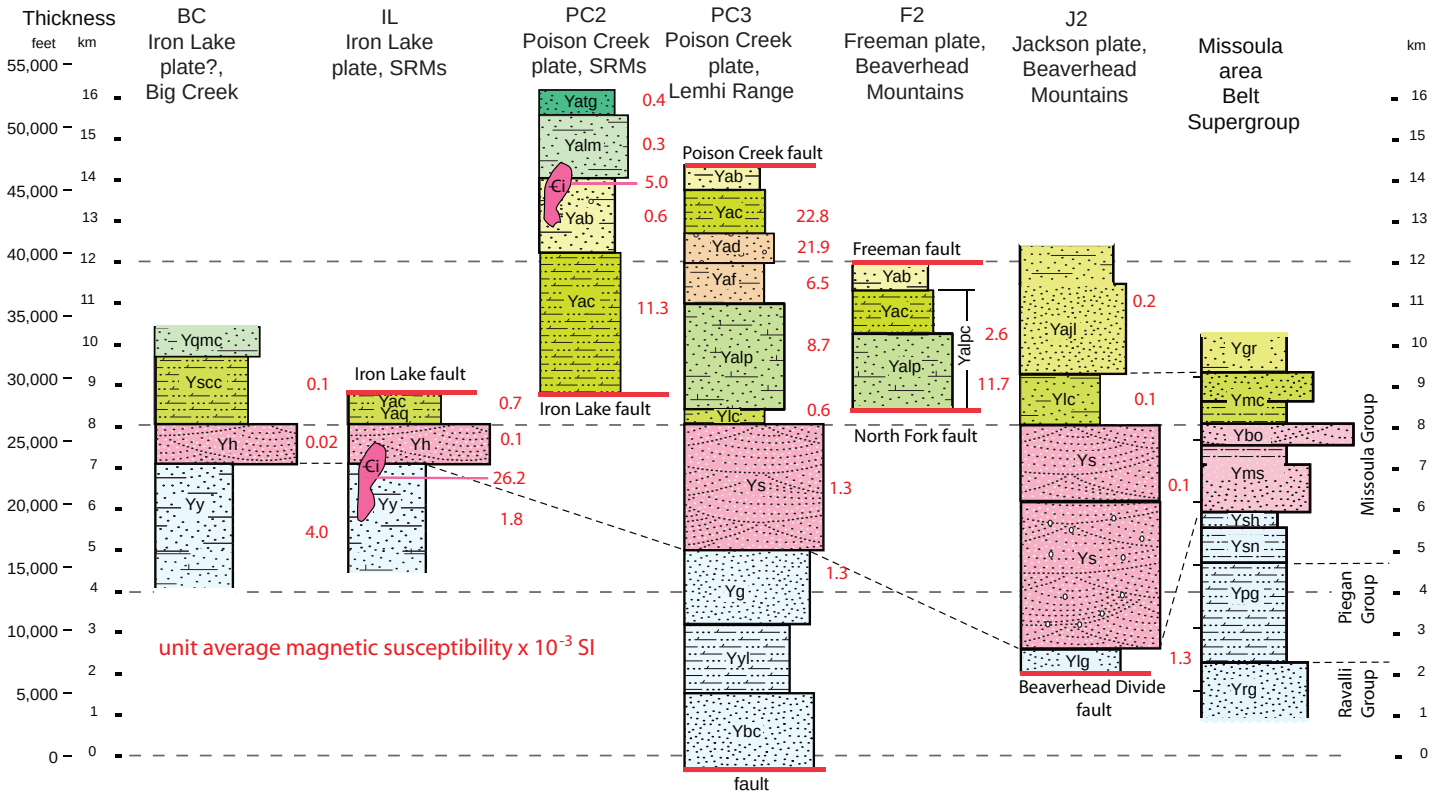

Figure 3. Stratigraphic columns across the Lemhi subbasin from west to east and the Missoula area section for the Belt Supergroup. Unit abbreviations are: Yab, banded siltite mbr, Apple Creek Formation; Yac, coarse siltite mbr, Apple Creek Formation; Yad, diamictite mbr, Apple Creek Formation; Yaf, fine siltite mbr. Apple Creek Formation; Yajl, Jahnke Lake mbr, Apple Creek Formation; Yalm, Lake Mountain mbr, Apple Creek Formation; Yalp, Lem Peak mbr, Apple Creek Formation; Yaq, argillaceous quartzite; Yatg, Trapper Gulch mbr, Apple Creek Formation; Ybc, Big Creek Formation; Ybo, Bonner Formation; Yg, Gunsight Formation; Ygr, Garnet Range Formation; Yh, Hoodoo Quartzite; Ylc, Lawson Creek Formation; Ylg, Lemhi Group; Ymc, McNamara Formation; Yms, Mt. Shields Formation; Ypg, Piegan Group; Yqmc, quartzite of Monumental Creek; Yrg, Ravalli Group; Ys, Swauger Formation; Yscc, siltite of Copper Camp; Ysh, Shepard Formation; Ysn, Snowslip Formation; Yy, Yellowjacket Formation; Yyl, Yellow Lake Formation. Columns aligned so top of Yh, Ys, and Ybo are at 8 km. Scale starts near base of lowest exposed rock in the Lemhi Range, which is likely not the base of the section, as no basement is known in the area. Big Creek section from descriptions in Stewart and others (2013) for rocks about 30 km (19 mi) northwest of the Iron Lake plate section near Yellowjacket, Missoula section from Lonn (2017), the others evolved from Burmester and others (2017).

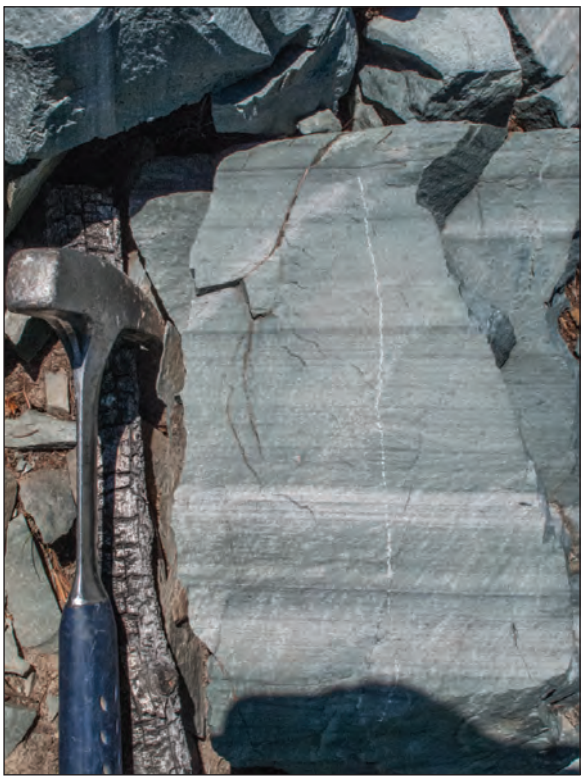

Figure 4. Parallel laminated very fine feldspathic quartzite of the fine siltite member, Apple Creek Formation, about 2.2 km (1.4 mi) east–northeast of Lem Peak. Hammer scratch reflects fine grain size and high feldspar content.

Figure 5. Siltite and argillite couplets of the coarse siltite member, Apple Creek Formation, on irrigation ditch cut above Hayden Creek. Bank is about 1 m high.

Figure 6. Angular to rounded argillite, siltite, and very fine quartzite clasts in muddy matrix of the diamictite member of the Apple Creek Formation about 2.9 km (1.8 mi) east–northeast of Lem Peak (Yafd on fig. 2).

Figure 7. Thick-bedded fine-grained feldspathic quartzite near the top of the Lem Peak member of the Apple Creek Formation (Yalp) about 1.2 km (0.75 mi) east–northeast of Lem Peak. Similar recessively weathering carbonate lamellae occur to the east near Hayden Creek and in at least one place in the Beaverhead Mountains but not to the northwest.

Figure 8. Pinch and swell quartzite to argillite couples and couplets of the banded siltite member, Apple Creek Formation (Yab), near the top of the unit above the Deep Creek Road 15 km (9.3 mi) east–southeast of the Blackbird mine. Garnets from the Deep Creek road 1.5 km (0.9 mi) to the west were dated at 1112 ± 3 Ma (Lu/Hf; Murphy and others, this volume).

Figure 9. Parallel and hummocky cross-laminated feldspathic quartzite of the Lake Mountain member, Apple Creek Formation (Yalm), with biotite concentrated in dark laminations. Location about 3.3 km (2 mi) south of Lake Mountain.

Figure 10. Thick-bedded very fine-grained biotite-feldspar quartzite of the Trapper Gulch member of Apple Creek Formation (Yatg) above Panther Creek about 5 km (3 mi) east–northeast of the Blackbird mine.

our view Swauger Formation equivalent, is overlain by the argillaceous quartzite of Ekren (1988), which we correlate with the Lawson Creek Formation (Ylc; fig. 11). The Lawson Creek is in turn overlain by the coarse siltite member of the Apple Creek Formation. The lowest members also have not been recognized in the Big Creek area west of the Cretaceous (?) and Eocene intrusions (Stewart and others, 2013) 28 km (17 mi) west–northwest of Yellowjacket, where units overlying the Hoodoo Quartzite that have been correlated with the coarse siltite and banded siltite members of the Apple Creek Formation are overlain by strata similar to the Lake Mountain member.

Lateral variations are evident to the northeast as well. Above the Swauger Formation east of the North Fork and Freeman thrusts in the Beaverhead Mountains (fig. 2), the Lawson Creek Formation has a higher concentration of spherical medium quartz grains than it does north of Lem Peak. The overlying Jahnke Lake member of the Apple Creek Formation was originally mapped around Jahnke Lake (JL, fig. 2) as three units (Yqf, Yqgr, and Yqpi; Lonn and others, 2009), but they differ from the strata that overlie the Lawson Creek Formation in the Lemhi Range. Yqf (figs. 12, 13) is broadly similar to the Lem Peak member north of Lem Peak but lacks carbonate and intervals of dark, thinner, and finer quartzite and siltite. Yqgr has more siltite and is plausibly correlative with the fine siltite member, although thicker bedded and argillite poor. Yqpi is mostly medium- to thick-bedded quartzite (fig. 14) with some mud chips, but lacks siltite and argillite couplets that characterize the coarse siltite member of the Lemhi Range and Salmon River Mountains. Farther south, the Yearian Creek member of the Apple Creek Formation overlies the Swauger Formation. Originally termed the siltite of Yearian Creek (Burmester and others, 2018), it has been correlated with the Lawson Creek Formation because it contains chert, mud chips and cracks, and spherical medium to coarse quartz grains (Lonn and others, 2019). However, the Yearian Creek member appears thicker than Lawson Creek elsewhere, and since all characteristics mentioned above except the chert are also found in the coarse siltite member, it likely includes coarse siltite member strata. If so, the Lem Peak, fine siltite, and diamictite members of the Apple Creek are missing.

Lateral variation for all units is consistent with variation within the Lem Peak member. Weathered-out carbonate laminae are prevalent west and east of Hayden Creek within the Lemhi Range, and present between the North Fork and Freeman thrusts in the Beaverhead Mountains, but not obvious immediately east of the Salmon River fault (fig. 15) or east of the Beaverhead Divide. Meter-scale intervals of dark, finer-grained material are similarly obvious near and southeast of Lem Peak but not elsewhere above the Lawson Creek Formation. These areal variations within strata overlying the Lawson Creek Formation, especially the absence of the Lem Peak, fine siltite, and diamictite members in some sections, document the complexity of the sediment distribution system. Perhaps it was like a giant delta with migration of distributaries influenced by concurrent faulting.

Figure 11. Flaser-bedded biotite-rich siltite and argillite plus quartzite with rounded medium quartz grains of the Lawson Creek Formation (Ylc) about 6.5 km (4 mi) northwest of Lem Peak near the Salmon River fault. Similar combination is found in the Lawson Creek (argillaceous quartzite) near Yellowjacket and on the east side of the Beaverhead Mountains (IL and J2, fig. 3) as well as within the Swauger Formation of Taylor Mountain (Iron Lake trip, this volume).

Strata below the Apple Creek

Below the Apple Creek Formation are the Lawson Creek and Swauger Formations, and below those, the Lemhi Group composed of the Gunsight, Yellow Lake, and Big Creek Formations (Lonn, 2017). The Lawson Creek and Swauger Formations have been widely recognized, but subdivisions of the Lemhi Group have been mapped only in the Lemhi Range in the Poison Creek thrust plate. The southwestern-most Lemhi Group rocks exposed on the Iron Lake plate are likely Yellow Lake Formation, but that unit has not been recognized within the type Yellowjacket Formation. A promising candidate for the Yellow Lake Formation on the North Fork plate is a phyllitic quartzite that Hillesland (1982) mapped northwest of

Figure 12. Heavy mineral laminations apparently contorted by scour and loading of the overlying quartzite bed low in the Jahnke Lake member of Apple Creek Formation (Yajl) on the ridge northwest of Jahnke Lake. Dark material is mostly hematite that may have been detrital magnetite.

Figure 13. Trough cross-bedded feldspathic quartzite of the Jahnke Lake member of Apple Creek Formation on the ridge north–northwest of Jahnke Lake.

Figure 14. Trough cross-bedded feldspathic quartzite of the Jahnke Lake member of Apple Creek Formation about 15 km (9.5 mi) east–northeast of Jahnke Lake. Some beds contain red mud chips but the lack of siltite and argillite couplets and mud-cracked tops discourages correlation with the coarse siltite member.

Figure 15. Thick-bedded feldspathic quartzite of the Lem Peak member of Apple Creek Formation above the Lawson Creek Formation (fig. 11) about 6.5 km (4 mi) northwest of Lem Peak near the Salmon River fault. This quartzite lacks carbonate and intervals of dark siltite found in Yalp east and southeast of Lem Peak (fig. 7).

the Beartrack mine, but we have not been able to map that phyllitic unit to the southeast. The thickness of the bottomless Lemhi Group section is unknown in the Lemhi Range due to faulting, and in the Salmon River Mountains due to unknown structural repetition, and intrusion by the Mesoproterozoic bimodal suite. The question of whether the Lemhi Range stratigraphy should be included in models of filling of, and correlation of units in, the Belt Basin applies to both the Lemhi Group and the Apple Creek Formation.

STRUCTURES AND THEIR HISTORY

A foremost problem is that Lemhi subbasin geology is a four-dimensional jigsaw puzzle with most of the pieces missing. The three-dimensional pieces are formed by faults that were active in the fourth dimension (time). Of the major tectonic episodes, the latest was Tertiary extension, which formed mostly steep, south-striking, west-dipping normal faults followed by low-angle detachment faulting along the northeast margin of the Salmon Basin (fig. 2). The next older structural episode was contraction during the Cretaceous that resulted in generally eastward transport on thrust faults, most of which strike southeast and dip southwest. Arrows shown on figure 2 show plunge direction of lineation, not direction of transport; ones pointed west mark motion up to the east. Much earlier extension in the Neoproterozoic during continental breakup produced mostly unseen, probably listric, normal faults with generally the same attitude as later thrusts, and probably transform faults linking them. Some or all of these Neoproterozoic and later faults probably cut and displaced Mesoproterozoic growth faults.

Were the Lemhi subbasin very narrow, one might imagine facies migrating northward and retreating southward to form sand wedges into finer-grained sediment. But if Cretaceous contraction exceeded later extension, the subbasin would have been wider than the present 185 km (115 mi) span of its present exposure. For reference, this is about the maximum width of the Mississippi River floodplain in Arkansas and Mississippi. Lateral variations within it might have extended farther north. Thus, the original continuity and therefore present correlation of units within the Lemhi subbasin with those in the main Belt Basin may not be as simple as using the nearest rocks or most complete sections from both basins.

North Fork and Trail Gulch–Freeman Thrusts

Some of the Apple Creek members have been mapped separately or lumped with others on the Trail Gulch plate near North Fork and the Freeman plate in the Beaverhead Mountains (fig. 2). Those plates are overridden and truncated by the North Fork plate. The Trail Gulch plate, which hosts strata with characteristics of the coarse and banded siltite members, is cut out at its northwest map extent where the North Fork thrust juxtaposes Lemhi Group against Swauger Formation. The Freeman plate, which in addition has carbonate-bearing quartzite currently correlated with the Lem Peak member, is cut out south of the middle of the Beaverhead Mountains where the North Fork thrust juxtaposes Lemhi Group against the Jahnke Lake member of the Apple Creek Formation. Those faults and their plates have different names because they are not continuous across the Carmen Creek stock but likely originally were a single fault and plate. Identification of specific Apple Creek members on those plates is hampered by complex deformation and varied metamorphism. Our current hypothesis is that the Trail Gulch–Freeman system is the remnant of a major thrust that juxtaposed western facies of the Apple Creek Formation, i.e., units now found in the Lemhi Range and Salmon River Mountains, against eastern facies of coarser-grained deposits above the Lawson Creek Formation, now the Jahnke Lake member of the Apple Creek Formation. When that thrust stalled, perhaps against the growing fold of the Beaverhead Divide, it spawned the out of sequence North Fork thrust that led to back-tilting and deformation of the North Fork plate (as suggested by Hansen, 2015).

Poison Creek Fault

The Poison Creek fault is a major structure that transects the Lemhi subbasin from northwest to southeast. What we think we know is that the Poison Creek fault had normal motion in the Neoproterozoic (Hansen, 2015; Hansen and Pearson, 2016). If that extensional fault had been listric, its hanging wall would have been riddled with other faults that accommodated rotation on a curved fault surface that did not have a constant radius (e.g., Erickson and others, 2001), so at least some of the faults mapped south of the Poison Creek fault likely date from the Neoproterozoic. Uplift and tilting to the northeast of its footwall led to erosion of some of the Swauger Formation, all of the Lawson Creek and Apple Creek Formations, and perhaps 5 km of overlying sediments from the Lemhi "Arch." Ordovician quartzite is preserved on both hanging wall to the south toward Gunsight Peak (fig. 2) where little Swauger is left, and with about 15° angular unconformity immediately to the north on the footwall (Hansen, 2015). Note that if the footwall's tilt was constant to the northeast, a 5-km-thick Apple Creek section could have been preserved only 20 km away, which is less than the current separation of the Poison Creek and North Fork faults. Thus, the Apple Creek strata now on the Trail Gulch and Freeman plates could be from that tilted fault block. Cretaceous contraction added a thrust component, which recovered some of the earlier displacement and involved the footwall of the Neoproterozoic fault (Hansen, 2015). The result of this and subsequent tilting to the southwest of the Poison Creek fault's footwall during North Fork thrusting was the opposite facing of younger strata on the southwest and older strata on the northeast that we see today. Hansen (2015) reported kinematics supporting east to northeast strain in the Poison Creek thrust complex south of Salmon, but there is no case

for the thrust coinciding with the Neoproterozoic normal fault everywhere.

The Poison Creek fault is mapped as the mylonitized contact between northeast-facing Apple Creek strata and southwest-facing Swauger and Lawson Creek formations 40 km (25 mi) north–northwest from where it crosses the Salmon River. Farther northwest to near Panther Creek and the Hot Springs fault (fig. 2), the Poison Creek fault appears to be within Mesoproterozoic megacrystic granite, whose intrusive contact with the Apple Creek on the southwest appears to dip northeast. Metamorphism near that contact (Bookstrom and others, 2016) could be attributed to the overlying intrusion north of the Blackbird mine; Aleinikoff and others (2012) interpreted the 1370 ± 4 Ma U-Pb age from cores of xenotime in the Merle prospect (Blackbird district) to date growth in a hydrothermal system driven by the nearby megacrystic granite. The northeast contact of that granite body is an unnamed top-to-the-southwest reverse fault (fig. 2). Lemhi Group strata to its northeast are overturned to the southwest, plausibly damage from back-tilting of the North Fork plate. That fault could also be collateral damage from that back-tilting, or it could be the Neoproterozoic Poison Creek normal fault rotated to its current attitude along with the Lemhi Group. If the latter, the Cretaceous thrust part of the Poison Creek fault may continue through the granite.

Anderson Creek and Coiner Faults

The south-striking Anderson Creek and Coiner faults near Gibbonsville and east of Panther Creek appear to have earlier dextral and later normal motion. Both are locally mineralized. The Coiner fault's dextral slip likely predates 68 Ma, and normal slip spanned at least 48–32 Ma (Lewis and others, 2022). The Poison Creek fault's thrust motion is constrained to 68–57 Ma ((U-Th)/He zircon cooling ages; Hansen, 2015). The Coiner is shown as offsetting the Poison Creek fault under Tertiary cover (fig. 2), but if these ages are accurate the opposite order of faulting could be true. Either way, the question remains of how relative northward motion of blocks west of those faults is related to northeastward or eastward motion of thrust sheets.

Salmon River Fault

The Salmon River fault south of Salmon appears to have a simple history as a normal fault that displaced Eocene Challis Group units and underlying Mesoproterozoic metasedimentary rocks down on its west side, with both hanging and footwall blocks tilting to the east (fig. 16 A–A'). However, steeply plunging, nearly isoclinal folds in Lemhi Group strata, and steep east dips in Swauger strata south of Williams Lake (Stop 3 of Lewis and others, Salmon to Challis trip, this volume) in the fault's hanging wall, are inconsistent with origin from simple listric faulting. Instead, they may record earlier strike-slip motion on a long-lived fault system. Farther south the Salmon River fault has a similar late history with Challis units down on the west against Mesoproterozoic strata. However, alignment of the Salmon River fault with lateral ramps in the Silurian and Ordovician strata in the footwall of the Poison Creek fault (Hansen, 2014; Hansen and Pearson, 2016) hints that the Salmon River fault (system) was older, likely Neoproterozoic (Hansen, 2015).

South of the Poison Creek fault attitudes of Mesoproterozoic strata are different on either side of the Salmon River fault. Strata on the east have northwest–southeast strikes and steep dips, some are overturned, and cleavage is well developed. In contrast, strata immediately to the west have more north–south strikes and gentler dips (Tysdal, 2002). That difference in attitudes hinders finding piercing points, but the contact between the fine siltite and diamictite members is offset approximately 4.5 km (2.8 mi) along the trace of the fault. Tysdal (2002) suggested that offset of units could be due to sinistral slip, but discounted fault drag as a cause of contrasting attitudes. Differences in displacement across such a tear fault during thrusting could account for the greater shortening from folding on its east side. If strike-slip motion was early and confined to the Poison Creek thrust plate, that fault should not extend north of the Poison Creek fault system. Tysdal's (2002) take was that normal fault motion reactivated this tear fault as part of the present throughgoing Salmon River normal fault.

An alternative mechanism for offset of Apple Creek Formation members and differences in their attitudes across the Salmon River fault is normal motion down on the west. Using a bedding dip of 60° east of the fault, normal slip would produce an offset of nearly 7.5 km but would not explain the differences in attitudes across the fault. However, the difference in attitudes and a smaller offset could be attributed to faulting of folded strata. Figure 16 B–B' imagines normal faulting of a now eroded syncline–anticline pair. Schematically, the offset of the Lem Peak–fine siltite contact is about 11,000 ft (3.4 km). For comparison, A–A' depicts the offset of Challis mafic lavas (Tlm) across the Salmon River fault north of the Poison Creek fault. The base of Tlm is not shown on the section, so the offset shown of about 9,000 ft (2.7 km) omits an unknown thickness of mafic lavas. A normal fault need not have the same displacement along its length, but this similarity of displacements supports the hypothesis above that the contrast across the Salmon River fault south of the Poison Creek fault is due to normal motion. Such a solution obviates the need for a Cretaceous sinistral transcurrent fault but does not rule out presence or reactivation of earlier Cretaceous, Neoproterozoic, or Mesoproterozoic faults. As diamictite concentrations may record block uplifts (Winston and others, 1999), proximity of the diamictite member of the Apple Creek Formation to the Salmon River fault makes proximal growth faults seem plausible. So, perhaps the Salmon River fault had gotten its start as a growth fault during deposition

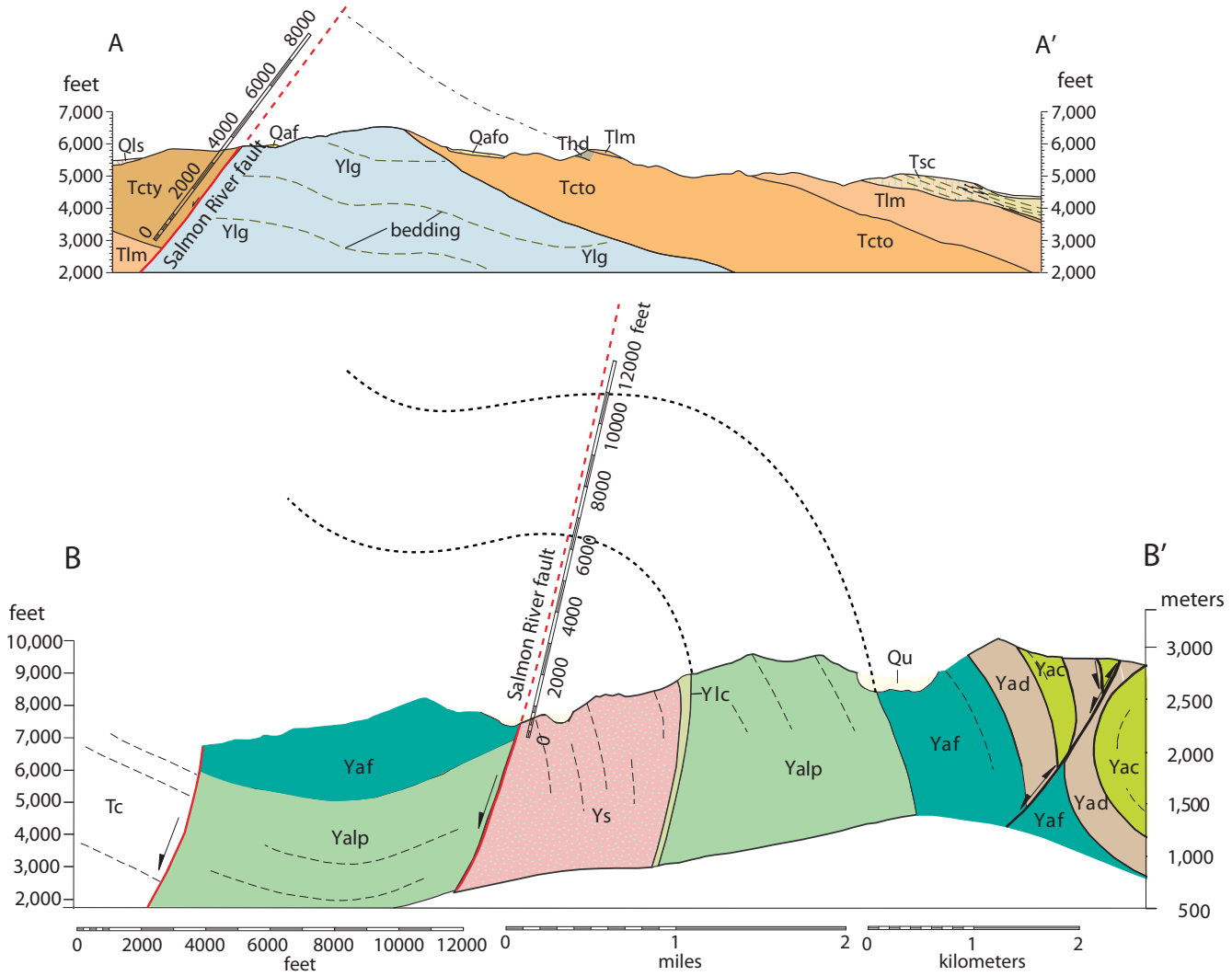

Figure 16. Cross sections across the Salmon River fault; locations shown on figure 2. A–A' is southwest to northeast across the Lemhi Range, modified from Tysdal's (2002) figure 5 section A–A' to omit the Lem Peak fault, change units and colors, and postulate folds above present surface that, when downfaulted, would reproduce repetition and gentle dips of units to the west. B–B' is southwest to northeast across the northern Lemhi Range modified from Lewis and others (2014). Scale along Salmon River fault is from top of Tlm on the west to base on the east so omits thickness of Tlm.

of the Apple Creek Formation. It may have been reactivated in the Neoproterozoic during extension, and in the Cretaceous as a dextral strike slip structure similar to the Coiner fault.

These generalizations leave some niggling details unresolved. Old structures we see on various thrust plates should have been transported along with those plates. A pre-thrusting Salmon River fault on the Poison Creek plate should have been transported northeast or east along with the plate relative to previously aligned structures in its footwall. Why then the apparent continuity of an ancient structure south of the Poison Creek fault with one to the north? Perhaps thrust motion on the Poison Creek fault had little eastward component so offset of an earlier structure is obscured between the Poison Creek and Goldbug thrusts. Alternatively, dextral slip on the Salmon River fault is younger than thrusting on the Poison Creek and Goldbug thrusts; alignment of lateral ramps between those two thrusts is from that lateral motion and not inherited, but the offset of the faults is small enough to be hidden under Tertiary cover as speculatively shown on figure 2.

BROADER VIEW AND NORTHWARD CHANGES

It is probable that the Mesoproterozoic intrusive suite northwest of Salmon intruded over several million years as separate bodies. Age range from zircons is 1379 ± 6 to 1359 ± 7 Ma (Doughty and Chamberlain, 1996, Aleinikoff and others, 2012). The mafic component is concentrated along the northeast contact west of North Fork (Spence, 1984), suggesting that there might be a crude intrusive stratigraphy with most of the intrusions exposed to the west being younger. Had the intrusions been laterally extensive into horizontal Mesoproterozoic strata, one might expect that at least the lower rocks now exposed to the northeast would be increasingly metamorphosed because they were deeper, but they are not. Lack of broader metamorphism might indicate that the intrusions were not laterally extensive or

that the strata were already or concurrently tilted (think lopolith) so those rocks to the east were not deeper or under the intrusion. Doughty and Chamberlain (1996) reported that zircons in partial melts in migmatite (fig. 17) near the northeast edge of the bimodal intrusive complex have upper intercept ages of 1370 ± 2 Ma. Metamorphic conditions in the migmatite were at pressures of approximately 220–350 MPa (8–13 km depth). Core-to-rim compositional difference in garnet was attributed to increase in pressure during garnet growth. That increase was attributed to increased depth by about 6 km due to burial by more sediment, but that conclusion was based on the main Belt Basin stratigraphy when the Yellowjacket was thought to be the Prichard Formation and the rest of the Belt could fill the role. That 6 km could instead be from very young Lemhi subbasin sediments that are nowhere preserved and/or intrusion of later granites above the sample locality. Garnet from that site was recently dated as 1353 Ma (Lu/Hf; Murphy and others, this volume) so it perhaps grew under peak metamorphic conditions after increase in pressure.

Metamorphic conditions existed away from and after the Mesoproterozoic intrusions too. Lu/Hf ages of garnets from the banded siltite member of the Apple Creek Formation on the Poison Creek and Trail Gulch plates are similar (1112 ± 3 Ma; Murphy and others, this volume) and 1173 ± 6 Ma (Lewis and others, 2019). This similarity, despite likely original separation greater than present 40 km (25 mi), is consistent with metamorphism being from burial as there is no evidence for magmatic activity nearby at that time. If conditions were like those in the garnet zone of pelitic rocks on the east coast (Whitney and others, 1996), temperature would have been around 475° C and depth 12–16 km (3–4 kbar). Some or all of that overburden could have been higher Apple Creek strata deposited before onset of magmatism mentioned above. This includes the 3 km of Lake Mountain and Trapper Gulch members above the banded siltite (fig. 3), leaving 9–13 km undocumented. Six km of that could have accumulated during or after magmatism to account for increase in pressure when garnet grew in the migmatite. Yet more might have accumulated in the late Mesoproterozoic.

To the northwest in the footwall of the Hot Springs fault, the Swauger Formation has not been recognized, so there the distinction between Apple Creek and Lemhi Group protoliths of the biotite gneiss and quartzite are obscured by metamorphism and deformation (fig. 18). Around Elk City 100 km (60 mi) to the northwest (fig. 1), augen gneiss, amphibolite, and enclosing gneisses and quartzites of the Elk City metamorphic sequence appear to be part of the Lemhi subbasin (Dragovich and others, 2009). Detrital zircons from a feldspathic quartzite near the east edge of the Elk City sequence have a young age peak at 1399 Ma (Di Fiori and others, 2022), which defines a maximum depositional age similar to that of the banded siltite near the Blackbird mine (1409 Ma; Aleinikoff and others, 2012). Thus, the protolith of the Elk City sequence is likely Apple Creek Formation. More extensive distribution at depth of Mesoproterozoic igneous rocks is recorded by the 1381 ± 6 Ma average age of inherited zircons in a megacrystic granodiorite east of Elk City (Gaschnig and others, 2013). The contact of the Elk City sequence with lower grade, more quartzitic rocks to the east is mapped as the Green Mountain fault with late (?) left lateral and up on the west motion (Di Fiori and others, 2022). Lund and others (2008) had called that contact the Brushy Gulch–Red River thrust fault. We think that any northeast vergence more likely is related to the North Fork and Trail Gulch thrusts (Trail Gulch field trip, Lonn and others, this volume). That would make those thrusts a major structure, juxtaposing the Lemhi subbasin strata of the Lemhi Range and Salmon River Mountains against more Belt-like strata of the Jackson plate.

Correlation with the Main Belt Basin

The right hand column in figure 3 is the nearest, most complete section from the main Belt Basin. Correlation of the Swauger and Lawson Creek Formations with the Bonner and McNamara Formations seems solid. The lower pair of units have thick beds of coarse quartzite in common; the upper ones have chert and/or porcellanite, which are absent or rare in other units. However, the main Belt Basin also has considerable lateral variation in units both above and below these (Lonn and others, 2020). Perhaps the section on the Jackson plate should be correlated with the Missoula section, and the Lemhi Range section with Belt strata in western Idaho.

Lateral changes in the Apple Creek Formation likely record spatial and temporal variation of depositional environments. Remember that these units are lithostratigraphic, so the environment for coarse siltite deposition could have existed at the same time as the Lem Peak, fine siltite, and diamictite environments, but farther west (in current coordinates). Suppose that following the influx of potassium feldspars from the Dillon block, and the well-rounded quartz grains from the pediment that supplemented the Big White Arc detritus during deposition of the Swauger and Bonner Formations, there was a flush of magnetite-bearing sediment from the Big White arc, and that a reason for this was renewed faulting. This could account for the high magnetic susceptibility of the Lemhi Range section, the coarse siltite in the Salmon River Mountains, and the Jahnke Lake member. A caution is that although magnetite is the only likely source of such high susceptibility, not all is necessarily detrital. On the flip side, some opaques in heavy mineral laminations in the Jahnke Lake member, e.g., figure 12, are hematite that do not contribute much to magnetic susceptibility but likely were magnetite before oxidation. The diamictite member that contains both magnetite and locally spherical medium quartz grains may record growth faults

Figure 17. Migmatite at locality B33 of Doughty and Chamberlain (1996) west of North Fork. Location is garnet symbol on figure 2 southeast of the Hot Springs fault on the Salmon River Road. Extent of metasediment there not shown, but location and dip to the west are consistent with this being on the North Fork plate.

Figure 18. Layered biotite–quartz–feldspar paragneiss (Ymt) along the Salmon River road about 4.5 km (2.8 mi) west of the edge of figure 2 that is likely metamorphosed Yab or Yac. The correlation is hindered by deformation and intrusion of Ymi. Subtle color grading within the layers likely due to original grading in siltite and argillite couplets. This is likely on the Poison Creek plate if such exists this far northwest.

activity at time of deposition; diamictite concentrations in the banded siltite and low in the Lake Mountain members may have been produced by faulting during their deposition too.

CONCLUSIONS

Mesoproterozoic strata vary widely across the Lemhi subbasin between thrust plates and even within them. Although the section in the Lemhi Range of strata on the Poison Creek plate seems the most complete and therefore the best choice for correlation with strata of the main Belt Basin, it is missing the highest units that are exposed in the Salmon River Mountains, and units of the Lemhi Group have not been recognized on the North Fork plate. Furthermore, the section of the Apple Creek Formation in the Lemhi Range bears only slight resemblance to that of the Jackson plate in and east of the Beaverhead Mountains, and key members are unknown on the same plate in the Salmon River Mountains or Iron Lake plate. Farther northwest the distinction between the Poison Creek and North Fork plates is obscured where the Poison Creek fault disappears into more highly deformed and metamorphosed Mesoproterozoic granites and metasediments. Similar rocks around Elk City to the north support former continuity of the Lemhi subbasin that far, at least for the Apple Creek. A major fault there separates those rocks from more Belt-like rocks to the east. That relationship is similar to the separation of rocks of the North Fork and Trail Gulch plates north of the Salmon River from the section of Swauger Formation and Jahnke Lake member of the Apple Creek Formation. Therefore, it seems likely that the Lemhi Range and Salmon River sections comprise a finer-grained part of the Lemhi subbasin that was juxtaposed against a coarser-grained part. Continuity to the northwest of this finer-grained part suggests that it should be correlated with western Belt units, if any, and that the Jackson plate section of Swauger, Lawson Creek, and Apple Creek Formations should be correlated with the Missoula section of the main Belt Basin. The similarity of the Swauger and Lawson Creek Formations on all plates suggests that extreme spatial variation may be limited to the Apple Creek Formation. Perhaps the Lemhi Group of the Lemhi Range can be correlated with the main Belt section below the Bonner Formation. If so, using the sand wedge into finer sediment model, one should expect the Gunsight and Big Creek Formations to disappear to the north and the Yellow Lake Formation to correlate with a unit below the Bonner that is dominated by siltite and argillite couplets, perhaps Snowslip and/or Shepard Formations.

REFERENCES CITED

Aleinikoff, J.N., Slack, J.F., Lund, K., Evans, K.V., Fanning, C.M., Mazdab, F.K., Wooden, J.L., and Pillers, R.M., 2012, Constraints on the timing of Co-Cu ± Au mineralization in the Blackbird district, Idaho, using SHRIMP U-Pb ages of monazite and xenotime plus zircon ages of related Mesoproterozoic orthogneisses and metasedimentary rocks: Economic Geology, v. 107, p. 1143–1175.

Anderson, A.L., 1961, Geology and mineral resources of the Lemhi quadrangle, Lemhi County, Idaho: Idaho Bureau of Mines and Geology Pamphlet 124, 111 p.

Bookstrom, A.A., Box, S.E., Cossette, P.M., Frost, T.P., Gillerman, V.S., King, G.R., and Zirakparvar, N.A., 2016, Geologic history of the Blackbird Co-Cu district in the Lemhi subbasin of the Belt-Purcell Basin, *in* MacLean, J.S., and Sears, J.W., eds., Belt Basin: Window to Mesoproterozoic Earth: Geological Society of America Special Paper 522, p. 1–35.

Burmester, R.F., Lewis, R.S., Lonn, J.D., and McFaddan, M.D., 2015, The Hoodoo is the Swauger and other heresies: Lemhi subbasin correlations and structures, east-central Idaho: Northwest Geology, v. 44, p. 1–19.

Burmester, R.F., Lonn, J.D., Lewis, R.S., and McFaddan, M.D., 2016, Stratigraphy of the Lemhi subbasin of the Belt Supergroup, *in* MacLean, J.S. and Sears, J.W., eds., Belt Basin: Window to Mesoproterozoic Earth: Geological Society of America Special Paper 522, p. 121–137.

Burmester, R.F., Lewis, R.S., and Lonn, J.D., 2017, Were we wrong? Second thoughts on geology of the Lemhi subbasin: Northwest Geology, v. 46, p. 7–14.

Burmester, R.F., Othberg, K.L. Stanford, L.R., Lewis, R.S., and Lonn, J.D., 2018, Geologic map of the Agency Creek quadrangle, Lemhi County, Idaho: Idaho Geological Survey Digital Web Map 182, scale 1:24,000.

Burmester, R.F., Lonn, J.D., and Lewis, R.S., 2020, Further speculation on Belt stratigraphy and structure around Salmon, Idaho: Alternative interpretations and tests: Northwest Geology, v. 49, p. 19–34.

Di Fiori, R.V., Lewis, R.S., Schmidt, K.L., Burmester, R.F., and Huttanus, H.M., 2022, Geologic map of the Elk City quadrangle, Idaho County, Idaho: Idaho Geological Survey Digital Web Map 206, scale 1:24,000.

Doughty, P.T., and Chamberlain, K.R., 1996, Salmon River Arch revisited: New evidence for 1370 Ma rifting near the end of deposition in the Middle Proterozoic Belt basin: Canadian Journal of Earth Sciences, v. 33, p. 1037–1052.

Dragovich, J., Burmester, R.F., and Lewis, R.S., 2009, Structure and metamorphism of the Elk City area, north-central Idaho: Idaho Geological Survey Technical Report 09-1, 33 p.

Ekren, E.B., 1988, Stratigraphic and structural relations of the Hoodoo Quartzite and Yellowjacket formation of Middle Proterozoic age from Hoodoo Creek eastward to Mount Taylor, central Idaho: U.S. Geological Survey Bulletin 1570, 17 p.

Erickson, S.G., Strayer, L.M., and Suppe, J., 2001, Mechanics of extension and inversion in the hanging walls of listric normal faults: Journal of Geophysical Research, v. 106, no. B11, p. 26,655–26,670.

Evans, K.V., 1998, The Yellowjacket Formation of east-central Idaho, *in* Berg, R.B., ed., Proceedings of Belt Symposium III-1993: Montana Bureau of Mines and Geology Special Publication 112, p. 17–30.

Gaschnig, R.M., Vervoort, J.D., Lewis, R.S., and Tikoff, B., 2013, Probing for Proterozoic and Archean crust in the northern U.S. Cordillera with inherited zircon from the Idaho batholith: GSA Bulletin, v. 125, no. 1–2, p. 73–88; doi:10.1130/B30583.1.

Hansen, Connor, 2015, An investigation into the Poison Creek thrust: A Sevier thrust with Proterozoic implications: M.S. thesis, Idaho State University, 80 p.

Hansen, C.M., and Pearson, D.M., 2016, Geologic map of the Poison Creek thrust fault and vicinity near Poison Peak and Twin Peaks, Lemhi County, Idaho: Idaho Geological Survey Technical Report T-16-1, scale 1:24,000.

Hillesland, L.L, 1982, The geology, mineralization, and geochemistry of the Pine Creek area, Lemhi County, Idaho: M.S. thesis, Oregon State University, 97 p.

Lewis, R.S., Othberg, K.L., McFaddan, M.D., Burmester, R.F., Stewart, D.E., Stanford, L.R., and Stewart, E.D., 2013, Geologic map of the Williams Lake quadrangle, Lemhi County, Idaho: Idaho Geological Survey Digital Web Map 162, scale 1:24,000.

Lewis, R.S., Othberg, K.L., Stanford, L.R., Burmester, R.F., Lonn, J.D., Stewart, D.E., and Stewart, E.D., 2014, Geologic map of the Sal Mountain quadrangle, Lemhi County, Idaho: Idaho Geological Survey Digital Web Map 170, scale 1:24,000.

Lewis, R.S., Burmester, R.F., and Lonn, J.D., 2019, Geologic map of the Ulysses Mountain quadrangle, Lemhi County, Idaho: Idaho Geologic Survey Digital Web Map 188, scale 1:24,000.

Lewis, R.S., Stewart, D.E., Burmester, R.F., Tkach, M.K., and Canada, A.S., 2022, Geologic map of the Jureano Mountain and Leesburg quadrangles, Lemhi County, Idaho: Idaho Geological Survey Digital Web Map 207, scale 1:24,000.

Link, P.K., Stewart, E.S., Steele, T., Sherwin, J., Hess, L.T., and McDonald, C., 2016, Detrital zircons in the Mesoproterozoic upper Belt Supergroup in the Pioneer, Beaverhead, and Lemhi Ranges, Montana and Idaho: The Big White arc, *in* MacLean, J.S., and Sears, J.W., eds., Belt Basin: Window to Mesoproterozoic Earth: Geological Society of America Special Paper 522, p. 163–183.

Lonn, Jeff, 2017, The Lemhi Group type section revisited and revised, east-central Idaho, Northwest Geology, v. 46, p. 15–28.

Lonn, J.D., Stanford, L.R., Burmester, R.F., Lewis, R.F., and McFaddan, M.D., 2009, Geologic map of the Goldstone Pass 7.5' quadrangle, Lemhi County, Idaho, and Beaverhead County, Montana: Montana Bureau of Mines and Geology Open-File Report 584, scale 1:24,000.

Lonn, J.D., Elliott, C.G., Stewart, D.E., Mosolf, J.G., Burmester, R.F., Lewis, R.S., and Pearson, D.M., 2019, Geologic map of the Bannock Pass 7.5' quadrangle, Beaverhead County, Montana, and Lemhi County, Idaho, Montana Bureau of Mines and Geology Geologic Map 76, scale 1:24,000.

Lonn, J.D., Burmester, R.F., Lewis, R.S., and McFaddan, M.D., 2020, The Mesoproterozoic Belt Supergroup, *in* Metesh, J.J., and Vuke, S.M., eds., Geology of Montana—Geologic History: Montana Bureau of Mines and Geology Special Publication 122, v. 1, 38 p. available at https://mbmg.mtech.edu/pdf/geologyvolume/Lonn_BeltFinal.pdf [Accessed 5/17/2023].

Lund, K., Aleinikoff, J.N., Yacob, E.Y., Unruh, D.M., and Fanning, C.M., 2008, Coolwater culmination: Sensitive high-resolution ion microprobe (SHRIMP) U-Pb and isotopic evidence for continental delamination in the Syringa Embayment, Salmon River suture, Idaho: Tectonics, v. 27, TC2009.

Murphy, J.P., Lewis, R.S., Vervoort, J.D., and Hämmerli, J., this volume, Multiple periods of metamorphism in the Salmon River Mountains as deduced from garnet Lu-Hf ages: Northwest Geology, v. 52.

Rogers, C., Mackinder, A., Ernst, R.E., and Cousens, B., 2016, Mafic magmatism in the Belt-Purcell Basin and Wyoming Province of western Laurentia, *in* MacLean, J.S. and Sears, J.W., eds., Belt Basin: Window to Mesoproterozoic Earth: Geological Society of America Special Paper 522, p. 243–282.

Ruppel, E.T., 1975, Precambrian Y sedimentary rocks in east-central Idaho: U.S. Geological Survey Professional Paper 889-A, 23 p.

Spence, J.G, 1984, Geology of the Mineral Hill interlayered amphibolite-augen gneiss complex, Lemhi County, Idaho: M.S. Thesis, University of Idaho, 240 p.

Stewart, D.E., Lewis, R.S., Stewart, E.D., and Link, P.K., 2013, Geologic map of the central and lower Big Creek drainage, Central Idaho: Idaho Geological Survey Digital Web Map 161, scale 1:75,000.

Tietbohl, D., 1986, Middle Proterozoic diamictite beds in the Lemhi Range, east-central Idaho, *in* Roberts, S.M., ed., Belt Supergroup: A Guide to Proterozoic Rocks of Western Montana and Adjacent Areas: Montana Bureau of Mines and Geology Special Publication 94, p. 197–207.

Tysdal, R.G., 1996a, Geologic map of parts of the Hayden Creek and Mogg Mountain quadrangles, Lemhi County, Idaho: U.S. Geological Survey Miscellaneous Investigations Series I-2563, scale 1:24,000.

Tysdal, R.G., 1996b, Geologic map of the Lem Peak quadrangle, Lemhi County, Idaho: U.S. Geological Survey Geologic Quadrangle Map GQ-1777, scale 1:24,000.

Tysdal, R.G., 2000, Stratigraphy and depositional environments of Middle Proterozoic rocks in northern part of Lemhi Range, Lemhi County, Idaho: U.S. Geological Survey Professional Paper 1600, 40 p.

Tysdal, R.G., 2002, Structural geology of western part of Lemhi Range, east-central Idaho: U.S. Geological Survey Profes-

sional Paper, v. 1659, 31 p.

Tysdal, R.G., 2003, Correlation, sedimentology, and structural setting, upper strata of Mesoproterozoic Apple Creek Formation and lower strata of Gunsight Formation, Lemhi Range to Salmon River Mountains, east-central Idaho, *in* Tysdal, R.G., Lindsey, D.A., and Taggart, J.E. Jr., eds., Correlation, sedimentology, structural setting, chemical composition, and provenance of selected formations in Mesoproterozoic Lemhi Group, Central Idaho: U.S. Geological Survey Professional Paper 1668-A, p. 1–22.

Tysdal, R.G., and Moye, F., 1996, Geologic map of the Allison Creek quadrangle, Lemhi County, Idaho: U.S. Geological Survey Geologic Quadrangle Map GQ-1778, scale 1:24,000.

Whitney, D.L., Mechum, T.A., Kuehner, S.M., and Dilek, Y.R., 1996, Progressive metamorphism of pelitic rocks from protolith to granulite facies, Dutchess County, New York, USA: Constraints on the timing of fluid infiltration during regional metamorphism: Journal of Metamorphic Geology, v. 14, p. 163–181.

Winston, D., Link, P.K., and Hathaway, N., 1999, The Yellowjacket is not the Prichard and other heresies: Belt Supergroup correlations, structure and paleogeography, east-central Idaho, *in* Hughes, S.S., and Thackray, G.D., eds, Guidebook to the geology of Eastern Idaho: Pocatello, Idaho Museum of Natural History, p. 3–20.

DEPOSITIONAL CHRONOLOGY AND PROVENANCE OF THE NORTHEASTERN BELT BASIN: EVIDENCE FOR EARLY MESOPROTEROZOIC NORTH AMERICAN DRAINAGE REORGANIZATION

Jaime A.M. Hirtz,[1] Kurt N. Constenius,[2] Brian K. Horton,[1,3] Victor A. Valencia,[4] and Brian R. Pratt[5]

[1]*Jackson School of Geosciences, University of Texas, Austin, Texas*
[2]*Department of Geosciences, University of Arizona, Tucson, Arizona*
[3]*Institute for Geophysics, University of Texas, Austin, Texas*
[4]*School of Earth and Environmental Sciences, Washington State University, Pullman, Washington*
[5]*Department of Geological Sciences, University of Saskatchewan, Saskatoon, Canada*

INTRODUCTION

The evolution of North America is punctuated by orogenic and magmatic activity in the Paleoproterozoic (ca. 2100–1800 Ma), Neoproterozoic (ca. 1100–900 Ma), and Phanerozoic (ca. 250–50 Ma) during amalgamation and breakup of the Columbia, Rodinia, and Pangea supercontinents (Zhao and others, 2002, 2004; Evans and Mitchell, 2011; Zhang and others, 2012; Meert and Santosh, 2017). These episodes formed extensive mountain ranges accompanied by erosion and deposition of thick successions in selected segments of Laurentia (Young and others, 1979). Mesoproterozoic metasedimentary successions include the Belt–Purcell Supergroup, U.S. and Canada (Winston and others, 1989), the Hess Canyon Group, Arizona (Doe and others, 2012, 2013), the Marqueñas Formation and Trampas Group, New Mexico (Jones and others, 2011, 2015; Daniel and others, 2013), the Muskwa assemblage, British Columbia (Ross and others, 2001), and the lower Fifteenmile Group, Yukon (Medig and others, 2014; Medig, 2016). However, reconstructions of sediment routing across Laurentia have largely focused on Phanerozoic to Neoproterozoic strata (Davis and others, 2010; Laskowski and others, 2013; Blum and Pecha, 2014; Linde and others, 2016; Rainbird and others, 2017; Saylor and Sundell, 2021).

Uncertainties remain for the geochronology and provenance of the Belt Basin. Most provenance studies have focused on potential western sources, including exotic (non-North American) terranes such as Siberia (Sears and Price, 2000; Sears and others, 2004; Link and others, 2007), Australia and East Antarctica (southwest U.S. to East Antarctica, SWEAT; Australia to southwest U.S., AUSWUS; and Australia to Mexico, AUSMEX hypotheses: Dalziel, 1991, 2013; Ross and others, 1992; Stewart and others, 2010; Halpin and others, 2014; Jones and others, 2015), and China (Missing Link hypothesis: Li and others, 1995, 2002; Zhang and others, 2012). However, Link and others (2016) assessed the potential contribution of North American sediments to the Lemhi subbasin (correlated with Belt–Purcell). Comparatively less is known about temporal variations in source regions and drainage dispersal patterns within Laurentia during basin evolution.

This study aims to refine the chronostratigraphic and provenance framework for the Belt–Purcell Supergroup by sampling all major units within a geographically limited area. Our objectives are to: (1) estimate the age, duration, and rate of sediment accumulation; (2) evaluate sediment provenance, routing patterns, and regional paleogeography; and (3) determine the occurrence and timing of potential shifts in source regions within the available Mesoproterozoic framework for North America and possible supercontinent reconfigurations. These results have implications for Laurentian paleogeographic reconstructions, the extent of Precambrian continental-scale drainage systems, and possible episodes of large-scale drainage reorganization prior to Grenville orogenesis.

GEOLOGIC AND STRATIGRAPHIC FRAMEWORK

The Mesoproterozoic Belt Basin of northwest U.S. and southwest Canada (Purcell Basin; fig. 1A) recorded accumulation of up to 17 km of predominantly fine-grained siliciclastic and carbonate rocks (Johns, 1970). With its depocenter near the Mission range, Montana (Harrison and others, 1974; Winston and others, 1989), the succession gradually thins to ~5 km northward near North Kootenay Pass, Alberta, Canada (Price, 1964; Fermor and Price, 1983; Sears, 2007; Fuentes and others, 2011).

The Belt–Purcell Supergroup is best exposed within the Lewis thrust sheet, in the Lewis and Livingston ranges, U.S., and Clarke range, Canada (fig. 1B). The Lewis sheet was translated >100 km northeastward during late Cretaceous–early Eocene crustal contraction (Fermor and Price, 1983; van der Velden and Cook, 1994; Constenius, 1996; Sears, 2007; Fuentes and others, 2011; Yonkee and Weil, 2015), and is spectacularly showcased in Glacier National Park (NP), Montana, and Waterton Lakes NP and Castle Wildland Provincial Park, Alberta.

The Belt–Purcell Supergroup within the Lewis thrust sheet consists of the Lower Belt, Ravalli Group, Piegan Group (Middle Belt Carbonate), and Missoula Group (fig. 2). Stratigraphic thicknesses and lithologic descriptions

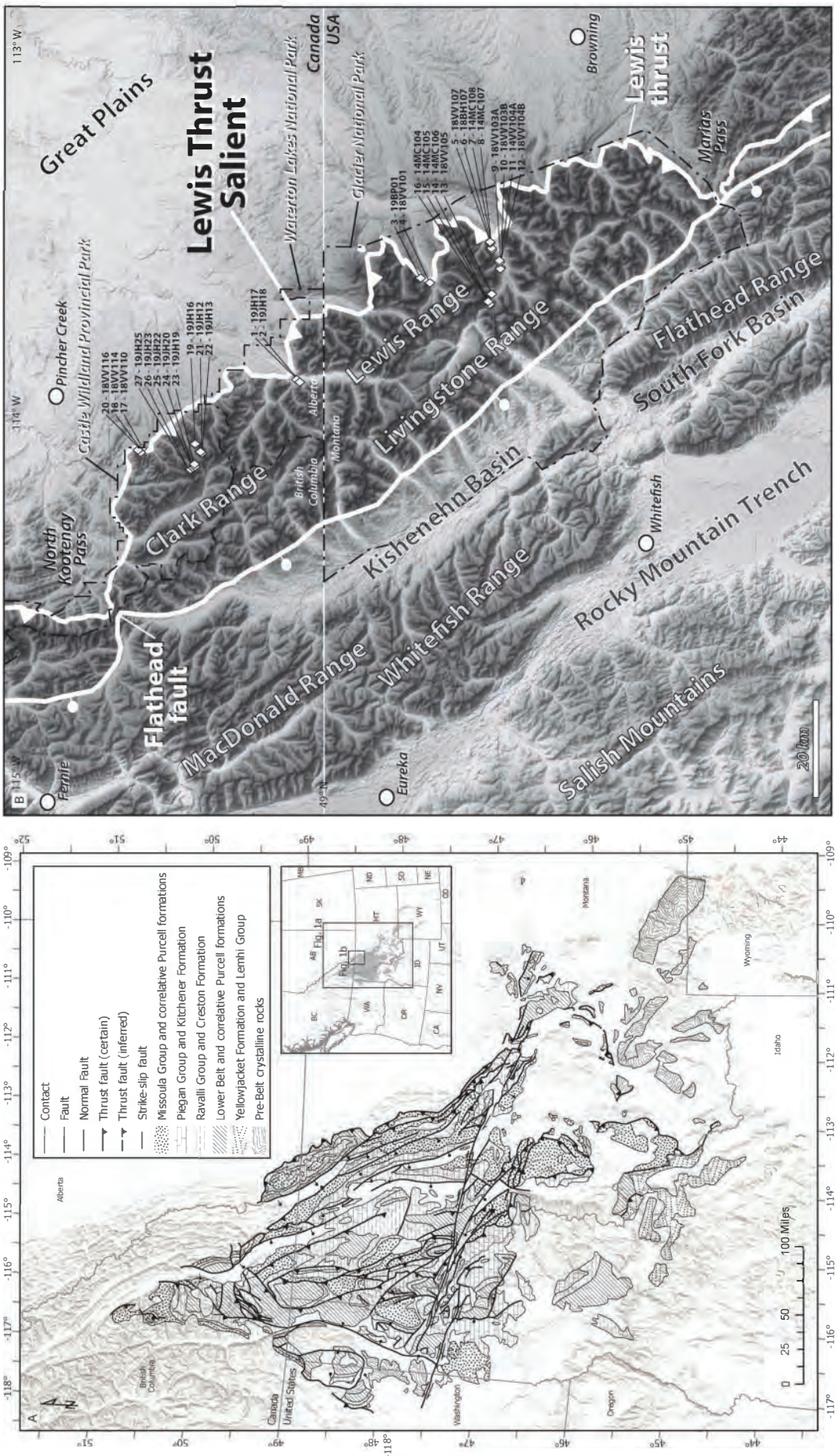

Figure 1. Study area shown by the (A) generalized geologic map of the Belt–Purcell Supergroup digitized from Winston and others (1989), and (B) digital elevation model of the Lewis thrust salient showing sample collection sites.

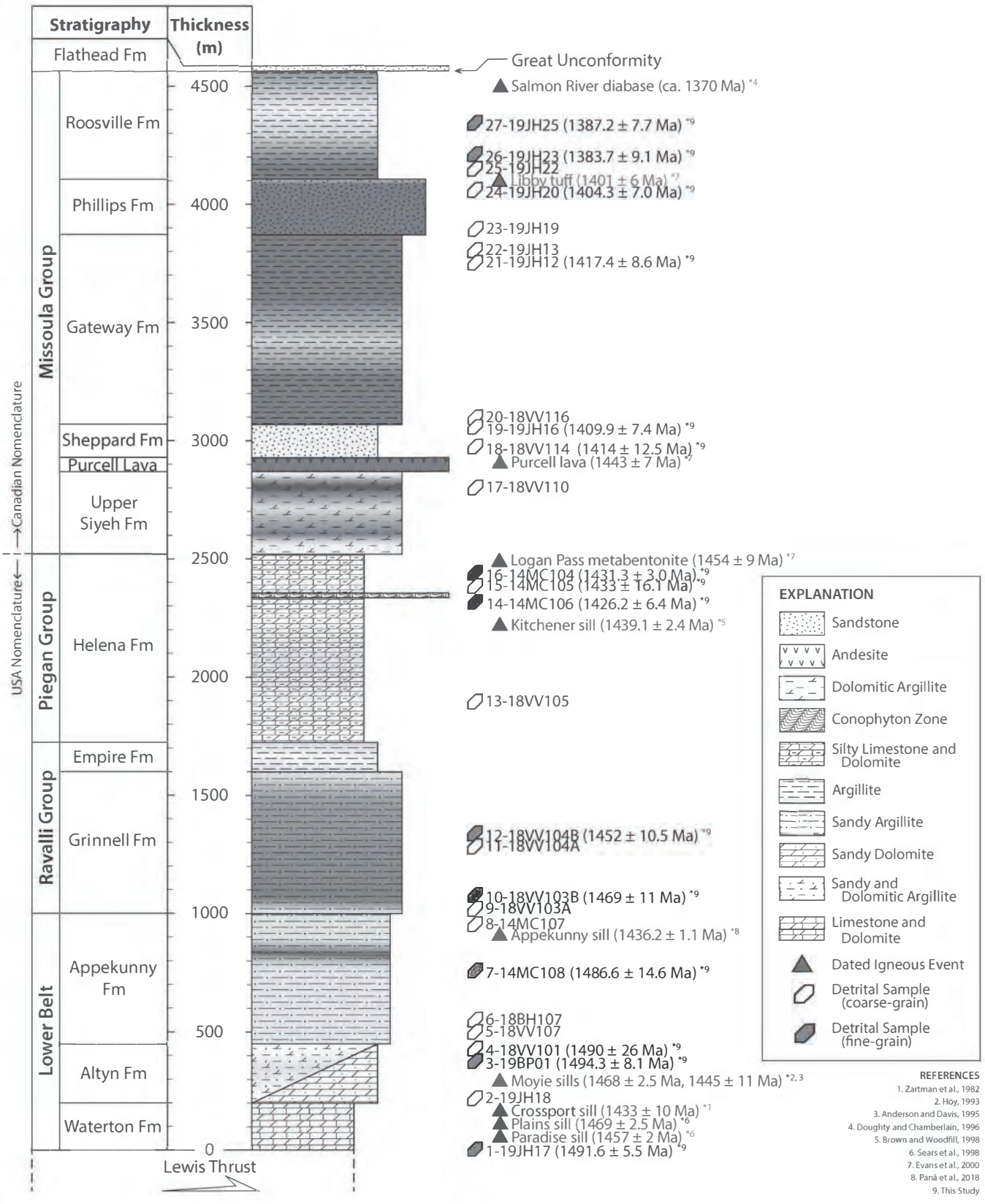

Figure 2. Lithostratigraphic framework for the Belt–Purcell Supergroup of the Lewis thrust salient modified from Ross (1959), Fermor and Price (1983, 1987), Winston and others (1989), Pratt and Ponce (2019), and Pratt and Rule (2021). Source of dated igneous rocks include Zartman and others (1982), Höy (1993), Anderson and Davis (1995), Doughty and Chamberlain (1996), Brown and Woodfill (1998), Sears and others (1998), Evans and others (2000) and Pană and others (2018).

for the Lewis, Livingstone, and Clark ranges and correlative strata in Montana and Idaho were compiled from Ross (1959), Fermor and Price (1983, 1987), Winston and others (1989), Pratt and Ponce (2019), and Pratt and Rule (2021). In the U.S., the Lower Belt is subdivided into the Waterton, Altyn, and Appekunny Formations. The Ravalli Group is composed of the Grinnell and Empire Formations. The Piegan Group consists of the Helena Formation, and the capping Missoula Group is subdivided in Canada into the Upper Siyeh Formation, Purcell Lava, and Sheppard, Gateway, Phillips, and Roosville Formations.

METHODS

Detrital zircon (DZ) U-Pb geochronological data were acquired using a laser ablation–inductively coupled plasma-mass spectrometer (LA-ICP-MS) for 27 samples (17 sandstones, 8 argillites, 1 oolitic grainstone, 1 metabentonite) spanning all stratigraphic units except the Empire Formation (fig. 2). Maximum depositional ages (MDA) calculated with detritalPy software (Sharman and others, 2018) for the DZ dataset provided new chronostratigraphic insights such as the basin age and sediment accumulate rates. We then compared the 27 Belt–Purcell sample results to a Laurentia-wide compilation of published igneous and metamorphic zircon U-Pb ages (n = 22, n = 12,362 concordant grains) for major Precambrian (>1000 Ma) tectono-magmatic provinces to evaluate North American sediment source inputs to the Belt Basin. Consideration of sediment provenance is evaluated qualitatively using multidimensional scaling (MDS) plots, and the relative mixing proportions are determined quantitatively using DZmix, a MATLAB-based inverse Monte Carlo mixture model (Sundell and Saylor, 2017).

RESULTS

New detrital U-Pb results for the Belt–Purcell Supergroup (fig. 3) and compiled igneous and metamorphic U-Pb data for potential Laurentian source regions are binned according to Proterozoic and Archean ages: Late Calymmian to Ectasian (LC-ET, 1480–1340 Ma), Early Calymmian (EC, 1600–1480 Ma), Late Statherian (LS, 1700–1600 Ma), Early Statherian (ES, 1800–1700 Ma), Orosirian (OS, 1920–1800 Ma), Siderian to Rhyacian (SD-RY, 2500–1920 Ma), and Archean (AR, 3500–2500 Ma).

Igneous and Metamorphic Zircon U-Pb Ages: Laurentia

Sediment sources to the north, northeast, and east constitute the bulk of the Canadian Shield, including the Slave craton, Taltson magmatic zone, Rae and Hearne cratons, Athabasca intrusives, Churchill province, Trans-Hudson orogen, Sask and North Atlantic cratons, Makkovik orogen, Medicine Hat province, Wyoming and Superior cratons, and Abitibi greenstone belt. They contain age populations dominated by the Archean eon (53%), and Paleoproterozoic Siderian–Rhyacian (20%) and Orosirian periods (19%), with no Mesoproterozoic groups.

Sources to the southeast and south include the Penokean and Grenville orogens, Anorogenic granites, Mazatzal terrane, Mazatzal–Yavapai transition, Yavapai province, Yavapai–Mojave intermediate zone, and Mojave crustal block. These Southern Provinces are characterized primarily by Early Statherian (26%), Late Statherian (34%), and Late Calymmian–Ectasian (25%), with negligible early Paleoproterozoic or Archean distributions.

Detrital Zircon U-Pb Ages: Belt–Purcell Supergroup

This study presents a comprehensive DZ U-Pb geochronologic dataset for the northeastern segment of the Belt Basin. Results yield a total of 3,123 individual grain analyses. Of these, 530 were >20% discordant and >5% reversely discordant, leaving a filtered total of 2,593 concordant ages for further analysis. These results are presented in stratigraphic order, from lower (samples 1-19JH17 to 13-18VV105) to intermediate (samples 14-14MC106 to 18-18VV114) and upper levels (samples 19-19JH16 to 27-19JH25; fig. 3).

Detrital zircon age distributions for the Waterton to lower Helena Formations (here the lower Belt–Purcell) have a high proportion of Archean (36%), Siderian–Rhyacian (13%), Orosirian (30%), and Early Statherian (15%) zircons, with negligible Mesoproterozoic contributions. In contrast, the middle Belt–Purcell succession (upper Helena to Sheppard Formations) reveal considerable diversity in age populations spanning the Archean eon (9%) and Orosirian (12%), Early Statherian (14%), Late Statherian (15%), Early Calymmian (15%), and Late Calymmian–Ectasian periods (33%). The upper Belt–Purcell succession (Gateway to Roosville Formations) is relatively uniform in exhibiting predominantly Orosirian (12%), Early Statherian (45%), and Late Statherian (18%) age spectra, with comparatively few Mesoproterozoic and early Paleoproterozoic to Archean grains.

Qualitative and Quantitative Provenance

Provenance of the Belt–Purcell Supergroup is evaluated qualitatively with MDS plots, graphical representations of the similarity or dissimilarity among sample U-Pb age distributions. Samples with similar age distributions plot in tight clusters, whereas dissimilar samples show considerable scatter. The MDS plots demonstrate that lower Belt–Purcell samples contain age distributions that resemble the Canadian Shield and are distinct from upper Belt–Purcell samples that are more similar to the Southern Provinces. In contrast, the transitional middle Belt–Purcell interval shows greater scatter.

This study also employs a statistical model (DZmix) to quantify potential contributions of Laurentian source regions throughout the depositional history of the Belt Basin (fig. 4). Significant contributions for the lower Belt–Purcell demonstrate derivation from the Canadian Shield

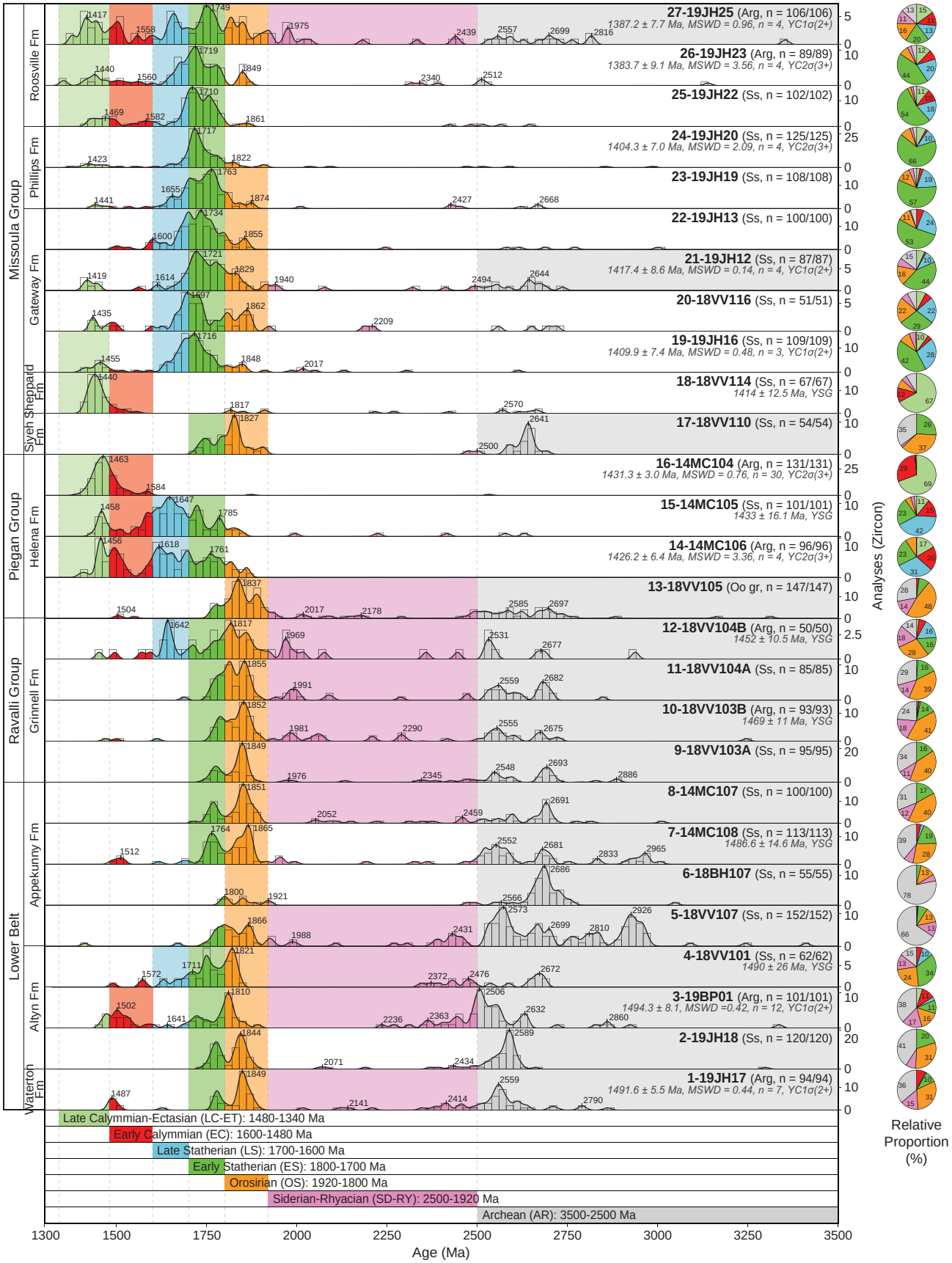

Figure 3. Detrital zircon U-Pb geochronology of the Belt–Purcell Supergroup. Probability density plots (curves), histograms (20 Myr bins), and pies (%) of zircon analyses (n) from the Precambrian (3500–1300 Ma) are listed in stratigraphic order from oldest (bottom) to youngest (top). Color bars and pie labels are illustrated when relative proportions of Proterozoic periods and Archean age populations (LC-ET, EC, LS, ES, OS, SD-RY, AR) are >10%. Maximum depositional age constraints (italicized), their mean square weighted deviations (MSWD), and method of analysis (YC1σ(2+), YC2σ(3+), YSG) are indicated for samples with interpreted syndepositional constraints.

to the northeast, principally the Churchill province (21%), Sask craton (18%), and Makkovik orogen (17%). The complex provenance record for the middle Belt–Purcell shows substantial variations between successive samples, potentially due to episodes of drainage reorganization and/or competing pulses from the Southern Provinces (samples 14-14MC106 to 15-14MC105), Canadian Shield (sample 17-18VV110), and a potentially unidentified source (samples 16-14MC104 and 18-18VV114). In sharp contrast to underlying units, the upper Belt–Purcell succession shows detrital contributions predominantly sourced from the Yavapai–Mojave transition (37%) and Mojave crustal terrane (31%) of the Southern Provinces.

INTERPRETATION AND DISCUSSION

Chronostratigraphy

Our detrital zircon U-Pb data enables refined calculations of the depositional chronology for the Belt–Purcell Supergroup (fig. 3). MDA values determined using detritalPy are based on: (a) the youngest cluster of at least two grains with 1σ uncertainty (YC1σ(2+)), (b) the youngest cluster of at least three grains with 2σ uncertainty (YC2σ(3+)), or where applicable, (c) the youngest single grain (YSG) ages. Collectively, the MDA results reveal a systematic upsection younging trend consistent with early Mesoproterozoic ages of ca. 1495–1380 Ma, from the Late Calymmian to Early Ectasian. These values suggest a depositional duration of ~115 Myr, and an average sediment accumulation rate of ~155 m/Myr when correlated with stratigraphy near the Mission Range where the basin attains its maximum thickness of ~17 km. Consideration of the effects of compaction require that these estimates are minimum values.

We interpret fine-grained sample 16-14MC104 (n = 131) of the Helena Formation from Logan Pass, Glacier NP, U.S. as a metabentonite that offers a new chronologic control for the Belt–Purcell Supergroup. This interpretation is supported by: (1) its distinctive lithology, as a thin olive-green argillite; (2) the presence of quartz shards (Moe and others, 1996); (3) its dominantly unimodal age distribution; and (4) its characteristic early Mesoproterozoic zircon population, which stands in stark contrast to the rest of the Belt–Purcell Supergroup (excluding sample 18-18VV114). Further investigation of its non-magnetic, heavy mineral separates reveals numerous needle-like, euhedral zircons with crystallographic c:a axis ratios of 20–15:1, widely understood to indicate a magmatic origin. Its volcanic nature was first noted by Moe and others (1996), and later by Evans and others (2000), who obtained zircon U-Pb-sensitive high-resolution ion microprobe (SHRIMP) ages on a metabentonite from Logan Pass (from Evans and others, 2000, sample 71-O-19, n = 18). However, although their data display a spread of values from 1492 to 1420 Ma, reanalysis of their data in detritalPy yields new MDAs of 1423 ± 8.5 Ma (YSG), 1423.7 ± 4.7 Ma (YC1σ(2+)), and 1437.5 ± 2.8 (YC2σ(3+)). Therefore, based on our estimate of 1431.3 ± 3.0 Ma (YC2σ(3+), MSWD = 0.76, n = 30; fig. 3) for the Helena metabentonite (sample 16-14MC104), we consider their reported age of 1454 ± 9 Ma to be ~25–30 Myr older than its true depositional age. Additionally, this sample coincides with a low coefficient of determination (R^2 = 0.63; fig. 4). This indicates that the recognized source regions prescribed to the cross-correlation test were insufficient to characterize sample 16-14MC104, suggesting an unaccounted zircon contributor. This unimodal age spectra roughly overlaps with the North American magmatic gap (ca. 1610–1490 Ma) that Precambrian provenance and paleotectonic studies have emphasized to highlight the presence of non-North American sediments; therefore, previously unrecognized sediment contributors (possibly volcanic) could include western exotic terranes (e.g., Australia, Antarctica, Siberia, China). Further testing of this option is outside the scope of this paper; however, if siliciclastic material of the Lewis thrust salient along northeastern Belt Basin exposures were derived from a western, non-Laurentian source, from the information above, we propose it might be present in the upper Helena Formation near the Conophyton zone. This interpretation has important implications for the evaluation of present and future Belt–Purcell chronostratigraphic and paleotectonic studies.

Continental-Scale Drainage Reorganization at ca. 1430–1410 Ma

The new DZ U-Pb data for 27 samples constrain depositional ages and sediment dispersal patterns during Mesoproterozoic evolution of the northeastern Belt Basin near the western (present coordinates) edge of paleo-Laurentia (fig. 5). The lower Belt–Purcell interval was deposited from ca. 1495–1430 Ma with sediment delivery from sources to the northeast. Given the inter-sample consistency for samples 1-19JH17 to 13-18VV105, we infer prolonged (at least ~65 Myr) drainage stability, where Laurentian transcontinental tributaries flowed from northeast to southwest. The middle Belt–Purcell succession (samples 14-14MC106 to 18-18VV114), deposited from ca. 1430–1410 Ma, recorded complex input from the Canadian Shield, newly contributing Southern Provinces, and a currently unidentified magmatic source. This variability indicates a period (~20 Myr) of fluvial catchment instability with a volcaniclastic influence. The upper Belt–Purcell (samples 19-19JH16 to 27-19JH25), deposited from ca. 1410–1380 Ma, recorded a switch to sediment delivery primarily from the southeast and south. The consistency among upper Belt–Purcell U-Pb age distributions attest to a second prolonged phase (at least ~30 Myr) of drainage stability in North America, with a renewed transcontinental fluvial network that instead flowed principally from the southeast to the northwest.

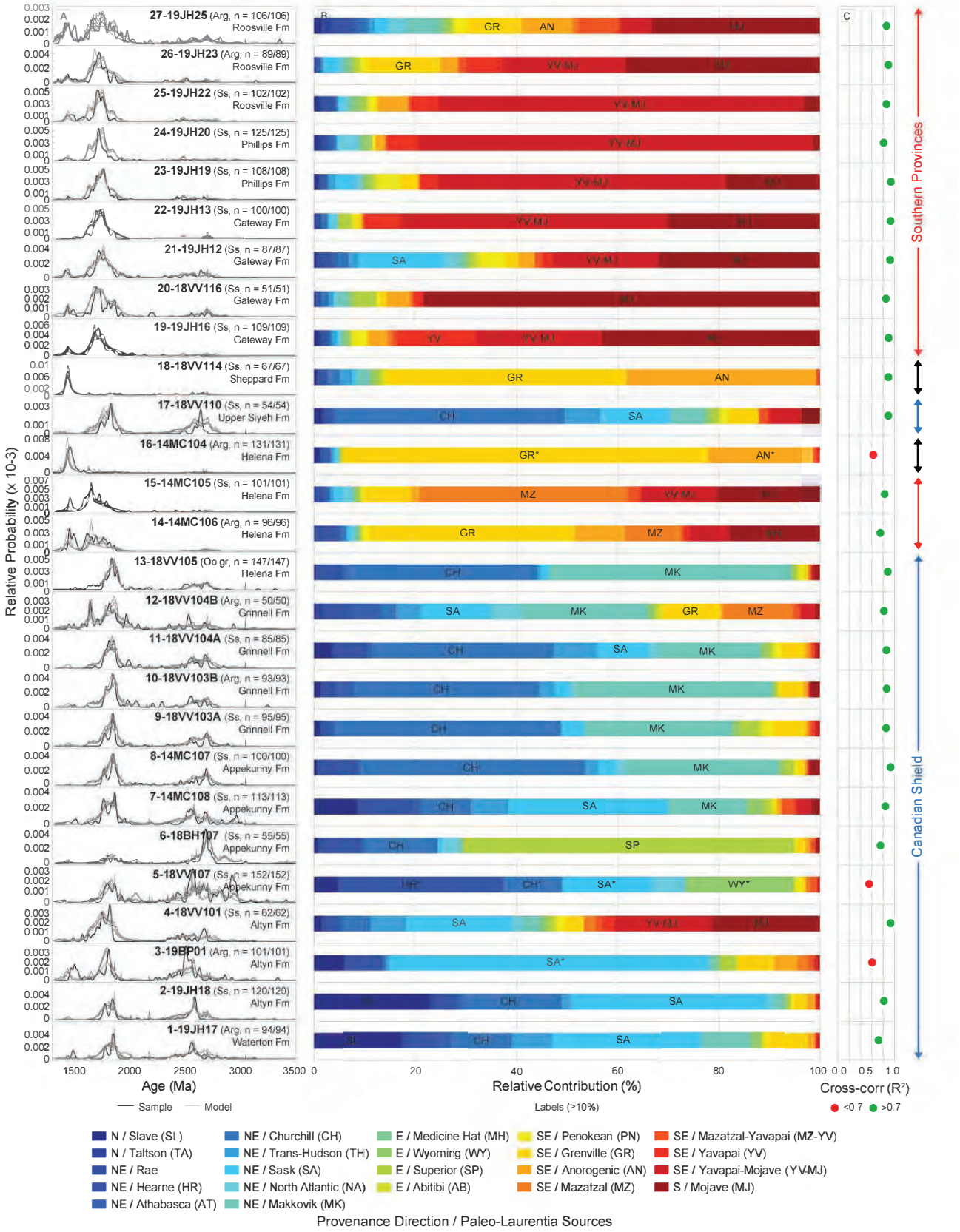

Figure 4. Inverse Monte Carlo mixture model results for the Belt–Purcell Supergroup illustrated by their (A) probability density plots (PDP) of our detrital analyses and top 5 statistical model outputs from 50,000 random combinations (curves), (B) cross-correlation model determined relative contributions (labeled when >10%), and (C) coefficient of determination (R2 >0.7, good fit; R2 <0.7, poor fit) for samples 1-19JH17 to 27-19JH25 (bottom to top). Provenance interpretations from the Canadian Shield (blue arrows; samples 1-19JH17 to 13-18VV105, and 17-18VV110), Southern Provinces (red arrows; samples 14-14MC106 to 15-14MC105, and 19-19JH16 to 27-19JH25), or undetermined source(s) (black arrows; samples 16-14MC104 and 18-18VV114) are shown on the right.

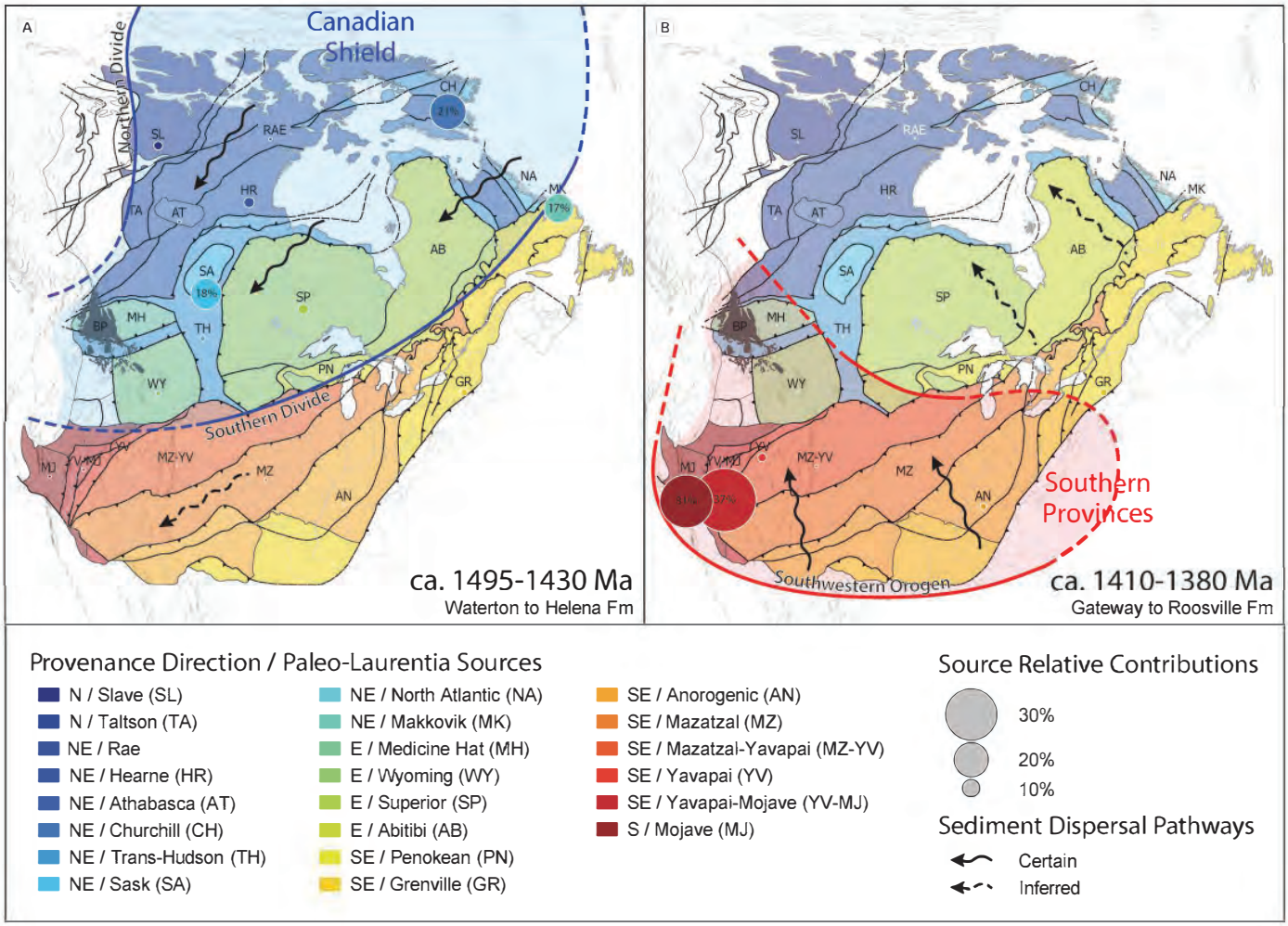

Figure 5. Generalized paleogeographic reconstruction for Laurentia during Belt Basin deposition indicating the general direction of transcontinental fluvial system flow (arrows) at (A) ca. 1495–1430 Ma and (B) ca. 1410–1380 Ma and inferred position of a southwestern orogen. Relative contributions (spherical size is proportional to sediment contribution) demonstrate that provenance of the Waterton to lower Helena Formations are dominated by the Churchill province, Sask craton, and Makkovik orogen (avg. 56%), whereas the Gateway to Roosville Formations exhibit a significant contribution of siliciclastic input from the Yavapai–Mojave transition and Mojave crustal block (avg. 68%). Therefore, we interpret this provenance shift to indicate the first observed instance of a continental-scale reorganization of the drainage network for paleo-North America during deposition of the Helena Formation in the early Mesoproterozoic at ca. 1430–1410 Ma.

The aforementioned early Mesoproterozoic provenance shift that lasted ~20 Myr during deposition of the upper Piegan Group to lower Missoula Group (upper Helena to Sheppard Formations) represents one of the first documented instances of a continental-scale drainage reorganization within North America (fig. 5). Specifically, the Lower Belt, Ravalli Group, and lower Piegan Group (Waterton to lower Helena Formations) were sourced predominantly from early Paleoproterozoic and Archean terranes, and this was succeeded by upper Missoula Group (Gateway to Roosville Formations) deposition from sources of late Paleoproterozoic and Mesoproterozoic terranes. This estimate (several tens of Myr) is equivalent to timescales necessary for comparable catchment reversals previously interpreted in North America (e.g., Cretaceous–Paleocene Mississippi; Blum and Pecha, 2014) and South America (e.g., Miocene Amazon; Hoorn and others, 1995), and highlights the notion that continental-scale drainage reorganizations are not instantaneous, but gradual (Parker and Hendrix, 2022).

Sedimentary Response to the Picuris Orogen

The continental-scale provenance shift postulated here was likely caused by a pre-Grenville orogen along southern Laurentia (fig. 5B). We propose the general provenance trend of the Belt–Purcell Supergroup records a sedimentary response at ca. 1430–1410 Ma, potentially influenced by a tectono-thermal event in present-day Arizona, New Mexico, and Colorado. Several candidates situated south of the Belt Basin have been introduced. Link and others (2016) infer that provenance for the Lemhi subbasin (correlated with Belt–Purcell) was the Big White arc, an accretionary magmatic arc and unroofed batholith of the Mazatzal–Yavapai orogen produced before ca. 1700 Ma. However, while our Missoula Group samples exhibit higher concentrations of ca. 1800–1650 Ma DZ ages, orogenic activity associated with the Big White arc likely ceased by the late Paleoproterozoic. Another possibility relates to the Picuris orogen of the southwest U.S., based on regional

amphibolite-facies metamorphism, deformation, magmatic intrusions, basin formation, and sedimentation between ca. 1500–1350 Ma (Daniel and others, 2013; Holland and others, 2016; Aronoff and others, 2016; Doe and Daniel, 2019; Kuiper and others, 2022). Therefore, based on the timing and geographic extent, we propose the paleo-North American drainage network reorganization was influenced by the Picuris orogen.

CONCLUSION

Based on 27 new samples containing 2,593 concordant DZ U-Pb ages, this study presents the single largest geochronologic dataset for northeastern exposures of the Belt basin to refine the chronostratigraphic and provenance characterization of the Belt–Purcell Supergroup. We conclude that: (1) the basin age spans from ca. 1495 to 1380 Ma (Late Calymmian–Early Ectasian); (2) deposition spanned ~115 Myr; (3) the average rate of sediment accumulation is ~155 m/Myr; and (4) a metabentonite from the upper Helena Formation (sample 16-14MC104) provides a new absolute age control (1431.3 ± 3.0 Ma) for the Belt Basin. Statistical modeling of new DZ data to 22 major Precambrian Laurentian basement provinces, compiled from 12,362 published igneous and metamorphic zircon U-Pb ages, support a drainage network in which: (5) provenance of the Waterton to lower Helena Formations is from the Canadian Shield (Churchill, Sask, Makkovik) and the Gateway to Roosville Formations is from the Southern Provinces (Mojave, Yavapai–Mojave); (6) at least two contrasting transcontinental river systems formed key components of the early Mesoproterozoic paleogeography; (7) Laurentia experienced a continental-scale drainage network reorganization at ca. 1430–1410 Ma during deposition of the upper Helena to Sheppard Formations; and (8) causes for this catchment reversal are likely tied to the Picuris orogen in southern Laurentia.

ACKNOWLEDGMENTS

This research was financially supported by an American Association of Petroleum Geologists Grants-in-Aid award through the R.E. McAdams Memorial Grant. The authors would like to thank Mark A. Helper and Ronald J. Steel for improving earlier versions of the manuscript, and Tyson M. Smith and Alan English for their thorough and constructive reviews.

REFERENCES

Anderson, H.E., and Davis, D.W., 1995, U–Pb geochronology of the Moyie sills, Purcell Supergroup, southeastern British Columbia: Implications for the Mesoproterozoic geological history of the Purcell (Belt) basin: Canadian Journal of Earth Sciences, v. 32, p. 1180–1193, doi:10.1139/e95-097.

Aronoff, R.F., Andronicos, C.L., Vervoort, J.D., and Hunter, R.A., 2016, Redefining the metamorphic history of the oldest rocks in the southern Rocky Mountains: Geological Society of America Bulletin, v. 128, p. 1207–1227, doi:10.1130/B31455.1.

Blum, M., and Pecha, M., 2014, Mid-Cretaceous to Paleocene North American drainage reorganization from detrital zircons: Geology, v. 42, p. 607–610, doi:10.1130/G35513.1.

Brown, D.A., and Woodfill, R.D., 1998, The Moyie industrial partnership project: Geology and mineralization of the Yahk–Moyie Lake area, southwestern British Columbia: British Columbia Geological Survey, p. 22.

Constenius, K.N., 1996, Late Paleogene extensional collapse of the Cordilleran foreland fold and thrust belt: Geological Society of America Bulletin, v. 108, p. 20–39, doi:10.1130/0016-7606(1996)108<0020:LPECOT>2.3.CO;2.

Dalziel, I.W.D., 1991, Pacific margins of Laurentia and East Antarctica–Australia as a conjugate rift pair: Evidence and implications for an Eocambrian supercontinent: Geology, v. 19, p. 598, doi:10.1130/0091-7613(1991)019<0598:PMOLAE>2.3.CO;2.

Dalziel, I.W.D., 2013, Antarctica and supercontinental evolution: Clues and puzzles: Earth and Environmental Science Transactions of The Royal Society of Edinburgh, v. 104, p. 3–16, doi:10.1017/S1755691012000096.

Daniel, C.G., Pfeifer, L.S., Jones, J.V. III, and McFarlane, C.M., 2013, Detrital zircon evidence for non-Laurentian provenance, Mesoproterozoic (ca. 1490–1450 Ma) deposition and orogenesis in a reconstructed orogenic belt, northern New Mexico, USA: Defining the Picuris orogeny: Geological Society of America Bulletin, v. 125, p. 1423–1441, doi:10.1130/B30804.1.

Davis, S.J., Dickinson, W.R., Gehrels, G.E., Spencer, J.E., Lawton, T.F., and Carroll, A.R., 2010, The Paleogene California River: Evidence of Mojave–Uinta paleodrainage from U-Pb ages of detrital zircons: Geology, v. 38, p. 931–934, doi:10.1130/G31250.1.

Doe, M.F., and Daniel, C.G., 2019, Evidence for Mesoproterozoic ca. 1470–1444 Ma regional deformation of the Mazatzal Group and equivalent rocks in the type area of the Mazatzal orogeny, Tonto Basin, Arizona, *in* Pearthree, P.A., ed., Geologic excursions in southwestern North America, Geological Society of America, v. 55, p. 0, doi:10.1130/2019.0055(10).

Doe, M.F., Jones, J.V., Karlstrom, K.E., Thrane, K., Frei, D., Gehrels, G., and Pecha, M., 2012, Basin formation near the end of the 1.60–1.45 Ga tectonic gap in southern Laurentia: Mesoproterozoic Hess Canyon Group of Arizona and implications for ca. 1.5 Ga supercontinent configurations: Lithosphere, v. 4, p. 77–88, doi:10.1130/L160.1.

Doe, M.F., Jones, J.V., Karlstrom, K.E., Dixon, B., Gehrels, G., and Pecha, M., 2013, Using detrital zircon ages and Hf isotopes to identify 1.48–1.45 Ga sedimentary basins and fingerprint sources of exotic 1.6–1.5 Ga grains in southwestern Laurentia: Precambrian Research, v. 231, p. 409–421, doi:10.1016/j.precamres.2013.03.002.

Doughty, P.T., and Chamberlain, K.R., 1996, Salmon River Arch revisited: New evidence for 1370 Ma rifting near the end of

deposition in the Middle Proterozoic Belt basin: Canadian Journal of Earth Sciences, v. 33, p. 1037–1052, doi:10.1139/e96-079.

Evans, D.A.D., and Mitchell, R.N., 2011, Assembly and breakup of the core of Paleoproterozoic–Mesoproterozoic supercontinent Nuna: Geology, v. 39, p. 443–446, doi:10.1130/G31654.1.

Evans, K.V., Aleinikoff, J.N., Obradovich, J.D., and Fanning, C.M., 2000, SHRIMP U-Pb geochronology of volcanic rocks, Belt Supergroup, western Montana: Evidence for rapid deposition of sedimentary strata: Canadian Journal of Earth Sciences, v. 37, p. 1287–1300, doi:10.1139/e00-036.

Fermor, P.R., and Price, R.A., 1983, Stratigraphy of the lower part of the Belt–Purcell Supergroup (Middle Proterozoic) in the Lewis thrust sheet of southern Alberta and British Columbia: Bulletin of Canadian Petroleum Geology, v. 31, p. 169–194.

Fermor, P.R., and Price, R.A., 1987, Multiduplex structure along the base of the Lewis thrust sheet in the southern Canadian Rockies: Bulletin of Canadian Petroleum Geology, v. 35, p. 159–185.

Fuentes, F., DeCelles, P.G., Constenius, K.N., and Gehrels, G.E., 2011, Evolution of the Cordilleran foreland basin system in northwestern Montana, U.S.A.: Geological Society of America Bulletin, v. 123, p. 507–533, doi:10.1130/B30204.1.

Halpin, J.A., Jensen, T., McGoldrick, P., Meffre, S., Berry, R.F., Everard, J.L., Calver, C.R., Thompson, J., Goemann, K., and Whittaker, J.M., 2014, Authigenic monazite and detrital zircon dating from the Proterozoic Rocky Cape Group, Tasmania: Links to the Belt–Purcell Supergroup, North America: Precambrian Research, v. 250, p. 50–67, doi:10.1016/j.precamres.2014.05.025.

Harrison, J.E., Griggs, A.B., and Wells, J.D., 1974, Tectonic features of the Precambrian Belt basin and their influence on post-belt structures: Washington, United States Government Printing Office, Geological Survey Professional Paper 866, 15 p.

Hoorn, C., Guerrero, J., Sarmiento, G.A., and Lorente, M.A., 1995, Andean tectonics as a cause for changing drainage patterns in Miocene northern South America: Geology, v. 23, p. 237–240, doi:10.1130/0091-7613(1995)023<0237:ATAACF>2.3.CO;2.

Holland, M.E., Karlstrom, K.E., Grambling, T.A., and Heizler, M.T., 2016, Geochronology of Proterozoic rocks of the Sandia–Manzano–Los Pinos Uplift: Implications for the timing of crustal assembly of the southwestern United States, *in:* The Geology of the Belen Area, Frey, B.A., Karlstrom, K.E., Lucas, S.G., Williams, S., Zeigler, K., McLemore, V., and Ulmer-Scholle, D.S., New Mexico Geological Society, Guidebook, 67th Field Conference, pp. 161–168, https://doi.org/10.56577/FFC-67.161.

Höy, T., 1993, Geology of the Purcell Supergroup in the Fernie west-half map-area, southeastern British Columbia: Victoria, Province of British Columbia, Ministry of Energy, Mines and Petroleum Resources.

Johns, W.M., 1970, Geology and mineral deposits of Lincoln and Flathead counties, Montana: Montana College of Mineral Science and Technology.

Jones, J.V. III, Daniel, C.G., Frei, D., and Thrane, K., 2011, Revised regional correlations and tectonic implications of Paleoproterozoic and Mesoproterozoic metasedimentary rocks in northern New Mexico, USA: New findings from detrital zircon studies of the Hondo Group, Vadito Group, and Marqueñas Formation: Geosphere, v. 7, p. 974–991, doi:10.1130/GES00614.1.

Jones, J.V. III, Daniel, C.G., and Doe, M.F., 2015, Tectonic and sedimentary linkages between the Belt–Purcell basin and southwestern Laurentia during the Mesoproterozoic, ca. 1.60–1.40 Ga: Lithosphere, v. 7, p. 465–472, doi:10.1130/L438.1.

Kuiper, Y.D., Aronoff, R.F., Daniel, C.G., and Bzdok, M., 2022, Exploring the nature and extent of the Mesoproterozoic Picuris orogeny in Colorado, USA, *in* Mahan, K.H., and Carpenter, L. eds., Field excursions in the Front Range and Wet Mountains of Colorado for Geological Society of America Connects 2022, Geological Society of America, p. 17–38, doi:10.1130/2022.0064(02).

Laskowski, A.K., DeCelles, P.G., and Gehrels, G.E., 2013, Detrital zircon geochronology of Cordilleran retroarc foreland basin strata, western North America: Tectonics, v. 32, p. 1027–1048, doi:10.1002/tect.20065.

Li, Z.X., Zhang, L., and Powell, C.M., 1995, South China in Rodinia: Part of the missing link between Australia–East Antarctica and Laurentia?: Geology, v. 23, p. 407–410, doi:10.1130/0091-7613(1995)023<0407:SCIRPO>2.3.CO;2.

Li, Z.X., Li, X., Zhou, H., and Kinny, P.D., 2002, Grenvillian continental collision in south China: New SHRIMP U-Pb zircon results and implications for the configuration of Rodinia: Geology, v. 30, p. 163–166, doi:10.1130/0091-7613(2002)030<0163:GCCISC>2.0.CO;2.

Linde, G.M., Trexler, J.H. Jr., Cashman, P.H., Gehrels, G., and Dickinson, W.R., 2016, Detrital zircon U-Pb geochronology and Hf isotope geochemistry of the Roberts Mountains allochthon: New insights into the early Paleozoic tectonics of western North America: Geosphere, v. 12, p. 1016–1031, doi:10.1130/GES01252.1.

Link, P.K., Fanning, C., Lund, K., and Aleinikoff, J.N., 2007, Detrital zircon populations and provenance of Mesoproterozoic strata of east-central Idaho, U.S.A.: Correlation with Belt Supergroup of southwest Montana, *in* Society for Sedimentary Geology, https://openresearch-repository.anu.edu.au/handle/1885/28426 [Accessed July 2021].

Link, P.K., Stewart, E.D., Steel, T., Sherwin, J.-A., Hess, L.T., and McDonald, C., 2016, Detrital zircons in the Mesoproterozoic upper Belt Supergroup in the Pioneer, Beaverhead, and Lemhi Ranges, Montana and Idaho: The Big White arc, *in* Geological Society of America Special Papers, Geological Society of America, v. 522, p. 163–183, doi:10.1130/2016.2522(07).

Medig, K.P.R., 2016, Sedimentology, geochemistry, and geochronology of unit PR1 of the lower Fifteenmile group and the Pinguicula Group, Wernecke and Ogilvie Mountains, Yukon, Canada: Mesoproterozoic environments and paleocontinental reconstructions [Thesis]: Science: Department of Earth Sciences, http://summit.sfu.ca/item/16901 [Accessed July 2021].

Medig, K.P.R., Thorkelson, D.J., Davis, W.J., Rainbird, R.H., Gibson, H.D., Turner, E.C., and Marshall, D.D., 2014, Pinning northeastern Australia to northwestern Laurentia in the Mesoproterozoic: Precambrian Research, v. 249, p. 88–99, doi:10.1016/j.precamres.2014.04.018.

Meert, J.G., and Santosh, M., 2017, The Columbia supercontinent revisited: Gondwana Research, v. 50, p. 67–83, doi:10.1016/j.gr.2017.04.011.

Moe, J.A., Ryan, P.C., Elliott, W.C., and Reynolds, R.C., 1996, Petrology, chemistry, and clay mineralogy of a K-bentonite in the Proterozoic Belt Supergroup of western Montana: Journal of Sedimentary Research, v. 66, p. 95–99, doi:10.1306/D42682C0-2B26-11D7-8648000102C1865D.

Pană, D.I., Rukhlov, A.S., Heaman, L.M., and Hamilton, M., 2018, Geochronology of selected igneous rocks in the Alberta Rocky Mountains, with an overview of the age constraints on the host formations: Alberta Energy Regulator/ Alberta Geological Survey, p. 67.

Parker, S.D., and Hendrix, M.S., 2022, Detrital zircon record of the Mesoproterozoic Belt basin and implications for horizontal and vertical tectonic models, *in* Foulger, G.R., Hamilton, L.C., Jurdy, D.M., Stein, C.A., Howard, K.A., and Stein, S., eds., In the footsteps of Warren B. Hamilton: New Ideas in Earth Science: Geological Society of America Special Paper 553, p. 159–176, doi: https://doi.org/10.1130/2021.2553(14).

Pratt, B.R., and Ponce, J.J., 2019, Sedimentation, earthquakes, and tsunamis in a shallow, muddy epeiric sea: Grinnell Formation (Belt Supergroup, ca. 1.45 Ga), western North America: Geological Society of America Bulletin, v. 131, p. 1411–1439, doi:10.1130/B35012.1.

Pratt, B.R., and Rule, R.G., 2021, A Mesoproterozoic carbonate platform (lower Belt Supergroup of western North America): Sediments, facies, tides, tsunamis and earthquakes in a tectonically active intracratonic basin: Earth-Science Reviews, v. 217, 103626, doi:10.1016/j.earscirev.2021.103626.

Price, R.A., 1964, The Precambrian Purcell System in the Rocky Mountains of southern Alberta and British Columbia: Bulletin of Canadian Petroleum Geology, v. 12, p. 399–426.

Rainbird, R.H., Rayner, N.M., Hadlari, T., Heaman, L.M., Ielpi, A., Turner, E.C., and MacNaughton, R.B., 2017, Zircon provenance data record the lateral extent of pancontinental, early Neoproterozoic rivers and erosional unroofing history of the Grenville orogen: Geological Society of America Bulletin, v. 129, p. 1408–1423, doi:10.1130/B31695.1.

Ross, C.P., 1959, Geology of Glacier National Park and the Flathead Region, northwestern Montana: U.S. Geological Survey, no. 296, doi:10.3133/pp296.

Ross, G.M., Parrish, R.R., and Winston, D., 1992, Provenance and U-Pb geochronology of the Mesoproterozoic Belt Supergroup (northwestern United States): Implications for age of deposition and pre-Panthalassa plate reconstructions: Earth and Planetary Science Letters, v. 113, p. 57–76, doi:10.1016/0012-821X(92)90211-D.

Ross, G.M., Villeneuve, M.E., and Theriault, R.J., 2001, Isotopic provenance of the lower Muskwa assemblage (Mesoproterozoic, Rocky Mountains, British Columbia): New clues to correlation and source areas: Precambrian Research, v. 111, p. 57–77, doi:10.1016/S0301-9268(01)00156-5.

Saylor, J.E., and Sundell, K.E., 2021, Tracking Proterozoic–Triassic sediment routing to western Laurentia via bivariate non-negative matrix factorization of detrital provenance data: Journal of the Geological Society, v. 178, p. 16, doi:10.1144/jgs2020-215.

Sears, J.W., 2007, Belt–Purcell Basin: Keystone of the Rocky Mountain fold-and-thrust belt, United States and Canada, *in* Special Paper 433: Whence the mountains? Inquiries into the evolution of orogenic systems: A volume in honor of Raymond A. Price, Geological Society of America, v. 433, p. 147–166, doi:10.1130/2007.2433(07).

Sears, J.W., and Price, R.A., 2000, New look at the Siberian connection: No SWEAT: Geology, v. 28, p. 423–426, doi:10.1130/0091-7613(2000)28<423:NLATSC>2.0.CO;2.

Sears, J.W., Chamberlain, K.R., and Buckley, S.N., 1998, Structural and U–Pb geochronological evidence for 1.47 Ga rifting in the Belt basin, western Montana: Canadian Journal of Earth Sciences, v. 35, p. 467–475.

Sears, J.W., Price, R.A., and Khudoley, A.K., 2004, Linking the Mesoproterozoic Belt–Purcell and Udzha basins across the west Laurentia–Siberia connection: Precambrian Research, v. 129, p. 291–308, doi:10.1016/j.precamres.2003.10.005.

Sharman, G.R., Sharman, J.P., and Sylvester, Z., 2018, detritalPy: A Python-based toolset for visualizing and analysing detrital geo-thermochronologic data: The Depositional Record, v. 4, p. 202–215, doi:http://dx.doi.org.ezproxy.lib.utexas.edu/10.1002/dep2.45.

Stewart, E.D., Link, P.K., Fanning, C.M., Frost, C.D., and McCurry, M., 2010, Paleogeographic implications of non–North American sediment in the Mesoproterozoic upper Belt Supergroup and Lemhi Group, Idaho and Montana, USA: Geology, v. 38, p. 927–930, doi:10.1130/G31194.1.

Sundell, K.E., and Saylor, J.E., 2017, Unmixing detrital geochronology age distributions: Geochemistry, Geophysics, Geosystems, v. 18, p. 2872–2886, doi:https://doi.org/10.1002/2016GC006774.

van der Velden, A.J., and Cook, F.A., 1994, Displacement of the Lewis thrust sheet in southwestern Canada: New evidence from seismic reflection data: Geology, v. 22, p. 819–822, doi:10.1130/0091-7613(1994)022<0819:DOTLTS>2.3.CO;2.

Winston, D., Horodyski, R.J., and Whipple, J.W., 1989, Middle Proterozoic Belt Supergroup, western Montana: American Geophysical Union, Field Trip Guidebook T334, 110 p., doi:10.1029/FT334.

Yonkee, W.A., and Weil, A.B., 2015, Tectonic evolution of the Sevier and Laramide belts within the North American Cordillera orogenic system: Earth-Science Reviews, v. 150, p. 531–593, doi:10.1016/j.earscirev.2015.08.001.

Young, G.M., Jefferson, C.W., Delaney, G.D., and Yeo, G.M., 1979, Middle and late Proterozoic evolution of the northern Canadian Cordillera and Shield: Geology, v. 7, p. 125–128, doi:10.1130/0091-7613(1979)7<125:MALPEO>2.0.CO;2.

Zartman, R.E., Peterman, Z.E., Obradovich, J.D., Gallego, M.D., and Bishop, D.T., 1982, Age of the Crossport C Sill near Eastport, Idaho: Idaho Bureau of Mines and Geology, Society of Economic Geologists Bulletin 24, p. 61–69.

Zhang, S., Li, Z.-X., Evans, D.A.D., Wu, H., Li, H., and Dong, J., 2012, Pre-Rodinia supercontinent Nuna shaping up: A global synthesis with new paleomagnetic results from North China: Earth and Planetary Science Letters, v. 353–354, p. 145–155, doi:10.1016/j.epsl.2012.07.034.

Zhao, G., Cawood, P.A., Wilde, S.A., and Sun, M., 2002, Review of global 2.1–1.8 Ga orogens: Implications for a pre-Rodinia supercontinent: Earth-Science Reviews, v. 59, p. 125–162, doi:10.1016/S0012-8252(02)00073-9.

Zhao, G., Sun, M., Wilde, S.A., and Li, S., 2004, A Paleo–Mesoproterozoic supercontinent: Assembly, growth and breakup: Earth-Science Reviews, v. 67, p. 91–123, doi:10.1016/j.earscirev.2004.02.003.

THE MESOPROTEROZOIC BELT–LEMHI CONNECTION, WESTERN MONTANA AND EAST-CENTRAL IDAHO

Jeffrey D. Lonn,[1] Russell F. Burmester,[2] and Reed S. Lewis[2]

[1]Montana Bureau of Mines and Geology, Butte, Montana
[2]Idaho Geological Survey, Moscow, Idaho

BACKGROUND AND PREVIOUS WORK

The Belt–Purcell Supergroup of western Montana, central and northern Idaho, southeastern British Columbia, and southwestern Alberta is one of the largest and best-studied Mesoproterozoic sedimentary basins in the world (fig. 1). Even so, its immense thickness of more than 15 km, its enormous extent covering >200,000 km^2, its repetitious and monotonous lithologies, its dismemberment by multiple tectonic events, and its obscuration by magmatism and metamorphism have confounded correlations across the basin. Correlations between typical Belt strata and the Mesoproterozoic Lemhi strata of east-central Idaho have been especially troublesome. The Lemhi strata, which include the Lemhi Group (Ruppel, 1975; Lonn, 2017) and overlying strata (Burmester and others, 2016b), are an equally thick (as much as 14 km) and even more monotonous succession of mainly feldspathic quartzite of Belt age (fig. 2). A plutonic–metamorphic complex separates the Lemhi strata from the typical Belt strata, and so the conventional interpretation was that they were deposited in separate basins that were later tectonically juxtaposed by major structures (Ruppel and others, 1993; Evans and Green, 2003; Ruppel and O'Neill, 2003; O'Neill and others, 2007). In contrast, Winston and others (1999) and Link and others (2007) proposed direct correlations between Belt and Lemhi strata (fig. 3), suggesting only one basin. In an attempt to resolve the controversy, in 2007 the Idaho Geological Survey (IGS) and the Montana Bureau of Mines and Geology (MBMG) began an ongoing mapping collaboration focused on revision of the Lemhi stratigraphic column to resolve structural problems. The collaboration used new 1:24,000-scale mapping, building on copious previous work (Ruppel and others, 1993; Tysdal, 1996a,b, 2000a, 2002, 2003; Tysdal and Moye, 1996; Tysdal and others, 2005; Evans and Green, 2003, and references therein), to suggest adding 4.5 km (2.8 mi) of strata to the top of the previously recognized Lemhi section (Burmester and others, 2016b) and removing 2.0 km (1.2 mi) of the lowest strata (figs. 2, 3; Lonn, 2017). The IGS–MBMG team demonstrated the continuity of the Lemhi rocks across the postulated terrane-bounding structures along the Idaho–Montana border into Montana (Burmester and others, 2016a,b; Lonn and others, 2016a,b, 2018; Lonn and others, 2020; fig. 1) and named this southern arm of the Belt Basin the Lemhi subbasin.

The Lemhi subbasin strata are much coarser-grained (sandier) than typical Belt strata. For example, the nearly 14 km of Lemhi strata in the eastern part of the Lemhi subbasin, north and east of Salmon and in southwestern Montana, are composed mainly of fine- to coarse-grained feldspathic quartzite (fig. 2) interpreted to have been deposited on vast alluvial aprons during storm-generated sheet floods (Winston, 2013, 2016). The finer-grained, thinner-bedded, siltite–argillite-rich marker units that separate similar sandy strata in the central Belt Basin are largely absent in the Lemhi subbasin (fig. 4).

Winston and others (1999) proposed correlations between the Belt and Lemhi strata (fig. 3) based on the Lemhi stratigraphy known at that time, but after major revisions were made to this stratigraphy (Burmester and others, 2016b), these correlations seemed less certain.

Burmester and others (2016b) proposed that the Swauger Formation, because it was the only medium- to coarse-grained quartzite formation in the Lemhi stack, could be used as a regional marker within the Lemhi strata. They also noted the lithologic similarities between the Swauger Formation of the Lemhi subbasin and the Bonner Formation of the Missoula Group, and tentatively correlated them. In addition, both the overlying Lawson Creek Formation of the Lemhi subbasin and McNamara Formation of the Missoula Group contain chert rip-ups and chert beds that are absent from the rest of the Belt, and so these, too, were correlated (fig. 4).

DETRITAL ZIRCON DATA

Meanwhile, detrital zircon (DZ) data became available that suggested the Missoula Group of the upper Belt Supergroup and the Lemhi strata shared the same provenance (Link and Fanning, 2003; Link and others, 2007, 2013, 2016; Gardner, 2008; Hendrix and others, 2016; Stewart and others, 2010, 2014; Lonn and others, 2018; Lonn and Mosolf, 2020). Importantly, Parker and Hendrix (2022) reviewed and analyzed all available Belt Supergroup DZ data, encompassing 50 samples from the Missoula Group and Lemhi subbasin that included 11 new samples. While they found that each Belt Group had somewhat diagnostic DZ signatures, geographic position in the basin was also important, especially at the formation level. They concluded that correlative stratigraphic units do not all have diagnostic DZ signatures, and that DZ results could not be reliably used to

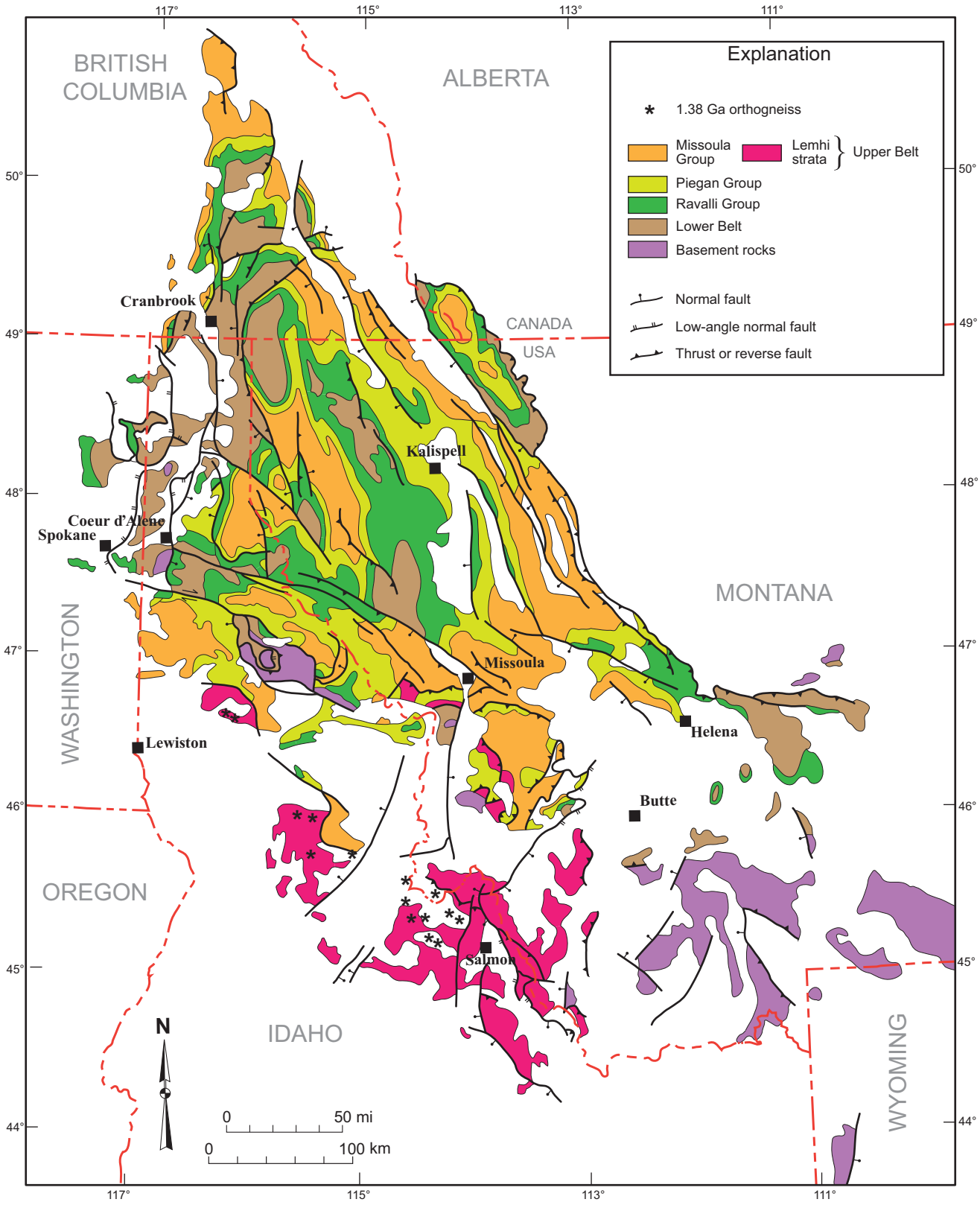

Figure 1. Map of the Belt Supergroup showing its division into three formal and two informal groups. Note that the Missoula Group and Lemhi subbasin strata in the southern part of map are postulated to be contemporaneous, and the contact shown between them is fuzzy across gradual facies changes. From Lonn and others (2020).

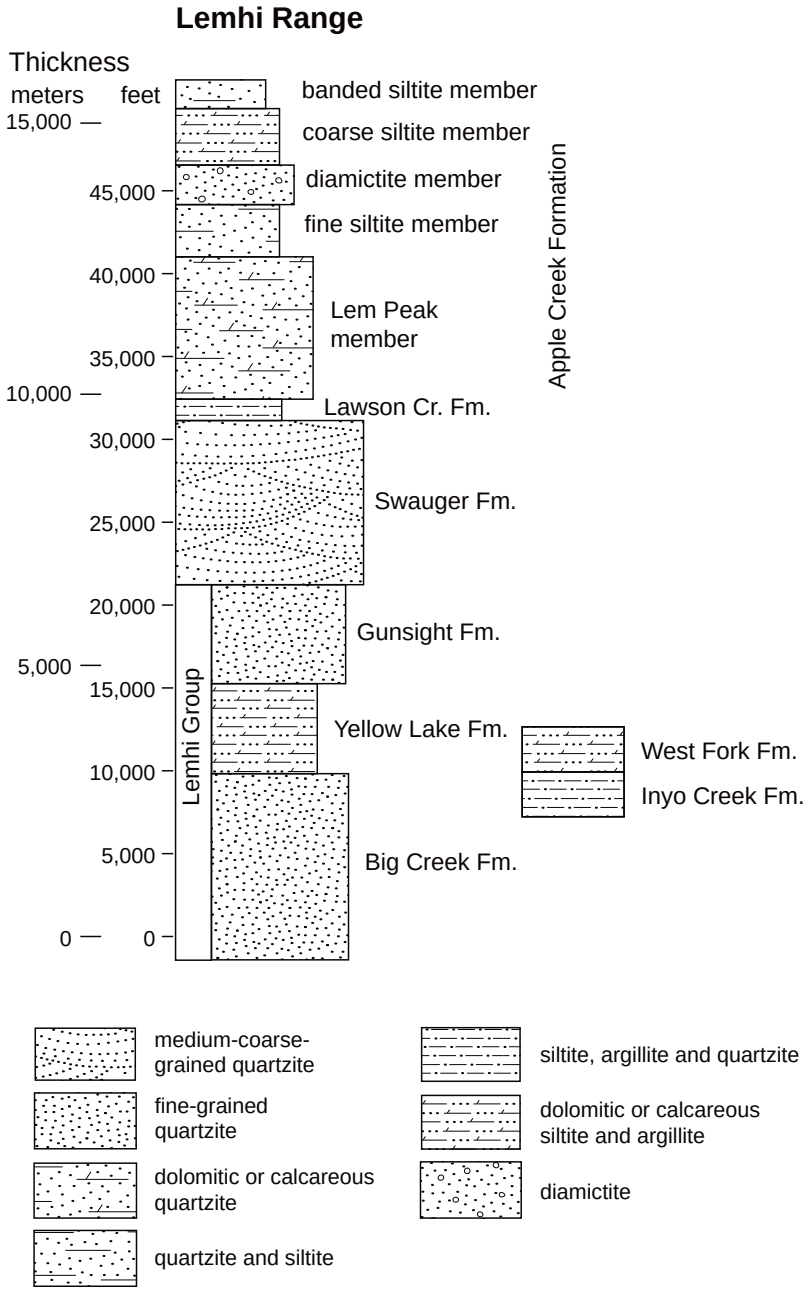

Figure 2. Composite Lemhi subbasin stratigraphic column showing that most of the 14-km-thick section in the Lemhi and Beaverhead ranges is composed of quartzite. Modified from Lonn (2017) to more clearly show that the bottom two of Ruppel's (1975) units are fault repetitions and do not add to the thickness of the Lemhi Group, which is unknown because no lower contact has been found.

distinguish formations. For example, conventional wisdom stated that pre-Missoula Group strata have a mix of Laurentian (1.7–1.8 Ga) and non-Laurentian, North American magmatic gap (NAMG) grains 1.51–1.62 Ga, while NAMG grains are absent in Missoula Group strata. But Parker and Hendrix (2022) found that some Missoula Group samples in the northwestern Belt Basin do contain NAMG grains. Another example of spatial variation is the presence of Archean grains in Lemhi–Missoula Group strata in the southeastern part of the basin, near the southeastern Belt Basin's margin with the Wyoming province/Dillon block, whereas Archean grains are scarce in the central and northern Belt Basin (Link and others, 2016). This probably reflects the proximity of the Archean Wyoming province source area to the southeastern samples.

Nonetheless, published DZ data show several commonalities between the Lemhi strata and Missoula Group that are not shared with lower strata of the Belt Supergroup (Piegan, Ravalli, and lower Belt groups). Both Lemhi and Missoula Group plots commonly display major peaks of 1.72–1.80 Ga, most lack significant NAMG grains (1.51–1.62 Ga), and most contain a number of grains younger than 1.44 Ga, with grains as young as 1.38 Ma, that constrain their maximum age of deposition to the upper Belt (Parker and Hendrix, 2022).

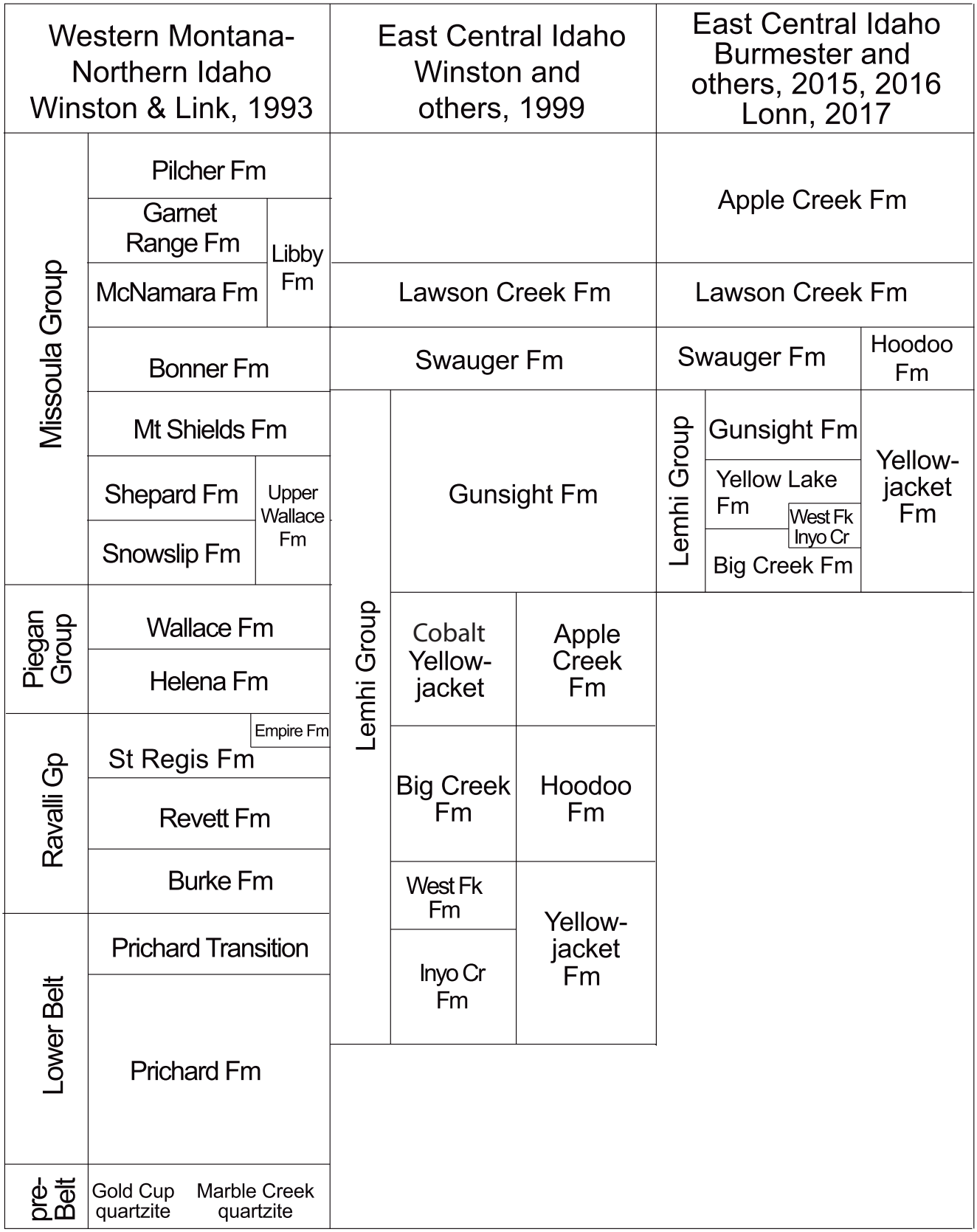

Figure 3. Postulated Belt Supergroup–Lemhi subbasin strata correlations. The column on the right is the interpretation presented herein. From Lonn and others (2020).

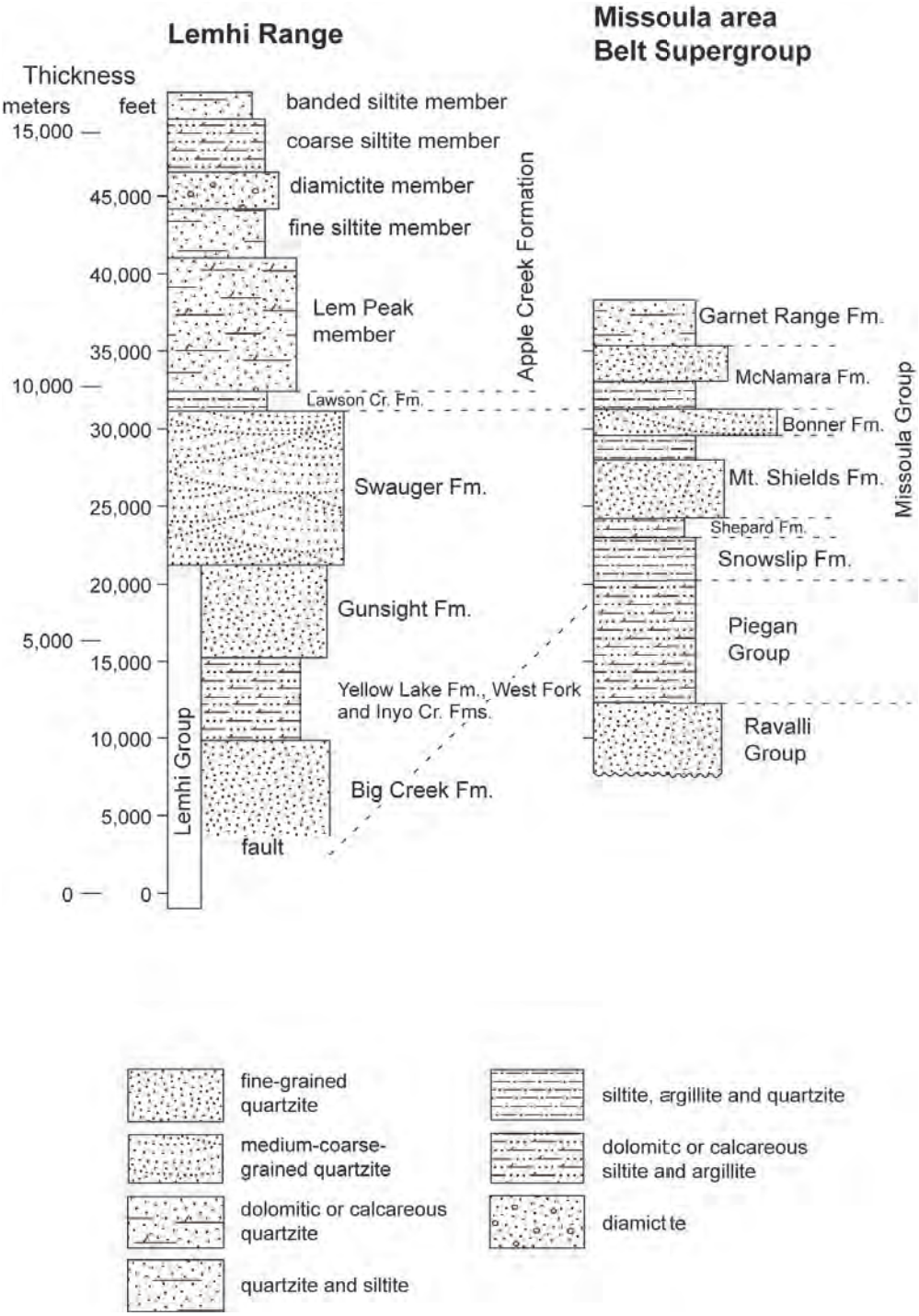

Figure 4. Belt Supergroup and Lemhi subbasin stratigraphic columns, with dashed connector lines showing postulated correlations. Note that the Missoula Group is much thinner and finer-grained than the correlative Lemhi strata. Modified from Lonn (2017).

NEW DETRITAL ZIRCON DATA

An important new DZ sample (JL-BC-01) came from the Big Creek Formation at the bottom of Ruppel's (1975) Lemhi Group type section in the Lemhi Range (fig. 5). Although the Big Creek Formation was postulated by both Winston and others (1999) and Lonn (2017) to be correlative with the Ravalli Group on the basis of lithology and stratigraphic position, the new data (fig. 6) suggest that it, too, is a Missoula Group equivalent. The sample contains the typical 1.7 Ga Missoula Group peak and only four NAMG grains, whereas both the Ravalli Group and the Piegan Group are characterized by a large number of NAMG grains. The sample also contains 12 grains in the 1.40 to 1.43 Ga range that make it too young to be in the Ravalli or Piegan Group and indicates that all Lemhi subbasin strata are Missoula Group equivalents.

NEW FIELDWORK INVESTIGATING THE BELT–LEMHI TRANSITION

Despite the above evidence for Missoula Group-Lemhi correlations, field observations giving direct support were few. This was partly because the Chief Joseph plutonic–

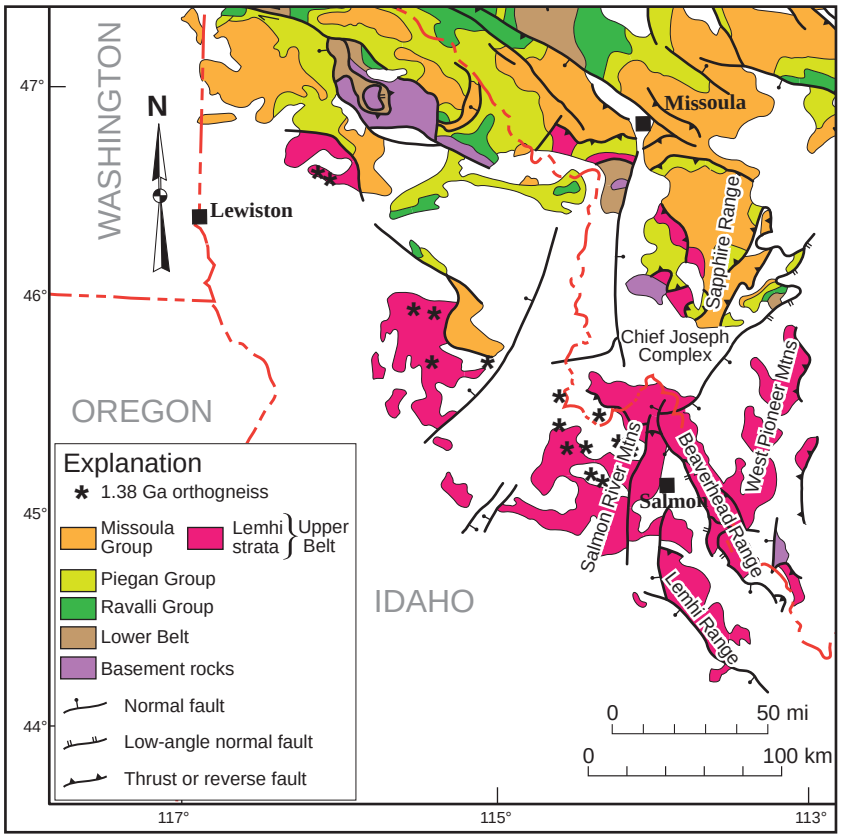

Figure 5. Map showing the southern part of figure 1 with locations discussed in text.

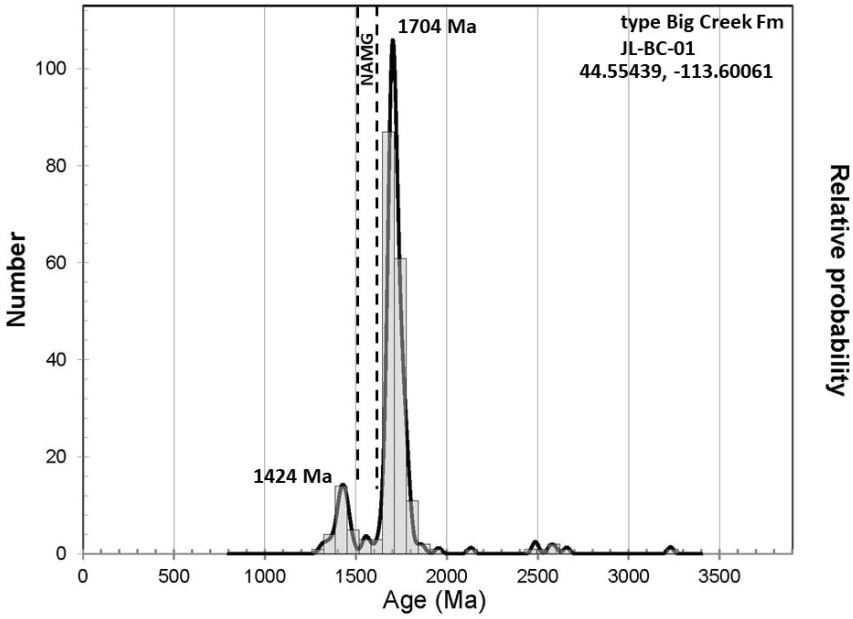

Figure 6. Detrital zircon plot for type Big Creek Formation showing a major peak at 1704 Ma and a minor peak at 1424 Ma, and few grains in the North American Magmatic Gap (NAMG). Sample prep and analysis by Jesse Mosolf using laser ablation inductively coupled plasma mass spectrometry at the University of California, Santa Barbara.

metamorphic complex largely separates the "true" Belt from the known Lemhi strata (fig. 5). However, previous maps of the Sapphire Range in western Montana (Wallace and others, 1986, 1989; Lewis, 1998; Lonn and others, 2003, 2010) had noted that Missoula Group units there were unusually sandy and thick. These sandy lithologies confounded geologists and were explained in various ways: by thrust repetition of sandy formations, by southward facies changes to coarser lithologies, by detachment faults that omitted section, or by combinations of the above. By far the simplest explanation seemed to be that the type Missoula Group section graded southward into the very sandy Lemhi section, so Lonn, living nearby, revisited selected areas where thick sandy sections had been explained by fault repetition or omission (Lonn, 2014; Lonn and others, 2016a; Lonn and Mosolf, 2020; Lonn, unpublished mapping 2014–2022). Important observations are:

In the south-central and southern Sapphire Range and the mountains west of Missoula, the top of the Piegan Group grades quickly up to a thick quartzite section that does not contain recognizable Snowslip or Shepard Formations, or member 3 of the Mount Shields Formation with their thin-bedded siltite–argillite lithologies.

In the central Sapphire Range, a 6000-m-thick sandy interval that had been called a Mt Shields–Bonner stratigraphic section (Wallace and others, 1986, 1989; Lewis, 1998; Lonn and others, 2003) is nearly identical to the Swauger–Lawson Creek–Apple Creek section in the Beaverhead and Lemhi Ranges, including the presence of chert diagnostic of Lawson Creek Formation in the middle part of these sections.

Northward, in the northern Sapphire Range and east-adjacent John Long Mountains, Snowslip, Shepard, and Mt Shields member 3 siltite–argillite lithologies make their southernmost appearances as thin intervals within the quartzite.

In the central Sapphire Range, McNamara Formation previously mapped (Wallace and others, 1986, 1989; Lewis, 1998; Lonn and others, 2003) on the basis of abundant chert rip-ups is dominated by medium-grained quartzite in contrast to the siltite–argillite-rich strata of the type McNamara Formation near Missoula.

Northwest of Missoula, the upper part of the Snowslip Formation contains a thick interval of fine-grained quartzite (Lonn, 2011) not present in other Snowslip Formation localities to the north and east.

Cretaceous and Tertiary tectonism disrupted the lateral continuity of the stratigraphy, complicating Missoula Group–Lemhi correlations. Without enough data for palinspastic reconstructions, these faults have been ignored in this paper, but facies changes are similar on all fault blocks.

INTERPRETATIONS

Using the new field data, a fence diagram can be constructed, extending south to north through the central Lemhi Range, the northern Beaverhead Range, and the length of the Sapphire Range (fig. 7). It hypothesizes that the thick sand units of the Lemhi subbasin grade into and interfinger with finer-grained, thinner-bedded units to the north as the Missoula Group type section is approached. The bottom of this succession is marked by the Piegan Group in the Sapphire Range, although it is not exposed farther south in the Beaverhead and Lemhi Ranges.

Winston (1986) drew a similar fence diagram from the West Pioneer Mountains in southwestern Montana into northwestern Montana and the Idaho panhandle (fig. 8). It shows essentially the same pattern: coarser, sandy Lemhi and Missoula Group units grade into and interfinger with increasingly finer-grained, thinner-bedded lithologies northwestward.

Figure 9 is a fence diagram drawn from the Lemhi Range west into the Salmon River Mountains that also shows sandy tongues interfingering with and grading into finer-grained, thinner-bedded units westward, suggesting that the axis of these northward-prograding sand tongues was in the eastern Lemhi subbasin.

The distribution of coarser-grained sand Lemhi units outline a giant sand tongue extending north–northwest into the main Belt Basin during Missoula Group time and westward into what was probably the center of the Lemhi subbasin (fig. 10). Winston (1986) envisioned enormous alluvial aprons carrying gravel and sand, alternately retreating and advancing northward into the Belt Sea. Where these megafans entered the Belt Sea, they were bordered by intermittently exposed mudflats of silt and desiccation-cracked mud that passed seaward to subaqueously deposited uncracked silt and mud and carbonate-bearing mud (fig. 11). Citing a lack of channels and the lateral continuity of the flat-laminated sand beds, Winston (2013) also proposed that the sandy Belt sediments were deposited in north-flowing sheet floods generated by storms over the barren landscape. Sears (2007b) used the Lemhi–Missoula Group's lack of significant NAMG detrital zircon grains, which are common in the lower Belt strata and thought to have a western source, as further evidence for a southeastern provenance for the Missoula Group. Wallace (1998) had also similarly proposed that the Missoula Group sediments were deposited in a northward-prograding river delta system, but one that entered the open ocean rather than an inland sea or lake.

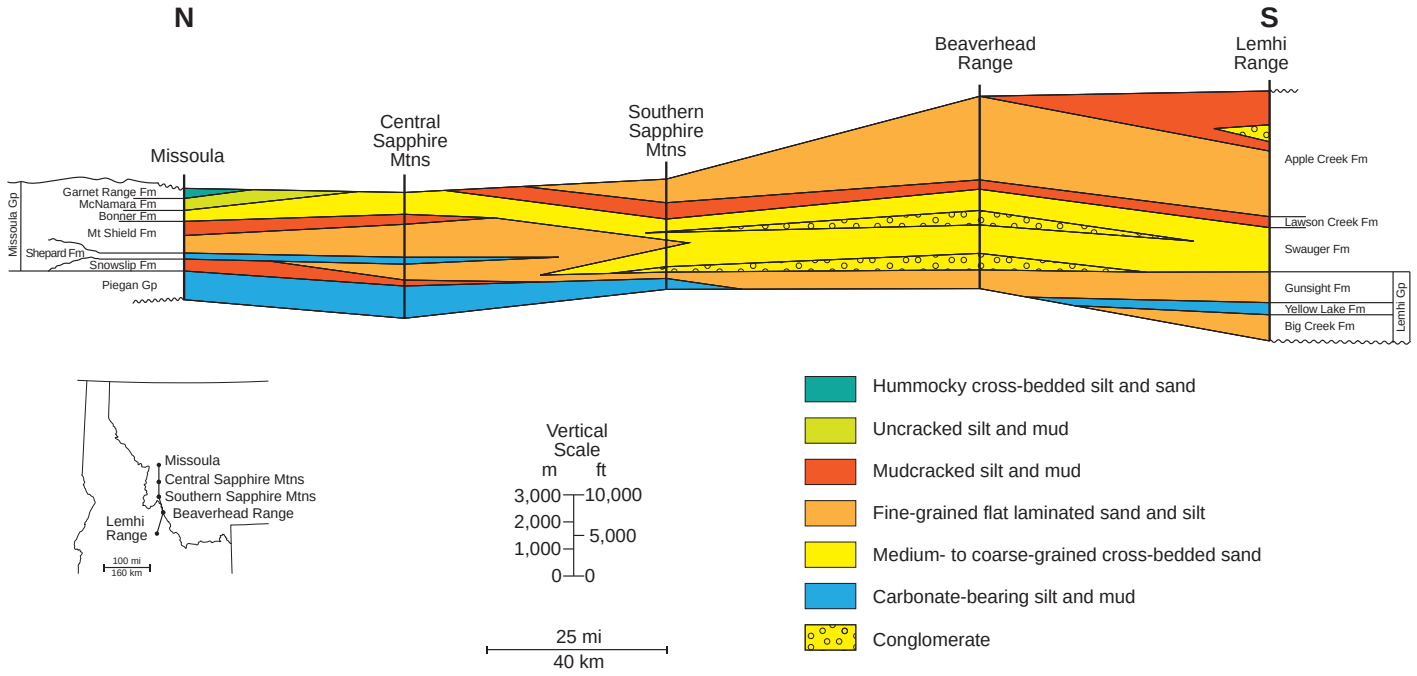

Figure 7. Cartoon fence diagram extending north–south from Missoula to the Lemhi Range shows postulated relationships between the type Missoula Group section and the Lemhi subbasin section. Sandy units are shown by brown and yellow colors. Wedge of conglomerate shown in the Apple Creek Formation is diamictite deposited in muddy debris flows, and differs from the sandy fluvial conglomerate in the rest of the sections. Modified from Lonn and others (2020).

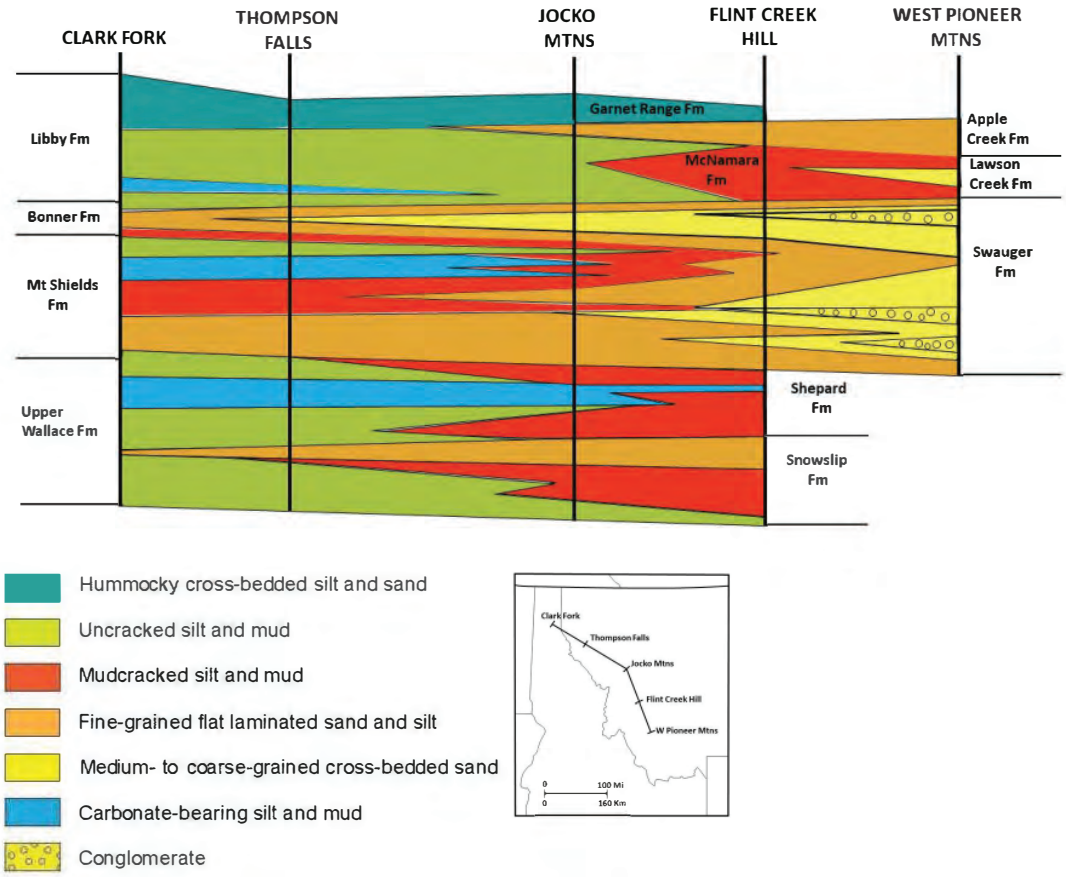

Figure 8. Cartoon fence diagram extending from the West Pioneer Mountains in southwestern Montana to the Idaho panhandle, showing the northwestward grain size and thickness decreases in sandy strata, similar to the figure 11 fence diagram. Sandy units are shown by brown and yellow colors. No vertical scale. Modified from Winston (1986).

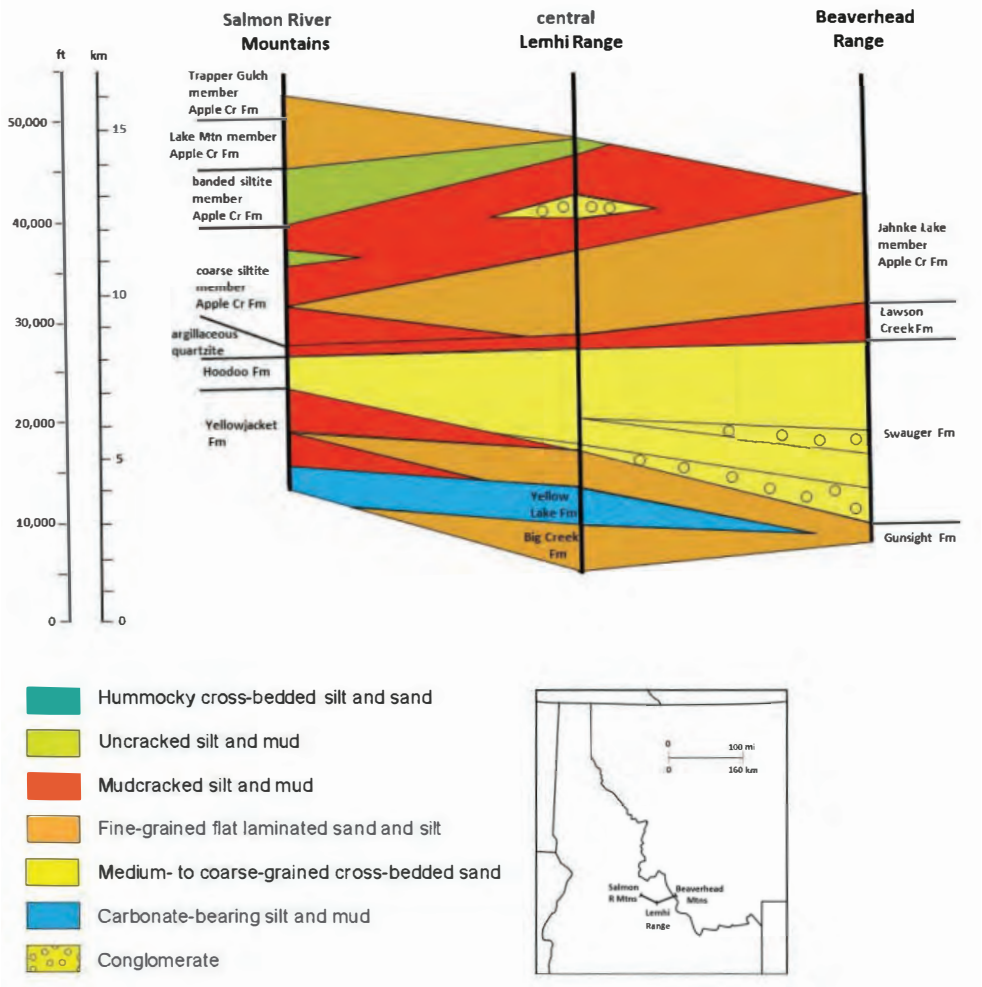

Figure 9. Cartoon fence diagram showing the differences in Lemhi strata from the Beaverhead Range to the Salmon River Mountains. Sandy units are shown by brown and yellow colors. Note that sand tongues get thinner and finer-grained westward, while the thickness of the Apple Creek Formation increases, due to either syndepositional faulting and subsidence or simply to differences in post-depositional erosion levels. Wedge of conglomerate shown in the Apple Creek Formation is diamictite deposited in muddy debris flows, and differs from the sandy fluvial conglomerate in the rest of the sections. Modified from Burmester and others (this volume).

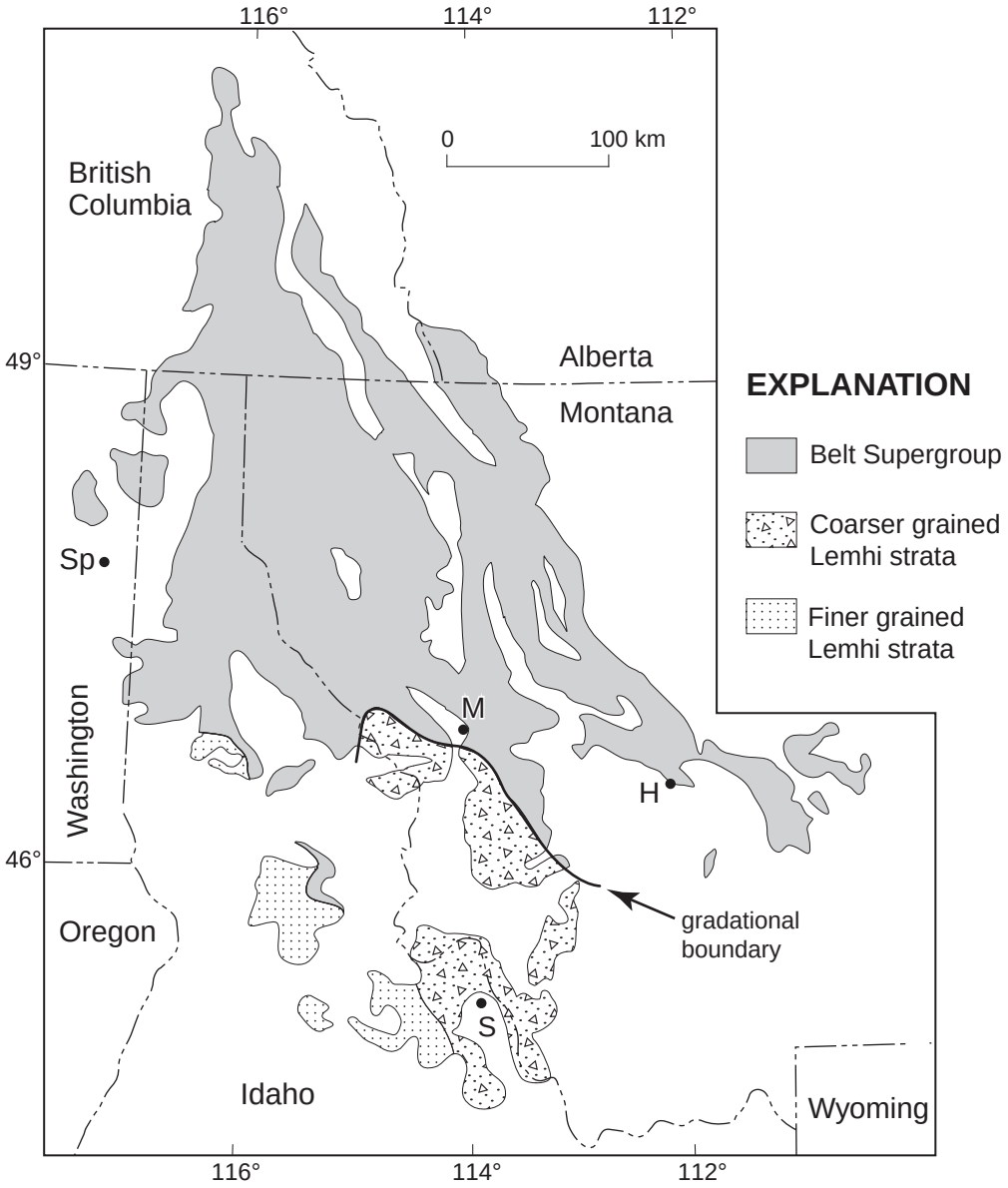

Figure 10. The Lemhi–Missoula Group alluvial apron varied in position and extent over time, but appears to have originated in modern-day east-central Idaho and southwestern-most Montana. It extended NNW into the main Belt Basin, interfingering with and grading into finer-grained sediments of the Missoula Group. Similarly, westward the alluvial apron also appears to interfinger with and grade into the finer-grained Lemhi sediments of the Salmon River Mountains (see fig. 9), which are the Yellowjacket, Hoodoo, and western Apple Creek Formations. H, Helena; M, Missoula; S, Salmon. Modified from Lonn and others (2016b).

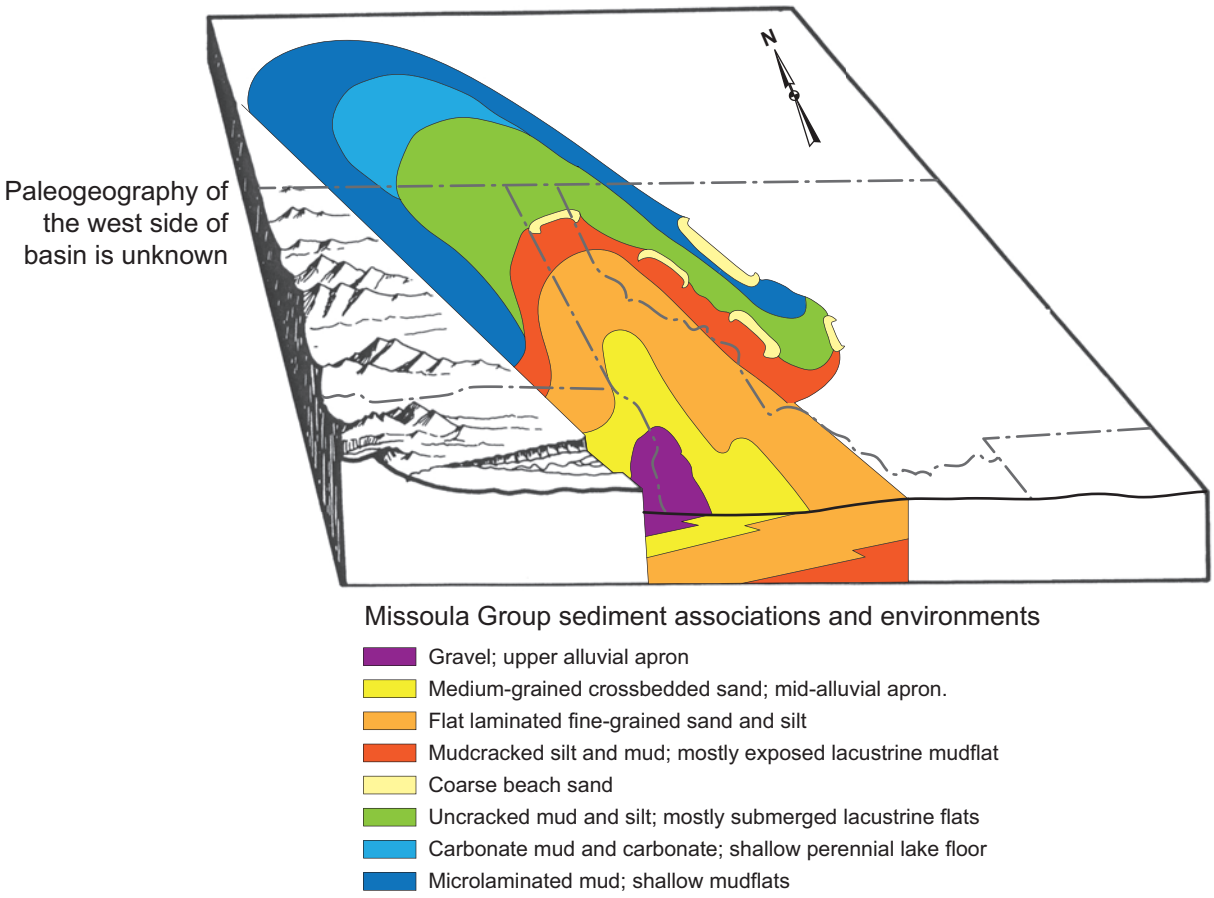

Figure 11. Block diagram shows postulated facies associations during deposition of the Missoula Group and Lemhi strata. Sand and gravel facies alternately prograded and retreated, bordered by exposed mudflats of silt and desiccation-cracked mud that passes seaward to uncracked silt and mud and carbonate-bearing mud. Not shown is probable gravel input from the southeast originating in the Wyoming province that bordered the southeast side of the Belt Sea and that mixed with sediment shown originating to the south. From Lonn and others (2020), modified from Winston (1986).

SPECIFIC FORMATION CORRELATIONS

Specific formation correlations between the Lemhi strata and the Missoula Group remain uncertain. Correlation of the bottom of the McNamara Formation with the bottom of the Lawson Creek Formation appears to have the most support (fig. 4). More speculative is a correlation between the Garnet Range/upper Libby Formation with the banded siltite member of the Apple Creek Formation; both are characterized by hummocky crossbeds created in a perennial water body where the bottom was within reach of storm waves. Don Winston (oral commun., 2011) had proposed correlation of the Yellow Lake Formation of the Lemhi subbasin with the Shepard Formation of the Missoula Group based on their relative stratigraphic positions and the presence of carbonate in both. However, their sedimentary features differ, and neither formation has been found within the thick quartzite succession of the southern Sapphire Mountains that separates their locations. Another problem with formation correlations is that the Lemhi subbasin lacks Piegan Group strata that mark the bottom of the Missoula Group father north, an observation supported by DZ data indicating that all Lemhi strata are younger than the Piegan Group.

GROWTH FAULTS

If Lemhi subbasin strata are equivalent to the Missoula Group, subsidence in the Lemhi subbasin must have been much faster in order to deposit as much as 14 km (8.7 mi) of sediment there versus the 3 km (1.9 mi) thickness of the type Missoula Group. Using thickness changes in the Belt Supergroup, Winston (1986) and Sears (2007a) postulated major growth fault locations, but show none that are helpful in explaining the Lemhi subbasin strata's thickness. Perhaps one Lemhi subbasin growth fault was located along the north–south-trending eastern margin of the Lemhi subbasin (fig. 1), labeled the 4th of July fault in Lonn and others (2020). The conglomeratic Black Lion Formation along this margin was interpreted as a Belt-aged, coarse-grained, basin-margin facies similar to the LaHood Formation (McMannis, 1963), but younger, of Lemhi subbasin age (McDonald and others, 2012; McDonald and Lonn, 2013). The Black Lion Formation contains mostly Archean grains (Link and others, 2016), many of them angular lithic fragments, that presumably were derived locally from the southeast-adjacent Archean Wyoming province. On the west side of the postulated 4th of July growth fault is a kilometers-thick section of Lemhi strata. Lonn and Elliott

(2017) described gritty intervals in the Swauger Formation there that are lithologically identical to gritty intervals in the Black Lion Formation, and suggested that debris flows of the Black Lion Formation fed parts of the Swauger Formation. The Swauger Formation in this area and along the northeast side of the Beaverhead Mountains also contains rounded pebbles and small cobbles of feldspar-poor quartzite with grains of Archean age (Link and others, 2016).

Rapid thickness changes in the sand units in the Sapphire Mountains also probably mark growth faults. For example, in the area south of Skalkaho Pass, medium- to coarse-grained quartzite between the underlying Piegan Group and the overlying McNamara–Lawson Creek Formation varies from 1 km to 4 km in thickness over a 10 km lateral distance with no intervening faults recognized (Lonn, unpublished mapping, 2018). This thickness variation must be the result of syndepositional faulting, but the orientation of a postulated growth fault could not be determined.

Muddy diamictite at various stratigraphic levels in the Apple Creek Formation (figs. 7, 9) was probably deposited in debris flows on the downdropped sides of growth faults. Note that the Apple Creek Formation thickens significantly from the Lemhi Range to the Salmon River Mountains (fig. 9), although grain size and bed thicknesses decrease. The thickness change could be the result of syndepositional faulting, different levels of post-depositional erosion, or truncation of the Lemhi Range section by the Poison Creek fault.

CONCLUSIONS

New and old fieldwork combined with detrital zircon data support the correlation of the entire Lemhi subbasin section with the Missoula Group of the upper Belt Supergroup. The Lemhi subbasin strata are much sandier and thicker than the equivalent Missoula Group strata and represent the upstream ends of immense alluvial aprons that originated to the south and southeast. These sand tongues alternately advanced and retreated into the Belt Sea during Missoula Group time. Similarly, the Lemhi strata also grade laterally westward into the finer-grained Mesoproterozoic rocks of the Salmon River Mountains. Although the Bonner Formation is tentatively correlated with the upper part of the Swauger Formation and the McNamara Formation is tentatively correlated with the Lawson Creek Formation, other specific formation correlations remain uncertain. During Missoula Group time, subsidence in the Lemhi subbasin must have been much faster than in the main Belt Basin in order to deposit the much thicker Lemhi section. No strata older than the Missoula Group are known in the Lemhi subbasin, and it is uncertain whether the Belt Basin extended this far south in pre-Missoula Group time. It is also uncertain whether the central Lemhi subbasin of the Salmon River Mountains was connected to the main Belt Basin, but the two are time correlative.

REFERENCES

Burmester, R.G., Lewis, R.S., Othberg, K.L., Stanford, L.R., Lonn, J.D., and McFaddan, M.D., 2016a, Geologic map of the western part of the Salmon 30 x 60 quadrangle, Idaho and Montana: Idaho Geological Survey Geologic Map 52, scale 1:75,000.

Burmester, R.F., Lonn, J.D., Lewis, R.S., and McFaddan, M.D., 2016b, Stratigraphy of the Lemhi subbasin of the Belt Supergroup, *in* MacLean, J.S., and Sears, J.W., eds., Belt Basin: Window to Mesoproterozoic Earth: Geological Society of America Special Paper 522, Chapter 5, p. 121–138, doi: 10, 1130/2016, 2522(05).

Burmester, R.F., Lewis, R.F., and Lonn, J.D., this volume (2023), The Lemhi subbasin of the Belt Supergroup: Northwest Geology, v. 52.

Evans, K.V., and Green, G.G., compilers, 2003, Geologic map of the Salmon National Forest and vicinity, east-central Idaho: U.S. Geological Survey Geologic Investigations Series, Map I-2765, 2 sheets, scale 1:100,000.

Gardner, D.W., 2008, Sedimentology, stratigraphy, and provenance of the Upper Purcell Supergroup, southeastern British Columbia, Canada: Implications for syn-depositional tectonism, basin models, and paleogeographic reconstructions: M.S. thesis, Victoria, British Columbia, University of Victoria, 85 p.

Hendrix, M.S., Winston, D., Crowley, J.L., and Schmitz, M.D., 2016, Detrital zircon results from Proterozoic and Paleozoic rocks of western Montana and implications for geologic evolution of the western North American margin: Geological Society of America Abstracts with Programs, v. 48, no. 6, doi: 10.1130/abs/2016RM-276264.

Lewis, R.S., 1998, Geologic map of the Butte 1° x 2° quadrangle: Montana Bureau of Mines and Geology Open-File Report 363, scale 1:250,000.

Link, P.K., and Fanning, C.M., 2003, Detrital zircon ages from the Yellowjacket, Apple Creek and Gunsight Formations, Blackbird mining district, Salmon River Mountains, central Idaho: Northwest Geology, v. 32, p. 206–207.

Link, P.K., Winston, D., and Boyack, D., 2003, Stratigraphy of the Mesoproterozoic Belt Supergroup, Salmon River Mountains, Lemhi County, Idaho: Northwest Geology, v. 32, p. 107–133.

Link, P.K., Fanning, C.M., Lund, K.I., and Aleinikoff, J.N., 2007, Detrital zircons, correlation and provenance of Mesoproterozoic Belt Supergroup and correlative strata of east-central Idaho and southwest Montana, *in* Link, P.K., and Lewis, R.S., eds., Proterozoic geology of western North America and Siberia: Society for Sedimentary Geology Special Publication 86, p. 101–128, doi:10.2110/pec.07.86.0101.

Link, P.K., Steele, T., Stewart, E.S., Sherwin, J., Hess, L.R., and McDonald, C., 2013, Detrital zircons in the Mesoproterozoic upper Belt Supergroup in the Beaverhead and Lemhi Ranges, MT and ID: Northwest Geology, v. 42, p. 39–43.

Link, P.K., Stewart, E.D., Steel, T., Sherwin, J., Hess, L.T., and McDonald, C., 2016, Detrital zircons in the Mesoprotero-

zoic upper Belt Supergroup in the Pioneer, Beaverhead, and Lemhi Ranges, Montana and Idaho: The Big White arc, *in* MacLean, J.S., and Sears, J.W., eds., Belt Basin: Window to Mesoproterozoic Earth: Geological Society of America Special Paper 522, Chapter 5, p. 121–138, doi: 10.1130/2016.2522(07).

Lonn, J.D., 2011, Belt rocks and structures of the Lewis and Clark Line in Alberton Gorge, western Montana: A river log: Northwest Geology, v. 40, p. 105–124.

Lonn, J.D., 2014, The northern extent of the Mesoproterozoic Lemhi Group, Idaho and Montana, and stratigraphic and structural relations with Belt Supergroup strata: Geological Society of America Abstracts with Programs, v. 46, no. 5, p. 72.

Lonn, J.D., 2017, The Lemhi Group type sections revisited and revised, east-central Idaho: Northwest Geology, v. 46, p. 15–28.

Lonn, J.D., and Elliott, C.G., 2017, Geologic map of the Stine Mountain 7.5' quadrangle, southwestern Montana: Montana Bureau of Mines and Geology Geologic Map 69, 1 sheet, scale 1:24,000.

Lonn, J., and Mosolf, J., 2020, Field guide to the geology of the Sleeping Child metamorphic complex, southern Sapphire Mountains, western Montana: Northwest Geology, v. 49, p. 35–56.

Lonn, J.D., McDonald, C., Lewis, R.S., Kalakay, T.J., O'Neill, J.M., Berg, R.B., and Hargrave, P., 2003, Preliminary geologic map of the Philipsburg 30' x 60' quadrangle, western Montana: Montana Bureau of Mines and Geology Open-File Report 483, 29 p., scale 1:100,000.

Lonn, J.D., McDonald, C., Sears, J.W., and Smith, L.N., 2010, Geologic map of the Missoula East 30' x 60' quadrangle, western Montana: Montana Bureau of Mines and Geology Open-File Report 593, 2 sheets, scale 1:100,000.

Lonn, J.D., Burmester, R.F., Lewis, R.S., and McFaddan, M.D., 2016a, Giant folds and complex faults in Mesoproterozoic Lemhi strata of the Belt Supergroup, northern Beaverhead Mountains, Montana and Idaho, *in* MacLean, J.S., and Sears, J.W., eds., Belt Basin: Window to Mesoproterozoic Earth: Geological Society of America Special Paper 522, Chapter 6, p. 139–162, doi: 10.1130/2016.2522(06).

Lonn, J.D., Lewis, R.S., Burmester, R.F., and McFaddan, M.D., 2016b, Mesoproterozoic Lemhi strata represent immense alluvial aprons that prograded northwest into the Belt Sea, Idaho and Montana: Geological Society of America Rocky Mountain Section Meeting, Moscow, Idaho, available at https://gsa.confex.com/gsa/2016RM/webprogram/Paper276082.html

Lonn, J.D., Elliott, C.G., Lewis R.S., Burmester R.F., McFaddan M.D., Stanford, L.R., and Janecke, S.U., 2018, Geologic map of the Montana part of the Salmon 30' x 60' quadrangle, southwestern Montana: Montana Bureau of Mines and Geology Geologic Map 75, 28 p., 1 sheet, scale 1:100,000.

Lonn, J.D., Burmester, R.F., Lewis, R.S., and McFaddan, M.D., 2020, The Mesoproterozoic Belt Supergroup, *in* Metesh, J.J., and Vuke, S.M., eds., Geology of Montana—Geologic History: Montana Bureau of Mines and Geology Special Publication 122, v. 1, 38 p., available at: https://mbmg.mtech.edu/pdf/geologyvolume/Lonn_BeltFinal.pdf

McDonald, C., and Lonn, J.D., 2013, Revisions of Mesoproterozoic and Cambrian stratigraphy in the Pioneer and Highland Mountains, southwestern Montana, and resulting implications for the Paleogeography of the Belt Basin: Northwest Geology, v. 42, p. 93–102.

McDonald, C., Elliott, C.G., Vuke, S.M., Lonn, J.D., and Berg, R.B., 2012, Geologic map of the Butte South 30′ x 60′ quadrangle, southwestern Montana: Montana Bureau of Mines and Geology Open-File Report 622, scale 1:100,000.

McMannis, W.J., 1963, LaHood Formation—A coarse facies of the Belt Series in southwestern Montana: Geological Society of America Bulletin, v. 74, p. 407–436.

O'Neill, J.M., Ruppel, E.T., and Lopez, D.A., 2007, Great Divide megashear, Montana, Idaho, and Washington—An intraplate crustal-scale shear zone recurrently active since the Mesoproterozoic: U.S. Geological Survey Open-File Report 2007-1280-A, 10 p.

Parker, S.D., and Hendrix, M.S., 2022, Detrital zircon record of the Mesoproterozoic Belt basin and implications for horizontal and vertical tectonic models, *in* Foulger, G.R., Hamilton, L.C., Jurdy, D.M., Stein, C.A., Howard, K.A., and Stein, S., eds., In the footsteps of Warren B. Hamilton: New ideas in earth science: Geological Society of America Special Paper 553, p. 159–176, doi: 10.1130/2021.2553(14).

Ruppel, E.T., 1975, Precambrian Y sedimentary rocks in east-central Idaho: U.S. Geological Survey Bulletin 889-A, 23 p.

Ruppel, E.T., and O'Neill, J.M., 2003, Early Tertiary detachment faulting in southwest Montana and east-central Idaho: Northwest Geology, v. 32, p. 222–223.

Ruppel, E.T., O'Neill, J.M., and Lopez, D.A., 1993, Geologic map of the Dillon 1° x 2° quadrangle, Idaho and Montana: U.S. Geological Survey Miscellaneous Investigations Series Map I-1803-H, scale 1:250,000.

Sears, J.W., 2007a, Belt-Purcell Basin: Keystone of the Rocky Mountain fold-and-thrust belt, United States and Canada, *in* Sears, J.W., Harms, T.A., and Evenchick, C.A., eds., Whence the mountains? Inquiries into the evolution of orogenic systems: A volume in honor of Raymond A. Price: Geological Society of America Special Paper 433, p. 147–166, doi: 10.1130/2007.2433(07).

Sears, J.W., 2007b, Destabilization of a Proterozoic epi-continental pediment by rifting: A model for the Belt-Purcell Basin, North America, *in* Link, P.K., and Lewis, R.S., eds., Proterozoic geology of western North America and Siberia: SEPM (Society for Sedimentary Geology) Special Publication no. 86, p. 55–64.

Stewart, E.D., Link, P.K., Fanning, C.M., Frost, C.D., and McCurry, M., 2010, Paleogeographic implications of non-North American sediment in the Mesoproterozoic upper Belt Supergroup and Lemhi Group, Idaho and Montana, USA: Geology, v. 38, p. 927–930.

Stewart, E.D., Steele, E.D., Stewart, D.E., and Link, P.K., 2014,

Geologic map of the Gibbonsville, Shewag Lake, and Allan Mountain quadrangles, and parts of the Lost Trail Pass and Big Hole Pass quadrangles, Lemhi County, Idaho, and Ravalli and Beaverhead Counties, Montana: Idaho Geological Survey Technical Report 14-2, scale 1:40,000.

Tysdal, R.G., 1996a, Geologic map of the Lem Peak quadrangle, Lemhi County, Idaho: U.S. Geological Survey Geologic Quadrangle Map GQ-1777, scale 1:24,000.

Tysdal, R.G., 1996b, Geologic map of parts of the Hayden Creek and Mogg Mountain quadrangles, Lemhi County, Idaho: U.S. Geological Survey Miscellaneous Investigations Series I-2563, scale 1:24,000.

Tysdal, R.G., 2000a, Stratigraphy and depositional environments of middle Proterozoic rocks, northern part of the Lemhi Range, Lemhi County, Idaho: U.S. Geological Survey Professional Paper 1600, 40 p.

Tysdal, R.G., 2000b, Revision of Middle Proterozoic Yellowjacket Formation, central Idaho: U.S. Geological Survey Professional Paper 1601-A, 13 p.

Tysdal, R.G., 2002, Structural geology of western part of Lemhi Range, east-central Idaho: U.S. Geological Survey Professional Paper 1659, 33 p.

Tysdal, R.G., 2003, Correlation, sedimentology, and structural setting, upper strata of Mesoproterozoic Apple Creek Formation and lower strata of Gunsight Formation, Lemhi Range to Salmon River Mountains, east-central Idaho: U.S. Geological Survey Professional Paper 1668-A, p. 1–22.

Tysdal, R.G., and Moye, F., 1996, Geologic map of the Allison Creek quadrangle, Lemhi County, Idaho: U.S. Geological Survey Geologic Quadrangle Map GQ-1778, scale 1:24,000.

Tysdal, R.G., Lindsey, D.A., Lund, K.I., and Winkler, G.R., 2005, Alluvial facies, paleocurrents, and source of the Mesoproterozoic Gunsight Formation, east-central Idaho and southwestern Montana: U.S. Geological Survey Professional Paper 1700-B, p. 21–39.

Wallace, C.A., 1998, Paleotransport directions and basin configurations, middle part of the Missoula Group (Belt Supergroup, middle Proterozoic), western Montana, *in* Berg, R., ed., Proceedings of Belt Symposium III: Montana Bureau of Mines and Geology Special Paper 112, p. 88–103.

Wallace, C.A., Schmidt, R.G., Lidke, D.J., Waters, M.R., Elliott, J.E., French, A.B., Whipple, J.W., Zarske, S.E., Blaskowski, M.J., Heise, B.A., Yeoman, R.A., O'Neill, J.M., Lopez, D.A., Robinson, G.D., and Klepper, M.R., 1986, Preliminary geologic map of the Butte 1^{o} x 2^{o} quadrangle, Montana: U.S. Geological Survey Open File Report 86-292, scale 1:250,000.

Wallace, C.A., Lidke, D.J., Waters, M.R., and Obradovich, J.D., 1989, Rocks and structure of the southern Sapphire Mountains, Granite and Ravalli Counties, western Montana: U.S. Geological Survey Bulletin 1824, 29 p., map scale 1:50,000.

Winston, D., 1986, Sedimentation and tectonics of the Middle Proterozoic Belt Basin and their influence on Phanerozoic compression and extension in western Montana and northern Idaho, *in* Peterson, J.A., ed., Sedimentation and Tectonics: American Association of Petroleum Geologists Memoir 41, p. 87–118.

Winston, D., 2013, Analysis of sheetflood fluvial systems in the middle Proterozoic Belt Supergroup, northern Idaho and northwestern Montana: Northwest Geology, v. 42, p. 71–74.

Winston, D., 2016, Sheetflood sedimentology of the Mesoproterozoic Revett Formation, Belt Supergroup, northwestern Montana, USA, *in* MacLean, J.S., and Sears, J.W., eds., Belt Basin: Window to Mesoproterozoic Earth: Geological Society of America Special Paper 522, p. 341–363, doi: 10.1130/2016.2522(01).

Winston, D., Link, P.K., and Hathaway, N., 1999, The Yellowjacket is not the Prichard and other heresies: Belt Supergroup Correlations, Structure and Paleogeography, east-central Idaho, *in* Hughes, S.S., and Thackray, G.D., eds., Guidebook to the geology of eastern Idaho: Pocatello, Idaho Museum of Natural History, p. 3–20.

MULTIPLE PERIODS OF METAMORPHISM IN THE SALMON RIVER MOUNTAINS REVEALED BY GARNET LU-HF AGES

John P. Murphy,[1] Reed S. Lewis,[2] Jeffrey D. Vervoort,[1] and Johannes Hammerli[1]

[1]*Washington State University, Pullman, Washington*
[2]*Idaho Geological Survey, Moscow, Idaho*

INTRODUCTION

Mesoproterozoic Belt Supergroup strata in the Salmon River Mountains of east-central Idaho have a complex metamorphic history. Zirakparvar and others (2007) reported lutetium-hafnium (Lu-Hf) ages of 151 ± 32 Ma for garnets from the Blacktail pit (BTg-1) immediately north of the Blackbird mine, and 113 ± 8 Ma (SCCg-1) for garnets from the Salmon Canyon Copper mine along the Salmon River (fig. 1). An additional Lu-Hf age of 94 ± 8 Ma (TRPg-1) was reported for garnets from a schistose biotitic mafic dike near the Tinkers Pride prospect north of the Blackbird mine (fig. 1; Zirakparvar and others, 2007). In contrast, preliminary work on a sample collected from north–northwest of Salmon as part of a geologic mapping effort yielded a >1100 Ma age (sample 12RBS56; J. Vervoort, written commun. in Burmester and others, 2016). Additional sampling of Lemhi subbasin metasedimentary rocks during this study further constrains the thermal history of the area as well as the spatial extent of Proterozoic and Cretaceous metamorphism in eastern Idaho. This information helps further understanding of the geologic evolution of the western margin of Laurentia and the age of ore mineralization within the Idaho Cobalt belt.

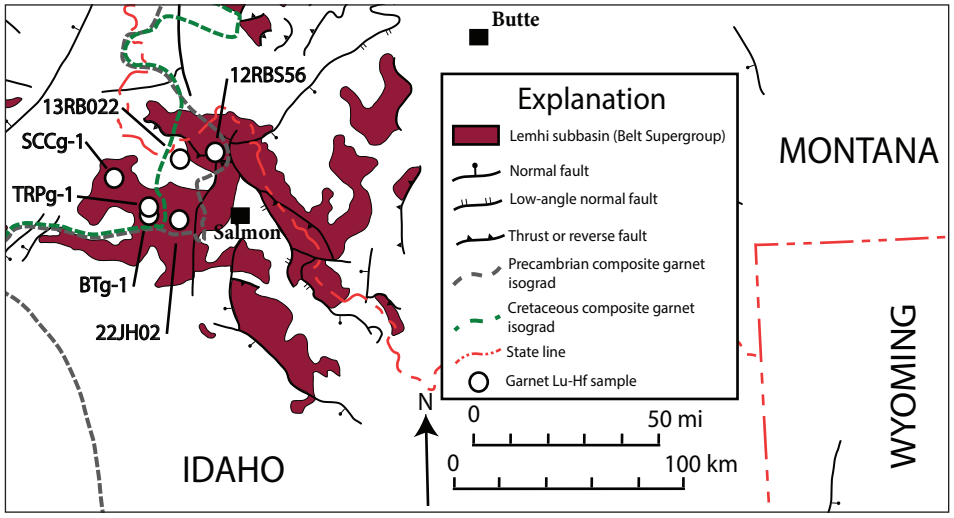

Figure 1. Map showing sample locations in the Lemhi subbasin near Salmon, Idaho. Map modified from Lonn and others (2020).

METHODS

Three garnet-bearing samples from the Salmon River Mountains were collected for analysis, and the data for the original Proterozoic-age sample (12RBS56) were revisited. Sample methodology consisted of standard crushing and mineral separation procedures performed at the School of the Environment, Washington State University. Once garnet mineral separates were obtained, both garnet fractions and whole-rock fractions were dissolved in the clean lab at the Radiogenic Isotopes and Geochronology Laboratory (RIGL), Washington State University, to produce garnet and whole-rock isochrons. For full discussion on the dissolution, spiking, chemical separation, and analysis, see Cheng and others (2008), Zirakparvar and others (2010), and Nesheim and others (2012). All sample locations are shown in figure 1.

RESULTS AND DISCUSSION

Of the three newly collected samples, only two produced straightforward Lu-Hf results. The oldest age of 1353 ± 4 Ma came from sample 13RB022 from northwest of Salmon (fig. 2). A younger age of 1135 ± 5 Ma was obtained for sample 12RBS56 from north of North Fork (fig. 3). Sample 22JH02 from west of Salmon along Deep Creek yielded an age of 1112 ± 3 Ma (fig.4).

These results further expand our knowledge of Mesoproterozoic garnet-grade metamorphism in east-central Idaho from the single Grenville-aged sample (12RBS56) and now span ~240 Ma from 1353 to 1112 Ma. The East Kootenay orogeny was first termed by McMechan and Price (1982) to describe granitic plutonism and metamorphism in the Purcell Basin of southeastern British Columbia during the Mesoproterozoic. Evans and Zartman (1990) reported on the southern extent of the East Kootenay orogeny where a pluton with an age of 1370 ± 10 intruded into the metasedimentary rocks of the Lemhi subbasin in east-central Idaho. A garnet Lu-Hf age of 1379 ± 8 Ma from a lower Belt mica schist exposed in the Priest River complex (Zirakparvar and others, 2010) is the maximum age constraint for the East Kootenay orogeny. A ^{207}Pb-^{206}Pb titanite age of 1325 ± 21 Ma from metamorphosed mafic sills located in southeastern British Columbia (Schandl and Davis, 2000) is the minimum age constraint for the orogeny. Magmatism during this

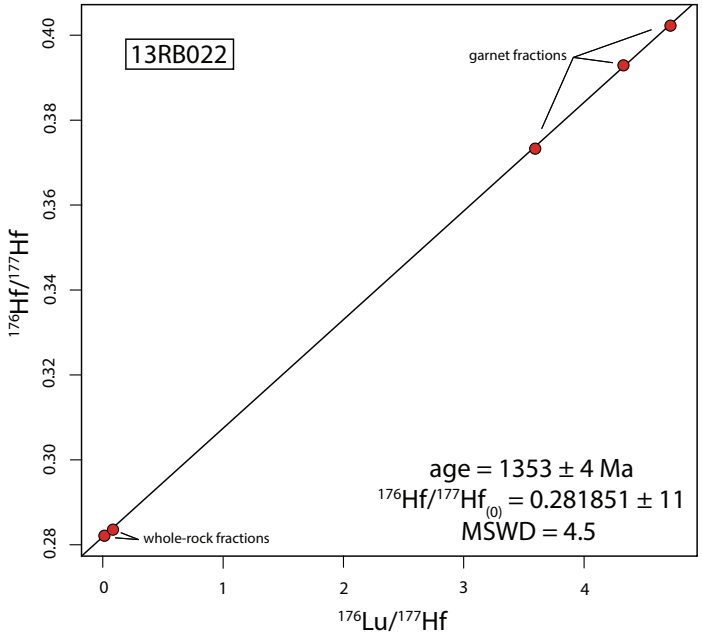

Figure 2. Lu-Hf isochron for sample 13RB022 showing three garnet fractions, a whole-rock bomb dissolution, and a whole-rock Savillex dissolution. Error ellipses are too small to be represented. Collected from Salmon River Road (45.3966° N, 114.1842° W, NAD27).

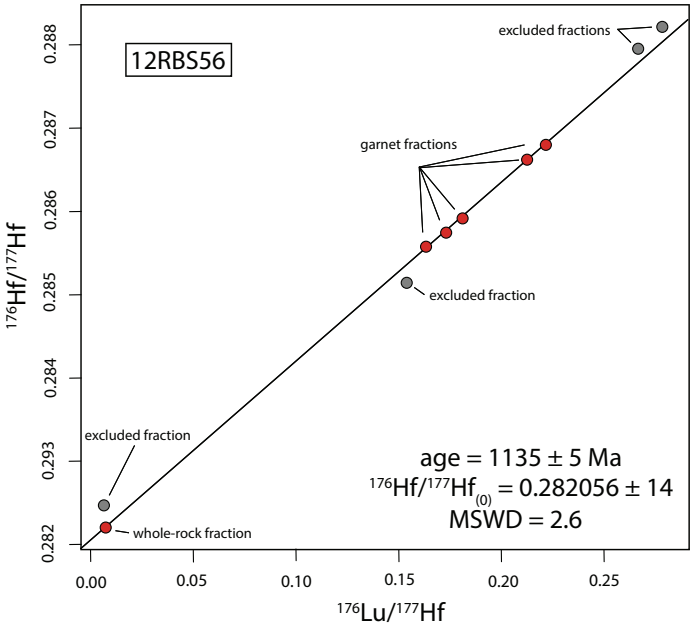

Figure 3. Sm-Nd isochron for sample 12RBS56 showing four garnet fractions, two excluded garnet fractions, a whole-rock bomb dissolution, and an excluded whole-rock Savillex dissolution. Error ellipses are too small to be represented. Collected from north of North Fork, Idaho (45.4344° N, 113.9902° W, NAD27).

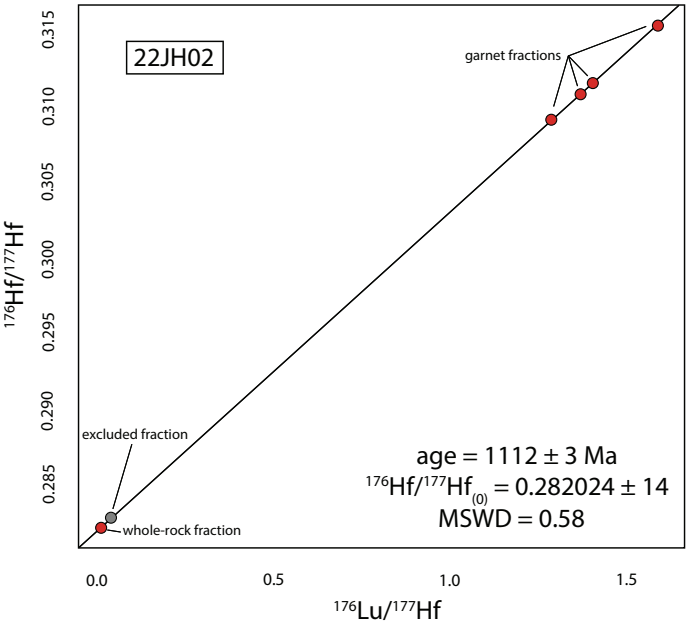

Figure 4. Lu-Hf isochron for sample 22JH02 showing four garnet fractions, a whole-rock bomb dissolution, and an excluded whole-rock Savillex dissolution. Error ellipses are too small to be represented. Collected from Deep Creek Road (45.1084° N, 114.1829° W, NAD27).

orogenic event has been further constrained through sensitive high-resolution ion microprobe (SHRIMP) U-Pb zircon and xenotime geochronology, with igneous zircon U-Pb ages ranging from 1383 ± 4 to 1359 ± 7 Ma (Aleinikoff and others, 2012) and xenotime U-Pb ages in oscillatory-zoned xenotime cores potentially recording initial cobaltite formation at 1370 ± 4 Ma (Aleinikoff and others, 2012). However, these ages were determined *in situ* from small areas on thin sections and extrapolating them to the entire Blackbird district within the Idaho Cobalt Belt could be problematic (Aleinikoff and others, 2012). Sample 13RB022 adds a garnet Lu-Hf age of 1353 ± 4 Ma to the area, corroborating the timing and extent of the East Kootenay orogeny in east-central Idaho.

Samples 12RBS56 (1135 ± 5 Ma) and 22JH02 (1112 ± 3 Ma) yield younger garnet Lu-Hf ages in the study area, and this falls within a Grenville-aged (ca. 1200–1000 Ma) tectonic event (Vervoort and others, 2005; Nesheim and others, 2012; Bookstrom and others, 2016). The samples from Vervoort and others (2005) and Nesheim and others (2012) are from in and near the Clearwater metamorphic complex in northern Idaho along the western margin of Laurentia. The similarity of the new dates presented here to the previously determined Grenville-aged garnet Lu-Hf ages indicate that the crustal thickening recorded in the Clearwater complex may have extended farther inland to present-day Salmon, Idaho on the ancient continent of Laurentia.

The Cretaceous Lu-Hf garnet ages reported by Zirakparvar and others (2007) and Bookstrom and others

(2016) in the study area span from 151 to 94 Ma. During the Mesozoic, two significant thermal events near the study area were oceanic island arc terrane accretion and the emplacement of the Atlanta lobe of the Idaho Batholith. Terrane accretion is likely responsible for the garnet Lu-Hf ages in this area that are older than 100 Ma, as the Blue Mountain province was accreted over an approximate range of 145–100 Ma (Gray and others, 2020). The garnet Lu-Hf age younger than 100 Ma is likely associated with the emplacement of the Idaho Batholith, which commenced at 98 Ma (Gaschnig and others, 2010). Additional monazite U-Pb ages in the study area determined by Aleinikoff and others (2012) at 110 ± 3 Ma and 92 ± 5 Ma are consistent with the Cretaceous garnet Lu-Hf ages in this area.

CONCLUSIONS

New garnet Lu-Hf ages coupled with existing geochronology are evidence of a complex metamorphic history in the Salmon River Mountains in east-central Idaho. In the Proterozoic, two thermal events are identified. A garnet Lu-Hf age of 1353 ± 4 Ma is in the age range of the East Kootenay orogeny (~1379–1325 Ma). Younger Proterozoic garnet Lu-Hf ages of 1135 ± 5 Ma and 1112 ± 3 Ma are within the age range of the Grenville tectonic event (~1200–1000 Ma). Lastly, Cretaceous ages relate to terrane accretion (>100 Ma) and the emplacement of the Idaho batholith (<100 Ma).

ACKNOWLEDGMENTS

A review by Russ Burmester is greatly appreciated.

REFERENCES

Aleinikoff, J.N., Hayes, T.S., Evans, K.V., Mazdab, F.K., Pillers, R.M., and Fanning, C.M., 2012, SHRIMP U-Pb ages of xenotime and monazite from the Spar Lake red bed-associated Cu-Ag deposit, western Montana: Implications for ore genesis: Economic Geology and the Bulletin of the Society of Economic Geologists, v. 107, no. 6, p. 1251–1274.

Burmester, R.F., Lewis, R.S., Othberg, K.L., Stanford, L.R., Lonn, J.D., and McFaddan, M.D., 2016, Geologic map of the western part of the Salmon 30 x 60-minute quadrangle, Idaho and Montana: Idaho Geological Survey Geologic Map 52, scale 1:75,000.

Bookstrom, A.A., Box, S.E., Cossette, P.M., Frost, T.P., Gillerman, V.S., King, G.R., and Zirakparvar, N.A., 2016, Geologic history of the Blackbird Co-Cu district in the Lemhi subbasin of the Belt-Purcell basin: Geological Society of America Special Papers, p. 185–219.

Cheng, H., King, R.L., Nakamura, E., Vervoort, J.D., and Zhou, Z., 2008, Coupled Lu-Hf and Sm-Nd geochronology constrains garnet growth in ultra-high-pressure eclogites from the Dabie orogen: Journal of Metamorphic Geology, v. 26, p. 741–758.

Evans, K.V., and Zartman, R.E., 1990, U-Th-Pb and Rb-Sr geochronology of Middle Proterozoic granite and augen gneiss, Salmon River Mountains, east-central Idaho: Geological Society of America Bulletin, v. 102, p. 63–73.

Gaschnig, R.M., Vervoort, J.D., Lewis, R.S., and McClelland, W.C., 2010, Migrating magmatism in the Northern U.S. Cordillera: In situ U–Pb geochronology of the Idaho Batholith: Contributions to Mineralogy and Petrology, v. 159, p. 863–883.

Gray, K.D., Isakson, V., Schwartz, D., and Vervoort, J.D., 2020, Orogenic link ~41°N–46°N: Collisional mountain building and basin closure in the Cordillera of western North America: Geosphere, v. 16, no. 1, p. 136–181, doi: https://doi.org/10.1130/GES02074.1.

Lonn, J.D., Burmester, R.F., Lewis, R.S., and McFaddan, M.D., 2020, The Mesoproterozoic Belt Supergroup, *in* Metesh, J.J., and Vuke, S.M., eds., Geology of Montana—Geologic History: Montana Bureau of Mines and Geology Special Publication 122, v. 1, 38 p.

McMechan, M.E., and Price, R.A., 1982, Superimposed low-grade metamorphism in the Mount Fisher area, southeastern British Columbia—Implications for the East Kootenay orogeny: Canadian Journal of Earth Sciences, v. 19, p. 476–489.

Nesheim, T.O., Vervoort, J.D., McClelland, W.C., Gilotti, J.A., and Lang, H.M., 2012, Mesoproterozoic syntectonic garnet within Belt Supergroup metamorphic tectonites: Evidence of Grenville-age metamorphism and deformation along northwest Laurentia: Lithos, v. 134-135, p. 91–107.

Schandl, E.S., and Davis, D.W., 2000, Geochronology of the Sullivan deposit: U-Pb and Pb-Pb ages of zircons and titanites: Chapter 8, *in* Lydon, J.W., Höy, T., Slack, J.F., and Knapp, M.E., eds., The geological environment of the Sullivan Deposit, British Columbia: Geological Association of Canada, Mineral Deposits Division Special Publication 1, p. 127–135.

Vervoort, J.D., McClelland, W.C., Watkinson, A.J., and Sha, G.S., 2005, Grenville-age metamorphism on the western margin of Laurentia, northern Idaho: Evidence from Lu-Hf garnet geochronology: Geological Society of America Abstracts with Programs, v. 37, no. 7, p. 89.

Zirakparvar, N.A., Bookstrom, A.A., and Vervoort, J.D., 2007, Cretaceous garnet growth in the Idaho cobalt belt: Evidence from Lu-Hf geochronology: Geological Society of America Abstracts with Programs, v. 39, no. 6, p. 413.

Zirakparvar, N.A., Vervoort, J.D., McClelland, W.C., and Lewis, R.S., 2010, Insights into the metamorphic evolution of the Belt-Purcell Basin; evidence from Lu-Hf garnet geochronology: Canadian Journal of Earth Sciences, v. 47, p. 161–179.

CLUES TO THE PROVENANCE AND LATER METAMORPHIC HISTORY OF THE BELT SUPERGROUP FROM MONAZITE PETROCHRONOLOGY

Richard Gaschnig,[1] Klementina Mato,[1] Aaron Leonard,[1] and Reed S. Lewis[2]

[1]Department of Environmental, Earth and Atmospheric Sciences, University of Massachusetts Lowell
[2]Idaho Geological Survey, Moscow, Idaho

The Mesoproterozoic Belt Supergroup has played an important role in efforts to reconstruct the paleogeography of the supercontinent Nuna. Detrital zircon studies have identified three major populations: (1) Archean zircons from relatively proximal Laurentian sources to the northeast through southeast; (2) Proterozoic zircons from more distal Laurentian sources to the south; and (3) Proterozoic zircons with ages between 1.49 and 1.61 Ga that lack a clear Laurentian source and are inferred to have originated from a now-removed western continent, possibly the combined cratons of East Antarctica, South Australia, and North Australia (Parker and Hendrix, 2022; Ross and Villeneuve, 2003; Stewart and others, 2010). While detrital zircon age analysis is undoubtedly a critical starting point for identifying sedimentary sources and exploring paleogeography, zircon provides a record that is biased toward intermediate to felsic magmatism and that largely misses the metamorphic history of source areas (Chew and others, 2020; Gaschnig, 2019). One important mineral that can help fill in these gaps is monazite. Monazite is chiefly a metamorphic mineral that is sometimes preserved in the detrital record, and it has been shown to have great potential in provenance research (e.g., Hietpas and others, 2010, 2011; Moecher and others, 2019; Mulder and others, 2019). Here, we present monazite U-Th-Pb geochronology and trace element results for samples from the Ravalli Group, Missoula Group, and strata of the Lemhi subbasin, building on the earlier detrital monazite results reported by Ross and others (1991, 1992) and González-Álvarez and others (2006).

Monazite analyses were conducted by LA-ICP-MS at the University of Massachusetts Lowell following the methods of Gaschnig (2019), with results summarized in figure 1. Abundant detrital monazite was found in one sample of the Ravalli Group, with major age peaks at ~1.50, 1.61, 1.67, and 1.77 Ga, whereas monazite in another Ravalli sample yielded ages and trace element geochemistry consistent with post-depositional metamorphic growth around 1.37 Ga. Missoula Group samples yielded detrital monazite with ages almost entirely between 1.65 and 1.8 Ga and closely paralleling detrital zircon ages. In the Lemhi subbasin, samples of the Swauger Formation *senso stricto* yield detrital monazite with age spectra nearly indistinguishable from monazite from the Missoula Group. However, monazite from the Hoodoo Quartzite, which has been correlated with the Swauger Formation, is predomi-

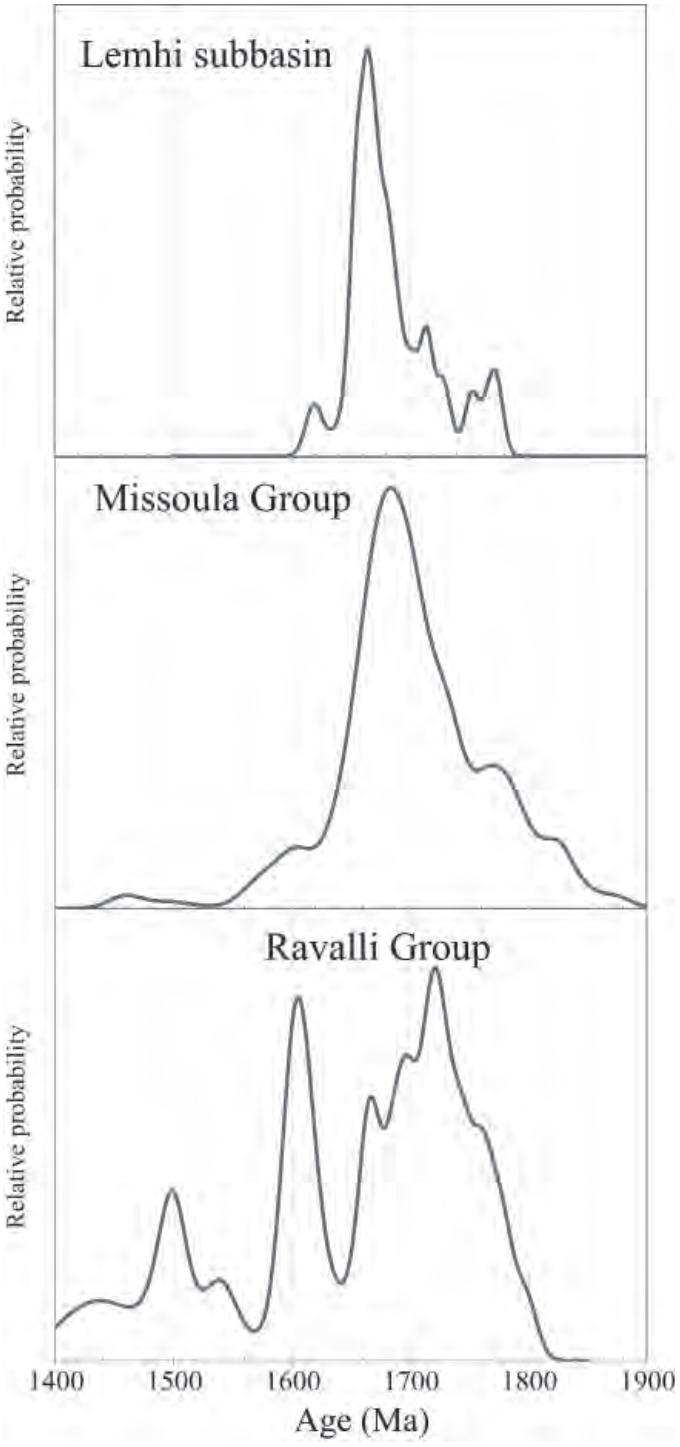

Figure 1. Detrital monazite ages from units of the Belt Basin. Metamorphic/hydrothermal grains with postdepositional ages were also observed and are discussed in the text.

nantly post-depositional in age, recording growth in the Early Paleozoic and also the Late Cretaceous.

The detrital monazite results for the Ravalli Group further strengthen previously proposed ties between the Belt and the Gawler craton (e.g., Ross and Villeneuve, 2003; Brennan and others, 2021), as all of the monazite age populations observed here have possible Gawler sources (Bockmann and others, 2022; Cutts and others, 2013). Detrital monazite from the Missoula Group and Lemhi units likewise strengthens proposed ties to sources in the southwest U.S. (e.g., Ross and Villeneuve, 2003; Link and others, 2007, 2016), as these match the timing of Yavapai orogeny (Whitmeyer and Karlstrom, 2007).

Both Ravalli and Lemhi samples contained monazite that grew *in situ* during metamorphism and/or hydrothermal activity. The 1.37 Ga growth episode seen in the Ravalli Group matches the age of widespread granitic magmatism that affected the Belt Basin area (Aleinikoff and others, 2012; Doughty and Chamberlain, 1996), and it is likely that monazite growth records fluid flow related to that magmatism. Unusually low Th content in these monazites is also consistent with hydrothermal growth. Postdepositional monazite in Hoodoo quartzite of the Lemhi subbasin records events in both the Paleozoic and Cretaceous. Most of the Paleozoic ages cluster around 509 Ma and have low Th and a positive Eu anomaly. These likely reflect an episode of fluid flow linked to the Early Paleozoic magmatism in central Idaho reported on by Lund and others (2010). In contrast, Late Cretaceous monazites cluster around 81 Ma, and have trace element characteristics more akin to monazite formed under regional metamorphic conditions, likely reflecting regional crustal thickening and thrusting.

REFERENCES

Aleinikoff, J.N., Slack, J.F., Lund, K., Evans, K.V., Fanning, C.M., Mazdab, F.K., Wooden, J.L., and Pillers, R.M., 2012, Constraints on the timing of Co-Cu ± Au mineralization in the Blackbird District, Idaho, using SHRIMP U-Pb ages of monazite and xenotime plus zircon ages of related Mesoproterozoic orthogneisses and metasedimentary rocks: Economic Geology, v. 107, no. 6, p. 1143–1175.

Bockmann, M.J., Hand, M., Morrissey, L.J., Payne, J.L., Hasterok, D., Teale, G., and Conor, C., 2022, Punctuated geochronology within a sustained high-temperature thermal regime in the southeastern Gawler Craton: Lithos, v. 430–431, 106860.

Brennan, D.T., Brian Mahoney, J., Li, Z.-X., Link, P.K., Evans, N.J., and Johnson, T.E., 2021, Detrital zircon U–Pb and Hf signatures of Paleo-Mesoproterozoic strata in the Priest River region, northwestern USA: A record of Laurentia assembly and Nuna tenure: Precambrian Research, v. 367, p. 106445.

Chew, D., O'Sullivan, G., Caracciolo, L., Mark, C., and Tyrrell, S., 2020, Sourcing the sand: Accessory mineral fertility, analytical and other biases in detrital U-Pb provenance analysis: Earth-Science Reviews, v. 202, p. 103093.

Cutts, K.A., Kelsey, D.E., and Hand, M., 2013, Evidence for late Paleoproterozoic (ca 1690–1665 Ma) high- to ultrahigh-temperature metamorphism in southern Australia: Implications for Proterozoic supercontinent models: Gondwana Research, v. 23, no. 2, p. 617–640.

Doughty, P.T., and Chamberlain, K.R., 1996, Salmon River Arch revisited: New evidence for 1370 Ma rifting near the end of deposition in the Middle Proterozoic Belt Basin: Canadian Journal of Earth Sciences, v. 33, p. 1037–1052.

Gaschnig, R.M., 2019, Benefits of a multiproxy approach to detrital mineral provenance analysis: An example from the Merrimack River, New England, USA: Geochemistry, Geophysics, Geosystems, v. 20, no. 3, p. 1557–1573.

González-Álvarez, I., Agnieszka Kusiak, M., and Kerrich, R., 2006, A trace element and chemical Th-U total Pb dating study in the lower Belt-Purcell Supergroup, Western North America: Provenance and diagenetic implications: Chemical Geology, v. 230, no. 1–2, p. 140–160.

Hietpas, J., Samson, S., Moecher, D., and Schmitt, A.K., 2010, Recovering tectonic events from the sedimentary record: Detrital monazite plays in high fidelity: Geology, v. 38, no. 2, p. 167–170.

Hietpas, J., Samson, S., and Moecher, D., 2011, A direct comparison of the ages of detrital monazite versus detrital zircon in Appalachian foreland basin sandstones: Searching for the record of Phanerozoic orogenic events: Earth and Planetary Science Letters, v. 310, no. 3–4, p. 488–497.

Link, P.K., Fanning, C.M., Lund, K.I., and Aleinikoff, J.N., 2007, Detrital-zircon populations and provenance of Mesoproterozoic strata of east-central Idaho, U.S.A.: Correlation with the Belt Supergroup of southwest Montana, *in* Link, P.K., and Lewis, R.S., eds., Proterozoic geology of western North America and Siberia, SEPM Special Paper 86, p. 101–128.

Link, P.K., Stewart, E.D., Steel, T., Sherwin, J.A., Hess, L.T., McDonald, C., MacLean, J.S., and Sears, J.W., 2016, Detrital zircons in the Mesoproterozoic upper Belt Supergroup in the Pioneer, Beaverhead, and Lemhi Ranges, Montana and Idaho: The Big White arc, *in* MacLean, J.S., and Sears, J.W., eds., Belt Basin: Window to Mesoproterozoic Earth, GSA Special Paper 522, p. 163–184.

Lund, K., Aleinikoff, J.N., Evans, K.V., duBray, E.A., Dewitt, E.H., and Unruh, D.M., 2010, SHRIMP U-Pb dating of recurrent Cryogenian and Late Cambrian-Early Ordovician alkalic magmatism in central Idaho: Implications for Rodinian rift tectonics: Geological Society of America Bulletin, v. 122, no. 3–4, p. 430–453.

Moecher, D.P., Kelly, E.A., Hietpas, J., and Samson, S.D., 2019, Proof of recycling in clastic sedimentary systems from textural analysis and geochronology of detrital monazite: Implications for detrital mineral provenance analysis: GSA Bulletin, v. 131, no. 7–8, p. 1115–1132.

Mulder, J.A., Halpin, J.A., Daczko, N.R., Orth, K., Meffre, S., Thompson, J.M., and Morrissey, L.J., 2019, A Multiproxy

provenance approach to uncovering the assembly of East Gondwana in Antarctica: Geology, v. 47, no. 7, p. 645–649.

Parker, S.D., and Hendrix, M.S., 2022, Detrital zircon record of the Mesoproterozoic Belt basin and implications for horizontal and vertical tectonic models, *in* Foulger, G.R., Hamilton, L.C., Jurdy, D.M., Stein, C.A., Howard, K.A., and Stein, S., eds., In the footsteps of Warren B. Hamilton: New ideas in earth science, GSA Special Paper 553, p. 159–176.

Ross, G.M., and Villeneuve, M., 2003, Provenance of the Mesoproterozoic (1.45 Ga) Belt basin (western North America): Another piece in the pre-Rodinia paleogeographic puzzle: Geological Society of America Bulletin, v. 115, no. 10, p. 1191–1217.

Ross, G.M., Parrish, R.R., and Dudas, F.O., 1991, Provenance of the Bonner Formation (Belt Supergroup), Montana: Insights from U-Pb and Sm-Nd analyses of detrital minerals: Geology, v. 19, no. 4, p. 340–343.

Ross, G.M., Parrish, R.R., and Winston, D., 1992, Provenance and U-Pb geochronology of the Mesoproterozoic Belt Supergroup (northwestern United States): Implications for age of deposition and pre-Panthalassa plate reconstructions: Earth and Planetary Science Letters, v. 113, no. 1, p. 57–76.

Stewart, E.D., Link, P.K., Fanning, C.M., Frost, C.D., and McCurry, M., 2010, Paleogeographic implications of non-North American sediment in the Mesoproterozoic upper Belt Supergroup and Lemhi Group, Idaho and Montana, USA: Geology, v. 38, no. 10, p. 927–930.

Whitmeyer, S.J., and Karlstrom, K.E., 2007, Tectonic model for the Proterozoic growth of North America: Geosphere, v. 3, no. 4, p. 220–259.

LA-ICPMS U-PB ZIRCON CRYSTALLIZATION AGES OF A 1380 MA GRANITE IN NORTH-CENTRAL IDAHO; WESTERNMOST EXTENT OF AUGEN GNEISS MEMBER OF THE MESOPROTEROZOIC BIMODAL INTRUSIVE SUITE

Emma Roberts,[1] Johannes Hammerli,[1] Russ Di Fiori,[2] and Jeff Vervoort[1]

[1]School of the Environment, Washington State University, Pullman, Washington
[2]Idaho Geological Survey, University of Idaho, Moscow, Idaho

ABSTRACT

New LA-ICP-MS U-Pb analyses of zircons from an augen gneiss along the South Fork of the Clearwater River reveal a weighted mean $^{207}Pb/^{206}Pb$ age of 1381 ± 4 Ma (n = 22), which is in excellent agreement with the upper Concordia intercept age of 1381 ± 4 Ma determined by Evans and Fischer (1986) for a similar sample collected 37 km to the east. Several ~1381 Ma zircons contain rims, which record a $^{206}Pb/^{238}U$ age of ~81 ± 1 Ma. An older population of zircon cores was identified, which returned an upper Concordia intercept age of 1709 ± 8. The 1381 Ma age is similar to the Mesoproterozoic granites found in the Salmon area, and the older cores suggest a Belt Supergroup component in the parental melt. The ~81 Ma ages of zircon rims suggest that a Cretaceous thermal event led to the partial resetting of the U-Pb system and zircon overgrowth in some instances. This thermal event can be linked to Cordilleran orogenesis coupled with the emplacement of the Idaho batholith.

INTRODUCTION

High-spatial resolution U-Pb zircon geochronology, when used in concert with detailed geologic mapping, is especially useful in regions where outcrop exposure is limited by dense foliage, deep soil cover, and where myriad similar-looking lithologies are not always easy to distinguish in the field. This is especially true when working with rocks that have been subjected to a protracted, polyepisodic, thermo-tectonic history. The geology of the Elk City area of north-central Idaho is characterized by such a complex of Mesoproterozoic metasedimentary and metaigneous rocks (fig. 1). Many of these lithologies can be easily conflated, especially where exposure is poor. Specifically, the common but variable gneissic rocks and localized zones of strained granodiorite can be difficult to discern. For instance, the paragneiss rocks are generally banded at the centimeter-scale and contain local crudely developed white lensoidal pods; the orthogneiss, similarly banded, contain well-developed pinkish-white augens; and the Cretaceous ductile-strained porphyritic biotite granodiorite also yields a banded appearance coupled with very coarse to megacrystic feldspar grains and grain aggregates that could be described as augens. While a certain amount of confidence can be achieved after weeks in the field, having *in situ* zircon geochronology provides more certainty when attempting to identify and catalogue these similar lithologic varieties. U-Pb zircon geochronology is a powerful tool that aids in the extraction of geologic data and augments the interpretations made in the field. The sample at the center of this paper is an example of this utility.

GEOLOGIC FRAMEWORK AND SAMPLE DESCRIPTION

Mesoproterozoic Belt Supergroup metasedimentary rocks across east-central Idaho, between latitudes 46°30' N to 44° N, have been intruded and cut by a bimodal igneous suite estimated to have been emplaced between ~1380 and 1370 Ma (Evans and Fischer, 1986; Doughty and Chamberlain, 1996; Aleinikoff and others, 2012). The bedrock of the Elk City area largely comprises polydeformed schist, paragneiss, calc-silicate granofels, and quartzite of the Mesoproterozoic metasedimentary rocks interpreted to be Lemhi subbasin strata of Belt Supergroup affinity (Lonn and others, 2020). These rocks have been intruded by dikes and sills composed of metaigneous augen gneiss (granite protolith) and amphibolite (mafic protolith; Evans and Fischer, 1986). The Augen gneiss and amphibolite lithologies have been intruded by a Late Cretaceous biotite granodiorite, which belongs to the Atlanta lobe of the Idaho Batholith, as well as by less abundant Eocene and Miocene hypabyssal rocks (e.g., Gaschnig and others, 2010; Di Fiori and others, 2022).

Sample 22RVD028 was collected from a south-facing roadcut along Idaho State Highway 14 (fig. 2), which parallels the South Fork of the Clearwater River near Golden, Idaho (fig. 1). This sample was chosen for analysis to aid in lithologic identification and to also help cultivate a robust geochronology dataset for the rocks of the region.

METHODS

Zircon Separation and Sample Preparation

The augen gneiss sample 22RVD028 was processed at the School of the Environment, Washington State University (WSU), using standard procedures to obtain a zircon separate. The sample was milled to a grain size of ≤500 μ with a disc mill followed by extraction of magnetic

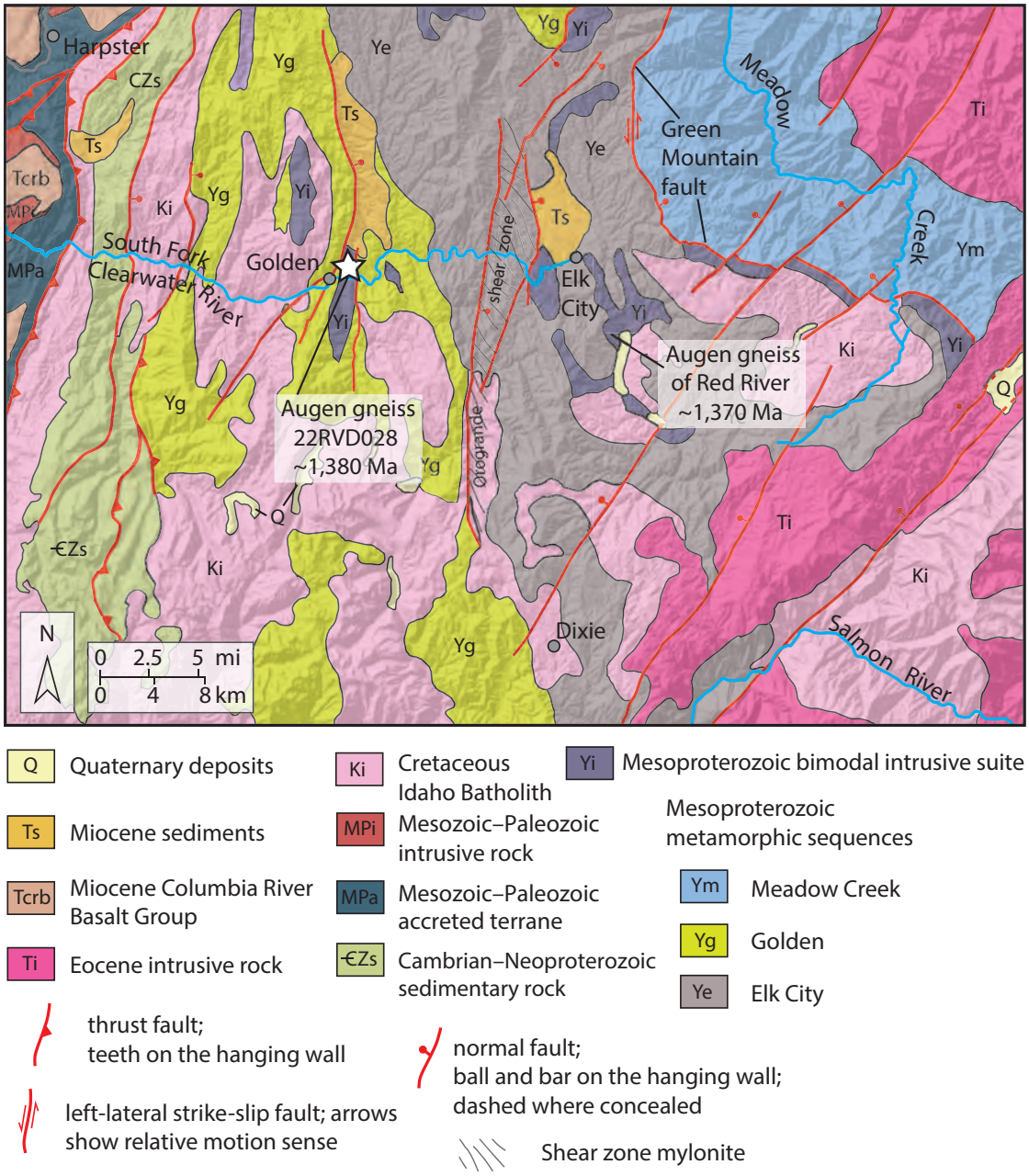

Figure 1. Simplified geologic map of study area, the Elk City 30' x 60' quadrangle. Map unit Yi (darkish purple) is the Mesoproterozoic bimodal igneous suite and the white star denotes sample 22RVD028. Augen gneiss of Red River age from Evans and Fischer (1986). Modified from Di Fiori and others (2022).

phases with a hand magnet. The sample was then panned to concentrate the heavy minerals. The separate was then transferred into a petri dish and zircon grains were carefully hand-picked and mounted onto a silicon tape. A 1-in mold was placed on the tape with the zircons located in the center. Epoxy was then poured into the mold to produce a disc. After curing the sample for 24 hours under 2-bar pressure to avoid the formation of bubbles in the epoxy, the sample was polished stepwise from 6 to 1 µ. After polishing the zircons, all grains were imaged in transmitted light to identify cracks and inclusions, which were to be avoided during LA-ICP-MS analyses. All zircons were subsequently CL-imaged via a JEOL 8500F HyperProbe at the Peter Hooper GeoAnalytical Lab at WSU to identify growth zoning and inherited cores.

U-Pb Analyses via LA-ICP-MS

U-Pb analyses were performed using via an Analyte G2 193 µm laser system coupled to a ThermoScientific Element 2 mass spectrometer at the Radiogenic Isotope & Geochronology Laboratory (RIGL) at WSU. A laser spot size of 25 µm was used and a pulse rate of 10 Hz and a fluence of 5–6 J/cm^2 was applied. Standard reference zircons 91500, FC1, GJ1, and Plesovice were analyzed. FC1 (1099 Ma, Paces and Miller, 1993) zircons were used as the primary standard for zircons ≥1.3 Ga and Plesovice (337 Ma, Sláma and others, 2008) zircons were used to standardize the younger zircon rims. 91500 and GJ1 zircons were used as secondary standards to monitor analytical performance. All data were reduced via the IOLITE 4 software pack-

Figure 2. Augen gneiss roadcut exposure along Idaho State Route 14 from which sample 22RVD028 was collected (45°48'37.12"N, 115°39'23.95"W; WGS84).

age (Paton and others, 2010). The mean $^{207}Pb/^{206}Pb$ age of 91500 zircon of 1,062 ± 14 (SD, n = 6) is in excellent agreement with the preferred $^{207}Pb/^{206}Pb$ age of 1,065 Ma (Wiedenbeck and others, 1995). Our GJ1 mean value of 606 ± 12 Ma (n = 5) agrees with the preferred U-Pb age of 609 Ma (Jackson and others, 2004).

RESULTS

The analyzed zircons are typically euhedral in shape and reach as much as 400 μm in length. The zircon grains are clear in transmitted light and some grains contain several inclusions. Cathodoluminescence images (fig. 3) revealed that many zircons contain oscillatory growth zonation, and some grains have cores. Younger overgrowth is typically seen as CL-light zones (fig. 3, analysis 14). We analyzed 25 individual zircons with a total of 32 measurements (fig. 4). The main zircon population has a weighted average mean $^{207}Pb/^{206}Pb$ age of 1381 ± 4 Ma with a MSWD of 2. Five grains contained older cores that produced an upper intercept age of 1709 ± 8 Ma. We measured three young zircon rims with a $^{206}Pb/^{238}U$ age of 81 ± 1 Ma (figs. 3, 4).

DISCUSSION AND CONCLUSIONS

Based on our results, sample 22RVD028 formed at approximately 1,381 Ma and thus is interpreted to be the augen gneiss of the Mesoproterozoic bimodal igneous suite. The older cores found in some of the zircons suggest that the magma had incorporated some Paleoproterozoic material, likely sourced from the Belt Supergroup sedimentary rock package, which is common in the region (fig. 1). The younger ~81 Ma rims suggest that a Cretaceous thermal event led to zircon recrystallization, likely related to Cordilleran orogenesis. This thermal event can be linked to the Late Cretaceous Idaho Batholith, which is a prominent feature of regional geology.

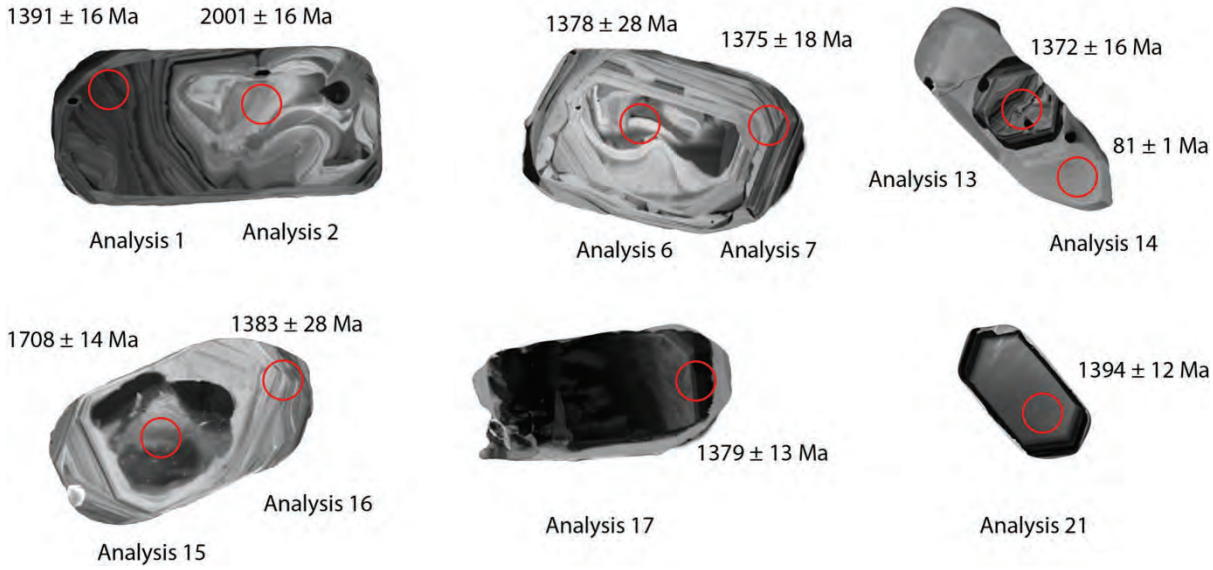

Figure 3. CL images of representative zircons from sample 22RVD028. Red circle shows location of laser ablation spots (25 µm).

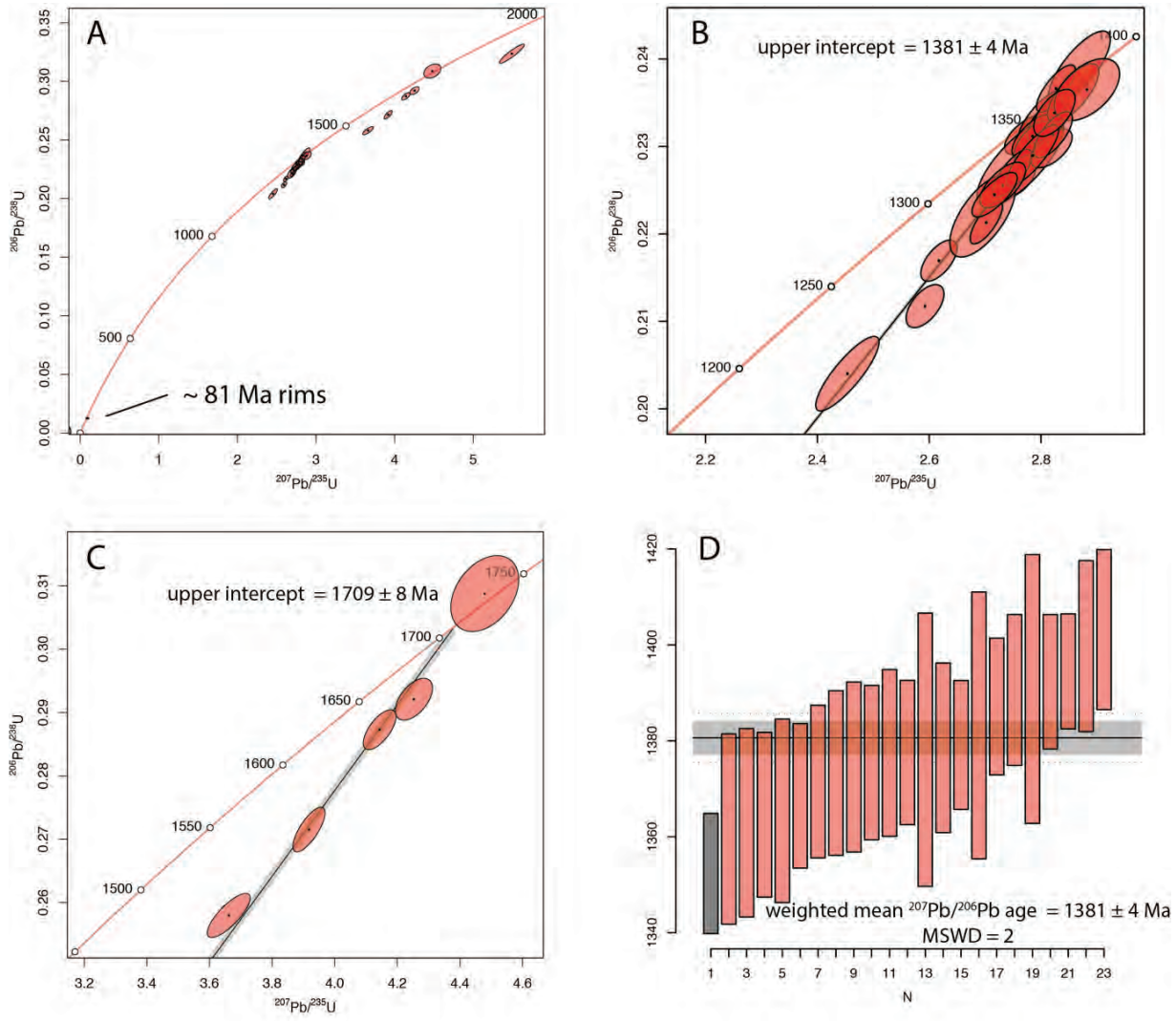

Figure 4. (A) Concordia diagram of all 32 U-Pb analyses, (B) upper intercept age of ~1380 Ma for the main zircon population (*n* = 23), (C) upper intercept age for older zircon cores, and (D) weighted mean age of main zircon population that overlap within uncertainty (2σ, n = 22) with one analysis being treated as an outlier (gray bar).

These new data add resolution to and expand the spatial footprint of the 1380–1370 Ma bimodal intrusive suite documented across east-central Idaho, marking the westernmost exposure of the Mesoproterozoic granite. Additionally, *in situ* U-Pb zircon geochronology of these complicatedly zoned zircon grains allow for a detailed set of time data that increases our understanding of the long-lived tectonic history of the interior of east-central Idaho.

ACKNOWLEDGMENTS

We thank Reed Lewis for kindly providing a review of this manuscript.

REFERENCES

Aleinikoff, J.N., Slack, J.F., Kund, K., Evans, K.V., Fanning, C.M., Mazdab, F.K., Wooden, J.I., and Pillers, R.M., 2012, Constraints on the timing of Co-Cu+/-Au mineralization in the Blackbird district, Idaho, using SHRIMP U-Pb age of monazite and xenotime plus zircon ages of related Mesoproterozoic orthogneisses and metasedimentary rocks: Economic Geology, v. 107, no. 6, p. 1143–1175.

Di Fiori, R.V., Lewis, R.S., Schmidt, K.L., Burmester R.F., and Huttanus, H.W., 2022, Geologic map of the Elk City 7.5' quadrangle, Idaho county, Idaho: Idaho Geological Survey Digital Web Map 206, scale 1:24,000.

Doughty, P.T., and Chamberlain, K.R., 1996, Salmon River arch revisited: New evidence for 1370 rifting near the end of deposition in the Middle Proterozoic Belt Basin: Canadian Journal of Earth Sciences, v. 33, p. 1037–1052.

Evans, K.V., and Fischer, L.B., 1986, U-Pb geochronology of two augen gneiss terranes, Idaho—New data and tectonic implications: Canadian Journal of Earth Sciences, v. 23, p. 1919–1927.

Gaschnig, R.M., Vervoort, J.D., Lewis, R.S., and McClelland, W.C., 2010, Migrating magmatism in the northern US Cordillera: in situ U–Pb geochronology of the Idaho batholith: Contributions to Mineralogy and Petrology, v. 159, p. 863–883.

Jackson, S.E., Pearson, N.J., Griffin, W.L., and Belousova, E.A., 2004, The application of laser ablation-inductively coupled plasma-mass spectrometry to in situ U–Pb zircon geochronology: Chemical Geology, v. 211, p. 47–69.

Lonn, J.D., Burmester R.F., Lewis, R.S. and McFaddan, M.D., 2020, The Mesoproterozoic Belt Supergroup: Montana Bureau of Mines and Geology Special Publication 122, v. 1, available at https://mbmg.mtech.edu/pdf/geologyvolume/Lonn_BeltFinal.pdf [Accessed 5/17/2023].

Paces, J.B., and Miller Jr., J.D., 1993, Precise U-Pb ages of Duluth Complex and related mafic intrusions, northeastern Minnesota: Geochronological insights to physical, petrogenetic, paleomagnetic, and tectonomagmatic processes associated with the 1.1 Ga Midcontinent Rift System: Journal of Geophysical Research: Solid Earth, v. 98, p. 13997–14013.

Paton, C., Woodhead, J., Hellstrom, J., Hergt, A., Maas, R., 2010. Improved laser ablation U-Pb zircon geochronology through robust downhole fractionation correction: Geochemistry, Geophysics, Geosystems.

Sláma, J., and others, 2008, Plešovice zircon—A new natural reference material for U–Pb and Hf isotopic microanalysis: Chemical Geology, v. 249, p. 1–35.

Wiedenbeck, M., Allé, P., Corfu, F., Griffin, W.L., Meier, M., Oberli, F., Quadt, AV., Roddick, J.C., and Spiegel, W., 1995, Three natural zircon standards for U-Th-Pb, Lu-Hf, Trace element and ree analyses: Geostandards Newsletter, v. 19, p. 1–23.

ELIMINATING THE UNNAMED FORMATION FROM THE KALISPELL 1° × 2° QUADRANGLE, MONTANA

Jeffrey L. Mauk, Grayce Gibbs, and Micah Hernandez

U.S. Geological Survey, Geology, Geophysics, and Geochemistry Science Center, Denver, Colorado

ABSTRACT

The unnamed formation was mapped in the Whitefish and Swan Ranges on the Kalispell 1° × 2° quadrangle in Montana by Harrison and others (1992). They describe the unit as:

> "Predominantly thin to thick beds of olive siltite and very fine grained quartzite speckled by brown spots of limonite after iron carbonate and perhaps magnetite. Lamination faint but generally even parallel; minor cross lamination. Contact placed above highest black argillite bed in underlying transition member of the Prichard. Unit unnamed because authors differ in interpretation of the rocks as a facies of either the Burke or the Appekunny Formation."

The U.S. Geological Survey is working to complete updated versions of geologic maps of the Wallace and Kalispell 1° × 2° quadrangles, and one of the major enigmas is how to classify the unnamed formation. The Burke Formation was named in the Coeur d'Alene mining district of Idaho by Ransome (1905) for exposures along Canyon Creek from Burke to Gem. Ransome and subsequent workers recognized that the Burke Formation grades downward into the underlying Prichard Formation, and grades upward into the overlying Revett Formation. Most workers recognize two or three parts. In a two-part system: (1) the lower part contains interstratified blocky to argillitic siltite and argillite, with argillite becoming more abundant downward toward the Prichard Formation, and (2) the upper part contains interstratified blocky to argillitic siltite, sericitic quartzite, and argillite, with the quartzite becoming more abundant upwards toward the Revett Formation. Toward the eastern limits of mapped extent of the Burke Formation, finer-grained rocks become more abundant, whereas coarser-grained rocks are more abundant in its type area in the Coeur d'Alene district.

The Appekunny Argillite was named for exposures at Apikuni Mountain in Glacier National Park by Willis (1902), and the name was changed to Appekunny Formation by Harrison (1972). In its type area on Apikuni Mountain, it abruptly overlies limestone of the Altyn Formation, and grades upwards into the Grinnell Formation. Detailed stratigraphic descriptions in the type area document five members (Whipple, 1992; Slotznick and others, 2016), and the most distinct lithology is vitreous quartzite in member 3. In the northern Swan Range, Clapp and others (2004) published a geologic map that showed the entire interval between the transition member of the Prichard Formation and the Empire Formation as Spokane Formation. We have not been able to locate other published geologic maps of the Whitefish and Swan Ranges that would help clarify the classification of the unnamed formation.

During the 2022 field season, we redescribed a stratigraphic section of the Appekunny Formation at the type area of Apikuni Mountain, and we also visited other localities of the Appekunny Formation in Glacier National Park. We undertook several traverses in the Whitefish and Swan Ranges that cross the unnamed formation. This work demonstrated that essential lithostratigraphic units, such as the vitreous quartzite in member 3 of the Appekunny Formation, do not occur in the unnamed formation. Instead, the lithostratigraphic package and stratigraphic succession most closely resembles the Burke Formation, with a mixture of argillitic siltite and blocky siltite near the base of the formation, and more abundant sericitic quartzite toward the top of the formation. We conclude that the preferred map unit for the unnamed formation in the Whitefish and Swan Ranges is the Burke Formation.

In closing, we recognize that there remain significant unresolved questions about stratigraphic correlations for lower Belt and Ravalli Group rocks, particularly on either side of the Rocky Mountain Trench. Available studies provide a firm foundation to build on (e.g., Mauk, 1983; Kuhn, 1987; Cronin, 1988; Slotznick and others, 2016; and references therein), but more careful work is required to resolve these stratigraphic correlations. And that work, which typically occurs through detailed descriptions of outcrop, must be translated into mappable criteria that can be used in the field where outcrop can be very limited, and sedimentary structures may be difficult to detect. At that point, careful consideration of time and funding constraints can help inform decisions about where further geologic mapping is most worthwhile.

REFERENCES

Clapp, K.K., Smith, L.N., MacLaughlin, M.M., and Miller, C.R., 2004, Geologic map of the Columbia Mountain area, northwest Montana: Montana Bureau of Mines and Geology Open-File Report 487, 1 sheet, scale 1:24,000, 11 p.

Cronin, C., 1988, Stratigraphy and sedimentation of the Ravalli Group (middle Proterozoic Belt Supergroup) in the Mission, Swan, and Flathead Ranges, northwest Montana: Missoula, Mont., University of Montana, M.S. thesis, 246 p.

Harrison, J.E., 1972, Precambrian Belt Basin of northwestern United States: Its geometry, sedimentation, and copper occurrences: Geological Society of America Bulletin, v. 83, no. 5, p. 1215–1240.

Harrison, J.E., Whipple, J.W., and Cressman, E.R., 1992, Geologic and structure maps of the Kalispell 1° × 2° quadrangle, Montana, and Alberta and British Columbia: U.S. Geological Survey Miscellaneous Investigations Series Map I-2267, scale 1:250,000.

Kuhn, J.A., 1987, The stratigraphy and sedimentology of the Middle Proterozoic Grinnell Formation, Glacier National Park and the Whitefish Range, NW Montana: Missoula, Mont., University of Montana, M.S. thesis, 113 p.

Mauk, J.L., 1983, Stratigraphy and sedimentation of the Proterozoic Burke and Revett Formations, Flathead Reservation, western Montana: Missoula, Mont., University of Montana, M.S. thesis, 91 p.

Ransome, F.L., 1905, Ore deposits of the Coeur d'Alene district, Idaho, *in* Emmons, S.F., and Hayes, C.W., eds., Contributions to Economic Geology, 1904: U.S. Geological Survey Bulletin 260, p. 274–303.

Slotznick, S.P., Winston, D., Webb, S.M., Kirschvink, J.L., and Fischer, W.W., 2016, Iron mineralogy and redox conditions during deposition of the mid-Proterozoic Appekunny Formation, Belt Supergroup, Glacier National Park, *in* MacLean, J.S., and Sears, J.W., eds., Belt Basin: Window to Mesoproterozoic Earth: Geological Society of America Special Paper 522, p. 221–242.

Whipple, J.W., 1992, Geologic map of Glacier National Park, Montana: U.S. Geological Survey Miscellaneous Investigations Series Map I-1508-F, scale 1:100,000.

Willis, B., 1902, Stratigraphy and structure, Lewis and Livingston ranges, Montana: Geological Society of America Bulletin, v. 13, no. 1, p. 305–352.

INTEGRATED GEOLOGIC INTERPRETATION OF BOUGUER GRAVITY RESIDUAL DATA FROM THE MADISON AND GALLATIN RANGES—SOUTHWESTERN MONTANA

Kevin Lielke

Independent Geologist, Ennis, MT

ABSTRACT

A gravity residual map generated from a legacy Bouguer gravity dataset was used to investigate the large-scale geologic structure of the Madison and Gallatin Ranges of southwestern Montana. Published aeromagnetic and surface geologic maps provide important constraints on the interpretation of the gravity residual data. The results of this analysis demonstrate the pervasive influence of preexisting structures, many with a Precambrian ancestry, on the geologic evolution of the region. In particular, major northwest and northeast-trending crustal scale features, such as the Spanish Peaks fault and the Madison mylonite zone, were repeatedly reactivated and controlled the deformation style and location of multiple generations of geologic structures. The locus of Mesozoic and Cenozoic volcanic activity, as well as the geometry of contemporary sedimentary depocenters, was also heavily influenced by preexisting structures. Gravity residual data provide an effective means of delineating the framework of complex crustal scale deformation especially in regions, such as the eastern half of the study area, covered by a surface veneer of younger glacial or volcanic deposits.

INTRODUCTION

Potential field, gravity, and magnetic data are a useful complement to surface geologic mapping in the sense that they can delineate subsurface features not evident from exposed rock bodies (Wetmore and others, 2021). Potential field methods are of particular use in identifying geologic features in areas obscured by surface glacial deposits or volcanic rocks, such as those associated with the Eocene Absaroka volcanic field and the Yellowstone hotspot. However, given the non-uniqueness of geophysical interpretations, broad geological knowledge of the area under examination is necessary in order to properly interpret such data. An integrated study including traditional geologic and potential field methods can provide new insight into even well-studied territory. In this paper, a legacy Bouguer gravity dataset is interpreted in the context of known regional geology in order to provide a better understanding of the tectonic evolution of the Madison and Gallatin Ranges of southwestern Montana. The results of this analysis point to several new lines of inquiry into the geology of this relatively well-studied region.

DATA AND METHODS

The primary dataset consists of 622 gravity stations collected and processed by the United States Geological Survey (USGS) between 1979 and 1982 (Hassemer and Kaufmann, 1984). A second geophysical survey, including aeromagnetic and new and legacy gravity data, was also conducted in this area by the USGS as part of a comprehensive study of the Gallatin National Forest (Wilson and others, 2005). However, the larger dataset of Hassemer and Kaufmann (1984) was not used in this report despite its denser coverage of the Madison and Gallatin Ranges. For this study, the original Hassemer and Kaufmann (1984) dataset was digitized and gravity residuals were calculated by removal of the regional gravity trend. This process removes that portion of the gravity field due primarily to deep crustal structure, highlighting the effect of the near-surface geology. Although there are different procedures for accomplishing this goal, a weighted least-squares regression of the data was employed in this analysis (LaFehr and Nabighian, 2012). Finally, the geophysical data were evaluated in the context of the known surface geology to construct the most probable interpretation of the geologic structure of this region—the end result of a complex history of overprinted tectonic events that extends far back into the Archean era.

GEOLOGIC INTERPRETATIONS

Several first-order geologic features are evident in the residual gravity data (figs.1, 2). The most prominent among these are the northwest-trending Spanish Peaks fault, the Hilgard thrust system along with its footwall sedimentary deposystem, the Cretaceous Lone Peak igneous suite, a northeast-directed trend centered on the Madison mylonite and Mirror Lake shear zones, as well as multiple intermontane basins. In addition to these structural features a number of processing artifacts, due to edge effects or sparse data, are also evident (fig. 2). These primarily take the form of linear anomalies located along the borders of the study area. These artifacts are unlikely to correspond to any actual geological structure and are therefore disregarded in this study. The gravity residual map was divided into north and south sections, which will be discussed in detail separately.

Long-wavelength aeromagnetic data highlight deep crustal structure at the expense of shallower sources (Mankinen and others, 2004). Aeromagnetic data from Montana (Sims and others, 2004) show regional northeast-trending features that appear to cross without deflection

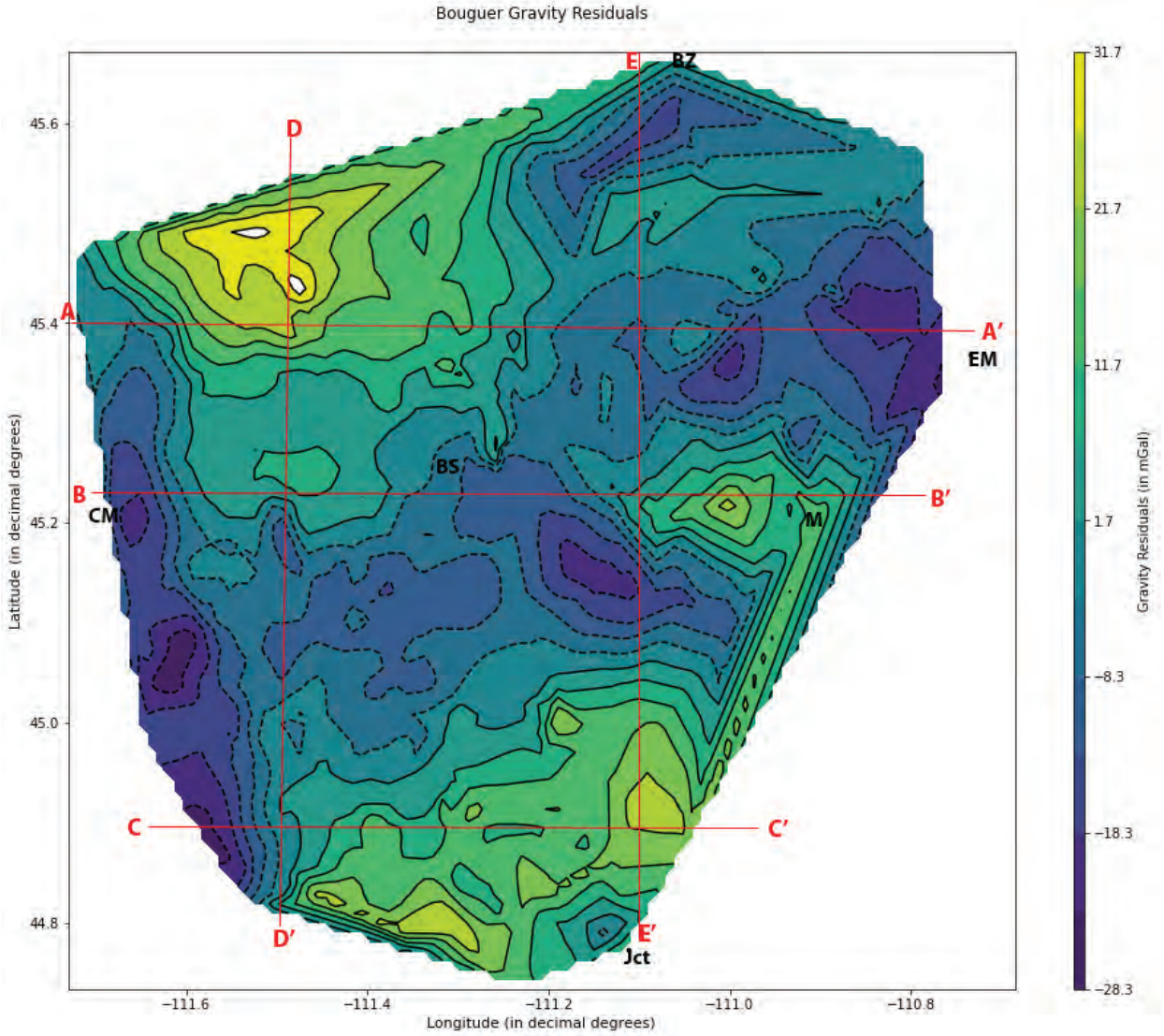

Figure 1. Bouguer residual map of Madison and Gallatin Ranges and adjacent areas, contour interval = 5 mGal. Localities on map: BS, Big Sky meadow village; BZ, Bozeman; CM, Cameron; EM, Emigrant; Jct, Junction of highway US 287 and US 191; M, Miner. Red lines represent gravity anomaly profiles shown in figures 5 and 6.

major oblique-slip, northwest-trending faults mapped at the surface and imaged by gravity data. The lack of offset of the long-wavelength aeromagnetic features suggests that they are rooted in the lower crust or upper lithospheric mantle, below the level of involvement of upper crustal faulting. If true, this means that care needs to be taken in correlating surface features, such as the Madison mylonite and Mirror Lake shear zones, and associated gravity anomalies across younger faults with a significant strike-slip component.

The Laramide Spanish Peaks oblique fault juxtaposes high-density Archean metamorphic rocks over predominately low-density Mesozoic sedimentary rocks (Vuke, 2013). This results in a pronounced northwest-trending gravity high that extends southeast into the Tom Miner Basin area. North of the Spanish Peaks fault several pronounced local gravity maxima occur, the most prominent of which are located in the Cherry Lake area of the northern Madison Range (fig. 2, area A). The gravity maxima observed here correspond to high aeromagnetic anomalies (USGS, 1982; Wilson and others, 2005) indicating the presence of high density, magnetite-bearing mafic rocks within the Archean basement. Younger intrusives are unlikely to account for this pattern since, although frequently magnetic, they are generally less dense than typical metamorphic lithologies.

Surface mapping in this area (Kellogg, 1993 a,b; Vuke, 2013), indicates the presence of amphibolites as well as irregular ultramafic bodies. Intriguingly, these rocks are associated with zones of ductile deformation, the Crooked Creek mylonite and Mirror Lake shear zone, as well as metasedimentary rocks, migmatic gneiss, and leucogranites (Kellogg and Williams, 2000; Kellogg, 1993 a,b), features frequently associated with orogenesis and crustal scale tectonism (Meen, 1992; Searle, 2013). The oldest (~3.2 to 3.3 Ga) rocks, formed during a period of extensive generation of felsic crust, have trace element and isotope signatures consistent with formation in an arc environment (Mogk and

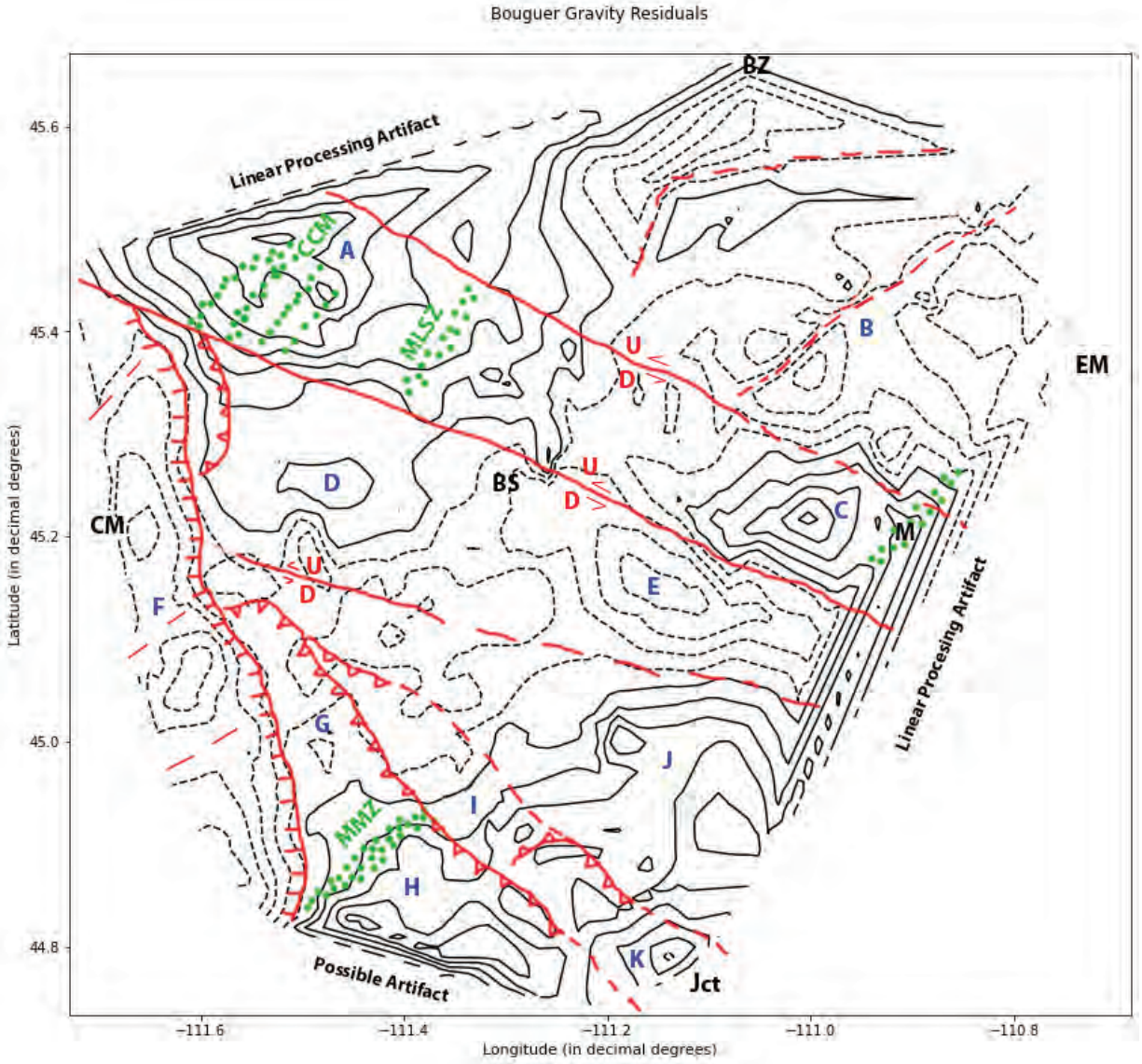

Figure 2. Primary geological features related to gravity anomalies, contour interval = 5 mGal. Solid red lines, known faults; dashed red lines, inferred faults; blue letters, gravity anomalies discussed separately in text; green dots, mylonite zones (MMR, Madison mylonite zone; CCR, Crooked Creek mylonite; MLSZ, Mirror Lake shear zone). Localities on map: BS, Big Sky meadow village; BZ, Bozeman; CM, Cameron; EM, Emigrant; Jct, Junction of highway US 287 and US 191; M, Miner.

others, 2020). Subsequently, during the Paleoproterozoic, crust in the Spanish Peaks underwent intense penetrative deformation and metamorphism up to granulite facies (Mogk and others, 2020; Spencer and Kozak, 1975). Rocks in the Gallatin Canyon area experienced intense ductile shearing and migmatization most likely during the ~2.45 Ga Beaverhead orogeny based on the age of anatectic melting of older gneiss (Mogk and others, 2020; Mueller and others, 2011). Regional deformation also occurred during the ~1.7 Ga Big Sky orogeny (Harms and Baldwin, 2021, 2023), possibly including strike-slip motion of the Spanish Peaks and other northwest-trending fault zones (Garihan and others, 1983).

To the northwest, within the Tobacco Root Range, along the trend of the Spanish Peaks/Bismarck fault system is another mafic sequence, the Sphuler Peak metamorphic suite (SPMS). The SPMS has been interpreted as a tectonically emplaced piece of ocean crust or island arc associated with the ~1.7 Ga Big Sky orogenic event (Harms and Baldwin, 2023; Harms and others, 2004). The Cherry Lake gravity anomaly in the Spanish Peaks may represent an older tectonically emplaced terrane. Along trend to the southeast, a similar, though less pronounced, gravity high occurs centered on Tom Miner Basin (fig. 2, area C), also associated with mylonite (Erslev, 1988; Vuke and others, 2007). These results indicate the Spanish Peaks fault zone has a long history as a crustal-scale discontinuity reaching far back into the Archean. Given its orientation parallel to the southeast-verging Big Sky orogeny (Burger, 2004), it likely accommodated Proterozoic deformation by strike-slip motion. This interpretation is consistent with prior estimates of ~9 km of Precambrian left-lateral movement on the Spanish Peaks fault (Garihan and others, 1983).

The middle portion of the Spanish Peaks fault lacks a

pronounced gravity signature compared to its northwest and southeast sections; however, linear low-amplitude gravity highs correspond to the surface presence of predominately felsic gneiss (Vuke, 2013). Perpendicular to this section of the Spanish Peaks fault, a northeast trend of gravity lows exits the sedimentary foreland of the Hilgard thrust system and bifurcates, with one branch headed east toward Emigrant and the other north towards the Gallatin Valley. Directly west of Emigrant, a pronounced gravity low occurs (fig. 2, area B), buried beneath Absaroka volcanic flows. This is interpreted as a remnant of the Cretaceous interior seaway possibly reactivated as a Cenozoic basin. The long linear gravity discontinuity along the northwest boundary of area B, between Palisades and Haylite Peak (fig. 3, localities 2, 3), suggests fault control or an incised valley rim. The apparent ponding of Eocene volcanics in area B also suggests the presence of a preexisting basin. A moderate gravity high between area B and the Gallatin Valley corresponds to the outcrop area of high-density Archean and Paleozoic lithologies (Vuke and others, 2007). The southeast-bounding fault of the Gallatin Valley appears to correspond to the subsurface extension of this basement block—buried beneath younger alluvial material.

South of the Spanish Peaks fault, predominately low gravity is observed, corresponding to the surface outcrop of low-density, predominately marine Cretaceous sediments (Kellogg and Williams, 2000; Vuke, 2013). This area was, pre-orogeny, the western shoreline of the Cretaceous interior seaway (Cobban and others, 1994; Vuke, 1984). Later, during Cretaceous compression, this area was transformed into the foreland basin of the Hilgard thrust system (Kellogg and others, 1995; Tysdal, 1986; Tysdal and others, 1986). The Hilgard thrust belt deposited thick alluvial and fluvial sediments, such as the Sphinx conglomerate, on top of the marine rocks (Tysdal, 1990). Igneous intrusives, localized at the junction of the Hilgard system and the Spanish Peaks fault, formed dacite laccoliths, dikes and sills within the Cretaceous sedimentary basin (Kellogg and Harlan, 2007; Tysdal, 1990; Vuke, 2013). The largest area of late Cretaceous intrusives occurs directly west of Big Sky in the Lone Mountain intrusive suite (fig. 2, area D). These dense magnetic igneous rocks account for the triangular gravity high whose corners roughly correspond to Lone Peak, Fan Mountain, and Cedar Mountain (fig. 3, localities 5–7). This area also corresponds to a pronounced mid-crustal aeromagnetic high (Wilson and others, 2005), which together with the gravity data suggests an extensive subsurface magma chamber beneath the surface exposures of dacitic sills (fig. 4, profile B–B', fig. 5, profile D–D'). The Spanish Peaks fault zone likely served as a conduit for magma sourced from the Tobacco Root batholith, which the Bismarck fault's northwestern extension intersects (Schmidt and others, 1990). Cogenetic northwest-trending faults in southwestern Montana performed a similar role throughout the Cenozoic, especially during Eocene Absaroka volcanism (Chadwick, 1970, 1981).

The middle of the southern section of the gravity residual data is dominated by negative values corresponding to thick deposits of low-density pre- and syn-tectonic sedimentary rocks (Kellogg and Williams, 2000). However, this larger basin is divided into a series of subbasins separated by moderate gravity highs. Moreover, the two principal Cretaceous high-angle reverse faults in this area, the Spanish Peaks and Buck Creek faults, appear to have influenced the development of these subbasins. In particular the prominent gravity low (fig. 2, area E) west of Cinnamon Mountain (fig. 6, locality 11) is bounded to the north and south, respectively, by these two faults (fig. 4, profile B–B', fig. 5, profile E–E'). This suggests that these preexisting structures influenced the development of the Cretaceous marine deposystem even before the onset of active deformation.

Along the west side of the map, the gravity pattern is dominated by the paired Hilgard thrust system and the parallel Madison Range extensional fault system. These two fault systems with opposite senses of motion are linked by the fact that the Madison Range fault zone has reactivated footwall ramps of the Hilgard thrust system as extensional fault planes, thereby stranding the easternmost sliver of the thrust sheet (fig. 2, area G, fig. 4, profile C–C') along the crest of the Madison Range front (Kellogg and others, 1995; Tysdal, 1986; Tysdal and others, 1986). The deep half-graben Madison Valley is clearly indicated by the negative north–south gravity anomaly along the western side of the map area (fig. 2, area F). The thin remnants of the thrust sheet correspond to a less obvious parallel line of low to moderate positive gravity residuals. Between Sphinx Mountain and Koch Peak (fig. 6, localities 9, 12) the thrust sheet is largely removed, most likely downdropped to the valley base (Kellogg and others, 1995; Schofield, 1981), corresponding to a local gravity low. Interestingly, directly to the west of this area a deep subbasin, as indicated by a prominent gravity low, occurs south of Cameron—possibly influenced by buried Precambrian crustal structures.

Evidence of Proterozoic northeast-trending structures is easily seen directly to the south of this area in the Madison mylonite zone (MMZ). This Proterozoic tectonic feature (Sumner and Erslev, 1988) is exposed south of Hilgard Peak (fig. 6, locality 13) and corresponds to the boundary of a northeast-trending block of higher density Precambrian and Paleozoic rocks (fig. 2, areas H–J). On trend to the northeast, Precambrian mylonitic rocks also outcrop in the Miner area (Erslev, 1988; Vuke and others, 2007). It should be noted, however, that these rocks, exposed north of the Spanish Peaks fault, are likely laterally displaced relative to rocks south of the fault, so a direct correlation is problematic. Cretaceous strike-slip movement along the Bismarck/

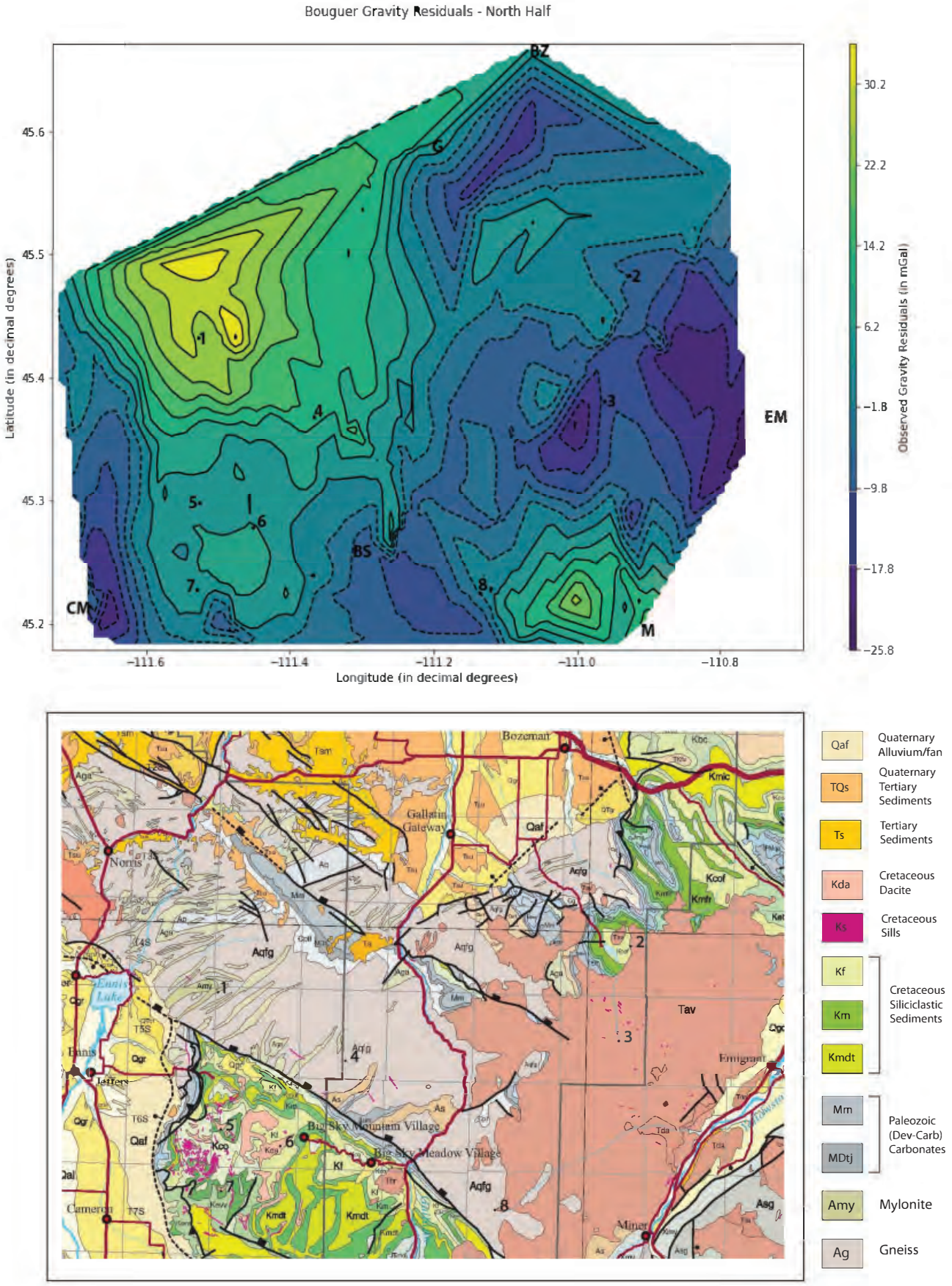

Figure 3. Top: north half of Bouguer residual map of Madison and Gallatin Ranges and adjacent areas, contour interval = 4 mGal. Bottom: geology modified from Vuke and others (2007). Localities on map: BS, Big Sky meadow village; BZ, Bozeman; CM, Cameron; EM, Emigrant; G, Gallatin Gateway; M, Miner. Topographic features: 1, Cherry Lake; 2, Palisades; 3, Hyalite Peak; 4, Gallatin Peak; 5, Fan Mountain; 6, Lone Mountain; 7, Cedar Mountain; 8, Eaglehead Mountain.

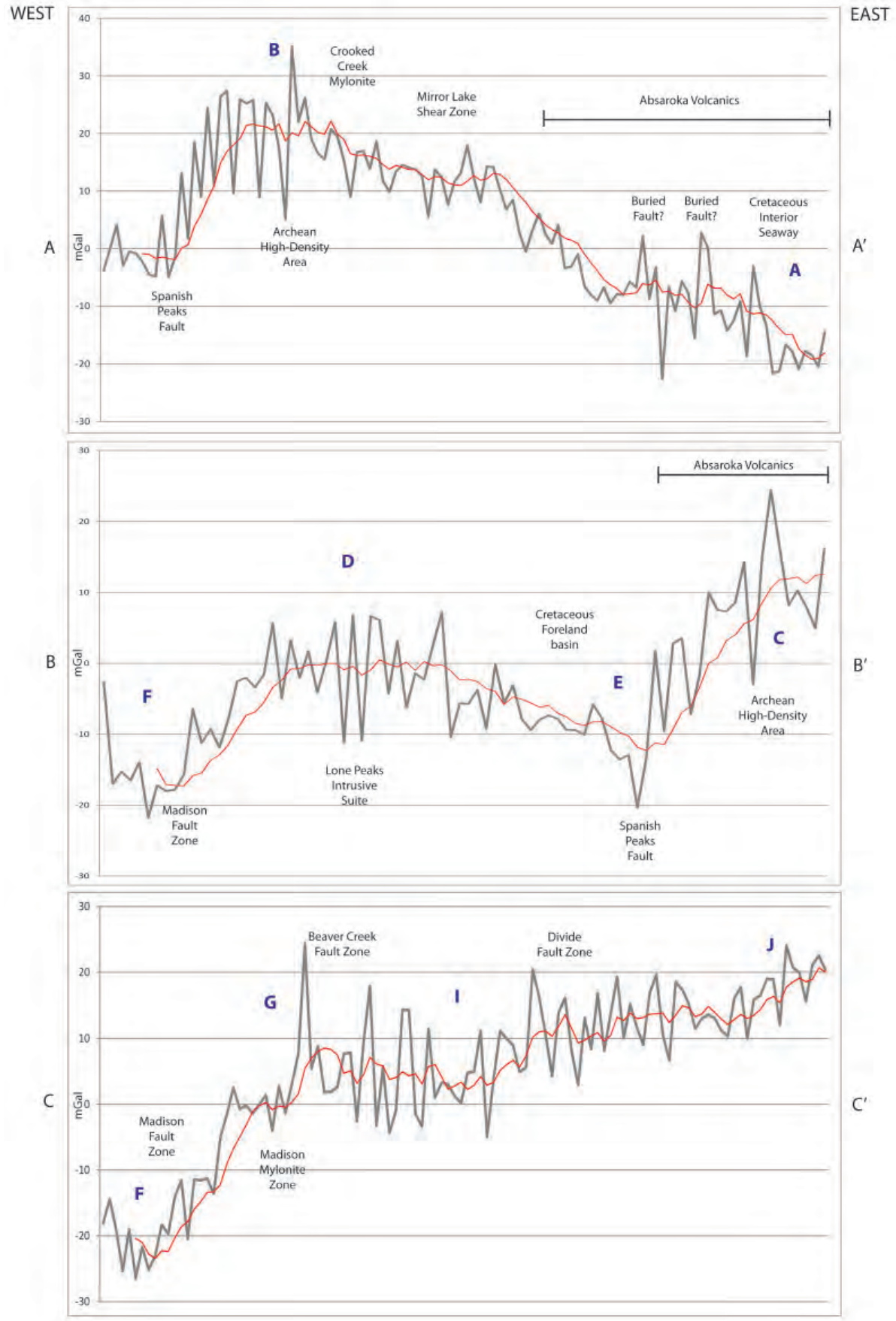

Figure 4. East to west gravity residual profiles in mGal (see fig. 1 for location of profiles). Intersections of selected known and projected geological features with associated gravity signals are shown. Blue letters refer to gravity residual anomalies in figure 2. Moving average shown in red in order to indicate average trend of gravity data. Data points within an approximately 0.02 decimal degrees of latitude window included within each profile line.

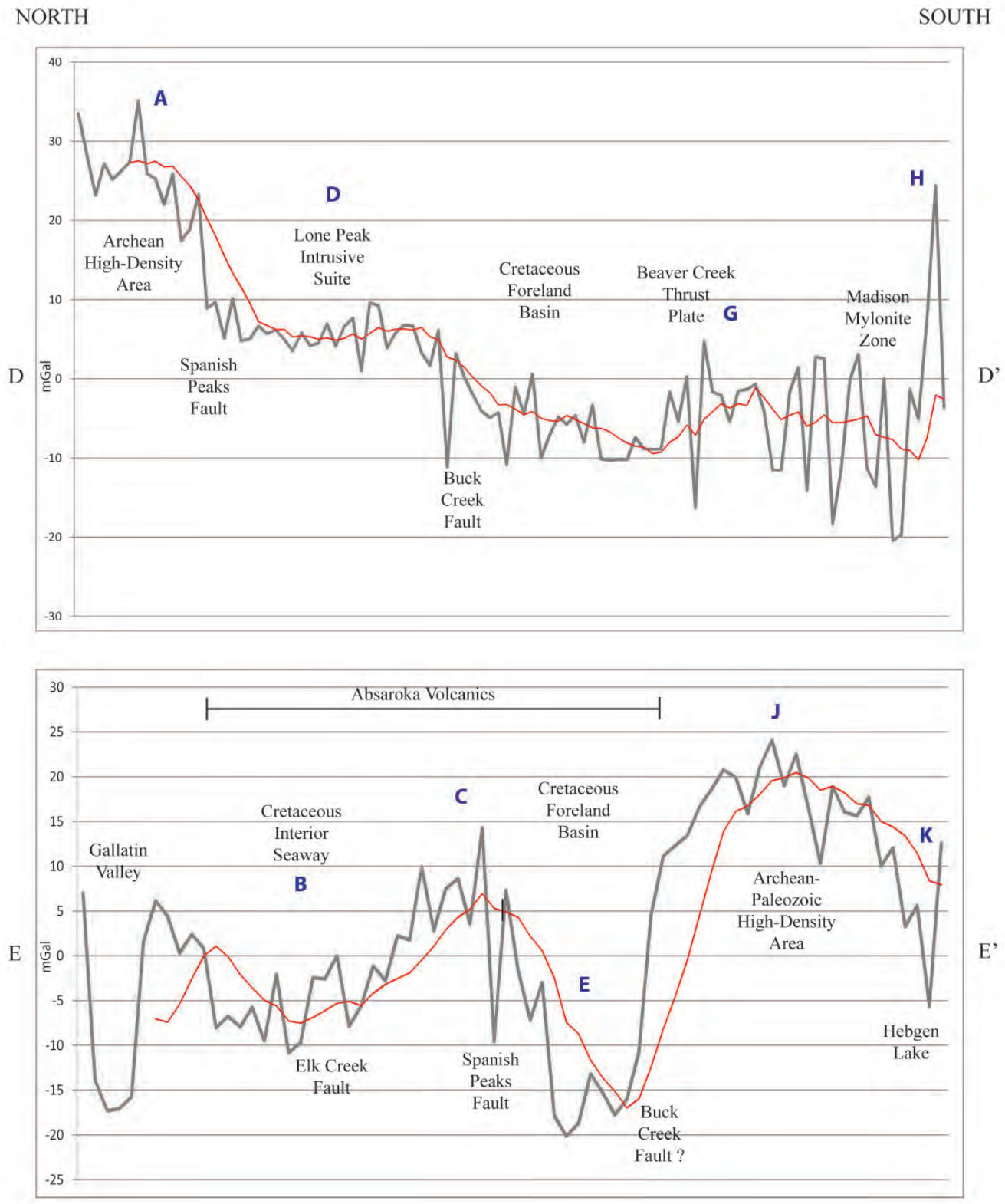

Figure 5. North to south gravity residual profiles in mGal (see fig. 1 for location of profiles). Intersections of selected known and projected geological features with associated gravity signals are shown. Blue letters refer to gravity residual anomalies in figure 2. Moving average shown in red in order to indicate average trend of gravity data. Data points within an approximately 0.02 decimal degrees of longitude window included within each profile line.

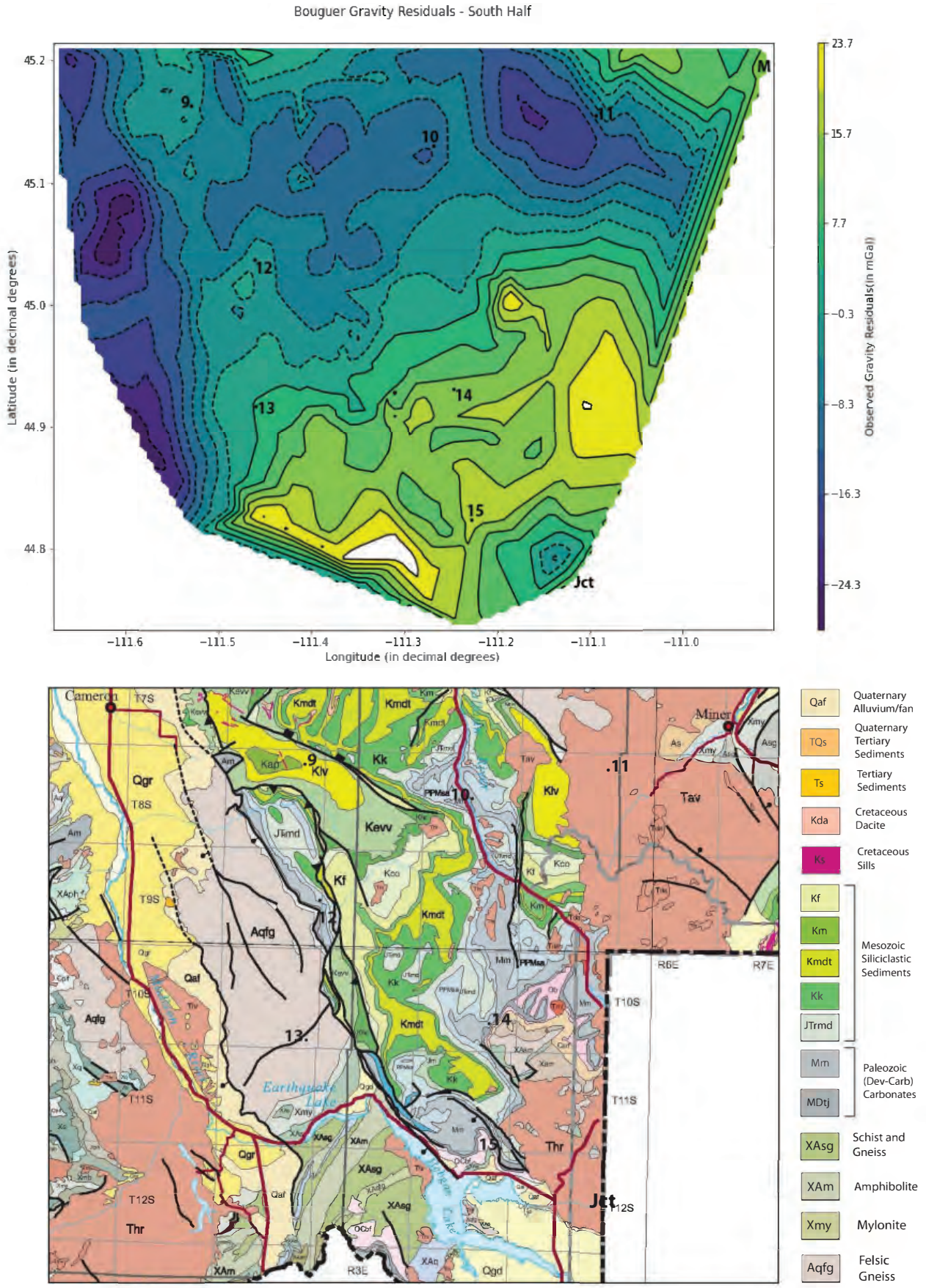

Figure 6. Top: South half of Bouguer residual map of Madison and Gallatin Ranges and adjacent areas, contour interval = 4 mGal. Bottom: Geology modified from Vuke and others (2007). Localities on map: BS, Big Sky meadow village; BZ, Bozeman; CM, Cameron; EM, Emigrant; Jct, Junction of highway US 287 and US 191; M, Miner. Topographic features: 9, Sphinx Mountain; 10, Ramshorn Peak; 11, Cinnamon Mountain; 12, Koch Mountain; 13, Hilgard Peak; 14, Sage Mountain; 15, Hebgen Mountain.

Spanish Peaks/Gardner fault system is ~3 to 5 km (Schmidt and Garihan, 1983) plus an estimated 9 km of Precambrian offset (Garihan and others, 1983). Strike-slip displacement along the more than 30 other Laramide northwest-trending faults is variable, ranging between <1 km and more than 10 km (Schmidt and Garihan, 1983), so the cumulative offset of older rocks separated by multiple faults is significant.

The gravity high bounded by the MMZ is abruptly terminated to the northeast, likely by the subsurface extension of the Buck Creek fault. Between Sage Mountain and Hebgen Peak (fig. 6, localities 14, 15) a section of highly deformed Cretaceous rocks occurs (O'Neill and Christiansen, 2002). The pattern of deformation suggests that this basement block (fig. 2, area J) acted as an immobile buttress during movement of the southern Hilgard thrust. A similar pattern of complex interaction between mobile belts and preexisting structures is observed throughout southwestern Montana (Schmidt and Garihan, 1983). The Beaver Creek and Divide thrust faults, terminated at the surface by the Red Rock normal fault, can be traced southward into the subsurface as linear gravity discontinuities. These two faults appear to bound the pronounced gravity low (fig. 2, area K) located beneath the eastern portion of Hebgen Lake.

CONCLUSIONS

The results of this study lead to the following conclusions:

(A) The principal tectonic features observed in the surface geology are also the primary influence on the pattern of the Bouguer residual anomalies. Moreover, the continuation of these surface faults can frequently be observed in the subsurface as linear patterns of gravity residuals. This is particularly useful for interpretation in the eastern and southern parts of the study area where the surface geology is obscured by volcanic flows.

(B) Cenozoic extensional basins, as well as the Cretaceous foreland, are broken into subbasins as indicated by localized gravity minima. Control by preexisting, in some cases demonstrably Precambrian, structures is suggested by the fact that several of these subbasins appear bounded by linear gravity discontinuities associated with known fault lines. Differential subsidence along Precambrian faults may have influenced sedimentary basin development even before the onset of Cretaceous deformation.

(C) The major thrust plates of the Hilgard thrust system, such as the Beaver Creek and Kirkwood plates, are identified as broad gravity maxima, especially where they contain high-density Precambrian metamorphic and Paleozoic carbonates in their hanging walls. Footwall synclines, composed predominately of Mesozoic clastic sediments, form less conspicuous paired gravity lows.

(D) The Lone Peak igneous intrusive system was fed by a magma chamber delineated by the triangular gravity high beneath Lone Peak, Fan Mountain, and Cedar Mountain. Given its proximity, the likelihood exists that the Spanish Peaks fault acted as a conduit for magma injection, possibly from the Tobacco Root batholith. During the Eocene, regional northwest-trending fault zones served a similar function, guiding emplacement of magma into southwestern Montana from the Absaroka volcanic field.

(E) The localization of prominent gravity lows underneath extensive overburden of Absaroka volcanics, especially west of Emigrant, suggests that these volcanics "ponded" in areas of preexisting basins. The occurrence of linear gravity features bounding several of these buried structures indicate they were either fault controlled, possibly reactivating Precambrian faults, or that they represent the rims of an incised valley system.

(F) Closely associated gravity highs and short-wavelength magnetic anomalies in the Archean basement, especially north of the Spanish Peaks fault, indicate the presence of high-density mafic material encased within more typical metamorphic lithologies. The occurrence of pronounced gravity maxima, associated with mylonite zones and amphibolite outcrops, along the Bismarck–Spanish Peaks–Gardiner fault zone seems significant. Northwest-trending crustal discontinuities in southwestern Montana likely have an Archean orogenic ancestry and a history of multiple reactivation from Precambrian to recent time.

(G) A discrepancy exists between deep-seated, throughgoing, northeast trending features seen on long wavelength aeromagnetic data, the surface geology and the shallow gravity anomalies of this study. In particular, surface mylonitic rocks were displaced laterally, probably multiple times, by strike-slip motion along northwest trending faults such as the Spanish Peaks fault. The original configuration of the Precambrian geology, before Cretaceous and Proterozoic lateral displacement, needs to be restored before accurate interpretations of Archean tectonic structures can be made.

ACKNOWLEDGMENTS

This paper was improved by the suggestions of reviewer Michael Stickney of the Montana Bureau of Mines and Geology, to whom I extend my thanks. I would also like to thank Reed Lewis of the University of Idaho and Alan English of the Montana Bureau of Mines and Geology for their editorial assistance. The initial processing of the raw gravity data was performed by the United States Geological Survey.

REFERENCES

Burger, H., 2004, General geology and tectonic setting of the Tobacco Root Mountains, *in* Brady, J., Burger, H., Cheney, J., and Harms, T., eds., Precambrian geology of the Tobacco Root Mountains, Montana: Geological Society of America Special Paper 377, p. 1–14.

Chadwick, R., 1970, Belts of eruptive centers in the Absaroka–Gallatin volcanic province, Wyoming–Montana: Geological Society of America Bulletin, v. 81, p. 267–274.

Chadwick, R., 1981, Chronology and structural setting of volcanism in southwestern and central Montana: Montana Geological Society 1981 Field Conference Guidebook, southwestern Montana, p. 301–310.

Cobban, W., Merewether, E., Fouch, T., and Obradovich, J., 1994, Some Cretaceous shorelines in the western interior of the United States, *in* Caputo, M., Peterson, J., and Franczyk, K., eds., Mesozoic systems of the Rocky Mountain region, USA: Rocky Mountain section–SEPM, p. 393–413.

Erslev, E., 1988, Precambrian geology and ductile normal faulting in the southwest corner of the Beartooth Uplift, Montana, *in* Bartholomew, M., Hyndman, D., Mogk, D., and Mason, R., eds., Basement Tectonics 8: Characterization and comparison of ancient and Mesozoic continental margins, p. 313–322.

Garihan, J., Schmidt, C., Young, S., and Williams, M., 1983, Geology and recurrent movement history of the Bismark–Spanish Peaks–Gardiner fault system, southwest Montana, *in* Lowell, J., and Gries, R., eds, Rocky Mountain foreland basins and uplifts: Rocky Mountain Association of Geologists, p. 295–314.

Harms, T., and Baldwin, J., 2021, Paleoproterozoic geology of Montana, *in* Metesh, J., and Vuke, S., eds, Geology of Montana, Volume 1—Geologic history: Montana Bureau of Mines and Geology Special Publication 122, 37 p.

Harms, T., and Baldwin, J., 2023, Paleoproterozoic geology of SW Montana: Implications for the paleogeography of the Wyoming craton and for the consolidation of Laurentia, *in* Whitmeyer, M., Kellett, D., and Tikoff, B., eds., Laurentia: Turning points in the evolution of a continent: Geological Society of America Memoir 220, p. 65–79.

Harms, T., Brady, J., Burger, H., and Cheney, J., 2004, Advances in the geology of the Tobacco Root Mountains, Montana, and their implications for the history of the northern Wyoming province, *in* Brady, J., Burger, H., Cheney, J., and Harms, T., eds., Precambrian geology of the Tobacco Root Mountains, Montana: Geological Society of America Special Paper 377, p. 227–243.

Hassemer, J., and Kaufmann, H., 1984, Principal facts for gravity stations in and near the Madison and Gallatin divide roadless areas, Montana: United States Geological Survey Open-File Report 84-847, 31 p.

Kellogg, K., 1993a, Geologic map of the Ennis Lake quadrangle, Madison County, Montana: United States Geological Survey Geologic Quadrangle Map GQ-1729.

Kellogg, K., 1993b, Geologic map of the Cherry Lake quadrangle, Madison County, Montana: United States Geological Survey Geologic Quadrangle Map GQ-1725.

Kellogg, K., and Harlan, S., 2007, New $^{40}Ar/^{39}Ar$ age determinations and paleomagnetic results bearing on the tectonic and magmatic history of the northern Madison Range and Madison Valley region, southwestern Montana, U.S.A.: Rocky Mountain Geology, v. 42, no.2, p. 157–174.

Kellogg, K., and Williams, V., 2000, Geologic map of the Ennis 30' x 60' quadrangle, Madison and Gallatin Counties, Montana and Park County, Wyoming: United States Geological Survey Geologic Investigations Series I-2690.

Kellogg, K., Schmidt, C., and Young, S., 1995, Basement and cover-rock deformation during Laramide contraction in the northern Madison Range (Montana) and its influence on Cenozoic basin formation: American Association of Petroleum Geologists Bulletin, v. 79, no. 8, p. 1117–1137.

LaFehr, T., and Nabighian, M., 2012, Fundamentals of gravity exploration: Society of Exploration Geophysicists Geophysical Monograph Series, no. 17, 218 p.

Mankinen, E., Hildenbrand, T., Zientek, M., Box, S., Bookstrom, A., Carlson, M., and Larsen, J., 2004, Guide to geophysical data for the northern Rocky Mountains and adjacent areas, Idaho, Montana, Washington, Oregon and Wyoming: United States Geological Survey Open-File Report 2004-1413, 34 p.

Meen, J., 1992, Evidence for the amalgamation of Archean oceanic and continental blocks to form the Beartooth Plateau, *in* Bartholomew, M., Hyndman, D., Mogk, D., and Mason, R., eds., Basement Tectonics 8: Characterization and comparison of ancient and Mesozoic continental margins, p. 299–311.

Mogk, D., Mueller, P., and Henry, D., 2020, The Archean geology of Montana, *in* Metesh, J., and Vuke, S., eds, Geology of Montana, Volume 1—Geologic history: Montana Bureau of Mines and Geology Special Publication 122, 45p.

Mueller, P., Wooden, J., and Mogk, D., 2011, 2450 Ma metamorphism recorded in 3250 Ma gneisses, Gallatin Range, Montana: Northwest Geology, v. 41, p. 63–70.

O'Neill, J., and Christiansen, R., 2002, Geologic map of the Hebgen Lake 30' x 60' quadrangle, Beaverhead, Madison and Gallatin Counties, Montana, Park and Teton Counties, Wyoming and Clark and Fremont Counties, Idaho: Montana Bureau of Mines and Geology Open-File Report 464.

Schofield, J., 1981, Structure of the Centennial and Madison Valleys based on gravitational interpretation: Montana Geological Society 1981 Field Conference Guidebook, southwest Montana, p. 275–283.

Schmidt, C., and Garihan, J., 1983, Laramide tectonic development of the Rocky Mountain in southwestern Montana, *in* Lowell, J., and Gries, R., eds, Rocky Mountain foreland basins and uplifts: Rocky Mountain Association of Geologists, p. 271–294.

Schmidt, C., Smedes, H., and O'Neill, J., 1990, Syncompressional emplacement of the Boulder and Tobacco Root batholiths

(Montana-USA) by pull-apart along old fault zones: Geological Journal, v. 25, p. 305–318.

Searle, M., 2013, Colliding continents: A geological exploration of the Himalaya, Karakoram and Tibet: Oxford University Press, 438 p.

Sims, P., O'Neill, J., Bankey, V., and Anderson, E., 2004, Precambrian basement geologic map of Montana—An interpretation of aeromagnetic anomalies: United States Geological Survey Scientific Investigations Map 2829, 14 p.

Spencer, E., and Kozak, S., 1975, Precambrian evolution of the Spanish Peaks area, Montana: Geological Society of America Bulletin, v. 86, p. 785–792.

Sumner, W., and Erslav, E., 1988, Late Archean thin-skinned thrusting of the Cherry Creek metamorphic suite in the Henry's Lake Mountains, southern Madison Range, Montana and Idaho, *in* Lewis, S., and Berg, R., eds., Precambrian and Mesozoic plate margins: Montana Bureau of Mines and Geology Special Publication 96, p. 69–79.

Tysdal, R., 1986, Thrust faults and back thrusts in Madison Range of southwestern Montana foreland: American Association of Petroleum Geologists Bulletin, v. 70, no. 4, p. 360–376.

Tysdal, R., 1990, Geologic map of the Sphinx Mountain quadrangle and adjacent parts of the Cameron, Cliff Lake and Hebgen Dam quadrangles, Montana: United States Geological Survey Miscellaneous Investigations Series Map I-1815.

Tysdal, R., Marvin, R., and DeWitt, E., 1986, Late Cretaceous stratigraphy, deformation, and intrusion in the Madison Range of southwestern Montana: Geological Society of America Bulletin, v. 97, p. 859–868.

United States Geological Survey, 1982, Aeromagnetic map of the Madison Range area, Montana: Open File Report OFR 82-946.

Vuke, S., 1984, Depositional environments of the early Cretaceous western interior seaway in southwestern Montana and the northern United States, *in* Stott, D., and Glass, D., eds., The Mesozoic of middle North America: Canadian Society of Petroleum Geologists Memoir 9, p. 127–144.

Vuke, S., 2013, Geologic map of the Fan Mountain, Lone Mountain, and Gallatin Peak 7.5' quadrangles, Madison Range, Madison and Gallatin Counties, Montana: Montana Bureau of Mines and Geology Open-File Report 633.

Vuke, S., Porter, K., Lonn, J., and Lopez, D., 2007, Geologic map of Montana: Montana Bureau of Mines and Geology Geologic Map 62.

Wetmore, P., Conner, C., Hastings, M., Mack, B., Gallant, E., Conner, L., Fallon, T., Nassir, R., and Malservisi, R., 2021, Gravity anomalies and alluvial fan areas of the Lost River Valley and implications for basin architecture and the dip of the Lost River Fault: Northwest Geology, v. 50, p. 23-49.

Wilson, A., Hammarstrom, J., and Van Gosen, B., 2005, Mineral and energy resource assessment of the Gallatin National Forest (exclusive of the Absaroka-Beartooth study area) in Gallatin, Madison, Meagher, Park and Sweet Grass counties, south-central Montana: United States Geological Survey Professional Paper 1654, 194 p.

AGE OF CARBONATITE-RELATED REE-NB MINERALIZATION IN THE SHEEP CREEK DISTRICT, SOUTHERN RAVALLI COUNTY, MONTANA

Christopher H. Gammons,[1] Sarah Risedorf,[1] Michael Gary,[1] Holly Stein,[2] and Jay M. Thompson[3]

[1]*Geological Engineering, Montana Technological University, Butte, Montana*
[2]*AIRIE, Applied Isotope Research for Industry and Environment, Fort Collins, Colorado*
[3]*U.S. Geological Survey, USGS LTRACE Laboratory, Denver, Colorado*

INTRODUCTION

Carbonatite-related REE-Nb mineralization in southern Ravalli County, Montana, was first described by Crowley (1960) and Heinrich and Levinson (1961). Over 30 narrow, discontinuous carbonate lodes occur in a ~10 km^2 area centered on Sheep Creek (fig. 1), a tributary to the headwaters of the West Fork of the Bitterroot River (WFBR). The deposits are contained in a belt that extends to the southeast into the Mineral Hill district of Lemhi County, Idaho (Kaiser, 1956; Anderson, 1960; Spence, 1984). Although first explored for columbite, the districts are now gaining attention for their locally high-grade REE mineralization. Previous workers (e.g., Crowley, 1960) proposed at least three contrasting ideas as to the origin of the REE-Nb-rich carbonate lodes: (1) carbonatite magmas; (2) hydrothermal replacement deposits; and (3) metamorphic segregation. The present authors prefer the term "carbonatite-related," in part to sidestep the debate as to whether the lodes formed by crystallization of a magma, or by precipitation from hydrothermal (or "carbothermal") fluids.

Gammons (2020) presented a reconnaissance mineralogy survey of samples collected on the dumps of the historic Crowley #1 and #3 adits (fig. 1A). Risedorf (2023) sampled all of the known carbonate bodies in the Sheep Creek district, and performed additional microscopy using XRD, automated SEM-EDS, and electron probe microanalysis (EPMA), as well as analysis of stable isotopes of matrix carbonate minerals. Gary (in progress) is examining the chemistry and mineralogy of heavy mineral separates of stream sediments in the upper WFBR watershed. The combined studies show that the deposits of Sheep Creek contain a complex assemblage of REE-bearing minerals, including monazite, allanite, ancylite, REE-F-carbonates (bastnaesite, parisite, synchysite), and trace Nb-REE minerals (aeschynite, fersmite). Sulfides, including molybdenite,

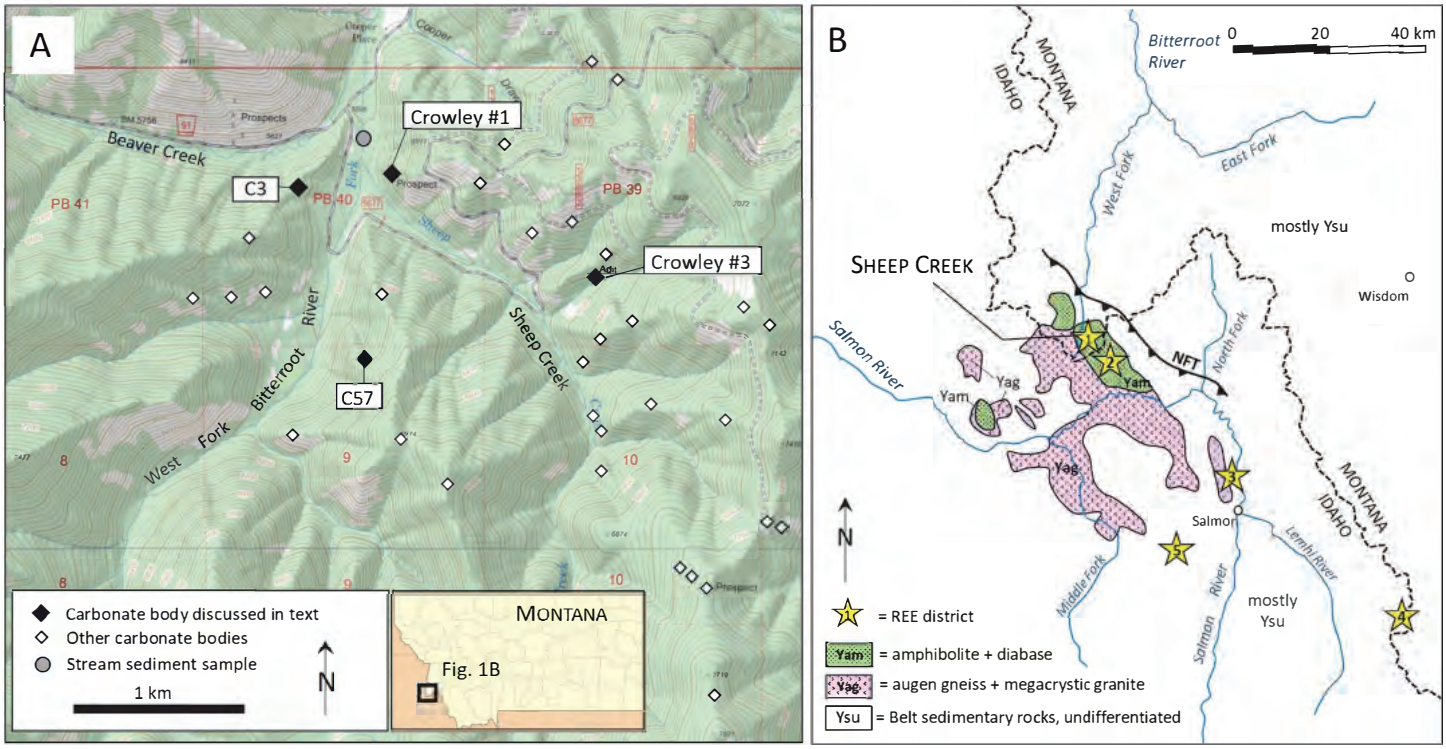

Figure 1. (A) Map of the Sheep Creek area showing the locations of carbonate bodies (from Risedorf, 2023) and locations mentioned in the text. (B) Simplified regional geology of the Sheep Creek area showing the distribution of 1.37 Ga granite/augen gneiss (Yag), diabase/amphibolite (Yam), undifferentiated Belt-aged sedimentary rocks (Ysu) and younger cover rocks, and REE-rich mining districts: (1) Sheep Creek; (2) Mineral Hill; (3) Diamond Creek; (4) Lemhi Pass; (5) Idaho Cobalt Belt. NFT, North Fork thrust fault.

are sparsely disseminated through the carbonate matrix, as are Fe-Ti oxides. The mineralization is contained within narrow, tabular bodies of calcite and dolomite **(**± barite, apatite, actinolite, quartz) that are crudely conformable to the foliation in the host meta-igneous rocks. The latter include augen gneiss, amphibolite, and relatively undeformed diabase (fig. 1B). The host rocks have been dated by zircon U-Pb and whole-rock Rb-Sr methods to ~1.37–1.38 Ga (Evans and Zartman, 1990; Doughty and Chamberlain, 1996). The only previously published dates for the REE mineralization are in the compilation of Jaffe and others (1959), who reported Pb-alpha dates of 90 to 99 Ma for three monazite samples from the Sheep Creek/Mineral Hill area. More recently, a set of monazite Th-Pb and molybdenite Re-Os dates were obtained on samples collected by Gammons (2020), Risedorf (2023), and Gary (in progress). The purpose of this short paper is to summarize the recent dates and discuss their implications.

METHODS

A polished plug containing a 0.5 cm monazite crystal from the dump at the Crowley #3 adit (sample SC-2018-35) was analyzed (May, 2019) by multiple collector laser ablation ICP-MS for U-Th-Pb geochronology at the University of California at Santa Barbara (UCSB). The sample contained negligible U (0 to 15 ppm) but sufficient ^{232}Th (0.6 to 1.3 wt%) and radiogenic ^{208}Pb (150 to 625 ppm) for dating. In February 2023, two samples of coarse-grained (>1 cm) monazite from the Crowley #1 and #3 adits (figs. 2A, 2B) were analyzed by LA-ICP-MS at the USGS LTRACE Laboratory in Denver. The measured ^{232}Th/^{208}Pb ratios were corrected for minor amounts of common lead by applying a ^{204}Pb correction and assuming a Stacey and Kramers (1975) model Pb composition at 100 Ma to yield ages with an approximate uncertainty of 2% (2 sigma). In the same session, a polished mount was analyzed that contained a non-magnetic, heavy-mineral fraction of stream sediment sourced from the WFBR downstream of the confluence of Sheep Creek (fig. 1). This sample, which was dominated by ilmenite, contained over 30 grains of monazite, as well as several grains of allanite and columbite. Separately, a hand sample of medium-grained molybdenite in a calcite–apatite matrix (fig. 3A), collected from the dump at Crowley #1 adit, was sent to AIRIE for Re-Os dating. A second molybdenite-rich sample collected from the C57 carbonate body (figs. 2C, 3B) by Risedorf (2023) was also sent to AIRIE. Both molybdenite samples were fresh, with no evidence of oxidation or weathering, and each sample gave a robust Re-Os date that replicated with a second analysis within two-sigma uncertainties.

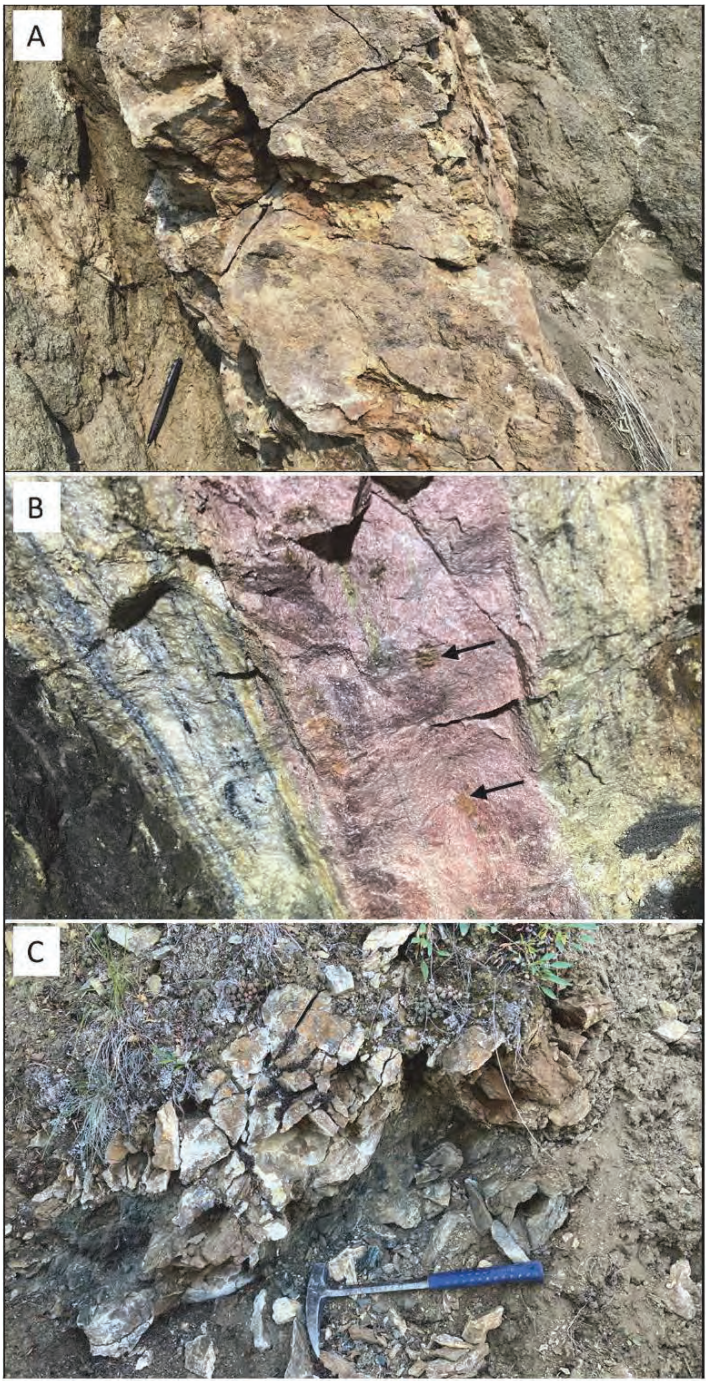

Figure 2. Field photographs of carbonate bodies sampled in this study. (A) Outcrop at the Crowley #1 adit. Crumbly rock on either side of the carbonate is biotite-rich fenite; (B) exposure of vein-dike at the Crowley #3 adit. The photo, roughly 0.6 m across, was taken underground in workings that are now inaccessible. Pink is ancylite-rich; arrows point to centimeter-sized monazite grains; (C) outcrop of C57 carbonate body (tan) with fenitized amphibolite (dark, crumbling). The molybdenite sample was collected from a shallow pit less than 20 m from this location.

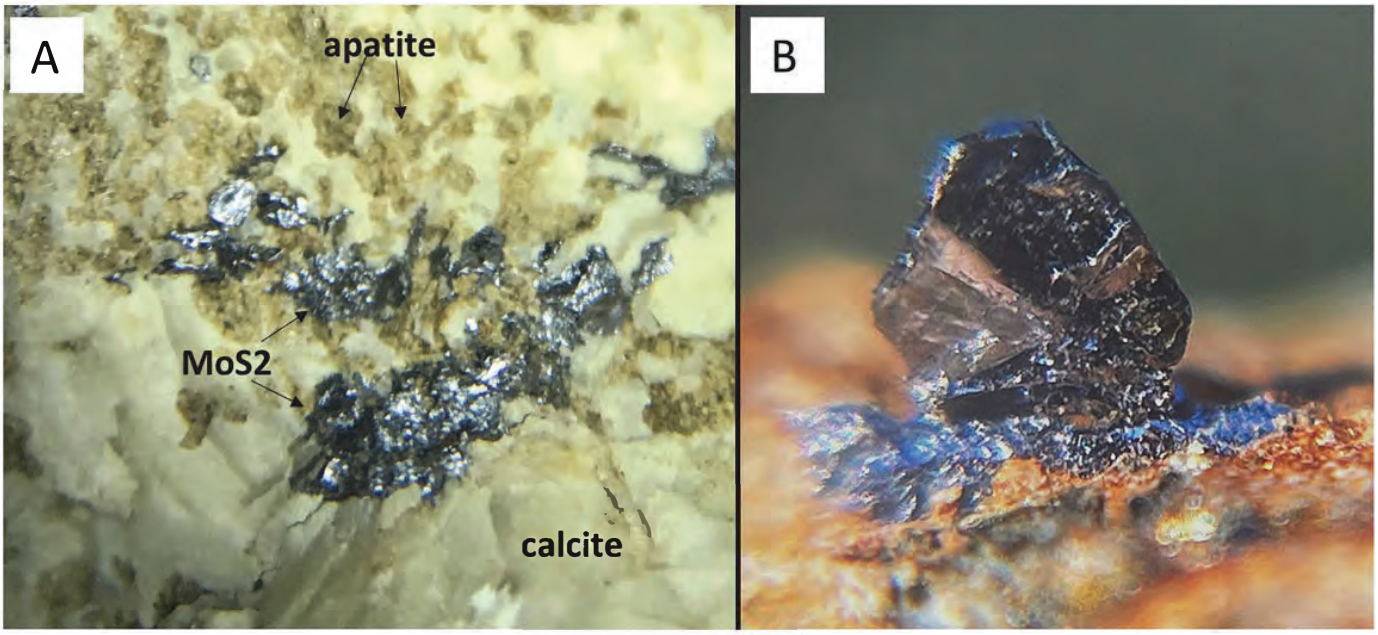

Figure 3. Photographs of dated molybdenite. (A) MoS2 intergrown with apatite and calcite from Crowley #1 adit, width of view roughly 1 cm; (B) euhedral molybdenite crystal (2 mm diameter) from C57 carbonatite body perched on a substrate of ferroan dolomite.

RESULTS

Figure 4 summarizes the ages obtained in this study. Each of the monazite samples analyzed by laser ablation shows a >60 m.y. range in ages. Each sample has a similar maximum age (~145–149 Ma) and then an uneven distribution to lower ages with clustering of dates at 110–125 Ma and 80–90 Ma. In general, the oldest ages were obtained from ablation spots near the center of the larger monazite grains (fig. 5). This was particularly true for the Crowley #1 sample (fig. 5A). Small, outlying monazite grains tended to give younger ages (e.g., <100 Ma), although there are exceptions. Analyses of 12 separate monazite grains from the WFBR stream sediment sample produced a similar spread of ages, with two older dates at 161 and 191 Ma. The Re-Os analyses of molybdenites from separate carbonate bodies gave distinctly different ages of 147.9 ± 0.6 and 108.0 ± 0.4/109.8 ± 0.4 Ma (the latter are two separate analyses from the same hand sample). Importantly, none of the samples analyzed, including the stream sediment, yielded any Precambrian ages.

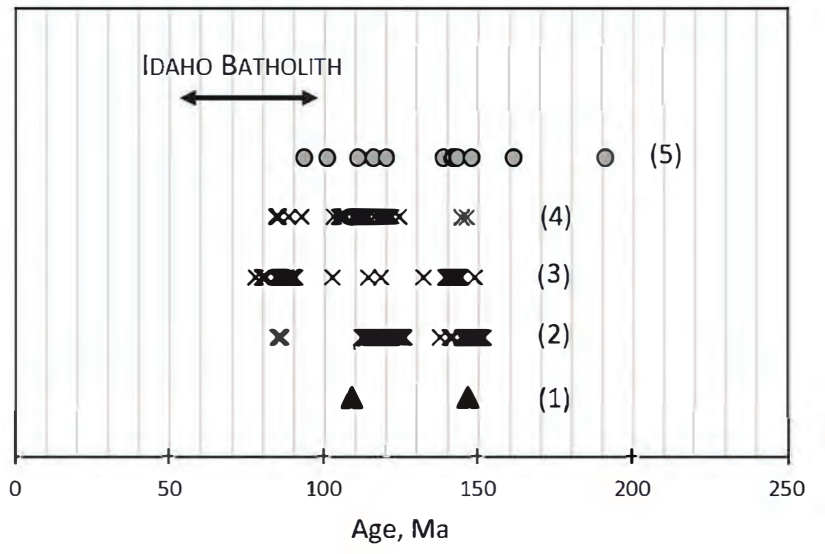

Figure 4. Dates obtained in this study: (1) Re-Os ages for molybdenite from Crowley #1 adit (147 Ma) and carbonatite C57 (109 Ma); (2) Th-Pb ages for monazite from Crowley #3 adit (UCSB lab); (3) Th-Pb ages for monazite from Crowley #1 adit (USGS lab); (4) Th-Pb ages for monazites from Crowley #3 adit (USGS lab); and (5) Th-Pb ages for monazites from the WFBR stream sediment sample (USGS lab). Age range shown for Idaho Batholith from Gaschnig and others (2010).

Figures 6A and 6B summarize REE profiles (obtained by LA-ICP-MS at the same time as the Th-Pb data) normalized to C1 chondrite for the Crowley #3 and #1 samples. The monazites have a typical carbonatite signature that is highly enriched in LREE and depleted in HREE, with no obvious Ce or Eu anomalies. Importantly, all of the analyses from these samples have nearly identical REE profiles, despite the fact that the same set of ablations produced a >60 m.y. range in ages. The simplest way to explain this result is if the entire monazite grain was chemically and isotopically homogenous when it crystallized (or was reset) at ~145 Ma, and then suffered episodic Pb loss without any change in the REE profile. In contrast, each separate monazite grain from the WFBR stream-sediment sample has a slightly different REE profile (fig. 6C). This suggests that the monazite grains, which likely eroded out of different carbonatite bodies in the watershed, grew during separate magmatic-hydrothermal events.

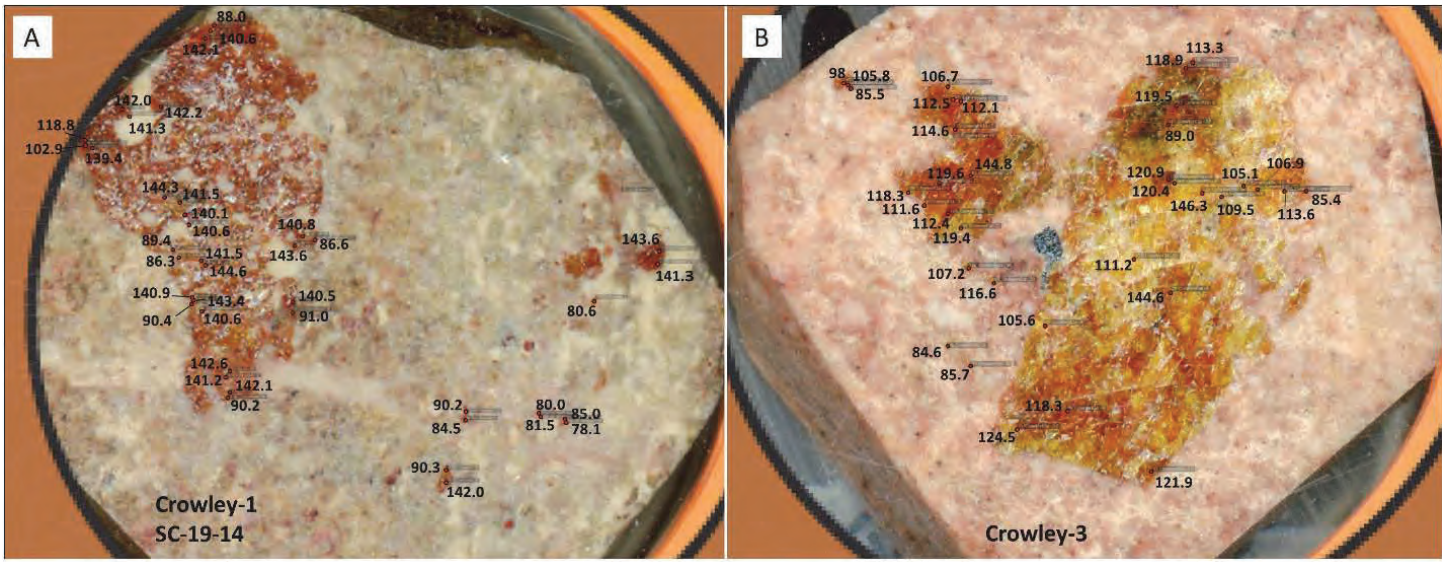

Figure 5. Photographs of Crowley #1 (A) and Crowley #3 (B) samples with Th/Pb dates adjacent to ablation pits (width of each view is 25 mm). Monazite is lustrous, honey brown. Matrix in A is a mix of calcite, quartz, barite, bastnaesite, parisite, and synchysite. White inclusions in large monazite grain are mostly calcite. Matrix in B is a fine-grained mix of calcite, barite, and ancylite.

DISCUSSION

The body of evidence presented in this paper suggests that REE mineralization in the carbonate bodies of Sheep Creek occurred episodically, between roughly 190 and 110 Ma. These ages straddle the Jurassic–Cretaceous boundary at 145 Ma. More data are needed to define discrete mineralizing episodes, although most of the samples analyzed in this study show evidence of an event at ~145–150 Ma. The fact that two molybdenite samples from two different carbonate bodies give different Re-Os ages (147 and 109 Ma) is strong evidence for multiple magmatic-hydrothermal events. The younger ages obtained in this study overlap with the onset of emplacement of the Atlanta Lobe of the Idaho Batholith (fig. 4). However, we are not aware of any dated igneous rocks in southwest Montana that fall in the 145–150 Ma time frame during which the coarse-grained monazites of figure 5 are most likely to have crystallized.

It is interesting to see how our dates correlate to previous geochronological work on REE mineralization to the south of Sheep Creek. As shown by figure 1B, the Diamond Creek and Lemhi Pass areas are on a trend that connects to Mineral Hill and Sheep Creek. Gillerman and others (2010) summarized dates from the Lemhi Pass area, and concluded that most of the REE-Th mineralization occurred in the Carboniferous (300–350 Ma), although a younger generation of monazite along rims and filling fractures in old monazite gave dates in the 150–90 Ma range (Gillerman, 2008). The 300–350 Ma age range is similar to most of the known carbonatites in western Canada (Millonig and Groat, 2013). Further south, Saintilan and others (2017) used the Re-Os isochron approach to date cobaltite mineralization in the Idaho Cobalt Belt at ~1.35 Ga, in agreement with previous work (summarized in Bookstrom and others, 2016). Aleinikoff and others (2012) used SHRIMP methods to obtain isotopic ages on xenotime and monazite from the Blackbird Mine. Whereas the xenotime had a wide range in ages from ~1.35 Ga to mid-Cretaceous, monazite gave solely Cretaceous ages with two clusters at 110 ± 3 and 92 ± 5 Ma. In addition, Zirakparvar and others (2007) reported Lu-Hf ages of 151 ± 32 Ma for garnets in the Blacktail pit, indicating a period of prograde metamorphism straddling the Jurassic/Cretaceous boundary. This metamorphism could have affected the Sheep Creek area as well, perhaps resetting the Th-Pb ages of the monazites. However, the Re-Os isotopic system is much less likely to be reset during metamorphism (Bingen and Stein, 2003; Saintilan and others, 2017). Therefore, the Re-Os dates of 147 and 109 Ma obtained from molybdenites in our study are strong evidence of primary mineralization during the dated time frame.

The fact that no Precambrian ages were obtained from the samples examined in this study is somewhat perplexing, given the intimate association between the carbonate lodes and the 1.37 Ga meta-igneous complex. No similar carbonatite-related REE-mineralization has been found in Belt-aged metasedimentary rocks that crop out to the immediate north and east of Sheep Creek. If the REE-rich carbonate bodies are true carbonatites sourced from the mantle or lower crust that intruded during the late Jurassic/early Cretaceous, it is hard to explain why they are only found in the meta-igneous complex, and not in the other rocks of the region. It is somewhat easier to imagine the carbonatites intruding during the 1.37 Ga rifting event that triggered the bimodal (gabbro/granite) igneous activity. However, this idea is weakened by the absence of peralkaline rocks in the meta-igneous suite. The gabbro/amphibolite has an unremarkable, tholeiitic composition (Spence, 1984), and the granite/augen gneiss has a composition typical of anorogenic "A-type" granites (Evans and Zartman, 1990).

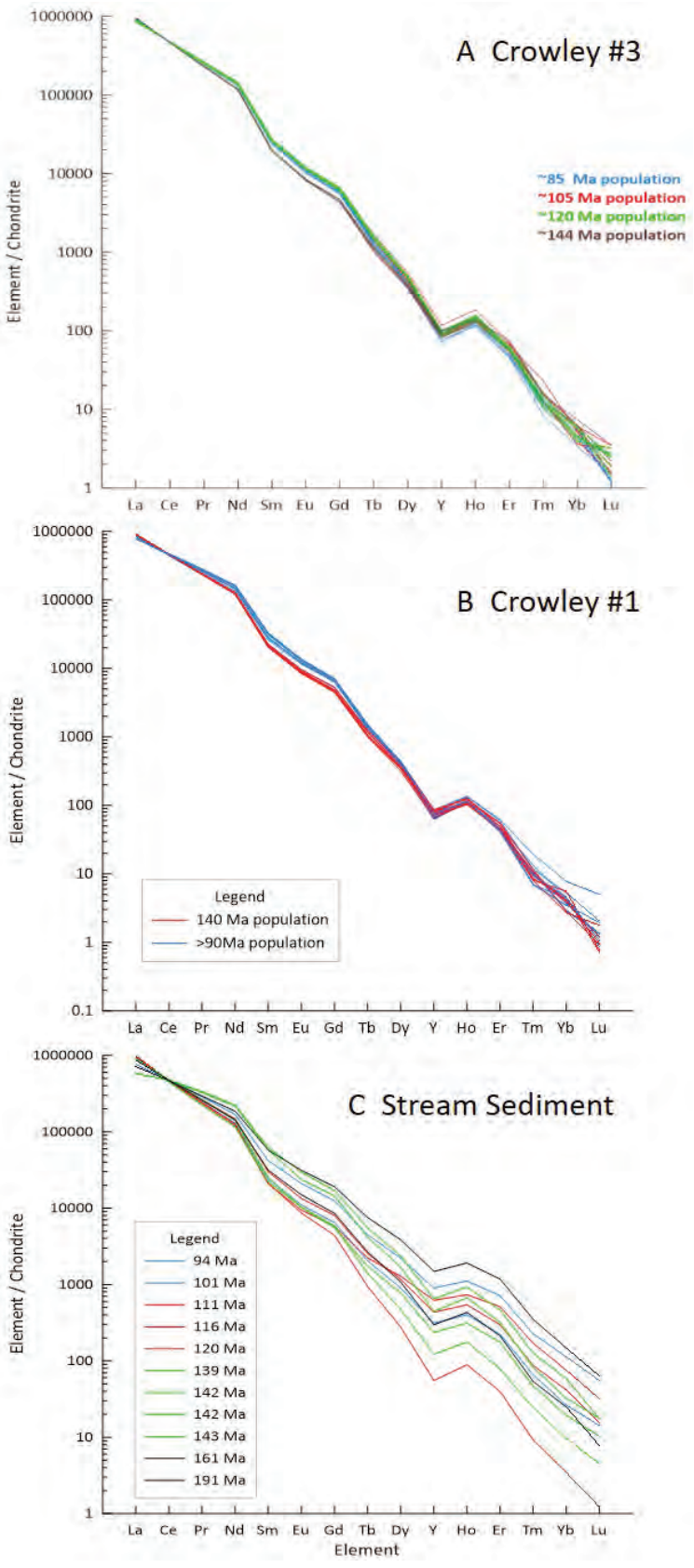

Figure 6. C1-normalized REE profiles for monazites; (A) Crowley #3 adit; (B) Crowley #1 adit (SC-14); (C) 12 individual grains of monazite collected from a heavy mineral concentrate of stream sediment from the WFBR.

If peralkaline igneous rocks exist in the region, they are yet to be recognized.

Early workers in the Sheep Creek and Mineral Hill districts recognized two distinct facies of carbonate rocks intercalated with the meta-igneous complex. Most of the mineralized carbonate bodies are coarse grained, with a banded or pegmatitic texture. Some of these mineralized carbonates have biotite-rich alteration envelopes (a type of "fenite") that extend for meters into the surrounding amphibolite (fig. 2A, see Risedorf, 2023). In contrast, both Crowley (1960) and Anderson (1960) noted another type of tabular carbonate body that lacks significant REE mineralization and has a fine-grained, strongly foliated fabric (e.g., the C3 carbonate body in fig. 1). The foliation is caused by alignment of apatite crystals intergrown with calcite/dolomite and an abundance of magnetite (Risedorf, 2023). Notably, the unmineralized carbonate bodies lack alteration envelopes. Kaiser (1956) and Crowley (1960) suggested that the foliated, fine-grained carbonate rocks could be sedimentary in origin. However, we argue against this idea, based on the C- and O-isotope compositions of the carbonate bodies, which are more consistent with a magmatic-hydrothermal origin (Risedorf, 2023).

Some speculative ideas are offered to spur additional research. (1) Is it possible that the fine-grained, foliated limestones are igneous, but were emplaced during a much older, Belt-aged or Paleozoic period of carbonatite activity? (2) Could the coarser-grained carbonate bodies rich in REE have formed by re-melting and/or hydrothermal re-mobilization of this early carbonatitic material during a late Jurassic/early Cretaceous thermal event? If these ideas are correct, then the REE-rich carbonate bodies (not necessarily true carbonatites) would have been locally derived, explaining their restricted geographic distribution. The foliated carbonates may be a type of "restite," from which the economically valuable elements (REE, Nb) were siphoned off, leaving a barren rock behind. Additional geochronological and geochemical studies are needed to test these hypotheses.

ACKNOWLEDGMENTS

Much of work in this study was funded by a grant from the Army Research Laboratory to Montana Tech. The views and conclusions contained in this document are those of the authors, and should not be interpreted as representing the official policies, either expressed or implied, of the Army Research Lab or the U.S. Government. We thank U.S. Critical Materials, especially Peter Mejstrick, for logistical support and sharing their bulk-rock geochemistry data with us. We also thank Jesse Mosolf (MBMG) and Andrew Kylander-Clark (UCSB) for performing the early MC-LA-ICP-MS analyses on a monazite specimen from Sheep Creek. Virginia Gillerman (IGS) and Danielle Olinger (USGS) made helpful edits on the paper.

REFERENCES CITED

Aleinikoff, J.N., Slack, J.F., Lund, K., Evans, K.V., Fanning, C.M., Mazdab, F.K., Wooden, J.L., and Pillers, R.M., 2012, Constraints on the timing of Co-Cu ± Au mineralization in the Blackbird district, Idaho, using SHRIMP U-Pb ages of monazite and xenotime plus zircon ages of related Mesoproterozoic orthogneisses and metasedimentary rocks: Economic Geology, v. 107, p. 1143–1175.

Anderson, A.L., 1960, Genetic aspects of the monazite and columbium-bearing rutile deposits in northern Lemhi County, Idaho: Economic Geology, v. 55, p. 1179–1201.

Bingen, B., and Stein, H., 2003, Molybdenite Re-Os dating of biotite dehydration melting in the Rogaland high-temperature granulites, S. Norway: Earth and Planetary Science Letters, v. 208, p. 181–195.

Bookstrom, A.A., Box, S.E., Cossette, P.M., Frost, T.P., Gillerman, V.S., King, G.R., Zirakparvar, N.A., 2016, Geologic history of the Blackbird Co-Cu district in the Lemhi subbasin of the Belt-Purcell Basin: Geological Society of America Special Paper 522, p. 185–219.

Crowley, F.A., 1960, Columbium-rare-earth deposits, southern Ravalli County, Montana: Montana Bureau of Mines and Geology Bulletin 18, 47 p.

Doughty, P.T., and Chamberlain, K.R., 1996, Salmon River Arch revisited: New evidence for 1370 Ma rifting near the end of deposition in the Middle Proterozoic Belt basin: Canadian Journal of Earth Sciences, v. 33, p. 1037-1052.

Evans, K.V., and Zartman, R.E., 1990, U-Th-Pb and Rb-Sr geochronology of middle Proterozoic granite and augen gneiss, Salmon River Mountains, east-central Idaho: Geological Society of America Bulletin, v. 102, p. 63–73.

Gammons, C.H., 2020, Mineralogical investigation of the Sheep Creek carbonatite veins, Ravalli County, Montana: Montana Bureau Mines and Geology Special Publication 121, p. 81–92.

Gary, M., in progress, Using indicator minerals from stream sediment to explore for REE mineralization in western Montana: M.S. thesis, Montana Technological University, Butte, Mont.

Gaschnig, R.M., Vervoort, J.D., Lewis, R.S., and McClelland, W.C., 2010, Migrating magmatism in the northern US Cordillera: in situ U–Pb geochronology of the Idaho batholith: Contributions to Mineralogy and Petrology, v. 159, p. 863–883.

Gillerman, V.S., 2008, Geochronology of iron oxide-copper-thorium-REE mineralization in Proterozoic rocks at Lemhi Pass, Idaho, and a comparison to copper-cobalt ores, Blackbird Mining District: Final Technical Report to the USGS, Grant 06HQGR0170, 148 p., available at https://www.usgs.gov/media/files/mrerp-report-06hqgr0170.

Gillerman, V.S., Schmitz, M.D., Jercinovic, M.J., and Reed, R., 2010, Cambrian and Mississippian magmatism associated with neodymium-enriched rare earth and thorium mineralization: Lemhi Pass district, Idaho [abs.]: Geological Society of America Abstracts with Programs, v. 42, no. 5.

Heinrich, E.W., and Levinson, A.A., 1961, Carbonatic niobium-rare earth deposits, Ravalli County, Montana: American Mineralogist, v. 46, p. 1424–1447.

Jaffe, H.W., Gottfried, D., Waring, C.L., and Worthing, H.W., 1959, Lead-alpha age determinations of accessory minerals of igneous rocks (1952-1957): U.S. Geological Survey, Bulletin 1097-B, p. 65–148.

Kaiser, E.P., 1956, Preliminary report on the geology and deposits of monazite, thorite, and niobium-bearing rutile of the Mineral Hill district, Lemhi County, Idaho: U.S. Geological Survey, Open-File Report 390, 41 p.

Millonig, L.J., and Groat, L.A., 2013, Carbonatites in Western North America—Occurrences and metallogeny: Society of Economic Geologists Special Publication v. 17, p. 245–264.

Risedorf, S., 2023, New investigations of the mineralogy and geochemistry of carbonatite-related REE-Nb mineralization in the Sheep Creek area, southern Ravalli County, Montana: M.S. thesis, Montana Technological University, Butte, Mont.

Saintilan, N.J., Creaser, R.A., and Bookstrom, A.A., 2017, Re-Os systematics and geochemistry of cobaltite (CoAsS) in the Idaho cobalt belt, Belt-Purcell basin, USA: Evidence for middle Mesoproterozoic sediment-hosted Co-Cu sulfide mineralization with Grenvillian and Cretaceous remobilization: Ore Geology Reviews, v. 86, p. 509–525.

Spence, J.G., 1984, Geology of the Mineral Hill interlayered amphibolite-augen gneiss complex, Lemhi County, Idaho: M.S. thesis, Univ. of Idaho, Moscow, ID, 239 p.

Stacey, J.S., and Kramers, J.D., 1975, Approximation of terrestrial lead isotope evolution by a two-stage model: Earth and Planetary Science Letters, v. 26, p. 207-221.

Zirakparvar, N.A., Bookstrom, A.A., and Vervoort, J. D., 2007, Cretaceous garnet growth in the Idaho cobalt belt: Evidence from Lu-Hf geochronology: Geological Society of America, Abstracts with Programs, v. 39(6), p. 413.

CRITICAL MINERAL RESOURCES IN LEMHI COUNTY, IDAHO: INVESTIGATING CARBONATITES AND THEIR RARE EARTH MINERALIZATION

Madeline A. Murchland,[1] Virginia S. Gillerman,[3] Reed S. Lewis,[2] Cody J. Steven,[2] and Thomas Williams[1]

[1]University of Idaho, Moscow, Idaho
[2]Idaho Geological Survey, Moscow, Idaho
[3]Idaho Geological Survey, Boise, Idaho

INTRODUCTION

The Mineral Hill district in northern Lemhi County, Idaho, is underlain by a complex of interlayered gneiss, paragneiss, and amphibolite rocks that extends northwest into Montana, where it is known as the Sheep Creek–Mineral Point mining district. Within both districts are multiple horizons and bodies of rare-earth-bearing carbonate rocks (Heinrich and Levinson, 1961; Spence, 1984). This belt of mineralization has been of both historic and modern interest to the Idaho Geological Survey (IGS), the United States Geological Survey (USGS), and mineral exploration companies due to its Nb, Ti, and rare earth element (REE) occurrences in the carbonate units. Previous studies on the Mineral Hill district, as well as current mineralogical work, have identified numerous critical elements, including Nb, Ti, Ba, Nd, Ce, La, and Pr present in the mineralized carbonate horizons (Abbot, 1954; Anderson, 1958, 1960; Gillerman, 2008; Kaiser, 1956; Sharp and Cavender, 1953; Spence, 1984; Sturm, 1954). With the increasing demand for economic occurrences of REEs and metals in the United States, these deposits are active and potential sites for critical mineral exploration (Verplanck and others, 2022). Critical minerals are commodities deemed crucial to the economic and national security of the country. Much of the research on domestic supplies of these resources is funded through the Earth Resources Mapping Initiative (Earth MRI), a program of the USGS that funds state surveys' work on characterizing and assessing domestic supplies of critical minerals. The IGS project to map and characterize the REE-Nb deposits of the Mineral Hill district is funded by Earth MRI and will build off historic work done in the area.

Much of the carbonate mineralization at the Mineral Hill and Sheep Creek districts is described as thin, tabular bodies originally characterized as replacement of marble lenses (Abbot, 1954; Sturm, 1954). However, later studies on the paragenesis of the mineralization determined an igneous origin for the deposits, with potential hydrothermal activity (Anderson, 1960; Spence, 1984). The rocks are calcite–dolomite dominant, with abundant magnetite and ilmenite (fig. 1), as well as reported minor amounts of apatite, monazite, ancylite, barite, bastnaesite, and Nb-bearing rutile (Abbot, 1954; Anderson, 1960). Carbonate-bearing rocks at three properties within the Mineral Hill district have been the subject of previous early studies: the Roberts, Roberts South, and Lee Buck prospects (Sharp and Cavender, 1953; Kaiser, 1956). However, much of this research was done before the 1960s, and the area remains understudied by modern methods. For our work, updated analytical methods will be used first to constrain the minerals that contain the REEs and other critical metals. One objective is to determine whether any of the occurrences are true igneous

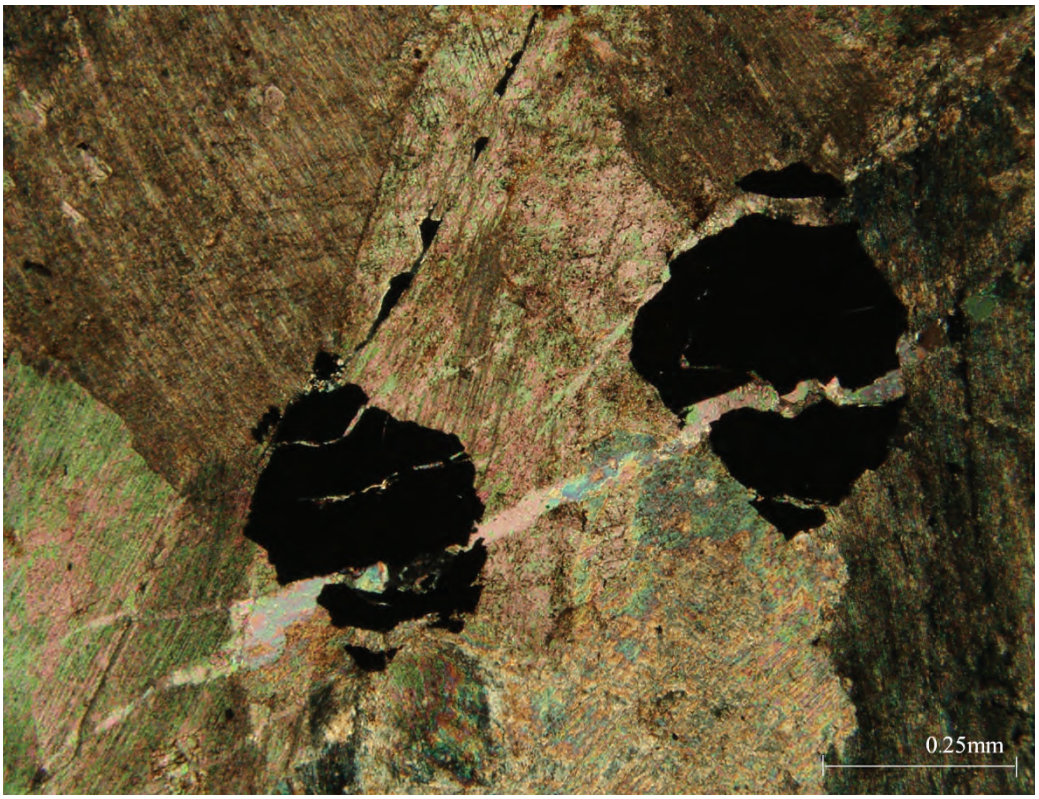

Figure 1. Photomicrograph of thin section 22MM001 (Roberts Prospect) in cross-polarized light, showing opaque magnetite grains in a matrix of calcite and dolomite.

carbonatites, which are typically characterized by their light REE enrichment. This work will ultimately aid in modern exploration efforts.

Preliminary study of samples from the Roberts, Roberts South, and Lee Buck properties has identified several REE-bearing phases, specifically allanite-(Ce) and monazite-(Ce). Ongoing work aims to characterize rare earth abundances to determine which of these deposits are carbonatite-hosted, chemically characterize the mineral phases of interest, understand episodes and controls on mineralization, and compare to other occurrences in east-central Idaho.

METHODS

The initial samples of this study are carbonatite float from the Roberts property (22MM001), collected by M. Murchland and C. Steven in September 2022, as well as six additional carbonate samples from the Mineral Hill district collected between 2007 and 2011 from the Lee Buck (01LB-3, 01LB-5), Roberts (07WP126, 07WP126A), and Roberts South (07WP127A, 07WP127B) properties by V. Gillerman. These rocks have been made into polished thin sections, the mineralogy of which has been initially characterized using microscopic methods and semi-quantitative chemical analysis. Optical petrography with a standard petrographic scope was used for initial mineral identification and textural description. Scanning electron microscopy and energy dispersive spectrometry (SEM-EDS) was then used for semi-quantitative chemical analysis of phases, as well as for identifying minor and trace phases of interest. To supplement the chemistry, mineral structures in the thin sections were identified using both powder X-ray diffraction (PXRD) and micro-XRD, with accompanying phase-analysis software (DiffracEva).

PRELIMINARY RESULTS

Preliminary work on thin sections from the Lee Buck, Roberts, and Roberts South properties revealed a variety of phases that are consistent with known carbonatite mineralogy (Yaxley and others, 2022). Thin section analysis of the float from the Roberts prospect (22MM001) showed that the major phases were carbonates, with large, opaque inclusions that had veinlets of carbonate through them (fig. 1). SEM-EDS analysis, accompanied with XRD, identified the major carbonates as intermixed calcite and dolomite, and the opaques as predominantly magnetite.

Thin section analysis of the Roberts South samples (07WP127A, 07WP127B) revealed abundant monazite and allanite (fig. 2), within a matrix of amphibole and carbonate. These phases were confirmed using SEM-EDS, which also showed that the monazite and allanite are Ce-dominated with accompanying light rare earths (fig. 3). Backscatter electron imaging (SEM-BSE) revealed textures of intermixed monazite, allanite, and apatite (fig. 4A); however, there are several grains of monazite that have been rimmed by fluorapatite and allanite (fig. 4B).

Preliminary analysis of the remaining Roberts and Lee Buck property samples has shown mineralogy similar to that of the Roberts float. They consist mainly of intermixed calcite and dolomite with numerous opaque inclusions of iron-oxide and ilmenite. SEM-EDS has revealed that several of these samples contain trace amounts of monazite, allanite, Nb-bearing rutile, and Sr-bearing barite.

PLANNED WORK

Fieldwork will be done by the IGS throughout the summers of 2023 and 2024 in the Shoup and Ulysses 7.5' quadrangles northwest of Salmon, Idaho, to sample and map in detail the previously documented carbonate occurrences, better understand the extent of related mineralization, and collect samples for mineralogical analysis using the previously described methods.

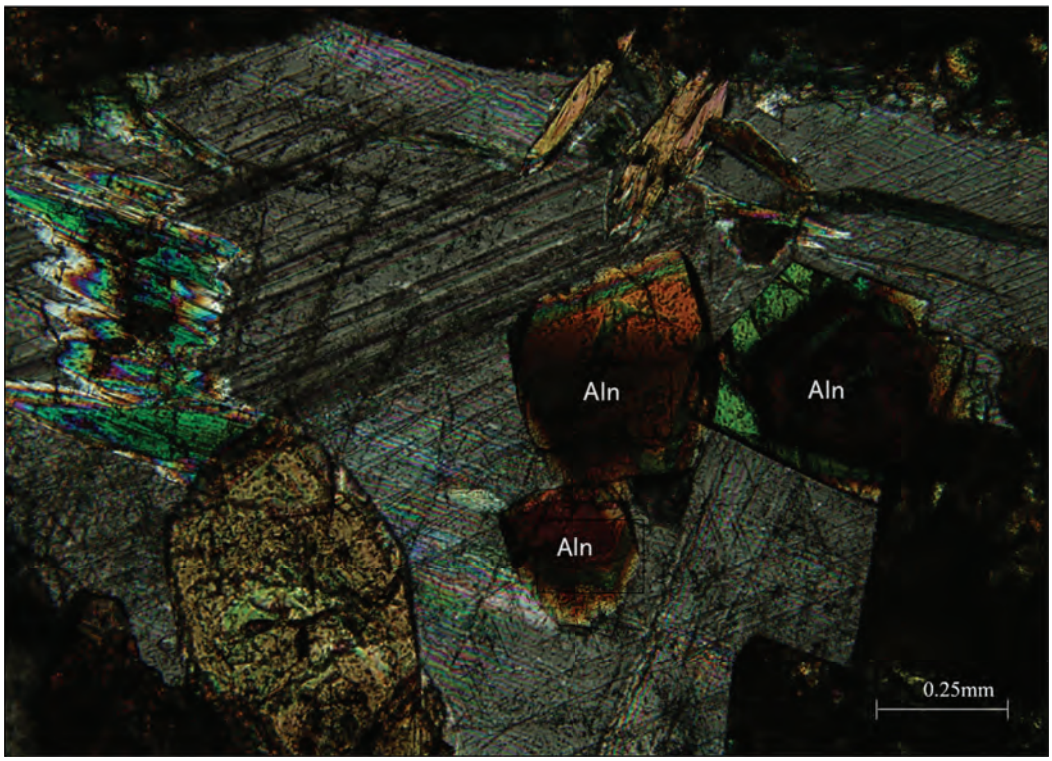

Figure 2. Photomicrograph of thin section 07WP127A (Roberts South) in cross-polarized light, showing euhedral allanite crystals (Aln) in carbonate.

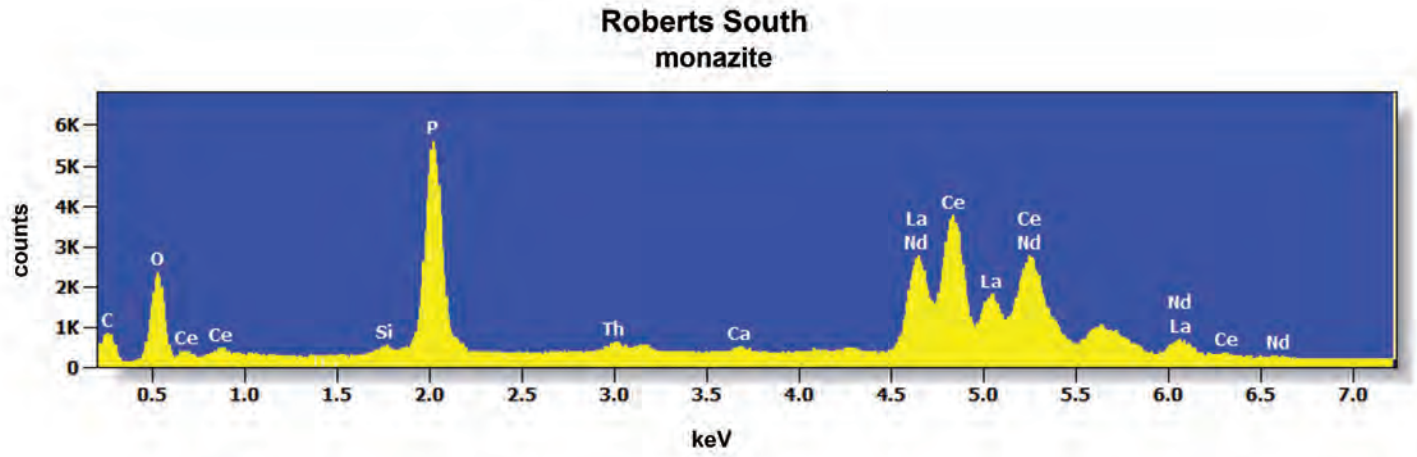

Figure 3. EDS spectrum of the monazite grain in figure 4A, showing a Ce-dominant monazite with additional REEs (La, Nd) and Th present above the SEM detection limit. C peak is the result of sample coating.

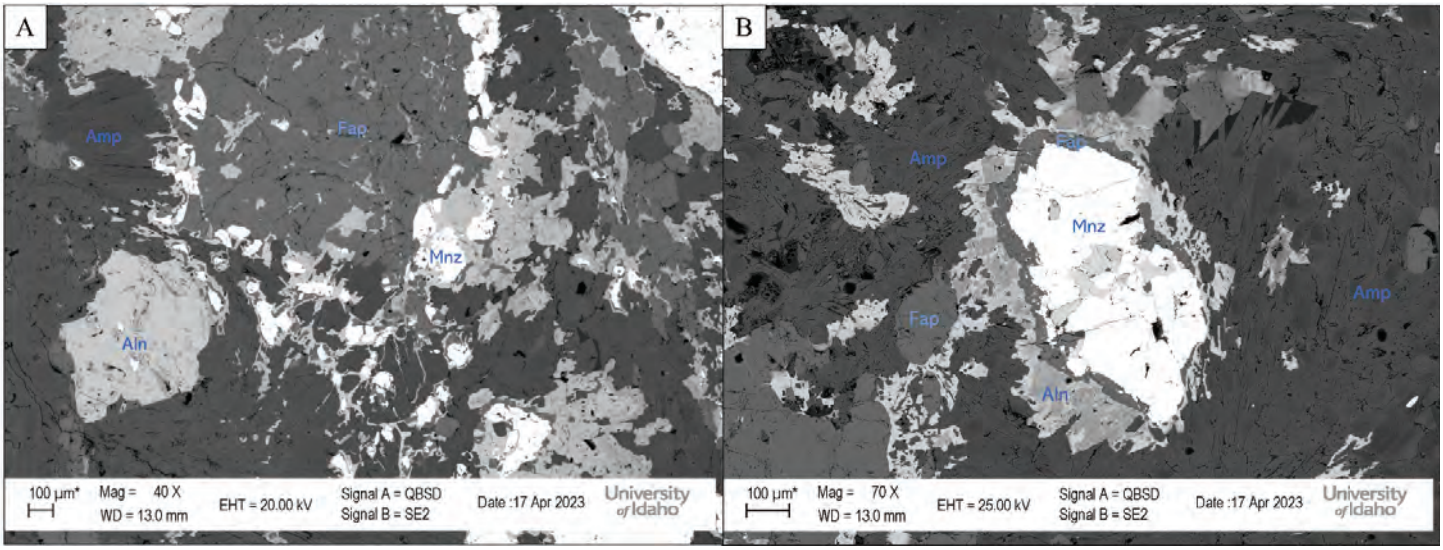

Figure 4. (A) SEM-BSE image of thin section from 07WP127A, showing the intermixed monazite-Ce grains (Mnz), fluorapatite (Fap), and allanite-Ce (Aln) in an amphibole-dominated matrix (Amp). (B) Monazite rimmed in fluorapatite and allanite, in amphibole matrix.

Electron probe microanalysis (EPMA) will be used to better characterize the chemistry of minor and trace mineral phases. This will supplement current SEM-EDS data for those minerals where REEs are either below EDS detection limits or require higher resolution to differentiate between individual elements. Wavelength dispersive X-ray fluorescence (WDXRF) will be used to determine the major elements in the bulk rock, while inductively coupled plasma mass spectrometry (ICP-MS) will be used for minor and trace elements, including specific abundances of REEs.

REFERENCES

Abbot, A.T., 1954, Monazite deposits in calcareous rocks, northern Lemhi Country, Idaho: Idaho Bureau of Mines and Geology Pamphlet 99, 24 p.

Anderson, A.L., 1958, Uranium, thorium, columbium, and rare earth deposits in the Salmon region, Lemhi Country, Idaho: Idaho Bureau of Mines and Geology Pamphlet 115, 81 p.

Anderson, A.L., 1960, Genetic aspects of the monazite and columbium-bearing rutile deposits in northern Lemhi County, Idaho: Economic Geology, v. 55, 22 p.

Gillerman, V.S., 2008, Geochronology of iron-oxide-copper-thorium-REE mineralization in Proterozoic rocks at Lemhi Pass, Idaho, and a comparison to copper-cobalt ores, Blackbird Mining District, Idaho: Final Technical Report to U.S. Geological Survey, 66 p.

Heinrich, E.W., and Levinson, A.A., 1961, Carbonatitic niobium-rare earth deposits, Ravalli County, Montana: The American Mineralogist, v. 46, p. 1424–1447.

Kaiser, E.P., 1956, Preliminary report on the geology and deposits of monazite, thorite, and niobium-bearing rutile of the Mineral Hill district, Lemhi County, Idaho: U.S. Geological Survey Open-File Report 56-69, 41 p.

Sharp, W.N., and Cavender, W.S., 1953, Preliminary report on the Mineral Hill monazite deposits, Lemhi County, Idaho: U.S. Geological Survey Trace Elements Memorandum Report 286, p. 1–13.

Spence, J.G., 1984, Geology of the Mineral Hill interlayered amphibolite-Augen gneiss complex, Lemhi County, Idaho: Moscow, Idaho, University of Idaho, M.S. thesis, 240 p.

Sturm, F.H., 1954, General geology of some replacement monazite deposits in Lemhi County, Idaho: Moscow, Idaho, University of Idaho, M.S. thesis, 64 p.

Verplanck, P.L., Farmer, G.L., Kettler, R.M., Lowers, H.A., Johnson, C.A., Koenig, A.E., and Blessington, M.J., 2022, Petrogenesis and rare earth element mineralization of the Elk Creek carbonatite, Nebraska, USA: Ore Geology Reviews, v. 146, p. 1–19.

Yaxley, G.M., Anenburg, M., Tappe, S., Decree, S., and Guzmics, T., 2022, Carbonatites: Classification, sources, evolution, and emplacement: Annual Review of Earth and Planetary Science, v. 50, p. 261–293.

PRELIMINARY OBSERVATIONS ON THE ORIGIN AND GEOLOGY OF MAGNETITE AT THE IRON CREEK CU-CO-FE DEPOSIT, LEMHI COUNTY, IDAHO

Virginia S. Gillerman,[1] Darin Schwartz,[2] Dan Pace,[3] and Frank Santaguida[4]

[1]*Idaho Geological Survey, Boise, Idaho*
[2]*Department of Geosciences, Boise State University, Boise, Idaho*
[3]*Revival Gold Inc., Salmon, Idaho*
[4]*Glencore Canada, Toronto, Ontario, Canada*

The Iron Creek Cu-Co deposit is located along the North Fork of Iron Creek at the southeast end of the Idaho Cobalt Belt in Lemhi County, Idaho. The deposit is approximately 30 km southwest of the town of Salmon. Since its early exploration in the 1970s, the Iron Creek property was distinguished for the presence of abundant magnetite horizons and occurrences in the host rocks, which are part of the Mesoproterozoic Apple Creek Formation, a monotonous sequence of siltites, argillites, and quartzites that also host the Blackbird Mining District to the northwest. Iron-rich rocks at Blackbird include biotite-rich horizons of enigmatic origin, but magnetite is rare (Bookstrom and others, 2016). The current study, undertaken with the cooperation of Electra Battery Materials, who is exploring the Iron Creek Cu-Co property, proposed to examine the magnetite occurrences to determine their origin and relationship to the copper–cobalt mineralization. A related question was whether magnetite geochemistry could be a useful exploration guide. Regional and district geology of Iron Creek, the Blackbird Mining District, and the Idaho Cobalt Belt has been described by multiple published references (Bookstrom and others, 2016; Lewis and others, 2021; Nash, 1989; Lund and others, 2011) and company reports (summarized in Perron and others, 2023, NI 43-101 report for Electra). For this study, selected magnetite-bearing rocks were collected from the surface and two drill holes through the Iron Creek deposit (IC 17-25 and IC 18-02) and one drill hole through the nearby Ruby zone (IC 22-02) occurrence at the Iron Creek property. Work to date has included optical petrography on 54 thin sections and analytical work by SEM-EDS and/or LA-ICPMS for mineralogy and trace elements on a subset of about a dozen thin sections. Results reported here are preliminary in nature.

Previous workers noted sedimentary accumulations of iron oxide grains within the Apple Creek Formation of the Lemhi subbasin, and recent work has mapped differences in magnetic susceptibility values (Lewis and others, 2021). Figure 1 shows an example of heavy mineral laminae from sedimentary host rocks near the Iron Creek deposit. The well-preserved sedimentary features and thin laminae of light and dark bands are common to much of the regional Apple Creek strata. Figure 2 shows magnetite preserved in a syn-sedimentary trough bed. However, cross-cutting magnetite veins are also present near Iron Creek. Figure 3

Figure 1. Polished thin section of unmineralized, finely bedded Mesoproterozoic Apple Creek Formation showing dark iron oxide-rich heavy mineral laminae and graded beds, brown argillaceous laminae, sedimentary scours, and possible syneresis cracks (Sample 333202).

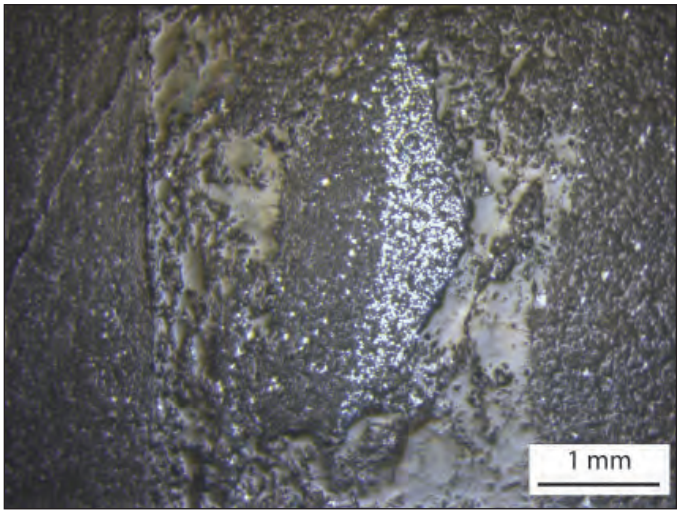

Figure 2. Magnetite grains (bright whitish gray) filling sedimentary trough in sample 333202; reflected light image of portion of section shown in figure 1.

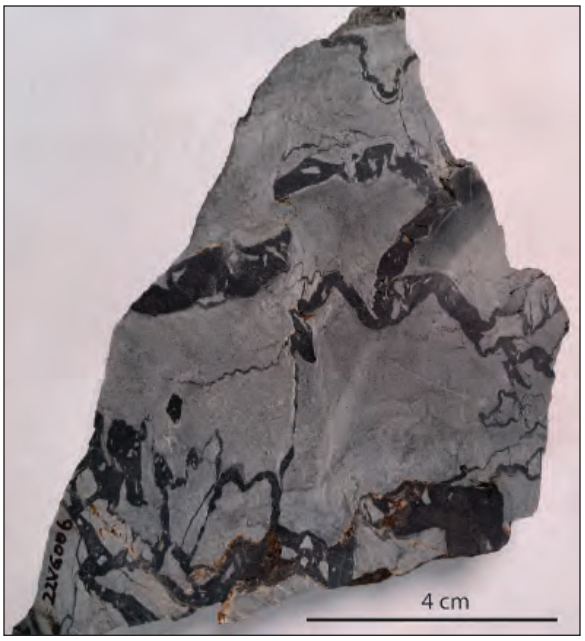

Figure 3. Outcrop sample 22VG006 showing discordant and folded black magnetite veins and breccias cutting Apple Creek Formation.

displays sample 22VG006, which does not contain copper or cobalt mineralization. The black, highly magnetic veins cross-cut and brecciate the dark argillaceous sedimentary rock, but the veins are also folded and offset along a faint axial planar cleavage. The dark veins and masses consist of an extremely fine-grained assemblage of quartz–tourmaline–magnetite with probable clay or sericite (fig. 4).

Cobalt at Iron Creek is hosted by cobaltiferous pyrite, with pyrite and magnetite typically coexisting in the same thin section. However, locally pyrite is overprinting or forming at the expense of the original finer-grained, earlier magnetite. An example of a well-mineralized horizon from the Ruby zone is shown in figures 5 and 6, where magnetite-rich, dark-colored material is the matrix to quartzite clasts and includes porphyroblasts of Co-rich pyrite. A meter below the sample in figure 6, the breccia (interpreted as originally a sedimentary breccia), is intensely flattened and sheared out. Multiple sections show strong deformation with pyrite porphyroblasts bordered by pressure shadows of quartz and calcite, which itself is locally lineated and stretched. Magnetite forms cracked masses that appear to have been broken, and gangue chlorite is locally foliated along what appears to be a Riedel shear fabric. Both pyrite and magnetite are interpreted as pre- to syn-tectonic in their formation, implying that the main Co and Fe mineralization predates the intense deformation and stretching. Chalcopyrite is more common in veins, and in one thin section an isoclinal folded quartz–chalcopyrite vein is cut off along a shear plane. Lund and others (2011) and earlier workers described intense deformation at the Blackbird Mine. At Iron Creek, there is also localized intense deformation, probably from the regional, Cretaceous-age thrusting and metamorphism—although earlier periods of deformation are possible. The abundant chlorite and micaceous alteration associated with the sulfides and oxides and argillaceous components may have localized the shearing in or near mineralized horizons.

Analytical work on magnetite geochemistry has been difficult due to inclusions and the very fine grain size of the magnetite, particularly in the sedimentary rocks. In general, magnetite seems most common in dark, argillaceous bands and in the matrix to sedimentary breccias, which were identified as diamictites by previous workers. The observed association of tourmaline and magnetite in early hydrothermal veins at Iron Creek suggests magnetite precipitation from a hydrothermal vent or "mud volcano" in the Proterozoic basin, perhaps along a rift margin fault. Preliminary results suggest that the magnetite compositions show only subtle differences, but the sample suite is limited to date. Trace elements used to discriminate magnetites from various ore-forming systems include Mg, Al, Ti, V, Cr, Mn, Co, Ni, Zn, and Ga (Nadoll and others, 2014; Dupuis and Beaudoin, 2011). At Iron Creek, all these trace elements show relatively large ranges within a single sample or for the suite as a whole. Overall, the trace element compositions in magnetite at Iron Creek are in the tens to hundreds of ppm. As shown in figure 7, plots of the Iron Creek magnetite compositions on the Al+Mn vs. Ti+V and Ni/(Cr+Mn) vs. Ti+V discriminant presented in Nadoll and others (2014) suggest that the Iron Creek magnetites overlap "BIF-Iron Ore; Hydrothermal-Metamorphic" and IOCG fields with formation tempera-

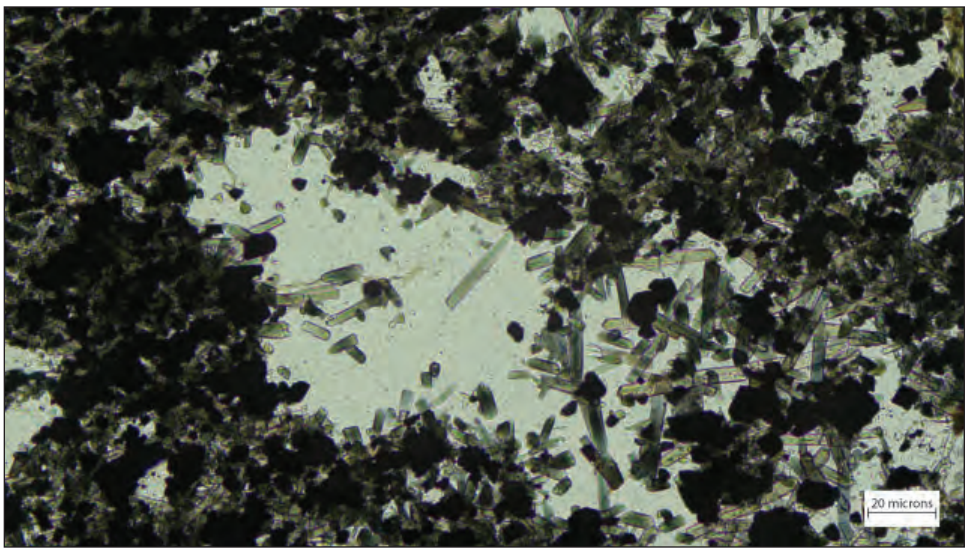

Figure 4. Photomicrograph (transmitted light) of sample 22VG006C showing black magnetite grains, and green tourmaline crystals in quartz matrix.

Figure 5. Drill core from Ruby zone showing weakly sheared, magnetite-matrix breccias with pyrite in quartz-rich siltite (Sample IC22-02-1013).

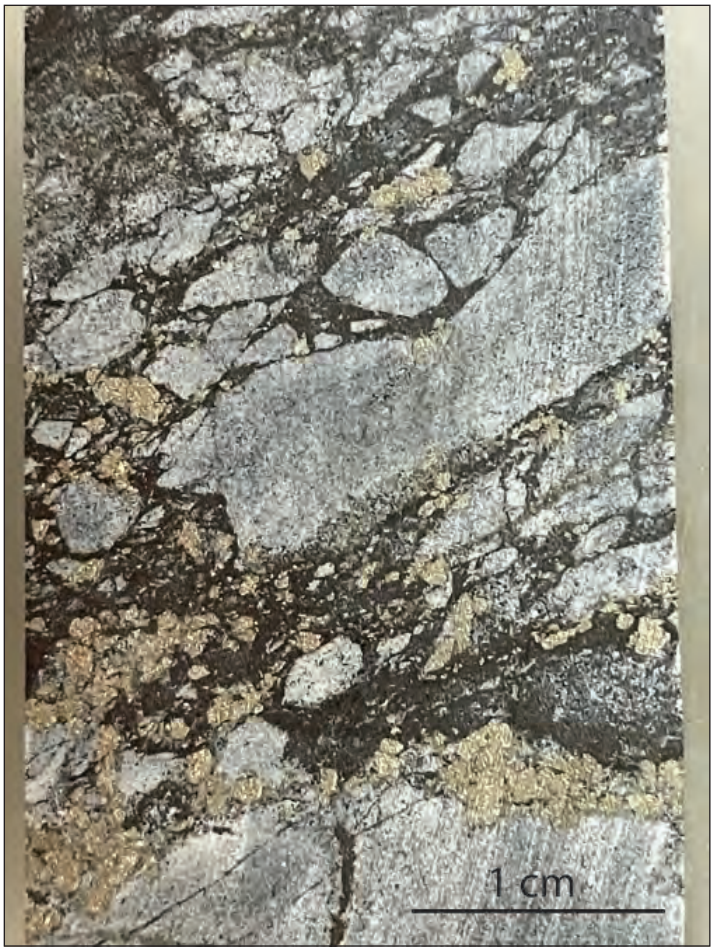

Figure 6. Magnetite–pyrite breccia in siltite, sample IC22-02-1020 billet.

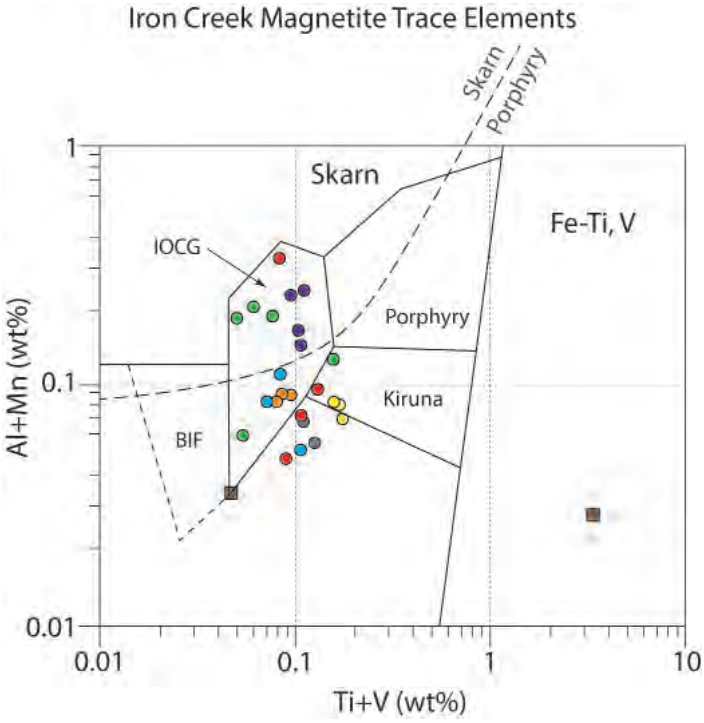

Figure 7. Graph of Al+Mn versus Ti+V (all in weight percent) of magnetite (colored circles) from Iron Creek. Squares are magnetite in single sample from unrelated, intrusive-hosted occurrence in the region. Mineral system fields from Nadoll and others (2014) and Dupuis and Beaudoin (2011).

tures in the upper 200°C to 300°C range, compatible with the observed greenschist metamorphic grade. Based on the limited data, Iron Creek magnetite trace element abundances appear to be significantly lower than magnetites from porphyry or Kiruna-type magmatic systems, though more work is needed at both the district and regional scale. Slack and others (2012) described the Idaho Cobalt Belt, which extends from Iron Creek to Blackbird and beyond, as a variant of the IOCG model and a strata-bound Fe-Co-Cu-Au-Bi-Y-REE deposit related to the 1370 Ma suite of megacrystic granitic plutons. The preliminary magnetite compositions could provide some credence to the IOCG (iron oxide–copper–gold) or a BIF (banded iron formation) iron setting as parts of the mineral system, but the Au and REEs are not present at Iron Creek, and the story would seem far more complex, due to petrographic evidence for overprinting of iron oxide-rich sedimentary rocks by hydrothermal fluids, metamorphism, and deformation. Rather a combination of Proterozoic sedimentary brines, hydrothermal circulation induced by Proterozoic plutons and overprinting, and remobilization by later Paleozoic alkalic plutonism and Mesozoic events is present along the Idaho Cobalt Belt and at Iron Creek.

REFERENCES

Bookstrom, A.A., Box, S.E., Cossette, P.M., Frost, T.P., Gillerman, V.S., King, G.R., and Zirakparvar, N.A., 2016, Geologic history of the Blackbird Co-Cu district in the Lemhi sub-basin of the Belt-Purcell Basin, *in* MacLean, J.S., and Sears, J.W., eds., Belt Basin: Window to the Mesoproterozoic Earth: Geologic Society of America Memoir 522, p. 185–219.

Dupuis, C., and Beaudoin, G., 2011, Discriminant diagrams for iron oxide trace element fingerprinting of mineral deposit types: Mineralium Deposita, v. 46, p. 319–335.

Lewis, R.S., Canada, A.S., Stewart, D.E., and Burmester, R.F., 2021, Geologic map of the Degan Mountain quadrangle, Lemhi County, Idaho: Idaho Geological Survey Digital Web Map 200, 1:24,000 scale, 1 plate.

Lund, K., Tysdal, R.G., Evans, K.V., Kunk, M.J., and Pillers, R.M., 2011: Structural controls and evolution of gold-, silver-, and REE-bearing copper-cobalt ore deposits, Blackbird District, east-central Idaho: Epigenetic origins: Economic Geology, v. 106, p. 585–618.

Nadoll, P., Angerer, T., Mauk, J.L., French, D., and Walshe, J., 2014, The chemistry of hydrothermal magnetite: A review: Ore Geology Reviews, v. 61, p. 1–32.

Nash, J.T., 1989, Geology and geochemistry of synsedimentary cobaltiferous-pyrite deposits, Iron Creek, Lemhi County, Idaho: U.S. Geological Survey Bulletin 1882, 33 p.

Perron, M., Beauvais, M.R., Kinnan, E., and Roy, P., 2023, NI 43-101 Technical report and mineral resource estimate for the Iron Creek cobalt-copper property, Lemhi County, Idaho, USA: InnovExplo Inc. report for Electra Battery Materials (www.electrabmc.com/our-business/iron-creek/), 196 p.

Slack, J.F., 2012, Strata-bound Fe-Co-Cu-Au-Bi-Y-REE deposits of the Idaho Cobalt Belt: Multistage hydrothermal mineralization in a magmatic-related iron oxide-copper-gold system: Economic Geology, v. 107, p. 1089-1113.

DRILLING THE DIAMOND CREEK RARE EARTH ELEMENT PROJECT, LEMHI COUNTY, IDAHO

Rob Morgan[1] and Rebecca Goddard[2]

[1]Vice President of Exploration, Idaho Strategic Resources, Couer d'Alene, Idaho
[2]Geologist, Idaho Strategic Resources, Couer d'Alene, Idaho

LOCATION

The Diamond Creek Rare Earth Element (REE) Project is located in the Eureka Mining district, approximately 8 mi (13 km) north–northwest of Salmon, Idaho. The project is comprised of 244 unpatented mining claims, covers approximately 4,554 acres, and is operated by Idaho Strategic Resources (IDR). The Diamond Creek Project lies in the center of the 70-mi-long Idaho Rare Earth Element-Thorium Belt (Idaho REE-Th Belt). The belt extends from Lemhi Pass in the southeast through Diamond Creek into the Mineral Hill District in the northwest (fig. 1).

HISTORY

The area was historically prospected for gold until the 1950s, when its unique geologic setting was recognized by the United States Geological Survey (USGS) and the Idaho Bureau of Mines and Geology (now Idaho Geological Survey, IGS). In the early 1950s the U.S. government sponsored country-wide exploration for nuclear power-related raw materials, which was overseen by the USGS and the Atomic Energy Commission. This campaign resulted in the discovery of thorium mineralization in areas of Lemhi County, including the REE occurrence in the Diamond Creek area. The efforts of the USGS, IGS, and other agencies resulted in the inclusion of the Diamond Creek mineralization into the country's critical minerals inventory.

Staatz and others (1979) estimated a probable potential resource at Diamond Creek of approximately 75,500 tons of total REE oxides (TREO), using an average grade of 1.22 percent (%). This resource calculation was derived solely from surface sample assays with values ranging from 0.59 to 5.51 percent TREO.

In 2012, US Rare Earths Inc. drilled two shallow core holes to depths of ~122 m (400 ft). One hole was reported to have encountered 0.5% TREO at 80 feet. Available information indicates that the second hole was left unlogged and unsampled.

Starting in 2019, geopolitical pressures have shown critical vulnerabilities in the U.S.'s supply chain economics. IDR recognized the immediate need for enhancing our critical mineral resources, and decreasing our reliance on foreign sources of these minerals. IDR targeted the Diamond Creek area for reasons such as its size, historic resource estimate, and unique mineralization. The series of REE prospects occurring along a 2.5-mi-long strike length with reported wide zones of mineralization up to 25 ft gives evidence of the potential size of the area. The historic resource estimate by Staatz and others (1979) was calculated using a value >1% TREO, which IDR considers to be ore grade. The project is also notable for its 10:1 high REE:low thorium ratios.

GEOLOGIC SETTING

The geologic setting at Diamond Creek (fig. 2) has been shaped over millions of years and with significant structural events. The lithology consists of two primary units, Mesoproterozoic metasediments belonging to the Lemhi Group (Gunsight Fm) and the Diamond Creek pluton. The metasediments are fine-grained, gray-colored, dirty quartzites with occasional siltite interbeds. The Diamond Creek pluton is a Mesoproterozoic megacrystic granite that is dated at 1,370 Ma (Evans and Zartman, 1990).

The largest structure in the area is the Diamond Creek fault. It is a thrust fault that places the megacrystic granite of the Diamond Creek pluton over the quartzite metasediments. This fault cuts across the area at a N60°W trend and dips westerly at 30-40°. The Contact fault is a secondary structure that links a series of REE prospects (Contact, Lucky Gem, Simer and Frank Burch) along its mapped 2.5 mi length (fig. 2). The structure was mapped by Biddle (1985) as the "Diamond fault," but IDR geologists changed the name to "Contact fault" to avoid confusion with the larger structure. The Contact fault has a N30°E strike, and while dips at surface are shown at ~65° to the west, drilling indicates a steepening of this fault at depth to ~79°W. The Diamond Creek fault and the Contact fault intersect just south of the Lucky Gem prospect area.

MINERALIZATION/ALTERATION

Age of the REE mineralization at Diamond Creek is unknown, but it is possibly sourced from deeply buried alkaline or carbonatite intrusions. REE mineralization occurs along fault and fracture systems as zones of weak to intense hydrofractured rock, eventually culminating with the full replacement of the country rock with brightly colored REE oxides (fig. 3).

Fenitization is a diagnostic REE alteration in the project area. This alteration manifests as white halos surrounding specularite-filled fractures (fig. 4). Outboard of these

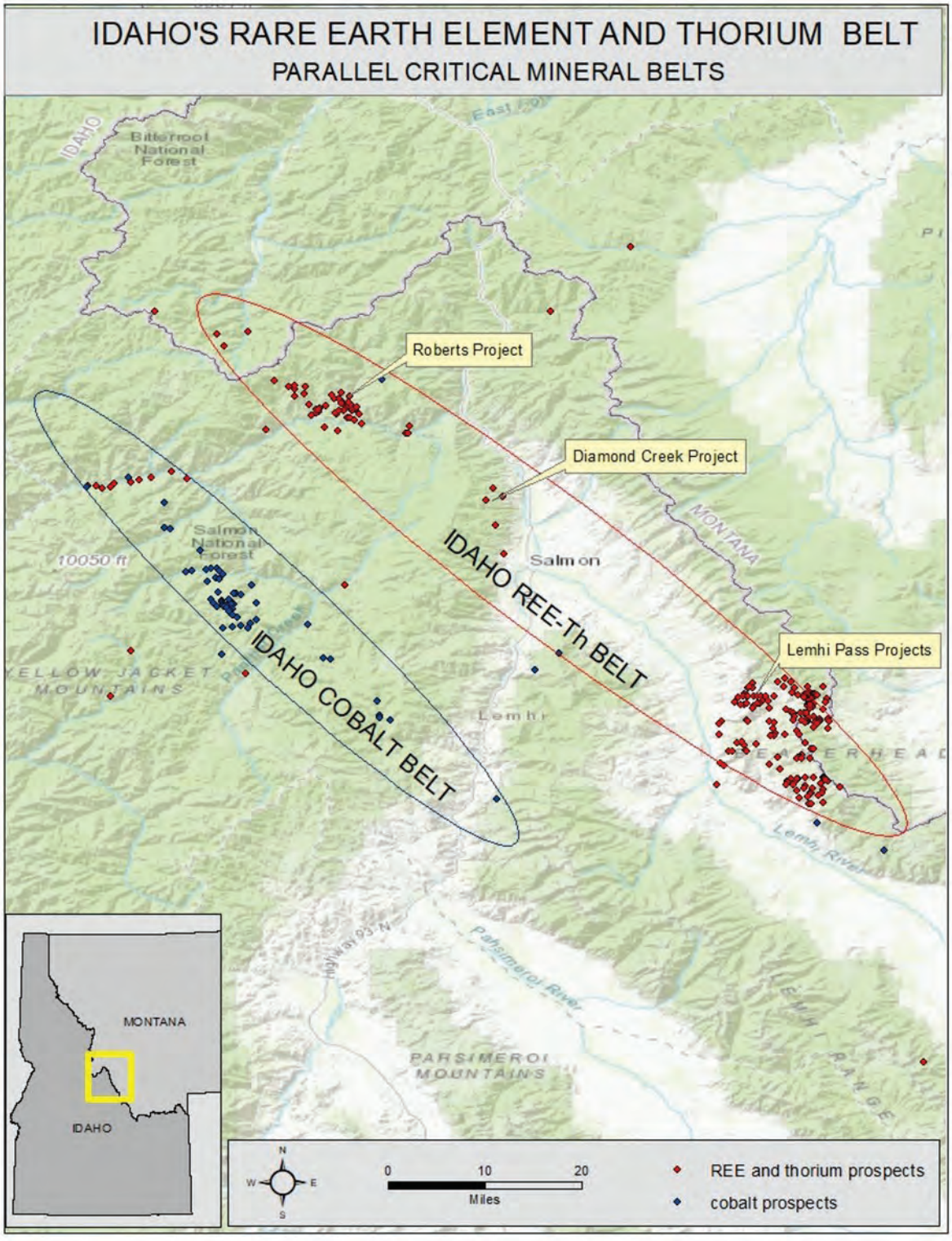

Figure 1. Idaho's critical mineral belts.

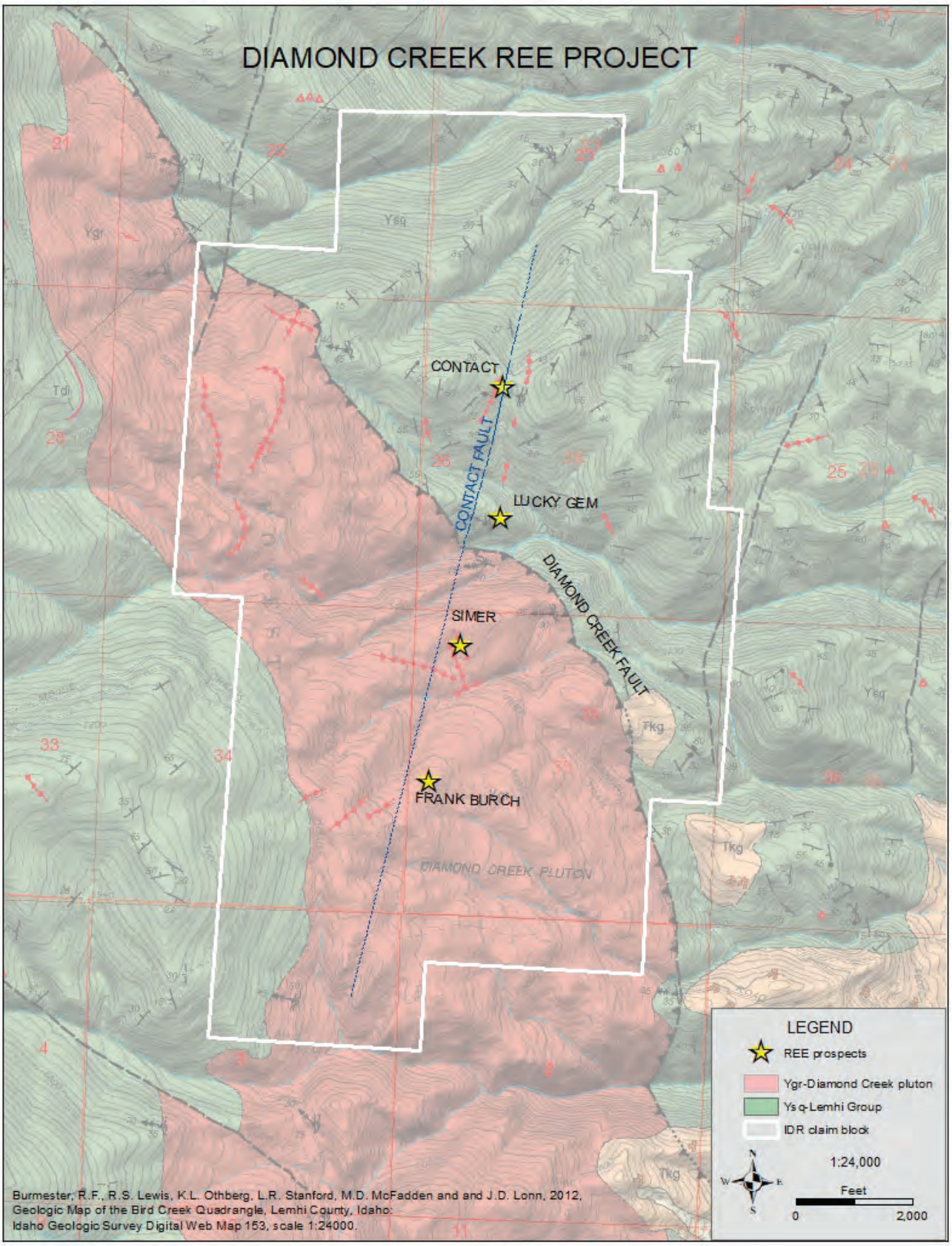

Figure 2. Geologic map of the Diamond Creek REE project area.

Figure 3. Drillcore (DC 22-8) showing complete replacement of country rock.

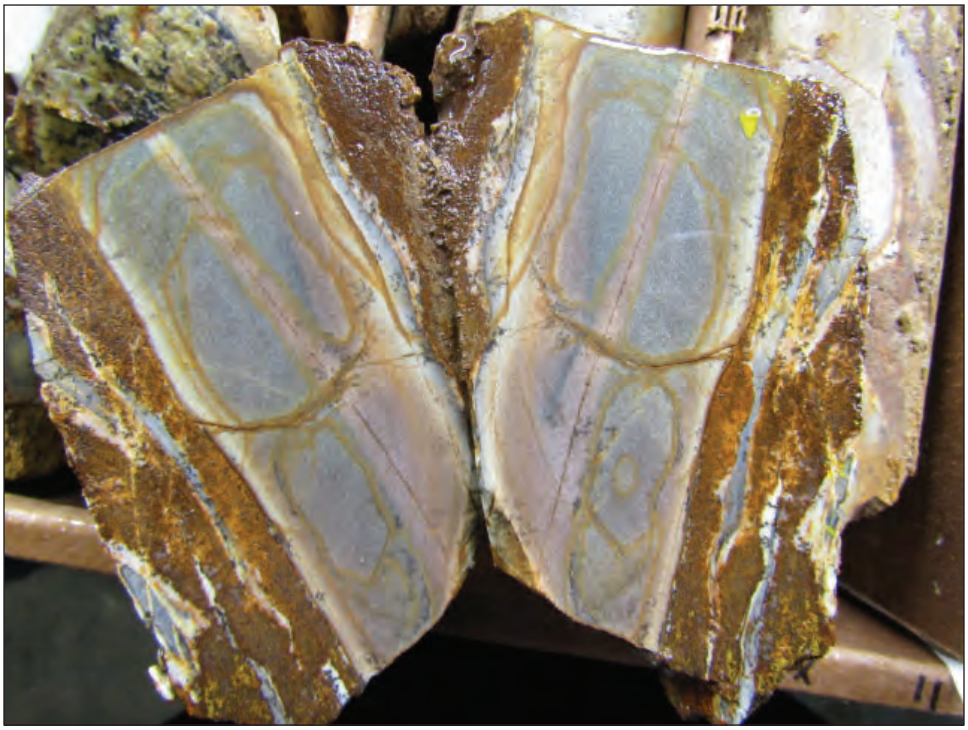

Figure 4. Sample of drillcore showing partial replacement along fractures, and fenitized halos.

fenitized fractures, the country rock displays a "sanded" texture possibly reflecting scapolite or widespread sodic replacement. Primary REE minerals include monazite, xenotime, and some allanite. Associated minerals include specular hematite, feldspars, quartz, barite, thorite, fluorite, and particularly goethite along mineralized fracture/shear zones. The REE minerals are generally only identifiable by microscopic analysis.

2022 DRILLING AND EXPLORATION

Between mid-September and late October of 2022, IDR completed a drilling program at Diamond Creek, with the goal of testing the resource potential of the area as estimated by Staatz and others (1979). The 2022 Diamond Creek drill program completed 12 core holes from 5 different pads for a total of 1,200 m (4,000 ft). Core drilling began in the Contact area and progressed south to the Lucky Gem prospect. In the Contact area, modest REE mineralization was encountered in moderately fractured country rock. However, the core drilling in the Lucky Gem area encountered strong REE mineralization at surface and at depth. A rough geometry developed from holes DC 22-5 to DC 22-7 indicated that the mineralization dipped shallow to the west. From this information, IDR positioned DC22-8 to drill down-dip through this replacement body. The drill hole collared in REE mineralization, which continued for 50.3 m before the hole was lost. The entire 50.3 m showed strongly anomalous to ore grade mineralization, including 11.3 m of 1.3 % TREO, which also includes 2.2 m of 2.1% TREO (fig. 5).

A valuable economic trait of Diamond Creek and other properties in the Idaho REE-Th Belt is the abundance of neodymium (Nd). In the above table, three values of Nd are greater than 0.3%. Neodymium, praseodymium (Pr), dysprosium (Dy), europium (Eu), terbium (Tb), and yttrium (Y) are critical rare earth elements widely considered to be of higher monetary value and essential to numerous low carbon and national defense technologies.

Also of note in the assay shown in figure 5 are elevated values of niobium (Nb), with 0.7% Nb over a 10.1-m interval. While niobium is an important critical mineral, it is not one of the 17 rare earth elements and is not included in TREO calculations. However, niobium may be a profitable byproduct of REE extraction. Anderson (1958) found niobium (columbium) associated with carbonatites in the Mineral Hill district. The niobium geochemical signature at Diamond Creek may point to a buried carbonatite at depth.

During Lucky Gem reclamation efforts, 32 m of REE mineralization was briefly exposed across a drill pad. The exposure displayed evidence of dynamic fluid movement along shears and fracture zones. The surface mineralization was continuous along strike and channel samples were collected every meter for the first 20 m of exposure, and then every 2 m for the last 12 m. Figure 6 shows the results of this surface sampling. The entire 32 m interval averages 1.28% TREO, including >2% TREO at 8 m and 12 m. Neodymium values average 0.5% between 4 m and 20 m, which includes 0.77% at 12 m. Again of note in the table below are the elevated credits of the more valuable REE elements such as Pr, Dy, Eu, Tb, and Y.

IDR's other surface exploration in 2022 included the continuation of mapping and sampling along the Contact fault to the southwest. Two other REE prospects occur along this southwestern extent of the fault: the Simer and Frank Burch. First pass surface outcrop sampling of these prospects returned some TREO values as high as 4.5% in the Simer area, and 5.4% in the Frank Burch area. These results indicate REE enrichment may be increasing toward the southwest.

CONCLUSION

Upon completion of the 2022 exploration program, IDR was able to calculate some dimensions for the Lucky Gem mineralized body. The surface exposure displayed a strike length of 32 m. First phase drilling defined its down-dip length to 50.3 m and DC22-7 gave it a true thickness of 3 m. These calculations make a rather good start in support of the potential REE resources estimated by Staatz and others (1979). Future work in Diamond Creek will build on the success at Lucky Gem, with more drill holes targeting mineralization further down-dip along this mineralized body. Additional drilling is planned in the Contact area, as well as in the Simer and Frank Burch areas, to test for mineral extension of the surface outcrops with assay results up to 5.4% TREO. IDR is continuing to systematically evaluate the Diamond Creek Project in hopes of delineating and identifying a large REE mineralized system.

DC22-8			MS81h																ICP61	S81h/XRF	TREO	TREO
			Ce	Dy	Er	Eu	Gd	Hf	Ho	La	Lu	Nd	Pr	Sm	Tb	Tm	Yb	Y	Sc	Nb		
from	to	thick (m)	ppm	ppm	ppm	ppm	ppm	ppm	ppm	ppm	ppm	ppm	ppm	ppm	ppm	ppm	ppm	ppm	ppm	ppm	ppm	%
2.9	3.8	0.9	2500	206	66	93	270	1	31	1235	4.2	1225	299	297	44.2	7.3	34.9	833	9	3320	7155	0.72
3.8	4.7	0.9	6510	412	131	205	572	0.5	62	3210	8.0	3060	821	700	90.4	14.2	67.9	1635	10	6400	17509	1.75
4.7	5.9	1.2	1945	276	90	112	336	0.5	42	811	5.4	1130	252	331	58.8	9.6	46.2	1140	10	6700	6596	0.66
5.9	6.6	0.7	2080	288	97	115	344	0.5	45	939	5.9	1155	266	332	60.5	10.5	51.0	1210	9	9100	7009	0.70
6.6	6.9	0.3	2300	280	90	116	348	0.5	43	1060	5.2	1275	295	358	59.4	9.7	47.0	1125	4	7600	7416	0.74
6.9	7.6	0.7	3470	429	138	183	539	0.5	65	1550	8.2	2010	455	569	91.3	14.9	70.4	1745	7	9300	11345	1.13
7.6	8.2	0.6	1220	230	80	83	263	0.5	36	497	4.7	727	161	236	47.3	8.7	41.3	976	5	4680	4616	0.46
8.2	9.6	1.4	4560	467	156	194	565	0.5	73	2180	9.1	2350	560	617	98.3	16.9	80.3	1905	6	8300	13838	1.38
9.6	10.1	0.5	4340	491	164	205	601	0.5	76	2010	9.7	2340	551	639	103.0	17.6	85.6	2030	12	10040	13675	1.37
10.1	11.3	1.2	4720	438	155	187	626	0.5	72	2290	10.0	2410	581	614	89.4	17.5	84.3	1825	15	9400	14134	1.41
11.3	12.0	0.7	6240	382	124	202	553	1	59	3160	8.3	2990	747	676	85.9	13.9	66.0	1410	26	5400	16744	1.67
12.0	13.1	1.1	7230	363	116	214	576	1	57	3900	7.7	3330	854	723	83.9	12.8	62.5	1395	22	3600	18947	1.89
13.1	14.2	1.1	9670	211	60	172	415	3	30	5680	4.0	3690	1040	643	54.0	6.5	32.6	745	18	1455	22474	2.25

Figure 5. Assay results from drillcore (DC22-8) showing rare earth elements plus yttrium and scandium for TREO, and niobium.

Diamond Creek Exposure from	to	Surface thick (m)	MS81h Ce ppm	Dy ppm	Er ppm	Eu ppm	Gd ppm	Hf ppm	Ho ppm	La ppm	Lu ppm	Nd ppm	Pr ppm	Sm ppm	Tb ppm	Tm ppm	Yb ppm	Y ppm	ICP61 Sc ppm	MS81h/XRF1 Nb ppm	TREO ppm	TREO %
0	1	1	5830	231	74	111	325	2.0	36	3520	4.6	2220	585	398	45.7	8.0	40	883	13	1555	14325	**1.4**
1	2	1	2990	169	56	76	237	4.0	26	1705	3.6	1245	307	260	33.4	6.0	30	649	11	1635	7809	0.8
2	3	1	2170	151	51	65	204	3.0	23	1145	3.4	990	235	217	28.9	5.6	28	578	12	1645	5910	0.6
3	4	1	5770	322	105	153	469	2.0	48	3110	6.1	2590	651	535	64.2	10.8	54	1210	12	3720	15112	**1.5**
4	5	1	6710	506	162	228	714	0.5	77	3430	9.3	3280	820	775	99.1	17.0	82	2000	8	6100	18918	**1.9**
5	6	1	5970	**718**	233	277	916	0.5	110	2850	13.5	3170	757	865	135.5	24.2	118	2850	9	5500	19016	**1.9**
6	7	1	6270	553	178	230	741	0.5	83	3090	10.4	3100	768	752	106.0	18.5	91	2140	8	5700	18139	**1.8**
7	8	1	7520	508	158	236	738	1.0	76	3940	9.25	3690	896	789	102	16.4	80	1925	9	4790	20693	**2.1**
8	9	1	5290	447	143	194	627	0.5	68	2660	8.49	2670	608	641	87.4	14.95	74	1765	10	5500	15308	**1.5**
9	10	1	5300	426	136	190	604	1.0	64	2650	7.8	2640	652	639	83.4	14.25	68	1660	9	5600	15144	**1.5**
10	11	1	6800	399	125	200	617	0.5	59	3670	7.16	3150	806	689	80.9	12.7	63	1495	11	4770	18184	**1.8**
11	12	1	6970	569	186	249	786	1.0	87	3510	11.2	3640	856	825	111.5	19.5	96	2250	16	7700	20183	**2.0**
12	13	1	4980	406	133	176	559	2.0	62	2460	7.81	2460	566	583	79.3	13.5	68	1615	13	5800	14184	**1.4**
13	14	1	5630	417	136	188	586	0.5	64	2860	8.1	2780	697	635	81.2	14.15	70	1635	11	5300	15812	**1.6**
14	15	1	4670	469	160	190	616	0.5	74	2260	9.5	2490	551	627	89.5	16.55	82	1935	9	4850	14248	**1.4**
15	16	1	4930	462	157	191	620	0.5	72	2400	9.26	2560	575	634	88	16.5	80	1935	9	4860	14739	**1.5**
16	17	1	3340	382	134	163	504	1.0	61	1495	7.39	1935	434	499	73.8	13.8	72	1620	12	3500	10746	**1.1**
17	18	1	4210	257	88	123	361	2.0	40	2110	5.03	1925	484	408	50.7	8.89	48	1025	14	3210	11160	**1.1**
18	19	1	3390	275	92	122	373	3.0	42	1730	5.21	1705	412	402	53.3	9.28	50	1135	14	2520	9813	**1.0**
19	20	1	5440	234	77	127	354	4.0	36	2830	4.79	2360	642	448	47.4	8	42	930	15	2020	13599	**1.4**
20	22	2	2360	84	26	50	140	5.0	13	1450	1.68	920	248	173	17.9	2.7	14	320	10	859	5834	0.6
22	24	2	1140	76	28	33	101.5	8.0	12	576	1.91	508	126.5	109.5	14.85	2.99	17	331	13	959	3100	0.3
24	26	2	2050	137	49	61	188.5	6.0	22	1160	3.26	909	230	203	27.1	5.21	29	587	11	2150	5678	0.6
26	28	2	2150	146	53	65	198.5	4.0	24	1195	3.51	963	244	210	28.7	5.58	31	622	10	2690	5953	0.6
28	30	2	3050	140	49	71	205	4.0	22	1685	3.21	1290	334	254	27.5	5.19	28	573	10	1710	7751	0.8
30	32	2	4700	124	39	73	201	6.0	19	3100	2.54	1615	464	265	26.2	3.9	22	490	12	1185	11161	**1.1**

Figure 6. Surface assay results at the Lucky Gem site, showing rare earth elements plus Yttrium and Scandium for TREO, and niobium.

REFERENCES

Anderson, A.L., 1958, Uranium, thorium, columbium, and rare earth deposits in the Salmon region, Lemhi County, Idaho: Idaho Bureau of Mines and Geology Pamphlet 115, 81 p.

Biddle, J.H., 1985, The geology and mineralization of part of the Bird Creek quadrangle, Lemhi County, Idaho: Moscow, Idaho, University of Idaho, M.S. thesis, 119 p.

Burmester, R.F., Lewis, R.S., Othberg, K.L., Stanford, L.R., McFadden, M.D., and and Lonn, J.D., 2012, Geologic map of the Bird Creek quadrangle, Lemhi County, Idaho: Idaho Geologic Survey Digital Web Map 153, scale 1:24,000.

Evans, K.V., and Zartman, R.E., 1990, U-Th-Pb and Rb-Sr geochronology of Middle Proterozoic granite and augen gneiss, Salmon River Mountains, east-central Idaho: Geologic Society of America Bulletin, v. 102, p. 63–73.

Staatz, M.H., Armbrustmacher, T.J., Olson, J.C., Brownfield, I.K., Brock, M.R., Lemons, J.F. Jr., Coppa, L.V., and Clingan, B.V., 1979, Principal thorium resources in the United States: U.S. Geological Survey Circular 805, 42 p.

REVIVAL GOLD'S BEARTRACK–ARNETT PROJECT: OROGENIC GOLD IN IDAHO

Steven T. Priesmeyer, Dan Pace, and Cameron Egan

Revival Gold, Inc., Salmon, Idaho

The Beartrack–Arnett Project is located in east-central Idaho, approximately 20 km west–northwest of the city of Salmon. Estimated historic placer gold production from the Napias Creek drainage, where both properties are located, is between 400,000 and 600,000 oz of gold. The Beartrack deposit was discovered in the 1980s, put into production during the late 1990s, and produced approximately 600,000 ounces of Au.

In 2017, Revival Gold acquired the Arnett and Beartrack properties and reinitiated exploration in the district. The current published resource at Beartrack–Arnett consists of an Indicated Mineral Resource of 65 million tonnes at 1.01 g/t gold containing 2.12 million oz of gold and an Inferred Mineral Resource of 46.2 million tonnes at 1.31 g/t gold containing 1.94 million oz of gold. The total minimum estimated gold endowment for the Mackinaw district is 5 million oz of gold. Exploration to expand the leachable resource at Arnett and to explore the high-grade underground potential at Beartrack are ongoing.

DISTRICT GEOLOGY

The bedrock geology in the Beartrack–Arnett area is dominated by two Mesoproterozoic rock units: metasedimentary rocks of the Lemhi Group, historically referred to as Yellowjacket Formation, and a rapakivi (megacrystic) granite. The Yellowjacket Formation consists predominantly of a thick sequence of very fine-grained non-calcareous quartzite, siltite, and argillite units that locally exhibit cross-bedding. The Yellowjacket Formation has been intruded by the Proterozoic rapakivi granite. The intrusive is medium to coarse grained, sub-equigranular to porphyritic, and is composed predominantly of quartz, potassium feldspar, plagioclase, and biotite.

Mesoproterozoic metasedimentary rocks have been intruded by the Cambro–Ordovician Arnett intrusive complex, a polyphase potassic intrusive complex located in the Arnett Creek drainage. The Arnett Creek intrusive complex hosts known mineralization in the Arnett area.

Thick accumulations of Tertiary conglomerate, sandstone, shale, and coal, with lesser amounts of mafic to felsic volcanic rocks, are present in the Leesburg Basin. The Leesburg Basin is a structurally developed half-graben that is in part localized by down-to-the-west extension along the Coiner fault. Tertiary facies are highly variable within the basin and include coarse clastic wedges (with cobble to boulder-sized clasts of Mesoproterozoic rock) indicative of multiple phases of rapid Tertiary exhumation and erosion. Volcanics within the package range from 48.3 Ma to 32.2 Ma (Lewis and others, 2022).

BEARTRACK

Gold mineralization at Beartrack lies along the Panther Creek shear zone (PCSZ), which is currently thought to be part of the regionally extensive Coiner fault system. The PCSZ has been active for an extended period. Evidence for this includes early ductile deformation, dikes of various composition, bull quartz veins, mineralized and unmineralized siliceous breccias and stockwork, and post-mineral faulting, all within the PCSZ.

Mineralization at Beartrack is sub-vertical and consists of disseminated and stockwork quartz–pyrite–arsenopyrite veinlets and mineralized siliceous breccias hosted primarily by the metasedimentary rocks and rapakivi granite. Gold occurs as very fine particles in arsenopyrite and in arsenic-rich growth bands in pyrite. Base metal sulfides, tellurides, and tungsten minerals are present in minor amounts. Hydrothermal alteration is dominated by quartz–sericite–pyrite alteration but silicification and K-feldspar alteration are important locally. Minor calcium and iron carbonates are present as gangue and alteration products. Geochemically, Beartrack is an Au-As (±Hg) system with a separate Ag-base metal event. Re-Os dating yielded a date of 68.2 ± -1.7 Ma for mineralization at Beartrack.

ARNETT

The current Mineral Resource in the Arnett area is the Haidee area, located approximately 6 km west of Beartrack. Mineralization at Haidee consists of widely spaced, moderately dipping, sheeted quartz–iron oxide (after pyrite) veins and veinlets striking to the northwest and dipping moderately to the southwest. All known mineralization at Haidee is hosted by Cambro–Ordovician Arnett intrusive complex. At Haidee, the primary host rock is a granite, informally called the "crowded porphyry." Alteration at Haidee consists of early secondary biotite–magnetite alteration, followed by the hypogene oxidation of magmatic and hydrothermal magnetite to specularite and, most closely related to mineralization, sericitic alteration of primary and secondary biotite. Although concentrations are low, Bi and Te are associated with Au at Haidee. The age of mineraliza-

tion at Haidee is 77–80 Ma based on K-Ar dates obtained from sericite.

Numerous other targets are present in the Arnett area. Mineralization in these targets exhibits similar characteristics to that at Haidee except for the orientation of mineralized structures, which is variable. In addition to the crowded porphyry, mineralization in these outlying areas may also be hosted by leucogranite or, more rarely, syenite.

DEPOSIT MODEL

Revival Gold considers Beartrack to be an orogenic Au system. Gold mineralization appears to be localized in extensional jogs and structural intersections within the PCSZ. Mineralization forms a large gold halo over more than 5 km of strike along the structure. Higher grade zones form steeply plunging shoots that are consistent with deposition during an early component of dextral strike-slip faulting along the Coiner fault/PCSZ. Post-mineral movement along the PCF dismembered portions of the system with both right lateral strike slip and down-to-the-west dip-slip motion. Ore-related mineral assemblages and alteration styles display no recognizable mineralogic and/or geochemical zonation over more than 5 km of strike and 750 m of vertical extent explored to date.

The deposit model for Haidee is less clear. Mineralized veins are similar in orientation to a large northwest-striking compressional structure (Poison Creek fault) that is mapped approximately 3 km south of the deposit. Subparallel structures have been inferred by some workers to occur in the Arnett system. If these structures do exist, they do not appear to dismember the intrusive complex based on the drilling completed to date and are not consistent with the current modeling of the depth extent of the intrusive system based on the aeromagnetic surveys. Mineralization occurs proximally to the margins of the Cambro–Ordovician intrusive complex, which has led some to imply a genetic relationship. The current age dates for mineralization at Haidee suggest the mineralizing system is significantly younger than any of the intrusive rocks identified to date. Nevertheless, the intrusions may play a key role in structural preparation and/or rheology contrast that controls the distribution of gold at Arnett. Northwest-striking and northeast-striking high-angle structures are also mapped within the deposit area, which have an unclear genetic relationship to mineralization. Mineralization exhibits characteristics of both an intrusion-related Au system and an orogenic Au system.

In addition to Beartrack, several other Idaho deposits or districts are thought to contain orogenic gold mineralization, including but not limited to the Lemhi deposit north of Beartrack, and the main stage of gold mineralization at Stibnite and Elk City. Mineralization in all four of these areas formed between 62 and 71 Ma. All of these districts overlie, or occur in close proximity to, north–south-trending basement structures.

ACKNOWLEDGMENTS

Reed Lewis provided a review of this text.

REFERENCE

Lewis, R.S., Stewart, D.E., Burmester, R.F., Tkach, M.K., and Canada, A.S., 2022, Geologic map of the Jureano Mountain and Leesburg quadrangles, Lemhi County, Idaho: Idaho Geological Survey Digital Web Map 207, scale 1:24,000.

FIELD GUIDES

GEOLOGY OF THE BELT SUPERGROUP AND CHALLIS VOLCANIC GROUP FROM SALMON TO CHALLIS, IDAHO

Reed S. Lewis, Russell F. Burmester, and Liam D. Knudsen

Idaho Geological Survey, Moscow, Idaho

INTRODUCTION

The Salmon River corridor between Salmon and Challis provides clues to a long and complex geologic history. The purpose of this trip is to see the two main Mesoproterozoic Belt Supergroup units exposed north (in the footwall) of the regionally important Poison Creek fault, and accessible units in its hanging wall to the south (fig. 1). Much of the inaccessibility is due to cover by volcanic rocks of the Eocene Challis Group, so we'll look at some of those too.

STRATIGRAPHY AND STRUCTURE

Mesoproterozoic strata around Salmon constitute the Lemhi subbasin of the Belt Supergroup (fig. 1), and reasonably correlate with the Missoula Group of the main Belt Basin. A stratigraphic column is shown in figure 2. The higher strata were described and named Apple Creek Formation in the Lemhi Range to the east of the Salmon River by Tysdal (2000). The exception we make to Tysdal's correlations is that the Big Creek Formation north of his Lem Peak fault is the Lem Peak member of the Apple Creek Formation (Burmester and others, 2016b). Above that are the fine siltite, diamictite, coarse siltite, and banded siltite members. All these are in the hanging wall of the Poison Creek fault, where the strata become younger to the north. However, the Lem Peak member is not known west of the Salmon River fault, where the fine siltite and diamictite members have but a token presence, and perhaps do not exist west of 114°W. North of the Poison Creek fault are lower strata, Swauger Formation, and Lemhi Group, which are younger to the southwest and locally are unconformably overlain by Ordovician units. This relationship documents pre-Ordovician, likely Neoproterozoic, down-on-the-southwest faulting that exposed the footwall to deeper erosion than the hanging wall. Subsequent thrust faulting affected

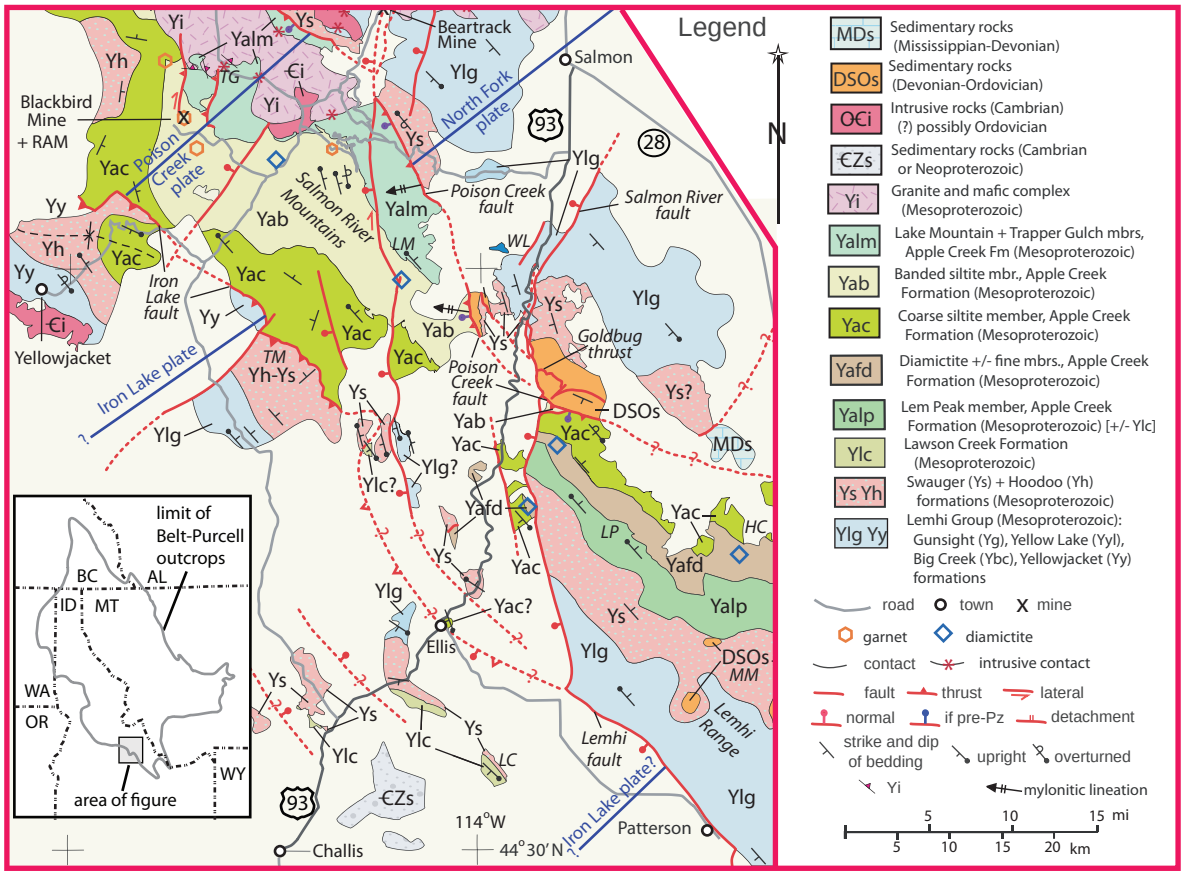

Figure 1. Simplified geologic map of parts of the Salmon River Mountains and northern Lemhi Range showing only Proterozoic and Paleozoic strata. Spans of thrust plates are blue lines. Geographic locations are in italics; HC, Hayden Creek; LC, Lawson Creek; LM, Lake Mountain (Yalm); LP, Lem Peak; MM, Mogg Mountain; TG, Trapper Gulch; WL, Williams Lake. Modified after Burmester and others (2020) to include insights from fieldwork in 2020 through 2022.

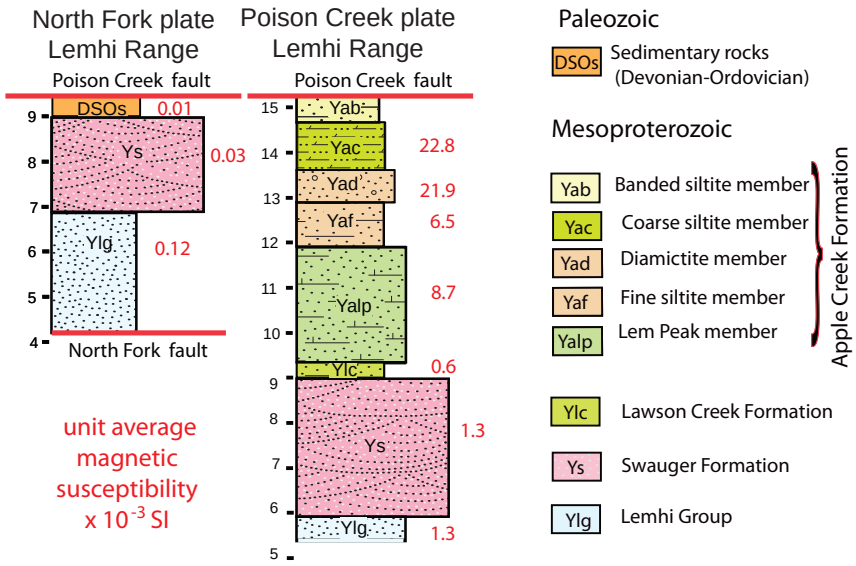

Figure 2. Stratigraphic column for the northern Lemhi Range. Colors and patterns are from figure 1. Vertical scale in kilometers, with 9 being arbitrary the top of the Swauger Formation. Magnetic susceptibilities are from across the Lemhi Range but not from south of about 44.625° N.

all rocks on both sides of the Salmon River and the ancestral Salmon River fault system, which appears to have been activated then (Hansen, 2015; Hansen and Pearson, 2016). The regional structure looks like a faulted syncline, but the southwest facing of footwall strata may be from back tilting as the footwall block rode up a ramp of a later thrust farther northeast (Hansen, 2015).

As shown in figure 3, the units of the Eocene Challis Volcanic Group have been simplified for this trip into those that are below the mafic lavas (Tcvl), the mafic lavas themselves (Tlm), and those overlying the mafic lavas (Tcvu). Although there are some thin mafic lava flows in the lower Challis, the vast majority are in the Tlm unit. These mafic lava flows are important regional markers and are remarkably widespread. The lower Challis units are only locally preserved and include dacite tuffs, flows, and domes, as well as thin mafic lavas and clastic rocks. The upper Challis is a series of mostly rhyolitic tuffs that grade upward into younger (Eocene to Oligocene) sedimentary strata.

ROAD LOG

Figures 3A, 3B, and 3C show the trip route and important rock units. Field trip stops are referenced to GPS coordinates (WGS84), and also with mileage at stops noted. Mileage to some highway mile posts should help you compensate for any side trips or odometer errors. The trip starts at the Sacajawea Interpretive, Cultural, and Educational Center parking lot exit on E. Main St. (Hwy 28) in Salmon. Turn right (NW) and go 1.2 mi to a left turn at the intersection with S. Challis St. (U.S. Highway 93; the first traffic light). Head 5.2 mi south past the BLM–USFS complex and the Salmon Airport (both on the left) to a right turn across the Salmon River on the Shoup Bridge.

6.4 mi US 93–NF 021 intersection. Reset odometer at the right turn. Figure 4 shows the route, stops, and points of interest mentioned in this log, starting here.

0.1 mi Cross the Salmon River on the Shoup Bridge. Drive due west on road NF 021, climbing up onto older alluvial fan deposits at about 0.6 mi to a Y intersection (0.8 mi) and park in the open space between roads.

0.8 mi Stop in the open area where the roads fork.

STOP 1

OVERVIEW OF SALMON BASIN AND NORTHERN LEMHI RANGE

(45.0986°N, 113.9101°W)

From here we can look eastward at the northern end of the Lemhi Range. Exposed rocks are Lemhi Group biotite–feldspar quartzite. Visible are some bare areas that are breccias along the Salmon River fault. Here the fault appears to have a simple (listric?) normal motion that tilted overlying Challis units eastward while dropping them down relative to the Lemhi Group bedrock of the Lemhi Range. See Burmester and others (2016a) for additional information of the geology around Salmon.

2.2 mi Possible detour up Perreau Creek (45.0989°N, 113.9392°W). Eocene or Oligocene conglomerate of Kriley Gulch on right resting on east-dipping Challis.

2.5 mi Tuffaceous sediments (45.0990°N, 113.9438°W).

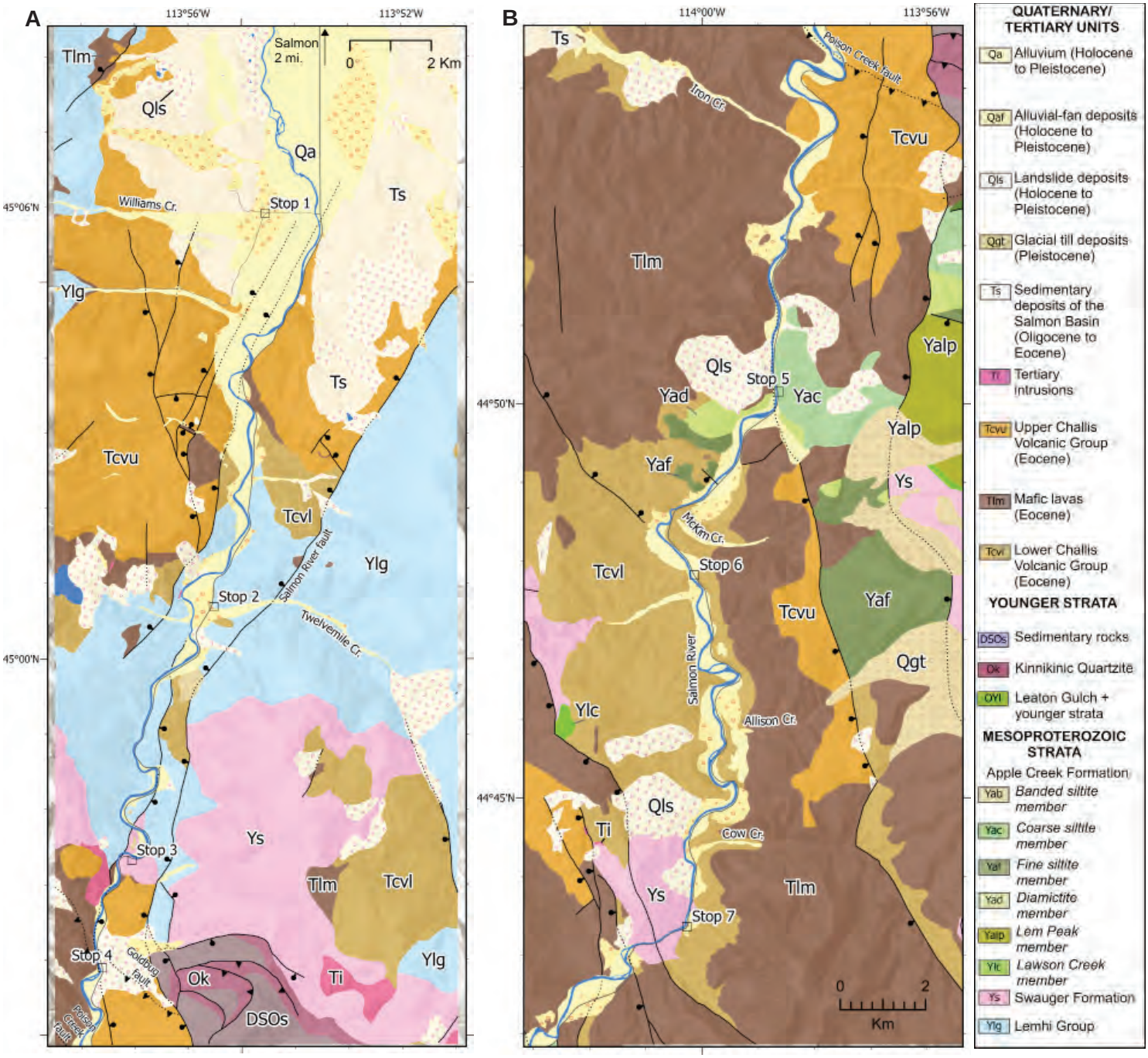

Figure 3. Geologic maps of the Salmon River corridor between Salmon and Challis Idaho: the legend shows units along the route; A shows stops 1-4; B stops 5-7; C stops 8-10. C on following page.

2.7 mi Pink biotite-plagioclase tuff (45.0992°N, 113.9482°W).

Return to US 93. Reset odometer. There are facilities immediately to the south at the Shoup Bridge Campground.

1.4 mi Sevenmile Creek. Much of the rock on the left is a biotite–plagioclase tuff with an average magnetic susceptibility of 2.2 SI x 10^{-3}.

2.1 mi Eightmile Day Use Area and river access.

2.7 mi East–northeast-dipping Challis mafic flow.

4.4 mi Tenmile Creek. Beyond are Mesoproterozoic rock of the Lemhi Group.

5.4 mi Elevenmile river access.

6.4 mi Greyhouse Inn B&B, and mile post 293.

6.6 mi Turn left onto Twelvemile (12 Mile) road and park on the right.

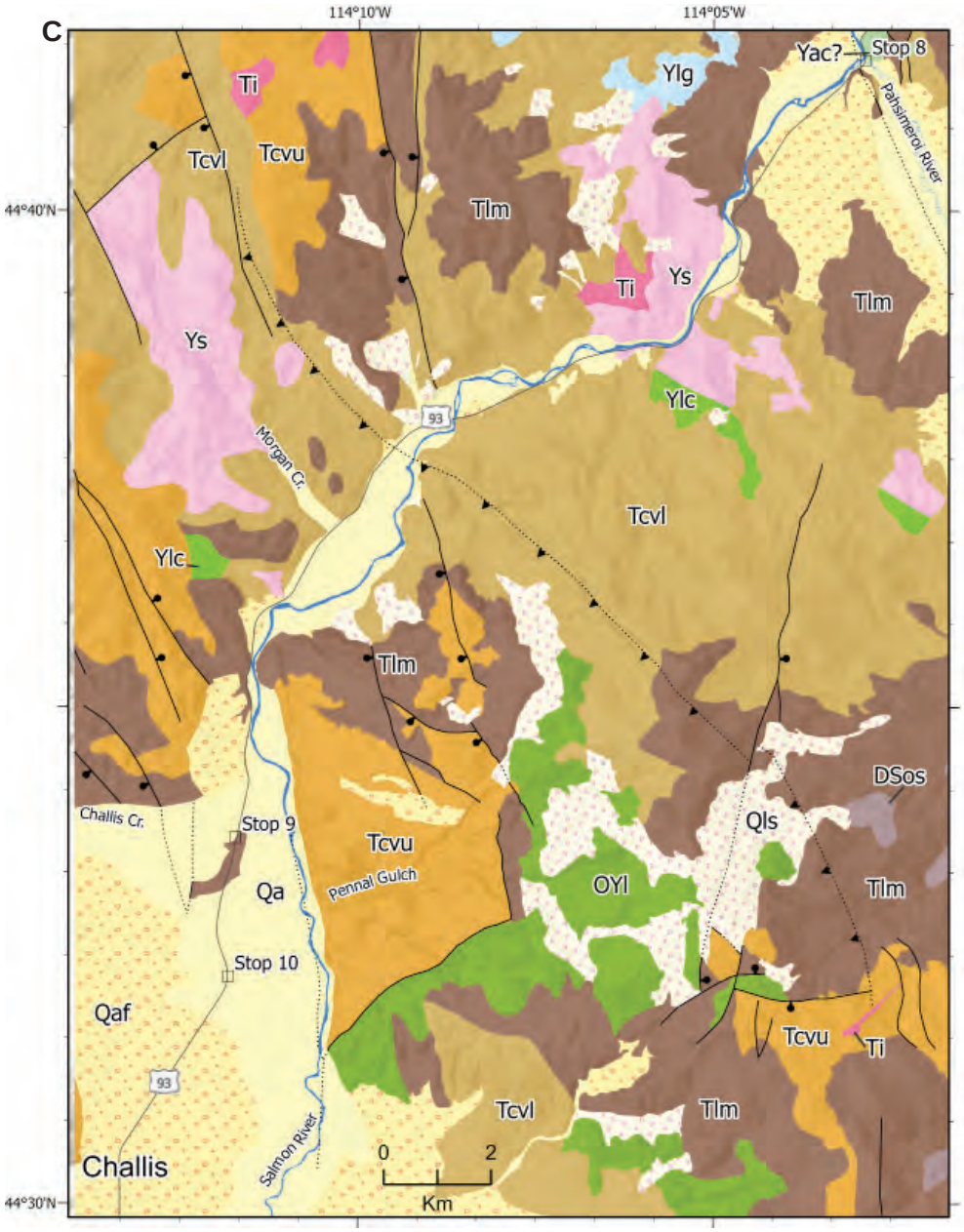

Figure 3. *Continued*.

Figure 4. Typical dark gray exposure of quartzite of the Lemhi Group at Stop 2 near the mouth of Twelvemile Creek.

STOP 2

LEMHI GROUP QUARTZITE AT TWELVEMILE CREEK

(45.0115°N, 113.9263°W)

We are on the North Fork plate, north of the Poison Creek fault. These rocks are below the Swauger Formation and were mapped here as Gunsight Formation of the Lemhi Group (Lewis and others, 2013). However, Ruppel's (1975) formalization of units in the Lemhi Group was in the Poison Creek plate to the south and we have been unable to recognize the Yellow Lake Formation, the fine-grained unit between the Gunsight and Big Creek formations, on the North Fork plate.

Here, look for grain size, bedding thickness, and any indication of which way is up (fig. 4).

Across the river to the west are Challis volcanics overlying the Lemhi Group (fig. 5).

7.5 mi 45th parallel, the south edge of the Salmon 1:100k map and our mapping along this road.

11.8 mi Pull out to the left at the Tree sign. Walk west to the outcrops of Swauger Formation.

STOP 3

SWAUGER FORMATION AT TREE POEM SIGN

(44.9554°N, 113.9519°W)

Thick-bedded quartzite of the Swauger Formation (fig. 6). Check for grain size, sorting, feldspar content, and crossbeds. Typical Swauger Formation contains well-rounded medium grains. What is the facing direction? There appears to be considerable structural complexity in this area, possibly due to faulting that roughly parallels the river (fig. 3A).

Figure 5. View west from Stop 2 of the road leading to Williams Lake. Exposures below the road and on the right edge of the photograph are quartzite of the Lemhi Group. Overlying rocks are Challis Volcanic Group. See Lewis and others (2013) and Burmester and others (2016a) for details.

Figure 6. Outcrop of quartzite of the Swauger Formation at stop 3 showing characteristic bedding style.

12.2 mi Tertiary and Quaternary cover for more than a mile.

13.4 mi Mile post 286.

13.5 mi Access to the Twin Peaks Guest Ranch on the right.

13.9 mi Waddington Creek river access (Google has this as Washington Creek). Pullout to the right.

STOP 4

LANDSLIDE BLOCKS OF KINNIKINIC QUARTZITE AT WADDINGTON CREEK

(44.9316°N, 113.9612°W)

Large blocks of quartzite in and east of the river (fig. 7) were transported to their current position by a significant landslide. Outcrops of Ordovician Kinnikinic Quartzite (Ok) are 1,100 ft above us to the east. This is about where Hansen and Pearson (2016) projected the Goldbug thrust. Across the river are columns in mafic lava, which are uncommon regionally (fig. 8).

14.6 mi Lime Creek. There is not much carbonate in the Mesoproterozoic stack, so lime is from Paleozoic strata above the Kinnikinic (Ok).

16.0 mi Idaho Hermits Historical Marker on right. Ahead are mafic lava flows (magnetic susceptibility 12.3 SI x 10^{-3}) and Elk Bend. Underneath is where Hansen (2015) and Hansen and Pearson (2016) projected the Poison Creek fault. The Salmon River fault is about 1.4 mi to the east.

17.5 mi Warm Spring Creek and access to Goldbug Hot Springs on left.

18.4 mi Mile post 281.

Figure 7. Large landslide-derived blocks of Kinnikinic Quartzite in and east of the Salmon River at Stop 4.

18.6 mi Iron Creek Bridge on the right. To access Iron Creek, cross the bridge and turn right. Thick sections of banded and coarse siltite members of Apple Creek Formation are mapped to the west, but no lower members or Lawson Creek Formation have been found on the Poison Creek plate in the Salmon River Mountains.

19.1 mi Poison Creek Road. Private but access to the northern end of the Poison Creek plate in the Lemhi Range.

19.9 mi Mafic lavas.

21.1 mi Outcrops on right are coarse siltite member of the Apple Creek Formation, but good parking is lacking. Magnetic susceptibility here (17.7 SI x 10^{-3}) is high relative to the average for Lemhi subbasin Mesoproterozoic strata (4.4 SI x 10^{-3}; n = 1746).

22.2 mi Talus of coarse siltite member and large pullout on left. Park near the concrete barrier.

STOP 5

TALUS OF COARSE SILTITE MEMBER OF APPLE CREEK FORMATION

(44.8358°N, 113.9782°W)

As Mark McFaddan would say, shop the talus for the variety of coarse siltite here (figs. 9, 10). This is close to the lower contact with the diamictite member. Average magnetic susceptibility measured here is 20.2 SI x 10^{-3}. We are now on the Allison Creek quadrangle, which was mapped in detail by Tysdal and Moye (1996).

22.8 mi Kilpatrick river access (44.8292°N, 113.9841°W). View across at diamictite member on the right (north) and fine siltite member on the left. Is there a difference in attitude? Implications? Magnetic susceptibility low in the diamictite where clasts are larger than directly across the river is 46.3. Magnetic susceptibility of the fine siltite is 0.2 lowest in the section as exposed but increases to 7.7 close to the diamictite contact (all SI x 10^{-3}). It is possible to walk up the alluvial fan to the east of the highway and see diamictite. Average magnetic susceptibility in two places there is 7.1 and 2.2 (SI x 10^{-3}).

Figure 8. Columns developed in mafic lavas of the Challis Volcanic Group west of the Salmon River at Stop 4.

23.4 mi Mile post 276.

23.8 mi Across river is a NW-striking, steeply dipping thick quartz vein, locally brecciated (44.8173°N, 113.9974°W). Mafic lavas on the left beyond that have average magnetic susceptibility of 30.0 SI x 10^{-3}.

25.7 mi McKim Creek Road, which provides access to coarse siltite and diamictite members west of the Salmon River fault as well as Swauger and Lawson Creek Formations, and Lem Peak and higher members of the Apple Creek Formation east of the fault. Park here and walk southeast to the roadcut.

STOP 6

TUFF OF ELLIS CREEK AT McKIM CREEK ROAD

(44.7970°N, 114.0032°W)

This outcrop of the tuff of Ellis Creek shows the characteristic light green color and darker green pumice

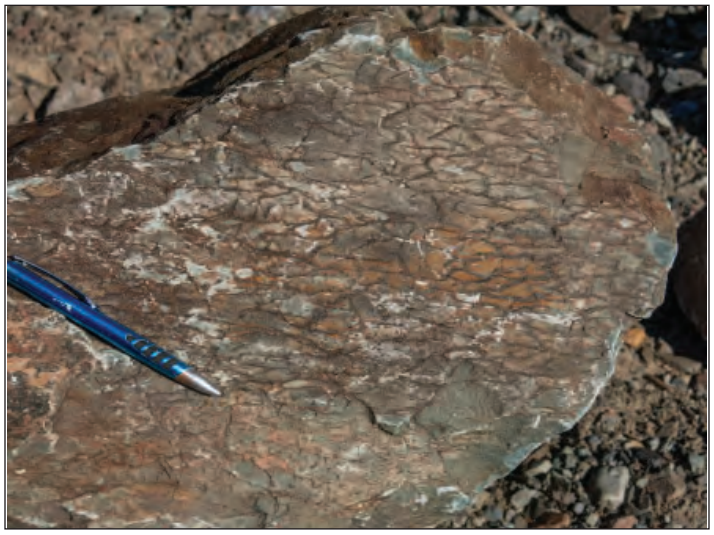

Figure 9. Stretched mudcracks in argillaceous layers within the coarse siltite member of the Apple Creek Formation at Stop 5.

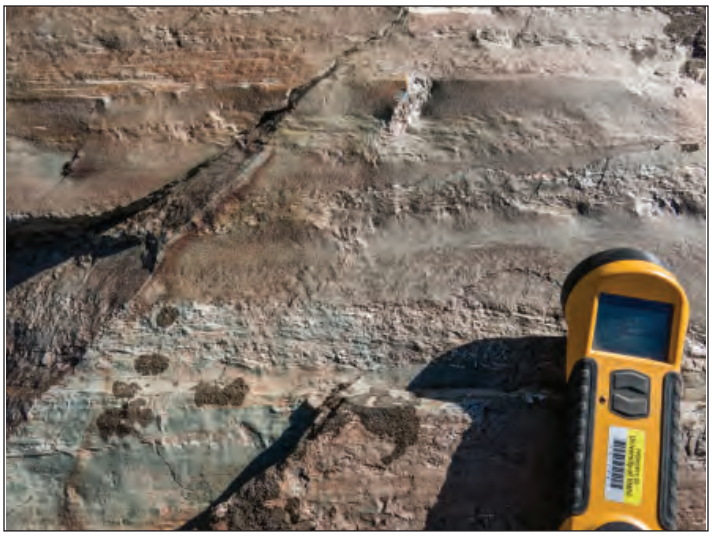

Figure 10. Mudchips deposited along bedding planes within the coarse siltite member of the Apple Creek Formation at Stop 5.

fragments. Exposure also shows a wood fragment caught up in the ash flow and now black carbon (fig. 11). Magnetic susceptibility measured here is 0.2 but a mile farther south is 2.0 (both SI x 10^{-3}).

25.9 mi Roadcut exposure showing an odd relationship of gravels of the Salmon River that appear to be under tuff of Ellis Creek. Why? One hypothesis is that the Ellis is not in place, having been transported downslope by a landslide. Across the river is Hat Creek.

27.0 mi More tuff of Ellis Creek on left.

27.8 mi Allison Creek Road. Access to Swauger and Lawson Creek Formations, and Lem Peak member of Apple Creek Formation. Look northwest across the river from here at light green volcaniclastic rocks interrupted by darker mafic lavas (fig. 12). Did those fill a gully in the tuff or do they occupy a small graben? Both are thought to be within the lower part of the Challis Volcanic Group below the tuff of Ellis Creek and are part of the "mixed unit" mapped to the southwest by Fisher and others (1992).

30.4 Mile post 269.

31.8 mi Narrows in river are the lower end of Cronks Canyon. To east is a stack of tuff of Ellis Creek overlain by mafic lavas.

32.2 mi Pullout to the left before entering Cronks Canyon (locally, the Royal Gorge).

STOP 7
CRONKS CANYON AND SWAUGER FORMATION QUARTZITE

(44.7227°N, 114.0054°W)

The main part of Cronks Canyon is formed by the Salmon River cutting through resistant quartzite of the

Figure 11. Exposure of the tuff of Ellis Creek at Stop 6 showing a carbonized piece of wood that was caught up in the ash flow tuff.

Figure 12. View looking north–northwest across the Salmon River north of the mouth of Allison Creek showing light-green tuffaceous rocks and brown mafic lavas (lower Challis volcanics).

Figure 13. View looking southwest up the Salmon River of Swauger Formation quartzite in Royal Gorge.

Swauger Formation (fig. 13). Check the dips—are they mostly shallow downriver? Here and farther upstream the Swauger protrudes above the Challis Volcanic Group and during Eocene time likely formed the high ridges in the area. A fault, mapped as down-on-the-southwest, is present on the southwest end of the gorge. See river guide by Knudsen and others (this volume) for geology from Cronks Canyon north to Kilpatrick river access (mile 22.8).

34.4 mi Mile post 265.

34.7 mi Bridge to the right leads to Deer Gulch campground and Hat Creek Road.

35.6 mi Intersection of US 93 and the Pahsimeroi River Road at Ellis. Turn left, cross a small bridge, and park on the right.

STOP 8

ENIGMATIC METASEDIMENTARY ROCKS AT ELLIS

(44.6919°N, 114.0486°W)

Rocks here were mapped as Apple Creek Formation by McIntyre and Hobbs (1987) using the stratigraphy of Ruppel (1975), which defined formal units within the Lemhi Group, which he also defined. Winston and others (1999) followed that stratigraphy, with which we disagree, because it had Apple Creek Formation both above and below the Swauger Formation. Our restriction of Apple Creek Formation to strata above the Swauger allowed renaming the section in the Lemhi Group to the Yellow Lake Formation. The rocks here could be Yellow Lake Formation. Broadly similar rocks, but perhaps with more carbonate, occur along Morse Creek 20 km (12.8 mi) southeast. Magnetic susceptibilities are similar (5.19 ± 8.34 SI x 10^{-3}, n = 20 there; 4.83 ± 7.45 SI x 10^{-3} n = 87 here). There the rocks are under a quartzite unit that is below the Swauger Formation. That puts them in the stratigraphic position of the Yellow Lake Formation. Those rocks are nearly along strike, but their northeast dip and facing direction are opposite of ones here. The apparent down-dip slip here (fig. 14) is consistent with these rocks being in the footwall of the Lemhi fault (Haller and Wheeler, 2010) that runs along the foot of the Lemhi Range so they could be Lemhi Group rocks in that fault's footwall. Assignment of these rocks to the Lemhi Group also reduces the need for a major fault between here and the closest similar rocks, which we have mapped up Ellis Creek as Lemhi Group, 3 km (1.9 mi) to the northwest. But there we saw generally thicker beds and no mudcracks, and measured an order of magnitude lower susceptibility (0.43 ± 0.83 SI x 10^{-3}, n = 91).

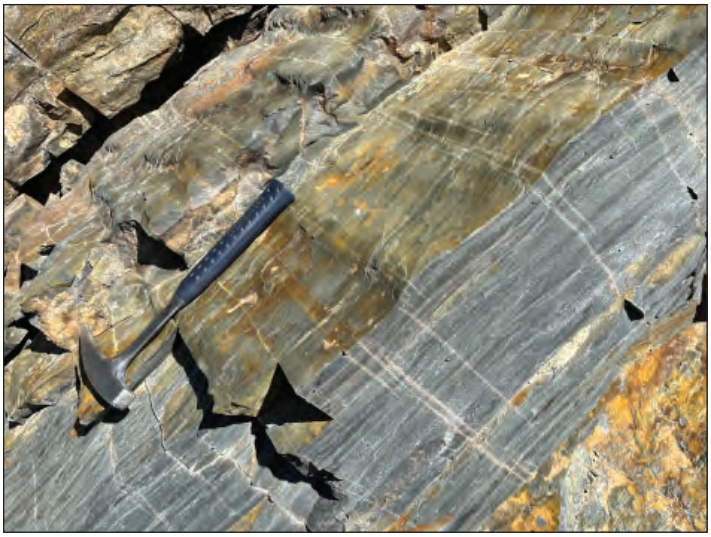

Figure 14. Fabric developed in Belt Supergroup strata at Stop 8 that is interpreted to show down-dip slip.

Alternatives are that the strata at this locality are above the Swauger, either Lawson Creek Formation or Apple Creek Formation. Mud cracks are known in the type Lawson Creek Formation (Hobbs, 1980) 14 km (8.7 mi) south–southeast of here, but that section is incomplete, with higher strata being obscured by Challis volcanics. The meter-thick, crossbedded feldspathic quartzite, red coloration, and sparse green porcellanite low in that section are not found here, and the susceptibility there is much lower (0.13 ± 0.05 SI x 10^{-3}, n = 30). Stretched mud cracks (fig. 15) and moderately high magnetic susceptibility (13.5 ± 13.2 SI x 10^{-3}, n = 147) occur in the coarse siltite member of the Apple Creek Formation 24 km (15 mi) to the north in the Degan Mountain quadrangle (Lewis and others, 2021). Well-rounded fine to medium quartz grains that are sparse but present here (fig. 16) also are in the

Figure 15. Stretched mudcracks in argillaceous layers of Belt Supergroup north of Ellis at Stop 8.

Figure 16. Siltite with thin lenses of well-rounded fine to medium quartz grains at Stop 8.

coarse siltite member under the Iron Lake fault near Quartzite Mountain (50 km, 31 mi) northwest of here; unpublished mapping, 2022). Although we saw no mud cracks, there were plenty of chips, thin bedding, and high susceptibility (9.42 ± 10.30 SI x 10^{-3}, $n = 100$), making the coarse siltite a viable unit for here.

However, assignment to the coarse siltite comes at a structural price. One solution is that the Swauger of Cronks Canyon is the core of an anticline such that from there to here we have been going upsection, probably with the help of a normal fault. The implication of this is that there is a major up-on-the-west fault between here and the Lemhi Group rocks up Ellis Creek. That could be the Iron Lake fault that farther southeast plausibly was reactivated as the Lemhi fault.

36.5 mi Mile post 263; canyon of Ellis Creek on the right where there is less tuff that bears its name than exposed better elsewhere.

37.8 mi Entrance to Cottonwood Recreation Site, a fine stop with facilities. Detouring here may add 0.6 mi to your odometer.

More mafic lavas on the left.

38.6 mi Eagle Rock. Quartzite of the Swauger Formation.

39.3 mi Shotgun Creek.

40.6 mi Sheep Creek Road. To the south is one section of the Lawson Creek Formation of Hobbs (1980). Out of Swauger for a short while. Tuff of Ellis Creek across the river ahead.

42.6 mi Waits Bridge. Boat ramp and facilities (?) across the bridge on the right.

44.6 mi Morgan Creek Road. Still more tuff of Ellis Creek, with overlying darker colored mafic lavas.

45.6 mi Private drive to right and small exposure of Swauger Formation.

45.8 mi More mafic lavas around Fuller Gulch. Up the gulch is another of Hobbs' (1980) Lawson Creek sections.

46.5 mi Large pullout on left. Mafic lavas, possibly latite, on right.

47.4 mi Stevens Gulch.

48.0 mi Challis Creek.

48.6 mi Stevens Lane (Road on Google maps). Also a sign for Mile High Outfitters on the east side of the highway. Pull over on right in small parking area west of the highway.

STOP 9

VIEW OF TUFFS OF PENNAL GULCH AND CHALLIS CREEK

(44.5614°N, 114.1964°W)

From the parking area, look east at the cliffs across the river (fig. 17). Most of the cliff faces are tuff of Pennal Gulch. The upper, red-weathering areas are tuff of Challis Creek. The tuff of Pennal Gulch consists of silicic, crystal-poor pyroclastic flows and tephra, both subaqueous and subaerial (McIntyre and Hobbs, 1987; Fisher and others, 1992). Unit includes pumice-bearing tuff as well as thin-bedded volcanic sandstone and mudstone. The tuff of Challis Creek consists of densely welded ash-flow tuff that contains 5 to 20 percent crystals of sanidine (commonly chatoyant), quartz (commonly smokey), and local minor plagioclase (McIntyre and Hobbs, 1987; Fisher and others, 1992).

50.2 mi North end River Rock Road and access to Pennal Gulch Birding Trail. Pull over on east side of highway.

Figure 17. View east across the Salmon River south of Challis Creek at Stop 9 showing the tuff of Pennal Gulch and overlying tuff of Challis Creek.

Figure 18. View east across the Salmon River at Pennal Gulch showing the tuff of Pennal Gulch and overlying tuff of Challis Creek as well as metasedimentary strata that at least in part post-date the Belt Supergroup (dark outcrops).

STOP 10

VIEW OF CHALLIS TUFFS AND OLDER METASEDIMENTARY STRATA

(44.5381°N, 114.1981°W)

Cliffs across the river are tuff of Pennal Gulch and the red rock above is the tuff of Challis Creek (fig. 18). Dark gray rocks in the distance are Mesoproterozoic to Ordovician quartzitic strata that have been uplifted along a northeast-striking normal fault. According to Pearson and others (2021), the ages of these rocks span from Mesoproterozoic at the older part of the section to about 1320 Ma (also Mesoproterozoic) at the upper part of the Leaton Gulch unit. These rocks are, in turn, overlain in angular unconformity by Neoproterozoic rocks and then eventually Ordovician strata.

50.8 mi South end River Rock Road and start of long straight stretch past the Challis Airport and into Challis.

52.7 mi Exxon station for those in need. It is across the street from the U.S. Forest Service Challis–Yankee Fork Ranger District office.

52.8 mi Intersection of US 93 and Main Street. Small city park.

Return to Salmon, picking up lost stops on the way as time and temperament allow. Beverages await.

ACKNOWLEDGMENTS

Paul Link kindly provided a manuscript review.

REFERENCES

Burmester, R.F., Lewis, R.S., Othberg, K.L., Stanford, L.R., Lonn, J.D., and McFaddan, M.D., 2016a, Geologic map of the western part of the Salmon 30 x 60-minute quadrangle, Idaho and Montana: Idaho Geological Survey Geologic Map 52, scale 1:75,000.

Burmester, R.F., Lonn, J.D., Lewis, R.S., and McFaddan, M.D., 2016b, Stratigraphy of the Lemhi subbasin of the Belt Supergroup, *in* MacLean, J.S., and Sears, J.W., eds., Belt Basin: Window to Mesoproterozoic Earth: Geological Society of America Special Paper 522, p. 121–137.

Burmester, R.F., Lonn, J.D., and Lewis, R.S., 2020, Further speculation on Belt stratigraphy and structure around Salmon, Idaho: Alternative interpretations and tests: Northwest Geology, v. 49, p. 19–34.

Fisher, F.S., McIntyre, D.H., and Johnson, K.M., 1992, Geologic map of the Challis quadrangle, Idaho: U.S. Geological Survey Miscellaneous Investigations Series Map I-1819, scale 1:250,000.

Haller, K.M., and Wheeler, R.L., compilers, 2010, Fault number 602a, Lemhi fault, Ellis section, *in* Quaternary fault and fold database of the United States: U.S. Geological Survey website, https://earthquakes.usgs.gov/hazards/qfaults [Accessed June 2023]

Hansen, C., 2015, An investigation into the Poison Creek thrust: a Sevier thrust with Proterozoic implications: Moscow, Idaho, Idaho State University, M.S. thesis, 80 p.

Hansen, C.M., and Pearson, D.M., 2016, Geologic map of the Poison Creek thrust fault and vicinity near Poison Peak and Twin Peaks, Lemhi County, Idaho: Idaho Geological Survey Technical Report T-16-1, scale: 1:24,000.

Hobbs, S.W., 1980, The Lawson Creek Formation of Middle Proterozoic age in east-central Idaho: U.S. Geological Survey Bulletin 1482-E, 12 p.

Knudsen, L.D., Lewis, R.S., Schmidt, K.L, and Stewart, D.E., this volume, Floating the river: Mesoproterozoic to Quaternary geology along the Salmon downstream from Ellis Idaho: Northwest Geology, v. 52.

Lewis, R.S., Othberg, K.L., McFaddan, M.D., Burmester, R.F., Stewart, D.E., Stanford, L.R., and Stewart, E.D., 2013, Geologic map of the Williams Lake quadrangle, Lemhi County, Idaho: Idaho Geological Survey Digital Web Map 162, scale 1:24,000.

Lewis, R.S., Canada, A.S., Stewart, D.E., and Burmester, R.F., 2021, Geologic map of the Degan Mountain quadrangle, Lemhi County, Idaho: Idaho Geologic Survey Digital Web Map 200, scale 1:24,000.

McIntyre, D.H., and Hobbs, S.W., 1987, Geologic map of the Challis quadrangle, Custer and Lemhi Counties, Idaho: U.S. Geological Survey Geologic Quadrangle Map GQ-1599, scale: 1:62,500.

Pearson, D.M., Montoya, L.M., and Link, P.K., 2021, Field guide to Mesoproterozoic to Ordovician rocks exposed east of Challis near Leaton Gulch, Idaho: Northwest Geology, v. 50, p. 95–106.

Ruppel, E.T., 1975, Precambrian Y sedimentary rocks in east-central Idaho: U.S. Geological Survey Professional Paper 889-A, 23 p.

Tysdal, R.G., 2000, Stratigraphy and depositional environments of Middle Proterozoic rocks in northern part of Lemhi Range, Lemhi County, Idaho: U.S. Geological Survey Professional Paper 1600, 40 p.

Tysdal, R.G., and Moye, F.J., 1996, Geologic map of the Allison Creek quadrangle, Lemhi County, Idaho: U.S. Geological Survey Geological Quadrangle Map GQ-1778, scale 1:24,000.

Winston, D., Link, P.K. and Hathaway, N., 1999, The Yellowjacket is not the Prichard and other heresies: Belt Supergroup correlations, structure and paleogeography, east-central Idaho, *in* Hughes, S.S., and Thackray, G.D., eds, Guidebook to the Geology of Eastern Idaho: Pocatello, Idaho Museum of Natural History, p. 3–20.

CHALLIS VOLCANICS, ASSOCIATED SEDIMENTS, AND VALLEY-FILLING LANDSLIDES IN THE WILLIAMS LAKE AREA NEAR SALMON, IDAHO

David E. Stewart,[1] Reed S. Lewis,[1] and Loudon R. Stanford[2]

[1]*Idaho Geological Survey, Moscow, Idaho*
[2]*Idaho Geological Survey, Moscow, Idaho, retired*

INTRODUCTION

This field trip will examine ash-flow tuffs, mafic lava flows, and related epiclastic sediments in the Challis volcanic section near Williams Lake, south of Salmon (fig. 1). These Eocene deposits are not only of interest for documenting volcanic activity at that time, but they also provide critically important marker beds that allow us to detect fault displacements in the Mesoproterozoic rocks that underlie them; rocks that contain markers best described as "ill-defined." Figure 1 shows the volcanics in relation to the Mesoproterozoic rocks they rest on. We will also see evidence of large landslides, some of which have filled valley floors and dammed streams. This trip involves mostly roadside stops with one short, strenuous hike at our final Stop 6.

This road log is modified from a previous TRGS trip in the Williams Lake area led by Reed Lewis, Kurt Othberg, Russ Burmester, Loudon Stanford, and Mark McFaddan in 2013 (Lewis and others, 2013a). It is based largely on geologic mapping by the Idaho Geological Survey in the Williams Lake quadrangle (Lewis and others, 2013b), the Lake

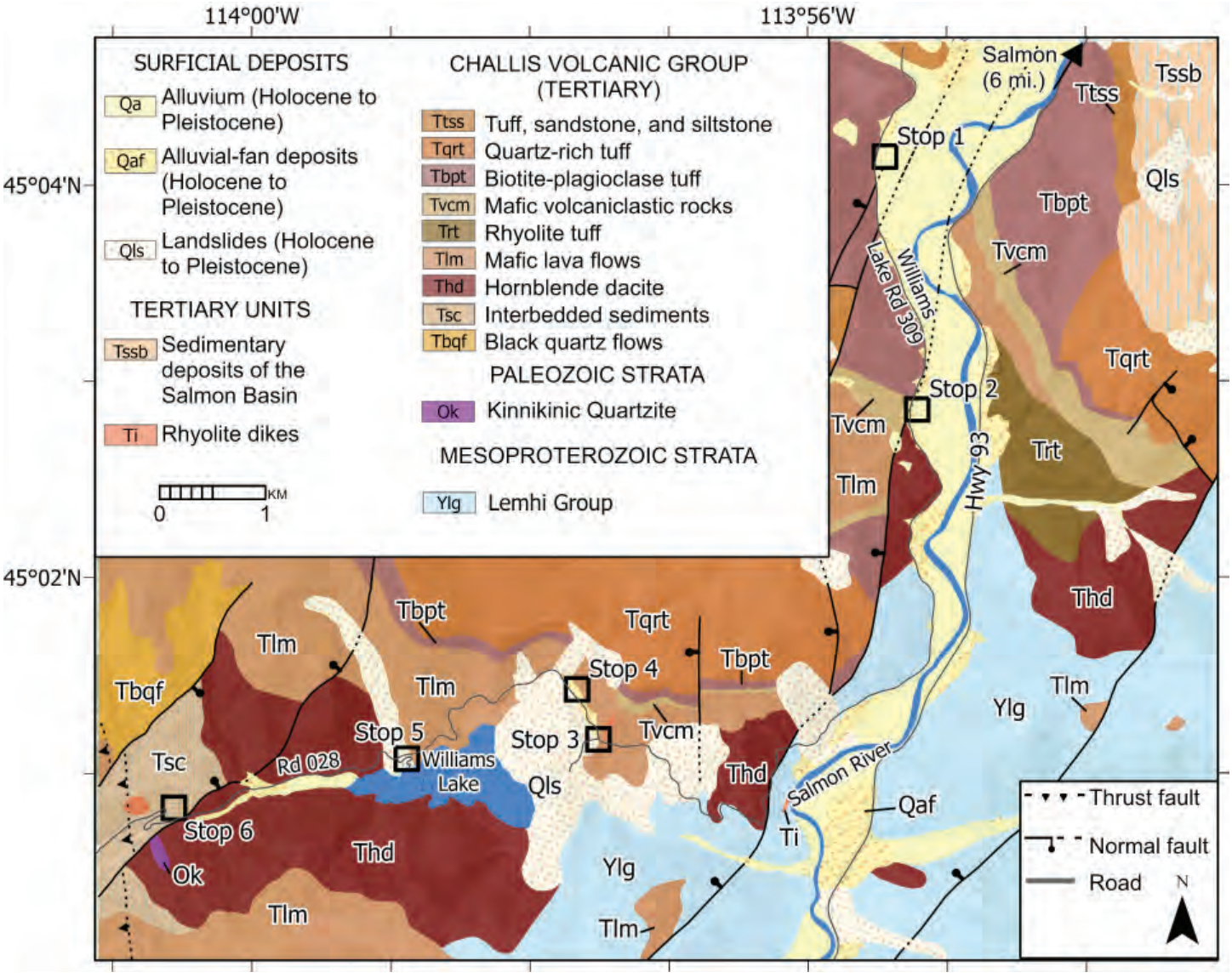

Figure 1. Geologic map showing stops on this field trip and distribution of Challis units. Based largely on Burmester and others (2016).

Mountain quadrangle (Stewart and others, in press) and the western part of the Salmon 30' x 60' quadrangle (Burmester and others, 2016).

REGIONAL GEOLOGY

Rocks of the Challis Volcanic Group formed from eruptions, intrusions, erosion, and deposition in the Eocene, about 51–44 Ma. They are widespread southwest of Williams Lake (fig. 1), where they were mapped in the Challis 1° x 2° quadrangle (Fisher and others, 1992). Blankenau (1999) established a stratigraphic section about 36 km (22 mi) east of Williams Lake, northwest of Lemhi Pass, which is also useful for mapping in this part of the volcanic field.

The oldest Challis units near Williams Lake are hornblende dacite (fig. 2) and tuff with quartzite lithics. The dacite is confined to the south in the area near the lake and the lithic tuff is present only to the north (southwest of Stop 6 and thus not shown on fig. 2). A much more regionally continuous series of mafic flows overlies both units. Capped locally by mafic volcaniclastic rocks, the flows are in turn overlain by units of welded tuff. The lowermost welded tuff contains biotite and plagioclase phenocrysts and is characterized by spherulites and lithophysae formed during extensive vapor-phase alteration. The next youngest unit is a quartz-rich tuff that forms the highest cliffs north of Williams Lake. To the north are less welded sanidine-bearing tuffs interlayered with sandstone and siltstone. Farther north, younger Tertiary sedimentary deposits of the Salmon basin overlie these Challis units (Burmester and others, 2016). See Stewart and Lewis (this volume, The Challis–Mesoproterozoic Unconformity, Challis Volcanics, and Related Sediments in the Williams Creek Vicinity) for discussion of the variation in Challis stratigraphy between the Williams Lake and Williams Creek areas and sections to the south.

Several down-to-the-west normal faults traverse the quadrangle (fig. 1). The most prominent fault crosses the upper part of Tenmile Creek 1.8 mi east of Stop 1, forming the range front that extends from there northeast into the adjoining Sal Mountain quadrangle. Not shown by Anderson (1956), but present on a later, unpublished map of his, this fault extends north to Salmon Hot Springs; to the south it apparently connects with a north–south structure termed the Salmon River fault (Tysdal, 2002) or the Allison Creek fault (Link and Janecke, 1999).

Exploration for uranium began in the area in the late 1950s, and several localities northeast of Williams Lake were found by prospectors to contain anomalous concentrations. All are in the uppermost part of the Challis Volcanic Group, either in the Sevenmile Creek area on the east side of the Salmon River, or northwest of the mouth of Williams Creek. Three Defense Minerals Exploration Administration (DMEA) reports discuss these exploration efforts. These DMEA reports (Dockets 4308, 4754, and 4899) are available for download (U.S. Geological Survey, 2021). Reconnaissance sampling in the 1970s during the National Uranium Resource Evaluation (NURE) Program also yielded anomalous uranium concentrations in the Sevenmile Creek area (Wodzicki and Krason, 1981).

ROAD LOG

Field trip stops are referenced to GPS coordinates (WGS84), Forest Service road names and numbers, and geographic names where possible, with mileage to stops noted.

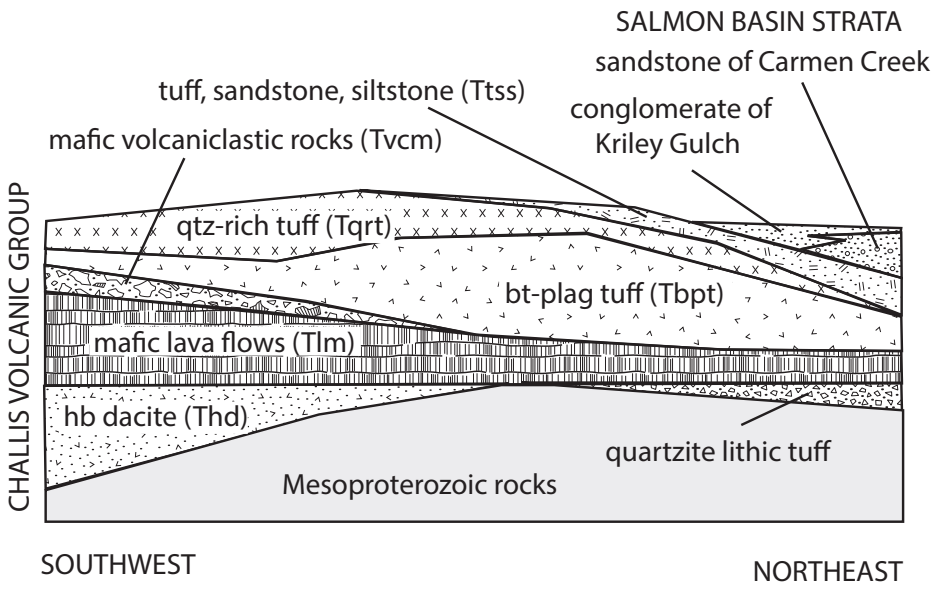

Figure 2. Schematic southwest to northeast cross section showing restricted extents of some Challis units as well as the overlying sediment and sedimentary rocks of the Salmon basin that are more widely exposed north of the field trip route. Modified from Lewis and others (2013).

Set odometer to zero at the intersection of Highways 93 and 28 in Salmon. Proceed south on Highway 93 to mile 5.2 and the intersection with Williams Creek Road 021. Turn right (west) onto Road 021 and immediately cross the Salmon River on the Shoup bridge, named after Idaho's first Governor, George Shoup. Continue west on Road 021, turning left (south) at 6.0 mi, passing through gravels of a higher terrace and the Eocene to Oligocene sandstone of Carmen Creek to a right-hand bend at 7.5 mi and the junction with Williams Lake Road 309 at mile 7.6. Turn left (south) on Road 309 continuing to mile 8.4 and into a pullout on the right side of the road for stop 1.

STOP 1—8.3 mi
BIOTITE–PLAGIOCLASE TUFF (Tbpt)

(45.0697° N; 113.9258° W)

This tuff, in addition to having phenocrysts of biotite and plagioclase, commonly shows extensive vapor-phase alteration as lithophysae or spherulites and distinct flow-banding. This is the lowest in a stack of ash-flow tuffs above the mafic lavas (Tlm) in the Williams Lake area. A sample collected near the mouth of Henry Creek about 1.4 mi farther south yielded a U-Pb zircon age of 48.27 ± 0.15 Ma on 14 of 15 youngest grains (Burmester and others, 2016; analytical work by Jesse Mosolf, MBMG, using facilities at the University of California, Santa Barbara).

Continue south on Road 309.

9.8 mi Henry Creek with public access.

At mile 10.2, on a left-hand turn, pull out along the road on the right for stop 2.

STOP 2—10.1 mi
OVERVIEW AND MAFIC EPICLASTICS (Tvcm)

(45.0474° N; 113.9221° W)

Light-colored rocks directly on the opposite side of the Salmon River are rhyolitic tuffs containing small phenocrysts of sanidine and quartz. They are well bedded and possibly water lain. Their stratigraphic position is uncertain, but they may be at the same level as the mafic flows (Tlm) or perhaps the hornblende dacite (Thd). The dark cliffs above are mafic lavas (Tlm) overlain by mafic volcaniclastic rocks (Tvcm) and capped by biotite–plagioclase tuff. The same strata are present on the west side of the river immediately to the northwest of this stop near the public access to Henry Creek. A down-to-the-west normal fault in the river valley to the north, one of several in the area, is likely responsible for the apparent offset. Walk back along the road to examine the green, bedded mafic epiclastic deposits (Tvcm) to the north. Return to the vehicles and continue south on Road 309.

10.5 mi Right bend around outcrop of vitrophyre. The contact between the Challis Volcanic Group and underlying Mesoproterozoic metasedimentary rocks is across the river to the east.

11.7 mi Point composed of Mesoproterozoic metasedimentary rock.

11.8 mi Cattle guard at end of pavement; start uphill on gravel road.

12.1 mi Lake Creek Road forks to the left. Keep to right.

12.2 mi Landslide with big blocks and large boulders. It appears to be a rockslide from steep slopes in the Challis quartz-rich tuff (Tqrt). Boulder distribution below the road shows that the slide debris capped a Pleistocene gravel terrace and probably entered the Salmon River. Younger alluvial fans are deposited on the landslide debris.

12.6 mi End landslide and begin cut in metasedimentary rocks.

13.2 mi Road bends around point with breccia of uncertain origin. Some of this breccia may have formed as talus in the Eocene, or perhaps as a vent breccia, rather than as a result of faulting.

13.3 mi More breccia; here it contains large blocks of both volcanic and metasedimentary rocks.

13.6 mi More metasedimentary rock, then breccia that is exclusively volcanic.

13.7 mi East edge of large landslide mass.

14.2 mi West edge of large landslide mass.

14.7 mi Faulted rhyolite dike in latite flow. At 14.5 mi pullout on the left for stop 3.

STOP 3—14.5 mi
FAULTED RHYOLITE DIKE IN LATITE (Tlm)

(45.0192° N; 113.9588° W)

Park on left just before junction of Road 028 and Skyline Road and walk back to light-colored biotite–quartz–feldspar dike that crosscuts the latite flow. The view to the southwest is the downstream side of the landslide that formed the Williams Lake dam. Two landslide masses form the dam: an older one from the south, and a younger, complex mass from the north (fig. 3). Lake water may have overtopped the low spot between these deposits, but there is little evidence of a dam failure caused by erosion of the landslide debris. This indicates that the material had sufficient permeability to balance the lake level with Lake Creek discharge.

Dark gray latite and andesite flows here are characteristic results of a widespread mafic flow event in the Challis. Interbeds of poorly exposed biotite–quartz tuff are present locally, as is flow breccia. Secondary chalcedony and calcite are common in vesicular intervals within the flows, which makes this a productive rock unit for rockhounds. The flows contain sparse 0.5–1

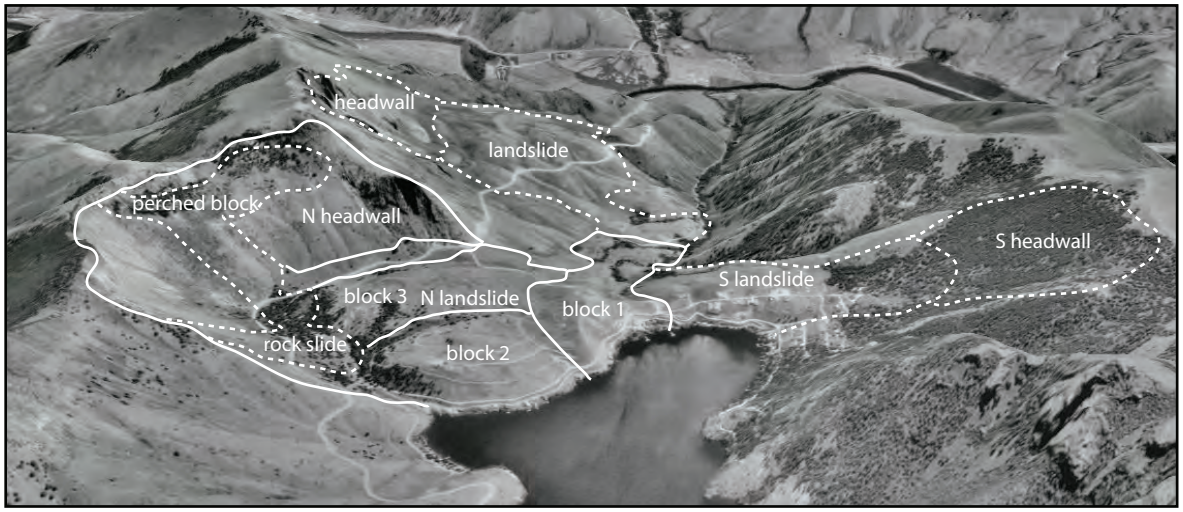

Figure 3. Oblique aerial view eastward of Williams Lake landslide dam annotated with interpretations of landslides, blocks, and headwalls. Source: Google Earth, 1998 black and white aerial photography. Modified from Burmester and others (2016), who provide a more detailed description, as do Lewis and others (2013a).

mm phenocrysts of clinopyroxene and altered olivine in a very fine-grained groundmass containing abundant plagioclase. Xenocrystic quartz and plagioclase are present locally, particularly in the upper part of unit. Quartz is highly embayed and has reaction rims; plagioclase is less embayed but is turbid and shows disequilibrium textures. Rocks here are likely correlative with the latite (Tl) unit mapped by Blankenau (1999); mafic flows mapped by Othberg and others (2011) northwest of Lemhi Pass; and Lewis and others (2012) near Salmon. These rocks are also correlative with the Tl unit of potassium-rich andesite, latite, and basalt flows in the Challis 1° x 2° quadrangle to the southwest (Fisher and others, 1992).

The rhyolite dike here is part of a north–south swarm of dikes that continue south for at least a mile. They contain phenocrysts of quartz, plagioclase, sanidine, and biotite. Note the chilled margin of the dike and the down-to-the-east normal fault in the latite.

14.9 mi Road forks; take the right fork. The left goes to a recreation site with facilities about 0.1 mi farther, almost within sight. Notice large boulders of tuff from cliff to the north but absence of boulders from the higher ground farther south. At mile 15.2 pull out on the left just before the cattle guard for Stop 4.

STOP 4—15.1 mi
PICNIC AREA AND LANDSLIDE DEBRIS

(45.0250°N; 113.9663°W)

The boulder field in the picnic area resulted from a partially airborne rockslide or rock avalanche originating from the cliffs of Tqrt (quartz-rich tuff), part of the Challis rocks above to the north. Most of the slide debris mantles the steep slope between the cliff and the road. This deposit and another rockslide just west around the bend are some of the youngest components of the landslide that dammed the northern side of Williams Lake. Continue west almost half a mile.

Sharp right turn in road. Parking on left. Look back at the landslide dam across Lake Creek. View shows older, smaller landslide mass from the south, and the younger, larger mass from the north. The younger, northern mass is the result of several events, but mainly three large slide blocks that appear to have moved at nearly the same time (fig. 3). The headwall area, seen high above the picnic area, includes an additional landslide block that has rotated and moved downslope somewhat. It is perched at the edge of the steep slope and could move catastrophically at any time, such as during earthquake shaking.

Continue west on Road 028.

16.4 mi East edge of large debris-flow deposit. At 16.7 mi turn left into boat ramp parking area.

STOP 5— 16.7 mi
LANDSLIDE DEBRIS AT BOAT RAMP, PICNIC FACILITIES, AND DACITE

(45.0178°N, 113.9835°W)

The stop here is within a debris-flow deposit that traveled nearly 1.25 mi from the source to the north. It originated in a stack of about seven subhorizontal Challis andesite/latite flows (Tlm). Levees on either side of the debris flow are readily apparent. Look back at the landslide dam across Lake Creek. View shows older, smaller landslide mass from the south, and the younger, larger, mass from the north. The younger, northern mass is the result of several events, but mainly three

Figure 3. View north from the Williams Lake road just east of Williams Lake. Dark brown and reddish brown rocks on the left are the mafic lava (Tlm). Green outcrops on the right are volcaniclastic rocks, and the cliffs above are the biotite-plagioclase tuff (Tbpt) capped by the quartz-rich tuff (Tqrt).

large slide blocks that appear to have moved nearly at the same time. The headwall area (fig. 4), seen high above the picnic area, includes an additional landslide block that has rotated and moved downslope somewhat. It is perched at the edge of the steep slope and could move catastrophically at any time, such as during earthquake shaking.

Hike west along the road to the first outcrops. These consist of hornblende dacite that is a lava flow, massive tuff, or a shallow intrusive material. A sample collected from this point by Jesse Mosolf (MBMG) yielded a weighted mean from the nine youngest grains of 48.79 ± 0.19 Ma using LA-ICPMS U-Pb zircon methods (Burmester and others, 2016; analytical work at University of California, Santa Barbara). If all but the oldest ages are included (29 of 30 analyses), the weighted mean is slightly older (49.45 ± 0.18 Ma). Dacite west of Lemhi Pass has been dated at 49.4 ± 0.5 Ma by the same methods (Burmester and others, 2018).

Continue west.

18.5 mi Switchback to the right and ranch road exits left. On the other side of Lake Creek a few hundred meters is an extensive outcrop of brecciated Ordovician Kinnikinic Quartzite associated with the Poison Creek fault. Stop here on the way out if you are so inclined. Continue up and pull out on the right at the left switchback at mile 18.2 for Stop 6.

STOP 6—18.2 mi
CHALLIS EPICLASTICS AND VOLCANICS (Tsc)

(45.0134°N, 114.0111°W)

Go up the gully to the north to see debris flows, a variety of epiclastic sediments including some with plant fossils, and intercalated tuffaceous beds. These are within a small graben and not laterally extensive.

End of trip. Return to Highway 93 and head north to Salmon.

ACKNOWLEDGMENTS

Liam Knudsen provided the digital rendition of Figure 1 and Russ Burmester provided a review.

REFERENCES

Anderson, A.L., 1956, Geology and mineral resources of the Salmon quadrangle, Lemhi County, Idaho: Idaho Bureau of Mines and Geology Pamphlet 106, 102 p.

Blankenau, J.J., 1999, Cenozoic structural and stratigraphic evolution of the southeastern Salmon basin, east-central Idaho: Utah State University M.S. thesis, 143 p., 3 plates.

Burmester, R.F., Lewis, R.S., Othberg, K.L., Stanford, L.R., Lonn, J.D., and McFaddan, M.D., 2016, Geologic map of the western part of the Salmon 30 x 60-minute quadrangle, Idaho and Montana: Idaho Geological Survey Geologic Map 52, scale 1:75,000.

Burmester, R.F., Mosolf, J., Stanford, L.R., Lewis, R.S., Othberg, K.L., and Lonn, J.D., 2018, Geologic map of the Lemhi Pass quadrangle, Lemhi County, Idaho, and Beaverhead County, Montana: Idaho Geological Survey Digital Web Map 183 and Montana Bureau of Mines and Geology Open-File Report 701, scale 1:24,000.

Fisher, F.S., McIntyre, D.H., and Johnson, K.M., 1992, Geologic map of the Challis quadrangle, Idaho: U.S. Geological Survey Miscellaneous Investigations Series Map I-1819, 39 p., scale 1:250,000.

Lewis, R.S., Othberg, K.L., Burmester, R.F., Stanford, L.R., McFaddan, M.D., and Lonn, J.D., 2012, Geologic map of the Salmon quadrangle, Lemhi County, Idaho: Idaho Geological Survey Digital Web Map 154, scale 1:24,000.

Lewis, R.S., Othberg, K.L., Burmester, R.F., Stanford, L.R., and McFaddan, M.D., 2013a, Challis volcanics, younger strata, and landslides in the Williams Lake area near Salmon, Idaho, *in* Lewis, R.S., Garsjo, M.M., and Gibson, R.I., eds., Belt Symposium V and other Papers: Northwest Geology, v. 43, p. 343–352.

Lewis, R.S., Othberg, K.L., McFaddan, M.D., Burmester, R.F., Stewart, D.E., Stanford, L.R., and Stewart, E.D., 2013b, Geologic map of the Williams Lake quadrangle, Lemhi County, Idaho: Idaho Geological Survey Digital Web Map 162, scale 1:24,000.

Link, P.K., and Janecke, S.U., 1999, Geology of east-central Idaho: Geologic road logs for the Big and Little Lost River, Lemhi and Salmon River valleys, *in* Hughes, S.S., and Thackray, G.D., eds., Guidebook to the geology of eastern Idaho: Pocatello, Idaho Museum of Natural History, p. 295–334.

Othberg, K.L., Lewis, R.S., Stanford, L.R., Burmester, R.F., and McFaddan, M.D., 2011, Geologic map of the Baker quadrangle, Lemhi County, Idaho: Idaho Geological Survey Digital Web Map 141, scale 1:24,000.

Stewart, D.E., Lewis, R.S, Burmester, R.F., Lonn, J.D., McFaddan, M.D., Tkach, M.K., and Canada, A.S., in press, Geologic map of the Lake Mountain quadrangle, Lemhi County, Idaho: Idaho Geological Survey Digital Web Map, scale 1:24,000.

Tysdal, R.G., 2002, Structural geology of western part of Lemhi Range, east-central Idaho: U.S. Geological Survey Professional Paper 1659, 33 p.

U.S. Geological Survey, 2021, Defense Minerals Exploration Administration (DMEA) available at: https://pubs.usgs.gov/ds/1004/ds1004_id.htm [Accessed 8 June 2023].

Wodzicki, A., and Krason, J., 1981, National uranium resource evaluation, Dillon quadrangle, Montana and Idaho: Bendix Field Engineering Corporation and U.S. Department of Energy, Grand Junction Office, Colorado, 67 p.

BRUSHY GULCH FAULT, EAST-CENTRAL IDAHO, REVISITED: FAULT OR FICTION?

Jeffrey D. Lonn,[1] Russell F. Burmester,[2] and Reed S. Lewis2

[1]*Montana Bureau of Mines and Geology, Butte, Montana*
[2]*Idaho Geological Survey, Moscow, Idaho*

INTRODUCTION

This half-day field trip near North Fork, Idaho, traverses a gradational metamorphic contact from lower-grade Mesoproterozoic Lemhi Group strata to migmatitic, high-grade metamorphic rocks, and then into the 1370 Ma igneous and meta-igneous rocks that drove the metamorphism. It involves 2 mi of off-trail hiking along the top of a ridge. Views are spectacular, and the rocks are highly varied.

GEOLOGIC SETTING/DISCUSSION

A few miles downstream along the Salmon River (west) from North Fork, Idaho, the monotonous succession of fine-grained quartzite that constitutes the Lemhi Group of the upper Belt Supergroup in this area gives way to a bimodal intrusive complex with U-Pb zircon crystallization ages from about 1383 to 1359 Ma (Doughty and Chamberlain, 1996; Evans and Zartman, 1990; Aleinikoff and others, 2012). The igneous/meta-igneous rocks are highly varied and include augen gneiss, megacrystic granite, trondhjemitic orthogneiss, amphibolite, diorite, and metagabbro (Spence, 1984). The complex intrusive relationships may have resulted from the comingling of mafic and felsic magmas (Doughty and Chamberlain, 1996). The igneous complex intrudes high-grade, locally migmatitic, regional metamorphic rocks (fig.1).

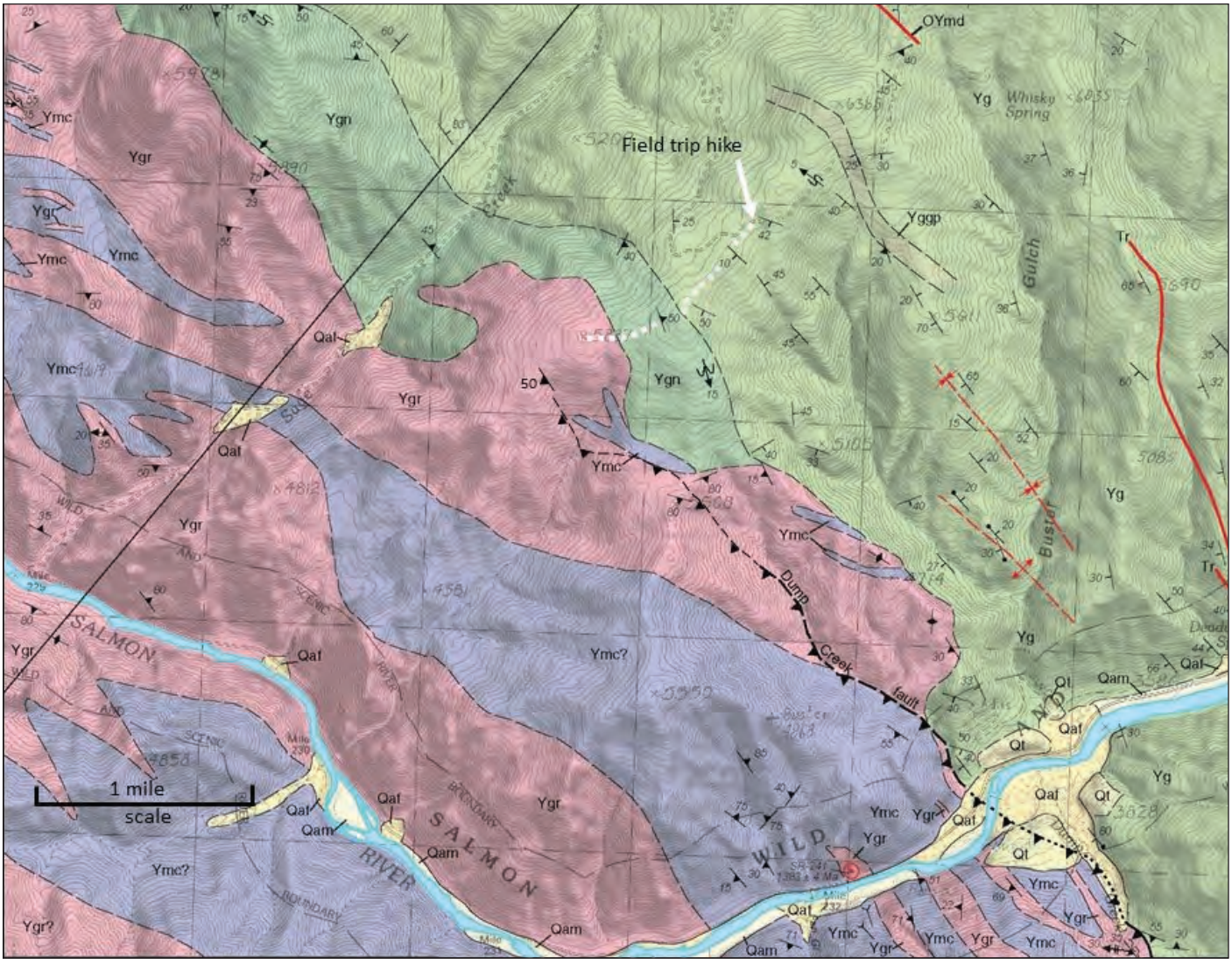

Figure 1. Geologic map of the field trip area. The hiking route is shown by the white dotted line. Ygr, megacrystic granite and augen gneiss; Ymc, mafic complex; Ygn, migmatitic gneiss; Yg, Gunsight Fm of the Lemhi Group; Yggp, garnet-bearing phyllite of the Lemhi Group; Tr, rhyolite dike; OYmd, mafic dike. Modified from Lewis and others (2019). Note that Yg, Gunsight Fm, is now interpreted more broadly as Lemhi Group, undivided, in this paper.

The boundary between the intrusive-metamorphic complex and the low-grade Lemhi Group quartzite has long been interpreted as a major northwest-striking, southwest-side-up, regional-scale reverse fault, the Brushy Gulch thrust, extending northwest from near Salmon, Idaho, across the Salmon River west of North Fork, and into the headwaters of the West Fork of the Bitterroot River in Montana (Berg, 1977; Lopez, 1982; Kaiser, 1956; Evans and Green, 2003; Lund and others, 2003). However, recent 1:24,000-scale mapping of this area (Lewis and others, 2019, 2021) suggests instead that the low-grade Lemhi Group strata grade into high-grade migmatite paragneiss as the intrusive contact is approached (figs. 1, 2), and that the high-grade metamorphic rocks are the result of large-scale contact metamorphism. Although there are some faults between the igneous complex and Lemhi Group rocks, they are discontinuous and do not comprise a throughgoing regional-scale structure. Instead, the recent mapping recognizes the North Fork thrust as the major structure of the region. The northwest-striking, southwest-dipping North Fork thrust is located 1–10 km northeast of, and subparallel to, the metamorphic-intrusive complex and the postulated Brushy Gulch fault (see Lonn and others, this volume; Burmester and others, this volume), and brings older Lemhi Group rocks (Gunsight Formation and lower units) intruded by the igneous complex up and over younger strata of the Lemhi subbasin (Swauger, Lawson Creek, and Apple Creek Formations) that do not host any 1370 Ma igneous rocks (fig. 2). Where the North Fork fault's trace is near the 1370 Ma intrusions, the thrust does form the boundary between high-grade and low-grade metamorphic rocks, but for most of its length it juxtaposes greenschist-facies metasediments, and can be very subtle (for example, see Lonn and others, this volume).

This field trip examines field relationships between the intrusive rocks, the high-grade metamorphic rocks, and the low-grade Belt strata, crossing the trace of the Brushy Gulch fault as mapped by Evans and Green (2003). The field trip also crosses exposures of several different 1380–1370 Ma igneous and meta-igneous rock types, including amphibolite, quartz–feldspar orthogneiss, and megacrystic granite.

There is little evidence here to support fault juxtaposition of the high-grade and low-grade rocks. Instead, the exposed gradational contact suggests that large-scale contact metamorphism, not regional Barrovian burial metamorphism, produced the high-grade rocks from the Lemhi Group country rocks. Zircons from granitic leucosomes yielded an age of 1370 ± 2 Ma (Doughty and Chamberlain, 1996) and garnets from migmatite in the same outcrop yielded a Lu-Hf age of 1353 ± 4 Ma (Murphy and others, this volume), indicating that metamorphism was coeval with, or shortly followed, intrusion. Whole-rock Sm-Nd data from both sides of the postulated Brushy Gulch fault are indistinguishable (Doughty and Chamberlain, 1996), further supporting a contact metamorphism interpretation.

Although the spatial association of regional metamorphism with intrusive activity has long been noted, it brings up the chicken or the egg question of: which came first, the plutons or the metamorphism? In other words, did the plutons and associated fluids provide the heat that drove metamorphism, or did tectonic burial and the resultant slow heating (Barrovian metamorphism) drive both the metamorphism and partial melting to form plutons? There is much recent literature discussing this question. Importantly, Viete and others (2011, 2013) reexamined the type locality of Barrovian regional metamorphism in Scotland and found it to be spatially and temporally related to several pulses of igneous intrusion, with no significant contribution from tectonic burial and the resultant slow heating. Viete and Lister (2017) and Ryan and Dewey (2019) argued that the short duration of many metamorphic events worldwide precludes

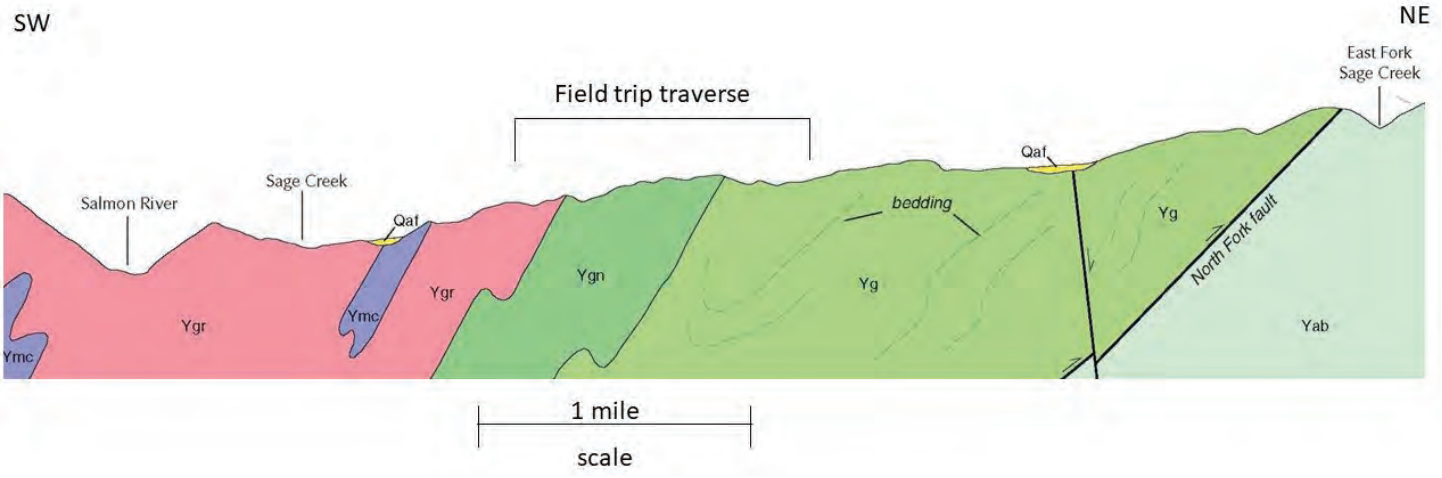

Figure 2. Cross-section in the field trip vicinity (see location in fig. 1) shows the contacts traversed on the hike. Although the North Fork thrust is a regional-scale fault, it is not a metamorphic boundary in this area. Ygr, megacrystic granite and augen gneiss; Ymc, mafic complex; Ygn, migmatitic gneiss; Yg, Gunsight Formation of the Lemhi Group; Yab, banded siltite member of the Apple Creek Fm. From Lewis and others (2019). Note that Yg, Gunsight Fm, is now interpreted more broadly as Lemhi Group, undivided in this paper.

their origin from tectonic burial and slow heating. Hamilton (1983) and Miller and Gans (1989) interpreted "regional" metamorphism in Idaho and Nevada, respectively, to be local, and spatially and temporally associated with and driven by igneous activity.

Similarly, tectonic overpressure/differential stress can produce local pressures higher than lithostatic pressure, locally forming higher pressure metamorphic minerals that overestimate burial depth (e.g., Mancktelow, 2008; Schmalholz and Podladchikov, 2014; Wheeler, 2014). For example, in this area, Doughty and Chamberlain (1996) used GASP (garnet–aluminum silicate–silica–plagioclase) geobarometry to estimate that the depth of metamorphism increased from 14 km to 20 km during metamorphism. They attributed the depth increase to renewed sedimentation, but either a sill-like geometry for the 1380–1370 Ma plutons or tectonism could have also caused burial, although there is no evidence for tectonism of this age. Because maximum exposed thickness of the Lemhi Group country rocks and overlying Belt strata is less than 14 km (Burmester and others, 2016), and maps (Lewis and others, 2019, 2021) show that the meta-Belt strata here were not at the bottom of the stack, it is possible that tectonic overpressure produced metamorphic mineral assemblages that overestimated depth.

The possibility of localized regional metamorphism is important. If regional metamorphism can be local, spatially and temporally associated with and driven by igneous intrusions, then the metamorphic conditions recorded may not be representative of the overall tectonic/metamorphic conditions in the crust. Viete and Lister (2017) asked: "Do the metamorphic facies series have the geological significance they are thought to have?" Most importantly for mappers like us (the authors), the concept of localized regional metamorphism eliminates the need or temptation to find significant structures separating nearby areas of high- and low-grade metamorphism.

While some of the high-grade rocks on the field trip suggest multiple generations of deformation, it is more likely that these hot, squishy rocks were just better able to record subtle and local variations in the stress fields, and/or they were more likely to experience and record plastic flow than the cooler, less ductile rocks nearby.

TO THE TRAILHEAD

Drive north from Salmon on US Highway 93 approximately 21 mi to the town of North Fork. North of the Tower Rock Campground, the Salmon River canyon is cut through Lemhi Group quartzite of the North Fork thrust hanging wall. Observe in passing the variety of bedding thicknesses, grading, and structures. Although Burmester and others' (2016) regional map shows a thick, undeformed gently west-dipping stratigraphic section of Lemhi Group in this area, note the two east-overturned folds visible from the highway before you reach North Fork. These indicate contraction, probably produced intraformational thrust and reverse faults that thickened the section. The monotonous lithology of the Lemhi Group here—dominantly fine-grained feldspathic quartzite— makes recognition of intraformational structures difficult.

At North Fork, turn left on the Salmon River Road. Just downstream from North Fork, note the road cut in nearly flat-lying fine-grained quartzite and darker siltite in beds 1–5 dm thick (fig. 3). Pass the Newlan Ranch where the down-to-the-west Monument Gulch fault (Lewis and others, 2019) is hidden under alluvium. The next few road miles proceed even further upsection through southwest-dipping, fine-grained, feldspathic quartzite that dominates the upper part of the Lemhi Group of the upper Belt Supergroup. Past Deadwater Picnic area, the canyon opens and abandoned mine works are visible on the hillside to the right (north). The mines are developed in the Lemhi Group quartzite near its intrusive contact with the Deadwater granite (Concordia Age = 1383 ± 4 Ma, Aleinikoff and others., 2012). On the ridge above the mines, both foliated and unfoliated megacrystic granite is in intrusive contact with Lemhi Group quartzite (fig. 4). Ahead, where the canyon narrows again, augen gneiss and megacrystic granite of the intrusive complex make their first appearance. In the narrow gulch hidden on the right are exposures of a strained contact between the quartzite and the augen gneiss that was interpreted as the Brushy Gulch fault (Lund and others, 2003), a major fault juxtaposing high-grade metamorphic rocks and the intrusive complex against the quartzite. We will not have time to

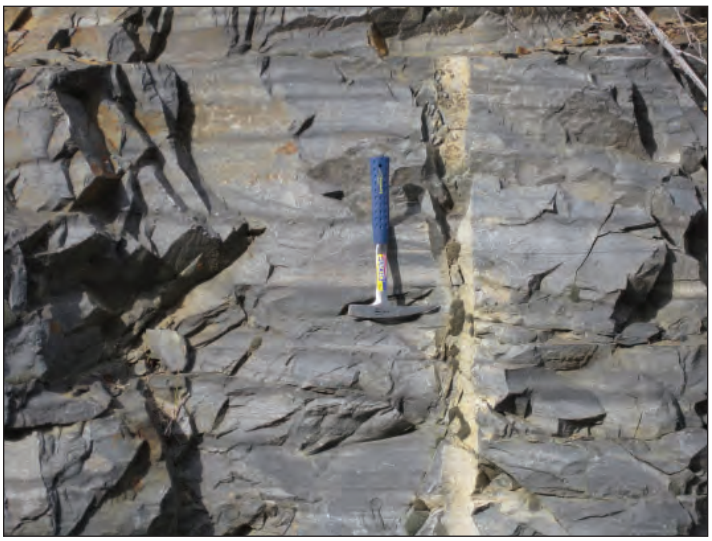

Figure 3. Road cut just downstream from North Fork showing beds of lighter colored very fine-grained quartzite and darker colored siltite of the Lemhi Group (Ylg) in the hanging wall of the North Fork thrust.

Figure 4. Xenolith of Lemhi Group quartzite (Yg) within undeformed megacrystic granite (Ygr) near the granite–quartzite contact above the mine adits.

examine this contact, but recent mapping (Lewis and others, 2019) shows that this high-strain zone does not coincide with the contact farther north, and instead is confined within the igneous complex. Consequently, Lewis and others (2019) renamed the zone the Dump Creek fault (figs 1, 5).

Continue a few more miles through amphibolite and megacrystic granite, turning right on the Sage Creek Road, a very steep dirt road that doubles back across the igneous–quartzite contact. About 4 mi up, just before the main road goes around a sharp hairpin, is a road angling back to the right. Take this road another 3 mi through a couple switchbacks to the ridgetop. Park in the flat timbered area just before you reach the ridge—there is no parking available on the ridgetop itself.

THE HIKE

Walk up the road to the ridgetop to view gently dipping Lemhi Group quartzite exposed in the roadcut. It is fine-grained, feldspathic, and contains disseminated metamorphic biotite and muscovite. Black planar laminations are common, and beds are as much as 0.5 m thick, some separated by thin finer-grained intervals that have been metamorphosed to biotite schist. Although metamorphosed to greenschist grade, bedding and sedimentary features are still preserved, and recent mapping (Lewis and others, 2019) shows that these rocks are in structural and stratigraphic continuity with the lower grade rocks we saw in the road cuts around North Fork.

Walk southwest along the ridgetop, viewing more quartzite float. A half mile of walking brings us to a hilltop where outcrops of higher grade rocks are exposed. Although this is predominantly quartzite too, bedding is no longer recognizable and the composition-

Figure 5. (A) Strained, mylonitic granite along the Dump Creek fault developed from the megacrystic granite visible in the upper part of photo; (B) Mylonite developed in megacrystic granite along the Dump Creek fault immediately south of the field trip hike. There the fault juxtaposes megacrystic granite and undeformed mafic igneous rock, both part of the 1380–1370 Ma igneous complex. The mylonitic fault's age is unknown—it is likely either Mesoproterozoic or late Cretaceous.

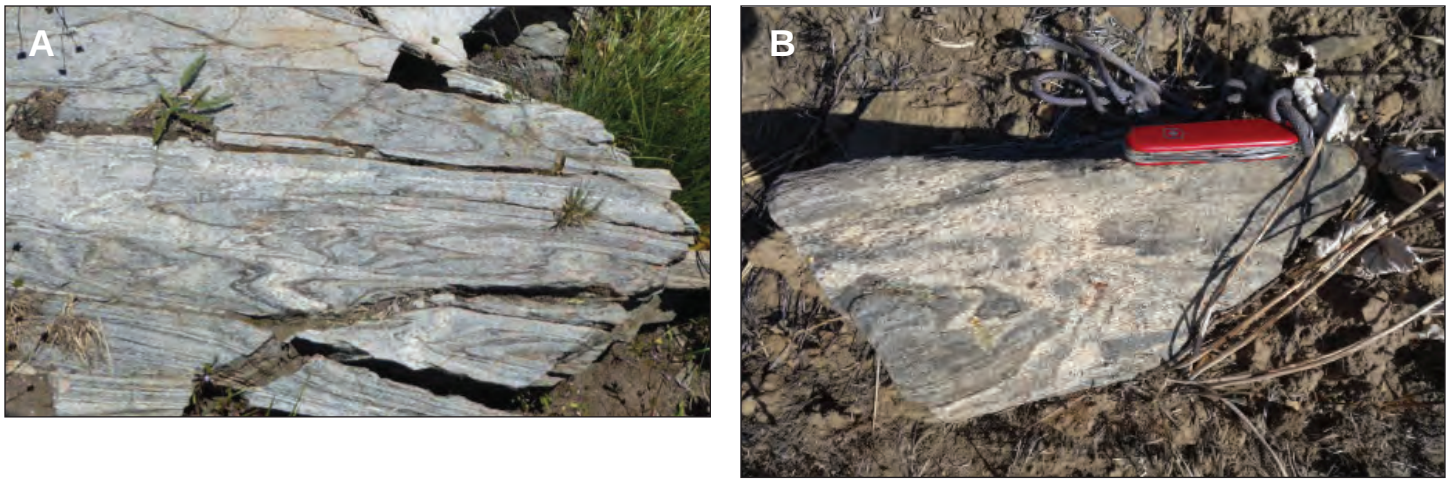

Figure 6. (A) Tightly folded Lemhi Group quartzite near the contact with the intrusive complex; (B) Deformed migmatitic quartzite with a Lemhi Group sandstone protolith. Some granitic stringers are probably intrusive. Leucosomes in similar rocks along the river about 8 km (5 mi) west yielded a U-Pb age of 1370 Ma (Doughty and Chamberlain, 1996), suggesting that metamorphism was coeval with intrusion.

al layering, probably relict bedding, is nearly vertical, striking northwest. Proceed downhill to the southwest; the rocks become increasingly deformed and migmatitic (fig. 6). They also are increasingly intruded by both fine-grained granitic rocks (trondhjemite?) and amphibolite (fig. 7)—both are components of the 1380–1370 Ma igneous complex (Spence, 1984). We'll try to find the large outcrop with complex cross-cutting relationships and textures that contains fine-grained granite, some feldspar megacrysts, amphibolite, and migmatitic quartzite.

As we approach the saddle, large, rounded outcrops of massive megacrystic granite become visible. Megacrystic granite also underlies the knob ahead. Medium-grained equigranular granite (trondhjemite?) appears to completely separate the rocks we have been walking through from the megacrystic granite, although the megacrystic granite is in direct contact with the quartzite in many nearby areas (fig. 8). The megacrystic granite is unfoliated here, but in other areas it has been deformed into augen gneiss, possibly by two processes: magmatic flow and later solid-state strain.

Fig. 7. Fine-grained granitic rock intruding migmatitic quartzite.

Proceed to the top of the knob, also underlain by massive megacrystic granite. However, a quarter mile to the southwest it is deformed into mylonitic augen gneiss interpreted to be developed along the northwestern extension of the Dump Creek fault discussed earlier (fig. 1).

The complexity of the 1380–1370 Ma igneous suite is baffling. Spence (1984) described metagabbro, diorite, amphibolite, tonalite, trondhjemite, hornblende gneiss, and several varieties of augen gneiss/megacrystic granite. The intrusions range from strongly foliated to not foliated at all. It is difficult to determine the relative

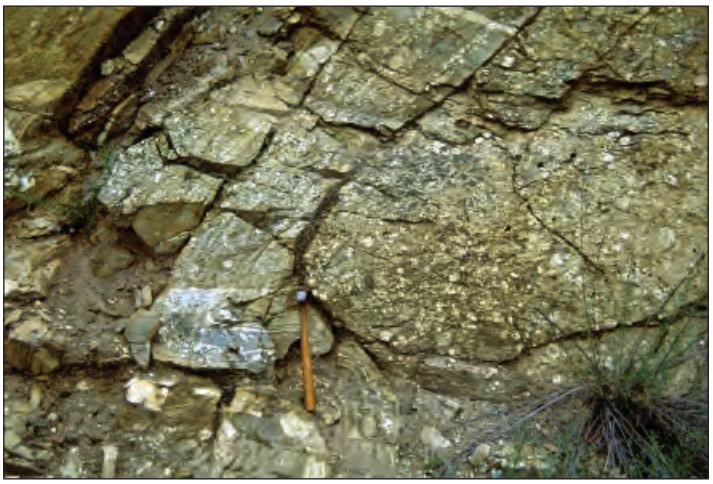

Figure 8. Folded contact between high-grade Lemhi Group quartzite on the left and megacrystic granite on the right. Note that feldspar megacrysts are developed within the quartzite too, suggesting that they formed through a replacement/recrystallization process. Glazner and Johnson (2013) provided strong evidence for late, low-temperature crystallization of K-spar megacrysts through a replacement/recrystallization process. Photo is from the Colson Creek area, about 20 km downriver from the field trip area.

timing of emplacement (fig. 9). Doughty and Chamberlain (1996) attributed the complex intrusive relationships to co-mingling of mafic and felsic magmas.

The top of the knob is the end of the trip. Retrace your route back to the vehicles.

ACKNOWLEDGMENTS

Reviews by Katie McDonald and Alan English are much appreciated.

Figure 9. Relative age relationships of the various igneous rock types in the 1380–1370 Ma intrusive complex are difficult to determine. (A) Contact between finer-grained granitic rock (trondhjemite?) and megacrystic granite gives few clues as to which came first; (B) xenolith of foliated amphibolite in megacrystic granite indicates that the amphibolite was emplaced and foliated first. Rocks of the intrusive complex range from strongly foliated to non-foliated.

REFERENCES

Aleinikoff, J.N., Slack, J.F., Lund, K., Evans, K.V., Fanning, C.M., Mazdab, F.K., Wooden, J.L., and Pillers, R.M., 2012, Constraints on the timing of Co-Cu ± Au mineralization in the Blackbird district, Idaho, using SHRIMP U-Pb ages of monazite and xenotime plus zircon ages of related Mesoproterozoic orthogneisses and metasedimentary rocks: Economic Geology, v. 107, p. 1143–1175.

Berg, R.B., 1977, Reconnaissance geology of southernmost Ravalli County, Montana: Montana Bureau of Mines and Geology Memoir 44, 39 p., map scale 1:40,000.

Burmester, R.F., Lonn, J.D., Lewis, R.S., and McFaddan, M.D., 2016, Stratigraphy of the Lemhi subbasin of the Belt Supergroup, *in* MacLean, J.S., and Sears, J.W., eds., Belt Basin: Window to Mesoproterozoic Earth: Geological Society of America Special Paper 522, Chapter 5, p. 121–138.

Burmester, R.F., Lewis, R.F., and Lonn, J.D., this volume (2023), The Lemhi subbasin of the Belt Supergroup: Northwest Geology, v. 52.

Doughty, P.T., and Chamberlain, K.R., 1996, Salmon River arch revisited: New evidence for 1370 Ma rifting near the end of deposition in the Middle Proterozoic Belt basin: Canadian Journal of Earth Sciences, v. 33, p. 1037–1052.

Evans, K.V., and Green, G.N., 2003, Geologic map of the Salmon National Forest and vicinity, east-central Idaho: U.S. Geological Survey Miscellaneous Investigations Map I-2765, scale 1:100,000.

Evans, K.V., and Zartman, R.E., 1990, U-Th-Pb and Rb-Sr geochronology of Middle Proterozoic granite and augen gneiss, Salmon River Mountains, east-central Idaho: Geological Society of America Bulletin, v. 102, p. 63–73.

Glazner, A.F., and Johnson, B.R., 2013, Late crystallization of K-feldspar and the paradox of megacrystic granites: Contributions to Mineralogy and Petrology, v. 166, p. 777–799, doi: 10.1007/s00410-013-0914-1

Hamilton, W., 1983, Metamorphism in the Riggins region, western Idaho: U.S. Geological Survey Professional Paper 436, 101 p.

Kaiser, E.P., 1956, Preliminary report on the geology and deposits of monazite, thorite, and niobium-bearing rutile of the Mineral Hill district, Lemhi County, Idaho: U.S. Geological Survey Open-File Report 56-69, 41 p.

Lewis, R.S., Burmester, R.F., and Lonn, J.D., 2019, Geologic map of the Ulysses Mountain quadrangle, Lemhi County, Idaho: Idaho Geological Survey Digital Web Map 188, 1 sheet, scale 1:24,000.

Lewis, R.S, Burmester, R.F, Lonn, J.D., Stewart D.E., and Canada, A.S., 2021, Geologic map of the Henderson Ridge 7.5' quadrangle, Lemhi County, Idaho, and Ravalli County, Montana: Idaho Geological Survey Digital Web Map 202, 1 sheet, scale 1:24,000.

Lonn, J.D., Burmester, R.F., and Lewis, R.S., this volume, 2023, Geologic field guide to the North Fork and Trail Gulch thrusts near North Fork, Idaho: Northwest Geology, v. 52.

Lopez, D.A., 1982, Reconnaissance geologic map of the Ulysses Mountain quadrangle, Lemhi County, Idaho: U.S. Geological Survey Miscellaneous Field Studies Map MF-1445, scale 1:48,000.

Lund, K., Evans, K.V., Doughty, P.T., Chamberlain, K.R., Link, P.K., and Winston, D., 2003, Geology of the Brushy Gulch fault and its hanging wall and footwall rocks, eastern Idaho: Northwest Geology, v. 32, p. 74–85.

Mancktelow, N.S., 2008, Tectonic pressure: Theoretical concepts and modelled examples: Lithos, v. 103, no. 1–2, p. 149–177, doi: 10.1016/j.lithos.2007.09.013

Miller, E.L., and Gans, P.B., 1989, Cretaceous crustal structure and metamorphism in the hinterland of the Sevier thrust belt, western U.S. Cordillera: Geology, v. 17, p. 59–62, available at https://pubs.geoscienceworld.org/gsa/geology/article-pdf/17/1/59/3511088/i0091-7613-17-1-59 [Accessed July 2023].

Murphy, J.P., Lewis, R.S., Vervoort, J.D., and Hämmerli, J., this volume, Multiple periods of metamorphism in the Salmon River Mountains Idaho as deduced from garnet Lu-Hf ages: Northwest Geology.

Ryan, P.D., and Dewey, J.F. 2019, The sources of metamorphic heat during collisional orogeny: The Barrovian enigma: Canadian Journal of Earth Sciences, v. 56, p. 1309–1317, doi: 10.1139/cjes-2018-0182

Schmalholz, S.M., and Podladchikov, Y., 2014, Metamorphism under stress: The problem of relating minerals to depth: Geology, v. 42, no. 8, p. 733–734.

Spence, J.G., 1984, Geology of the Mineral Hill interlayered amphibolite–augen gneiss complex, Lemhi County, Idaho: Moscow, Idaho, University of Idaho, M.S. thesis, 241 p.

Viete, D.R., and Lister, G.S., 2017, On the significance of short duration regional metamorphism: Journal of the Geological Society, v. 174, p. 377–392, doi: 10.1144/jgs2016-060

Viete, D.R., Forster, M.A. and Lister, G.S., 2011, The nature and origin of the Barrovian metamorphism, Scotland: $^{40}Ar/^{39}Ar$ apparent age patterns and the duration of metamorphism in the biotite zone: Journal of the Geological Society, London, v. 168, p. 133–146, doi: 10.1144/0016-76492009-164

Viete, D.R., Oliver, G.J.H., Fraser, G.L., Forster, M.A., and Lister, G.S., 2013, Timing and heat sources for the Barrovian metamorphism, Scotland: Lithos, v. 177, p. 148–163.

Wheeler, J., 2014, Dramatic effects of stress on metamorphic reactions: Geology, v. 42, no. 8, p. 647–650, doi: 10.1130/g35718.1

EOCENE CHALLIS VOLCANICS, RELATED SEDIMENTS, AND THE COINER FAULT IN THE IRON CREEK VICINITY, EAST-CENTRAL IDAHO

David E. Stewart and Reed S. Lewis
Idaho Geological Survey, Moscow, Idaho

On this field trip we will look at Eocene Challis Volcanic Group ignimbrites and lava flows, fossiliferous and other Challis-related sediments, the Coiner fault at three localities, and end with a glorious view from Sheephorn lookout. The trip involves mostly roadside stops with two short off-trail hikes to see the Coiner fault, and an optional section of rough road to our final stop at Sheephorn Lookout.

Figure 1 shows the field trip route on a geologic map of the area. The oldest Challis unit here is the tuff of Ellis Creek. Farther south, a mixed series of dacitic rocks, thin mafic flows, and epiclastic rocks are preserved below the Ellis tuff (Knudsen and others, this volume). Locally above the Ellis tuff are sediments, and these are in turn overlain by mafic lavas. Higher still is an unaltered olivine basalt of uncertain age.

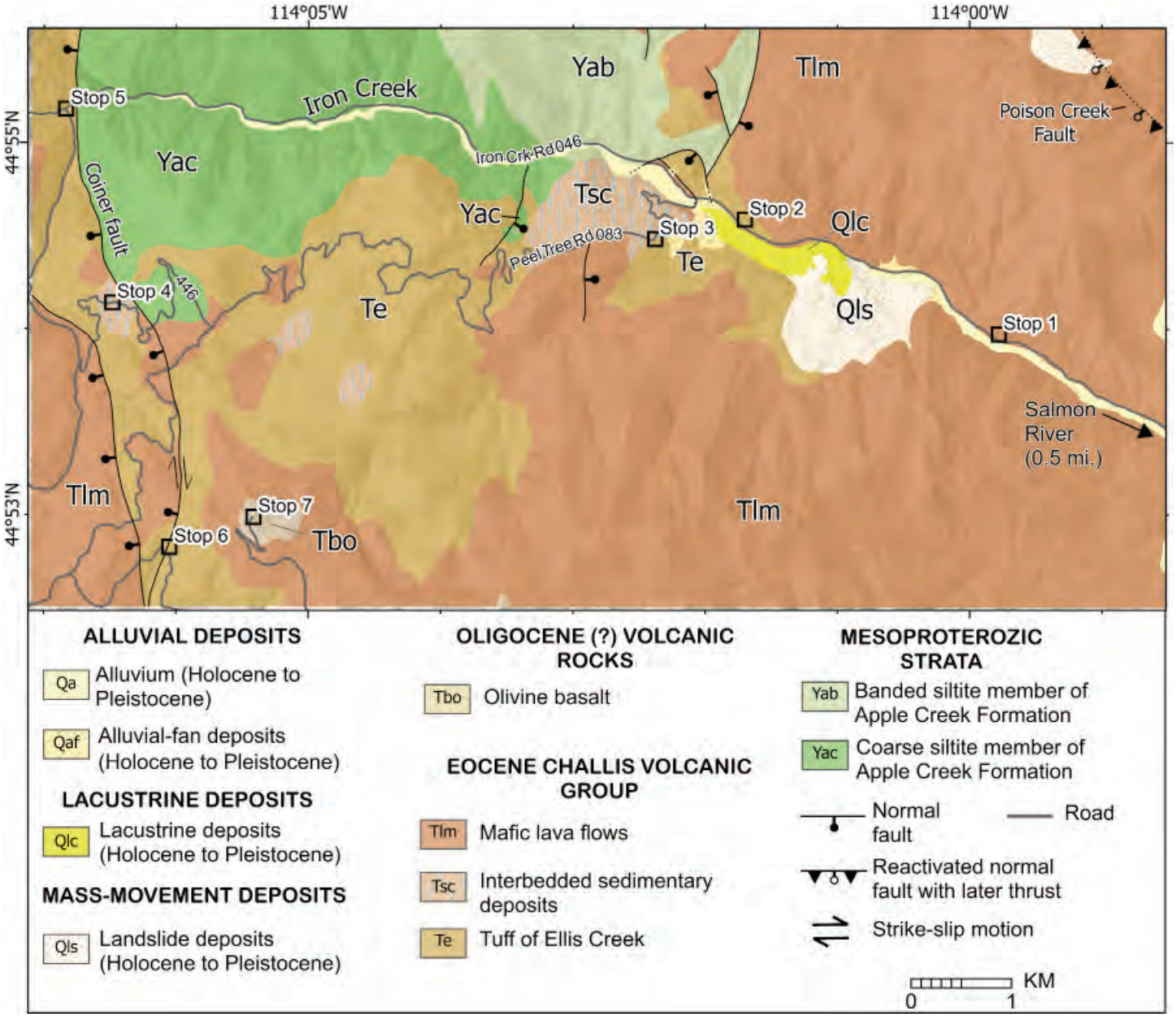

Figure 1. Geologic map of the Iron Creek area showing field trip stops. Modified from Lewis and others (2021).

ROAD LOG

Set odometer to zero at the junction of Highways 93 and 28 in Salmon and proceed south on Highway 93 24.2 mi to the junction of Highway 93 with Iron Creek Road 045. Turn right (west) onto Iron Creek Road 045, cross the Salmon River, and then turn right (north) to stay on Road 045. Continue on Road 045 to mile 26.1 and turn into the wide pullout on the right for Stop 1.

STOP 1—26.1 mi
MAFIC LAVAS (Tlm)

(44.8995° N; 113.9972° W)

Here there are several good outcrops of vesicular andesite. Most is aphyric, but you might find some phenocrysts of pyroxene or possibly olivine. Twenty meters (~66 ft) farther up the road is an autoclastic breccia. The mafic lavas, and the underlying Ellis tuff that we will see at Stop 2, are both distinctive and laterally continuous at this locale. These units are important marker beds within the Eocene volcanics in this area; without them, it can be very difficult to find one's place in the section.

Continue west on Road 045 with cliffs of Tlm above you to a pullout on the right at mile 28.1 for Stop 2.

STOP 2—28.1 mi
TUFF OF ELLIS CREEK (Te)

(44.9097° N; 114.0292° W)

The tuff of Ellis Creek is crystal-rich with white plagioclase, biotite, acicular hornblende, and minor quartz. It also contains flattened pumice and lithics. The entire volcanic package in this area dips gently to the east, and by driving west we have gone down-section into the Ellis tuff, which lies stratigraphically below Tlm at Stop 1. See figure 2 for a view of the Ellis in the outcrops above this stop. Notice that there is also Ellis tuff cropping out across Iron Creek to the south behind the house.

Continue west on Road 045 to mile 28.4 and the junction with Peel Tree Road 083 coming in from the left. Turn left onto Road 083 and cross Iron Creek, climbing switchbacks to where the road tops out on a ridge at mile 29.5. Pullout to the left, parking in the sagebrush for Stop 3.

STOP 3—29.5 mi
TERTIARY SEDIMENTS (Tsc) AND OVERVIEW OF LANDSLIDE

(44.9080° N; 114.0405° W)

Walk 30 m (100 ft) back down the road to see rounded cobbles of Mesoproterozoic quartzite and perhaps a few clasts of Ellis tuff. The top of the deposit to the south is littered with clasts of Tlm, but these are derived from an outcrop of Tlm to the south. The sediments appear to be post-Ellis and pre-Tlm in age. Look east back down the valley to where, on the north side, red-brown Tlm rests on white Ellis tuff. Also visible is a landslide that moved from the south and dammed Iron Creek (about where the large, metal-roofed shed is located), which formed a shallow, probably short-lived lake, deposits of which make for the rich green meadows below you. The craggy skyline ridge to the southeast is composed of dacite megabreccia and was probably a vent.

Continue climbing up Road 083 past Tsc with cobbles, dark reddish Tlm, and light-colored Te to mile 35.5 and the junction with the South Fork cutoff Road 446 coming in from the right. Turn right (west) onto Road 446 and descend to mile 37.3 and pull out on the left for Stop 4.

STOP 4—35.5 mi
CHALLIS SEDIMENTS (Tsc) WITH PLANT FOSSILS, COARSE SILTITE MEMBER OF THE APPLE CREEK FORMATION (Yac), AND THE COINER FAULT

(44.9023° N; 114.1090° W)

Walk up and down the road observing rounded quartzite clasts in Tsc in a sand, silt, and mudstone matrix. The light-tan-colored siltstone to mudstone with iron

Figure 2. Outcrop of upper part of tuff of Ellis Creek near Stop 2.

staining commonly contains molds of plant fragments; needle molds, probably of sequoia, have been found at this locality. After looking at the sediments walk east a third of a kilometer to where the Coiner normal fault places Yac (coarse siltite member of the Apple Creek Formation) as footwall rocks to the east in contact with Tlm, Te, and Tsc to the west in the downdropped hanging wall.

Continue descending, turning right on Road 047 at mile 38.2, to mile 40.2, where we cross Iron Creek and Road 046 joins from the left. Turn left on 046 and park in the wide spot on the immediate right for Stop 5.

STOP 5—40.2 mi
ELLIS TUFF, APPLE CREEK FORMATION, AND THE COINER FAULT

(44.9196° N; 114.1142° W)

Walk east back along Road 047 to look at Te, which is very crystal-rich here, and then north down Road 047 to the cattle guard, where the Coiner fault again places Yac in the footwall to the east against Ellis tuff to the west in the hanging wall.

Turn around and return east back up Road 047 and 446 to the junction with Road 083 at the saddle at mile 44.9. Turn right (south) onto Road 083 continuing to another saddle, cattle guard, and intersection at mile 47.6. Turn left (southeast) onto Sheephorn Lookout Road 050 and continue to where, at mile 48.5, the road turns right through a gulch and park in the wide spot on the left for Stop 6.

STOP 6—48.5 mi
COINER FAULT, MAFIC LAVAS (Tlm), AND ELLIS TUFF (Te)

(44.8804° N; 114.1018° W)

Hike up the gulch 300 vertical feet to trace the Coiner fault. Notice that the outcrop in front of the vehicles is Ellis tuff, while we have been driving in Tlm. Climb northwest up a cow trail on the left (south) side of the gulch to Sheephorn Spring. The spring is on the fault contact between Tlm and Te. Go around and past the spring on the right and continue northeast on a cow trail that follows an old jeep road, all in Tlm, to where you start to see light-colored Te float. Follow the contact north to where there are outcrops. The Te east of the fault here is continuous with the Te in front of the vehicles below.

Return to vehicles and continue up Sheephorn lookout road.

!!WARNING!! The road to the lookout is rough—you will need good tires and clearance. The turnaround at the lookout can accommodate no more than 4–5 vehicles.

Continue to the dead end at Sheephorn lookout for Stop 7 (mile 53.2).

STOP 7—53.2 mi
OLIVINE BASALT (Tbo)

(44.8828° N; 114.0911° W)

This basalt is fresher looking than the rocks of Tlm, and, while it has not been dated, is probably younger than Eocene in age (Oligocene?). See if you can find green olivine phenocrysts. The view is quite fine, with the Lemhi and Beaverhead Ranges to the east and the high country of Taylor Mountain to the west.

ACKNOWLEDGMENTS

The authors appreciate the drafting of figure 1 by Liam Knudsen as well as a review by Jesse Mosolf.

REFERENCES

Knudsen, L.D., Lewis, R.S., Schmidt, K.L, and Stewart, D.E., this volume, Floating the river: Mesoproterozoic to Quaternary geology along the Salmon downstream from Ellis Idaho: Northwest Geology, v. 52.

Lewis, R.S., Canada, A.S., Stewart, D.E., and Burmester, R.F., 2021, Geologic map of the Degan Mountain quadrangle, Lemhi County, Idaho: Idaho Geologic Survey Digital Web Map 200, scale 1:24,000.

GEOLOGY OF THE BELT SUPERGROUP FROM IRON LAKE NORTH TO PHELAN MOUNTAIN, EAST-CENTRAL IDAHO

Russell F. Burmester,[1] Reed S. Lewis,[1] David M. Pearson,[2] and Liam D. Knudsen[1]

[1]Idaho Geological Survey, Moscow, Idaho
[2]Idaho State University, Pocatello, Idaho

INTRODUCTION

The Salmon River Mountains expose Mesoproterozoic Belt Supergroup rocks that have a long and complex history. The purpose of this trip is to see examples of the three main Apple Creek Formation members exposed in the Salmon River Mountains on the Poison Creek plate (coarse siltite, banded siltite, and Lake Mountain), look at the Poison Creek fault and its footwall, and the Iron Lake fault and its hanging wall (fig. 1).

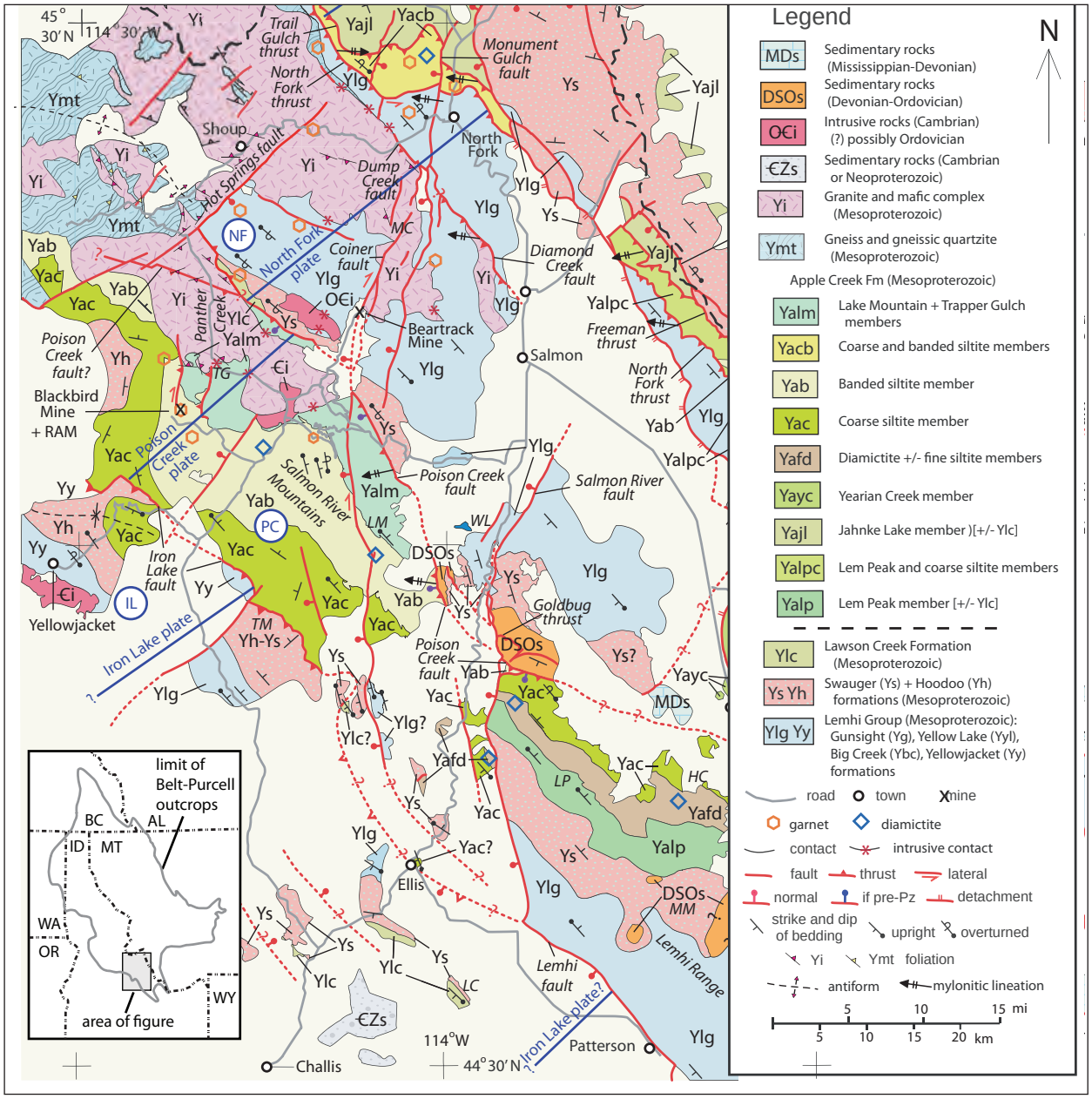

Figure 1. Pre-Mesozoic bedrock geology around Salmon, Idaho. The coarsest clastic unit (Ys = Yh) separates lower formations of the Lemhi Group (in blue) from higher Lawson Creek and Apple Creek Formations (greens and yellows). Units are combined where scale or previous mapping makes separating them impractical. Codes in circles are locations of stratigraphic columns in figure 2. Geographic locations are in italics; those for type or reference sections have units in parentheses: *HC*, Hayden Creek [*Yafd (Yaf+Yad), Yac*]; *LC*, Lawson Creek (Ylc); *LM*, Lake Mountain (Yalm); *LP*, Lem Peak (Yalp); *MC*, Moose Creek; *MM*, Mogg Mountain (Ys); *TG*, Trapper Gulch (Yatg); *TM*, Taylor Mountain; *WL*, Williams Lake. Modified after Burmester and others (2020) to include insights from fieldwork in 2020 through 2022.

REGIONAL STRATIGRAPHY AND STRUCTURE

Mesoproterozoic strata around Salmon, Idaho constitute the Lemhi subbasin of the Belt Supergroup, and reasonably correlate with the Missoula Group of the main Belt Basin (Lonn and others, 2020). The higher strata in the subbasin were described and named Apple Creek Formation in the Lemhi Range to the east and correlated with those in the Salmon River Mountains by Tysdal (2003). The exception we make to Tysdal's naming in the Salmon River Mountains is that the Gunsight Formation is the Lake Mountain member of the Apple Creek Formation (fig. 2). Below that are the banded siltite and coarse siltite members. All these Apple Creek members are in the hanging wall of the Poison Creek fault, and young stratigraphically to the north (fig. 1). Across the Poison Creek fault in its footwall are stratigraphically lower Swauger Formation and Lemhi Group strata that young to the southwest and locally are unconformably overlain by Ordovician units. This relationship documents pre-Ordovician, likely Neoproterozoic, down-on-the-southwest faulting that exposed the footwall to deeper erosion than the hanging wall. This is best documented in the Lemhi Range where subsequent thrust faulting affected all rocks, but evidence also is preserved west of the Salmon River and the ancestral Salmon River fault south of Salmon, which appears to have been activated prior to the Ordovician (Hansen, 2015). However, farther northwest near Panther Creek, the location and role of the Poison Creek fault are more difficult to discover. What is consistent is the opposite facing of younger rocks to the southwest and older southwest-facing rocks on the northeast. This makes the regional structure look like a faulted syncline, but the southwest facing may be from back tilting of the footwall block as it rode up a ramp of a later thrust farther northeast (Hansen, 2015).

LOCAL GEOLOGY

The Poison Creek plate extends southwest in the Salmon River Mountains from the Poison Creek fault to the Iron Lake fault (fig. 1). Units below the coarse siltite, the diamictite, fine siltite, and Lem Peak members of the Apple Creek Formation are missing, but whether they pinched out across the Salmon River fault system or are under the Iron Lake fault is unknown. The lowest strata are graded siltite and argillite couplets and minor thin feldspathic quartzite beds of the coarse siltite member. The argillite is greenish to brown (where weathered). Sedimentary structures include mud cracks and ripples. High but varied magnetic susceptibility is characteristic ($11.11 \pm 11.26 \times 10^{-3}$ SI; $n = 351$). This is due to uneven concentration, even between beds, of magnetite that is commonly visible. For comparison, the average susceptibility for Lemhi subbasin Mesoproterozoic strata is 4.4 SI $\times 10^{-3}$; $n = 1746$.

The gradationally overlying banded siltite member also has siltite and argillite couplets and locally couples, and beds of very fine-grained feldspathic quartzite. Differences from the coarse siltite member are that the argillite is dark gray to black and has ptygmatically folded, discontinuous silt to sand dikelets that taper downward. Bedding is much more uneven, undulose to pinch and swell, and cross lamination in the quartzite and siltite are smaller and much more intricate. Concentrations of diamictite, like those of the diamictite member of the Apple Creek Formation in the Lemhi Range, but typically with more angular quartzite clasts, are scattered throughout. Magnetic susceptibilities are generally very low ($0.44 \pm 1.48 \times 10^{-3}$ SI; $n = 288$). An exception is low in the unit near Iron Creek south of this trip.

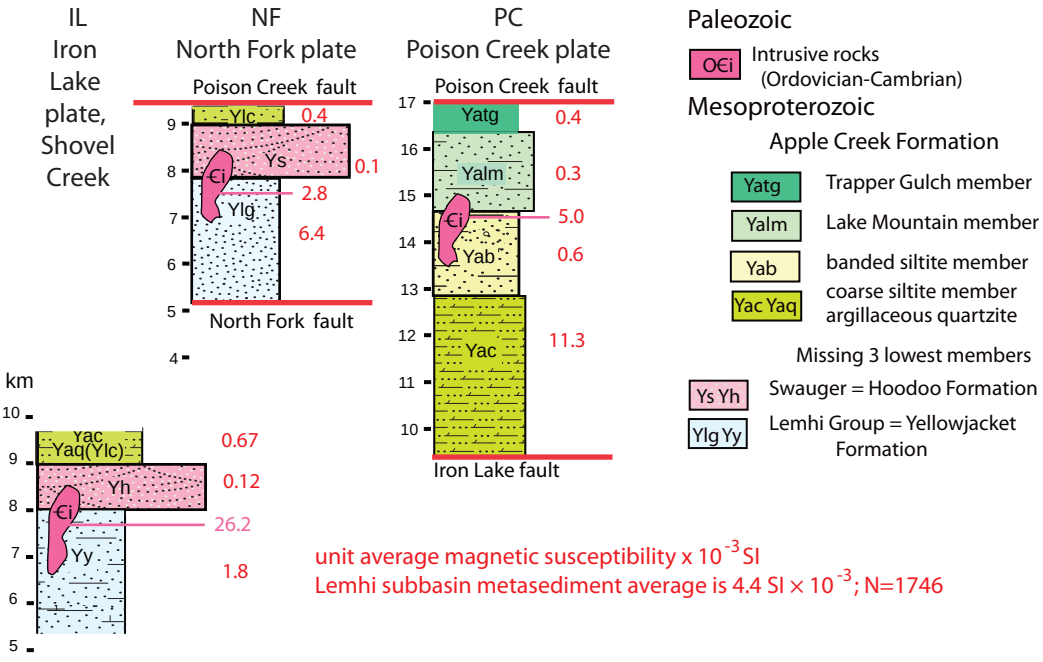

Figure 2. Stratigraphic column for the Salmon River Mountains.

The gradationally overlying Lake Mountain member is mostly very fine-grained, well-sorted feldspathic quartzite. Biotite is common on bedding surfaces and in laminae, generally parallel to bedding surfaces but also showing low- and high-angle cross laminations throughout. Hummocky cross lamination, diamictite, and soft-sediment deformation are found near the lower contact. Magnetic susceptibilities are low ($0.25 \pm 0.22 \times 10^{-3}$ SI; $n = 46$). The overlying Trapper Gulch member is the highest unit known in the Lemhi subbasin but is not exposed in the field trip area. It can be seen along Panther Creek northeast of the Ram deposit (Jervois Global's Idaho cobalt operations). It has marginally higher magnetic susceptibilities ($0.39 \pm 0.19 \times 10^{-3}$ SI; $n = 9$) than the banded siltite member, likely due to higher biotite content. On either side of the Poison Creek plate are Swauger Formation and Lemhi Group strata, and locally Lawson Creek Formation.

Strata at Iron Lake are the coarse siltite member of the Apple Creek Formation in the footwall of the Iron Lake fault, and Swauger Formation quartzite in its hanging wall. The Swauger Formation of the Iron Lake plate is varied pale pink to white, fine- to medium-grained, poorly sorted quartzite with as much as 50 percent feldspar, and contains small red grains, possibly jasperoid or chert. Quartz grains are well rounded to spherical. Feldspar grains are interstitial or blocky. Bedding is thin to thick, and planar to trough cross bedded. Ripples and large mud cracks exist but are not common. Several intervals of dark gray, fine-grained, and thinly laminated argillite, siltite, and quartzite 1 to 10 m thick (fig. 3) are similar to the Lawson Creek Formation in the Lemhi Range. Magnetic susceptibilities are low ($0.13 \pm 0.24 \times 10^{-3}$ SI; $n = 25$). The Swauger here was previously mapped as Hoodoo Quartzite (Ekren, 1988; Tysdal, 2003), but continuity with the Swauger of the Lemhi Range makes retaining that term difficult.

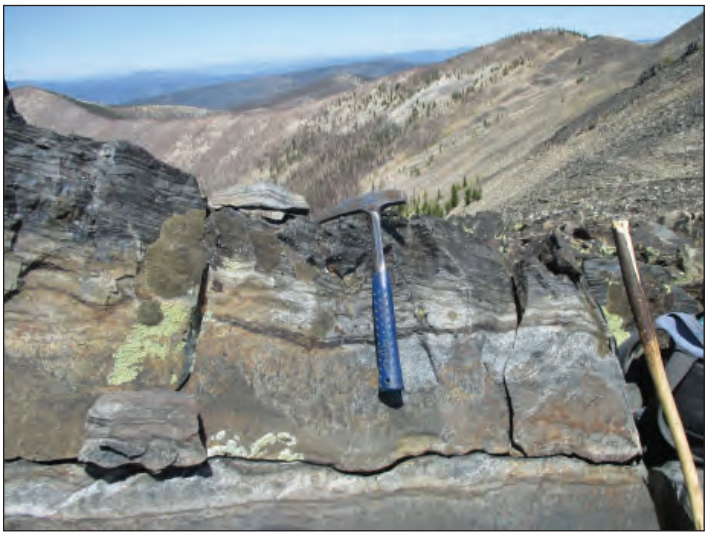

Figure 3. Thin beds with uneven and flaser lamination of darker and finer material within the Swauger Formation about 0.6 km (0.4 mi) south of Taylor Mountain, out of the picture to the right. Similar are strata of the Lawson Creek Formation in the Lemhi Range to the east. Photo by Dave Stewart.

The quartzite at Williams Creek Summit and to the north on Phelan Mountain has been mapped as Ordovician Kinnikinic Quartzite (Shockey, 1957), Big Creek Formation (Connor and Evans, 1986), and Swauger Formation (Evans and Green, 2003). We side with the Swauger call because in comparison with published descriptions and what we have seen elsewhere, it is too coarse to be Big Creek Formation and too poorly sorted and feldspathic to be Kinnikinic, and contains red accessory grains that appear elsewhere in the Swauger.

ROAD LOG

Field trip stops are referenced to GPS coordinates (WGS84), and with mileage at stops noted. The trip starts at the Sacajawea Interpretive, Cultural, and Educational Center parking lot exit on E. Main St. (Hwy 28) in Salmon. Turn right (NW) and go 1.2 mi to a left turn at the traffic light at the intersection with S. Challis St. (US Highway 93). Head 5.2 mi south past the BLM–USFS complex and the Salmon Airport (both on the left) to a right turn across the Salmon River on Shoup Bridge.

6.4 mi Reset odometer at the right turn. Figure 4 shows the route, stops, and points of interest mentioned in this log, starting here.

0.1 mi Cross the Salmon River on the Shoup Bridge. Drive due west, climbing up onto older alluvial fan deposits at about 0.6 mi to a Y intersection (0.9 mi). Take the left fork and follow the paved road as it winds south to southwest for about 1.6 mi over terrace gravels and Tertiary sediments before a right bend to the west. Continue past the intersection with the Williams Lake Road about 2.4 mi from the bridge into steeply east-dipping biotite–plagioclase tuff of the Challis Volcanic Group. At its base, resting on Mesoproterozoic rocks, is a sliver of basal mafic lavas. We'll see more of this on the ridge 6 mi west and 3,500 ft higher.

STOP 1—4.5 mi
Lemhi Group—optional

(45.0821°N, 113.9657°W)

We are on the North Fork plate, northeast of the Poison Creek fault. We originally mapped the rocks below the Swauger Formation as "siltite and quartzite" instead of assigning it a formal name (Lewis and others, 2012). In later mapping, we assigned these rocks below the Challis to the Gunsight Formation of the Lemhi Group (Lewis and others, 2013). Most recently, we have been assigning these strata to the Lemhi Group. The reason for this is that Ruppel's (1975) formalization of units in the Lemhi Group was in the Poison Creek plate in the Lemhi Range, but we have been unable to recognize

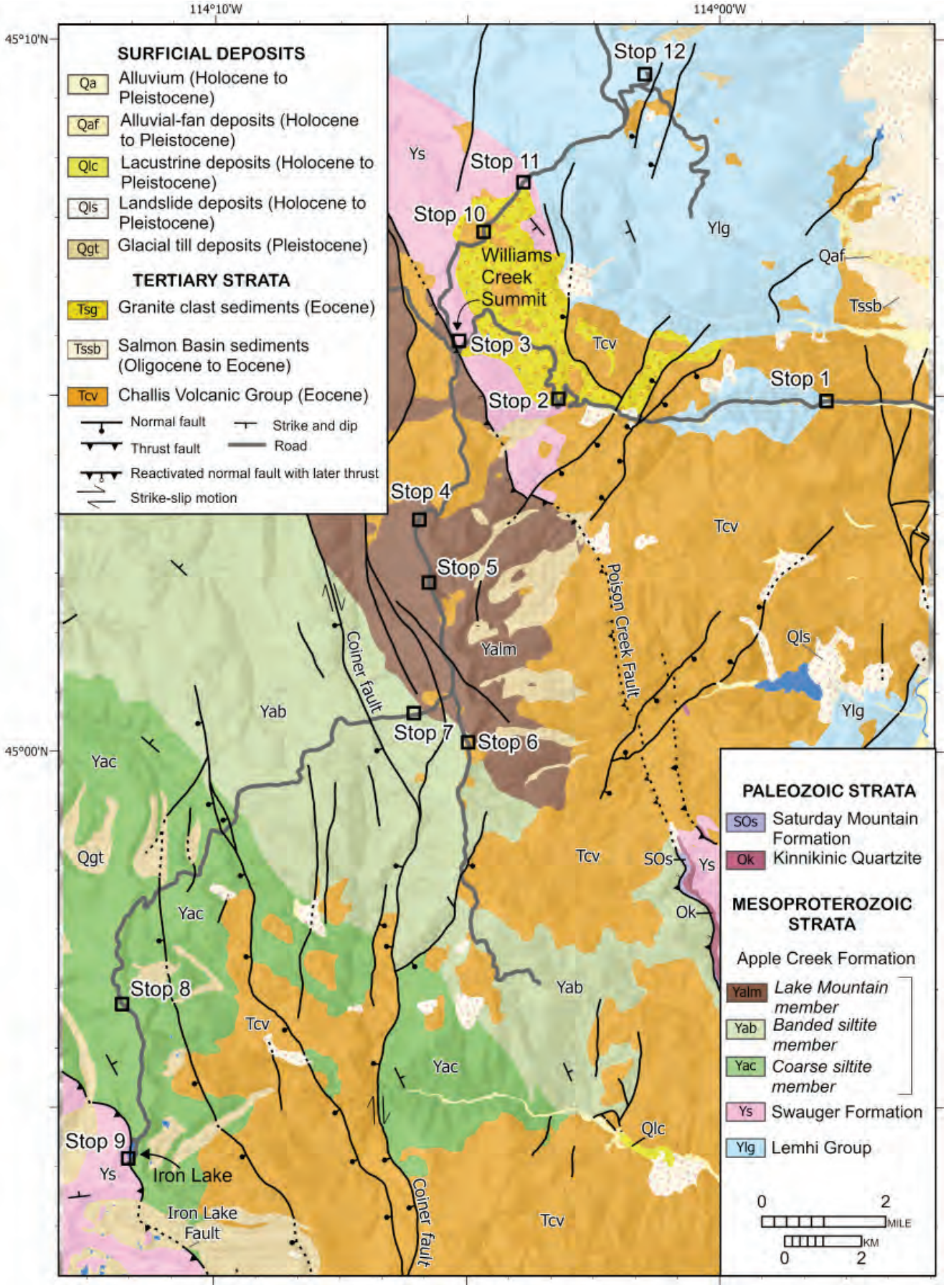

Figure 4. Geologic map of field trip from west of Shoup Bridge showing stops. Map sources include 1:24,000-scale geologic maps of the Williams Lake (Lewis and others, 2013), Lake Mountain (Stewart and others, 2023, in press), Cobalt (Lewis and others, 2021a), Degan Mountain (Lewis and others, 2021b), and Taylor Mountain (Stewart and other, 2021) 7.5′ quadrangles.

those separate lithologic packages on the North Fork plate.

7.0 mi Pass the fork up the South Fork Williams Creek. On the right there are cliffs of conglomerate at the base of the Challis section. Proceed up through two sets of switchbacks and varied Challis and Quaternary units. Look for nearly horizontal lake bed(?) deposits above one right turn. The last right switchback (10.3 mi) is at Cougar Point.

7.7 mi First set of short switchbacks. A double set follows in another mile and a half.

STOP 2—10.4 mi
Swauger Formation—optional

(45.0826°N, 114.0542°W)

This is a small picnic area (Cougar Point Recreation Site). Outcrop is at the hairpin turn. From there and west to the Poison Creek fault, Swauger Formation quartzite has intervals of south-striking mylonite dipping 20 to 40 degrees west with down-dip lineations. This was Stop 2 on a 2013 TRGS field trip (Burmester and others, 2013). The coarser grain size (some medium rather than entirely fine to very fine) is characteristic of the Swauger Formation, and we are now near the southeastern end of the Swauger exposures within the Williams Creek Summit block. Sericite is concentrated along spaced shear surfaces (C) that are at an angle to the foliation (S), so if they were formed during evolving strain as shear surfaces, motion would have been top-to-the-west and thus anomalous. The hill visible to the southwest is the same material. The eastern contact is obscured by a Challis tuff. The eastern steep slope has mylonitic fabric similar to what we see here. The steep west side of the hill is silicified quartzite with mylonite foliation that dips gently (15°) east. Below that is poorly exposed scapolitic gray, fine-grained quartzite. The saddle to the west has float of mylonite, and farther west is dark, very fine-grained feldspathic quartzite. The hill about 1.1 mi due west of Cougar Point is similar. Nonuniformly distributed mylonite dips gently (20°) southeast. Kinematics on these hills seem similar to what we find here, suggesting top-to-the-west motion throughout. Perplexing are why the fabric appears synformal and why is the apparent sense of motion opposite the regional top to the east?

13.0 mi After a sharp left there is a steep slope and road cut on the right. There may be nothing in place, but rocks here have medium round quartz grains and some pink grains that are typical of the Swauger Formation northeast of Lemhi Pass.

Proceed to Williams Creek Summit (13.7 mi). Turn right on USFS Rd 020 and proceed about 0.1 mi north, and park on side road on right that leads to a small quarry in quartzite.

STOP 3—13.8 mi
Quarry and Poison Creek fault

(45.0962°N, 114.0870°W)

The quarry has sparse exposures of quartzite mylonite with a very steep foliation and north-plunging lineation (fig. 5). This is different from both the top-to-the-west motion apparent in the Swauger quartzite at and west of Cougar Point, and the regional top-to-the east motion.

Zircon grains from the hanging wall of the Poison Creek fault underwent (U-Th)/He analysis at the University of Arizona to constrain the timing and magnitude of rock exhumation, which we infer resulted from thrusting (fig. 6). (U-Th)/He thermochronometry of zircon generally reflects the time since cooling of the zircon below ~180 °C (Reiners, 2005). Assuming a reasonable geothermal gradient of 20-25°C/km, this dates when rocks were exhumed through depths of ~6–9 km. One sample was collected from the Cambrian alkali-feldspar syenite of the Deep Creek pluton near the intersection of Deep Creek and Panther Creek ~10 km west of this quarry; that pluton was dated by U-Pb zircon to 492 ± 4.4 Ma (Link and others, 2017). Another sample was collected ~30 km southeast of here from mylonitized fine-grained Mesoproterozoic quartzite of the coarse siltite member of the Apple Creek Formation of the Belt Supergroup (Hansen and Pearson, 2016). For the mylonitic quartzite sample collected in the hanging wall of the Poison Creek thrust, six detrital

Figure 5. View north at Swauger Formation quartzite with vertical mylonitic foliation and 35° NNW-plunging lineation in quarry north of Williams Creek Summit. Poison Creek fault contact with the Lem Peak member of the Apple Creek Formation is about 250 m (800 ft) to the left.

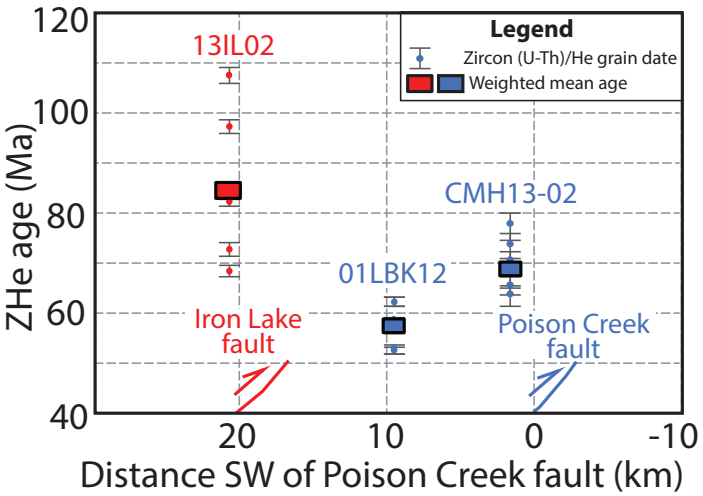

Figure 6. (U-Th)/He plot for zircons collected on the Poison Creek and Iron Lake plates. Individual zircon (U-Th)/He grain dates (small circles) and weighted mean ages (larger squares) of samples analyzed within the field trip area. Ages are interpreted to constrain the timing of thrusting as rocks were exhumed through depths of ~6–9 km.

Figure 7. Block of Lake Mountain member of Apple Creek Formation quartzite with parallel lamination defined by concentrations of biotite. Location is about 8 km (5 mi) north of Lake Mountain.

zircons yielded very similar (U-Th)/He dates, ranging between 77.5 ± 2.8 Ma and 63.6 ± 1.9 Ma, and a well-constrained weighted mean age of 68.4 ± 0.9 Ma (fig. 6, above). The five grains from the pluton, which was sampled at a lower elevation in the hanging wall of the Poison Creek fault, produced similar dates ranging between 62.4 ± 0.9 Ma and 52.5 ± 0.7 Ma and a weighted mean age of 56.8 ± 0.7 Ma (fig. 6). These results suggest that the thrusting along the Poison Creek fault occurred in Late Cretaceous to early Cenozoic time.

Return to Williams Creek Summit. Make use of the last restroom for a while. Reset odometer.

0.0 mi Williams Creek Summit. Follow USFS Rd 020 south.

0.7 mi Keep left. USFS Rd 232 turns off to the right.

1.0–1.3 mi Look to the east at the nearly bare slope of quartzite talus. Among the talus high and towards the south are vertical flatirons of quartzite mylonite that are probably southward continuations of the Poison Creek fault we saw in the quarry at Stop 1.

2.5 mi Challis mafic lava in roadcuts on the left.

STOP 4—3.4 mi
View of Salmon River Mountains and Ram deposit

(45.0543°N, 114.1001°W)

USFS Rd 106 takes off to the right. Stay left, and park just beyond the turnoff. This stop affords a view of the Salmon River Mountains, including the Jervois Global Ram deposit 21 km to the west–northwest. Closer (8 km) slightly south of west on this side of Panther Creek is the Blackpine mine; the area is currently being explored by Koba Resources. The Coiner fault is this side of the proximal, Pepper Creek Ridge. Here, loose blocks east of the road display a range of sedimentary structures and typical laminations of biotite concentrations (fig. 7, above).

STOP 5—4.5 mi
Lake Mountain member of Apple Creek Formation

(45.0396 N, 114.0969 W)

Relatively steep dips here in characteristic biotite-bearing quartzite of the Lake Mountain member.

5.9 mi Road to left goes to Lake Mountain.

6.3 mi China Spring intersection. Road to left (USFS Rd 045) goes to Degan Mountain, right (USFS Rd 020) to Iron Lake. Reset odometer.

Side trip to see diamictite in Lake Mountain member of the Apple Creek Formation and the Salmon aviation navigation facility. Lots of blocks of Lake Mountain quartzite but not much in place.

STOP 6—0.9 mi
Lake Mountain member diamictite

(45.0022°N, 114.0839°W)

Park in grassy area on left for access to stop. Hike about 200 m northeast, crossing through the woods to open block-rich slopes (45.0038 N, 114.0828 W). The diamictites are characterized by angular to rounded clasts of lighter quartzite in darker argillaceous siltite matrix (fig. 8) here near the lower contact of the Lake Mountain member of Apple Creek Formation. Some

Figure 8. Diamictite at Stop 6 with angular to rounded clasts of lighter quartzite in darker argillaceous siltite matrix near the lower contact of the Lake Mountain member of Apple Creek Formation.

clasts are folded and are carbonate-bearing (fig. 9) and blocks with soft-sediment deformation (fig. 10) are present about 140 m farther northeast.

Return to China Spring intersection and reset odometer.

Main trip on USFS Rd 020, to Iron Lake

0.0 mi Road intersection.

0.1 mi China Spring on right.

0.3 mi Trailhead on left for North Fork Iron Creek.

Figure 9. Carbonate-bearing diamictite clast at Stop 6 near the lower contact of the Lake Mountain member of Apple Creek Formation.

Figure 10. Contorted laminated feldspathic quartzite near the lower contact of the Lake Mountain member of Apple Creek Formation.

STOP 7—0.7 mi
Banded siltite of Apple Creek Formation

(45.0090°N, 114.1018°W)

Park on right. Hike north about 50 m to outcrop visible from road. Note characteristic bedding style (fig. 11).

1.5 mi Saddle. Minor amounts of chalcedonic quartz in float. Coiner fault, which had Tertiary down-on-the-west motion and probably Cretaceous right-lateral motion, likely comes through this topographic depression but is not well expressed.

Follow USFS Rd 020 another half mile and stay left at that intersection. Then in another half mile stay right, and yet another half mile, stay left. All the rocks you haven't seen are the banded siltite member. At about

Figure 11. Thin beds of white feldspathic quartzite, some grading up to dark siltite and argillite tops, and some discontinuous, others with undulatory bases and "pinch-and-swell" geometry.

4.7 mi from the China Spring intersection (44.9863°N, 114.1601°W) the road crosses into the coarse siltite member of the Apple Creek Formation and stays in it to the road's end at 12.6 miles at the south end of Iron Lake. Below the road to the east along the way the rocks look like those shown in figure 12.

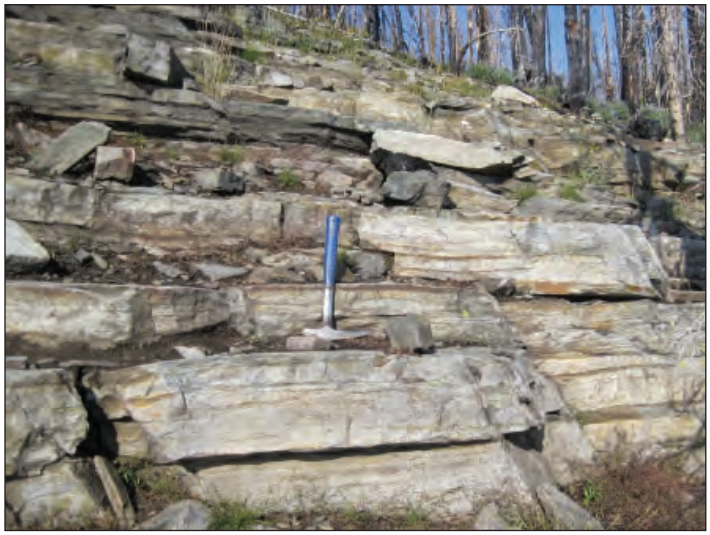

Figure 12. View northwest of nearly horizontal thin quartzite beds and siltite and argillite couples and couplets of the coarse siltite member of Apple Creek Formation about 2 km (1.2 mi) north of Iron Lake.

STOP 8—9.6 mi
Coarse siltite member of Apple Creek Formation

(44.9408°N, 114.1978°W)

Observe lithology, intense cleavage, and high magnetic susceptibility ($22.0 \pm 9.8 \times 10^{-3}$ SI). See any magnetite octahedra? See mud chips or cracks, ripples? Drive to the Iron Lake Campground.

STOP 9—12.4 mi
Swauger Formation near the Iron Lake Campground

(44.9042°N, 114.1946°W)

Figure 13 shows a detailed geologic map of the Iron Lake area. At the campground, the Iron Lake fault places the Swauger Formation on the west against the coarse siltite member of the Apple Creek Formation on the east.

Walk to the west side of the lake and shop the talus for Swauger quartzite. What are the varieties there? About 1 km (0.6 mi) to the southwest the Swauger contains dark red to black argillite and siltite interbeds.

Detrital U-Pb zircon analysis (n = 100) from a sample of the Swauger Formation collected on the western shore of Iron Lake (44.9084 N, 114.1954 W) produced two dominant age-peaks at ~1680-1740 Ma and ~1470 Ma, with several older ages (fig. 14); the youngest mode of the kernel density estimation (five grains) defines a maximum depositional age (MDA) of ~1451 Ma. Additional published U-Pb DZ data from rocks previously mapped as the Hoodoo Formation and now correlated with the Swauger Formation (from Quartzite Mountain and Taylor Ranch, ID; Link and others, 2007) have indistinguishable age modes and MDAs and collectively define an MDA of ~1447 Ma. Similarly, U-Pb DZ results from rocks mapped as the Swauger Formation east of the Salmon River in east-central Idaho yield major age modes at ~1722 Ma and ~1449 Ma (Link and others, 2016). These results support the correlation of the Hoodoo with the Swauger Formation that is based on lithofacies, and regional stratigraphic relationships documented elsewhere (Burmester and others, 2016).

Bushwhacking about 250 m north of Iron Lake would allow one to observe a locally laminated, green-gray phyllite of the coarse siltite member of the Apple Creek Formation that we interpret to have been deformed within a broad shear zone that defines the Iron Lake fault. There, fine-grained footwall rocks exhibit 1- to 2-cm-scale crenulation folds with a prominent, moderately (35°–40°) west-dipping axial planar cleavage. In some outcrops, faint and irregularly oriented, north-

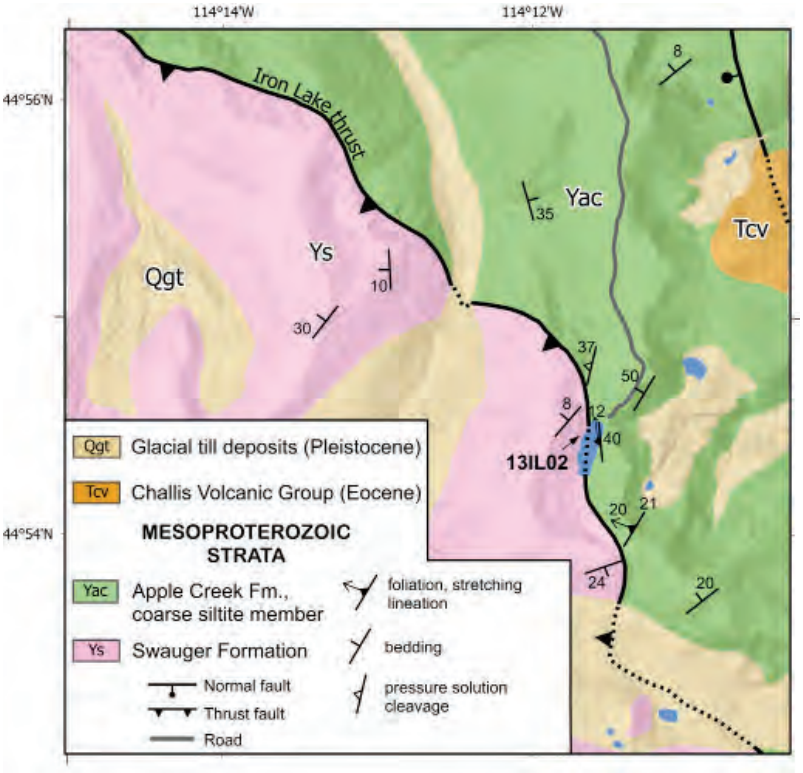

Figure 13. Detailed geologic map of the Iron Lake area. Based on Stewart and others (2021) and unpublished mapping by D. Pearson.

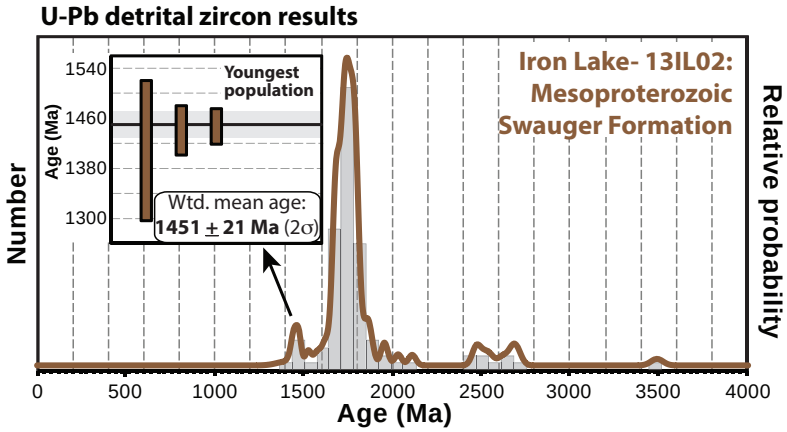

Figure 14. Detrital zircon age histogram and probability distribution plot for the Swauger Formation west of and above Iron Lake in the hanging wall of the Iron Lake fault. Maximum depositional age is 1451 ± 21 Ma.

west-plunging stretching lineations were observed, with possible S-C fabrics interpreted as a top-to-the-east/southeast sense of displacement across shallowly west-dipping shear surfaces (fig. 15).

Walk the trail on the east side of Iron Lake southward a little over half a mile and climb about 400 ft to point 9238 on the Taylor Mountain topographic map (44.8984°N, 114.1910°W). This is a more scenic locality to observe the "invisible" Iron Lake fault. Go west to outcrops of Swauger Formation and look for evidence of faulting as well as more views of the variety of quartzite there. If time permits, wander farther west to see more varieties in the felsenmeer on the ridge. Reconnaissance fieldwork and oriented thin sections from rocks collected from the coarse siltite member of the Apple Creek Formation along this ridge in the footwall of the Iron Lake fault identified possible S-C deformation fabrics within the Iron Lake fault zone (fig. 15). These fabrics are interpreted to indicate top-to-the-east thrust displacement along the Iron Lake fault. Structural analysis of thin sections reveals dynamic recrystallization fabrics with larger quartz grains surrounded by smaller sub-grains, which suggests that bulging recrystallization (Passchier and Trouw, 2005) was the dominant deformation mechanism; this constrains deformation temperatures to ~300°C during faulting. This is in accord with metamorphic mineral assemblages that indicate a greenschist-facies equivalent metamorphic grade.

Zircon grains from the hanging wall of the Iron Lake fault (sample 13IL02) also underwent (U-Th)/He analysis to constrain the timing and magnitude of rock exhumation in the hanging wall of the Iron Lake fault, which we infer resulted from thrusting (fig. 6). The five zircons dated using zircon (U-Th)/He thermochronometry yielded dates ranging from 107.6 ± 1.5 Ma to 68.5 ± 1.3 Ma; uncertainties consist of 2σ analytical error. These results give a weighted mean age of 84.3 ± 1.3 Ma. If the youngest individual grain dates of ~70 Ma (n = 2) constitute the "most reset" grains, then thrust-related exhumation along the Iron Lake fault may have occurred at that time.

Return to Williams Creek Summit. Reset odometer and, if time allows, continue north, following USFS road 020, which goes up a ridge held up mostly by the light-colored medium-grained quartzite interpreted as Swauger. Below the road at about mile 0.8, there is folded and mylonitized Swauger quartzite close to the fault contact with the Lake Mountain member of the Apple Creek Formation. Up the road another half mile (1.6 mi) float of Swauger Formation includes thin-bedded almost schistose, biotite-rich material. Such is found at various levels within the Swauger on Taylor Mountain and elsewhere.

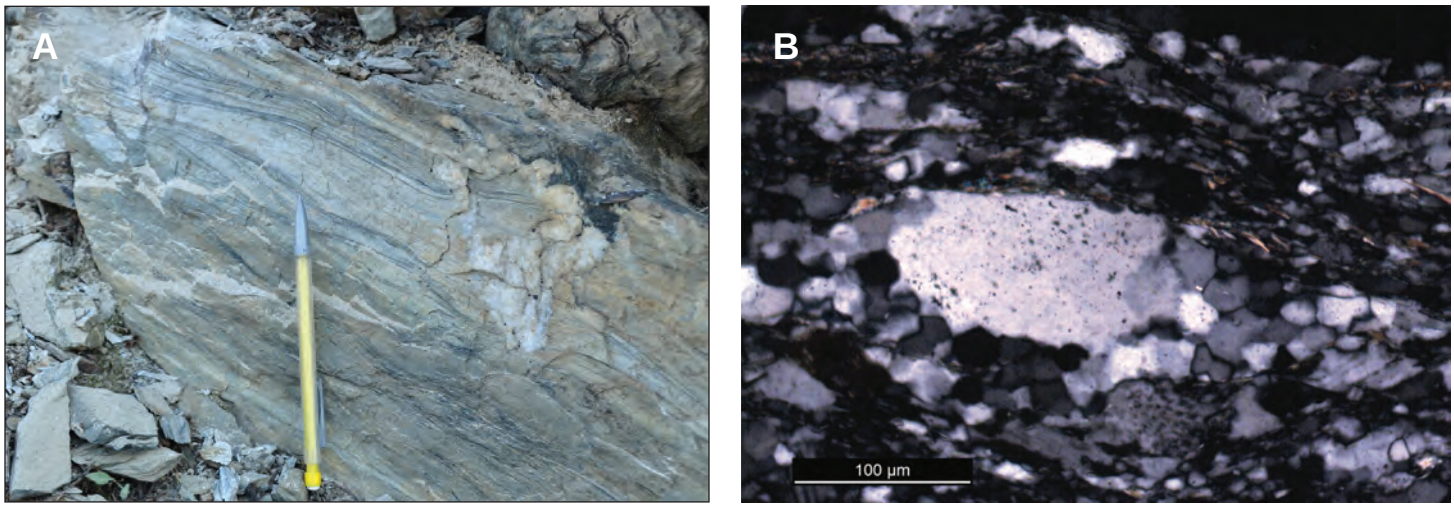

Figure 15. Coarse siltite member of the Apple Creek Formation in the footwall of the Iron Lake fault. (A) Photo of rocks in the immediate footwall of the Iron Lake fault that are interpreted to be sheared; view looking southeast. (B) Photomicrograph of a thin section showing dynamic recrystallization fabrics with larger quartz grains surrounded by smaller subgrains. Petrographic analysis supports the field interpretation that the rocks are mylonitized.

2.0 mi Sharp right turn in a saddle. Note that there is a spur straight ahead that continues to the base of Phelan Mountain. Continue east then north around a Challis mafic lava flow.

STOP 10—2.5 mi
Mafic lava and granite boulders—optional

(45.1217°N, 114.0789°W)

Parking looks possible in a wide spot in the road and a cleared swath to the left. Stop here to look at mafic Challis lava flow we just passed and explore the saddle between it and Phelan Mountain for Mesoproterozoic megacrystic granite. Is the granite in place, i.e., intrusive into or in fault contact with the Swauger (look for fabric in the granite), or is it just lag from Tertiary erosion? Our current interpretation is that the boulders are weathering from a sedimentary deposit below the mafic lavas. Boulders of this granite litter saddles and ridges southwest to near Yellowjacket, the slopes west and northwest of Salmon, and mark a river system that extends at least 65 km (40 mi) to the southeast at Lemhi Pass (Janecke and others, 2000). At Lemhi Pass, the same relationship exists, with boulders of megacrystic granite restricted to a deposit that is directly below mafic lavas (Burmester and others, 2018).

2.8 mi A logging spur goes to the right. If drivable, this is an alternate way to see the Swauger Formation. Proceed 0.6 mi to past where the road bends left from going southeast to northeast. Some pieces are close enough in place that top directions can be determined from crossbeds. A sample from here has a mode of 95 percent quartz, 4 percent potassium feldspar, and 1 percent plagioclase. Look for variations in grain size and feldspar and mica content. The contact with underlying Lemhi Group is 0.8 mi farther along the road on the other side of West Fork Perreau Creek.

STOP 11—3.6 mi
Swauger Formation on Phelan Mountain—optional

(45.1333°N, 114.0658°W).

Park in clearing and walk west to the base of Phelan Mountain. Outcrops and blocks here show typical bedding style of the Swauger Formation. Look for small red to pink grains.

5.6 mi Turnoff to Baldy on right. Take this. Proceed 0.9 mi (6.5 mi) and take left on USFS Rd 200. Proceed 0.4 mi to Baldy communication towers and park.

STOP 12—6.9 mi
Lemhi Group—optional

(45.1586°N, 114.0257°W).

These strata are typical of the upper Lemhi Group below the Poison Creek fault in having a dark color, fine grain size, and high feldspar content. Note atypical concretions are present (fig. 16) just east of the communication facilities.

Return to Salmon.

Figure 16. Concretions in Lemhi Group quartzite northwest of Baldy.

ACKNOWLEDGMENTS

A manuscript review by Stuart Parker is greatly appreciated.

REFERENCES CITED

Burmester, R.F., McFaddan, M.D., Lewis, R.S., and Lonn, J.D., 2013, What's the Swauger Formation doing in the eastern Salmon River Mountains, Idaho?: Northwest Geology, v. 42, p. 197–198.

Burmester, R.F., Lonn, J.D., Lewis, R.S., and McFaddan, M.D., 2016, Stratigraphy of the Lemhi subbasin of the Belt Supergroup, *in* MacLean, J.S., and Sears, J.W., eds., Belt Basin: Window to Mesoproterozoic Earth: Geological Society of America Special Paper 522, p. 121–137.

Burmester, R.F., Othberg, K.L., Stanford L.R., Lewis, R.S., and Lonn, J.D., 2018, Geologic map of the Lemhi Pass quadran-

gle, Lemhi County, Idaho: Idaho Geological Survey Digital Web Map 183, scale: 1:24,000.

Connor, J.J., and Evans, K.V., 1986, Geologic map of the Leesburg quadrangle, Lemhi County, Idaho: Geological Survey Miscellaneous Field Studies Map MF-1880, 19 p., scale 1:62,500.

Ekren, E.B., 1988, Stratigraphic and structural relations of the Hoodoo Quartzite and Yellowjacket Formation of Middle Proterozoic age from Hoodoo Creek eastward to Mount Taylor, central Idaho: U.S. Geological Survey Bulletin 1570, 17 p.

Evans, K.V., and Green, G.N., 2003, Geologic map of the Salmon National Forest and vicinity, east-central Idaho: U.S. Geological Survey Geologic Investigations Series Map I-2765, 19 p., scale 1:100,000.

Hansen, C., 2015, An investigation into the Poison Creek thrust: A Sevier thrust with Proterozoic implications: Moscow, Idaho, Idaho State University, M.S. thesis, 80 p.

Hansen, C., and Pearson, D.M., 2016, Geologic map of the Poison Creek thrust fault and vicinity near Poison Peak and Twin Peaks, Lemhi County, Idaho: Idaho Geological Survey Technical Report, v. 16–1.

Janecke, S.U., VanDenburg, C.J., Blankenau, J.J., and M'Gonigle, J.W., 2000, Long-distance longitudinal transport of gravel across the Cordilleran thrust belt of Montana and Idaho: Geology, v. 28, no. 5, p. 439–442.

Lewis, R.S., Othberg, K.L., Burmester, R.F., Stanford, L.R., McFaddan, M.D., and Lonn, J.D, 2012, Geologic map of the Salmon quadrangle, Lemhi County, Idaho: Idaho Geologic Survey Digital Web Map 154, scale 1:24,000.

Lewis, R.S., Othberg, K.L., McFaddan, M.D., Burmester, R.F., Stewart, D.E., Stanford, L.R., and Stewart, E.D., 2013, Geologic map of the Williams Lake quadrangle, Lemhi County, Idaho: Idaho Geological Survey Digital Web Map 162, scale 1:24,000.

Lewis, R.S., Stewart, D.E., Burmester, R.F., and Canada, A.S., 2021a, Geologic map of the Cobalt quadrangle, Lemhi County, Idaho: Idaho Geological Survey Digital Web Map 199, scale 1:24,000.

Lewis, R.S., Canada, A.S., Stewart, D.E., and Burmester, R.F., 2021b, Geologic map of the Degan Mountain quadrangle, Lemhi County, Idaho: Idaho Geological Survey Digital Web Map 200, scale 1:24,000.

Link, P.K., Fanning, C.M., Lund, K.I., and Aleinikoff, J.N., 2007, Detrital-zircon populations and provenance of Mesoproterozoic strata of east-central Idaho, USA: Correlation with the Belt Supergroup of southwest Montana: Special Publication-SEPM, v. 86, p. 101–128.

Link, P.K., Stewart, E.D., Steel, T., Sherwin, J.A., Hess, L., and McDonald, C., 2016, Detrital zircons in the Mesoproterozoic upper Belt Supergroup in the Pioneer, Beaverhead, and Lemhi Ranges, Montana and Idaho: The Big White arc, *in* MacLean, J.S., and Sears, J.W., eds., Belt Basin: Window to Mesoproterozoic Earth: Geological Society of America Special Paper, v. 522, p. 163–183.

Link, P.K., Todt, M.K., Pearson, D.M., and Thomas, R.C., 2017, 500–490 Ma detrital zircons in Upper Cambrian Worm Creek and correlative sandstones, Idaho, Montana, and Wyoming: Magmatism and tectonism within the passive margin: Lithosphere, v. 9, no. 6, p. 910–926, doi:10.1130/l671.1

Lonn, J.D., Burmester, R.F., Lewis, R.S., and McFaddan, M.D., 2020, The Mesoproterozoic Belt Supergroup, *in* Geology of Montana: Montana Bureau of Mines and Geology Special Publication 122, v 1: Geologic History, available at: https://mbmg.mtech.edu/pdf/geologyvolume/Lonn_BeltFinal.pdf [Accessed July 2023].

Passchier, C.W., and Trouw, R.A.J., 2005, Microtectonics: Springer, doi:10.1007/3-540-29359-0

Reiners, P.W., 2005, Zircon (U-Th)/He Thermochronometry, *in* Reiners, P.W., and Ehlers, T.A., eds., Thermochronology, Reviews in Mineralogy and Geochemistry, v. 58, p. 151–176.

Ruppel, E.T., 1975, Precambrian Y Sedimentary Rocks in East-Central Idaho: U.S. Geological Survey Professional Paper 889-A, 23 p.

Shockey, P.N., 1957, Reconnaissance geology of the Leesburg quadrangle, Lemhi County, Idaho: Idaho Bureau of Mines and Geology Pamphlet 113, 42 p.

Stewart, D.E., Canada, A.S., Burmester, R.F., and Lewis, R.S., 2021, Geologic map of the Taylor Mountain quadrangle, Lemhi County, Idaho: Idaho Geological Survey Digital Web Map 201, scale 1:24,000.

Stewart, D.E., Lewis, R.S., Burmester, R.F., Lonn, J.D., McFaddan, M.D., Tkach, M.K., and, Canada, A.S., 2023, in press, Geologic map of the Lake Mountain quadrangle, Lemhi County, Idaho: Idaho Geological Survey Digital Web Map, scale 1:24,000.

Tysdal, R.G., 2003, Correlation, sedimentology, and structural setting, upper strata of Mesoproterozoic Apple Creek Formation and lower strata of Gunsight Formation, Lemhi Range to Salmon River Mountains, east-central Idaho, *in* Tysdal, R.G., Lindsey, D.A., and Taggart, J.E., Jr., eds., Correlation, sedimentology, structural setting, chemical composition, and provenance of selected formations in Mesoproterozoic Lemhi Group, central Idaho: U.S. Geological Survey Professional Paper 1668-A, p. 1–22.

RETURN TO THE RIVER OF NO RETURN CORRIDOR: NEW INSIGHTS FROM MESOPROTEROZOIC ROCK ALONG THE SALMON RIVER FROM NORTH FORK TO CORN CREEK, EAST-CENTRAL IDAHO

Russell F. Burmester,[1] Cody J. Steven,[1] Keegan L. Schmidt,[2] Reed S. Lewis,[1] Richard M. Gaschnig,[3] and Madeline Murchland[4]

[1]Idaho Geological Survey, Moscow, Idaho
[2]Lewis-Clark State College, Lewiston, Idaho
[3]University of Massachusetts Lowell, Lowell, Massachusetts
[4]University of Idaho, Moscow, Idaho

INTRODUCTION

The Salmon Canyon transect from North Fork to Corn Creek (fig. 1) spans an enigmatic part of the Lemhi subbasin of the Mesoproterozoic Belt–Purcell Basin. Relatively unmetamorphosed quartzite, siltite, and minor argillite of the Lemhi Group (Ylg) constitute the section nearest North Fork. To the west they are intruded by Mesoproterozoic mafic and granitic dikes, sills, and plutons (Yi). These intrusions belong to a bimodal suite with A-type granites that appears confined to the Lemhi subbasin. All of those rocks are cut by faults and are more metamorphosed and deformed in the west, resulting in garnet–sillimanite grade

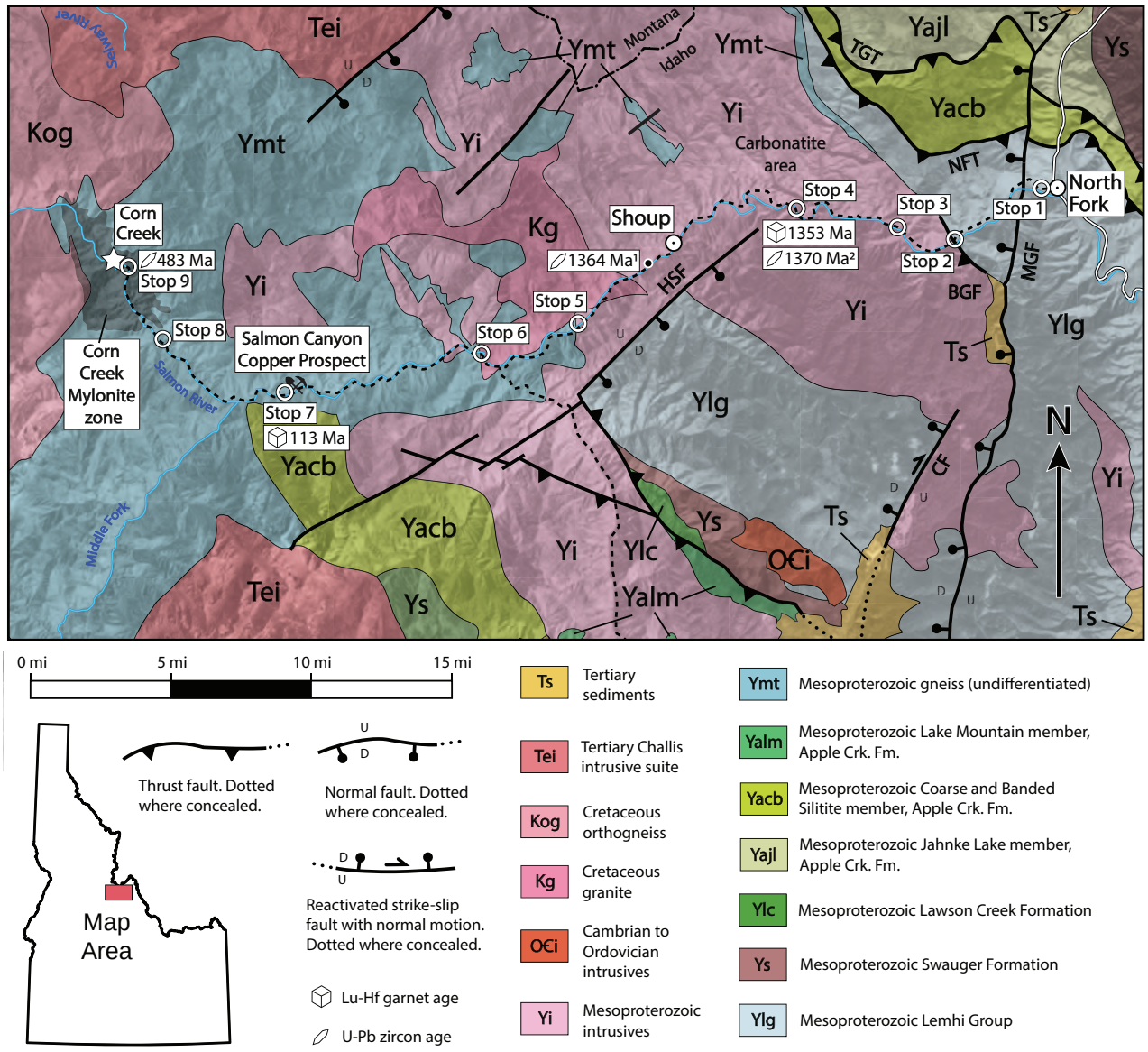

Figure 1. Geologic map showing field trip stops along the transect from North Fork west to Corn Creek. Geology modified from Schmidt and others (1994) and Burmester and others (this volume, Lemhi subbasin stratigraphy and structure: An update). Ages by [1]Evans and Zartman (1990) and [2]Doughty and Chamberlain (1996).

paragneisses, schists, and migmatites (Ymt) intercalated with orthogneiss and augen gneiss. Within this geologic setting, exhalative metal sulfide mineralization occurs in localized clusters throughout the region. Protoliths of the Lemhi Group and the Apple Creek Formation have been identified within the metasedimentary rocks (Yacb), but the contact between the two has not been identified. Near Corn Creek, hypabyssal intrusions and Eocene deformation are prevalent. Affected rocks also include a newly dated Ordovician orthogneiss. The goal of this trip is to see these rocks in the context of new and recently published ages that others have written about from reconnaissance mapping.

GEOLOGIC BACKGROUND

The Mesoproterozoic Belt–Purcell Basin is of interest for its varied and rich mineral deposits (Lydon, 2007) and evolution of Laurentia. Detrital zircons from western facies include ages not known from Laurentia (the North American magmatic gap, or NAMG), suggesting that their sources are included in parts rifted away in the Neoproterozoic. Mesoproterozoic strata around Salmon in the Lemhi subbasin have long been correlated and miscorrelated with those of the main Belt Basin, with direct connections severed by intrusion of the Bitterroot lobe of the Idaho Batholith and faults. Current thinking is that the subbasin is age-equivalent only to the youngest of the main Belt Basin (see Lonn and others, this volume, The Mesoproterozoic Belt–Lemhi connection, western Montana and east-central Idaho). West of Salmon, Lemhi subbasin strata have intrusive contacts with 1380–1370 Ma granites that are unknown in the main Belt Basin but are known near Elk City and toward Moscow. West of North Fork the Salmon River cuts through the Mesoproterozoic igneous complex and its host rocks south of the Bitterroot lobe.

ROAD LOG

The trip starts at the Sacajawea Interpretive, Cultural and Educational Center parking lot exit on E. Main St. (Hwy 28) in Salmon. Turn right (NW) and go through Salmon on US Highway 93 about 23 mi to North Fork. This field guide starts at North Fork and follows the same route west down the Salmon River Road as a similar trip for Belt Symposium V (Schmidt and others, 2013). Some stops repeat those from that trip, but most are new. Field trip stops are referenced to mileage from North Fork and GPS coordinates (WGS84).

STOP 1—0.4 mi
LEMHI GROUP

(45.4066°N, 114.0053°W)

Park at pullout on south side of the road, walk back east to first roadcut. If there is insufficient parking, go another 0.1 mi to a wider spot. Here we will look at Lemhi Group metasedimentary rocks (fig. 2). Notice the intricate laminations, grading from light quartzite bases to dark siltite and argillite tops. Are these rocks upright? Imagine what they would look like when more metamorphosed. These have been mapped as Apple Creek Formation (Evans and Green, 2003), and Yellowjacket Formation by Winston and others (1999) continuing from similar rocks mapped in the Beaverhead Mountains by Ruppel and others (1993). In Ruppel's (1975) stratigraphy, the Apple Creek was below the Swauger Formation, so we all agree that these are Lemhi Group.

1.0 mi Donnelly Gulch. The Monument Gulch fault (fig. 1, MGF) mapped on the Ulysses Mountain quadrangle (Lewis and others, 2019) crosses here. Lemhi Group rocks west of it are typically thicker bedded than at Stop 1 and have moderate dips to the southwest. You may notice trees and brush on either side of the road as far as Panther Creek that burned during the human-caused 2022 Moose Creek fire.

STOP 2—4.7 mi
BIMODAL IGNEOUS COMPLEX

(45.3801°N, 114.0698°W)

Park at the river access point on the left side of the road. Zircons from a diabase dike about 0.5 km (0.3 mi) farther west (fig. 3) yielded an upper intercept age of 1379 ± 1 (Doughty and Chamberlain, 1996) and from the granite a Concordia age of 1383 ± 4 Ma (Aleinikoff and others, 2012). The similarity of these ages and of mafic inclusions within the granitic to mafic dikes nearby (Evans and Zartman, 1990) suggest a genetic relationship. The mafic complex appears concentrated near the northeast side of the complex (Spence, 1984), giving the impression of a crude igneous stratigraphy. Look at some of the rock blocks here,

Figure 2. Outcrop at Stop 1 of Lemhi Group (mi 0.4). Lighter parts are intricately crossbedded quartzite; darker horizons have more siltite and argillite with biotite, commonly as graded tops to beds.

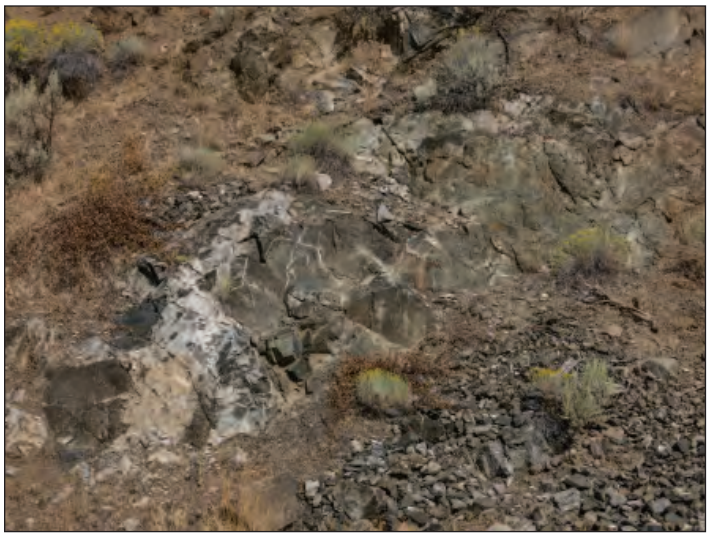

Figure 3. Diabase of Mesoproterozoic mafic complex west of Stop 2 dated near here at 1379 ± 1 Ma (Doughty and Chamberlain, 1996).

and carefully cross the road to see more.

This is the Brushy Gulch fault Stop 3 of Lund and others (2003). Above here and across the river well-developed mylonite locally separates mylonitized granite (fig. 4) from Lemhi Group, which may be part of the reason this was thought to be a regional fault. However, the mine workings to the north are near an intrusive contact, which is easier to access on the ridge above (Lonn and others, this volume, Brushy Gulch fault, east-central Idaho, revisited: Fault or fiction). Therefore, this mylonite zone, named the Dump Creek fault, and other faults that separate Lemhi Group from the igneous complex, may reflect deformation concentrated where rheology of the rocks contrast and are not a major tectonic boundary.

5.7 mi Moose Creek on the left.

Figure 4. Mylonitic Mesoproterozoic granite south of the Salmon River near the lower part of Dump Creek. White augen 2–3 cm across were potassium feldspar megacrysts. Sharp contact of such rock with Lemhi Group quartzite is the Dump Creek fault.

STOP 3—7.4 mi
UNDEFORMED MEGACRYSTIC GRANITE

(45.3881°N, 114.1141°W)

The pullout on the left allows access to Mesoproterozoic granite without penetrative deformation but minor mylonite and shears. Contrast this with the Mesoproterozoic augen gneiss that we'll see later.

7.9 mi Sage Creek Road on the right with access to the North Fork and Trail Gulch thrust faults (fig. 1) in the Ulysses Mountain quadrangle.

10.3 mi Indianola Ranger Station and Indian Creek Road (dead ends).

STOP 4—11.6 mi
MIGMATITE WITHIN AUGEN GNEISS

(45.3958°N, 114.1850°W)

Where the road heads due north after two right-hand bends, look for wide spots on the left, pull off, and stop across from Sawlog Gulch. This is a small septum of tightly folded migmatitic sillimanite–garnet–biotite quartzite (fig. 5) within the augen gneiss. Sillimanite grows with garnet and is randomly oriented on foliation planes. Relict skeletal kyanite porphyroblasts have been observed in samples from here. This was Stop 5 of Lund and others (2003) and Stop 3 of Schmidt and others (2013). Doughty and Chamberlain (1996) obtained a U/Pb age of 1370 Ma ± 1 Ma from zircons in a leucosome within the migmatite, and GASP peak temperature and pressure estimates of 680–690˚C and 6.5 kilobars from the metamorphic assemblage. Garnets sampled here in 2021 yielded a Lu/Hf age of 1353 Ma

Figure 5. Migmatite at Stop 4 (mi. 11.6). Black dot on left side is a borehole about 3 cm in diameter. Zircons from the leucosome material were dated at 1370 Ma (Doughty and Chamberlain, 1996). Garnets were recently dated at 1353 Ma (Murphy and others, this volume).

± 4 Ma (Murphy and others, this volume), which might date peak metamorphism. Note that figure 1 shows the Hot Springs fault ending south of the river east of here. Does the apparent high grade of the rocks here in contrast to low grade before Sage Creek indicate that we are on that fault's footwall?

13.5 mi On the right and up the hill about 600 ft is the Roberts REE property, the southwestern most occurrence in the Sheep Creek–Mineral Hill mineral belt. The belt hosts thin REE-bearing carbonatite horizons and carbonate-hosted Nb-bearing rutile deposits of unknown age and origin. The Idaho Geological Survey is conducting new geologic mapping and geochemical sampling in two quadrangles within the belt, funded by the U.S. Geological Survey Earth–MRI program.

14.4 mi Schistose gneiss with alternating mica-poor and mica-rich centimeter-scale layers, possibly relict siltite and argillite couplets? Garnets are present here too (fig. 6).

15.1 mi Very pink, little deformed, megacrystic granite. Pink color may be the result of replacement of potassium feldspar with hematite-bearing sodic feldspar (albite).

17.1 mi Augen gneiss or just deformed megacrystic granite? Consider the contorted aplite and pegmatite dikes: original shape or deformed along with the granite host?

18.1 mi This is still augen gneiss but has an L-S fabric with lineation plunging to the southwest. The old town of Shoup is just ahead.

18.7 mi This is the Shoup Cemetery granitic augen gneiss dated as 1362 ± 8 (Aleinikoff and others, 2012).

Figure 6. Schistose gneiss with alternating mica-poor and mica-rich centimeter-scale layers northeast of Shoup (mile 14.4).

Continue west and cross the bridge at Pine Creek, then cross the contact from augen gneiss to Cretaceous granodiorite and dark, micaceous metasediments (biotite quartzite). An optional side trip is to look at the Hot Springs fault. The augen gneiss here continues about 1.7 mi southeast up Pine Creek to where the fault juxtaposes it against much less deformed quartzite, siltite and argillite of the Lemhi Group.

STOP 5—22.6 mi
AUGEN GNEISS

(45.3377°N, 114.3422°W)

Excellent exposure of augen gneiss on the south side of the road (fig. 7). Look for evidence of brittle versus plastic strain. South of here, Hillesland (1982) observed that potassium feldspar "crystals" appeared to be broken phenocrysts rather than true augen. Are there any kinematic indicators?

23.6 mi Muscovite–biotite quartzite just east of pictograph site. Protolith likely siltite and argillite couplets.

26.5 mi Panther Creek and Duncan's outpost just over a marathon from North Fork. Road clips Cretaceous biotite granodiorite not far ahead.

Figure 7. Mesoproterozoic augen gneiss at Stop 5.

STOP 6—27.3 mi
CRETACEOUS(?) GRANODIORITE AND BIOTITE QUARTZITE

(45.3225°N, 114.4166°W)

This is Stop 5 of Schmidt and others (2013) at a contact between the granodiorite we've been in and host rocks. Park near Cove Creek bridge and walk upstream to granodiorite, downstream to quartzite. Age of this intrusive is uncertain but suspected to be Cretaceous based on lithologic similarity to some phases of the Idaho Batholith. Note that fabric in granodiorite parallels that developed in quartzite. Road crosses river for the last time.

29.2 mi Fairly shallow foliation in biotite quartzite with suggestion by folded pegmatites of top to the east shear (fig. 8), but are these sheath folds from north-south elongation instead?

31.4 mi Ram's Head Cafe and Lodge.

33.6 mi Chinook Drive population concentration and Colson Creek.

STOP 7—35.7 mi
SALMON CANYON COPPER PROSPECT

(45.3002°N, 114.5581°W)

Park on south side of road and walk back east to dirt road on north side. Alternatively, park on north side of the road 0.45 mi east from this stop. Stop 6 of Schmidt and others (2013). The rocks are recrystallized siltite and argillite with platy parting on biotite-rich surfaces. Note the biotite-rich zones that contain garnet (fig. 9). These garnets have been dated at 112.7 ± 7.7 Ma

Figure 8. View north of north-plunging folds of pegmatites in biotite gneiss (mi. 29.2). Lowest pegmatite is 1–2 cm thick. Do folds support top-to-the-east shear, or are they sheath folds from north–south extrusion?

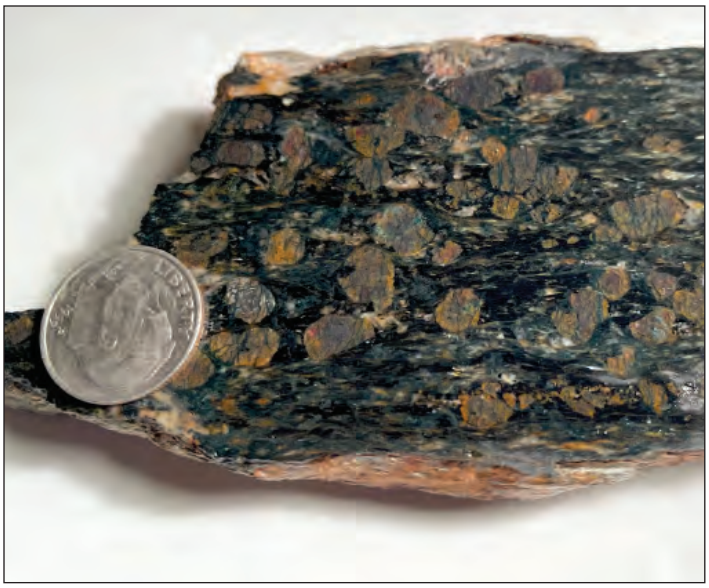

Figure 9. Hand sample of garnet–biotite schist from the Salmon Canyon copper prospect. Garnet-rich samples from the prospect commonly contain interstitial metal-sulfides. Garnets are rimmed by chlorite, indicating late-stage disequilibria with biotite.

(Zirakparvar and others, 2007; Murphy and others, this volume). Electron backscatter image of a mineralized sample from the dump shows chalcopyrite as well as bismuthinite (fig. 10). The association with copper and cobalt mineralization with Apple Creek Formation in the Blackbird district and in the Ulysses Mountain quadrangle (Lewis and others, 2019) and proximity to Apple Creek mapped to the south (Yacb, fig. 1) indicates that we passed from the Lemhi Group to the Apple Creek somewhere, perhaps between stops 4 and 5?

The historic Salmon Canyon Copper mine produced several hundred tonnes of copper–cobalt ore between

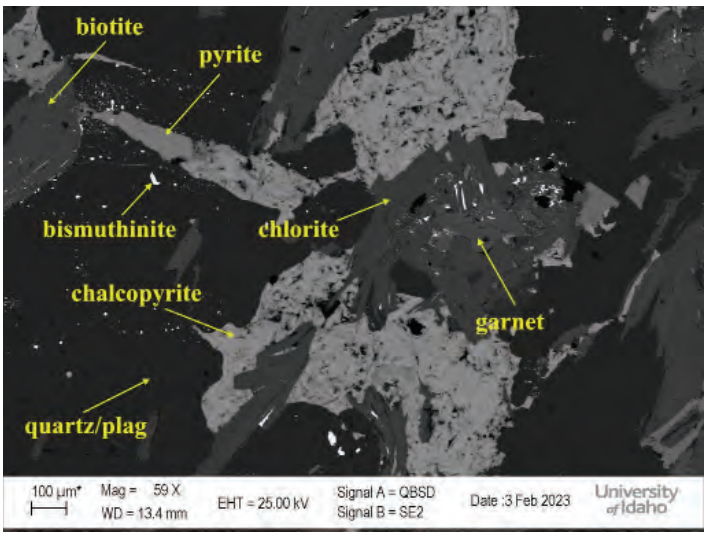

Figure 10. Backscatter image of mineralized sample from Salmon Canyon copper mine. Sample contains significant amounts of chalcopyrite and minor bismuthinite. Pyrite and chalcopyrite display infilling textures between metamorphic minerals in contrast with bismuthinite, which appears to be less mobile.

1964 and 1979 from 3,000 ft of underground development (Johnson and others, 1998). In late 2017, New World Cobalt Ltd. acquired a 100% interest in the property (New World Cobalt, 2019). Their 2018 efforts included drilling 12 holes to test for the immediate extensions of the deposit, soil sampling, and ground geophysics (IP) surveying. Drilling intersected cobalt and copper sulfides and validated that IP anomalies were associated with cobalt–copper mineralization. The property was subsequently included in the Colson cobalt–copper project of Koba Resources Ltd., who reported maximum values from underground sampling of 0.59% Co, 5.33% Cu, and 2.24 g/t Au over a width of 2.5 m (Koba Resources, 2022).

37.4 mi Steeply dipping layered biotite quartzite at 45.2969 N, 114.5870 W (fig. 11). Interpretation of grading from biotite-poor to biotite-rich in layers as relict from siltite and argillite couplets suggest tops to the west here.

37.8 mi Middle Fork Salmon River.

38.1 mi Steeply dipping layered biotite quartzite as east of the Middle Fork, but grading interpreted as relict from siltite and argillite couplets suggest tops to the east here (45.2981 N, 114.5988 W).

38.4 mi New (fall of 2022) foot bridge across the Salmon River. It is on the Corn Creek fault mapped by Schmidt and others (1994).

38.7 mi Isoclinal fold with steep axial surface here helps explain apparent opposite facing of strata on either side of the Middle Fork (45.2998 N, 114.6096 W). Eocene dikes are increasingly common beyond here.

40.7 mi Cache Bar boat ramp and congestion.

Figure 11. Steeply dipping biotite quartzite at mile 37.4 with centimeter- to decimeter-thick layers of quartz and feldspar separated by thinner layers richer in biotite. Layers are likely relict bedding.

STOP 8—41.3 mi
MAFIC DIKE CUTTING MIGMATITE

(45.3266°N, 114.6478°W)

Lamprophyre (variety spessartite) cutting migmatite on northeast side of road (fig. 12A). The dike contains hornblende, biotite, and plagioclase, along with tremolite pseudomorphs after olivine. Age uncertain but given the state of recrystallization (fig. 12B) it is unlikely Tertiary as is a lamprophyre sampled 7 mi east of Riggins, Idaho along the Salmon River that yielded a $^{40}Ar/^{39}Ar$ age of 46.77 Ma (Buddington and others, 2021). More likely its age is similar to either a Cambrian (534 Ma) pyroxene porphyry lamprophyre near Lemhi Pass (Gillerman, 2008; Gillerman and others, 2010) or the Ordovician orthogneiss at Stop 9. Either way, the migmatite would be older yet and possibly the same age as the migmatite at stop 4.

Continue west 3.5 mi.

STOP 9—44.8 mi
MYLONITIC DACITE AND ORDOVICIAN ORTHOGNEISS

(45.3659°N, 114.6752°W)

Roadcuts here contain mylonitized Eocene dacites intercalated with Ordovician orthogneiss (fig. 13). In thin section, gneiss shows subgrain development (fig. 14), presumably related to the mylonitic event. (Stop 7 of Schmidt and others, 2013).

Orthogneiss sampled here yielded a U/Pb age of 483 Ma ± 7 Ma (fig. 15). This age is similar to the ages of syenites and theralites that occur throughout the region. One zircon rim gave a Late Cretaceous age of 88.9 Ma and likely records metamorphism, which is consistent with its low Th/U of 0.005 (compared to an average Th/U of 0.4 for the Ordovician age components). $^{87}Sr/^{86}Sr$ at 483 Ma was 0.70914 (Vincent Isakson, written commun., 2017) and the average zircon εHf(i) isotope composition, determined by LA-MC-ICP-MS at Washington State University is -8.5. Both parameters are indicative of significant crustal contamination in the production of the orthogneiss magma. Eocene dacite dikes at this stop are locally mylonitic as well as undeformed (fig. 16).

Proceed west for approximately 1 mi and turn around at Corn Creek Campground.

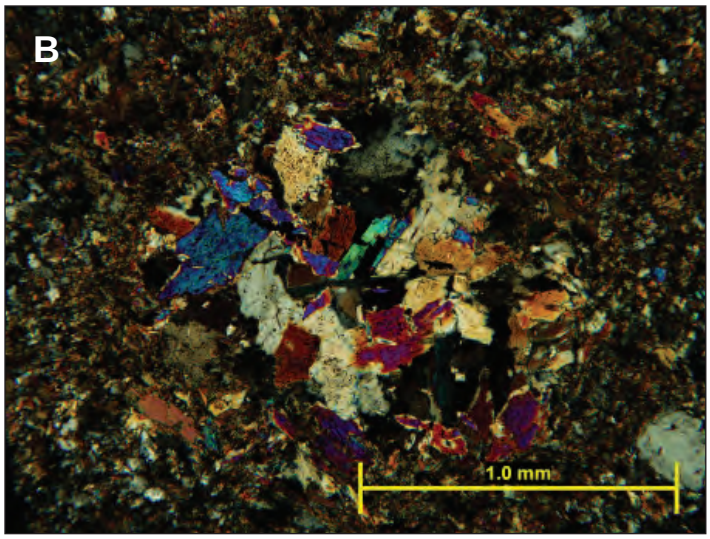

Figure 12. Mafic dike (likely lamprophyre) cutting migmatite at Stop 8 (A, outcrop; B, photomicrograph). The mafic dike contains fine amphibole, plagioclase, and biotite matrix, with round clusters of tremolite.

Figure 13. Outcrop of Ordovician orthogneiss at Stop 9. View looking north of centimeter-scale mylonitic layering. Superficially similar to the Mesoproterozoic augen gneiss seen upriver to the east, but this rock has less quartz and has been dated as Ordovician (fig. 15).

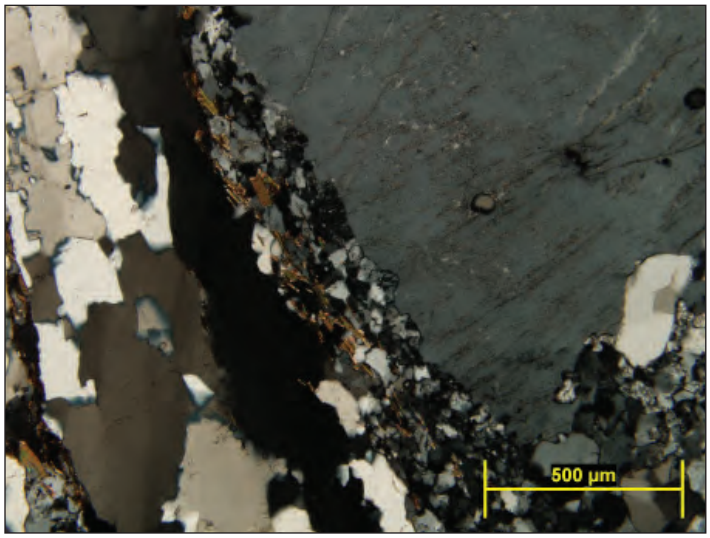

Figure 14. Photomicrograph of Ordovician orthogneiss showing subgrain development of K-spar, and grain boundary migration of quartz.

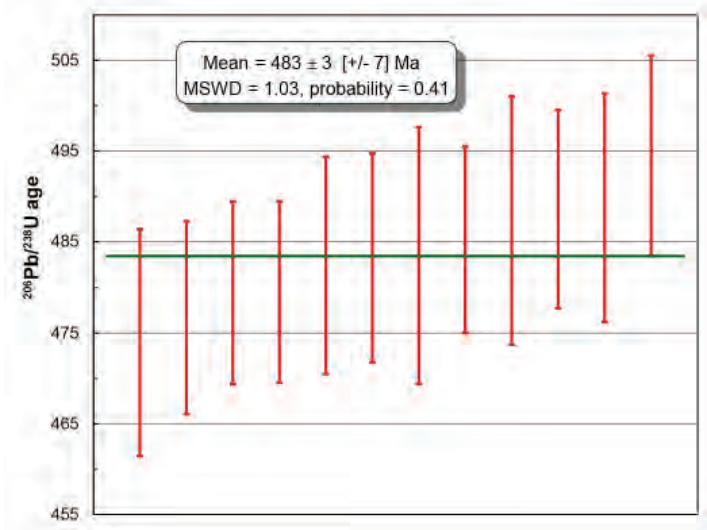

Figure 15. Weighted average U-Pb age plot for Ordovician orthogneiss. Error bars represent the internal 2 standard error uncertainty. The total uncertainty incorporating reproducibility of the primary standard is given in brackets. Zircons were dated by LA-ICP-MS at Washington State University. In addition to the Ordovician population shown here, a single zircon rim yielded a likely metamorphic age of 88.9 Ma.

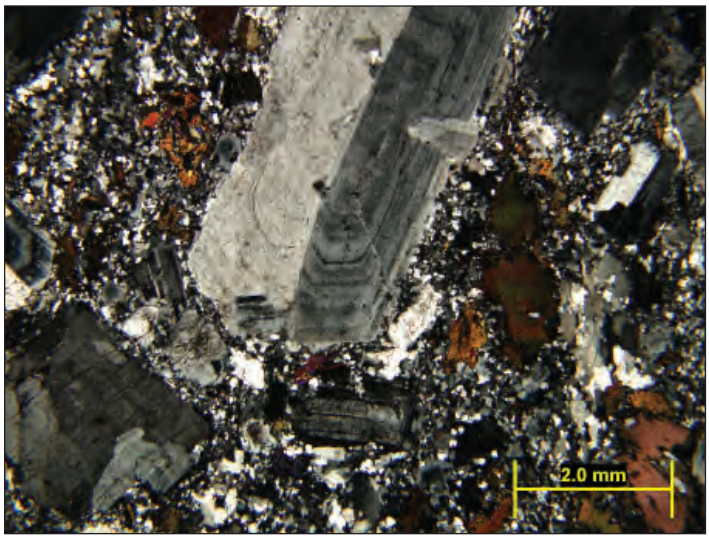

Figure 16. Photomicrograph of an undeformed dacite dike at Stop 9.

ACKNOWLEDGMENTS

Russ Di Fiori kindly provided a review.

REFERENCES

Aleinikoff, J.N., Slack, J.F., Lund, K., Evans, K.V., Fanning, C.M., Mazdab, F.K., and Pillers, R.M., 2012, Constraints on the timing of Co-Cu±Au mineralization in the Blackbird district, Idaho, using SHRIMP U-Pb ages of monazite and xenotime plus zircon ages of related Mesoproterozoic orthogneisses and metasedimentary rocks: Economic Geology, v. 107, no. 6, p. 1143–1175.

Buddington, A.M., Steven, C.J., Tikoff, B., and Gaschnig, R.M., 2021, Lamprophyre dikes of northern Idaho and northeastern Washington: Idaho Geological Survey Technical Report 21-01, 17 p.

Burmester, R.F, Lewis, R.S., Lonn, J.D., and McFaddan, M.D., this volume, Lemhi subbasin stratigraphy and structure: An update.

Doughty, P.T., and Chamberlain, K.R., 1996, Salmon River arch revisited: New evidence for 1370 Ma rifting near the end of deposition in the Middle Proterozoic Belt basin: Canadian Journal of Earth Sciences, v. 33, p. 1037–1052.

Evans, K.V., and Green, G.N., 2003, Geologic map of the Salmon National Forest and vicinity, east-central Idaho: U.S. Geological Survey Geologic Investigations Series Map I-2765, 19 p., scale 1:100,000.

Evans, K.V., and Zartman, R.E., 1990, U-Th-Pb and Rb-Sr geochronology of Middle Proterozoic granite and augen gneiss, Salmon River Mountains, east-central Idaho: Geological Society of America Bulletin, v. 102, p. 63–73.

Gillerman, V.S., 2008, Geochronology of iron oxide-copper-thorium-REE mineralization in Proterozoic rocks at Lemhi Pass, Idaho, and a comparison to copper-cobalt ores, Blackbird mining district, Idaho: Final technical report to U.S. Geological Survey.

Gillerman, V.S., Schmitz, M.D., Jercinovic, M.J., and Reed, R., 2010, Cambrian and Mississippian magmatism associated with neodymium-enriched rare earth and thorium mineralization, Lemhi Pass district, Idaho: Geological Society of America Abstracts with Programs, v. 42, no. 5, p. 334.

Hillesland, L.L, 1982, The geology, mineralization, and geochemistry of the Pine Creek area, Lemhi County, Idaho: Corvallis, Ore., Oregon State University, M.S. thesis, 97 p.

Johnson, R., Close, T., and McHugh, E., 1998, Mineral resource appraisal of the Salmon National Forest, Idaho: U.S. Geological Survey Open-File Report 98-478, 277 p.

Koba Resources, 2022, Colson Project. Available at: https://kobaresources.com/projects/united-states/colson-project/ [Accessed 3 May 2023].

Lewis, R.S., Burmester, R.F., and Lonn, J.D., 2019, Geologic map of the Ulysses Mountain quadrangle, Lemhi County, Idaho: Idaho Geologic Survey Digital Web Map 188, scale 1:24,000.

Lonn, J.D., Burmester, R.F., and Lewis, R.S., this volume, The Mesoproterozoic Belt-Lemhi connection, western Montana and east-central Idaho.

Lund, K., Evans, K.V., Doughty, P.T., Chamberlain, K.R., Link, P.K. and Winston, D., 2003, Geology of the Brushy Gulch fault and its hanging wall and footwall rocks: Northwest Geology, v. 32, p. 74–82.

Lydon, J.W., 2007, Geology and metallogeny of the Belt-Purcell Basin, *in* Goodfellow, W.D., ed., Mineral deposits of Canada: A synthesis of major deposit types, district metallogeny, the evolution of geological provinces, and exploration methods: Geological Association of Canada, Mineral Deposits Division, Special Publication 5, p. 581–607.

Murphy, J.P., Lewis, R.S., Vervoort, J.D., and Hämmerli, J., this volume, Multiple periods of metamorphism in the Salmon River Mountains, Idaho as deduced from garnet Lu-Hf ages.

New World Cobalt, 2019, Annual Report, 30 June 2019, available at: https://www.asx.com.au/asxpdf/20190930/pdf/4491xlnnjdqw43.pdf [Accessed 3 May 2023].

Ruppel, E.T., 1975, Precambrian Y sedimentary rocks in east-central Idaho: U.S. Geological Survey Professional Paper 889-A, 23 p.

Ruppel, E.T., O'Neill, J.M., and Lopez, D.A., 1993, Geologic map of the Dillon 1° x 2° quadrangle, Idaho and Montana: U.S. Geological Survey Miscellaneous Investigations Series Map I-1083-H, scale 1:250,000.

Schmidt, K.L., Lewis, R.S., Burmester, R.F., and Lang, R.A., 1994, Reconnaissance geologic map of the Shoup and Horse Creek Area, Lemhi and Idaho Counties, Idaho: Idaho Geological Survey Technical Report 94-3, scale 1:50,000.

Schmidt, K.L., Lewis, R.S., and Burmester, R.F., 2013, Into the River of No Return corridor: Mesoproterozoic rock along the Salmon River from North Fork to Corn Creek, east-central Idaho: Northwest Geology, v. 42, p. 215–228.

Spence, J.G., 1984, Geology of the Mineral Hill interlayered amphibolite-augen gneiss complex, Lemhi County, Idaho: Moscow, Idaho, University of Idaho, M.S. thesis, 170 p.

Winston, D., Link, P.K., and Hathaway, N., 1999, The Yellowjacket is not the Prichard and other heresies–Belt Supergroup correlations, structure, and paleogeography, east-central Idaho, *in* Hughes, S.S., and Thackray, G.D., eds., Guidebook to the geology of eastern Idaho: Pocatello, Idaho, Idaho Museum of Natural History, p. 3–20.

Zirakparvar, N.A., Bookstrom, A.A., and Vervoort, J.D., 2007, Cretaceous garnet growth in the Idaho cobalt belt: Evidence from Lu-Hf geochronology: Geological Society of America Abstracts with Programs, v. 39, no. 6, p. 413.

FIELD GUIDE TO THE POPE-SHENON MINE, LEMHI COUNTY, IDAHO

Skip Yates

Consulting Geologist, Lolo, Montana
Mine Owner, Neuma International Inc.

INTRODUCTION

The Pope–Shenon mine is developed along several east–west-trending, northward-dipping veins in brecciated shear zones in Mesoproterozoic Gunsight Formation quartzites. The mineralization occurs as quartz–sulfide and sulfide veinlets and veins up to 10 ft in width. The primary copper minerals include chalcopyrite, pyrite, and delafossite, with lesser amounts of bornite, chalcocite, specular hematite, galena, and sphalerite. Secondary copper minerals are malachite, azurite, cuprite, chrysocolla, brochantite, and libethenite. Wall rocks are highly fractured to brecciated, and are moderately to highly altered, showing green biotite, bleaching, sericite, chlorite, silicification, and argillization, along with ubiquitous iron oxides, and hematite-limonite veining in fracture and breccia zones.

The Pope–Shenon mine is in the Eureka Mining district at the northern end of Lemhi Range in Lemhi County, Idaho. The mine is approximately 7 mi south of the town of Salmon, Idaho and is accessible via the Hot Springs Road to the Pope–Shenon Road (fig. 1).

HISTORY

Most of the mining history relies heavily on the "History of the Pope–Shenon Mine, Lemhi County, Idaho"

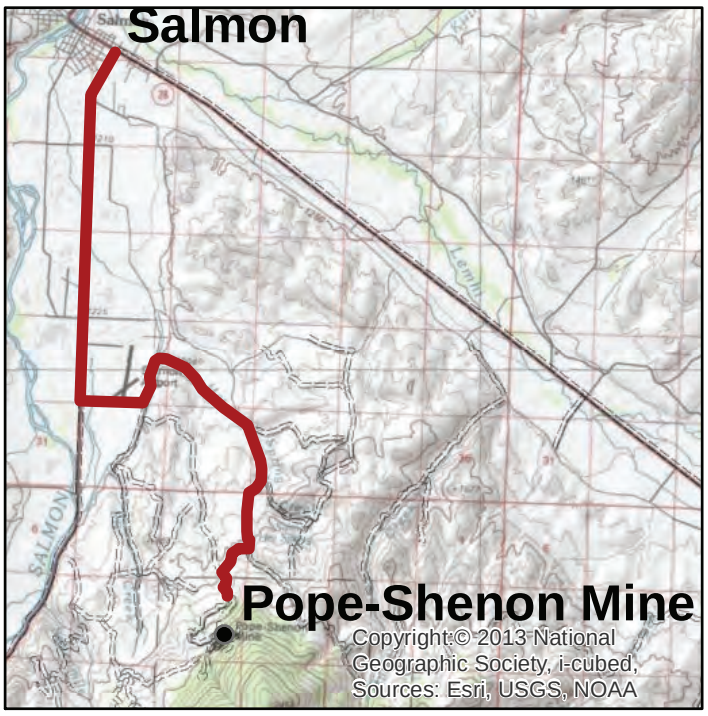

Figure 1. Location of the Pope–Shenon Mine near Salmon, Idaho.

(Mitchell, 1997). The mine area was first staked for gold in the early 1890s by two prospectors, Lige Stroud and James Fennin. In the mid-1890s the first copper claims were located by a group including Thomas Pope at the future site of the Pope–Shenon Mine. Philip Shenon acquired a 2/3 interest in the property sometime before mining commenced in 1908. The mine produced minor shipments of mostly hand-sorted ore from a succession of owners and lessees until 1921, when a 50 ton-per-day leach mill was constructed for the secondary copper ore. The leach mill proved unsuccessful and was converted into a gravity mill in 1922.

The mine was developed by six tunnels spaced approximately at 100-ft levels. The mine and mill were expanded throughout the 1920s, and by 1923 the Pope–Shenon mine was the fourth largest copper producer in Idaho, later culminating in the second largest Idaho copper producer in 1928, and was the largest copper producer by 1929. Mining operations slowed dramatically during the Great Depression, then picked up once again during World War II and the Korean War. The mine experienced sporadic development and production through the late 1970s, especially by Grandview Metals, who developed the 800-level tunnel and drilled several underground holes.

Three Pope–Shenon Mine veins (North Pope–Shenon, South Pope–Shenon and Taft veins) were primarily mined on six levels: from the top down, the 300, 400, 500, Intermediate, 600 and 800 Level tunnels (figs. 2, 3). The ore was mostly secondary copper in the upper levels, while sulfide ores dominated in the 600 and 800 tunnels. In all, over 4.5 million lbs of copper, 24,700 oz of Ag, 500 oz of Au, 22,000 lbs of Pb, and 15,000 lbs of Zn were produced from the mine between 1908 and 1990. Recorded production in 1970 saw a shipment of 882 tons averaging 2.37% Cu and 0.57 opt Ag with minor Au. Historical reserves in 1953 totaled 65,000 tons at 2.37% Cu and 0.57 opt Ag (unpub. report, Centrida Mining, 1954). Western Uranium Corp., in their 1962 OME loan application, stated "In summary, probable and possible reserves above the 600 level are in the order of at least several tens of thousands of tons. Similar reserves between the 600 level and the proposed [800] level are 50,000 to 100,000 tons. All of this ore is estimated to average about 2.5% Cu. These figures do not take in account the possible very large reserves below the proposed [800] level."

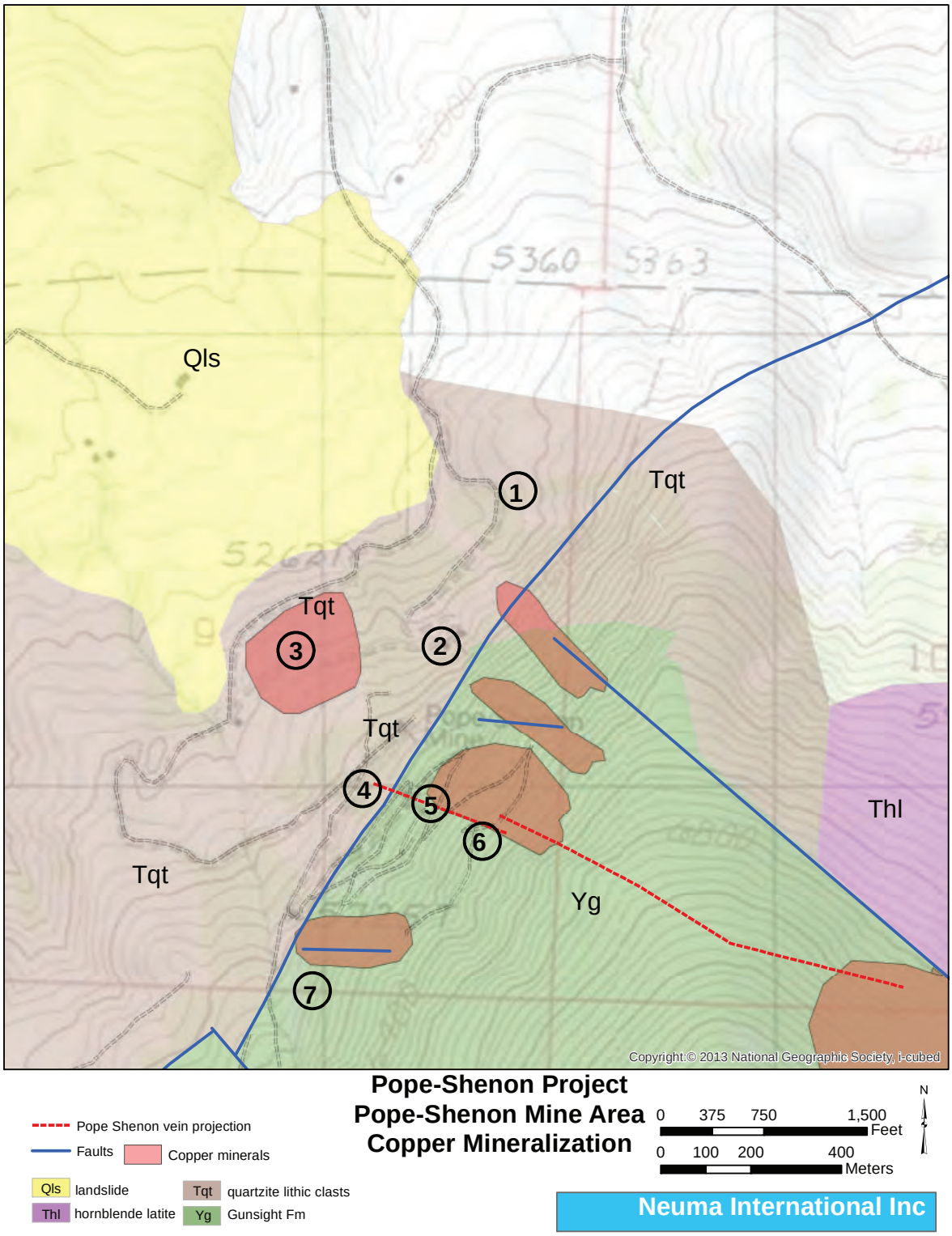

Figure 2. Pope–Shenon mine levels and vein surface projections. Geologic basemap modified from Lewis and others, 2014.

GEOLOGICAL SETTING

The Pope–Shenon Mine is located on the western slope at the northern end of the Lemhi Range. The core of the mountain range is composed of Mesoproterozoic metasedimentary rocks, while the surrounding foothills are composed of younger Eocene (46 to 50 my) Challis volcanic rocks. The Mesoproterozoic clastic rocks are Gunsight Formation, which is part of the Lemhi Group of the Belt Supergroup.

The Gunsight Formation is a thick (>5000 ft) sequence of clastic metasedimentary rocks composed of fine-grained, feldspar-rich, micaceous quartzites with siltite and argillite. For the most part, these rocks are a dark gray to black, thin-bedded to laminated sequence of fine-grained clastic sediments with scattered coarser-grained channel deposits. Siltites and argillites are typically darker with well-developed foliation. Common mud cracks, ripple marks, and cross lamination indicate their shallow water origin. The rocks are

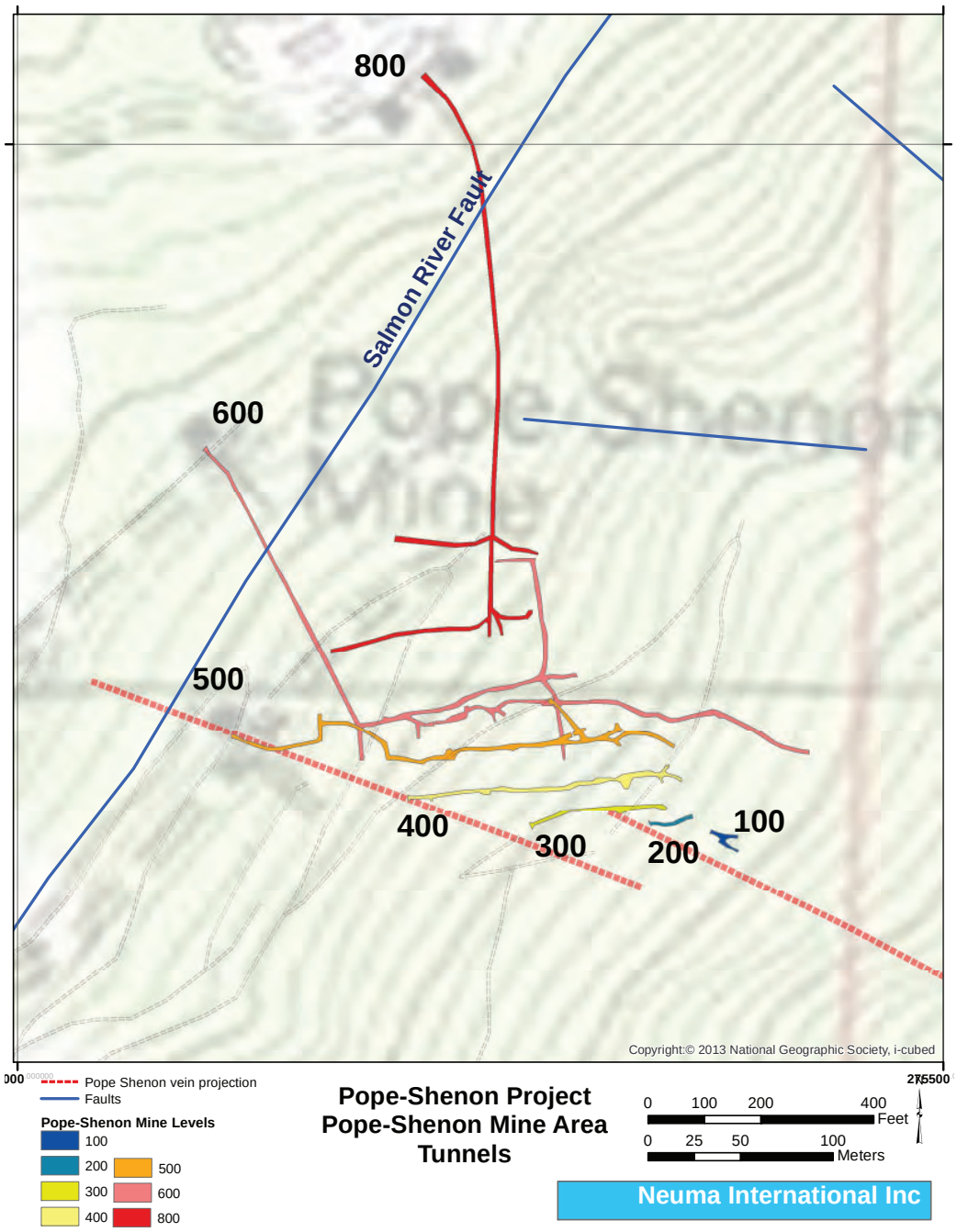

Figure 3. Copper mineralization noted at the surface and field trip stops.

extensively foliated and fractured, making bedding surfaces difficult to recognize (Burmester and others, 2016).

The quartzites/siltites are a green-gray to dark green-gray color in the vicinity of the Pope–Shenon mine. This green color is probably due to alteration of biotite. Where hydrothermally altered, the Gunsight generally is bleached, with visible sericite and chlorite, along with iron oxides in fractures and as matrix in brecciated rock.

Challis volcanic rocks intrude, overlap, and are in fault contact with the older Gunsight Fm Near the Pope–Shenon Mine; the volcanics are felsic and commonly contain phenocrysts of quartz, feldspar, hornblende, and biotite in an aphanitic groundmass. Two subtypes are most notable in the area of the mine:

Tqt—Rhyolite containing abundant angular to sub-rounded, dark gray to black quartzite lithic fragments. Abundant quartz phenocrysts are euhedral to rounded (quartz eyes), and the unit also contains phenocrysts of alkali feldspar and plagioclase. Mafic minerals are rare. Almost always altered to some degree, making identification difficult from Thl. Near the Gunsight contact lithic clasts are more common.

Thl—Hornblende quartz latite. Contains few to no lithic clasts of dark quartzite. Abundant hornblende and biotite phenocrysts, with fewer quartz, alkali feldspar and plagioclase phenocrysts.

MINERALIZATION

Copper, with accessory gold, silver, lead, zinc, and cobalt mineralization, is primarily hosted in brecciated, fractured, intensely altered Gunsight Formation and in surrounding Challis volcanics. This mineralization appears to be structurally controlled by large north–northeast-trending faults (Salmon River fault) and by secondary east–west-trending faults, veins, and wide breccia zones. These east–west zones were likely created by rotation caused by movement on the north–northeast faults. The exposed vertical range of exposed copper mineralization is a minimum of 3,000 ft (900 m) but is probably much greater.

The mineralization is Eocene in age and related to Challis volcanism. Gunsight lithic fragments found in the volcanic rocks are not altered unless the surrounding volcanics are also altered; nor do iron–oxide–quartz veins cut Gunsight lithic fragments unless they also cut the surrounding volcanic rock. Both primary copper sulfides and secondary copper minerals have been observed in Challis volcanic rocks and intrusives, particularly at the Pope–Shenon Mine. Intense alteration, including acid leaching, argillization, silicification, and chalcedony veins can be found in Challis rocks surrounding the Gunsight as well as along structures over a mile away from the Gunsight–Challis contacts. Most conclusively, Challis volcanic diatremes and breccia pipes, some copper bearing, intrude into and alter Gunsight metasediments.

Chalcopyrite and delafossite ($CuFeO_2$) are primary copper minerals at the mine. The veins also contain lesser amounts of bornite, pyrite, magnetite, specular hematite, galena, and sphalerite. Gangue minerals include quartz, hematite, barite, sericite, biotite, epidote, and chlorite (Anderson. 1956). More recent underground sampling shows the veins average 4 to 5% copper and can range up to 20% copper. Mined ore averaged around 1.0 opt Ag, and 0.01 opt Au. The copper veins are structurally controlled in east–west-trending shear zones largely constrained by foliation in the Gunsight Fm. At least three mineralized shear zones have been identified; the overall shear zone has a width approaching 200 ft. Grades and widths appear to be determined by intersecting shear zones and splits. Sulfide veinlets show little to no alteration selvages, suggesting there may be little difference of temperature or chemistry between the ore-bearing fluids and wall rocks.

Lower grade copper is exposed at the surface for up to 2,500 ft surrounding the Pope–Shenon mine. Secondary copper minerals can be found along fractures and in breccia zones (Stop 7). Quartz-copper vein material, likely related to the Salmon River fault, is also noted at Stop 3. This wider copper zone suggests that a low-grade, bulk-tonnage deposit, with possible secondary enhancement at depth, may exist surrounding the Pope–Shenon.

ROAD LOG

From the stoplight in Salmon, drive south on US Hwy 93 towards Challis. At approximately 4 mi, turn left onto Airport Road. Go past the airport to the stop sign and turn left. Stay on the paved road for 1.8 mi, then turn right onto Hot Spring road, which is graveled. Stay on the main graveled road for 2.3 mi, to where the road splits into the upper and lower Pope–Shenon Roads (may show as Road 004 on map software).

STOP 1

On the upper Pope–Shenon Road. Exposures of altered Challis volcanic rocks and altered Gunsight Formation. Challis rocks are mostly Tqt, with dark lithic fragments of Gunsight. Gunsight rocks are highly fractured with iron–oxide veinlets, are bleached, and may be sericitic or chloritic.

STOP 2

800 level of the Pope–Shenon mine. The 800-level tunnel was developed as a long crosscut before intercepting the Taft and Pope–Shenon veins. Take a short walk over the dumps to the portal entrance to see good examples of alteration and mineralization for both Gunsight and Challis rocks. Vein material and copper minerals are scattered across the waste pile.

STOP 3

Lower Pope–Shenon Road. Sagebrush-covered hill with abundant copper–quartz vein material. These veins appear different from the Pope–Shenon veins, which appear to be oriented north–northeast instead of east–west, and may be related to the Salmon River fault. Both primary and secondary copper minerals have been noted in the quartz. The copper here is over 2,500 ft from the Pope–Shenon veins. There is also an intensely bleached and argillized thin volcanic dike(?) that cuts through the section. This is a good spot to see the various levels of the Pope–Shenon mine.

STOP 4

Park here and walk the road to visit various tunnel levels. There is a tight turnaround and we'll need to park the vehicles close together. Walk a short distance north on level ground to the 600-level tunnel. The tunnel entrance often forms an ice sheet in July that slowly melts by the end of summer. There are good specimens of the vein material below the adit, and mineralized Challis volcanic rock can be found on the dump.

STOPS 5 and 6

Hike a bit more than a mile up the road for a spectacular view of the Salmon valley and to visit level 300, level 400 and level 500 workings; all three levels were developed on surface exposures of the vein. It appears that there are two portals at the 500 level, though both are caved in and covered by talus. There is quite a bit of intensely altered Challis rock next to the portals here—bleached white, argillic with cryptocrystalline quartz veins. A few sparse copper spots have been noted in these rocks. There are good blue and green specimens of secondary copper minerals, plus rare cuprite and chalcocite.

The portals at level 300 and level 400 are still open. Please do not enter any open tunnels. There are large overhanging boulders that could drop at any time. Secondary copper minerals are common around these tunnels, including cuprite and chalcocite. These portals will afford the best view of the Pope–Shenon vein.

Note that there is a large area of visible copper minerals around the road between level 400 and level 300. This continues at least 1,000 ft north beyond the Pope–Shenon vein and could signify a lower grade, bulk-tonnage deposit adjacent to the vein.

STOP 7

As we return, this is a short walk up the road along the creek. There is copper mineralization scattered throughout the talus slope. If anyone wants to hike up through the talus to the east–west cliff wall above, there is secondary copper along almost every fracture surface. My hypothesis is that this represents a recent rock fall from the cliff face and the newly exposed copper minerals have not yet had time to oxidize further. There is also quite a bit of primary barite, quartz, and specular hematite in the talus along all of the roads in the mine area.

ACKNOWLEDGMENTS

Neuma International allowed publication of this information and Reed Lewis provided a review.

REFERENCES

Anderson, A.L., 1956, Geology and mineral resources of the Salmon quadrangle, Lemhi County, Idaho: Idaho Bureau of Mines and Geology Pamphlet 106, 105 p.

Burmester R.E., and others, 2016, Stratigraphy of the Lemhi subbasin of the Belt Supergroup, *in* MacLean, J.S., and Sears, J.W., eds., Belt Basin: Window to the Mesoproterozoic Earth: Geological Society of America Special Paper 522, p 121–137.

Lewis, R.S., and others, 2014, Geologic map of the Sal Mountain quadrangle, Lemhi County, Idaho: Idaho Geological Survey Digital Web Map 107, scale 1:24,000.

Mitchell, V.E., 1997, History of the Pope–Shenon mine, Lemhi County, Idaho: Idaho Geological Survey, Staff report 97-15, 20 p.

FIELD TRIP GUIDE TO IRON CREEK, LEMHI COUNTY, IDAHO

Katharina Pfaff,[1] Daniel Schmidt,[1] George King,[2] William Stone,[2] and Thomas Monecke[1]

[1]Center to Advance the Science of Exploration to Reclamation in Mining (CASERM), Department of Geology and Geological Engineering, Colorado School of Mines, Golden, Colorado

[2]Electra Battery Materials Corporation, Toronto, Canada

INTRODUCTION AND GEOLOGIC SETTING

The Idaho Cobalt belt (ICB) is a northwest-trending belt of cobalt ± copper-bearing deposits and prospects in the Salmon River Mountains of east-central Idaho, and is an important domestic cobalt mineral resource (fig. 1A; Landis and Hofstra, 2012). The host rocks of the ICB are part of the Belt–Purcell Supergroup, a Mesoproterozoic meta-sedimentary succession extending across the Idaho–Montana border into southern Canada (Perron and others, 2023).

The Iron Creek deposit is a strata-bound Co-Cu deposit in the southeastern portion of the ICB. Mineralization is hosted within a lower greenschist grade succession of interbedded siltite–argillite with quartzite-rich units of the lacustrine Mesoproterozoic Apple Creek Formation (Ristorcelli and Schlitt, 2019). The banded siltite member is the principal host rock to mineralization and contains abundant quartz, muscovite, biotite, and chlorite, with minor amounts of apatite, plagioclase, and Fe-Mn-oxides. Pyrite, pyrrhotite, chalcopyrite, and magnetite are associated with thin, cross-bedded quartzite layers in the banded siltite member. Cobalt is mainly held in pyrite, and Cu in chalcopyrite.

Current indicated mineral resources at Iron Creek are 4.5 million tonnes grading 0.19% cobalt and 0.73% copper, and inferred mineral resources are 1.2 million tonnes grading 0.08% cobalt and 1.34% copper (Perron and others, 2023). Ongoing research within the Center to Advance the Science of Exploration to Reclamation in Mining (CASERM) is striving to improve our understanding of the geologic framework of the ICB and its cobalt mineral resources in three dimensions and to aid exploration and assessments of (critical) mineral resources. The aim of this study is to better understand the mineralization and alteration mineralogy, geochemistry, and magnetic susceptibility of the subsurface and deposit-forming processes at Iron Creek.

HISTORY

The history of the Iron Creek Property is summarized from the technical report by Ristorcelli and Schlitt (2019). The first mining claims were staked in the Iron Creek area in 1967 on copper-stained material in what later became known as the "No Name" Zone and is now considered to be the upper zone of the broader Iron Creek mineralization. In 1970, these claims were leased to Sachem Prospects Corporation (Sachem) of Salt Lake City, Utah. Sachem completed 11 diamond-core drill holes and excavated three underground exploratory drifts. Hanna Mining optioned the Iron Creek Property in 1972 through its wholly owned subsidiaries, Coastal Mining Co. and Idaho Mining Co., and then acquired it outright in 1973 from Sachem.

From 1979 through 1996, the Property was explored by Noranda Exploration, Inc., Inspiration Mines, Inc., Centurion Gold, and Cominco American Resources, Inc. Various campaigns of drilling, geophysical surveys, and surface and underground geochemical sampling were conducted. Between all these programs, a total of 57 holes were drilled on the property prior to 1996.

Between 1996 and 2016, the patented and unpatented claims were acquired by the Chester Mining Company. Scientific Metals Corp. optioned the Iron Creek patented property from Chester Mining Company in 2016 and staked claims surrounding the Iron Creek patents. Scientific Metals Corp. changed its name to U.S. Cobalt in 2017. U.S. Cobalt conducted exploration drilling in 2017 and 2018 prior to being acquired by First Cobalt in 2018. First Cobalt acquired the patented claims and continued the exploration drilling into 2019. First Cobalt subsequently changed its name to Electra Battery Materials Corporation and completed a drill program in 2021.

ONGOING RESEARCH

Samples for an ongoing study within CASERM and in collaboration with the U.S. Geological Survey and Electra Battery Materials Corporation were collected from two drill holes: one from the Iron Creek Project (IC-17-28) and one from the nearby Ruby Zone (IC-22-02) intercepting high-grade Cu-Co mineralization (fig. 1B; Schmidt and others, 2023). Thirteen additional field samples representing host rock units in the ICB were also collected.

Based on continuous X-ray fluorescence data, the 293-m-long drill hole from the Iron Creek Project intersects the high-grade portions of the Cu-Co-rich mineralized zone between 63 and 87 m and two Co-rich ore zones between 116 and 145 m and 178 and 216 m, respectively. The 374-m-long drill hole from the Ruby Zone intersects

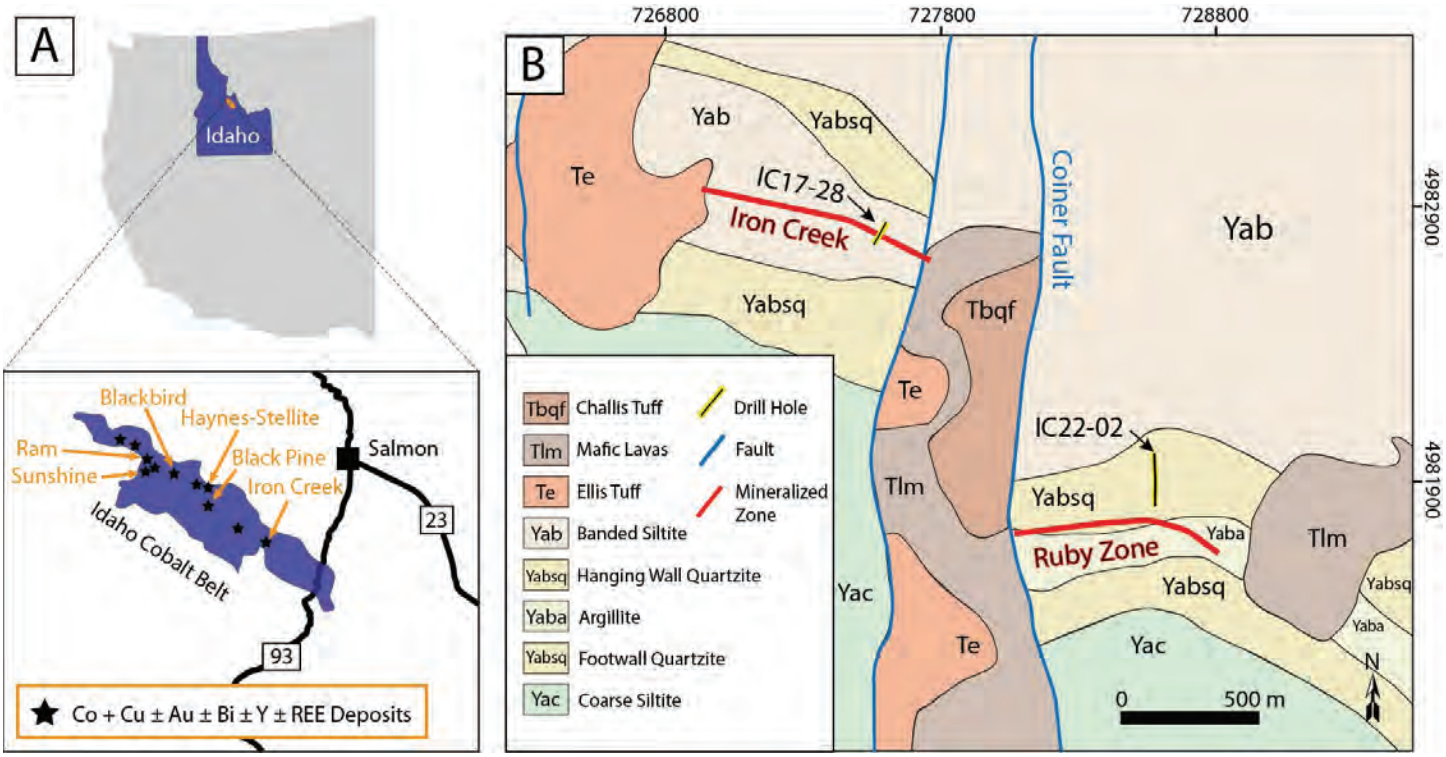

Figure 1. (A) Idaho Cobalt belt and (B) Iron Creek deposit with the Iron Creek Project and the Ruby Zone drill collars indicated (after Schmidt and others, 2023).

two Co-rich mineralized zones between 308 and 313 m and between 364 and 365 m. This dataset also indicates that Co has a strong positive correlation with As and Se, whereas Cu shows positive correlations with Te, Pb, and Zn. A detected Cr and Ni halo around the Co mineralized zones could represent a useful tool for vectoring toward Co mineralization. Short-wave infrared core scanning revealed a significant increase in Fe-rich chlorite-group minerals around mineralized zones, whereas muscovite and illite are predominant in unmineralized host rocks.

Magnetic susceptibility data show a significant property contrast between the host rock above and below the mineralized zones, and the mineralized zones themselves. At Ruby, values acquired on core outside the mineralized zones range from 0.85 x 10^{-3} to 0.002 x 10^{-3} SI, whereas values from the mineralized zones range from 1.37 x 10^{-3} to >2000 x 10^{-3} SI. The magnetic susceptibility data acquired on mineralized intercepts are consistently high across the entire ore zone.

Petrographic observations on high-grade ore samples by Schmidt and others (2023) show a distinct succession of ore and alteration minerals, including five discrete pyrite generations. Early cobaltiferous pyrite predates the main mineralization stage and is ubiquitous in samples from mineralized zones in the Iron Creek Project, whereas early magnetite and lesser pyrite are abundant in samples from mineralized intercepts in the Ruby Zone. Both early pyrite and early magnetite are associated with abundant biotite. Main stage ore minerals are represented by cobaltiferous pyrite with ubiquitous Bi-telluride inclusions, and chalcopyrite with minor cattierite–vaesite accompanying pyrite. Post-mineralization pyrite forms a porous overgrowth on main-stage pyrite. Main-stage alteration consists of Fe-rich chlorite and muscovite. Late-stage, possibly syn-metamorphic silicification and quartz veining is host to cobaltiferous pyrrhotite and minor galena and sphalerite. Subsequent alteration caused pyrrhotite to be replaced by marcasite/pyrite and goethite. Supergene oxidation and weathering of pyrite led to the formation of jarosite, hematite, and other secondary minerals. Cobalt and Ni originally hosted in primary pyrrhotite was liberated during the pyrrhotite breakdown and form discrete cobaltite–vaesite minerals.

At Iron Creek, Co-Cu mineralization is hosted in interlayered siltite, biotite phyllite, and quartzite of the banded siltite member of the Apple Creek Formation. Sediment deposition in the area is bracketed between ~1445 Ma (U-Pb on detrital zircons from the underlying Hoodoo Formation; Link and others, 2007) and ~1409 Ma (U-Pb on detrital zircons from the uppermost part of the banded siltite member; Aleinikoff and others, 2012). Based on these ages as well as the findings of Bookstrom and others (2016), Saintilan and others (2017), and Schmidt and others (2023), it is proposed that early cobaltiferous pyrite at the Iron Creek Project and early magnetite at the Ruby Zone formed before the main stage of mineralization and was followed by an epigenetic main-stage mineralization forming event linked to the emplacement of a ~1383–1359 Ma suite of bimodal gabbro-granite intrusions: Big Deer Creek, bordering the northeastern margin of the ICB, dated at ~1377 ± 4 Ma (U-

Pb on xenotime and monazite; Aleinikoff and others, 2012; Slack, 2012). Re-Os dates on cobaltite from the Blackbird Mine, the Haynes–Stellite Mine, and the Black Pine Mine (fig. 1A; located to the northwest of Iron Creek in the ICB) led Saintilan and others (2017) to propose a mineralization model involving the influx of Mesoproterozoic evaporitic brines and magmatic-hydrothermal fluids and multi-stage REE-Y-Co-Cu-Au mineralization at around 1370 to 1349 Ma.

MINERALIZATION PROCESSES

According to Schmidt and others (2023), main-stage mineralization (cobaltiferous pyrite and chalcopyrite) at the Iron Creek deposit might be comparable to the formation of the sediment-hosted Black Butte Co-Cu deposit on the eastern side of the Belt–Purcell Basin. The Black Butte Cu-Co deposit is considered to have formed by moderate-temperature, reduced basinal brines, which entered pre-mineralized horizons and caused the formation of main-stage pyrite and chalcopyrite (Graham, 2011; Pfaff and Graham, 2013; Saintilan and others, 2021). Saintilan and others (2021) suggested that Cu mineralization at Black Butte coincided with an increased thermal gradient in the eastern portion of the Belt–Purcell Basin caused by intrusion of a tholeiitic dike swarm around 1455 Ma (Re-Os isochron age). Studies at Iron Creek agree with a Mesoproterozoic origin of main-stage Cu-Co mineralization. Cretaceous metamorphism in the ICB led to a greenschist (Iron Creek) to amphibolite (Blackbird) facies overprint (Lund and others, 2011) and associated silicification and quartz veining found in the Iron Creek deposit and elsewhere in the ICB (Nash and Hahn, 1989; Aleinikoff and others, 2012). Evidence put forward by Saintilan and others (2017) suggests that Cretaceous deformation and metamorphism during the Cordilleran Orogeny remobilized metals in the ICB, as represented at the Iron Creek deposit by cobaltiferous pyrrhotite, sphalerite, and galena deposited together with quartz in late structures.

FIELD TRIP STOPS

Figure 2 shows the locations of the field trip stops on a geologic basemap. This field trip begins officially at the road junction near the confluence of the North and South Forks of Iron Creek. This location is reached by travelling 24.3 mi south on Highway 93 from the Intersection of Highways 93 and 28, and then turning west off of the highway and proceeding roughly 8 mi in a generally westerly direction up the Iron Creek Road (USFS Road 45). The road trip proceeds in a generally northerly direction along USFS Road 45, which follows the North Fork of Iron Creek up to patented claims held by Electra Battery Materials, which will be the final stop on this road trip.

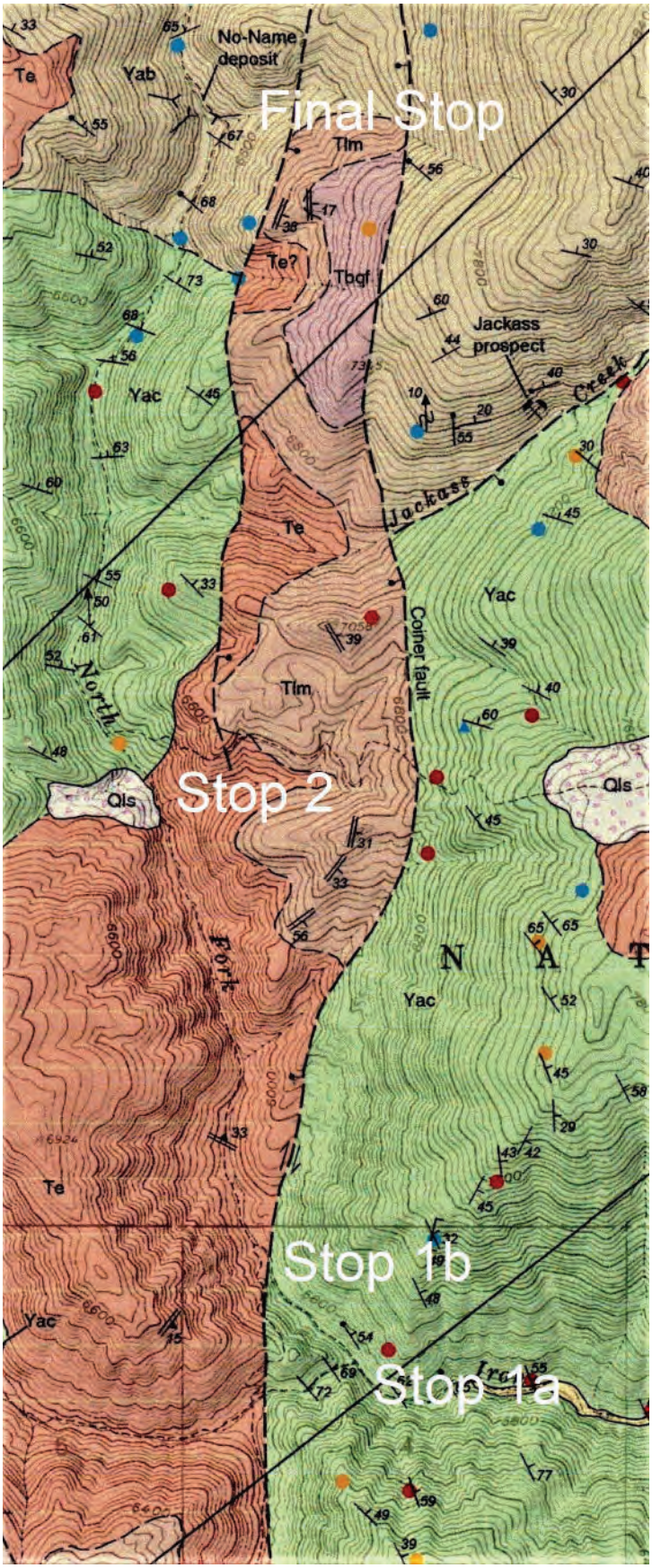

Figure 2. Iron Creek field trip stops, Geology from Lewis (2021).

STOPS 1a–1b—0 mi
Junction of North and West Forks of Iron Creek (USFS roads 45 and 456, respectively)

(45.9256°N, 114.1142°W)

This is an example of steeply northeast-dipping strata of the coarse siltite member of the Apple Creek Formation. The lower part of the coarse siltite member is characterized by tabular beds of quartzite up to 30 cm in thickness (fig. 3). These are readily visible from the road junction.

Figure 3. Steeply dipping tabular beds of quartzite exposed along the West Fork of Iron Creek a short distance west of the road junction.

STOP 2—0.3 mi
On North Fork of Iron Creek Road

(45.9214°N, 114.1097°W)

This stop is at the trace of the northerly trending Coiner fault, which coincides with the contact between the Apple Creek Formation and the Tuff of Ellis Creek Unit of the Eocene Challis Volcanics (fig. 2).

STOP 3—1.4 mi

45.9406°N, 114.1194°W

The road leaves the Challis Volcanic stratigraphy about 1.1 mi north of the Coiner fault and once again traverses the coarse siltite member of the Apple Creek Formation (fig. 4). There is a Quaternary landslide mapped near this contact. This is the upper part of the coarse siltite member of the Apple Creek Formation, and mud cracks occur in this vicinity between this point and Jackass Creek. The banded siltite member of the Apple Creek Formation begins about 0.3 mi below Adit 1 on the Iron Creek patents. The banded siltite member is the host for the Iron Creek deposit and other prospects

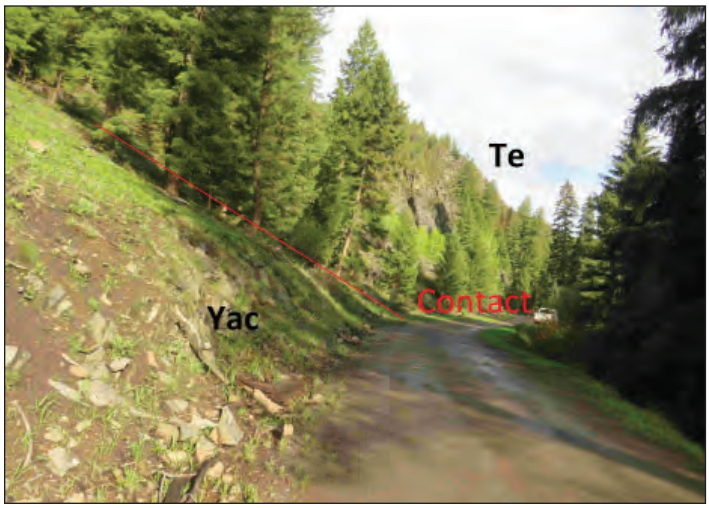

Figure 4. Stop 2 looking south along North Fork of Iron Creek Road, contact between Challis Volcanic and Apple Creek Formation.

and deposits in the area. It contains frequent occurrences of rhythmic couplets of argillaceous and coarser silty material, and frequent sand diking and other soft sediment bedding disruptions.

STOP 4—3.1 mi
The Laydown Area Near the Portals at the No Name Deposit (Final Stop)

(45.9622°N, 114.1161°W)

The tour concludes at the laydown area near the adit portals at the No Name Zone of the Iron Creek Deposit. This location is within the Banded Siltite Member stratigraphy and portions of the No Name Zone are exposed in outcrop in this vicinity. There are two historic adits dating from the early 1970s in this vicinity.

ACKNOWLEDGMENTS

This study and field trip is supported by the Center to Advance the Science of Exploration to Reclamation in Mining (CASERM), which is an industry–university collaborative research center between Colorado School of Mines and Virginia Tech funded under NSF award numbers 1822108 and 1822146. We thank Dan Pace for sample access and fruitful discussions; Reed Lewis for support with logistics, fieldwork, and discussions; and Kelsey Livingston and Filip Kasprowicz for their invaluable assistance with expedient sample preparation. Russ Burmester provided a helpful review.

REFERENCES

Aleinikoff, J., Slack, J.F., Lund, K., Evans, K.V., Fanning, C.M., Mazdab, F.K., Wooden, J.L., and Pillers, R.M., 2012, Constraints on the timing of Co-Cu ± Au mineralization in the Blackbird district, Idaho, using SHRIMP U-Pb ages of monazite and xenotime plus zircon ages of related Me-

soproterozoic orthogneisses and metasedimentary rocks: Economic Geology, v 107, p. 1143–1175.

Bookstrom, A.A., Box, S.E., Cossette, P.M., Frost, T.P., Gillerman, V., King, G., and Zirakparvar, N.A., 2016, Geologic history of the Blackbird Co-Cu district in the Lemhi subbasin of the Belt-Purcell Basin, *in* Maclean, J.S., and Sears, J.W., eds., Belt Basin: Window to Mesoproterozoic Earth. Geologic Society of America, Idaho, p. 185–219.

Graham, G.E., 2011, Geologic and stable isotope investigation of the Sheep Creek Cu-(Co-Ag) deposit with comparison to other sediment-hosted base metal deposits in Mesoproterozoic basins: Golden, Co., Colorado School of Mines, PhD Thesis.

Landis, G.P., and Hofstra, A.H., 2012, Ore genesis constraints on the Idaho cobalt belt from fluid inclusion gas, noble gas isotope, and ion ratio analyses: Economic Geology, v. 107, p. 1189–1205.

Lewis, R.S., Canada, A.S., Stewart, D.E., and Burmester, R.F., 2021, Geologic map of the Degan Mountain quadrangle: Idaho Geologic Survey Digital Web Map 200, scale 1:24,000.

Link, P.K., Fanning, C.M., Lund, K.I., and Aleinikoff, J.N., 2007, Detrital zircon populations and provenance of Mesoproterozoic strata of east-central Idaho, U.S.A.: Correlation with Belt Supergroup of southwest Montana: Society for Sedimentary Geology (SEPM) Special Publication, p. 101–128.

Lund, K., Tysdal, R.G., Evans, K.V., Kunk, M.J., and Pillers, R.M., 2011, Structural controls and evolution of gold-, silver-, and REE-bearing copper-cobalt ore deposits, Blackbird district, east-central Idaho—Epigenetic origins: Economic Geology, v. 106, p. 585–618.

Nash, J.T., and Hahn, G.A., 1989, Stratabound Co-Cu deposits and mafic volcaniclastic rocks in the Blackbird mining district, Lemhi County, Idaho: Geological Association of Canada Special Paper 36, p. 339–356.

Perron, M., Beauvais, M.R., and Kinnan, E., 2023, NI 43-101 Technical report and mineral resource estimate for the Iron Creek Cobalt-Copper Property, Lemhi County, Idaho, USA: NI 43-101 technical report prepared for Electra Battery Materials, available at https://electrabmc.com/wp-content/uploads/2023/03/Iron-Creek-Tech-Report-2023-Final.pdf [Accessed July 2023].

Pfaff, K., and Graham, G.E., 2013, The Black Butte Cu-(Co-Ag) deposit, Montana: A thermodynamic model: GSA 2023 Annual Meeting & Exposition, Denver, Colo.

Ristorcelli, S.J., and Schlitt, J., 2019, Amended technical report and estimate of mineral resources for the Iron Creek Cobalt-Copper Project, Lemhi County, Idaho, USA: NI 43-101 technical report prepared for First Cobalt Corp.

Saintilan, N.J., Creaser, R.A., and Bookstrom, A.A., 2017, Re-Os systematics and geochemistry of cobaltite (CoAsS) in the Idaho cobalt belt, Belt-Purcell Basin, USA: Evidence for middle Mesoproterozoic sediment-hosted Co-Cu sulfide mineralization with Grenvillian and Cretaceous remobilization: Ore Geology Reviews, v. 86, p. 509–525.

Saintilan, N., Sheldrake, T.E., Creaser, R.A., Selby, D., Zieg, J., Boyce, A., and Chelle-Michou, C., 2021, Synsedimentary to diagenetic Cu±Co mineralization in Mesoproterozoic pyritic shale driven by magmatic-hydrothermal activity on the edge of the Great Falls tectonic zone–Black Butte, Helena embayment, Belt-Purcell Basin, USA: Evidence from sulfide Re-Os isotope geochemistry: Lithosphere 2021, 7866186.

Schmidt, D., Lehman, M., Pfaff, K., Monecke, T., Hofstra, A., Phelps, G., Lewis, R., Kocher, S., Jobe, Z., Gillerman, V., Day, W., Caddick, M., Anderson, E., Harrison, J., and Pace, D., 2023, The Iron Creek deposit in the Idaho Cobalt Belt: On a quest for cobalt: Peer-reviewed extended abstract, Soceity for Geology Applied to Mineral Deposits Meeting, 2023.

Slack, J., 2012, Strata-bound Fe-Co-Cu-Au-Bi-Y-REE deposits of the Idaho Cobalt belt: Multistage hydrothermal mineralization in a magmatic-related iron oxide copper-gold system: Economic Geology, v. 107, p. 1089–1113.

GEOLOGIC FIELD GUIDE TO THE NORTH FORK AND TRAIL GULCH THRUSTS NEAR NORTH FORK, IDAHO

Jeffrey D. Lonn,[1] Russell F. Burmester,[2] and Reed S. Lewis[2]

[1]*Montana Bureau of Mines and Geology, Butte, Montana*
[2]*Idaho Geological Survey, Moscow, Idaho*

INTRODUCTION

This trip repeats the Trail Gulch field trip of 2013 TRGS/Belt Symposium V (Lonn and others, 2013a) because structural and stratigraphic interpretations have been greatly revised since then. This all-day hike totals about 5 mi with 1,600 ft of elevation gain through grassland and open forest typical of the lower elevations of the Salmon, Idaho region. Most of the hiking is on game trails, and because elevations top out at only 5,500 ft, temperatures in summer will be hot, probably near 90°F. No water is available along the route, and participants are advised to camel up! But efforts will be rewarded by good exposures of the major thrust system of this region and of the Mesoproterozoic Lemhi subbasin strata, upper Belt Supergroup.

GEOLOGIC SETTING

The mountains surrounding this location are underlain by low-grade Mesoproterozoic metasedimentary rocks of the Lemhi subbasin of the Belt Basin (fig. 1). These strata are correlated with the Missoula Group of the upper Belt Supergroup (Lonn and others, 2020). The main players here are the Lemhi Group, which is everything below the Swauger Formation, the Swauger and Lawson Creek Formations, and overlying Apple Creek Formation, which is subdivided into informal members. The strata are cut by a complex array of northwest-striking faults that extends from near Lemhi Pass into the headwaters of the West Fork of the Bitterroot River in Montana. The North Fork thrust (NFT), first recognized in the field trip area (Lonn and others, 2013b), is now interpreted as a significant thrust that has been traced from the field trip area northwest into Montana, where it is cut by Tertiary–Cretaceous igneous rocks of the Idaho Batholith (fig. 2). Southeast of the field trip area, it is covered by Tertiary volcanic and sedimentary rocks in the hanging wall of the Salmon Basin fault (SBF), but it re-emerges in the SBF footwall on the west side of the Beaverhead Mountains and appears to continue southeast toward Lemhi Pass. For a broader view of unit distribution and faults exposed in the Beaverhead Mountains between here and Lemhi Pass, refer to Burmester and others (2016).

The NFT carries Lemhi Group intruded by an extensive 1380–1370 Ma bimodal igneous complex (Doughty and Chamberlain, 1996) over younger Lemhi subbasin strata

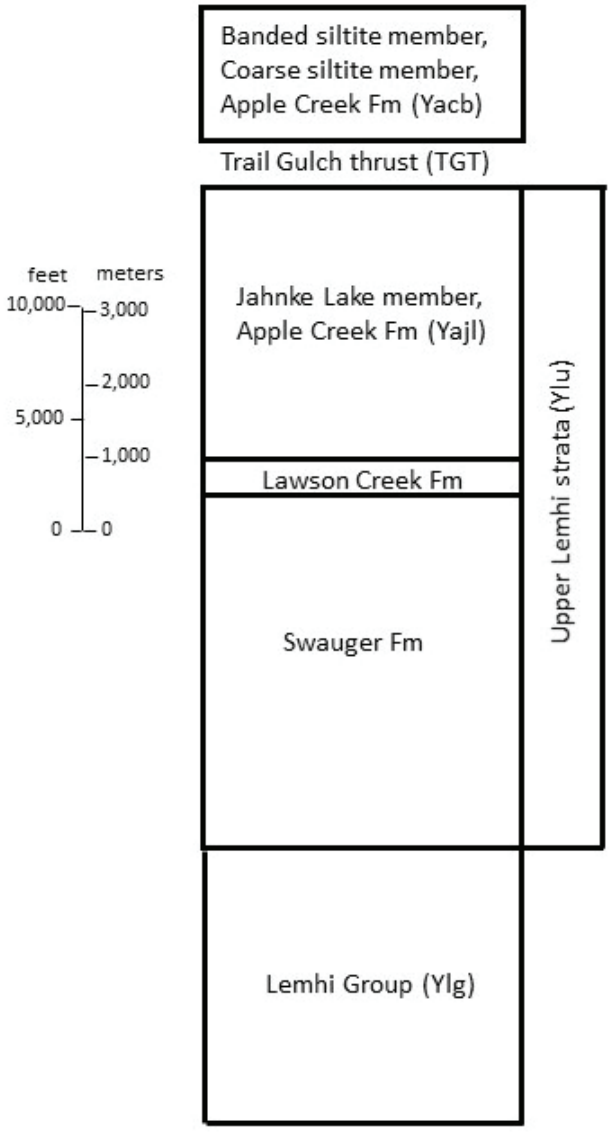

Figure 1. Stratigraphic column showing rocks of the Lemhi subbasin, upper Belt Supergroup, that underlie the region surrounding the field trip. The banded siltite member, Apple Creek Fm, is separated from the Jahnke Lake member, Apple Creek Fm, by the Trail Gulch thrust. While the two members have not been found in stratigraphic contact in the North Fork region, the banded siltite member is thought to be younger based on stratigraphy exposed in the Lemhi and Salmon River Mountains.

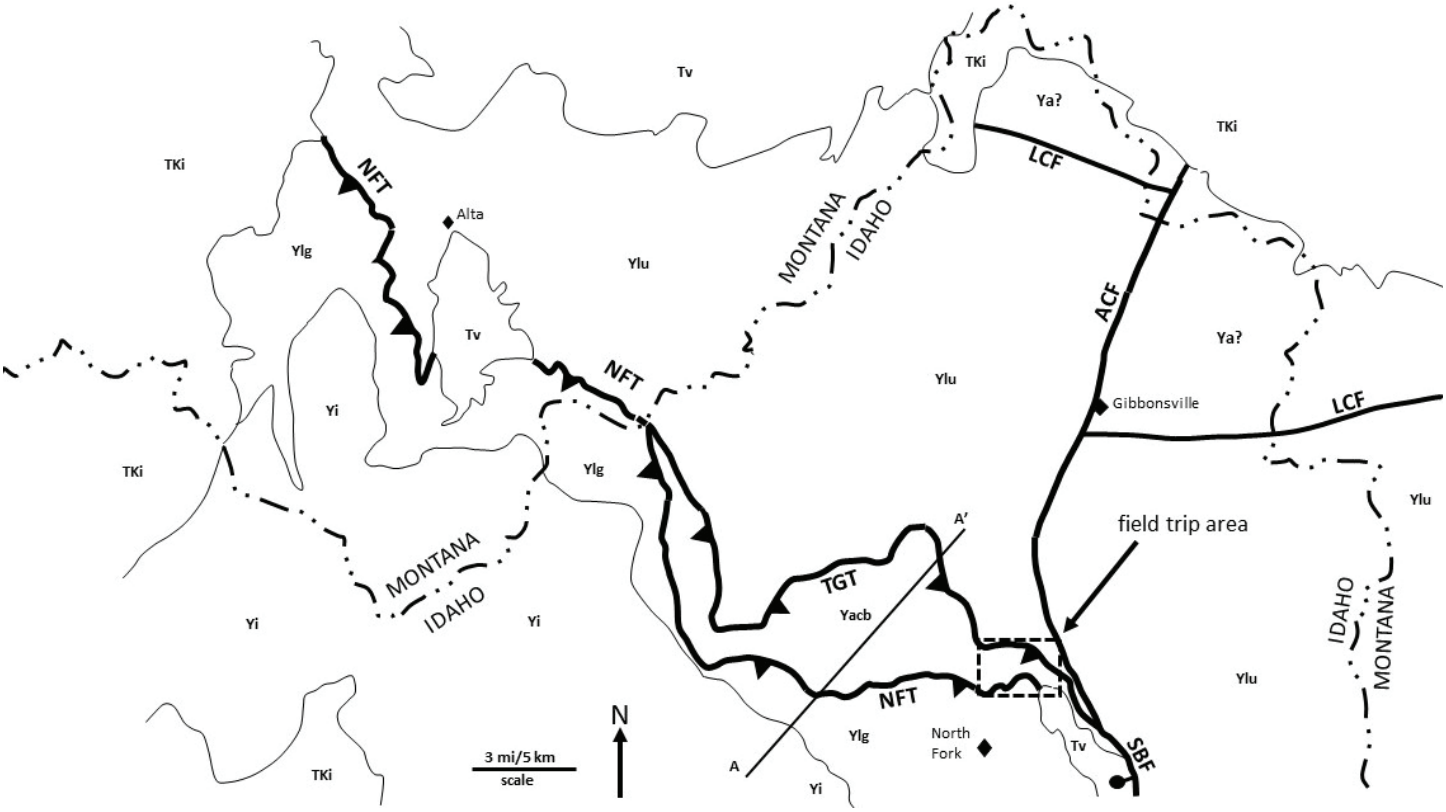

Figure 2. Simplified geologic map of the North Fork thrust system (NFT) near North Fork, Idaho. The NFT places older Lemhi strata (Ylg) intruded by the 1370 Ma intrusive complex (Yi) over younger Lemhi strata. The NFT is truncated by the Salmon Basin fault (SBF) on the SE and the Idaho batholith (TKi) on the NW. Note the subparallel Trail Gulch thrust (TGT) in part of the NFT footwall. AA', location of cross section shown in fig. 4; ACF, Anderson Creek fault; LCF, Lick Creek fault; NFT, North Fork thrust; TGT, Trail Gulch thrust; SBF, Salmon Basin fault; TKi, Idaho batholith; Tv, volcanic rocks; Yi, 1370 Ma intrusive suite; Ya, Apple Creek Fm; Yacb, coarse siltite and banded siltite members, Apple Creek Fm; Ylg, Lemhi Gp; Ylu, upper Lemhi subbasin strata, includes Swauger, Lawson Creek, and Apple Creek Fms. Map compiled from Lonn and others (2013b); Lewis and others (2019, 2021); Berg and Lonn (1996); and Lonn (2020–2022 unpublished mapping).

that lack Mesoproterozoic intrusions (figs. 1, 2). In the area of the field trip (fig. 3), the NFT's footwall contains a subparallel thrust, the Trail Gulch thrust (TGT), that carries a fault slice of banded siltite member of the Apple Creek Formation in between the Lemhi Group of the NFT hanging wall and the Jahnke Lake member of the Apple Creek Formation of the TGT footwall (fig. 4). Both the NFT and TGT contain discontinuous mylonitic zones with nearly due-east lineations and top-to-the-east shear sense indicators (fig. 5). Because these thrusts strike southeast and dip southwest, the lineations do not rake directly down the dip of the fault planes, and so these faults are interpreted to have components of both left-lateral and reverse slip movement that was oblique to the fault planes in a sinistral transpressive sense.

TO THE TRAILHEAD

Drive north from Salmon on US Highway 93 approximately 21 mi to the town of North Fork. North of the Tower Rock Campground, the Salmon River canyon is cut through Lemhi Group of the NFT hanging wall. Observe in passing the variety of bedding thicknesses, grading, and structures. Although Burmester and others' (2016) regional map shows a thick, undeformed gently west-dipping stratigraphic section of Lemhi Group in this area, note the two east-overturned folds visible from the highway before you reach North Fork. These indicate contraction that probably produced intraformational thrust and reverse faults that thickened the section. The monotonous lithology of the Lemhi Group here—dominantly fine-grained feldspathic quartzite—makes recognition of intraformational structures difficult.

Continue past North Fork for 2.8 mi and turn right into the Trail Gulch trailhead (45.4469°N, 113.9871°E), marked by a brown Forest Service sign.

THE HIKE

Figure 6 is a view of much of the hiking route. Start by walking north along base of the hill towards the gully that enters the valley north of the parking lot. The parking lot contains pieces of dark-colored, phyllitic, thin-bedded (centimeter–millimeter scale) siltite and argillite from the fault slice between the NFT and TGT. A better look at this phyllitic unit is in the nearby bulldoz-

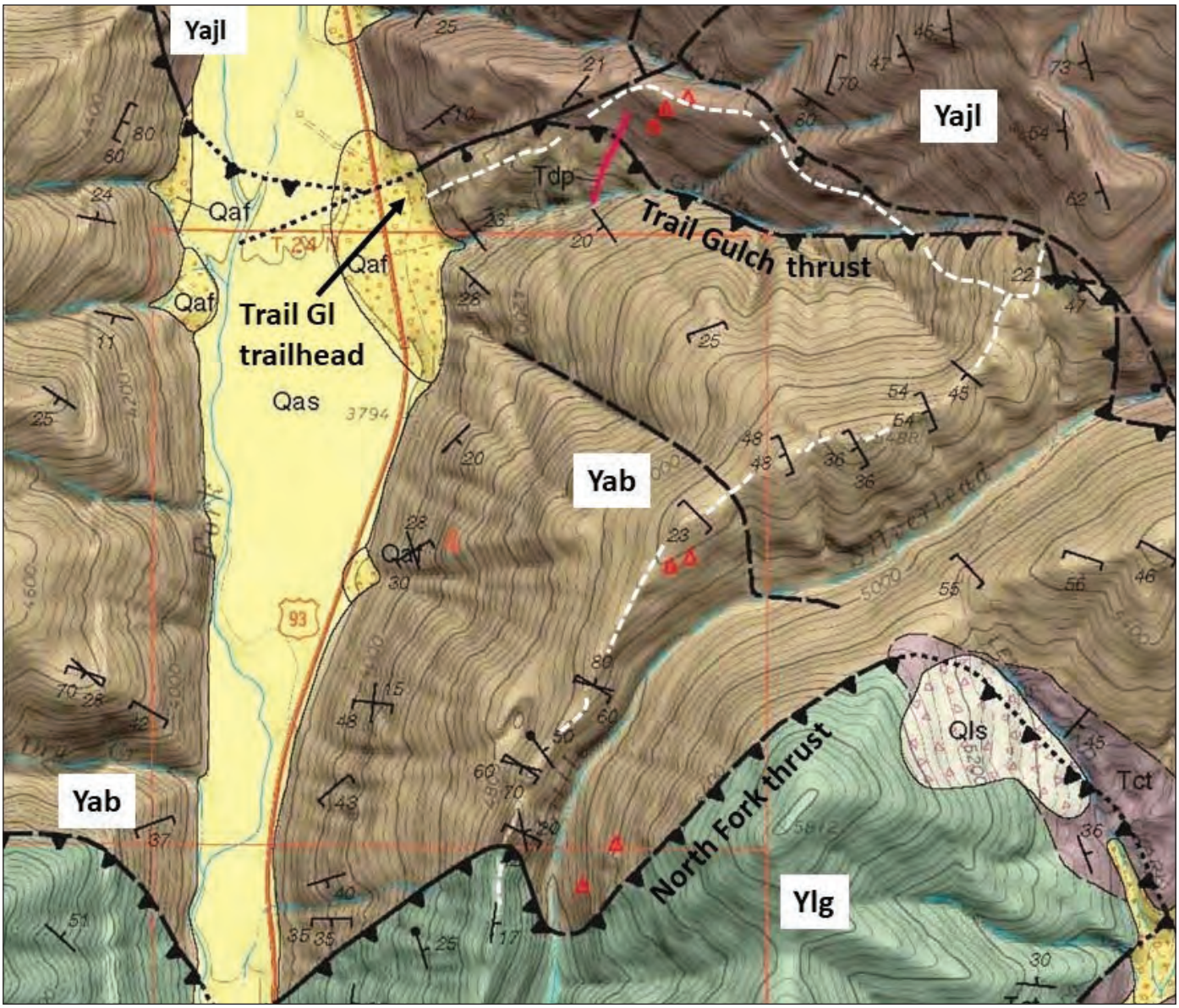

Figure 3. Geologic map of the field trip area with the hiking route shown by the dashed white line. Yab, banded siltite member, Apple Creek Fm; Yajl, Jahnke Lake member, Apple Creek Fm; Ylg, Lemhi Gp. Map from Lonn and others (2013b).

er prospects that cross the trace of the TGT. The phyllite is correlated with the banded siltite member of the Apple Creek Formation (fig. 1) based on lithology and the presence of diamictite in the west-adjacent Ulysses Mountain quadrangle (Lewis and others, 2019). The Apple Creek Formation contains the only known such diamictite occurrences in the Belt Supergroup.

Near the mouth of the gully is an outcrop of brecciated, very fine-grained feldspathic quartzite in the footwall of the TGT. The hill north of the gully is composed entirely of similar brecciated, pink, fine-grained quartzite. The quartzite is correlated with the Jahnke Lake member of the Apple Creek Formation (fig. 1).

Proceed up the hill on the south side of the gully, crossing grussy granitic rock, feldspar porphyry, and phyllite. The igneous rocks appear to have intruded the TGT and probably controlled the mineralization in the many prospects. Continue upward past a few ponderosa pines to a metal post. Along the way, note the float of lineated mylonite developed in the fault zone. The metal post is in breccia and quartz vein, and marks the trace of the TGT. The slope above is composed of brecciated, pink, very fine-grained Jahnke Lake quartzite (Yajl). Although no outcrops of the mylonite could be located, the fault plane forms a dip slope on the north side of Trail Gulch (figs. 6, 7), so here the fault strikes east–southeast and dips moderately (30°–40°) to the southwest.

The mylonite developed in the phyllite contrasts with the brecciated quartzite. Did the brittle and ductile fabrics develop simultaneously during shear along the TGT, or is the breccia related to the high-angle normal faults that postdate the TGT?

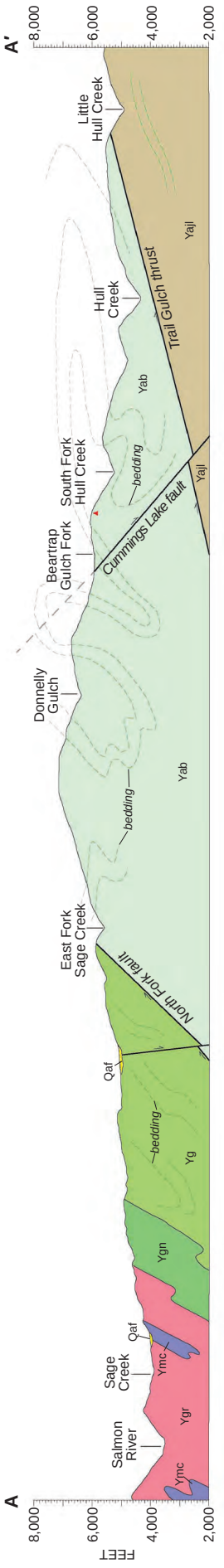

Figure 4. Cross-section from the west-adjacent Ulysses Mountain 7.5' quadrangle (Lewis and others, 2019) showing the geometry of the Trail Gulch and North Fork thrusts and the 1370–1380 Ma intrusive complex that intrudes the North Fork thrust hanging wall. See figure 2 for location. Yab, banded siltite member, Apple Creek Fm; Yajl, Jahnke Lake member, Apple Creek Fm; Yg, Gunsight Fm; Ygn, gneiss; Ygr, megacrystic granite; Ymc, mafic intrusive complex.

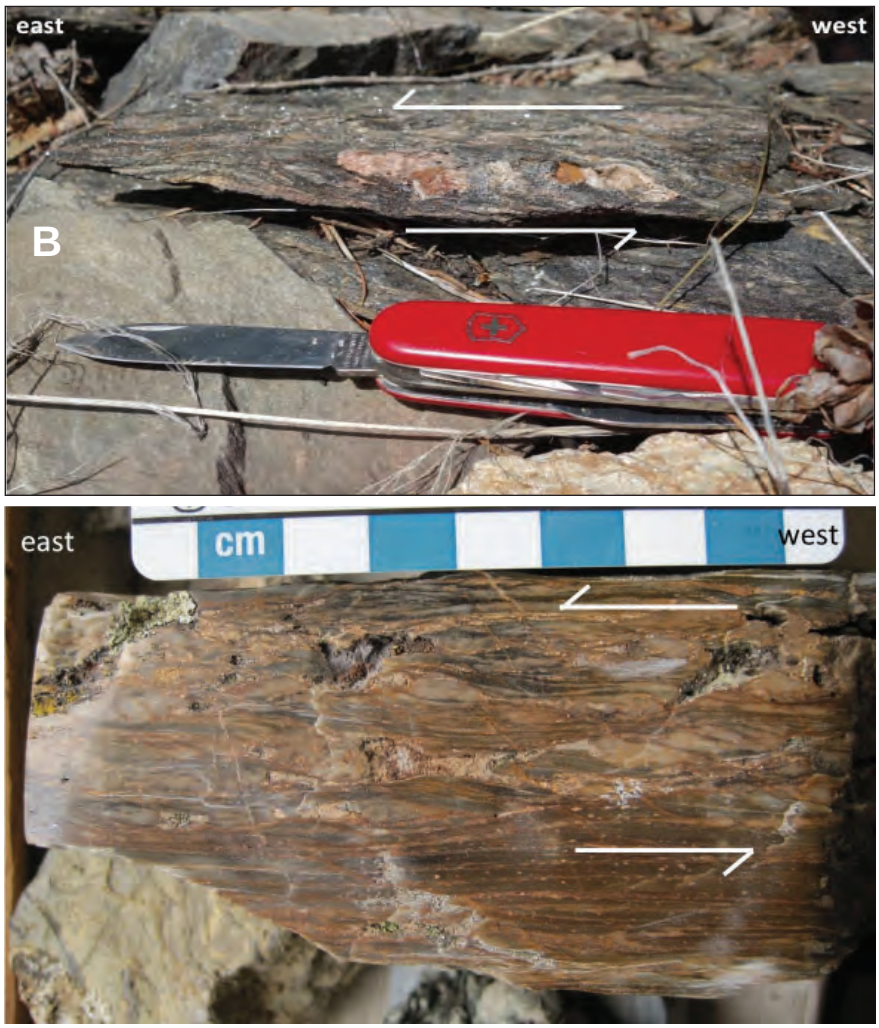

Figure 5. Cross-sectional views of mylonite cut parallel to lineations showing top-to-the east shear sense for both (A) the North Fork thrust, and (B) the Trail Gulch thrust. Both have nearly due east lineations.

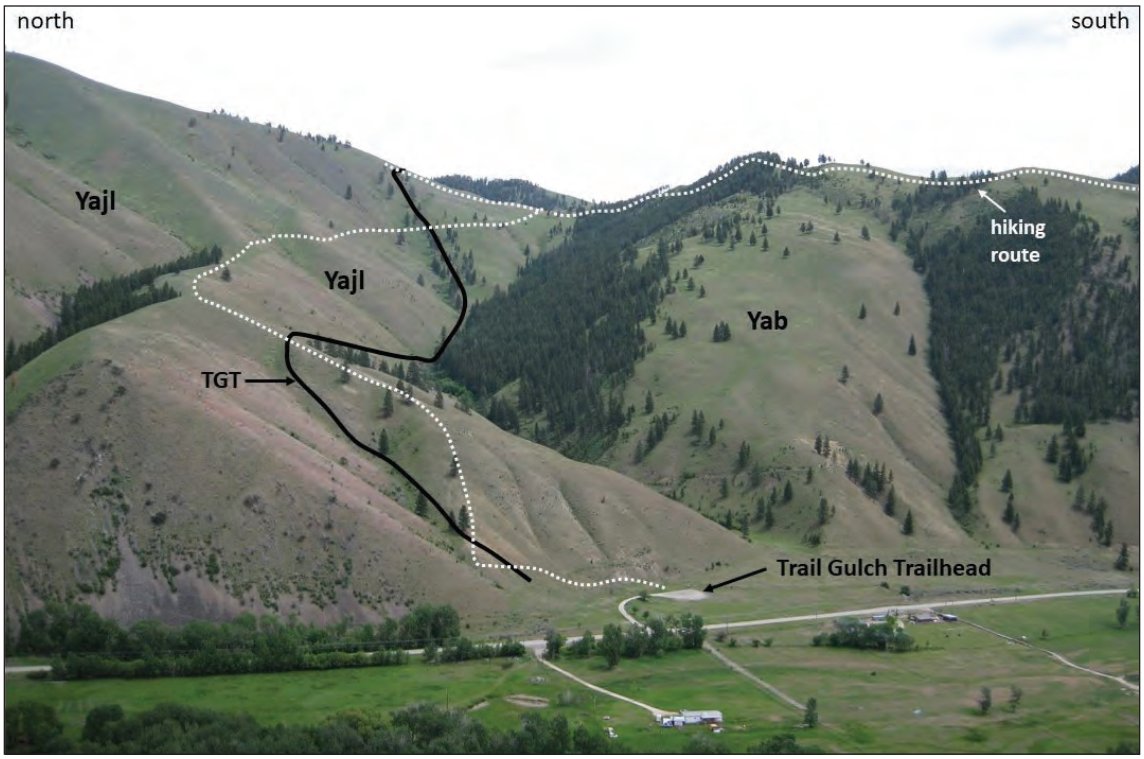

Figure 6. Eastward view of the Trail Gulch area shows trace of the Trail Gulch thrust in black and field trip hiking route as the white dotted line. TGT, Trail Gulch thrust; Yab, banded siltite member, Apple Creek Fm; Yajl, Jahnke Lake member, Apple Creek Fm.

Continue up the slope and follow the ridge east to the base of the steep slope, walking through brecciated pink quartzite with some intrusions (?) of porphyry. The base of the steep slope is thought to mark the trace of a down-to-the-southwest normal fault that postdates the TGT (fig. 3).

Just before the slope steepens, take the obvious game trail that contours to the right (south), heading back to Trail Gulch and the Lewis and Clark Trail. This game trail is remarkable for its continuity and level grade, and will take you across Trail Gulch and the TGT, then upward a short distance to the main trail. Once on the main trail, you are back in phyllite of the hanging wall. Proceed upward on the trail to the saddle. Looking back down Trail Gulch, the TGT plane forms a dip slope on the right side of the valley, climbs the lower part of the slope above the ponderosa pines, and continues across the North Fork of the Salmon River, where it traces the top of the lower cliffs (fig. 7). Therefore, the fault strikes west–northwest through Trail Gulch, then swings northward on the other side of the river where it dips gently to moderately southwest to west. The NFT lies structurally above and nearly parallel to the TGT (fig. 4), but is difficult to pick out from here.

From the saddle, go left (northeast) and continue up the ridge; two knobs will become visible a short distance ahead. Proceed to the south knob, traversing from phyllite to quartzite and back to phyllite as you cross the gently dipping thrust. On this knob are outcrops of strongly cleaved phyllite that is mylonitic near the thrust. Lineations are difficult to locate, but those visible bear nearly due east. Oriented samples cut parallel to the lineations and perpendicular to foliation show top-to-the-east shear sense (fig. 5). In places such as this, where the TGT strikes west–northwest, lineations are nearly horizontal, and movement was therefore south-side-to-the-east, or left-lateral. In those places where the TGT strikes north or northwest, movement was mostly southwest-side-up, or reverse sense. Therefore, the west–northwest-striking segments are here interpreted as left-lateral ramps, but an alternative interpretation is that they are parts of the thrust tilted south during later folding.

Just upslope from the knob, where the slope steepens again, is quartzite of the footwall. The TGT here juxtaposes rocks of very different lithologies, and so it is easy to put your finger on it, in contrast to the NFT that we will view later. The TGT continues southeastward across the valley of Little Silverlead Creek and passes through the not-so-obvious saddle to the southeast, where it has been cut off by a down-to-the-southwest normal fault (fig. 3).

Return to the saddle and follow a game trail that contours along the northwest side of the ridge. The trail gains the ridge and then ascends through phyllitic rocks to a small summit. From the summit, you can look south through the prominent saddle into a basin that preserves Tertiary volcanic rock, and beyond into the

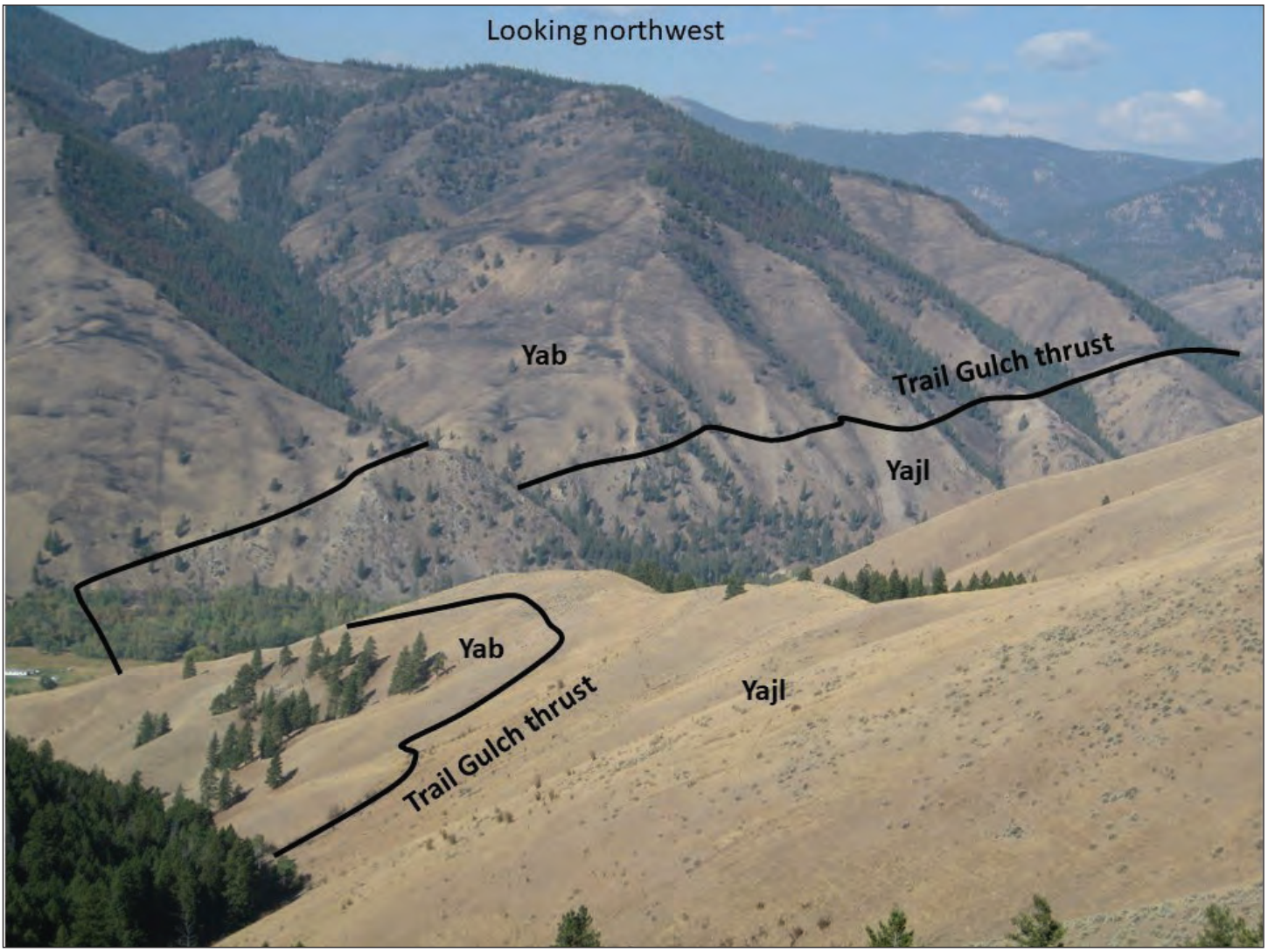

Figure 7. View northwest from the saddle across the North Fork Salmon River valley shows the trace Trail Gulch thrust. The North Fork thrust is out of view to the left. Yab, banded siltite member, Apple Creek Fm; Yajl, Jahnke Lake member, Apple Creek Fm.

Salmon Basin. The west-dipping detachment fault that controls the Salmon Basin (SBF on fig. 2) is also obvious, forming the gentle west slope of the Beaverhead Range. The most prominent peak is Copperhead, with Freeman beyond and just to its right; both are underlain by Jahnke Lake quartzite in the footwall of the NFT. In the foreground, the prominent saddle across the valley marks the NFT; the saddle to its left (east) marks the down-to-the-southwest normal fault that cuts the TGT, and the saddle still farther left (east), below the logging roads, marks the Salmon Basin fault that juxtaposes coarse-grained Swauger Formation quartzite to the northeast against the younger Janhke Lake quartzite (fig. 1).

Continue down the ridge to the rocky outcrops. Sedimentary characteristics are hard to discern in the phyllite due to strong cleavage and iron oxide stain, but we will be able to see more in the area ahead. Tiny metamorphic garnets are common and yielded Lu-Hf ages of 1135 ± 5 Ma (Murphy and others, this volume), postdating metamorphism associated with the 1,370 Ma intrusive complex. These garnets also predate the top-to-the-east oblique shear fabric associated with the TGT and NFT that is thought to be Cretaceous.

In the area of the low saddle and the knob beyond, breccia and iron oxide stain are common, and interpreted to be developed along a normal(?) fault that appears as a dashed line on the map (fig. 3). The ridge then becomes rockier, and some of the sedimentary characteristics of the phyllitic unit can be seen. It appears to be dominated by couplets and couples of light gray siltite grading up to purple-black argillite. Desiccation cracks are present, but rare. A few thicker, very fine-grained quartzite beds from 0.2 to 0.5 m thick are also present. Locally, this lithology contains diamictite (Lewis and others, 2019), although so far none has been found along this traverse. The sedimentary features and presence of diamictite have led us to correlate rocks of the hanging wall of the TGT with the banded siltite member of the Apple Creek Formation (fig. 1). The quartzite

beds in these outcrops show complex folding, and it is likely that all the phyllite we have walked through is similarly deformed.

Continue scrambling along the ridge through an area burned in the 2012 Mustang fire. The highest rocky point is still within the phyllite, but a severely brecciated and iron-stained zone on the southwest side of this point probably is on the North Fork thrust trace. Beyond this breccia zone, the rock weathers into blocky pieces of siltite and very fine-grained quartzite, and contains no dark-colored phyllite. This rock is interpreted to belong to a different unit: Lemhi Group (Ylg on figs. 2, 3) in the hanging wall of the NFT (fig. 2). Across Little Silverlead Canyon is a similar rocky interval of breccia and complexly folded rocks along the southeastward continuation of the thrust. It appears to be gently to moderately dipping like the TGT. To the northwest, across the North Fork of the Salmon River, the fault trace is even more subtle: it is located between the rocky outcrops and the smooth slope south of Dry Creek. Its trace is marked by bulldozer prospects near the bottom of Dry Creek upstream from its mouth; from there it traverses westward up the Dry Creek valley. Its trace is obscure in the covered slopes. This fault illustrates some of the problems inherent in mapping these rocks in this region: even though the country is steep, useful outcrops are scarce, and the differences in lithology are often subtle. Although the NFT is only marked by breccia zones here, in other places mylonite with due east lineations and top-east shear sense is present (fig. 5).

Continue along the ridge to the final rocky point marked by two Douglas fir trees. Here you are out of the brecciated zone and into undeformed gently dipping Lemhi Group that underlies the area around North Fork, the mountains west of Salmon, and the western slope of the Beaverhead Mountains. It consists of decimeter- to meter-scale planar beds of siltite and fine-grained quartzite, with minor argillite. This unit has been shown on previous maps as Lemhi Quartzite (Anderson, 1959), Yellowjacket Formation (Ruppel and others, 1993), or Apple Creek Formation (Evans and Green, 2003). However, we assign these rocks to the Lemhi Group because, in the mountains west of Salmon, rocks in structural and stratigraphic continuity with these were mapped in depositional contact with the overlying Swauger Formation (Evans and Green, 2003; Burmester and others, 2013, 2016). They were boldly correlated with the Gunsight Formation of the upper Lemhi Group (Ruppel, 1975) that underlies the Swauger Formation in the Lemhi Range. However, units below the Gunsight Formation defined there (Ruppel, 1975) have not been recognized in this area, so we instead use the term Lemhi Group, leaving formation divisions within the North Fork plate to future workers.

Return to the trailhead by retracing your steps along this ridge to the saddle where the Lewis and Clark Trail crosses. Turn left on the trail and follow it down; fortunately, it is mostly shady. About 30 min of walking will take you back to your vehicle.

ACKNOWLEDGMENTS

Katie McDonald and Alan English kindly reviewed the manuscript.

REFERENCES

Anderson, A.L., 1959, Geology and mineral resources of the North Fork quadrangle, Lemhi County, Idaho: Idaho Bureau of Mines and Geology Pamphlet 118, 92 p.

Berg, R.B., and Lonn, J.D., 1996, Preliminary geologic map of the Nez Perce Pass 30' x 60' quadrangle, Montana: Montana Bureau of Mines and Geology Open-File Report 339, scale 1:100,000.

Burmester, R.F., McFaddan, M.D., Lewis, R.S., and Lonn, J.D., 2013, What's the Swauger Formation doing in the eastern Salmon River Mountains, Idaho?: Northwest Geology, v. 42, p. 187–198.

Burmester, R.F., Lewis, R.S., Othberg, K.L., Stanford, L.R., Lonn, J.D., and McFaddan, M.D., 2016, Geologic map of the western part of the Salmon 30' x 60' quadrangle, Idaho and Montana, Idaho Geological Survey Geologic Map 52, scale 1:75,000.

Doughty, P.T., and Chamberlain, K.R., 1996, Salmon River Arch revisited: New evidence for 1370 Ma rifting near the end of deposition in the Middle Proterozoic Belt basin: Canadian Journal of Earth Sciences: v. 33, p. 1037–1052.

Evans, K.V., and Green, G.N., 2003, Geologic map of the Salmon National Forest and vicinity, east-central Idaho: U.S. Geological Survey Geologic Investigations Series Map I-2765, 19 p., scale 1:100,000.

Lewis, R.S., Burmester, R.F., and Lonn, J.D., 2019, Geologic map of the Ulysses Mountain quadrangle, Lemhi County, Idaho: Idaho Geological Survey Digital Web Map 188, 1 sheet, scale 1:24,000.

Lewis, R.S, Burmester, R.F, Lonn, J.D., Stewart D.E., and Canada, A.S., 2021, Geologic map of the Henderson Ridge 7.5' quadrangle, Lemhi County, Idaho, and Ravalli County, Montana: Idaho Geological Survey Digital Web Map DWM-202, 1 sheet, scale 1:24,000.

Lonn, J.D., Lewis, R.S., Burmester, R.F., and McFaddan, M.D., 2013a, Geologic field guide to the Trail Gulch area near North Fork, Idaho: Northwest Geology, v. 42, p. 205–214.

Lonn, J.D., Othberg, K.L., Lewis, R.S., Burmester, R.F., Stanford, L.R., and Stuart D.E., 2013b, Geologic map of the North Fork 7.5' quadrangle, Lemhi County, Idaho: Idaho Geological Survey Digital Web Map 160, scale 1:24,000.

Lonn, J.D., Burmester, R.F., Lewis, R.S., and McFaddan, M.D., 2020, The Mesoproterozoic Belt Supergroup, *in* Geology of Montana: Montana Bureau of Mines and Geology Special Publication 122, v. 1: Geologic History, available at: https://mbmg.mtech.edu/pdf/geologyvolume/Lonn_BeltFinal.pdf [Accessed July 2023].

Murphy, J.P., Lewis, R.S., Vervoort, J.D., and Hämmerli, J., this volume, Multiple periods of metamorphism in the Salmon River Mountains Idaho as deduced from garnet Lu-Hf ages.

Ruppel, E.T., 1975, Precambrian Y sedimentary rocks in east-central Idaho: U.S. Geological Survey Bulletin 889-A, 23 p.

Ruppel, E.T., O'Neill, J.M., and Lopez, D.A., 1993, Geologic map of the Dillon 1º x 2º quadrangle, Idaho and Montana: U.S. Geological Survey Miscellaneous Investigations Series Map I-1803-H, scale 1:250,000.

THE CHALLIS–MESOPROTEROZOIC UNCONFORMITY, CHALLIS VOLCANICS, AND RELATED SEDIMENTS IN THE WILLIAMS CREEK VICINITY, EAST-CENTRAL IDAHO

David E. Stewart and Reed S. Lewis

Idaho Geological Survey, Moscow, Idaho

INTRODUCTION

On this field trip we will visit the basal Challis unconformity where quartzites of the Mesoproterozoic Lemhi Group (Ylg) are overlain by conglomerates (Tcgl) and the brick tuff (Tbt) unit of the Challis Group, other Challis volcanic units, related sediments (including one extensive deposit that contains boulders of Mesoproterozoic rapakivi granite), mylonitized Mesoproterozoic Swauger quartzite, and an exposure of the Coiner fault. This trip involves mostly roadside stops with two short off-trail hikes. Figure 1 shows a geologic map of the area and stops.

This trip is one of four field trips that demonstrate rapid lateral changes in the Challis volcanic section at locations west and south of Salmon. Figure 2 is a comparison of these sections and includes rocks seen on this field trip. As is readily apparent, only the mafic lavas (the Tlm unit) appear in all of the sections.

Mapping has shown that the mafic lavas are widespread. Does it seem reasonable that the mafic lavas, which are relatively thin lava flows and so confined to topographic lows, are more consistently present than the intermediate to silicic ash-flow tuffs that it overlies, tuffs that should blanket topography and not be confined topographically? The four localities (the ridge does not expose a tuff beneath Tlm) are only 4–14 km apart from each other. How can each one have a different tuff underlying Tlm? Three of the localities have sediments present, as Tsc or Tsg, at the horizon below Tlm resting on the different tuff sequences.

The most likely explanation for these observations is erosion of tuffs. Prior to deposition of the sediments and mafic lavas, the area in question experienced active faulting, which formed a graben at Lake Creek and a half-graben at Iron Creek, and high-relief topography, such as along Williams Creek. That led to local preservation of tuffs in lowlands and stripping of them from other parts of the area. The fact that there are different tuffs underlying the mafic

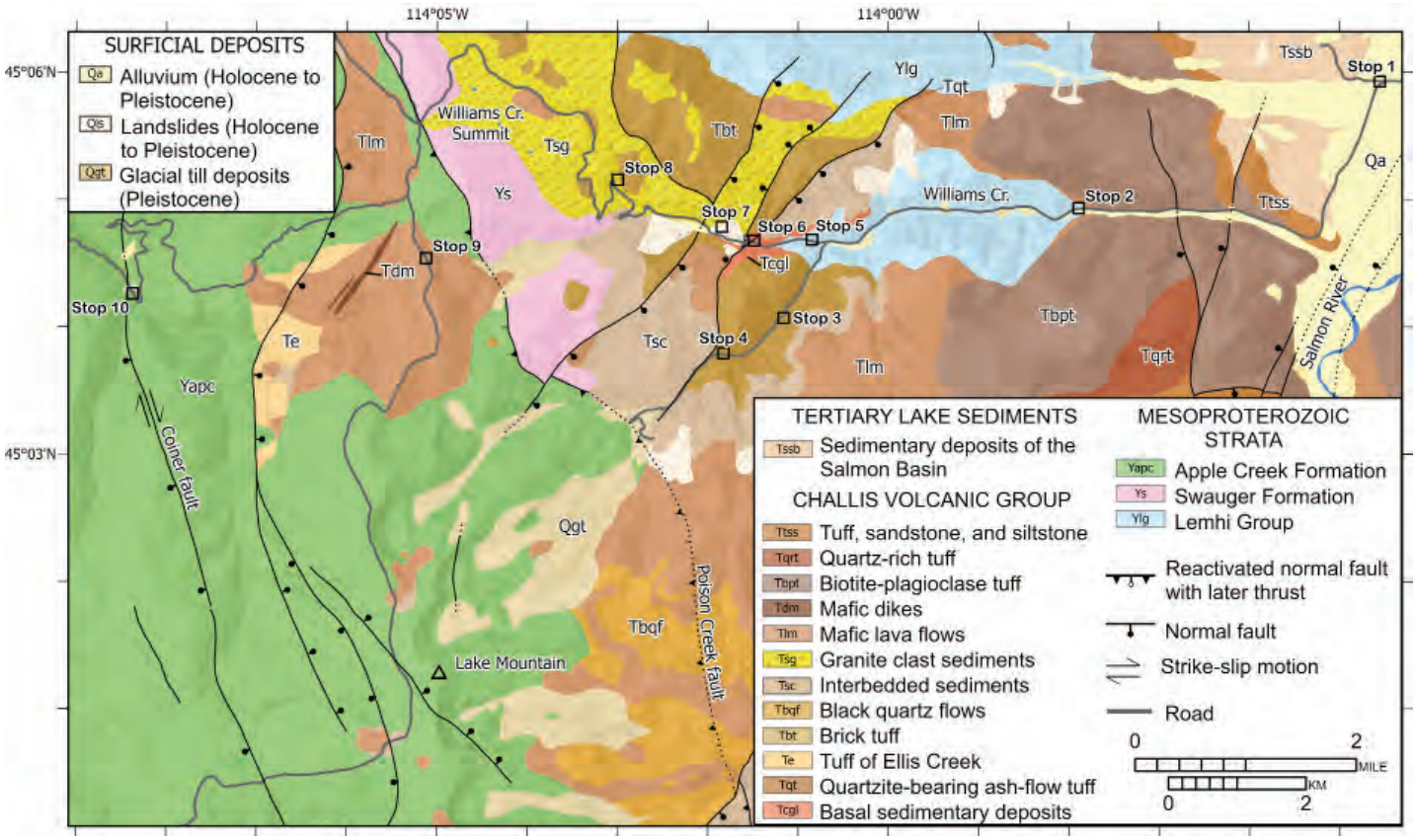

Figure 1. Geologic map showing stops on this field trip and distribution of Challis units. Based on Lewis and others (2012, 2013, 2021, and in press) and Burmester and others (2016).

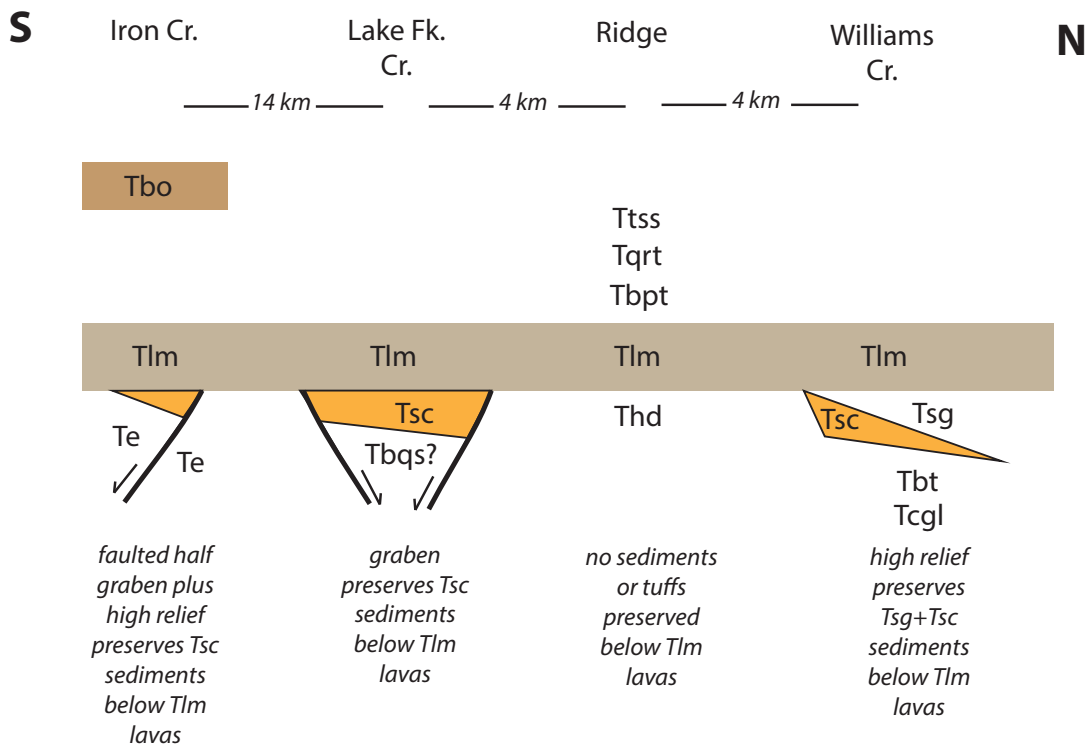

Figure 2. Schematic south to north stratigraphic sections showing restricted extents of some Challis Volcanic Group units in separate basins. In contrast, the mafic lava unit (Tlm) is widespread.

lavas and sediments at different localities demonstrates that the faults were not active at the same time and therefore did not preserve the same tuff. Lack of sediments intercalated with the tuffs suggests very rapid, almost collapse-like activity on the faults.

After this period of intense intermediate to silicic volcanic and fault activity ended, Tsc was deposited in fault-bounded basins at Lake Creek and Iron Creek and a topographic low at Williams Creek. This was in turn followed by a stable erosional period that largely leveled the topography and allowed development of a large river system capable of carrying the Mesoproterozoic granite boulders of Tsg southeast across Lemhi Pass. The leveled topography also allowed subsequent volcanic activity, now mafic in character, to blanket the low-relief surface with Tlm. The next phase of volcanic activity was eruption of intermediate to silicic magmas and deposition of the tuffs above the Tlm that are preserved along Napias Creek and on the ridge between Lake Fork and Williams Creeks. Perhaps the evacuation of large volumes of volcanic material from magma chambers high in the crust to produce the tuffs led to the intense faulting, while the mafic lavas, being generated at deeper levels, were erupted without notable accompanying fault activity.

This road log is an outgrowth of geologic mapping at 1:24,000 scale by the Idaho Geological Survey (IGS). Published maps along the route include the following quadrangles: Salmon (Lewis and others, 2012), Williams Lake (Lewis and others, 2013), Lake Mountain (Stewart and others, in press), and Cobalt (Lewis and others, 2021). All are available for free download from the IGS website (https://idahogeology.org/). For a discussion of the regional Tertiary stratigraphy of the Salmon area, see Burmester and others (2016).

ROAD LOG

Set odometer to zero at the junction of Highways 93 and 28 in Salmon and proceed south on Highway 93 to mile 5.2 and junction of Williams Creek Summit Road 021. Turn right (west) onto Road 021 and immediately cross the Salmon River on the Shoup bridge, named for George Shoup, a Salmon resident and Idaho's first Governor. At 6.0 mi Road 021 turns left (south) and Perreau Creek Road 027 joins from the west. Park in the large parking area immediately west of the junction of 021 and 027 for Stop 1.

STOP 1—6.0 mi
VIEW OF SALMON RIVER TERRACES

(45.0986°N; 113.9100°W)

Alluvial gravel terraces and remnants of terraces are common along the Lemhi and Salmon Rivers, forming a sequence of terraces that are 3–180 m (10–600 ft) above present-day streams. At this stop, older Perreau Creek alluvial fan deposits bury gravels of the second terrace, which were deposited by the Salmon River during the Pleistocene. Commonly, the mainstream gravels interfinger with and are overlain by fan gravels

wherever major tributaries have built alluvial fans into the valley. Across the floodplain from here, the first terrace is extensive, widening northward into the city of Salmon. The airport is on the second terrace just above a low alluvial scarp.

South of here a few remnants of higher terraces occur along the west edge of the valley. Remnants of the highest terrace form the low ridge viewed across the Salmon River valley 4 km (2.5 mi) northeast (beyond the airport). The high terrace gravels rest unconformably on fine-grained sediments of the late Eocene–Oligocene siltstone of Wimpey Creek. Only scattered remnants of this highest terrace are known, and their distribution suggests that when those gravels were deposited, the stream valley geometry was similar to that of today. Well logs and exposures show that the Quaternary alluvial gravel deposits do not constitute a thick valley fill. On the contrary, the gravel deposits are relatively thin, typically only a few meters (up to 30 ft) thick, which is consistent with stepwise downcutting during the Quaternary.

Continue south on Road 021, passing Williams Lake Road 028 coming in from the left on a right-hand bend, then continue on 021 westward to mile 9.8 and park in a large pullout on the right for Stop 2.

STOP 2—9.8 mi
BIOTITE–PLAGIOCLASE TUFF (Tbpt)

(45.0822° N, 113.9657° W)

The biotite–plagioclase tuff occurs relatively high in the Challis volcanic section (fig. 1), above the mafic lavas (Tlm). It is a pinkish, crystal-rich, mostly densely welded tuff. At this locality look for flow-banding, dense, "vitrophyric" specimens, and vapor-phase alteration in the form of lithophysae or spherulites.

Continue west up Road 021 to mile 12.2 and the junction with the South Fork of Williams Creek and junction with Road 028. Turn left (south) on Road 028 and continue to mile 13.2 and pull out on the left for Stop 3.

STOP 3—13.2 mi
BRICK TUFF (Tbt)

(45.0677° N; 114.0212° W)

The brick tuff is the lowest tuff exposed along Williams Creek; its base is only exposed at our Stop 5, where it rests gradationally on conglomerates with volcanic clasts and matrix (Tcgl). Low content of very small crystals, sparse small (1 mm) pumice, and numerous small voids that give the rock a low-density "brick-like" feel characterize this unit.

Continue south up Road 028 to mile 13.9 and pull out on the right for Stop 4 just before a ranch road takes off to the right.

STOP 4—13.9 mi
EPICLASTIC SEDIMENTS AND ASH BEDS WITHIN THE CHALLIS SECTION (Tsc)

(45.0632° N; 114.0314° W)

Walk up the ranch road, through the gate (still on Forest Service land, and the rancher's son is a chum), and then north up the gulch with the white hoodoos (fig. 3). These conglomeratic sandstones, silts, and tuffaceous beds were deposited in an erosional basin on the brick tuff. Plant fossils have been recorded at this site but have not been positively identified or dated.

Turn around and go north back down Road 028 and return to the junction with Road 021 at 15.4 miles. Turn left (west) up Road 021 to mile 15.6 and pull out on the left for Stop 5.

Figure 3. West-dipping Eocene conglomeratic sandstones, silts, and tuffaceous beds at Stop 4.

STOP 5—15.7 mi
BASAL CHALLIS UNCONFORMITY (Ylg + Tcgl)

(45.0780° N; 114.0161° W)

The Mesoproterozoic metasedimentary rocks exposed here were shown as Gunsight Formation (Yg) on the Salmon Forest map of Evans and Green (2003). The IGS has been somewhat more circumspect to date, most recently calling them Lemhi group (Ylg), which is basically anything under the Swauger quartzite. Go up the gulch to the north where you can see the conglomeratic deposits (Tcgl) resting on the Ylg. There may be thin sandstones beneath the conglomeratic material. Note the conglomerate matrix—at some localities it is very rich in plagioclase feldspar, and at others

resembles the brick tuff. Both indicate that these are not pre-Challis but rather initial or basal Challis deposits with volcanic input.

Continue up Road 021 to mile 16.2 and pull out on the right at the base of the first switchback for Stop 6.

STOP 6—16.2 mi
DEBRIS FLOWS (Tcgl) AND JOINTED BASAL BRICK TUFF (Tbt)

(45.0779° N; 114.0256° W)

The cliffs both north and south of the road here expose debris flows (lahars?) with clasts of Ylg and matrix with volcanic affinities. The debris flows grade upward into vertically jointed brick tuff, which caps the cliffs to the north. These deposits are only found at this one locality, and do not contain clasts of Mesoproterozoic rapakivi granite that characterize younger deposits that we will examine at the next stop.

Continue up the switchbacks to mile 16.8 and turn right at a sign that says "Trail Access." Proceed 120 m (400 ft) to a turnaround at mile 17.0 and Stop 7.

STOP 7—17.0 mi
GRANITE-BEARING SEDIMENTS (Tsg)

(45.0797° N; 114.032° W)

We have already seen two Challis-related sediments, Tsc and Tcgl; now here is a third (Tsg), this one with distinctive boulders and cobbles of Mesoproterozoic rapakivi granite (Ygr) in addition to the more abundant metasedimentary quartzite clasts. Walk north up the gulch for a few minutes to a large Ygr boulder. These sediments rest on the brick tuff, contain Tbt clasts at some localities, and are overlain by Eocene Challis Mafic lavas (Tlm). The closest granite that could be source rock for the boulders is currently exposed 30 km to the northwest near the headwaters of Napias Creek. The Ygr boulder-bearing sediments occur discontinuously from west of Leesburg to Lemhi Pass in the Beaverhead Range, and, while Challis ash-flow deposits below Tlm are generally not continuous laterally and appear to be limited to local, mostly fault-bounded basins, the Ygr-bearing sediments (Tsg) and the Tlm flows above them are encountered quite widely, apparently marking a cessation of basin subsidence following eruption of the brick tuff and its equivalents.

Return to Road 021 and continue west, noticing more Ygr boulders along the way, to mile 18.5 and a left turn at a switchback; pull out on the right at the switchback for Stop 8.

STOP 8—18.5 mi
GRANITE-BEARING SEDIMENTS (Tsg), BRICK TUFF (Tbt), DIKES (Ta), AND BRECCIAS

(45.0858° N; 114.0516° W)

Here we take a short hike north and east, contouring down through Tsg from the switchback and across the creek, crossing it and into a welter of Challis units. First is a volcanic breccia or debris flow that is either beneath the Tbt, and so Tcgl, or within it—we haven't enough exposure to tell. Then uphill to several jointed andesite dikes, brick tuff, and more Tsg.

Continue up Road 021 to Williams Creek Summit.

Williams Creek Summit—22.5 mi.
Turn left and proceed south on ridge Road 020.

Junction with Road 231 coming in from the right at mile 23.2. Continue south on Road 020 for 0.8 mi.

STOP 9—24.0 mi
MAFIC LAVAS (Tlm)

(45.0736° N; 114.0853° W)

Hike north a short distance along the east side of the fence line to see the mafic lava unit. Here it includes some flow breccias, which are common elsewhere too. Regionally the mafic flows contain xenocrystic quartz and plagioclase feldspar crystals; have a look here to see if they are present.

Return to vehicles and return north to Road 231. Turn left. Proceed 5.2 miles, descending to cross Deep Creek, and be stopped at a slide across the road for Stop 10.

STOP 10—5.2 mi from Road 020
COINER NORMAL FAULT

(45.0717° N; 114.1411° W)

Go up the slope to see breccias, altered fault rock, and springs weeping out of the brecciated zone (fig. 4). The Coiner fault here places the banded siltite member of the Mesoproterozoic Apple Creek Formation in the west against the Lake Mountain member of the Apple Creek Formation in the east (Lewis and others, 2021). Fault displacement likely includes an early, right-lateral component based on displacement of the Yab–Yalm contact. Preservation of a Challis tuff on its west side 3 km north of here supports later down-on-the-west displacement. The Coiner fault hosts Cretaceous mineralization at the Beartrack mine 18 km (11 mi) to the north (Lewis and others, 2022).

Figure 4. Breccia and altered fault rock along the Coiner fault west of Deep Creek. Road 231 (on left) has been abandoned beyond this point because of a slide.

ACKNOWLEDGMENTS

A manuscript review by Russ Burmester is greatly appreciated. Liam Knudsen kindly drafted the geologic map.

REFERENCES

Burmester, R.F., Lewis, R.S., Othberg, K.L., Stanford, L.R., Lonn, J.D., and McFaddan, M.D., 2016, Geologic map of the western part of the Salmon 30 x 60-minute quadrangle, Idaho and Montana: Idaho Geological Survey Geologic Map 52, scale 1:75,000.

Evans, K.V., and Green, G.N. 2003, Geologic map of the Salmon National Forest and vicinity, east-central Idaho: U.S. Geological Survey Geologic Investigations Series Map I-2765, 19 p., scale 1:100,000.

Lewis, R.S., Othberg, K.L., Burmester, R.F., Stanford, L.R., McFaddan, M.D., and Lonn, J.D, 2012, Geologic map of the Salmon quadrangle, Lemhi County, Idaho: Idaho Geologic Survey Digital Web Map 154, scale 1:24,000.

Lewis, R.S, Othberg, K.L., McFaddan, M.D., Burmester, R.F., Stewart, D.E., Stanford, L.R., and Stewart, E.D., 2013, Geologic map of the Williams Lake quadrangle, Lemhi County, Idaho: Idaho Geological Survey Digital Web Map, in preparation, scale 1:24,000.

Lewis, R.S., Burmester, R.F., Stewart, D.E., and Canada, A.S., 2021, Geologic map of the Cobalt quadrangle, Lemhi County, Idaho: Idaho Geologic Survey Digital Web Map 199, scale 1:24,000.

Lewis, R.S., Stewart, D.E., Burmester, R.F., Tkach, M.K., and Canada, A.S., 2022, Geologic map of the Jureano Mountain and Leesburg quadrangles, Lemhi County, Idaho: Idaho Geological Survey Digital Web Map 207, scale 1:24,000.

Stewart, D.E., Lewis, R.S, Burmester, R.F., Lonn, J.D., McFaddan, M.D., Tkach, M.K., and Canada, A.S., in press, Geologic map of the Lake Mountain quadrangle, Lemhi County, Idaho: Idaho Geological Survey Digital Web Map, scale 1:24,000.

MESOPROTEROZOIC TO TERTIARY GEOLOGY FROM SALMON IDAHO TO THE BEARTRACK MINE

Reed S. Lewis, Russell F. Burmester, David E. Stewart, and Liam D. Knudsen

Idaho Geological Survey, Moscow, Idaho

INTRODUCTION

The road from Salmon to the Beartrack mine traverses the eastern part of the Salmon River Mountains and provides numerous easily accessible road cuts (fig. 1). The oldest rocks are Mesoproterozoic metasedimentary of the Belt Supergroup that were intruded by a bimodal suite that includes A-type granites and mafic rocks. They are intruded by Cambrian and Ordovician syenitic plutons and overlain by Eocene volcanic and sedimentary rocks of the Challis Volcanic Group. The volcanic rocks, which dominate the group, are interbedded with and overlain by sedimentary rocks that vary from cobble–boulder conglomerate to silt. Two major fault systems transect the area. The Poison Creek fault history includes Cretaceous thrusting that recovered only some of the fault's earlier normal motion. The north–south Coiner and Rabbit Creek faults offset the Poison Creek fault in an apparent right-lateral sense and are also responsible for a small Eocene or younger basin developed by down-to-the-west faulting in the Napias Creek area, immediately south of the Beartrack mine. Mineralization at the mine is Cretaceous, as is mineralization at the Arnett Creek syenitic suite 2–8 km to the west.

This road log is an outgrowth of geologic mapping at the 1:24,000 scale by the Idaho Geological Survey (IGS). Published maps along the route include the following quadrangles: Salmon (Lewis and others, 2012), Williams Lake (Lewis and others, in prep.), Lake Mountain (Stewart and others, in press), Cobalt (Lewis and others, 2021), and Jureano and Leesburg (Lewis and others, 2022). All are available for free download from the IGS website (https://idahogeology.org/). For a regional discussion of the Mesoproterozoic stratigraphy of the Salmon area, see Burmester and others (2016b).

ROAD LOG

Field trip stops are referenced to GPS coordinates (WGS84), and with mileage at stops noted. The trip starts at the Sacajawea Interpretive, Cultural and Educational Center parking lot exit on E. Main St. (Hwy 28) in Salmon. Turn right (NW) and go 1.2 mi to a left turn at the traffic light at the intersection with S. Challis St. (US Highway 93). Head south past the BLM–USFS complex and the Salmon Airport (both on the left) to a right turn across the Salmon River on Shoup Bridge.

6.4 mi Reset odometer at the right turn. Figure 1 shows the route, stops, and points of interest mentioned in this log, starting here.

0.1 mi Cross the Salmon River on the one-lane Shoup Bridge. Drive due west, climbing up onto older alluvial fan deposits at about 0.8 mi to a Y intersection. Park on the right just as the road turns south.

STOP 1—0.8 mi
SALMON BASIN OVERVIEW

(45.0986°N, 113.9100°W)

Take the left fork and follow the paved road as it winds south to southwest for about 1.6 mi over terrace gravels and Tertiary sediments before a right bend to the west.

2.4 mi Williams Lake Road takes off to the left. Continue west on NF 021 up Williams Creek into east-dipping biotite–plagioclase tuff of the Challis Volcanic Group.

STOP 2—4.5 mi
CHALLIS VOLCANIC GROUP

(45.0821°N, 113.9657°W)

Near the end of the long straight road segment, we crossed a thin deposit of mafic lava (Tlm 1), which here is the lowest unit of the Challis section. It is thicker on the ridge to the north where it overlies a black quartzite lithic tuff correlated with a thicker section of lithic-rich tuff in Withington Creek, 9 mi to the east–southeast. From the ridge to this point, the overall dip of the base of the Challis is little more than 10°, less than the 20° dip measured on vesicular basalt on the ridge. Above the mafic lava (and in talus here) is a pink biotite–plagioclase tuff.

Here we originally mapped the rock below the Challis as "siltite and quartzite" (Ysq) instead of assigning it a formal name (Lewis and others, in prep.). Later we assigned it to the Gunsight Formation of the Lemhi Group (Burmester and others, 2016a). Most recently we have taken a more conservative approach and now call it the Lemhi Group, undivided. The talus provides a good sampling of rock types that are up the hill, and

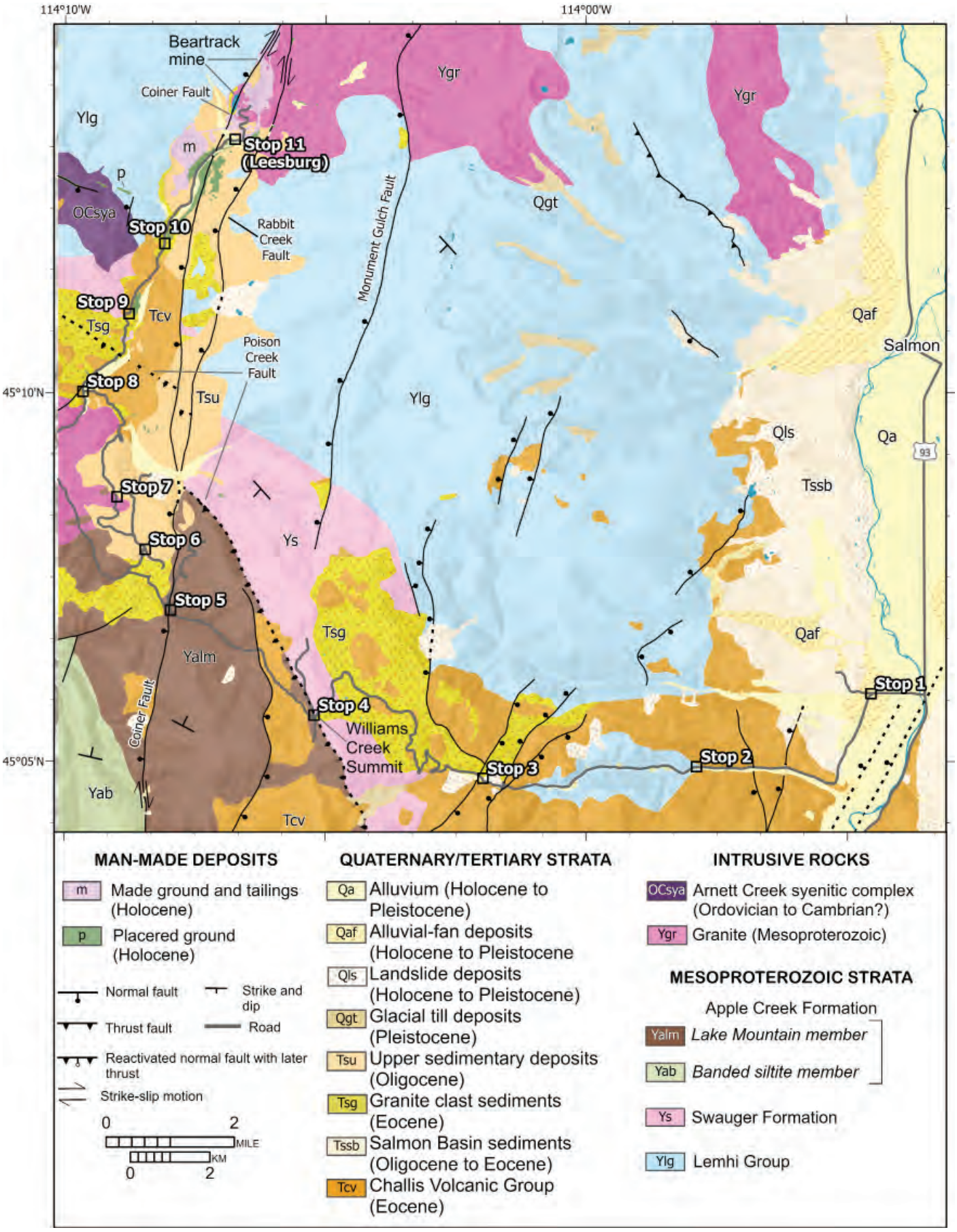

Figure 1. Geologic map of the Salmon River Mountains in the vicinity of Williams Creek Summit and the Beartrack mine. Map is annotated with field trip stop locations.

folded rocks are in place a short walk up the road to the west.

6.3 mi **Optional Stop**
(45.0813°N, 14.0009°W) Cross longitude 114° W. This gets us onto the Leesburg 15' quadrangle where Swauger (Ys) and Ysq were mapped as Big Creek (Yb) and the upper part of the upper Yellowjacket (Yyuu) Formations, respectively (Conner and Evans, 1986).

7.0 mi Pass the fork up the South Fork Williams Creek.

7.7 mi First set of short switchbacks. Continue to 8.4 mi where a two-track road takes off to the right to a trailhead. Park on the right.

STOP 3—8.4 mi
WILLIAMS CREEK OVERVIEW

(45.0795°N, 114.0339°W)

Hike east to top of small hill overlooking the valley below: 45.0793°N, -114.0299°W.

The lowermost rocks in the view downstream are quartzite and siltite of the Lemhi Group. Well-indurated conglomerate (lowermost Challis Volcanic Group) is visible directly to the east and along the sides of the Williams Creek canyon south of the creek. A close-up view is shown in figure 2. Importantly, clasts consist entirely of Proterozoic metasedimentary rock; no Mesoproterozoic granite or Eocene volcanic clasts are present. The conglomerate is discontinuous here and not widespread regionally. The lowermost volcanic unit here is rhyolite tuff (quartz–sanidine "brick" tuff), seen here to the left of, and in fault contact with, the conglomerate. Above this is poorly indurated and poorly sorted matrix-supported cobble and boulder conglomerate characterized by conglomeratic sandstone to siltstone matrix with non-imbricated and typically subrounded to subangular clasts of quartzite and less abundant clasts up to boulder size of Mesoproterozoic granite. Some of these boulders are visible on the hillside to the northwest and along the road toward Williams Creek Summit. At the Beartrack mine, the uppermost part of Tsg contains a biotite tuff dated at 48.30 ± 0.06 Ma (Lewis and others, 2022). To the south, sediments of likely similar age, but different provenance (no granite clasts) are present. These consist of poorly to moderately consolidated mudstone, siltstone, and conglomeratic sandstone with intercalated debris flows, ash beds, and minor thin tuffs or mafic lava flows. Plant fossils are present locally. Notably, no outcrops of Mesoproterozoic granite are present in the upper Williams Creek drainage. The nearest potential source is 11.5 km (7 mi) to the northwest (at Stop 7) over the divide between Williams Creek and the Panther Creek drainage. Granite boulders can be traced to a narrow gap in the ridge 3.2 km (2 mi) north–northeast of Williams Creek Summit, where they are overlain by the mafic lavas. Down-on-the-west faulting west of the divide has now cut off the source area. The same conglomerate with distinctive Mesoproterozoic granite boulders can be traced across the Beaverhead Range at Lemhi Pass and is a remnant of an Eocene river system that fed into Montana prior to the Oligocene downdropping of the Salmon basin (Janecke and others, 2000).

The uppermost Challis strata visible here are mafic lava flows, which cap the ridge to the southeast. These are characterized by red-weathering, mostly andesitic lava flows that are sparsely porphyritic to aphyric with less than 5 percent phenocrysts of pyroxene and olivine. The lower part consists mostly of flows characterized by partially resorbed xenocrystic quartz and xenocrystic plagioclase with reaction rims. Top not exposed here, but to the southeast near Williams Lake rhyolitic units overlie the mafic lavas. These lavas are the most widespread and voluminous unit in the Challis Volcanic Group and are likely correlative with the latite unit mapped by Blankenau (1999) in the Lemhi Pass

Figure 2. Conglomerate at the base of the Challis Volcanic Group on the north side of Williams Creek.

area and the Tl unit of potassium-rich andesite, latite, and basalt lava in the Challis 1° x 2° quadrangle to the southwest (Fisher and others, 1992). At Lemhi Pass the mafic lava flows cap the conglomerate that contains Mesoproterozoic boulders, the same relationship as found north of Williams Creek Summit.

Return to vehicles and continue west toward Williams Creek Summit.

8.9 mi Williams Creek Picnic Site on left.

9.3 mi Switchback to right.

9.8 mi Switchback to left.

10.3 mi Switchback to right at Cougar point. Exposures in the cliffs southwest of the road consist of sericitic quartzite, lighter in color and coarser grained than anything we passed on the way. The coarser grain size is characteristic of the Swauger Formation, and we are now near the southeastern end of the Swauger exposures within the Williams Creek Summit block. See Burmester and others (2013) for a detailed discussion of this locality.

10.4 mi Entrance to Cougar Point Campground on right. Exposures in the next few miles are poor but we are traversing through the Challis Volcanic Group consisting here of sedimentary deposits containing boulders of Mesoproterozoic granite, overlying mafic lavas, and underlying quartz–sanidine rhyolite "brick" tuff.

13.0 mi After a sharp left there is an east-facing steep slope and road cut on the right. There is little rock in place, but the float here has medium round quartz grains and some pink grains that are typical of the Swauger Formation in the Beaverhead Mountains and Lemhi Range.

Proceed to Williams Creek Summit (13.7 mi). Turn right and follow NF road 020 0.1 mi and pull out on the right at the outhouse.

STOP 4—13.7 mi
RESTROOM STOP AND THE POISON CREEK FAULT

(45.0938°N, 114.0879°W)

The quartzite at Williams Creek Summit and to the north on Phelan Mountain has been mapped as Ordovician Kinnikinic Formation (Shockey, 1957), Big Creek Formation (Conner and Evans, 1986), and Swauger Formation (Evans and Green, 2003). We side with the Swauger call because in comparison with published descriptions and what we have seen elsewhere, it is too coarse to be Big Creek Formation and too poorly sorted to be Kinnikinic. It also contains minor amounts of feldspar locally, a characteristic not typical of the Kinnikinic.

Reset odometer at Williams Creek Summit and continue west on NF Road 021. Road soon crosses from Lake Mountain member of the Apple Creek Formation into mafic lavas of the Challis Volcanic Group. A down-on-the-east normal fault at 1.5 mi brings the Lake Mountain member back up. Dark (biotite-rich) talus for the next 2 mi is fine-grained feldspathic quartzite, characteristic of this unit. The quartzite is generally fine grained and well sorted. The unit is named after Lake Mountain about 8 km (5 mi) south of Williams Creek Summit. Previously included in upper unit of the Yellowjacket Formation by Conner and Evans (1986), and Gunsight Formation of the Salmon River Mountains by Tysdal (2003) and Evans and Green (2003).

2.8 mi Y intersection; take the right fork, staying on NF Road 021. The left fork is truck route to Deep Creek and Panther Creek (NF Road 101).

3.0 mi Park on right and walk northwest along the road to roadcuts ahead.

STOP 5—3.8 mi
COINER FAULT

(45.1175°N, 114.1337°W)

Brecciated quartzite of the Lake Mountain member of the Apple Creek Formation in roadcut. Better exposures are visible in an abandoned USFS quarry a bit to the north and up the hill (45.1194°, -114.1343°). American Gold Resources Corporation used the term Coiner fault during their exploration work in the late 1980s for a north–northeast fault with this orientation (Watts, Griffis, and McOuat Limited, 1989, p. 35) and the fault was also shown on the map of Conner and Evans (1986). Fault displacement likely includes an early, right-lateral component based on displacement of contacts between Mesoproterozoic units. Preservation of boulder-rich sediments and volcanics of the Eocene Challis Volcanic Group on its west side support later down-on-the-west displacement. A stroll back toward the intersection with the truck route road provides a look at float of the Lake Mountain member of the Apple Creek Formation.

Continue NNW toward Napias Creek.

3.7 mi Road down Moccasin Creek (FS 076) turns off to the left; continue north on FS098 toward Napias Creek.

4.3 mi Pullout on left and park opposite tan roadcut.

STOP 6—4.3 mi
OLIGOCENE ASH

(45.1312°N, 114.1418°W)

Massive tan mudstone capped by light-gray ash (fig. 3). Locally contains minor sandstone and conglomerate and local pebble–cobble lag. Conglomeratic intervals are largely in the upper part of unit and some of these have been placered for gold. Also present in several drill holes south of the Beartrack mine and exposed in a roadcut along Napias Creek 0.7 mi southwest of Leesburg (mile 12.3). Mudstone likely has major tuffaceous component. Like at this locality, a light-gray ash bed within the mudstone is exposed along an old logging road on the south side of Phelan Creek, 1 km (0.6 mi) northeast of this stop. Four of five zircons from this ash bed, dated by CA-TIMS methods, yielded a weighted average age of 32.19 ± 0.02 Ma (Lewis and others, 2022). Drillcore data from south of the Beartrack mine indicate an approximate thickness of 50 m (170 ft).

Continue NW toward Napias Creek.

5.8 mi Pullout on right; walk back along the road to the first roadcuts of granite.

STOP 7—5.8 mi
MESOPROTEROZOIC GRANITE

(45.1431°N, 114.1509°W)

This locality shows medium- to coarse-grained, variously porphyritic granite. Regionally this unit contains megacrysts 3 to 8 cm in length, typically blocky or ovoid (ellipsoidal granite) or deformed into variously elongate augen. Some are entirely microcline, while others are microcline rimmed with albite (rapakivi texture). Spheroidal weathering of outcrops is common, typically producing coarse grus with intact microcline phenocrysts. Zircons from a Ygr outcrop along Moose Creek about 10 km (6 mi) to the north–northeast of Leesburg yielded a weighted average age of 1359 ± 7 Ma from 11 of 12 SHRIMP analyses (Aleinikoff and others, 2012, locality D). Zircons from that same outcrop had previously yielded a TIMS age of approximately 1367 Ma (Evans and Zartman, 1988).

Figure 3. Oligocene ash (light-colored horizon) in silt-rich sediments along the road into Napias Creek.

Continue northwest and at 8.3 mi cross bridge over Napias Creek and pull out on either side of road.

STOP 8—8.4 mi
CHALLIS VOLCANIC GROUP ALONG NAPIAS CREEK

(45.1669°N, 114.1618°W)

Two units of the Challis Volcanic Group are accessible from this stop. Exposures west of the creek are pumice-rich dacite tuff with conspicuous light-colored, well-flattened pumice lapilli as much as 4 cm in length. Small sparse phenocrysts consist of light-colored blocky plagioclase, pyroxene, black tabular hornblende, largely altered pseudohexagonal biotite, and rare quartz. Groundmass is welded ash and lapilli. Lithics are angular, as much as 1 cm across, and primarily consist of dark fine-grained feldspathic quartzite with lesser volcanic fragments. Average magnetic susceptibility from two exposures and two hand samples was 1.71×10^{-3} SI (Lewis and others, 2022). Thickness 365 m (1,200 ft) or less. Walk east of the creek and back up the road to a black to dark-gray olivine basalt lava flow. Phenocrysts here consist of olivine along with minor plagioclase and pyroxene. As much as 50 m (165 ft) thick. Sample collected here is basalt (49.45 percent SiO_2; Lewis and others, 2022). A sample collected to the north near the mouth of Arnett Creek had relatively high magnetic susceptibility (18×10^{-3} SI). Unit thickness is likely less than 30 m (100 ft).

Continue north along Napias Creek (FS242) and at 10.7 mi park on right opposite light-colored roadcut and prior to left turn in road.

STOP 9—10.0 mi
LITHIC TUFF ALONG NAPIAS CREEK

(45.1844°N, 114.1471°W)

White to light-gray ash-flow tuff with sparse but distinctive small, dark-gray lithics (fig. 4). Light-gray pumice lapilli are typically not flattened. Lithics are 1 to 5 mm, subangular to angular, and 80 percent are of

Figure 4. Lithic tuff of the Challis Volcanic Group along Napias Creek. U-Pb zircon age of 49.2 Ma (Richard Gaschnig, written commun., 2023).

dark Mesoproterozoic feldspathic quartzite to siltite with the remaining 20 percent of light-colored quartzite or rare volcanic fragments. The unit is massive with very faint welding horizons. A U-Pb zircon age of 49.2 Ma was determined using laser-ablation ICP-MS techniques (Richard Gaschnig, written commun., 2023). As much as 275 m (900 ft) thick.

Continue north along Napias Creek and at 12.1 mi park on right, opposite roadcut with large boulders.

STOP 10—11.3 mi
EOCENE BOULDER CONGLOMERATE ALONG NAPIAS CREEK

(45.2003°N, 114.1357°W)

This roadcut exposes Eocene sedimentary deposits with distinctive granite clasts identical to those found east of Williams Creek Summit near Stop 3. Here the deposits are poorly indurated and matrix-supported. At depth in drillcore, they are slightly more indurated. Characterized by very poorly sorted, non-imbricated, and typically angular to subangular clasts of quartzite (Ylg) and less abundant clasts of granite (Ygr) up to boulder size (fig. 5). Previously mapped as glacial deposits (Shockey, 1957). Conglomeratic sandstone to siltstone matrix. Locally contains abundant woody debris, notably near the mouth of Missouri Gulch and in several of the drill holes south of the Beartrack mine. The upper part of unit contains a biotite tuff approximately 8 m (25 ft) thick that is only recognized in core from southwest of the Beartrack mine. Zircons from this tuff, dated by CA-TIMS methods, have a weighted average age of 48.30 ± 0.02 Ma from 4 of 7 analyses (Lewis and others, 2022). Conglomeratic intervals are interpreted to be debris flows based on poor sorting, amount of matrix, and large clast size. Drillcore data indicate an apparent thickness of 180 m (600 ft). True thickness may be as much as 550 m (1,800 ft) locally.

11.8 mi Road up Arnett Creek enters from left. Ordovician syenite of the Arnett Creek syenitic complex is exposed along this road.

12.3 mi Silt-rich sediments, likely Oligocene.

13.1 mi Road to left leads to a gate, beyond which is the Beartrack tailing pile and heap leach pads. Continue to mile 13.5. Park in Leesburg viewpoint area on left and check out the signage for Leesburg.

STOP 11—13.5 mi
LEESBURG VIEWPOINT

(45.2239°N, 114.1133°W)

Gold placer deposits are widespread along and east of Napias Creek as well as in the Arnett Creek drainage. The initial discovery was along Napias Creek at the mouth of Ward Gulch, just east of Leesburg, in 1866 (Umpleby, 1913; Lorain and Metzger, 1939). A gold rush followed, and the population of Leesburg reached

Figure 5. Poorly consolidated Eocene sediments along Napias Creek. Note the large Mesoproterozoic granite boulders. Mistaken for glacial deposits by earlier mappers.

about 2,000 in 1867 before dropping to 180 in 1870 (Wells, 1983). Placer gold constituted most of the production, although O.E. Kirkpatrick, who arrived in 1898, operated a ten-stamp mill near Wards Gulch on and off for 40 years to process lode gold from veins. That mill site was later engulfed by the Beartrack open-pit mine. Placer operations up through the 1930s are described in detail by Lorain and Metzger (1939). Shockey (1957) noted that the richest placer gold occurs in the lower few feet of coarse gravels that overlie the Tertiary "ash deposits" here mapped as Tsu. The gravels he referred to are relatively thin (a few tens of feet at most) and in the uppermost part the Tsu unit.

The Beartrack open-pit gold mine, north of Leesburg, operated between 1994 and 2000. Remnants of the mining activity include the south pit, now partly filled with water (fig. 6), and the largely reclaimed north pit. Robert Perry with Canyon Resources discovered the bulk-mineable Beartrack mine in 1984 (Perry and Childs, 2003; Bookstrom and others, 2013). Mining produced over 609,000 oz of gold (Revival Gold, 2020). Exploration at depth and south along strike of the ore zone has continued since mining ceased, most recently by Revival Gold Inc., who commenced diamond drilling in 2018. That exploration work is ongoing. See Priesmeyer and others (this volume) for additional information on the Beartrack mine and the Arnett Creek project just to the west.

Return to Salmon.

ACKNOWLEDGMENTS

The authors would like to thank Russ Di Fiori for a review of the manuscript.

Figure 6. View looking north of the Beartrack mine from above the mouth of Arnett Creek. The south pit is in the distance and the tailings pile from the heap-leach operation is on the left.

REFERENCES

Aleinikoff, J.N., Slack, J.F., Lund, K., Evans, K.V., Fanning, C.M., Mazdab, F.K., Wooden, J.L., and Pillers, R.M., 2012, Constraints on the timing of Co-Cu ± Au mineralization in the Blackbird district, Idaho, using SHRIMP U-Pb ages of monazite and xenotime plus zircon ages of related Mesoproterozoic orthogneisses and metasedimentary rocks: Economic Geology, v. 107, p. 1143–1175.

Blankenau, J.J., 1999, Cenozoic structural and stratigraphic evolution of the southeastern Salmon basin, east-central Idaho: Logan, Utah, Utah State University, M.S. thesis, 143 p., 3 plates.

Bookstrom, A., King, G., Perry, R., and Childs, J., 2013, Field guide to selected sites along the Idaho cobalt belt (ICB) and to the Beartrack gold deposit, in the eastern Salmon River Mountains, *in* Lewis, R.L., Garsjo, M.M., and Gibson, R.I., eds., Belt Symposium V and other papers, 38th Annual Tobacco Root Geological Field Conference: Northwest Geology, v. 42, p. 163–186.

Burmester, R.F., McFaddan, M.D., Lewis, R.S., and Lonn, J.D., 2013, What's the Swauger Formation doing in the eastern Salmon River Mountains, Idaho?: Northwest Geology, v. 42, p. 197–198.

Burmester, R.F., Lewis, R.S., Othberg, K.L., Stanford, L.R., Lonn, J.D., and McFaddan, M.D., 2016a, Geologic map of the western part of the Salmon 30 x 60-minute quadrangle, Idaho and Montana: Idaho Geological Survey Geologic Map 52, scale 1:75,000.

Burmester, R.F., Lonn, J.D., Lewis, R.S., and McFaddan, M.D., 2016b, Stratigraphy of the Lemhi subbasin of the Belt Supergroup, *in* MacLean, J.S., and Sears, J.W., eds., Belt Basin: Window to Mesoproterozoic Earth: Geological Society of America Special Paper 522, p. 121–137.

Connor, J.J., and Evans, K.V., 1986, Geologic map of the Leesburg Quadrangle, Lemhi County, Idaho: Geological Survey Miscellaneous Field Studies Map MF-1880, 19 p., scale 1:62,500.

Evans, K.V., and Green, G.N., 2003, Geologic map of the Salmon National Forest and vicinity, east-central Idaho: U.S. Geological Survey Geologic Investigations Series Map I-2765, 19 p., scale 1:100,000.

Evans, K.V., and Zartman, R.E., 1988, Early Paleozoic alkalic plutonism in east-central Idaho: Geological Society of America Bulletin, v. 100, p. 1981–1987.

Fisher, F.S., McIntyre, D.H., and Johnson, K.M., 1992, Geologic map of the Challis quadrangle, Idaho: U.S. Geological Survey Miscellaneous Investigations Series Map I-1819, scale 1:250,000.

Janecke, S.U., VanDenburg, C.J., Blankenau, J.J., and M'Gonigle, J.W., 2000, Long-distance longitudinal transport of gravel across the Cordilleran thrust belt of Montana and Idaho: Geology, v. 28, no. 5, p. 439–442.

Lewis, R.S., Othberg, K.L., Burmester, R.F., Stanford, L.R., McFaddan, M.D., and Lonn, J.D, 2012, Geologic map of the Salmon quadrangle, Lemhi County, Idaho: Idaho Geologic Survey Digital Web Map 154, scale 1:24,000.

Lewis, R.S, Othberg, K.L., McFaddan, M.D., Burmester, R.F., Stewart, D.E., Stanford, L.R., and Stewart, E.D., in prep., Geologic map of the Williams Lake quadrangle, Lemhi County, Idaho: Idaho Geological Survey Digital Web Map, scale 1:24,000.

Lewis, R.S., Burmester, R.F., Stewart, D.E., and Canada, A.S., 2021, Geologic map of the Cobalt quadrangle, Lemhi County, Idaho: Idaho Geologic Survey Digital Web Map 199, scale 1:24,000.

Lewis, R.S., Stewart, D.E., Burmester, R.F., Tkach, M.K., and Canada, A.S., 2022, Geologic map of the Jureano Mountain and Leesburg quadrangles, Lemhi County, Idaho: Idaho Geological Survey Digital Web Map 207, scale 1:24,000.

Lorain, S.H., and Metzger, O.H., 1939, Reconnaissance of placer-mining districts in Lemhi County, Idaho: U.S. Bureau of Mines Information Circular 7082, 81 p.

Perry, R.V., and Childs, J.F., 2003, On the way to Beartrack (Parts I-II), *in* Lageson, D.R, and Christner, R.B., eds., 2003, Tobacco Root Geological Society Field Conference at the Belt Symposium IV: Northwest Geology, v. 32, p. 86–92.

Priesmeyer, S.T., Pace, D., and Cameron, E., this volume, Revival Gold's Beartrack–Arnett project: Orogenic gold in Idaho.

Revival Gold, 2020, Press Release: Revival Gold delivers substantial resource increase at Beartrack–Arnett, February 3, 2020, available at https://revival-gold.com/ [Accessed February 18, 2020].

Shockey, P.N., 1957, Reconnaissance geology of the Leesburg quadrangle, Lemhi County, Idaho: Idaho Bureau of Mines and Geology Pamphlet 113, 42 p.

Stewart, D.E., Lewis, R.S, Burmester, R.F., Lonn, J.D., McFaddan, M.D., Tkach, M.K., and Canada, A.S., in press, Geologic map of the Lake Mountain quadrangle, Lemhi County, Idaho: Idaho Geological Survey Digital Web Map, scale 1:24,000.

Tysdal, R.G., 2003, Correlation, sedimentology, and structural setting, upper strata of Mesoproterozoic Apple Creek Formation and lower strata of Gunsight Formation, Lemhi Range to Salmon River Mountains, east-central Idaho, *in* Tysdal, R.G., Lindsey, D.A., and Taggart, J.E., Jr., eds., Correlation, sedimentology, structural setting, chemical composition, and provenance of selected formations in Mesoproterozoic Lemhi Group, central Idaho: U.S. Geological Survey Professional Paper 1668-A, p. 1–22.

Umpleby, J.B., 1913, Geology and ore deposits of Lemhi County, Idaho: U.S. Geological Survey Bulletin 528, 182 p.

Watts, Griffis, and McOuat, Limited, 1989, Review of American Gold Resources Corp. properties, Lemhi County, Idaho: Idaho Geological Survey Mineral Property File MPF-EC1184_006, available at https://idahogeomap.nkn.uidaho.edu/Data/MineDocs/EC1184_006.pdf [Accessed February 18, 2020].

Wells, M.W., 1983, Gold camps & silver cities: Nineteenth century mining in central and southern Idaho: Idaho Geological Survey Bulletin 22, 175 p.

FLOATING THE RIVER: MESOPROTEROZOIC TO QUATERNARY GEOLOGY ALONG THE SALMON DOWNSTREAM FROM ELLIS, IDAHO

Liam D. Knudsen,[1] Reed S. Lewis,[1] Keegan L. Schmidt,[1,2] and David E. Stewart[1]

[1]Idaho Geological Survey, Moscow, Idaho
[2]Lewis-Clark State College, Lewiston, Idaho

INTRODUCTION

The Salmon River from the Deer Gulch boat ramp near Ellis to the Kilpatrick boat ramp flows between the eastern base of the Salmon River Mountains and the western base of the Lemhi Range. The oldest rocks are Mesoproterozoic metasedimentary rocks of the uppermost part of the Belt Supergroup. Along this stretch of river, the Belt Supergroup is overlain by Eocene volcanic rocks of the Challis Volcanic Group. Quaternary landslide and alluvial fan deposits occur along the river and multiple normal faults are crossed while floating downstream. This river log is an outgrowth of in-progress geologic mapping at 1:24,000 scale by the Idaho Geological Survey (IGS).

RIVER LOG

Field trip stops are referenced to GPS coordinates (WGS84), with mileage by river at stops noted. The trip starts at the Deer Gulch Access boat ramp that is about 40 misouth of Salmon, Idaho (1 mi north of the Ellis Post Office) and across the Hat Creek bridge. It continues downstream by river to the Kilpatrick boat ramp. Figure 1 shows stops and illustrates the geology of the trip.

0.0 mi Deer Gulch River Access.

Immediately downstream of the Deer Gulch Access is a small alluvial fan on the right side of the river; Salmon River alluvium is exposed on the left side. The slopes on both sides of the river above the alluvium are underlain by the mafic lava unit of the Tertiary Challis Volcanic Group (fig. 1, Tlm). The mafic lavas range in color from dark gray to dark green-gray and dark brown and consist primarily of aphanitic lava flows. The mafic lavas provide a distinct stratigraphic marker within the Challis volcanics. For this field trip, the Challis volcanics above Tlm are lumped together as Tertiary Challis volcanics upper (fig. 1, Tcvu) and the Challis volcanics below Tlm are lumped together as Tertiary Challis volcanics lower (fig. 1, Tcvl).

North-striking normal faults intersect the river 0.8 and 1.3 mi downstream from the Deer Gulch boat ramp. Could these normal faults be responsible for the broad valley that is visible looking upstream? The valley is within the half-grabens created by sub-parallel normal faults (down to the west). These normal faults brought the relatively soft Challis volcanics down and the erosion-resistant Swauger Formation up. One possible explanation for the topography here is that the river preferentially removed the down-faulted Challis volcanics. Note that as the river enters the Swauger Formation, the canyon steepens and narrows.

1.9 mi Enter Cronks Canyon.

1.9 mi downstream from the boat ramp the river enters Cronks Canyon, a steep canyon with walls of light orange and white quartzite of the Swauger Formation on both sides of the river. The erosionally resistant Swauger Formation quartzite formed a paleo-topographic high in the Eocene, around which Challis volcanic rocks were emplaced. Quartzite of the Swauger Formation commonly contains rounded medium-sized quartz grains and less rounded potassium feldspar grains.

STOP 1—2.9 mi
Swauger Formation

(44.7237°N, 114.0060°W)

After the section of swift water through the top of Cronks Canyon, pull over on the left side of the river to observe the Swauger Formation. Note the low feldspar content that gives the quartzite its clean appearance. Also note the medium grain size and rounded quartz grains (“ball-bearing quartz”). Look for large-scale cross-bedding.

As we drift downstream out of Cronks Canyon, deposits from a large landslide can be seen along the left hillside.

On river right, the contact between the tuff of Ellis Creek (here included at the top of Tcvl) and overlying Tlm can be seen.

4.4 mi View 1. Near Colston Boat ramp.

The Challis volcanics dip eastward. Just upstream on river right the tuff of Ellis Creek at the top of Tcvl can

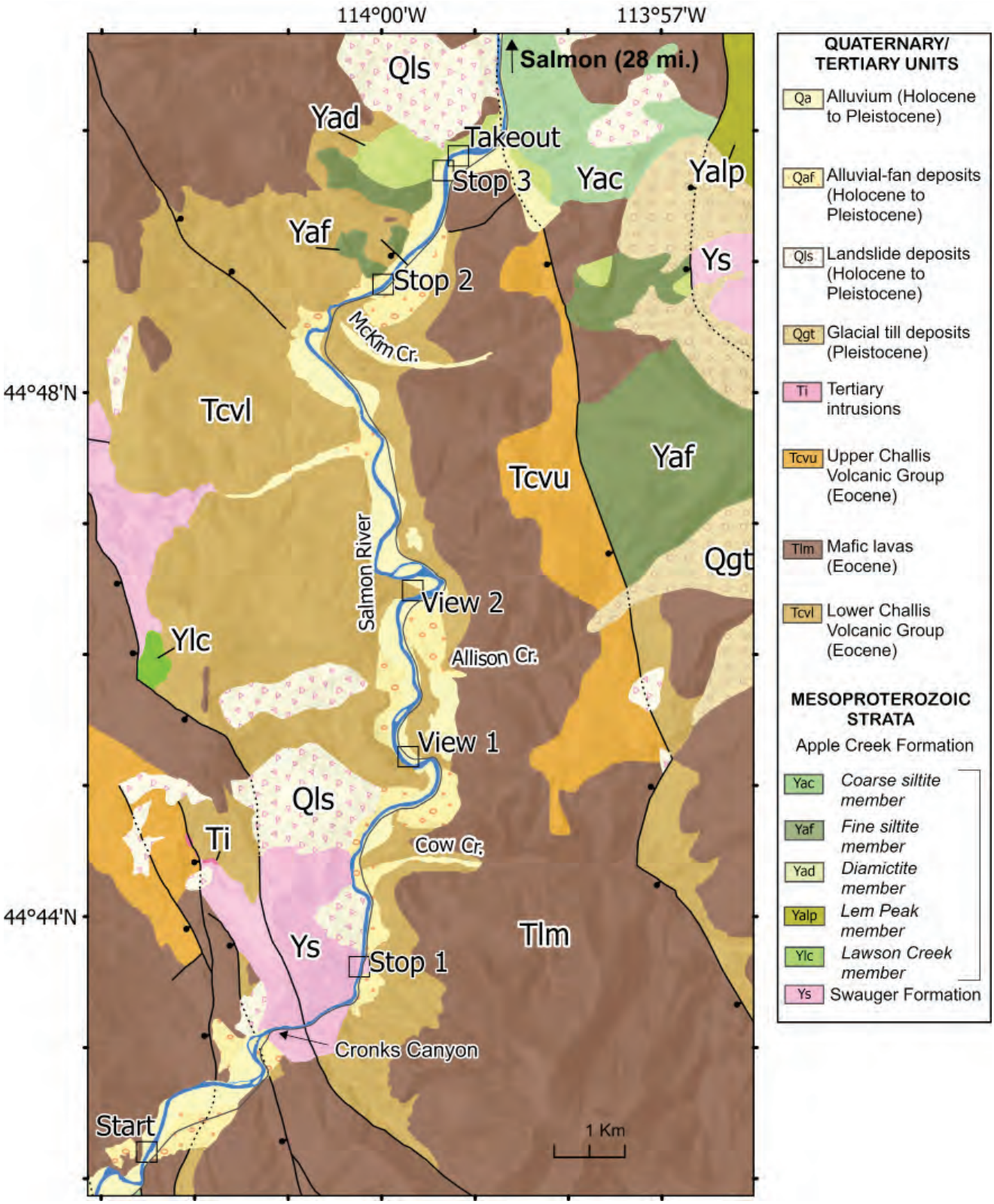

Figure 1. Geologic map of the field trip route showing stops.

be seen once again overlain by mafic lavas (Tlm). The outcrop on river left immediately across from the boat ramp is an autoclastic brecciated lava within Tcvl.

6.0 mi View 2. Lower Challis mixed zone.

On the top of the small ridge on river left a red lava can be seen overlying a lapilli tuff. Both the red lava and lapilli tuff are part of the lower Challis mixed zone unit, here lumped within unit Tcvl. The lower Challis mixed zone is a mixture of mafic and dacitic lavas, flow breccia, and tuffs (Fischer and others, 1992).

STOP 2—10.4 mi
Apple Creek Formation (fine siltite member) and Challis volcanics

(44.8139°N, 114.0004°W)

At river mile 10.4 pull over on the left at the sandy beach within the stand of ponderosa pines. Here we can walk around and observe several rock units. The cliffs above the beach are composed of the fine siltite member of the Apple Creek Formation (fig. 2). The fine siltite member of the Apple Creek Formation is planar-laminated siltite, ripple cross-laminated siltite, and argillite. Beds 1–2 cm thick are commonly graded from siltite upward into argillite (Tysdal, 2003). Within walking distance upstream of the beach are outcrops of the lower Challis mixed zone (Tcvl), including dacite. Farther up the slope above the beach, the contact between the lower Challis mixed zone and the overlying tuff of Ellis Creek can be observed.

Return to the boats for lunch.

Looking downstream from Stop 2, a large quartz vein can be seen as a resistant rib on the left side of the river. This vein, on private property, cuts the fine siltite member of the Apple Creek Formation (fig. 3).

Continue downstream by boat to observe the vein from the river.

At river mile 11.5, rocks of the diamictite member of the Apple Creek Formation are exposed downstream of a small gulch (Ezra Creek). Continue downstream past the private property and pull over on river left to observe the diamictite member at Stop 3.

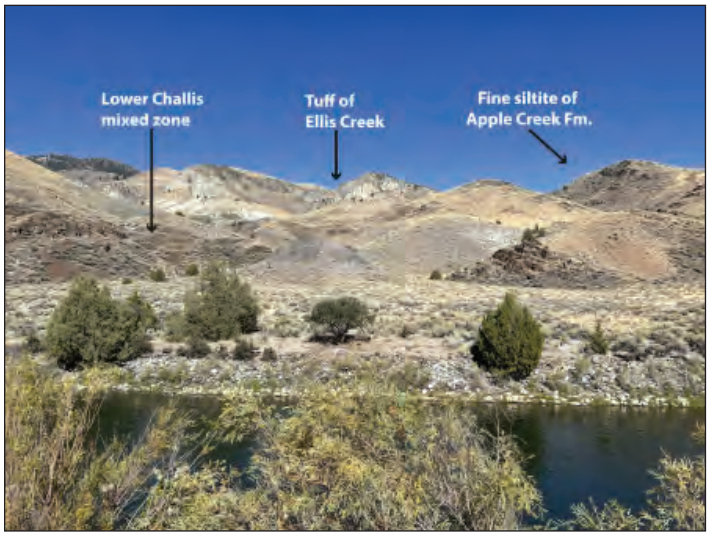

Figure 2. View of left bank of the Salmon River on the upstream side of the beach at lunch stop, showing locations for rocks of lower Challis mixed zone, tuff of Ellis Creek, and fine siltite member of the Apple Creek Formation.

Figure 3. Looking southwest upstream across the river at the quartz vein cutting the fine siltite member of the Apple Creek Formation.

STOP 3—11.6 mi
Apple Creek Formation, diamictite member

(44.830 °N, 113.990 °W)

If desired, walk up the scree slope to observe the diamictite member in outcrop. Alternatively, look at the large talus blocks of diamictite on the alluvial bench. The diamictite is matrix supported with 30–40 percent clasts of quartzite and siltite. At this location, the diamictite member is foliated. It contains stretched clasts from millimeter to decimeter scale and has relatively high magnetic susceptibility (48.5 x 10^{-3} SI), likely from magnetite within the matrix.

Cross to the right side of the river and takeout at the Kilpatrick boat ramp. (44.83001°N, 113.9872°W)

ACKNOWLEDGMENTS

We appreciate a review from Russell Burmester.

REFERENCES

Fisher, F.S., McIntyre, D.H., and Johnson, K.M., 1992, Geologic map of the Challis quadrangle, Idaho: U.S. Geological Survey Miscellaneous Investigations Series Map I-1819, scale 1:250,000.

Tysdal, R.G., 2003, Correlation, sedimentology, and structural setting, upper strata of Mesoproterozoic Apple Creek Formation and lower strata of Gunsight Formation, Lemhi Range to Salmon River Mountains, east-central Idaho, *in* Tysdal, R.G., Lindsey, D.A., and Taggart, J.E., Jr., eds., Correlation, sedimentology, structural setting, chemical composition, and provenance of selected formations in Mesoproterozoic Lemhi Group, Central Idaho: U.S. Geological Survey Professional Paper 1668-A, p. 1–22.

FIELD GUIDE TO CARBONATE MYLONITES AND REACTIVATED BASEMENT FAULTS OF THE LEADORE AREA

Stuart D. Parker[1] and David M. Pearson[2]

[1]*Montana Bureau of Mines and Geology, Butte, Montana*
[2]*Idaho State University, Pocatello, Idaho*

INTRODUCTION

Situated in the central Beaverhead Mountains, south of the Idaho–Montana border, the northern part of the 1:24,000-scale Leadore quadrangle hosts complicated contractional and extensional structures that highlight a long history of persistent basement and stratigraphic weaknesses within the interior of the North American Cordillera (figs. 1, 2). Early stage carbonate mylonites define shear zones that follow thin lithologic horizons above a regional unconformity, which we interpret to have formed during a phase of Cretaceous thrusting that was characterized by a thin-skinned structural style. In contrast, Mesoproterozoic to Ordovician quartzites and plutonic rocks of the Lemhi arch basement high were carried by brittle thrusts that cut across lithologic boundaries at moderate to high angles; these thrusts are characteristic of a thick-skinned structural style,

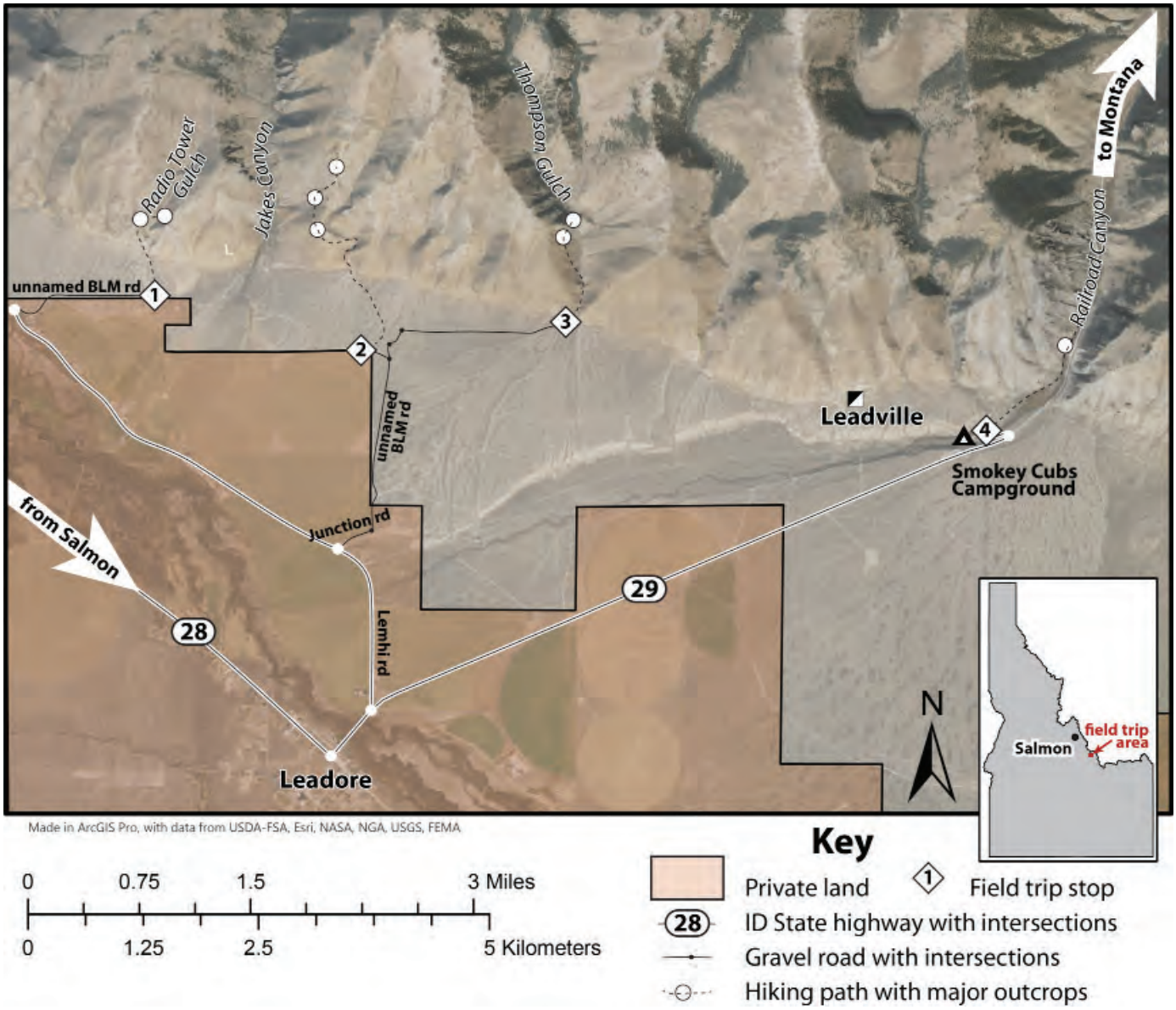

Figure 1. Map showing field trip stops and outcrops described in this field guide. The inset map shows location in relation to Salmon, Idaho. Note that road names may be incorrect on mapping applications.

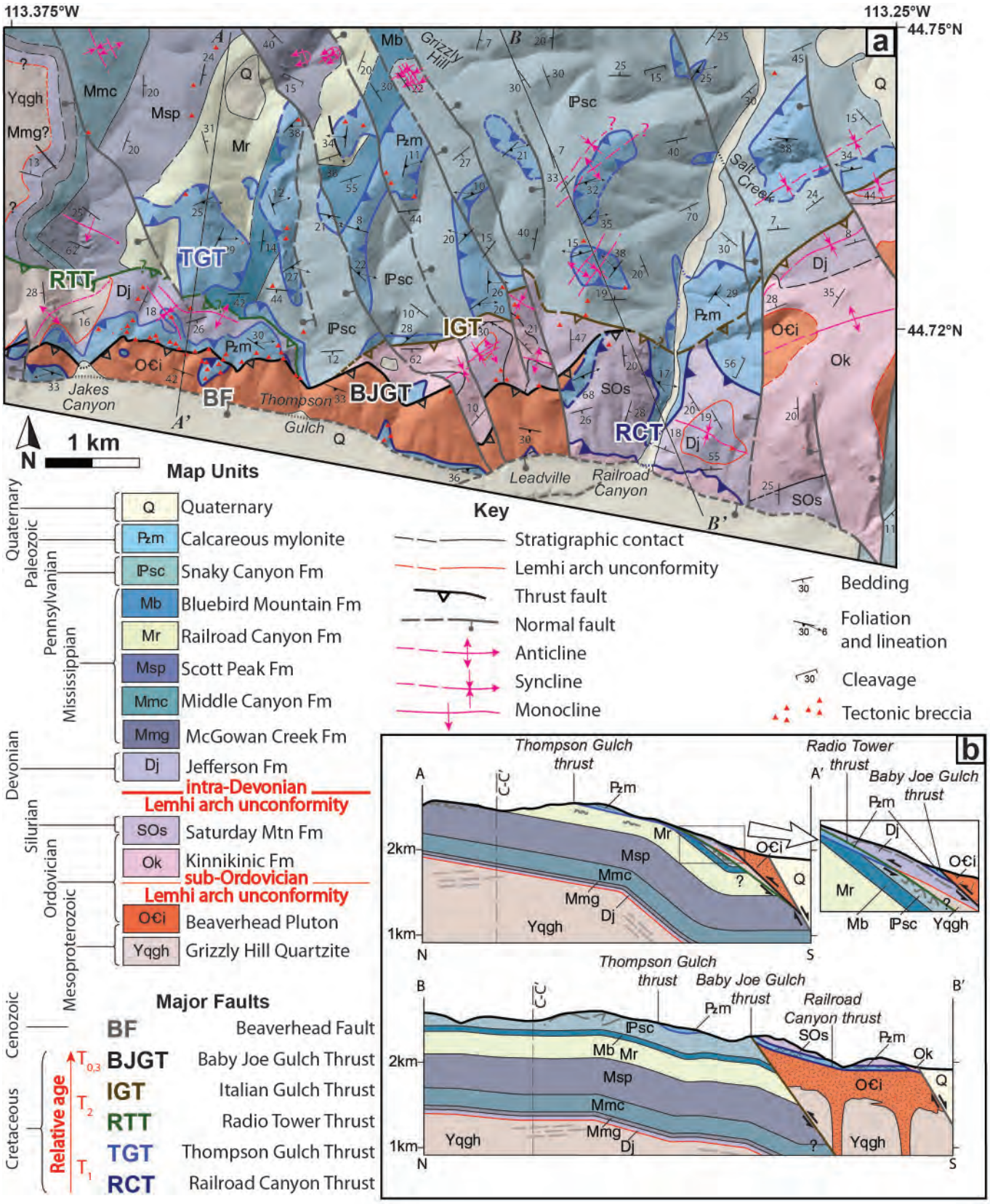

Figure 2. Simplified geologic map of the northern part of the Leadore quadrangle and cross sections, modified from Parker and Pearson (2021). See Parker and Pearson (2020) for detailed 1:24,000-scale map. Abbreviated unit names are used on subsequent figures.

and truncate the older carbonate mylonites. We interpret that burial heating during thrusting and foreland basin sedimentation resulted in elevated temperatures that accentuated the strength contrast between weak carbonate rocks that deformed plastically, and structurally lower, mechanically strong quartzites and igneous rocks that deformed brittlely. This strength contrast not only localized early thin-skinned deformation to within mechanically weak carbonates at the bottom of the regionally continuous middle Paleozoic passive margin succession above the Lemhi arch, but also resulted in a bewildering variety of outcrop-scale structures that make the region an excellent field trip locality.

In this field guide we will highlight the numerous stratigraphic and structural weaknesses that coincide with later thrust fault detachments, near the basement/cover rock contact of the Lemhi arch. We hope to convince participants that overlapping thin- and thick-skinned structural styles are not confined to the foreland of southwestern Montana, but instead occur throughout the Idaho–Montana fold-thrust belt, particularly where sedimentary rocks drape the underlying basement.

GEOLOGIC BACKGROUND

The North American Cordillera is a type example of an ancient orogenic belt formed during ocean–continent convergence. Horizontal shortening in the Idaho–Montana fold-thrust belt occurred mostly in the Cretaceous, from ca. 135 to 55 Ma (e.g., Yonkee and Weil, 2015). Weak, layered sedimentary rocks of the continental passive margin deformed mostly as imbricated thrust sheets bounded by a series of décollements and low-angle-to-bedding thrusts that cut up stratigraphy in the direction of transportation. This structural style is often described as "thin-skinned," although individual thrust sheets may be kilometers thick. Stronger, more massive metasedimentary and igneous rocks of the underlying basement deformed mostly as broad uplifts, with mid-crustal detachments linked to high-angle thrusts or reverse faults that cut indiscriminately through the upper crust. This structural style is often described as "thick-skinned." The Idaho–Montana fold-thrust belt contains a broad "overlap zone" of both thin- and thick-skinned thrusts, which in recent years has been central to debates regarding the role of flat-slab subduction in the Sevier–Laramide orogeny (e.g., Garber and others, 2020; Orme, 2020). Recent work in the Leadore quadrangle (Parker and Pearson, 2020, 2021) has suggested that the overlap zone between thin- and thick-skinned thrusts spans most of the Idaho–Montana fold-thrust belt. Within the northern part of the Leadore quadrangle, we can see exposures of the lower structural levels of the Idaho–Montana fold-thrust belt, allowing us to investigate the role that stratigraphic and structural weaknesses play in determining structural style.

STRATIGRAPHY

The stratigraphy of the field trip area lies near the hinge line of the Laurentian passive margin, separating thin sedimentary cover rocks atop the craton to the east (Montana) from thicker strata deposited on extended crust of the rift-passive margin to the west (Idaho). In the Leadore quadrangle (fig. 2), a ~2-km-thick (6,500 ft) section of Devonian to Pennsylvanian carbonate and siliciclastic rocks rests in angular unconformity on fine-grained Mesoproterozoic (?) quartzite (Lonn and others, 2019; Parker and Pearson, 2021). This intra-Devonian Lemhi arch unconformity (fig. 2; Sloss, 1954; Scholten, 1957) defines a basement high that is interpreted as a horst within the rift margin (e.g., Link and others, 2017). The Devonian Jefferson Formation records flooding of the Lemhi arch, which remained a topographic high during deposition of the early passive margin (e.g., Ruppel, 1986). This thin, discontinuous stratigraphic section of the hinge line occurs throughout much of the Beaverhead and Tendoy Mountains (fig. 3).

A thicker, more complete stratigraphic section lies to the south, in fault contact with the condensed section described above (fig. 3). The ca. 500 Ma Beaverhead pluton intruded into the tilted Mesoproterozoic quartzites (fig. 2) that locally make up the sub-Ordovician Lemhi arch unconformity (e.g., Scholten and Ramspott, 1968; Link and others, 2017). This is overlain by the well-cemented Ordovician Kinnikinic Quartzite and a thick section of Silurian to Devonian reef-bearing dolostones. In contrast to the Devonian section that flooded the Lemhi arch, this section is much thicker, older, continuous, and was deposited in deeper water. Exposures in the neighboring Lemhi Range, only about 17 km (11 mi) away, are characteristic of much of east-central Idaho and suggest that the total passive margin section was about twice as thick as the corresponding section in the Beaverhead Range (fig. 3). Within the northern Leadore quadrangle, these contrasts in thickness, completeness, and depositional environment pinpoint the fault-bounded hinge line of the Lemhi arch near its highest point (fig. 3).

STRUCTURE

Shortening during the Cretaceous juxtaposed these two segments of the Lemhi arch, resulting in the complicated structures visible today (fig. 2). The local stratigraphic thickness of a few kilometers is comparable to those found throughout the foreland of southwestern Montana, where deformation is entirely brittle. However, carbonates of the Leadore quadrangle deformed plastically, forming impressive carbonate mylonites that indicate higher temperatures during deformation (fig. 4). Maximum temperature estimates of around 280°C (±25) for the Devonian Jefferson Formation suggest that the apex of the Lemhi arch was buried to at least about 6.5 km (~21,000 ft) during the Cretaceous (Parker and others, 2022). This is part of a regional

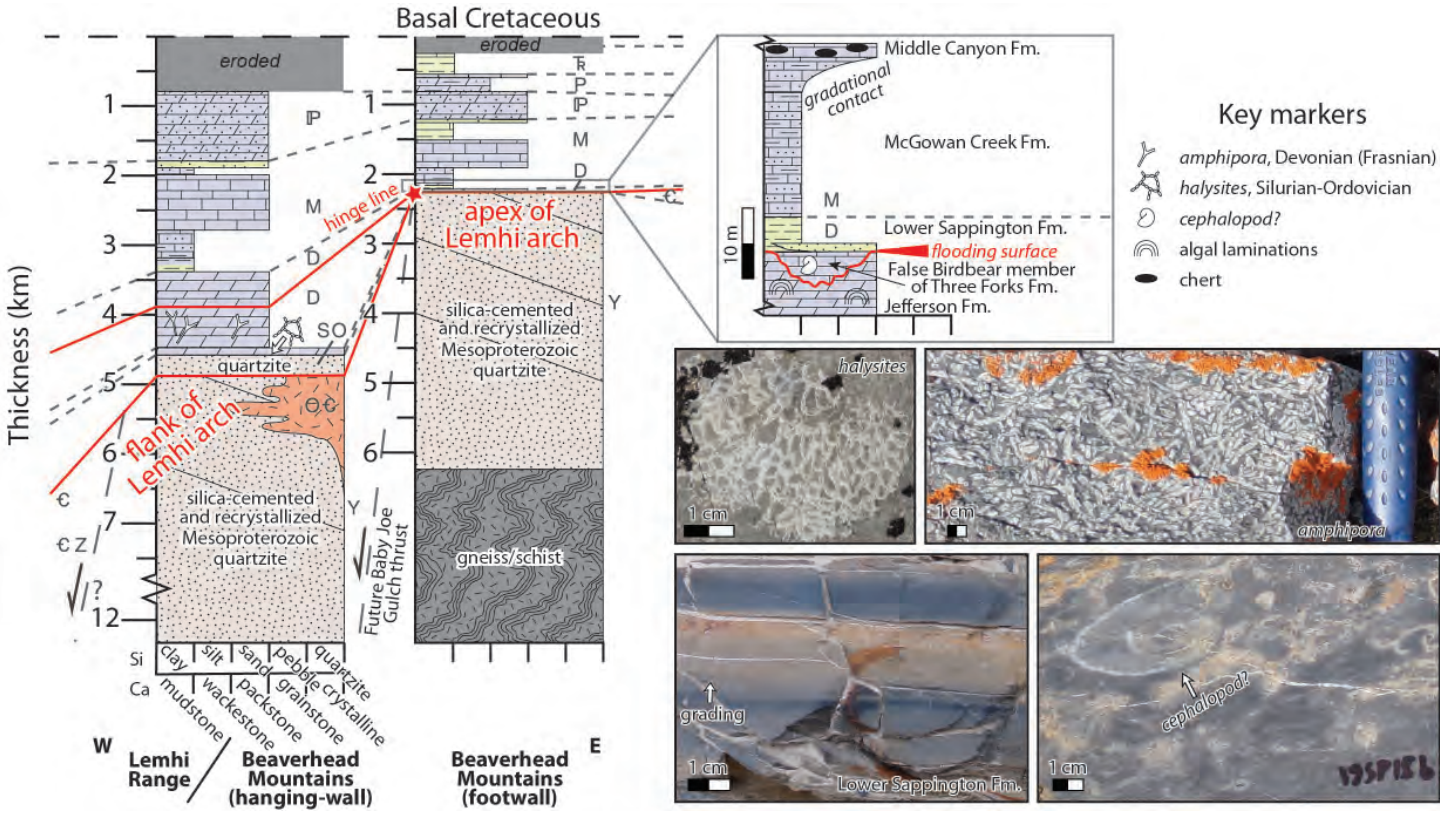

Figure 3. Simplified stratigraphic columns and key markers of the Leadore area, modified from Parker and Pearson (2021). Predominantly siliciclastic units shown in yellow-green; carbonate units shown in purple. General unit correlations and relative age shown by dashed lines, with Lemhi arch unconformities shown in red. Inset shows detailed Devonian to Mississippian stratigraphy (see Grader and others, 2016). Note the abrupt thickness and stratigraphic changes across the hinge line, and the pre-Devonian normal fault we interpret was later reactivated as the Baby Joe Gulch thrust.

temperature trend, interpreted as widespread syntectonic burial during initial shortening and wedge-top deposition in the Idaho–Montana fold-thrust belt (ca. 135–80 Ma; Parker and others, 2022).

Among the oldest fold-thrust structures are carbonate mylonites of the Thompson Gulch and Railroad Canyon thrusts, which structurally overlie a continuous section of the Lemhi arch (Lonn and others, 2019). The low-angle fault contact shallowly cuts upsection toward the east. The fault trace connects to the regional-scale Fritz Creek thrust and its imbricates (Pass Peak and Dry Canyon thrusts of Lucchitta, 1966; Skipp, 1988). This regional detachment generally parallels the Devonian flooding surface above the Lemhi arch and served as the décollement to the early Idaho–Montana fold-thrust belt (Hait, 1965; Beutner, 1968; Parker and Pearson, 2021). Sub-horizontal east–west-stretching lineations and kinematic indicators give a top-to-the-east sense of shear for this thin-skinned thrust system (fig. 5a).

The Radio Tower and Italian Gulch thrusts cut the mylonite (fig. 2), demonstrating that they are younger (Parker and Pearson, 2020). These later thrusts cut across bedding of well-cemented quartzites of the Kinnikinic Quartzite and Quartzite of Grizzly Hill at a high angle, indicating a thick-skinned style. However, the Radio Tower thrust is partly detached in the Devonian Jefferson Formation, just above the mylonite of the Thompson Gulch thrust, in a thin-skinned style. The Baby Joe Gulch thrust cuts across the Radio Tower and Italian Gulch thrusts, signifying it is the youngest in the area. The Baby Joe Gulch thrust cuts indiscriminately across mylonitic rocks and the Beaverhead pluton, characteristic of a thick-skinned style. It is one short segment of a broader anastomosing system between the Poison Creek and Hawley Creek thrusts (Lund, 2018). Provenance studies and low-temperature thermochronology suggest that the Baby Joe Gulch thrust system was active by ca. 67 Ma (Garber and others, 2020; Kaempfer, 2021). Stratigraphic disparities across the Baby Joe Gulch, Italian Gulch, and Radio Tower thrusts suggest reactivation of older normal faults related to the Lemhi arch (Parker and Pearson, 2021). The trace of this thick-skinned fault system also mimics the modern Beaverhead normal fault. Stranded chips of the hanging wall of the basement-involved Baby Joe Gulch thrust occur in the footwall of the Beaverhead normal fault along its trace, suggesting normal reactivation of Cretaceous thick-skinned thrusts during Basin and Range extension.

Horizontal shortening in the Leadore area generally evolved from a more thin- to a more thick-skinned structural style, as deeper detachment horizons were activated during progressive mountain building (Parker and Pearson,

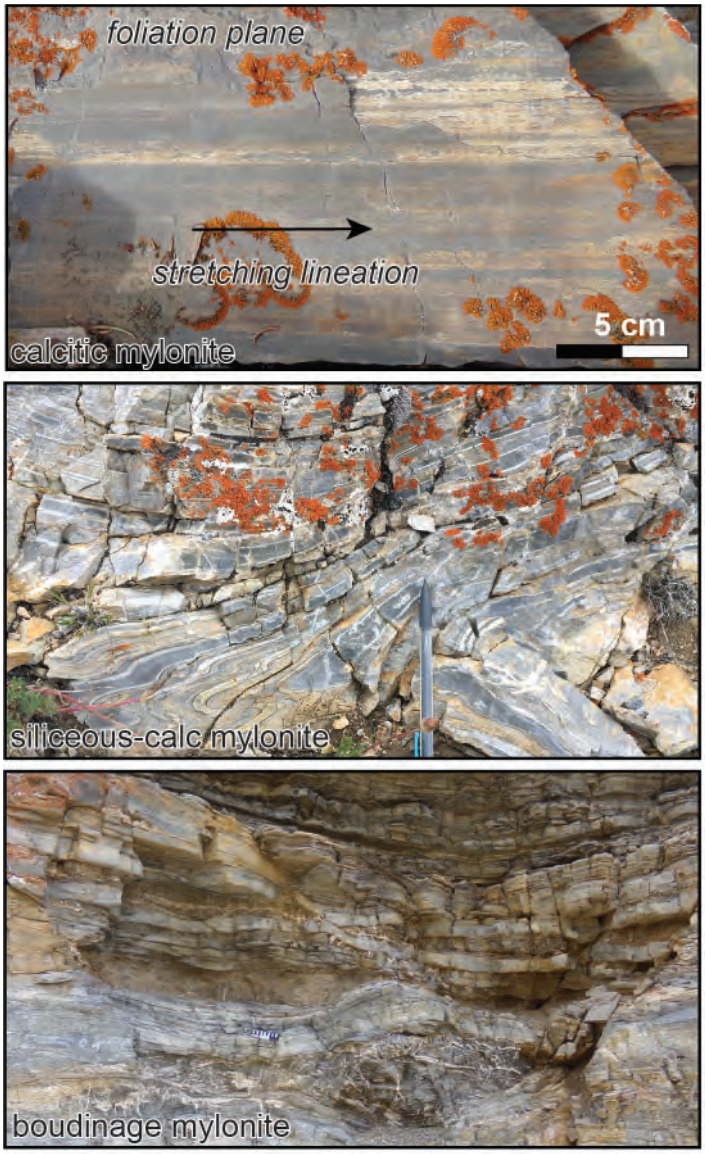

Figure 4. Calcitic, partly siliceous, and boudinaged mylonite tectonofacies of the Thompson Gulch and Railroad Canyon thrusts. Siliceous layers are likely deformed chert. Note upper photo shows planar view, whereas bottom photos show cross-section view. Scale bar in lower photo is 15 cm long, with 1 cm increments.

2021). Thin-skinned deformation of the cover rocks above the Lemhi arch was followed by thick-skinned thrusting of the basement, terminating with reactivation of a preexisting normal fault. Similar patterns of overlapping thin- to thick-skinned thrusts occur throughout the Idaho–Montana fold-thrust belt (e.g., Schmidt and Perry, 1988), but with variable ages that predate flat-slab subduction in the Sierra Nevada (e.g., Orme, 2020). Synthesizing structural interpretations of the Leadore quadrangle with work in the foreland led Parker and Pearson (2021) to propose a double-decker geometry for the Idaho–Montana fold-thrust belt. In this view, the Idaho–Montana fold-thrust belt consists of an upper level of older thin-skinned thrusts that overlap with a lower level of younger thick-skinned thrusts, formed simply by advancing a wedge-shaped deformation zone through a thinly covered basement high.

MINING HISTORY AND ECONOMIC GEOLOGY

This field trip traverses the Leadville (aka Junction) mining district, a small historic lead–silver district along the range front of the Beaverhead Mountains just north of Leadore, Idaho (See Mitchell, 2004 for summary; see Cox and Antonioli, 2017 for field guide). The namesake Leadville (aka Sunset) mine was staked in 1904 and developed the following year (Umpleby, 1913). By 1920, around $100,000 ($1.7 million today) of lead and silver was produced in the district, mostly between 1908 and 1911 during initial production of the Leadville mine (Bell, 1920). While the district was relatively small and short-lived, it hosted numerous shafts, a tunnel, a 25-ton concentrating mill on site, and year-round residents.

Ore consists of argentiferous galena [(Pb, Ag), S] with uncommon pyrite, which replaced brecciated carbonates just above and below fault contacts with the Beaverhead pluton (Umpleby, 1913). The main mineralized zone in the Leadville lode is planar, with a dip of 35–40° toward the south–southwest, likely following permeable zones along the Baby Joe Gulch thrust contact or the adjacent carbonate breccia. Adjacent mylonite contains pyrite with strain fringes, which are concentrated in offset veins (fig. 8 of Parker and Pearson, 2021). This demonstrates that pyrite crystals were rigid during ductile deformation, suggesting that some mineralization could be pre- or syn-kinematic. Mineralization clearly predates the Beaverhead fault, which cuts the deposit in a normal sense. Based on detailed descriptions of Umpleby (1913), the "Calcareous Breccia" unit of Parker and Pearson (2020) is likely the main host rock. Elsewhere, this permeable tectonic breccia has been replaced by dark silica (jasperoid), which has understandably been mistaken for chert (e.g., Ruppel, 1968). While it is clear that mineralization was greatly influenced by the faulting history and tectonostratigraphy within the Leadville mining district, the extraordinary complexity of the geology has proven difficult to predict in the subsurface.

AVAILABLE MAPPING

The 1:62,500-scale Leadore quadrangle was mapped by Ruppel (1968), who identified in the southern portion of his map—and beyond the southern extent of the 1:24,000-scale Leadore quadrangle—a succession of Mesoproterozoic quartzites and siltites that are overlain unconformably by Ordovician through Devonian strata. In the northern portion of his map, which includes the 1:24,000-scale Leadore quadrangle, Ruppel (1968) mapped granite of an uncertain age, complicated thrusts, and "chert" breccias. Mapping at 1:100,000 scale, Ruppel (1998) and Evans and Green (2003) improved upon this work by identifying the Cambrian/Ordovician Beaverhead pluton and simplifying thrust geometries. Using legacy 1:50,000-scale mapping, Lund (2018) identified and named the Baby Joe Gulch and Thompson Gulch thrust systems and reinterpreted the

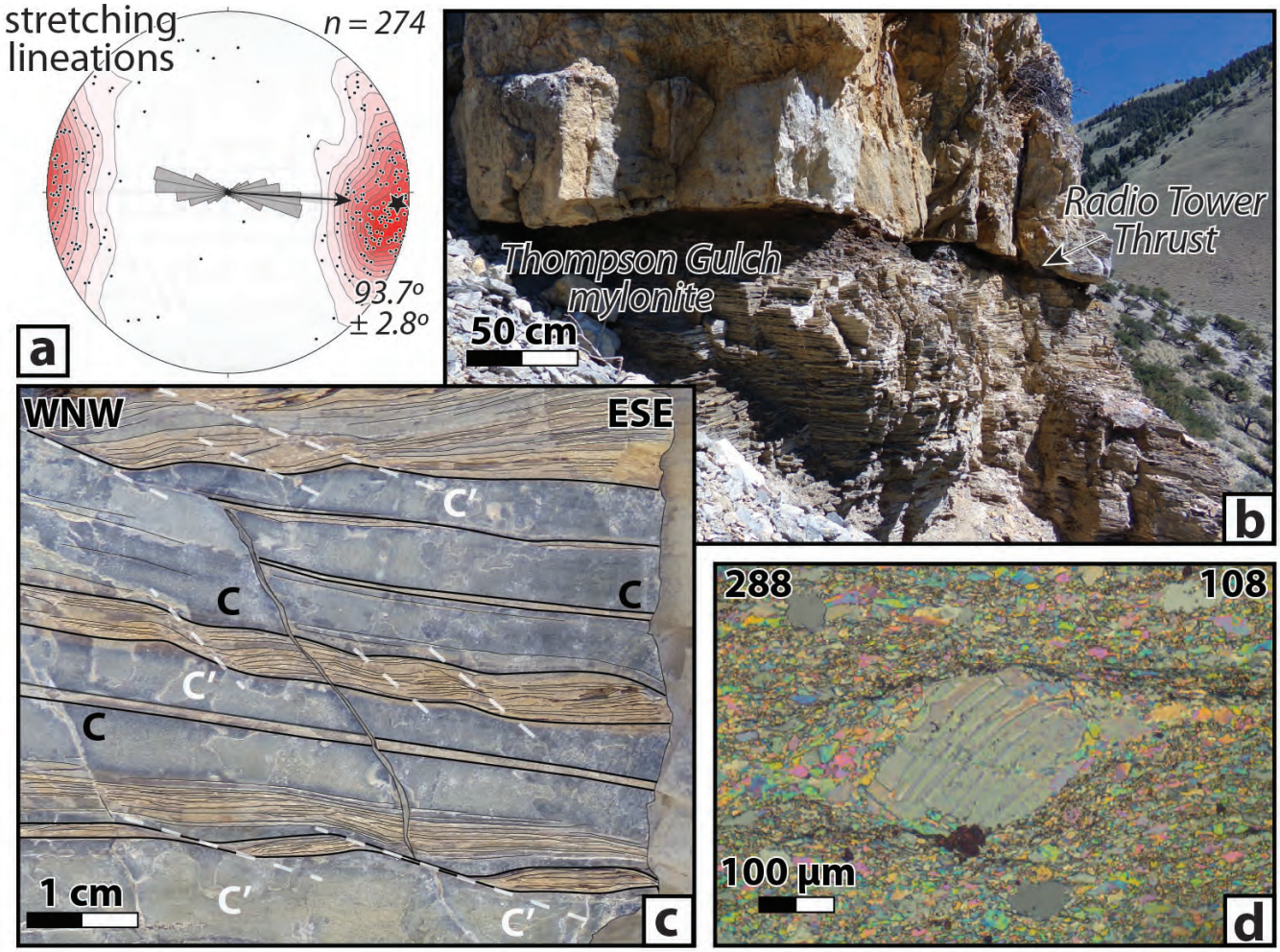

Figure 5. Deformation features of the Thompson Gulch thrust mylonite (Stop 3). (a) Lower hemisphere stereographic projection showing all measured stretching lineations within the Leadore quadrangle. Labeled star shows mean orientation. Inset rose diagram shows mean trend and uncertainty, with data grouped into 10° bins. Kamb contouring at 2σ uncertainty levels. (b) Sharp thrust contact at Stop 2. Note that the black siliceous rock thickens and thins below the Radio Tower Thrust contact. (c) Calcitic mylonite of Thompson Gulch, showing ductile shear planes (C) and antithetic shear bands (C'), which give a top-to-the-right sense of slip. (d) Twinned calcite σ-clast with dynamically recrystallized tails, giving a top-to-the-right sense of slip within the mylonite shown in c. Modified from Parker and Pearson (2021).

lower contact of Paleozoic-on-Mesoproterozoic rocks as an unconformity rather than a fault contact. Further mapping at 1:24,000-scale of the adjacent Bannock Pass quadrangle to the north by Lonn and others (2019) documented that above this newly documented unconformity, middle Paleozoic strata are predominantly east- and southeast-dipping, defining a regional homocline that was inferred to continue southward into the northern Leadore quadrangle. Within this simplified regional geologic context and with the detailed stratigraphic framework of the Jefferson Formation in mind (Grader and others, 2016), Parker and Pearson (2020) mapped the northern part of the Leadore quadrangle at 1:24,000 scale.

Parker and Pearson (2020) recognized that structurally lower rocks within the northern part of the map are structurally overlain by carbonate mylonites along many of the ridges. These mylonites are characterized by a systematic tectonostratigraphy, which reduced the total number of required thrust faults and allowed for individual thrusts to be correlated, defining klippen across much of the map. Parker and Pearson (2020) also identified small-offset, north–northwest-striking normal faults that cut across all other faults, except the modern range-bounding Beaverhead normal fault. Lastly, Parker and Pearson (2020) recognized that two major regional unconformities were likely superimposed upon each other within the map: the sub-Ordovician Lemhi arch unconformity in the south and the intra-Devonian Lemhi arch unconformity to the north. Juxtaposition of strikingly different strata across the Baby Joe Gulch thrust system suggests that older structures were reactivated during Mesozoic and younger faulting in the region and the inherited, pre-thrusting stratigraphic framework likely had a primary influence on the style of thrusting during the Cretaceous (Parker and Pearson, 2021). Given the complexity of the structures within the area, the thinness and heterogeneity of the stratigraphy, and locally poor exposure, future work is likely to continue to refine the mapping, regional stratigraphy, and structural interpretations within the Leadore quadrangle.

ROAD LOG

From the Salmon River in Salmon, Idaho, travel southeast on ID 28 (Main St.), to Leadore, Idaho. It is a 46 mi (74 km), about 45 min, drive. At Leadore, set your odometer to zero, and reset it after each stop. See figure 1 for an overview map of the field trip stops.

0.0 mi (0.0 km) From Leadore, take a left (northeast) on Old ID 28/ID 19 (Dillon St.), following signs toward Smokey Cubs Campground.

0.3 mi (0.5 km) After crossing the Lemhi River, bear left on Old ID 28 (Lemhi Rd.) at the 4-point intersection.

3.2 mi (5.2 km) Continue past the left-hand curve. After passing the last farm field on the right, take a sharp right onto an unnamed dirt BLM road, toward Yearian Cemetery.

4.1 mi (6.7 km) Follow the dirt road up the bench. Bear right, heading toward the "L" and the mouth of Jakes Canyon. Park at the small (Yearian) cemetery, where the road curves to the right, down the bench. This is Stop 1 (fig. 1).

STOP 1

Tectonostratigraphy near the Lemhi arch unconformity

(44.712943°, -113.373260°)

From the parking spot, hike northwest up the alluvial fan toward the small canyon with the dirt road. The contact of interest forms a dip slope on the western side of this small drainage. Follow the small game trail up the ridge, left (west) of the road through the tight canyon, for about 0.5 mi (0.8 km). Where the game trail intersects the highpoint of the road, you'll see a large patch of disturbed ground on the dip slope above, on the hillslope to the right (northeast). Follow the ridge uphill, toward the outcrops above the disturbed patch but on the west side of the ridge, at about 6,530 ft elevation.

Outcrop 1a: Lemhi arch unconformity

(44.718577°, -113.377441°)

Walking along the game trail avoids multiple generations of normal and thrust faults that intersect in Radio Tower Gulch. Structurally beneath these faults, the intact stratigraphy of the Lemhi arch can be observed. Here, a quartzite pebble to cobble conglomerate lies just above the Devonian Lemhi arch unconformity. Clasts are generally well rounded and in matrix support. This compositionally mature conglomerate is only about 1–3 m (3–10 ft) thick, overlying the vitreous upper unit of the Quartzite of Grizzly Hill (Parker and Pearson, 2020). In some places it contains large, meter-scale boulders. The age (Mesoproterozoic?) of the Quartzite of Grizzly Hill and the conglomerate bed above the unconformity is unconstrained (Lonn and others, 2019; Parker and Pearson, 2020).

This unconformity forms a prominent dip slope, with bedding dipping moderately (20–30°) toward the south–southeast. As you walk down the dip slope, upsection, you will encounter laminated dolostones of the Jefferson Formation disconformably overlying this quartzite conglomerate. Near Grizzly Hill, about 5 mi (8 km) north, the unconformity is strongly angular with a northeast-facing direction of about 20°. At this stop, the exceptional thinness of the Jefferson Formation, which is characteristic of the unit at the lowest structural levels, characterizes the apex of the Lemhi arch (Grader and others, 2016). Within the Jefferson Formation, rare tabular beds of matrix-supported dolomite breccias interrupt otherwise intact sedimentary rocks, suggesting layer-parallel slip within very weak beds with high pore-fluid pressures. Rare outcrops of dolomitic sandstones and the Devonian Lemhi arch unconformity are useful pinning points for the numerous north–northwest-striking normal faults that slightly offset the dip panel in an apparent left-lateral sense.

Walk east for about 0.1 mi (0.2 km), down the dip slope and up the other side of the small drainage. Head toward the largest outcrop with patchy trees on the skyline, at about 6,570 ft elevation.

Outcrop 1b: Mylonite above the Lemhi arch unconformity

(44.718059°, -113.374547°)

On the east side of the drainage, the section passes from dolostones of the Jefferson Formation to an overlying carbonate mylonite. These impressive outcrops of carbonate mylonite have a strong foliation and lineation, with late-stage boudins, veins, and normal-sense shear zones (fig. 4). Foliation generally dips to the south–southeast at about 30–40°, parallel with the underlying dip slope. Sub-parallel east–west-stretching lineations are common. Black siliceous intervals form boudins, with pervasive calcite veins indicating late-stage brittle fracturing and filling. In contrast, clean gray calcareous intervals are brilliantly foliated and lineated, with evidence of earlier plastic strain and dynamic recrystallization. Field relationships elsewhere within the northern Leadore quadrangle suggest that mylonitic foliations and lineations formed during a phase of Cretaceous thrusting. Normal-sense brittle-ductile shear zones, boudins, veins, and late-stage faults

exposed here may have formed either during vertical flattening and horizontal extension concurrently with the bedding-parallel shear zone, or during early, post-contractional extensional tectonism that exploited the older mylonite. Consider these possible interpretations as we see more of these normal-sense shear zones throughout this trip.

The composition of the mylonite, intact footwall stratigraphy, and contact geometry are consistent with a thin-skinned structural style, with the detachment following the flooding surface of the Lemhi arch, near the thin Sappington and McGowan Creek Formations (fig. 3). Parker and Pearson (2021) hypothesized that this shear zone represents the décollement to the early Idaho–Montana fold-thrust belt. Toward the hinterland, this décollement is likely continuous with a regional thrust flat that forms impressive fold trains in the neighboring Lemhi and Lost River Ranges (e.g., Hait, 1965; Beutner, 1968). As you will see throughout the field trip, this tectonostratigraphy is remarkably consistent throughout the mylonite of the Leadore area, supporting the interpretation of a regional décollement rooted in the thin strata above the Lemhi arch (Parker and Pearson, 2021).

Return to the cars, reset odometer, and drive to stop 2.

0.0 mi (0.0 km) From the cemetery, backtrack to Lemhi Rd. (Old ID 28).

0.9 mi (1.5 km) Take a left (southeast) on Lemhi Rd. (Old ID 28), toward Leadore.

2.9 mi (4.7 km) After the farm fields on the left, near the bench, take a left (east) onto Junction Rd.

3.1 mi (5.1 km) After the center pivot farm field, take an immediate left (north) onto the unnamed dirt BLM road, heading toward the range front. Follow the fence line north.

4.1 mi (6.6 km) At the unmarked intersection, park on the left, before the gate and just outside the northeastern corner of the private section of land. This is Stop 2 (fig. 1).

STOP 2
Tectonostratigraphy near the Baby Joe Gulch thrust

(44.709425°, -113.353993°)

Follow the dirt road uphill, weaving through the small draw and contouring into the side of Jakes Canyon. Once the road begins to contour into Jakes Canyon, head uphill (east) to gain the ridge. Follow the ridge uphill (north), until you reach an old prospecting road that contours across the ridge at about 7,170 ft elevation. Outcrop 2a is on the ridge just below this road, a 1.2 mi (2.0 km) hike from the parking spot.

Outcrop 2a: Footwall tectonostratigraphy

(44.721890°, -113.357528°)

These dolostone outcrops of the Jefferson Formation, in the footwall of the Baby Joe Gulch thrust, are continuous with the stratigraphic section of the previous stop. Primary sedimentary structures, such as fine algal laminations, mud chips, and rare solution breccias, suggest an upright position and a shallow water, restricted depositional environment. These units most likely belong to the Famennian upper Jefferson Formation (D5 and D6 of Grader and others, 2016), which contains abundant anhydrite in a nearby drill hole (e.g., M'Gonigle, 1982). On the hill above, several brecciated outcrops within the Jefferson Formation dot the hillside, structurally just below the shear zone of the Railroad Canyon thrust.

As you walk down the ridge, you'll generally go upsection through the folded tectonostratigraphy of the footwall of the Baby Joe Gulch thrust. Rare outcrops of mottled thick-bedded nodular crinoidal (lime) wackestone with cephalopods (fig. 3) occur just above dolostone of the Jefferson, signifying a change to open marine conditions (Grader and others, 2016). This discontinuous unit is correlative with the False Birdbear member of the Three Forks Formation (Trident Limestone in Montana; Grader and others, 2016). Better exposures on the next hill east show 7 m (23 ft) of black-lavender mudstone and black chert in centimeter-scale layers above, likely correlative to the Sappington Formation (fig. 3; Grader and others, 2016). The disconformity beneath the Sappington Formation is a regional sequence boundary, marking the flooding of the Lemhi arch following Famennian uplift and faulting (Beaverhead uplift of Grader and others, 2016). Above this unit, 5 m (16 ft) of gray-yellow-weathering silty limestone and dolostone, with wavy cleavage and fossil fragments, are tentatively correlative with the McGowan Creek Formation. Above these units you encounter the carbonate mylonite of the Railroad Canyon thrust. While thin, these units are important markers, and this tectonostratigraphy seems to be consistent throughout much of the Leadville mining district.

Structurally above the mylonite, carbonate breccia forms an outcrop belt of cohesive cataclasite. The south-dipping tabular body has subrounded dolomite clasts supported in a calcitic matrix. Unlike the mylonite, which is very fine grained and dynamically recrystallized, a field acid test shows that the breccia is very permeable. This brecciated unit hosts lead–silver

ore throughout the Leadville mining district (Umpleby, 1913). Similar breccias have been described in the Gilmore mining district (M'Gonigle, 1982). Rare chert and mylonite clasts are present within the breccia, but overall it is remarkably monolithologic and in many places occurs between undeformed beds, perhaps reflecting deformation and replacement of evaporite beds (M'Gonigle, 1982).

Continue walking down the ridge. After the last brecciated outcrops, keep an eye on the float. Find the contact between the red-weathering slopes of the Beaverhead pluton and the gray to yellow limestone breccia, at about 6,830 ft elevation. Follow this contact down (west) into Jakes Canyon, where it intersects the contouring road at about 6,710 ft elevation.

Outcrop 2b: Baby Joe Gulch Thrust

(44.719372°, -113.359532°)

This prominent color change marks the Baby Joe Gulch thrust, making it easy to trace through the landscape. The view to the west, across Jakes Canyon, shows the cross-sectional geometry of the fault (fig. 6). The fault plane dips to the south–southwest (198°) at 38°. In the footwall, the fault cuts across a section of mylonite that lies below the breccia that marks the fault contact here. The complete section of mylonite, the Devonian Jefferson Formation, and Mesoproterozoic (?) Quartzite of Grizzly Hill have been folded in an open anticline. Note that the quartzite outcrop is truncated by the steep Radio Tower Gulch thrust, with apparent thrust (or left-lateral) offset.

In contrast to the Devonian unconformity we have seen in the footwall of the Baby Joe Gulch thrust, nearby the hanging wall stratigraphy consists of Beaverhead pluton intruded into Mesoproterozoic quartzite, nonconformably underlying Ordovician Kinnikinic Quartzite (Lund and others, 2010). These two sections represent the apex and flank of the Lemhi arch, respectively, bracketing the hinge line (fig. 3). These stratigraphic relationships suggest normal fault offset before the latest Devonian, with thrust reactivation during the Cretaceous (Parker and Pearson, 2021).

Continue walking down the road (south), contouring around the left (east) and into the small drainage. At about 6,650 ft elevation, you'll see a mylonite outcrop uphill (northeast) of the road.

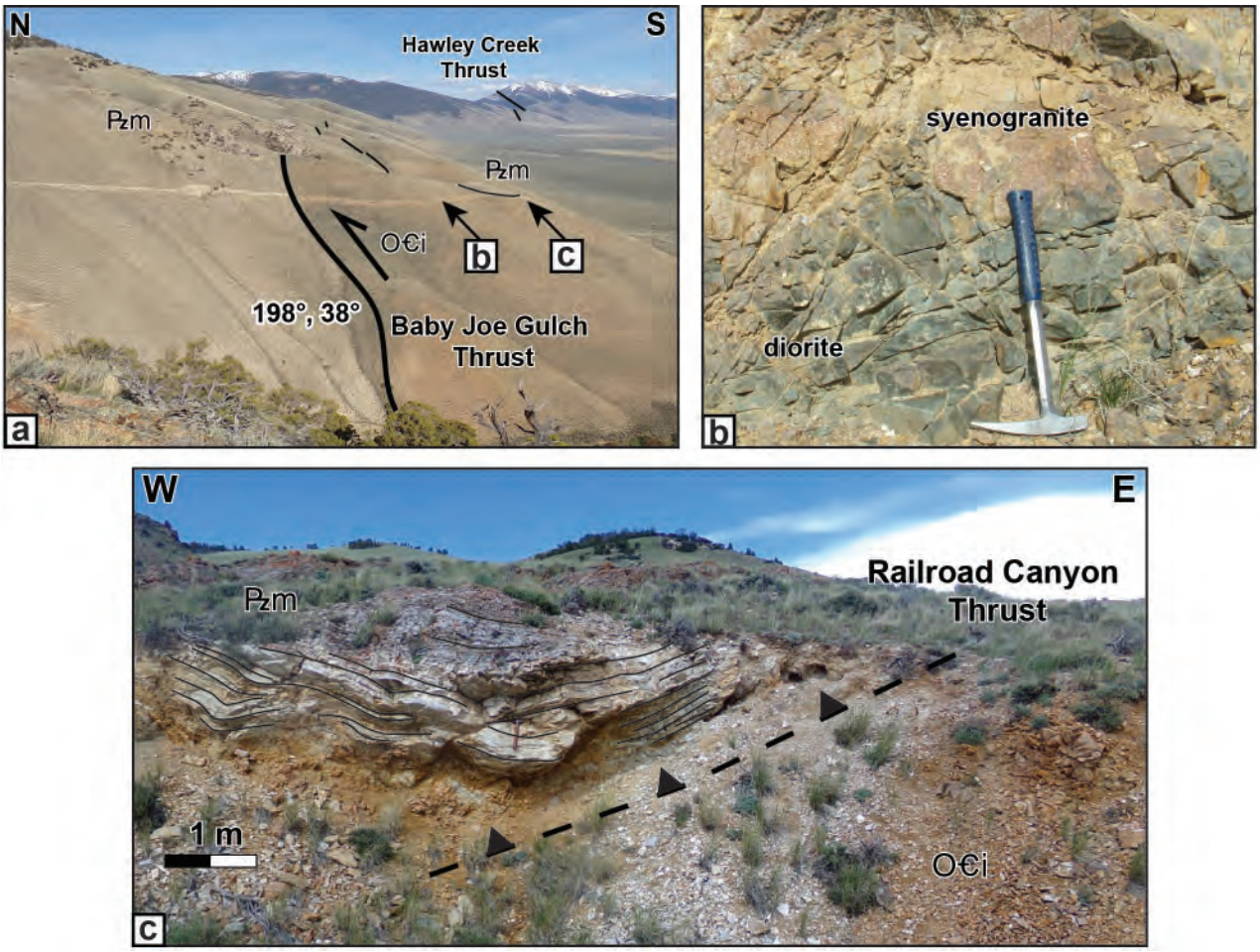

Figure 6. Annotated photo of faults in Jakes Canyon, looking west from Stop 2. Modified from Parker and Pearson (2021). See figure 2 for abbreviated unit names. Modified from Parker and Pearson (2021).

Outcrop 2c: Beaverhead pluton and hanging wall mylonite

(44.717235°, -113.358676°)

Along the road, between outcrops 2b and 2c, there are rare outcrops of the Beaverhead pluton, where clasts of pink potassium–feldspar-rich syenogranite are included in dark-green, altered diorite (fig. 6). Often the pluton is concealed by reddish, sparsely vegetated slopes like seen along this road. Where it crops out near Hawley Creek (fig. 7), the Beaverhead pluton yielded a mean U-Pb zircon age of 488 ± 5 Ma (Lund and others, 2010).

At the next road cut, a klippe of mylonite overlies the poorly exposed Cambrian/Ordovician Beaverhead pluton (fig. 6). This cryptic outcrop is typical of the Railroad Canyon thrust, the structurally highest mylonite in the field trip area. This younger-on-older relationship is interpreted as a bedding-parallel thrust fault, like the one observed at stop 1. It is unclear whether the omitted tectonostratigraphy (e.g., Jefferson Formation, breccia, Kinnikinic, etc.) is the consequence of a nonconformity, attenuation in the shear zone, or local downcutting in the direction of transport during thrusting.

In detail, the mylonitic foliation parallels abundant similar folds, many of which are sheath folds. The foliation, and in places a weak lineation, has been folded by open outcrop-scale folds and in places is truncated by late-stage brittle faults. See if you can find any dolomite clasts within the calcitic mylonite. Follow the slightly irregular fault contact, between the mylonite and the Beaverhead pluton, around this small outcrop to get a sense of the low-angle fault geometry.

In summary, the tectonostratigraphy suggests that the Railroad Canyon thrust is detached in weak silty limestones, mudstones, and possibly evaporites, just above the uppermost Jefferson Formation. The consistency of this tectonostratigraphy suggests that the shear zone, defined by mylonite and breccia, follows a major unconformity in a thin-skinned fashion. The Baby Joe Gulch thrust postdates the Railroad Canyon thrust, dips moderately to the south, cuts across all lithologic markers, and exposes plutonic rocks in its hanging wall, giving it a thick-skinned structural style. The Baby Joe Gulch thrust apparently reactivated an older Paleozoic normal fault of the Lemhi arch.

Hike 0.8 mi (1.3 km) back down to the parking spot, reset odometer.

0.0 mi (0 km) From the parking area for stop 1, drive east along unmarked roads. Aim for the mouth of the next major canyon to the east, Thompson Gulch.

1.0 mi (1.66 km) Park at the intersection at the mouth of the canyon.

STOP 3
Radio Tower thrust and Thompson Gulch mylonite

(44.711244°, -113.334105°)

Hike about 0.5 mi (0.8 km) into Thompson Gulch. Just after the bedrock constriction, contour up the slope on the left, toward the pinnacles at about 6,780 ft.

Outcrop 3a: Radio Tower thrust contact

(44.717119°, -113.334947°)

The pinnacle exposes the sharp contact of the Radio Tower thrust, marked by a yellow-tan dolostone breccia on top of the Thompson Gulch thrust mylonite (fig. 5).

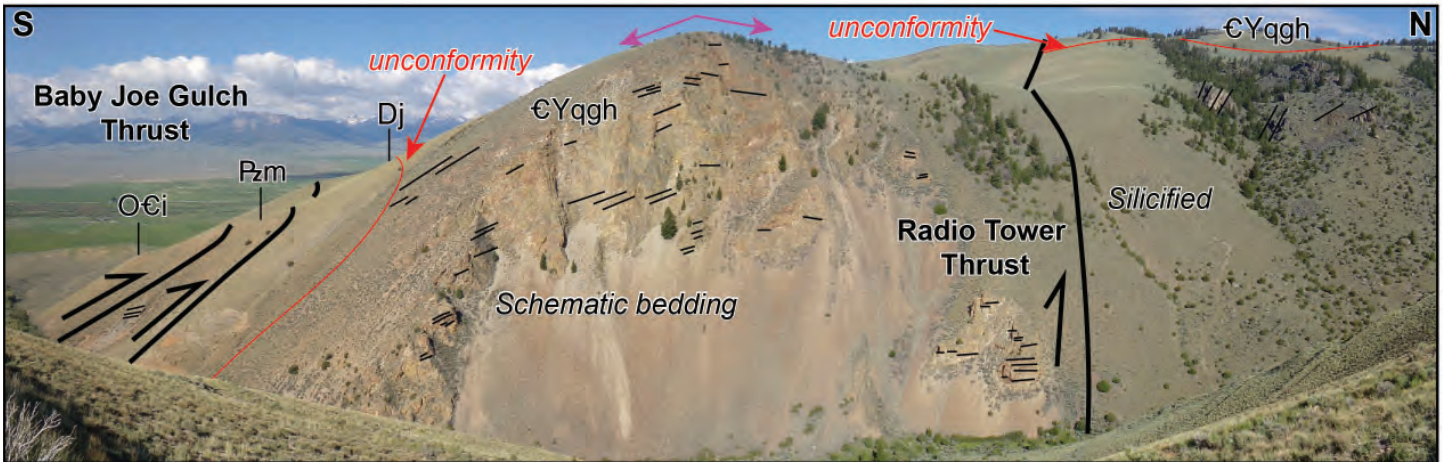

Figure 7. Annotated photos showing rocks of Stop 1. (a) Cross-section of Baby Joe Gulch thrust, as viewed from the west side of Jakes Canyon. Note correlative Hawley Creek thrust to the east. (b) Intrusive contact between syenogranite and diorite of the Beaverhead pluton. (c) Railroad Canyon Thrust contact, which puts younger carbonate mylonite on the older Beaverhead pluton. See figure 2 for abbreviated unit names. Modified from Parker and Pearson (2021).

In places, the contact cuts downsection slightly, leaving behind large blocks of black siliceous rocks. Variably thick fault gouge marks the base of the fault contact. A polished, lineated clay layer a few centimeters thick underlies the fault gouge in some spots, possibly representing a late-stage brittle fault in siliceous rocks. Mylonitic chips within this damage zone are often imbricated or inclined. The base of the outcrop is a clean carbonate mylonite, with stretching lineations and C–C' fabrics that suggest a top-to-the-east-southeast thrust sense of motion (fig. 5). In thin sections, σ-clasts and strain fringes give the same sense of slip.

The hanging wall consists of about a meter of tabular breccia, similar to those observed at previous stops. Above, dolostone of the Jefferson Formation is fractured, but upright sedimentary structures are still visible, including flat laminations, mud chips, ooids, scours, mud cracks, and possible stromatolites. On the ridge above, rare outcrops of the thick-bedded, mottled limestone and overlying fine-grained sandstone signify the transition from restricted to open shelf and shoreface conditions during flooding of the Lemhi arch (False Birdbear member and Sappington Formation). In the footwall, the clean gray and tan banded calcite mylonite is likely deformed McGowan Creek Formation. Dark, more siliceous intervals may be deformed Sappington Formation.

Though the stratigraphic offset clearly has a thrust-sense, normal-sense shear zones are common throughout the outcrop. As discussed earlier, this may be representative of either late-stage extension or syn-contractional flattening within the shear zone, which is common in weak ductile rocks, particularly when they are bounded by much stronger units. The temperature conditions during faulting were such that dolomite and siliceous rocks were brittle, whereas calcitic rocks deformed plastically. This observation agrees well with maximum temperature constraints from the field trip area, which range from 244 to 281°C (±25) in the Pennsylvanian to Devonian section (Parker and others, 2022). The minor thrust offset (<50 m) of the Radio Tower thrust suggests that it may be a late-stage brittle imbricate to the Thompson Gulch thrust, perhaps accommodating strain variations between stronger dolostones and weaker limestones. To the west, the Radio Tower thrust can be traced into the high-angle thick-skinned fault contact observed in Jakes Canyon (fig. 2), suggesting the fault-geometry transitions from a more thin- to a more thick-skinned segment as it encountered much stronger quartzites of the Lemhi arch.

Contour north, across the hill slope to the spur ridge, and follow it down toward Thompson Gulch.

Outcrop 3b: Thompson Gulch mylonite

(44.718369°, -113.334110°)

Along this spur ridge you'll walk downsection through the Radio Tower thrust fault zone, into mylonite of the Thompson Gulch thrust. This extensive mylonite forms klippen throughout the field trip area, defining the shear zone of the Thompson Gulch thrust. It varies from clean calcite mylonite to brilliantly banded siliceous–calcitic mylonite, likely reflecting chert-rich intervals that are common in the Mississippian Middle Canyon and Scott Peak Formations. The mylonite of the Thompson Gulch thrust is about 37 m (120 ft) thick here. Eventually you'll get into Pennsylvanian Snaky Canyon Formation in the footwall.

Hike out of Thompson Gulch, back to the parking spot, reset odometer.

0.0 mi (0 km) From the parking area for Stop 2, reverse course back to the 4-way intersection of Old ID 28 (Lemhi Rd.) and ID 29.

3.0 mi (4.8 km) Take a left (northeast) on ID 29, toward Smokey Cubs Campground (fig. 1).

6.4 mi (10.3 km) Take a left into Smokey Cubs Campground. Bear right, away from the bathrooms, to cross the creek.

6.7 mi (10.8 km) Park on the right, near the water pump.

STOP 4
Railroad Canyon mylonite

(44.703965°, -113.293063°)

Hike northeast along the flat dirt road, into Railroad Canyon (aka Canyon Creek), for as long as you'd like. Head back when you've seen enough mylonite.

Outcrop 4a: Railroad Canyon mylonite and Lemhi arch flank stratigraphy

(44.709658°, -113.285414°)

The canyon mouth marks the Beaverhead (normal) fault, with outcrop bands of Ordovician Kinnikinic Quartzite and Beaverhead pluton marking remnants of truncated thrust faults. The prospect pits along the range front continue to the Leadville Mine, less than a mile (1.6 km) to the west. In contrast to previous stops, here quartzite of the Ordovician Kinnikinic and fossiliferous dolostone of the Ordovician/Silurian Saturday Mountain Formation occur above the Beaverhead pluton. In the float, look for Halysites (chain coral), a tabulate coral that is diagnostic of the Ordovician and

Silurian (fig. 3). The overlying Jefferson Formation is at least 150 m thick (490 ft) and contains reefs and impressive thick-bedded cycles containing amphipora (spaghetti rock fossils), which last occurred in Frasnian (Late Devonian) time (fig. 3; Grader and others, 2016).

This older, thicker, more complete stratigraphic section represents the western flank of the Lemhi arch, which is typical of east-central Idaho. In this more basinward section, the younger (Devonian) Lemhi arch unconformity is less pronounced (fig. 3). The stratigraphic discontinuity across the Baby Joe Gulch thrust and its imbricates suggests pre-Devonian (Famennian) normal offset, which downdropped the flank of the Lemhi arch (Beaverhead uplift of Grader and others, 2016). Thrust reactivation of the Baby Joe Gulch fault (and possibly its imbricates) in the Cretaceous shortened this important hinge line, while later Basin and Range normal faulting seems to have reactivated it again in the Cenozoic.

The constriction of the canyon marks the Railroad Canyon thrust contact, where steep mylonite outcrops (fig. 8a) have an apparent thickness of up to 80 m (260 ft). In detail, foliation parallels axial surfaces of flattened sheath folds and rootless folds (fig. 8b), suggesting local shear zone flattening. Rare boudins of dark, more siliceous rock, within attenuated mylonite layers (fig. 8c), suggests similar rheologic contrasts as discussed at previous stops. Gently plunging east–west-stretching lineations are indistinguishable with those of the Thompson Gulch thrust.

The Railroad Canyon thrust contact dips about 30° to the southeast (fig. 8a), wrapping around the canyon. It can be traced to the west, structurally above the Beaverhead pluton, in the hanging wall of the Baby Joe Gulch thrust (fig. 2). Removing slip on the Baby Joe Gulch thrust and its imbricates establishes continuity between the Thompson Gulch and Railroad Canyon thrusts. This suggests that they were once part of the

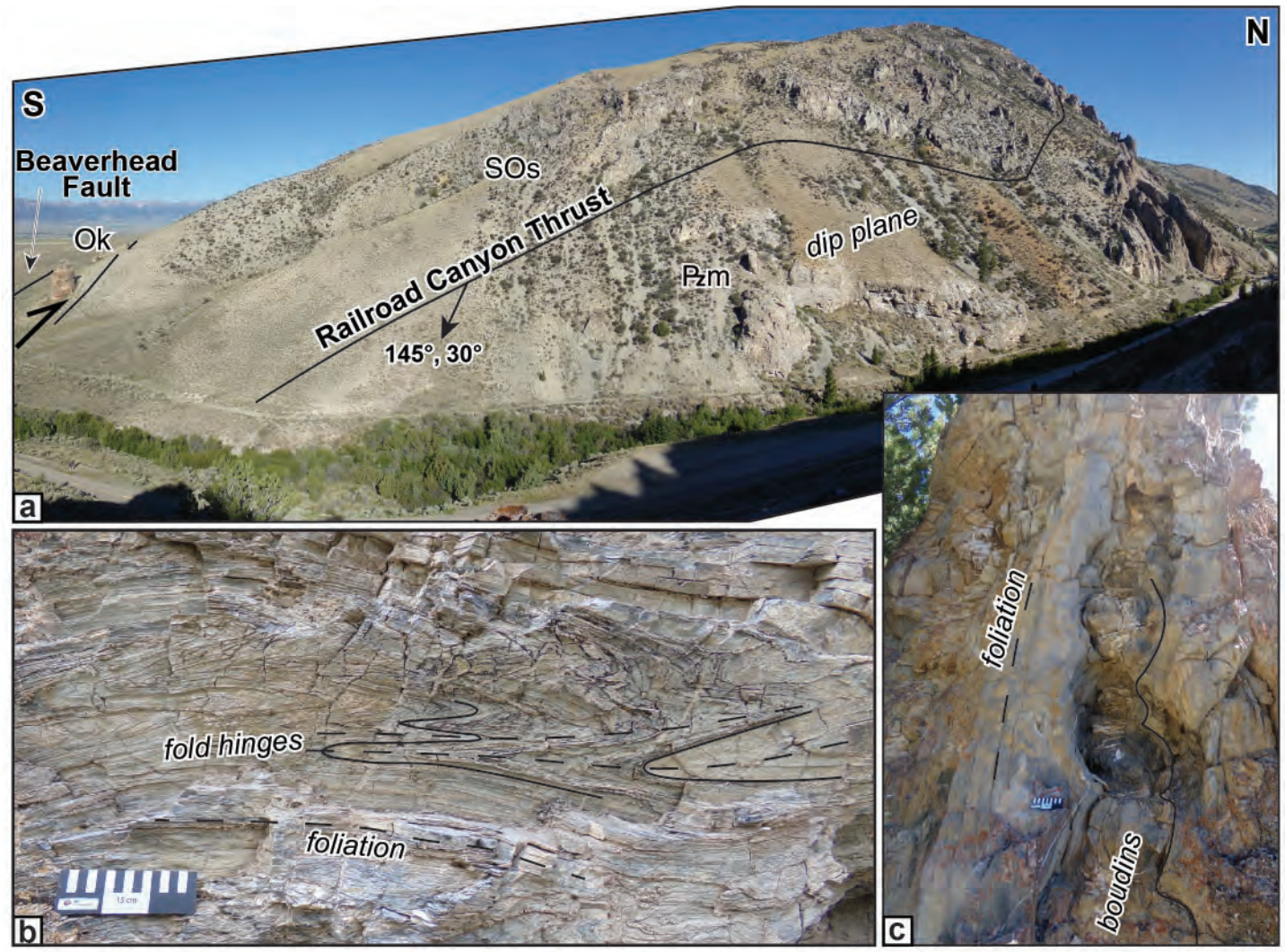

Figure 8. Annotated photos of Railroad Canyon thrust (Stop 4). (a) Fault relationships as viewed from the eastern side of Railroad Canyon, with label on the hanging wall. Mean dip of the thrust plane shown by labeled arrow. See figure 2 for abbreviated unit names. (b) Flattened similar folds within the mylonite showing high ductile strain. Resistant siliceous bands highlight folds. (c) Rheological contrasts between brittle, more siliceous boudins, and ductile, more calcitic mylonites.

same thin-skinned thrust, with a detachment following nonconformities and disconformities up and over the low-relief Lemhi arch.

The complicated relationships observed during this field trip within the northern Leadore quadrangle can be summarized by a simple series of deformation events. The stratigraphy suggests pre-Devonian normal faulting, with the resultant Lemhi arch basement high persisting until it was flooded in the latest Devonian (Famennian; Grader and others, 2016). During the Cretaceous, top-to-the-east motion along the Thompson Gulch–Railroad Canyon thrust system occurred in a thin-skinned fashion at depths of around 6–9 km (4–6 mi; Parker and others, 2022). A lateral ramp, following weak rocks near the base of the carbonate package, likely connected the detachment across the variable hinge line strata that drape the Lemhi arch. Late thick-skinned slip along the Baby Joe Gulch thrust and its imbricates cut this mylonite, during more north–south-oriented shortening above a deeper detachment within basement rocks of the Lemhi arch. Normal slip along the Beaverhead fault may have taken a shortcut and rooted into the thick-skinned Baby Joe Gulch thrust at depth, leaving behind a "perched basement wedge" (Sales, 1983; Lageson, 1989). In addition to being persistent weaknesses, the stratigraphically controlled thin-skinned thrusts of the Thompson Gulch–Railroad Canyon thrust system and the reactivated thick-skinned thrusts of the Baby Joe Gulch thrust system seem to be important conduits and seals that focused mineralization in the small but complex Leadville mining district.

REFERENCES

Bell, R.N., 1920, Twenty-first annual report of the mining industry of Idaho for the year 1919: Report of inspector of mines, 180 p.

Beutner, E.C., 1968, Structure and tectonics of the southern Lemhi Range, Idaho: State College, Penn., Pennsylvania State University, Ph.D. thesis, 106 p., 3 plates.

Cox, B., and Antinioli, T., 2017, Ore controls of the Leadville (Junction) and Gilmore mining districts, Lemhi County, Idaho: A field trip guide: Northwest Geology, v. 46, p. 93–100.

Evans, K.V., and Green, G.N., 2003, Geologic map of the Salmon National Forest and vicinity, east-central Idaho: U.S. Geological Survey Geologic Investigations Series, I-2765, 2 sheets, scale 1:100,000.

Garber, K.L., Finzel, E.S., and Pearson, D.M., 2020, Provenance of synorogenic foreland basin strata in southwestern Montana requires revision of existing models of Laramide tectonism: North American Cordillera: Tectonics, v. 39, 26 p.

Grader, G.W., Isaacson, P.E., Doughty, P.T., Pope, M.C., and Desantis, M.K., 2016, Idaho Lost River shelf to Montana craton: North American Late Devonian stratigraphy, surfaces, and intrashelf basin, *in* Playton, T.E., Kerans, C., and Weissenberger, J.A.W., eds., New advances in Devonian carbonates: Outcrop analogs, reservoirs, and chronostratigraphy: Society of Sedimentary Geology Special Publication 107, p. 347–379.

Hait, M.H., 1965, Structure of the Gilmore area, Lemhi Range, Idaho: State College, Penn., Pennsylvania State University, Ph.D. thesis, 134 p., 3 plates.

Kaempfer, J.M., 2021, Deep-time tectono-thermal history of the northern US Cordillera: Understanding zircon (U-Th)/He thermochronology and its application to Idaho–Montana basement rocks: Ph.D. thesis, University of Illinois, 141 p.

Lageson, D.R., 1989, Reactivation of a Proterozoic continental margin, Bridger Range, southwestern Montana, *in* French, D.E., and Grabb, R.F., 1989 Field conference guidebook: Geologic resources of Montana: Montana Geological Society, p. 279–298.

Link, P.K., Todt, M.K., Pearson, D.M., and Thomas R.C., 2017, 500–490 Ma detrital zircons in upper Cambrian Worm Creek and correlative sandstones, Idaho, Montana, and Wyoming: Magmatism and tectonism within the passive margin: Lithosphere, v. 9, no. 6., p. 910–926.

Lonn, J.D., Elliott, C.G., Stewart, D.E., Mosolf, J.G., Burmester, R.F., Lewis, R.S., and Pearson, D.M., 2019, Geologic map of the Bannock Pass 7.5' quadrangle, Beaverhead County, Montana, and Lemhi County, Idaho: Montana Bureau of Mines and Geology Geologic Map 76, 1 sheet, scale 1:24,000.

Lucchitta, B.K., 1966, Structure of the Hawley Creek area, Idaho-Montana: State College, Penn., Pennsylvania State University, Ph.D. thesis, 203 p., 2 plates.

Lund, K., 2018, Geologic map of the central Beaverhead Mountains, Lemhi County, Idaho, and Beaverhead County, Montana: U.S. Geological Survey Scientific Investigations Map 3413, 1 sheet, scale 1:50,000.

Lund, K., Aleinikoff, J.N., Evans, K.V., duBray, E.A., Dewitt, E.H., and Unruh, D.M., 2010, SHRIMP U-Pb dating of recurrent Cryogenian and Late Cambrian–Early Ordovician alkalic magmatism in central Idaho: Implications for Rodinian rift tectonics: Geological Society of America Bulletin, v. 122, p. 430–453.

M'Gonigle, J.W., 1982, Devonian carbonate-breccia units in southwestern Montana and Idaho; A review of brecciating mechanisms, *in* Powers, R.B., ed., Geologic studies of the Cordilleran thrust belt: Rocky Mountain Association of Geologists, v. 2, p. 677–690.

Mitchell, V.E, 2004, History of the Leadville, Kimmel, and Baby Joe Mines, Lemhi County, Idaho: Idaho Geological Survey Staff Report 04-1, 35 p.

Orme, D.A., 2020, New timing constraints for the onset of Laramide deformation in southwest Montana challenge our understanding of the development of a thick-skinned structural style during flat-slab subduction: Tectonics, v. 39, no. 12., 8 p.

Parker, S.D, and Pearson, D.M., 2020, Geologic map of the northern part of the Leadore quadrangle, Lemhi County,

Idaho: Idaho Geological Survey Technical Report T-20-03, 1 sheet, scale 1:24,000.

Parker, S.D, and Pearson, D.M., 2021, Pre-thrusting stratigraphic control on the transition from a thin-skinned to thick-skinned structural style: An example from the double-decker Idaho–Montana fold-thrust belt: Tectonics, v. 40, no. 5., 31 p.

Parker, S.D, Pearson, D.M., and Finzel, E.S., 2022, A thermal profile across the Idaho–Montana fold-thrust belt reveals a low-relief orogenic wedge that developed atop a pre-orogenic basement high: Lithosphere, v. 2022, 28 p.

Ruppel, E.T., 1968, Geologic map of the Leadore quadrangle, Lemhi County, Idaho: U.S. Geological Survey Geologic Quadrangle map GQ-733, 1 sheet, scale 1:62,500.

Ruppel, E.T., 1986, The Lemhi arch: A Late Proterozoic and early Paleozoic landmass in central Idaho: AAPG Memoir, v. 41, p. 119–130.

Ruppel, E.T., 1998, Geologic map of the eastern part of the Leadore 30' x 60' quadrangle, Montana and Idaho: Montana Bureau of Mines and Geology Open-File Report 372, 1 plate, scale 1:100,000.

Sales, J.K., 1983, Collapse of Rocky Mountain basement uplifts, *in* Lowell, J.D., ed., Rocky Mountain foreland basins and uplifts: Rocky Mountain Association of Geologists, p. 79–97.

Schmidt, C.J., and Perry, W.J., 1988, Interaction of the Rocky Mountain foreland and the Cordilleran thrust belt: Geological Society of America Memoir, v. 171, 582 p.

Scholten, R., 1957, Paleozoic evolution of the geosynclinal margin north of the Snake River Plain, Idaho–Montana: Geological Society of America Bulletin, v. 68, p. 151–170.

Scholten, R., and Ramspott, L.D., 1968, Tectonic mechanisms indicated by structural framework of central Beaverhead Range, Idaho–Montana: Geological Society America Special Paper, v. 104, 59 p.

Skipp, B, 1988, Cordilleran thrust belt and faulted foreland in the Beaverhead Mountains, Idaho and Montana, *in* Schmidt, C.J., and Perry, W.J., eds., Interaction of the Rocky Mountain foreland and the Cordilleran thrust belt: Geological Society of America Memoir, v. 171, 2 plates, p. 237–266.

Sloss, L.L., 1954, Lemhi arch, a mid-Paleozoic positive element in south-central Idaho: Bulletin of the Geological Society of America, v. 65, p. 365–368.

Umpleby, J.B., 1913, Geology and ore deposits of Lemhi County, Idaho: U.S. Geological Survey Bulletin, v. 528, 182 p.

Yonkee, W.A., and Weil, A.B., 2015, Tectonic evolution of the Sevier and Laramide belts within the North American Cordillera orogenic system: Earth-Science Reviews, v. 150, p. 531–593.

HUMBOLT ANTICLINE, SOUTHWEST MONTANA PIONEER MOUNTAINS: KEY STRATIGRAPHIC EVIDENCE FOR BREAKUP OF SUPERCONTINENT RODINIA

James W. Sears,[1] Michael H. Hofmann,[1] and Catherine McDonald[2]

[1]*University of Montana, Missoula, Montana*
[2]*Montana Bureau of Mines and Geology, Butte, Montana*

The field trip examines the Ediacaran–Cambrian stratigraphy of the Humbolt Anticline in the Pioneer Mountains of southwestern Montana. This Sevier/Laramide anticline is an inverted paleo-graben that captured >500 m of Ediacaran and Early Cambrian clastic sediment, as documented by recent paleontological findings (Kovalchuk, 2017; McDonald and Yakovlev, 2019; Trippe, 2019). The paleo-graben provides key stratigraphic evidence for breakup of supercontinent Rodinia, and for the rift-to-drift transition of Laurentia's Cordilleran margin. It occupies the east flank of the early Paleozoic Lemhi arch of central Idaho and is equivalent to a similarly inverted Neoproterozoic paleo-graben on the west flank of the arch in the Bayhorse area, ~100 km to the southwest (Brennan and others, 2020).

From the base up, the inverted graben exposes the following informal map units: (1) the 250-m-thick "Quartzite of Argenta" (which rests directly on metamorphic basement in a borehole; see fig. 1 for borehole location); (2) the 350-m-thick Cryogenian (?) through Ediacaran Phyllite unit, and (3) the > 300-m-thick Early Cambrian Quartzite unit. These rocks were previously assigned to the Mesoproterozoic Belt Supergroup (Meyers, 1952; Pearson and Zen, 1985; Ruppel and others, 1993). The Middle Cambrian Flathead, Wolsey Shale (equivalent to Silver Hill Formation), and Hasmark Formations onlapped the tilted and

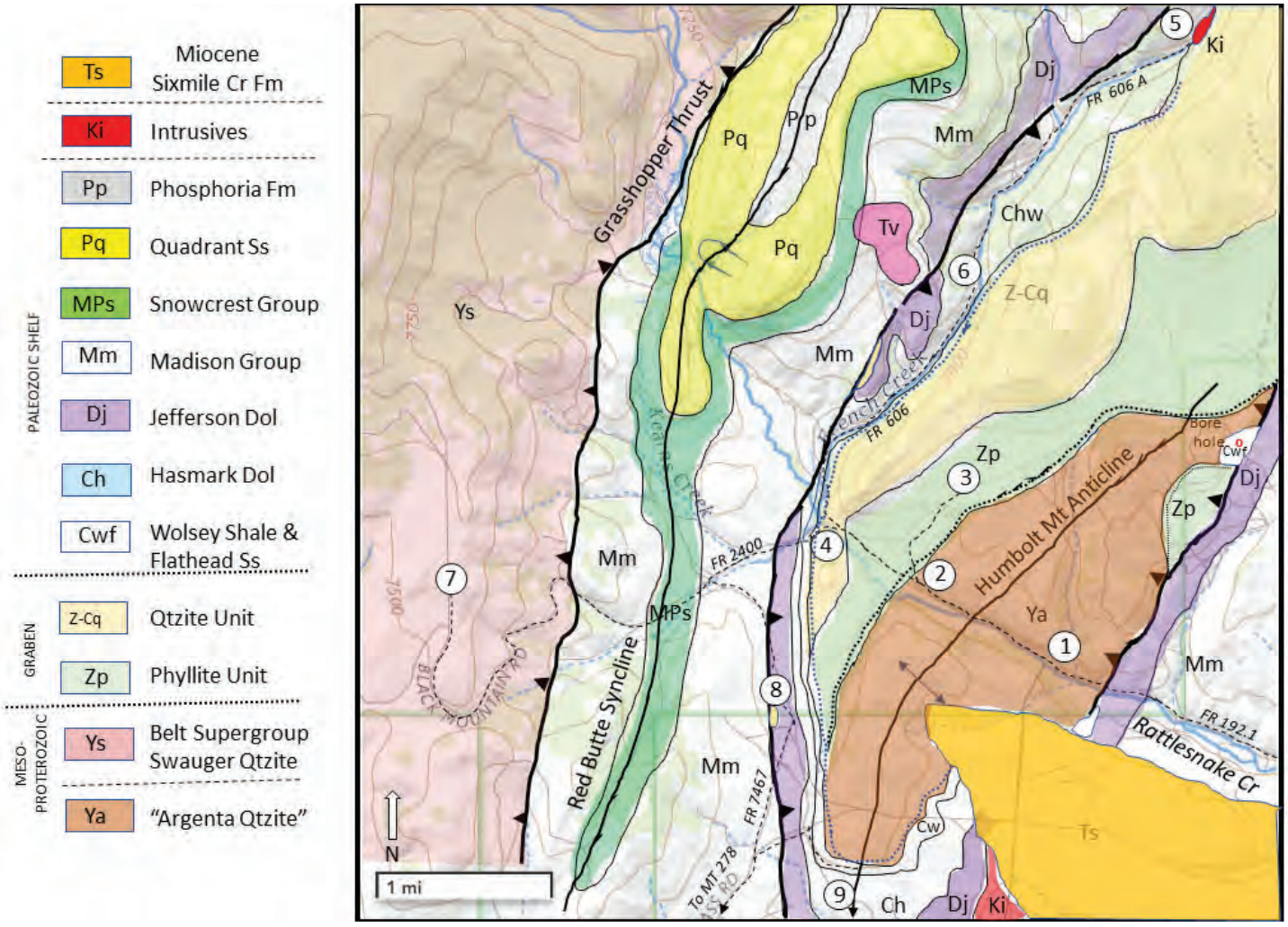

Figure 1. Simplified geologic map of Humbolt Anticline in Rattlesnake Creek area. Circled numbers, field trip stops. Dashed lines, roads. Dotted lines, unconformities. Tv, Eocene volcanic rocks. Small red circle, borehole. After field camp maps by Sears, 2010–2022.

lithified graben fill, which formed a paleo-high during the Sauk transgression. The graben lies 3 km east of Mesoproterozoic Belt Supergroup in the Kelley/Grasshopper thrust plate (fig. 1).

The paleo-graben field trip begins with stops in the Quartzite of Argenta, and continues upsection with stops in the Phyllite and Quartzite units. The angular unconformity at the base of the Middle Cambrian section will be documented with stops in the Flathead Sandstone, Wolsey Shale, and Hasmark Dolomite. The Belt Supergroup will be visited with a stop in the Kelley/Grasshopper thrust plate.

The paleo-graben may record several aspects of the main phases of the Cordilleran margin breakup as outlined by Beranek (2017): (1) Pre-rift; (2) 750–640 Ma (?) Early Rift phase; (3) 640–570 Ma Early Sag phase; (4) 570–540 Ma Late Rift phase; (5) 540–520 Ma Breakup phase; and (6) post-520 Ma Late Sag phase.

Pre-rift—The Quartzite of Argenta, its underlying metamorphic basement, and the Belt Supergroup represent the pre-breakup units of the field trip area. The Quartzite of Argenta crops out in the core of the Humbolt Anticline. The field guide describes an exposure along Rattlesnake Creek at Stops 1, 2a, and 2b. Basement rocks were encountered at a depth of 280 m in a borehole that penetrated the quartzite, an underlying phyllite, and a basal feldspathic quartzite and conglomerateon the east limb of the anticline (Pearson, 1996). The Quartzite of Argenta may correspond to the Neihart Quartzite of the Little Belt Mountains, which may represent part of an epicontinental sheet of clean quartz sandstone (Sears and Link, 2007; Sears and others, 2010). It contrasts sharply with the feldspathic Swauger Quartzite of the Mesoproterozoic Belt Supergroup, which occupies the Kelley thrust sheet on Black Mountain ridge at Stop 7 (Lonn and others, 2019). The Kelley thrust may follow the reactivated rift margin of the Lemhi subbasin of the Belt Basin. It approximately defines the east edge of the Lemhi Arch.

Early Rift phase—The basal "Phyllite unit," seen at Stop 2b, unconformably overlies the Quartzite of Argenta. It includes a thin, immature conglomerate that contrasts sharply with the immediately underlying clean Quartzite of Argenta. The conglomerate contains lithoclasts of rhyolite and trachyte, and coarse grains of monocrystalline microcline, implying nearby magmatic sources (Trippe, 2019). The unit may be equivalent to the Neoproterozoic Windermere Supergroup, a thick rift facies recognized along the Cordilleran margin from Death Valley north to Canada's Yukon. The Windermere Supergroup occurs 200 km southwest of the field trip area in central Idaho, where it includes ~700 to 670 Ma continental-rift affinity basalt, trachyte, and rhyolite (Yonkee and others, 2014). A group of 665–650 Ma syenite–diorite stocks intruded the Belt Supergroup on the flank of the rift in central Idaho, about 100 km southwest of the field trip area (Lund and others, 2010).

Early Sag phase—The upper Phyllite unit, seen at Stop 3, is interpreted as a system of turbidites captured in the subsiding graben (Trippe, 2019). Neoproterozoic trace fossils indicate correlation with the upper part of the Windermere Group, during a hiatus in igneous activity.

Late Rift phase—The uppermost Phyllite unit records a marginal-marine profile transitional into a wave-dominated, very shallow-marine depositional setting. It may record the open marine conditions for the rift. Abundant mat-ground trace fossils appear, including varieties of Helminthoides, correlated with late Ediacaran (570 Ma). Kovalchuk (2017) concluded the mat-grounds were microbially induced, and suggested that the rocks are most likely to be Neoproterozoic. Trippe (2019) considered them to be late Ediacaran.

Breakup phase—The "Quartzite unit" is seen at Stop 4. It is a compositionally super-mature and texturally pure, non-feldspathic quartz–arenite, and lacks bedforms within thick, tabular, massive beds (McDonald and Yakovlev, 2019; Trippe, 2019). It is most indicative of intracontinental fluvial origins, as it accumulated in the subsiding paleo-graben. It includes a thin bed of argillite with a rich ichnofossil assemblage (McDonald and Yakovlev, 2019) that includes *Treptichnus pedum,* which dates it to earliest Cambrian (Trippe, 2019). The Quartzite unit is 300 m thick in the field trip area. It is continuous to Birch Creek, 9 mi to the north. It forms a series of peaks, including Humbolt Mountain, but also forms wide areas of blocky alpine felsenmeer. It probably brackets the breakup phase as presented by Beranek (2017), 540–520 Ma, when the paleo-graben captured thick, clean quartz sand.

Late Sag phase—The Quartzite unit was well-lithified before deposition of the Middle Cambrian Flathead Sandstone and Wolsey Shale, when the Sauk transgression reached western Montana at ~500 Ma (Link and others, 2017). Angular clasts of the Quartzite unit are found in Flathead conglomerate on the east limb of the anticline. The paleo-graben fill was tilted by faulting, and the extremely resistant Quartzite unit formed a strike-ridge, parallel to the paleo-graben axis. A boulder conglomerate seen at Stop 5 was shed down the west limb of the ridge. The conglomerate and ridge were ultimately buried on an angular unconformity by the Wolsey Shale and Hasmark Dolomite as seen at Stops 6, 8, and 9, as sea level rose and the Cordilleran margin thermally subsided, perhaps in response to global seafloor spreading as Rodinia's fragments drifted apart. Basement crops out 20 km to the south in the Armstead anticline, and in the Ruby, Blacktail, and Highland mountains 40–50 km to the east (Vuke and others, 2007). In those areas, the high-grade basement rocks are directly overlain by coarse-grained, fossiliferous, Middle Cambrian Flathead Sandstone. (Link and others, 2017).

ROAD LOG

Begin at intersection of I-15 exit ramp 59 and Montana Highway 278. Take MT Highway 278 west toward Bannack State Park and Jackson.

7.0 mi Turn right toward Argenta on wide gravel road RD 64. Argenta Flats is the outwash plain of the Rattlesnake Creek glacier of the Pioneer Mountains.

9.0 mi Turn left at gravel road intersection onto RD 1.

11.7 mi Village of Argenta.

12.5 mi Cross Rattlesnake Creek. Outcrops of a Late Cretaceous granite sill. Silver mines to left at contacts of Cretaceous granite and Paleozoic carbonates. Large white outcrop to south is Mississippian Madison Group marble, contact-metamorphosed by granite sill.

13.3 mi Enter Beaverhead–Deerlodge National Forest (road becomes FR 192.1). Stapleton Gulch on right. East-dipping, thin-bedded and kink-folded Mississippian Lodgepole Limestone on east side of gulch, Devonian Three-Forks Shale in gulch, and Devonian Jefferson Dolomite on west side of gulch.

13.7 mi Fault contact of Quartzite of Argenta and Cambrian Hasmark Dolomite in gulch on right. Reactivated graben-bounding fault. Enter canyon of Rattlesnake Creek, cut through gently dipping, red Quartzite of Argenta.

STOP 1—14.0 mi
QUARTZITE OF ARGENTA

Mouth of Clarks Canyon at FR 192.1. Park on Forest Service road. Walk short distance up Clarks Canyon to view prominent cliff outcrop on right (fig. 2).

The Quartzite of Argenta is exposed in a near-vertical cliff (outcrop height is approximately 200 ft) along Clarks Canyon, a small tributary to Rattlesnake Creek (view is to the east). Sandstones are mainly medium-grained (ranging from fine-grained to coarse-grained) and are intensely crossbedded. Crossbeds range in height from 10 to 15 cm. Most quartz grains are subround and sorting changes from moderately well sorted to poorly sorted. Bed thickness increases from bottom (reddish unit in lower cliff) to top (lighter colored unit in upper cliff). Beds in the lighter color (upper) parts of the cliff forming united are largely amalgamated. No trace fossils have been observed in the Quartzite of Argenta.

Continue west on FR 192.1.

Figure 2. Stop 1. Quartzite of Argenta in Clark Canyon, a small northern tributary to HumRattlesnake Creek. The near-vertical cliff is approximately 200 ft high (view is to the east).

STOP 2a, b—15.0 mi
QUARTZITE OF ARGENTA AND BASE OF PHYLLITE UNIT

Pull off at dirt road on right, at west end of quartzite-walled canyon. Climb to base of red quartzite outcrops.

The outcrops are in the upper part of the Quartzite of Argenta. The following lithologic description is modified from Trippe (2019). The upper package is dominated by tabular, moderately silicified, highly resistant, often cliff-forming non-micaceous, non-feldspathic, quartz–arenitic orthoquartzite. Beds are very thick to medium-bedded, trough cross-stratified, high to low-angle, and horizontally planar cross-stratified. The rock is very light pink to dark pinkish-red, and mostly consists of rounded, very fine to medium grains of quartz, that are tightly packed and very well cemented. It contains discontinuous lenses of rounded, milky quartz–pebble conglomerate, and sand chips on bedding surfaces.

Previous workers have correlated the Quartzite of Argenta with the Flathead Sandstone or the Belt Supergroup. Sears and Link (2007) suggested a correlation with the lithologically similar Neihart Quartzite of the Little Belt Mountains, rather than younger members of the Belt Supergroup or the Flathead Sandstone. Sears and others (2010) presented detrital zircon U-Pb age dates that were compatible with Neihart Quartzite correlation. That range contrasts with most upper Belt quartzites, which typically contain 1400 Ma detrital zircons. Mapping demonstrates that the unit cannot be Flathead, as it is overlain by diverse strata, truncated by a profound angular unconformity, and unconformably onlapped by Wolsey Shale and thin patches of Flathead (fig. 1). The Quartzite of Argenta is interpreted as a predominantly fluvial system, its sediments transported

and deposited by intra-cratonic braided and meandering streams, over a broad plain.

Traverse ~ 100 yards west across small gulch to float and small outcrops of base of Phyllite unit.

The following lithologic description is modified from Trippe (2019, p. 30–31). The basal Phyllite unit is a clast-supported, rounded to well rounded, quartz–pebble and quartz–arenite pebble conglomerate. It contains mylonite clasts, and is non-feldspathic. It is overlain by maroon, arkosic, small pebble to granule, matrix-supported conglomerate, in an immature, micaceous matrix. Clasts consist of mostly rounded, milky quartz, with lesser angular to rounded, euhedral, pink, optically clear feldspar grains, and lithic–volcanic clasts of rhyolite and lesser quartz–trachyte.

It is overlain by a sequence of very fine- to medium-grained maroon sandstone, with symmetrical wave-dominated and oscillation ripple marks, interpreted as a reworked Quartzite of Argenta. It was deposited as a fluvial channel-lag axial drainage deposit, paralleling the graben's structural axis, during late-stage rift-margin development. The rounded quartz pebbles are interpreted as recycled from the Quartzite of Argenta and other intracratonic sources. The small pebble- to granule-sized lithic–volcanic clasts are interpreted as from syn-rift, bimodal(?) activity along the developing rift margin.

Take the dirt road to right of Rattlesnake Creek Road FR 192.1 on west edge of quartzite cliffs.

15.7 mi Intersection with dirt road on left.

STOP 3
SEDIMENTARY STRUCTURES OF UPPER PHYLLITE UNIT

Trippe (2019) described this package of tan, silty sandstone with gutter casts, wave-dominated ripples, syneresis cracks, gutter molds, groove casts, and unidirectional tool marks. Small-scale soft-sediment loading and dewatering structures, and truncation surfaces are also seen. Microbial structures include petees, filled-sand cracks, wrinkle structures, gas domes, and microbial mat chips. Rare bioturbation, mostly interpreted as varieties of Helminthoides, indicate a transitional, marginal-marine depositional profile passing into a wave-dominated, very shallow-marine depositional setting, that may record the initial exposure of the rift margin shoulder to open marine conditions. The Phyllite unit was examined by Kovalchuk (2017), who concluded that it was Neoproterozoic. Helminthoidichnites and Helminthopsis trace fossils in the upper half of the Phyllite unit imply that the upper section is no older than late Ediacaran (575 Ma).

The Phyllite unit marks the beginning of the late rift phase of the Cordilleran margin breakup as presented by Beranek (2017). In Idaho, trachybasalt and bi-modal volcanics erupted from ~580 Ma to 540 Ma, the possible timespan of the Phyllite and upper Quartzite units. Final breakup occurred from 540 Ma to 520 Ma, when the lithified sedimentary fill of the graben was faulted and tilted into resistant ridges that shed boulder conglomerate down the dip-slope. By 500 Ma, sea level rose as recorded by the Cambrian transgression. The tilted grabenfill formed an island until buried by the Wolsey Shale and Hasmark Dolomite.

Return to main Rattlesnake Creek Road (FR 192.1).

16.3 mi Turn right on FR 192.1.

STOP 4—16.6 mi
"QUARTZITE UNIT"

Park near intersection of FR 192.1 and FR 2400 roads. Large white cliffs are the Quartzite unit. Examine large fallen blocks near road.

The Quartzite unit is a compositionally and texturally pure, very light gray, non-feldspathic quartz–arenite, with very massive bedding. These properties would be most indicative of an intracontinental stable craton petrofacies. A thin argillite layer within the quartzite on Humbolt Mountain has an ichnofossil assemblage that includes *Treptichnus pedum, Treptichnus isp., Planolites, Monomorphichnus, Palaeophycus, Bergaueria,* and *Helminthopsis* (Trippe, 2019).

Reset odometer at intersection of FR 192.1 and FR 2400 roads, then continue on FR 192.1.

0.3 mi Turn right onto French Creek Road (FR 606).

Canyon of French Creek. Silver and gold mines on left. Road proceeds along contact between west-dipping Quartzite of Argenta (on right) and Hasmark Dolomite (on left). Gold and silver mines on left in Devonian Jefferson Dolomite and Three Forks Shale.

2.5 mi Take dirt road on right (FR 606 A), proceed up Trout Creek canyon.

STOP 5—3.0 mi
CAMBRIAN BOULDER CONGLOMERATE AND SYENITE–TRACHYTE PORPHYRY SILL

The boulder conglomerate likely records erosion of resistant ridges of quartzite of the graben that stood

above wave-base during the Middle Cambrian transgression. It is overlain by Middle Cambrian Wolsey Shale, which has thin interbeds of flaggy sandstone. The Wolsey Shale is overlain by Hasmark Dolomite. The section is intruded by a syenite–trachyte porphyry sill.

Return toward FR 2400.

STOP 6—4.2 mi
HASMARK DOLOMITE SANDSTONE FACIES
Small cliff road cut on right.

This unit of sandstone is thought to lie within the Hasmark Dolomite (fig. 3). Compared to the Quartzite of Argenta and the Flathead Sandstone, the Hasmark Sandstone is finer-grained and indicates a distinctly different paleoflow direction (due south, see rose diagram in fig. 4). Sorting is moderate to well sorted. Grains are largely subround. Quartz–arenite is most common, but feldspathic arenite is present. Bed thickness varies from centimeter-scale to massive. The contact of the sandstone to the underlying units is not exposed. The upper contact is below the first carbonate bed, distinctly different from the upper contacts of the Quartzite of Argenta and the Flathead Sandstone, which both are overlain by siliciclastic strata.

Return to intersection of FR 2400. Reset odometer at intersection of FR 2400, then turn right on FS 2400 (Black Mountain Road).

0.8 mi Intersection of FS 7467, continue on FS 2400. (Return to this intersection after Stop 5.)

1.4 mi Enter canyon. Inverted Madison Group limestone in footwall of Grasshopper Thrust exposed on the right (north).

2.0 mi Cross Grasshopper Thrust at gap. Red-

Figure 3. Stop 5. Sandstone beds in Hasmark Formation along French Creek Road.

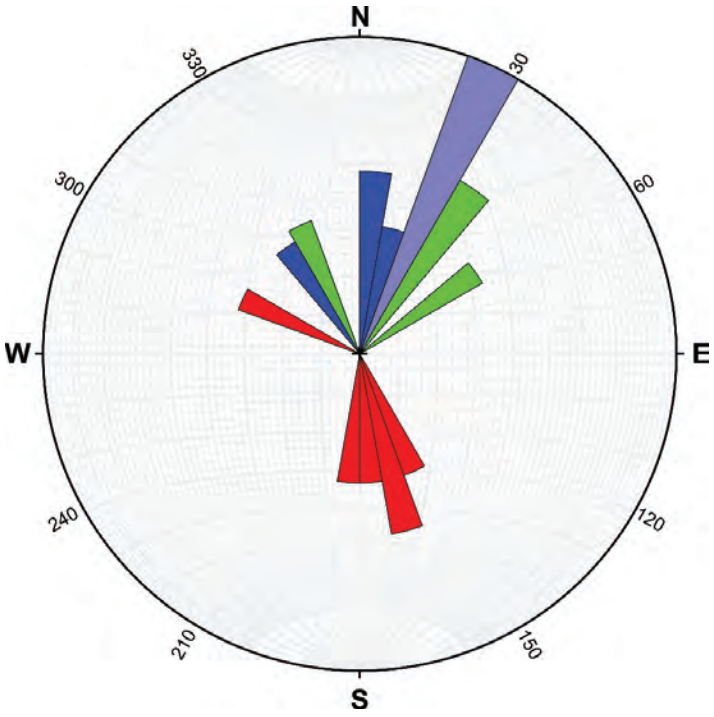

Figure 4. Paleoflow measurements from various sandstone units in the field trip area. The measurements from the Quartzite of Argenta (green; Stop 1) in Clarks Canyon trend to the north, in line with the measurements taken from the Flathead Sandstone in the trench near Argenta (light blue; Stop 9), and from outside the field trip area near Clark Canyon Reservoir (dark blue). A distinctly different paleoflow direction (due south) is observed for the sandstone unit observed in the Hasmark Dolomite in French Creek (red; Stop 6). It needs to be noted that the number of measurements taken from each unit are very small. Therefore, these values should be just used as general trends until more data is available to confirm these paleoflow patterns.

weathering Mesoproterozoic Belt Supergroup thrust over gray Mississippian Madison Group.

4.0 mi Park along straight stretch of road and hike about 0.1 mi up hill, east to crest of ridge.

STOP 7
SWAUGER QUARTZITE OF BELT SUPERGROUP

Great views of Pioneer Mountains. View east—Prominent forested ridge at French Creek is dip-slope of Quartzite of Humbolt on west limb of Humbolt anticline, continuing north to Humbolt Mountain. Note forested quartzite wrapping to crest of anticline. East of the forested ridge, the grassy area is the Phyllite unit, and in Rattlesnake Creek Canyon is terrace of Quartzite of Argenta in core of anticline. East limb of anticline is cut by thrust fault with quartzite over Paleozoic limestone. West of forested ridge are gray Paleozoic carbonates continuing to south. Three forest patches to south are on Quartzite of Argenta on west limb of Humbolt anticline. To south, the nose of the south-plunging Humbolt anticline can be seen, where the carbonates wrap around the reddish quartzite ridge. The carbonates

clearly cut downsection from north to south on the west limb of the anticline.

The Swauger Quartzite is a unit within the Lemhi subbasin of the Belt Supergroup. It is likely equivalent to the Mt. Shields Formation and Bonner Quartzite of the Missoula Group. Here it is a medium-to-coarse feldspathic and micaceous quartzite, locally conglomeratic. It commonly contains red argillite chips eroded from interlayered argillite beds. It exhibits centimeter- to decimeter-scale trough crossbeds and small channels. It was likely deposited as widespread sheet floods with only small channelization. The unit fines to the north, indicating generally northward sedimentary transport, likely captured in a broad continental rift system.

These are the easternmost outcrops of the Belt Supergroup in this part of Montana. The Belt thickens westward to >15 km. This likely marks the eastern edge of the Belt Basin, thrust-transported tens of kilometers eastward in the Laramide orogeny. The Grasshopper/Kelley Thrust of the Pioneer Mountains is equivalent to the Lewis Thrust of Glacier National Park. On the Black Mountain to the west, the Belt Supergroup is overlain by thick quartz arenite thought to be of Neoproterozoic to early Cambrian age (Lonn and others, 2019). If it is equivalent to the Quartzite unit of the graben, the unit would have cut eastward across the Belt Basin to the Phyllite unit in the Humbolt graben.

Return to FR 7467 intersection. Reset odometer at FR 7467 intersection, then turn right.

1.2 mi Pull over at intersection of dirt road on left.

STOP 8
VIEW OF ANGULAR UNCONFORMITY

Ridge to east is gently dipping Quartzite of Argenta in axis of anticline. Valley to north is Phyllite unit. Low ridge to north is the Quartzite unit. The Cambrian Wolsey Shale, Hasmark Dolomite, and Devonian Jefferson Dolomite overlie an angular unconformity that cuts downsection from west to east from the graben's Quartzite unit, across the Phyllite unit, to the Quartzite of Argenta.

Continue on FR 7467.

1.9 mi Take hard left on gravel road.

2.2 mi Gravel crossroad. Take right road.

STOP 9—2.7 mi
FLATHEAD SANDSTONE IN TRENCH

Park along dirt road. Walk ~200 ft north to trench.

The Flathead Sandstone exposed in the trench contains two distinct sandstone intervals separated by siltstone and mudstone units. The beds are nearly vertical dipping in the left (west) part of the trench, and nearly horizontal in the center part. Coarse- to medium-grained, crossbedded quartz arenite occurs in the lower sandstone unit. Many beds are normally graded. Sorting is moderate to poor in these lower sandstone beds and grains are subangular to subround. Crossbeds are accentuated by abundant mud rip-up clasts. Paleoflow measurements indicate paleotransport to the north–northeast (see rose diagram in fig. 4). Ripples are present throughout the quartz arenites, and best developed along the upper bedding planes of many individual beds. The grain size in the upper interval is largely medium-grained, with fine-grained sandstone becoming more common towards the top of the interval. Grains are subround, and sorting is well to medium. Glauconite is present in some intervals. Trace fossils are present throughout the interval. Average elemental concentrations of selected elements in the Flathead Sandstone and Quartzite of Argenta are compared in figure 5.

Return to crossroad intersection.

3.2 mi Turn left at crossroad intersection. Return to FR 7467.

3.5 mi Turn left on FR 7467. This road takes you to MT HWY 278 at Badger Pass.

6.9 mi T-intersection with RD 57. Turn left.

7.3 mi Intersect MT HWY 278. Turn left to return to I-15.

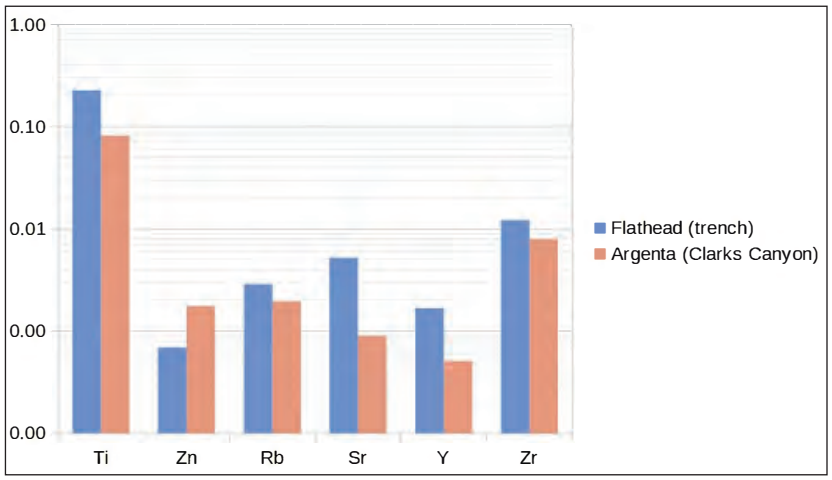

Figure 5. Average elemental concentrations (y-axis in wt%) for selected elements (x-axis) in the Flathead Sandstone (blue; trench section Stop 9) and Quartzite of Argenta in Clarks Canyon (red; Stop 1). All elements presented in this plot are from sandstones only. Other facies are not included to allow for better comparison. The distinct elemental concentration differences between the two units are potentially indicating different source areas. Similar to the paleoflow data, the number of samples is small and these averages only represent general trends. Additional data are required to confirm these initial observations.

END OF FIELD TRIP (FIND YOUR WAY HOME!)

REFERENCES

Beranek, L.P., 2017, A magma-poor rift model for the Cordilleran margin of western North America: Geology, v. 45, p. 115–118, doi: https://doi.org/10.1130/G39265.1

Brennan, D.T., Pearson, D.M., Link,P.K., and Chamberlain, K.R., 2020, Neoproterozoic Windermere Supergroup near Bayhorse, Idaho: Late-stage Rodinian rifting was deflected west around the Belt Basin: Tectonics, v. 39, issue 8, doi: https://doi.org/10.1029/2020TC006145

Kovalchuk, O., 2017, Microbial mat-related structures: Laboratory experiments and observations from the Mesoproterozoic Belt Supergroup, southwestern Montana, U.S.A.:Edmonton, Alberta, University of Alberta, M.S. thesis, 105 p.

Link, P.K., Todt, M.K., Pearson, D.M., and Thomas, R.C., 2017, 500-490 Ma detrital zircons in Upper Cambrian Worm Creek and correlative sandstones, Idaho, Montana, and Wyoming: Magmatism and tectonism within the passive margin: Lithosphere, v. 9, no. 6, p. 910–928, doi: https://doi.org/10.1130/L671.1

Lonn, J.D, Elliott, C.G., Lewis, R.S., Burmester, R.F., McFadden, M.D., Stanford, L.R., and Janecke, S.U., 2019, Geologic Map of the Montana Part of the Salmon 30' x 60' quadrangle, southwest Montana: Montana Bureau of Mines and Geology Geologic Map 75, scale 1:100,000.

Lund, K.L., Aleinikoff, K.V., duBray, E.A., Dewitt, E.H., and Unruh, D.M.., 2010, SHRIMP U-Pb dating of recurrent Cryogenian and Late Cambrian-Early Ordovician alkalic magmatism in central Idaho: Implications for Rodinian rift tectonics: Geological Society of America Bulletin, v. 122, p. 430-453.

McDonald, C., and Yakovlev, P., 2019, Geologic map of the Twin Adams Mountain 7.5' quadrangle, southwestern Montana: Montana Bureau of Mines and Geology Geologic Map 73, 1 sheet, scale 1:24,000.

Myers, W.B., 1952, Geology and mineral deposits of the northwest quarter of the Willis quadrangle and adjacent Brown's Lake area, Beaverhead County, Montana: U.S. Geological Survey Open-File Report 52-105, 46 p., 1 sheet, scale 1:31,680.

Pearson, R.C., and Zen, E-an, 1985, Geologic map of the Eastern Pioneer Mountains, Beaverhead County, Montana: U.S. Geological Survey Miscellaneous Field Studies Map 1806-A, scale 1:50,000.

Pearson, R.C., 1996, Cambrian(?), Middle Proterozoic, and Archean rocks penetrated in a borehole near Argenta, Beaverhead County, Montana, and some paleogeographic and structural implications: U.S. Geological Survey Bulletin 2121-B, 15 p.

Ruppel, E.T., O'Neill, J.M., and Lopez, D.A., 1993, Geologic map of the Dillon 1° x 2° quadrangle, Idaho and Montana: U.S. Geological Survey Miscellaneous Investigations Series Map I-1803-H, scale 1:250,000.

Trippe, R.R., 2019, A record of the Precambrian–Cambrian transition in southwest Montana: A Late Neoproterozoic to Early Cambrian stratigraphic window, Fortunian biostratigraphic assemblage and *Treptichnus pedum*: Missoula, Mont., University of Montana, M.S. thesis, 115 p.

Sears, J.W., Link, P.K., Balgord, E.A., and Mahoney, J.B., 2010, Quartzite of Argenta, Beaverhead County, Montana, revisited: Definitive evidence of Precambrian age indicates edge of Belt basin: Northwest Geology, v. 39, p. 41-48.

Sears, J.W., and Link, P.K., 2007, Quartzite of Argenta: Neihart Quartzite equivalent?, *in* Thomas, R.C., and Gibson R., eds., Geologic history of Southwest Montana: Northwest Geology, v. 36, p. 221–230.

Vuke, S.M., Porter, K.W., Lonn, J.D., and Lopez, D.A., 2007, Geologic map of Montana: Montana Bureau of Mines and Geology Geologic Map 62-A, 73 p., 2 sheets, scale 1:500,000.

Yonkee, W.A., Dehler, C.D., Link, P.K., Balgord, E.A., Keeley, J.A., Hayes, D.S., Wells, M.L., Fanning, C.M, and Johnston, S.M., 2014, Tectono-stratigraphic framework of Neoproterozoic to Cambrian strata, west-central U.S.: Protracted rifting, glaciation, and evolution of the North American Cordillera: Earth-Science Reviews, v. 136, p. 59–95.

FIELD GUIDE TO THE CHALLIS VOLCANIC GROUP IN THE AGENCY CREEK AND LEMHI PASS AREAS, IDAHO AND MONTANA

Jesse Mosolf,[1] Reed S. Lewis,[2] and Russell F. Burmester[2]

[1]Montana Bureau of Mines and Geology, Butte, Montana
[2]Idaho Geological Survey, University of Idaho, Moscow, Idaho

INTRODUCTION

This field guide explores the geology of Lemhi Pass along the Idaho–Montana border in the central Beaverhead Mountains, focusing on the Eocene Challis Volcanic Group (CVG). Volcano-sedimentary deposits of the CVG record eruptive activity and related sedimentation during a transitory period of tectonism in the northern Cordillera as Cretaceous–Paleogene crustal shortening ended and extension began (fig. 1; e.g., VanDenburg, 1997). The oldest rocks exposed at Lemhi Pass are Mesoproterozoic-age metasedimentary strata in the Lemhi subbasin of the Belt Supergroup (Burmester and others, 2016a). These rocks were generally tilted, faulted, and folded during contraction prior to Eocene magmatism (Burmester and others, 2016b, 2018a,b). The older contractional structures were then overprinted during Cenozoic extension and contemporaneous Challis magmatism, which together formed extensional half-grabens filled with volcanogenic deposits preserved near Lemhi Pass (fig. 2; e.g., Vandenburg and Janecke, 1998). The Bitterroot–Anaconda metamorphic core complexes and associated extensional structures that developed during Eocene time greatly modified the paleolandscape (figs. 1, 2) and are postulated to have produced major southeasterly flowing river systems that transported boulders of megacrystic granite (~1380 Ma) from an area in the present-day Salmon River Mountains through Lemhi Pass (Chetel and others, 2011).

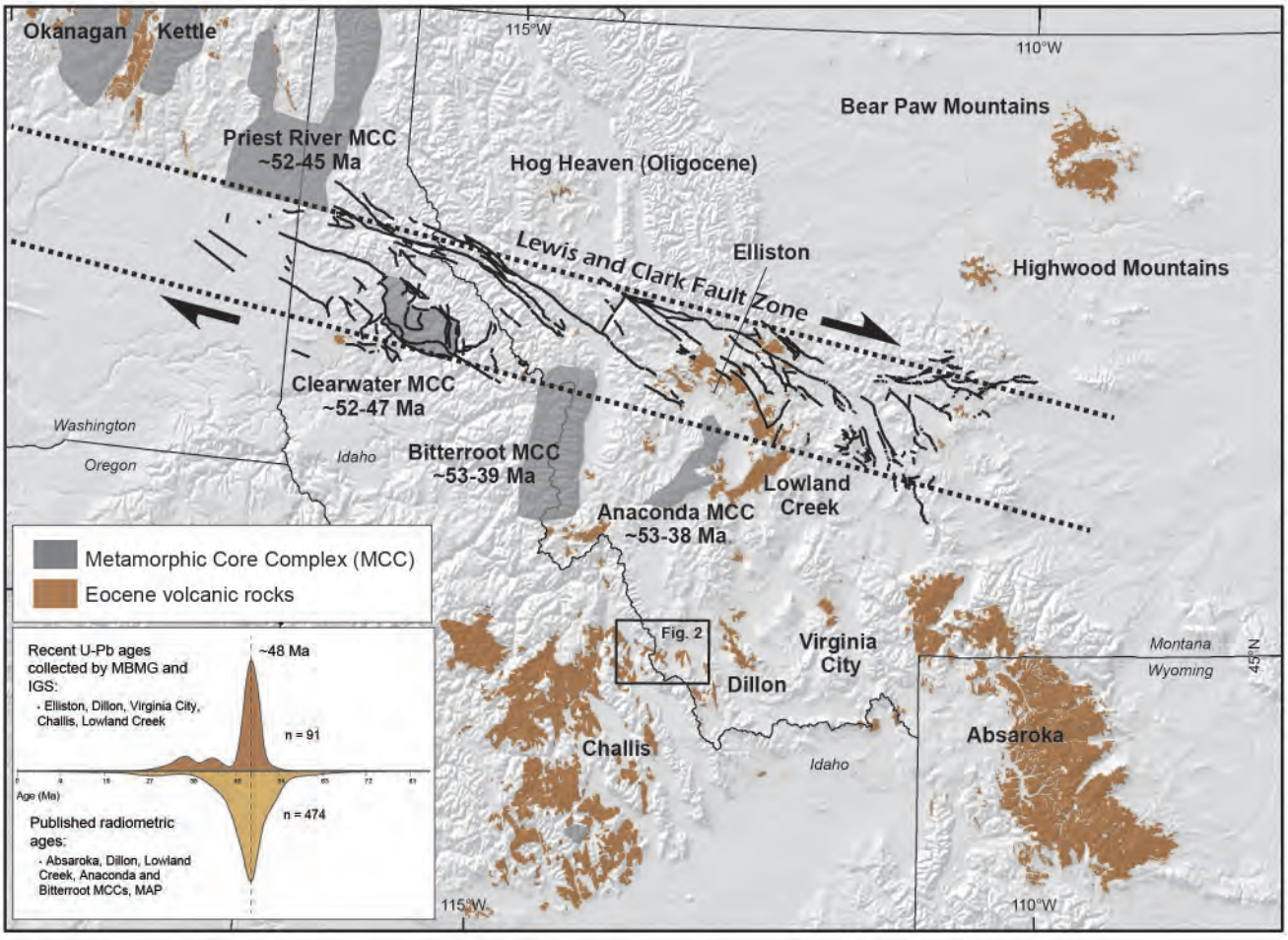

Figure 1. Simplified tectonic map showing the regional extent of Eocene extrusive volcanic rocks of the Challis–Kamloops volcanic belt and contemporaneous metamorphic core complexes recognized throughout the North American Cordillera. Major volcanic fields are labeled. The location of figure 2 is shown by the black box. Inset plot is compilation of published radiometric ages. Simplified geologic map was compiled from Case and others (2013), Lewis and others (2012), Massey and others (2005), Schuster (2005), Vuke and others (2007), and Walker and MacLeod (1991).

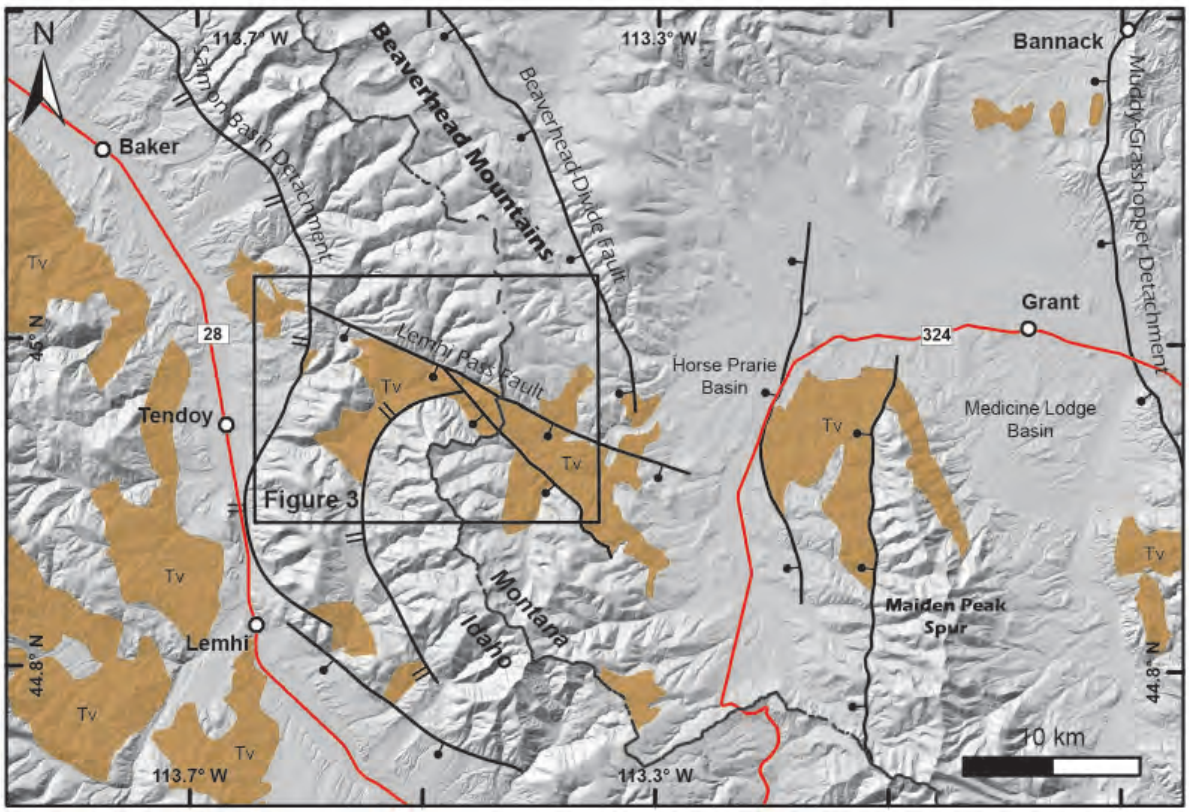

Figure 2. Physiographic map showing the extent of Challis volcanic deposits (brown) and major extensional faults flanking the central Beaverhead Mountains. Black box shows the location of figure 3.

Many of these tectonic elements and major units of the CVG are easily viewed along a historic road that crosses Lemhi Pass at the Montana–Idaho border, affording an excellent opportunity for field trip participants to examine Eocene volcanogenic sequences, and to ponder their magmatic origin within the context of extensional tectonism. This day-long trip begins in the town of Salmon and travels south on Highway 28 through the scenic Lemhi Valley. The field guide route turns east at Tendoy, Idaho, and follows the Agency Creek Road to Lemhi Pass, crossing the state line into Montana. Participants are urged to be cognizant of traffic—most of the field trip stops are along gravel roads that are narrow in places and accommodate a fair amount of Lewis-and-Clark tourism. A vehicle with a sturdy chassis capable of driving on rough gravel roads is recommended. The last two stops entail moderate off-trail hikes (~1 mi each, optional). Participants should bring food, water, hiking apparel, rock hammer, hand lens, and enthusiasm for igneous rocks.

The field trip materials are mostly derived from a cooperative mapping project between the Idaho Geological Survey and Montana Bureau of Mines and Geology that was supported by the USGS STATEMAP Program. Geologic maps of both the Agency Creek and Lemhi Pass 7.5' quadrangles were published at the Idaho Geologic Survey (Burmester and others, 2018a,b). The regional geology north of Lemhi Pass is available at 1:75,000 scale (Burmester and others, 2016b) and a discussion of the regional Precambrian stratigraphy is given in Burmester and others (2016a). A companion field guide focused on rare earth element (REE) occurrences near Lemhi Pass was previously published by Lewis and others (2017).

TECTONIC SETTING

Eocene magmatic rocks exposed throughout Idaho and Montana form the southeasterly part of the Challis–Kamloops volcanic belt (CKVB) that stretches over 10 degrees of latitude in the North American Cordillera. The CKVB comprises several large volcanic fields, including the Buck Creek, Kamloops, Penticton, Princeton, Colville, Clarno, Challis, Absaroka, and Montana alkalic fields (fig. 1), most of which were erupted between ~55 and 40 Ma and exhibit a wide range of compositional trends, with most having elevated- to high-potassium, calc-alkaline geochemical signatures. Contemporary tectonomagmatic models attempt to reconcile spatially and compositionally diffuse Eocene magmatism in the southern CKVB, with most linking magmatism to North America's active plate margin. More traditional models evoke magmatism at a subduction margin, including: flat slab subduction followed by slab rollback (e.g., Constenius, 1996); slab foundering (Humphreys, 1995; Feeley, 2003); and subduction of a slab window (Breitsprecher and others, 2003). Other models don't invoke melts generated by subduction processes, but instead suggest widespread magmatism in the southern CKVB is the product of heating and decompression melting of the crust in response to the extensional collapse of

the Cordilleran orogenic belt (e.g., Meen and Eggler, 1987; Dudas, 1991; Norman and Mertzman, 1991; Morris and Hopper, 2000). Interestingly, many of the Eocene magmatic centers in the northern Cordillera overlap regions of pronounced crustal attenuation and the formation of metamorphic core complexes (fig. 1), perhaps signifying a relationship between magmatism and crustal extension (Foster and others, 2007).

CHALLIS VOLCANIC GROUP

Volcanogenic deposits of the CVG currently cover an area of ~25,000 km^2 (e.g., Moye and others, 1988); however, wide distribution of Eocene plutons suggest the Challis magmatic center may have sprawled over an area greater than 100,000 km^2 (Lewis and others, 2012), making it one of the largest Eocene volcanic fields in the northwestern United States. Volcanic intervals generally have calc-alkaline affinities and were erupted over an irregular surface underlain by Precambrian crystalline rocks, metasedimentary Belt Supergroup, Paleozoic sedimentary rock, and Cretaceous Idaho Batholith (Moye and others, 1988; Rodgers and Janecke, 1992). The CVG comprises an intertonguing sequence of intermediate to mafic lava flows, pyroclastic ash-flows, rhyolite domes, and volcaniclastic deposits, most of which were deposited ca. ~50–46 Ma. Stratigraphic relationships within the CVG are generally complex due to its irregular basal surface, and to extensional faulting that occurred during and after Challis magmatic activity (McIntyre and others, 1982; Kiilsgaard and others, 1986, 2000; Snider, 1995; Janecke and others, 1997). Dated primary volcanic deposits are generally younger than ~50 Ma, but U-Pb ages for detrital zircons collected from modern streams in the CVG suggest that volcanic activity may have commenced as early as ~52 Ma (Stroup and others, 2008). U-Pb ages on the plutonic rocks dated thus far span a slightly wider interval than the volcanic rocks (51–43 Ma; Gaschnig and others, 2010).

Eocene volcano-sedimentary rocks occurring near the Montana–Idaho border were previously assigned to the CVG (e.g., Staatz, 1979), with volcanogenic intervals in the Horse Prairie Valley and Lemhi Pass areas being especially well exposed and studied (M'Gonigle and Dalrymple, 1996; VanDenburg, 1997; Blankenau, 1999; Burmester and others, 2018a,b). Here, volcanic and volcaniclastic intervals rest unconformably on Mesoproterozoic metasedimentary rocks of the Belt Supergroup near Lemhi Pass, and on Archean crystalline basement rocks along the eastern margin of the Horse Prairie basin. Primary volcanic deposits include mafic-to-intermediate lavas (52.6–59.75 wt. % SiO_2), rhyo-dacitic ash-fall and ash-flow deposits (48.6–45.9 Ma), and associated dacitic intrusions (49.4 Ma; 64.0 wt. % SiO_2). Extensive rhyolitic intrusions, domes, and flows (~48.7 Ma) occur along the eastern margin of the Horse Prairie basin but are largely absent near Lemhi Pass. Sedimentary strata are intercalated with primary volcanic intervals locally; Janecke and others (2000), and Chetel and others (2011) postulated that an Eocene paleoriver transported sedimentary detritus southeastward across the Beaverhead Range near Lemhi Pass before the Salmon basin formed. Magmatism, sedimentation, and crustal extension were closely associated in this region, and Eocene volcanic and sedimentary strata appear to have accumulated in subsiding, fault-controlled basins (e.g., VanDenburg and others, 1998; Burmester and others, 2018a,b). Early studies linked extensive REE and thorium mineralization near Lemhi Pass to Challis magmatism (e.g., Staatz, 1972, 1979; Staatz and others, 1972), but more recent geochronology work yielded complex mineralization ages, some of which are clearly Paleozoic (Gillerman, 2008, 2011; Gillerman and others, 2008, 2010, 2013).

ROAD LOG

Travel south from Salmon, Idaho, 20.4 mi to Tendoy. Road log and milage begin in Tendoy. Travel east, following signs to Agency Creek. All field trip stops and the geology of Lemhi Pass are shown in figure 3. Latitudes and longitudes listed below use the WGS84 datum.

1.9 mi Deformed rocks on the left are Mesoproterozoic strata in the footwall of the Salmon Basin detachment (fig. 4). We will be in the same but less deformed until Stop 3.

STOP 1—2.4 mi
Yearian Creek member of Apple Creek Formation

(44.948°N, 113.594°W).

The stratigraphic position of this Mesoproterozoic unit was uncertain and was therefore named the siltite of Yearian Creek (Burmester and others, 2018b). Our current terminology includes this unit as a member in the Apple Creek Formation. This unit comprises graded siltite and argillite couplets with scattered beds and cosets of quartzite. Diagnostic features include undulating, graded, uncracked couplets and rarer couples of medium-green siltite and light-green to gray argillite (fig. 5). Cracked couplets are rarer, but look for mud cracks and angular light-colored mud chips. Mud chips are in bases of some beds along with well-rounded fine to spherical medium quartz grains in dark-green scour channels a few centimeters wide and as thick as 1 cm (0.4 in). Some chips and thin layers are chert. Look for those because they provide a good tie with the Lawson Creek Formation, a likely correlative to this unit. The Lawson Creek is correlative to the McNamara Formation of the main Belt Basin (Burmester and others, 2016a; Lonn and others, this volume, The Mesoproterozoic Belt–Lemhi connection, western Montana and

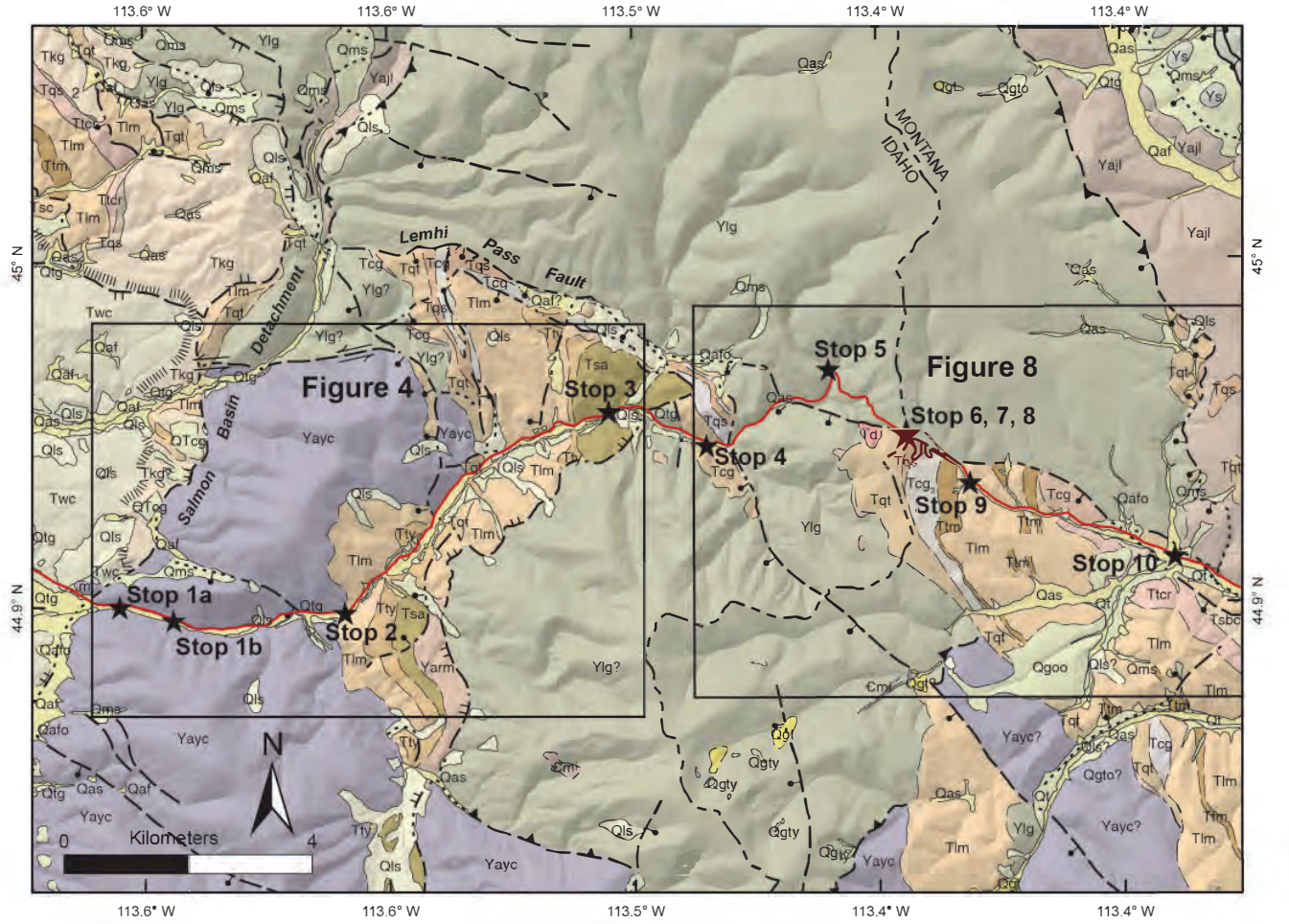

Legend

Contacts and faults

- Contact
- Gradational contact
- Normal fault, ball and bar on downthrown block
- Strike-slip fault, arrows show relative motion
- Thrust fault, sawteeth on upper plate
- Detachment fault, hachures on upper plate

Quaternary sedimentary and manmade deposits

- m — Manmade ground
- Qas — Side-stream alluvium
- Qaf — Alluvial-fan and debris-flow deposits
- Qalc — Fine-grained alluvial and lacustrine deposits
- Qafo — Older alluvial-fan deposits
- Qt — Terrace deposits, undivided
- Qgt — Till of last glacial maximum
- Qgty — Young glacial and periglacial deposits
- Qgoo — Glacial outwash gravels
- Qls — Landslide deposits
- Qms — Mass-movement deposits

Post-Challis sedimentary deposits

- Tkg — Conglomerate of Kriley Gulch
- Twc — Siltstone of Wimpey Creek
- Tsa — Sedimentary deposits of Agency Creek
- Tcg_4 — Uppermost conglomerate
- Tsbc — Sediments of Bear Creek basin, undivided

Challis volcanic and sedimentary deposits

- Tty — Younger Challis tuff, undivided
- Tqs_2 — Younger quartz-sanidine welded tuff
- Ttcr — Tuff of Curtis Ranch
- Tlm — Mafic lava flows
- Tuff, associated with mafic lava
- Tcg_3 — Upper conglomerate
- Tqs_1 — Older quartz-sanidine welded tuff
- Tcg_2 — Middle conglomerate
- Tqt — Quartzite-bearing ash-flow tuff
- Tcg_1 — Basal conglomerate

Mesoproterozoic strata

- Ylg — Lemhi Group
- Ys — Swauger Fomation
- Yajl — Jahnke Lake member of Apple Creek Formation
- Yarm — Ramsey Mountain member of Apple Creek Formation
- Yayc — Yearian Creek member of Apple Creek Formation

Intrusions

- Td — Dacite intrusive rocks
- €sy — Syenite
- €mi — Mafic intrusive rocks

- Lemhi road
- ★ Field trip stop

Figure 3. Simplified geologic map of the Agency Creek and Lemhi Pass area showing field trip stops. Map data derived from Burmester and others (2018a,b).

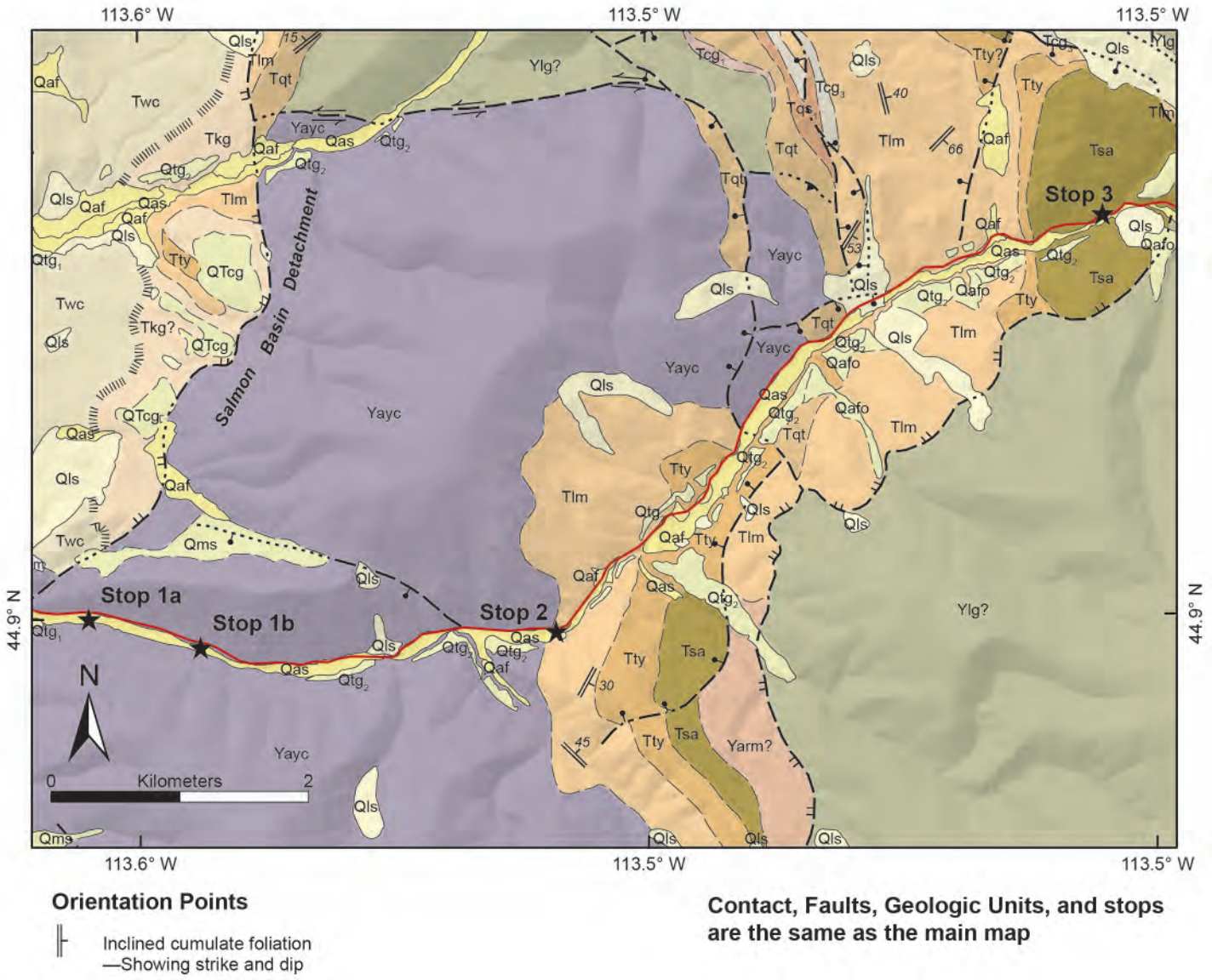

Figure 4. Simplified geologic map showing field trip stops 1–3. See figure 3 for legend. Map data derived from Burmester and others (2018a, b) and unpublished mapping by the authors.

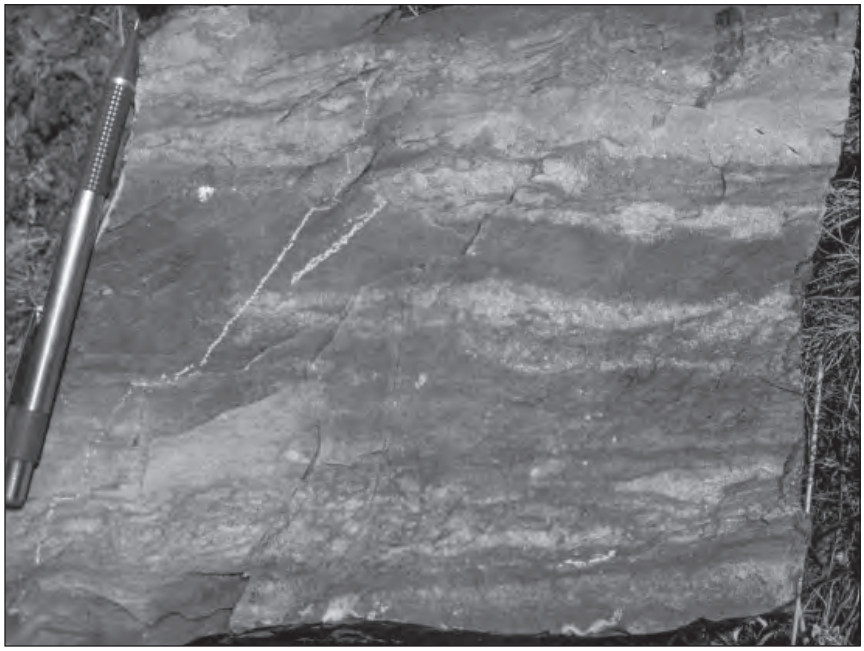

Figure 5. Yearian Creek member of Apple Creek Formation at Stop 1. Note uneven graded darker siltite to lighter argillite couplets. Darkest lenses and layers have concentrations of spherical medium quartz grains and light mud chips.

east-central Idaho). Common to this unit along Agency Creek road are 10–30 cm (4–12 in) beds of green to white, very fine- to fine-grained feldspathic quartzite, some with ripple tops and ripple cross lamination. Also common in some intervals are centimeter-scale, intricately interbedded, white and green quartzite with wide variation of grain sizes and feldspar content. Lower contact is faulted against an anomalously thin section of Swauger Formation.

4.2 mi Cow Creek is to the right. For most of its lower reach, Cow Creek follows closely the basal contact of the Challis section on the Yearian Creek member of Apple Creek Formation we saw at Stop 1. As we approach Stop 2, observe the flatirons of mafic lavas east of Cow Creek. These rocks appear to have been rotated to their eastward tilt in the hanging wall of the Agency–Yearian Detachment.

STOP 2—4.6 mi
Mafic to intermediate flows of the Challis Volcanic Group

(44.9492°N, 113.5588°W).

Parking on the right before the curve is sketchy, so it is safer to park in the BLM campground (mi 4.7, 44.950°N, 113.558°W) and walk back.

Mafic to intermediate flows such as these are a widespread and important stratigraphic marker in the region (fig. 6). The rock locally contains round to irregular vesicles or amygdules and flow breccias, and flows are intercalated with thin, discontinuous rhyolitic tuffs. Secondary chalcedony and calcite are common, and xenocrystic quartz and plagioclase are found locally. Compositions include basalt, basaltic trachyandesite, trachyandesite, and andesite. Phenocrysts are primarily pyroxene and olivine, although Staatz (1972) also reported minor amounts of biotite and plagioclase in some of the flows. Equivalent to Tl unit of Blankenau (1999) and Tcl unit of VanDenburg (1997), and correlative with Tl unit of potassium-rich andesite, latite, and basalt lava in the Challis 1° x 2° quadrangle to the southwest (Fisher and others, 1992). We will visit this unit again on the east side of Lemhi Pass later in the field trip (Stop 9). Staatz (1972) reported a thickness of about 1,000 m (3,300 ft).

6.0 mi Narrow water gap through Challis mafic flows (44.955°N, 113.552°W).

7.4 mi Contact of Mesoproterozoic metasedimentary rocks with tuff (44.969°N, 113.535W°).

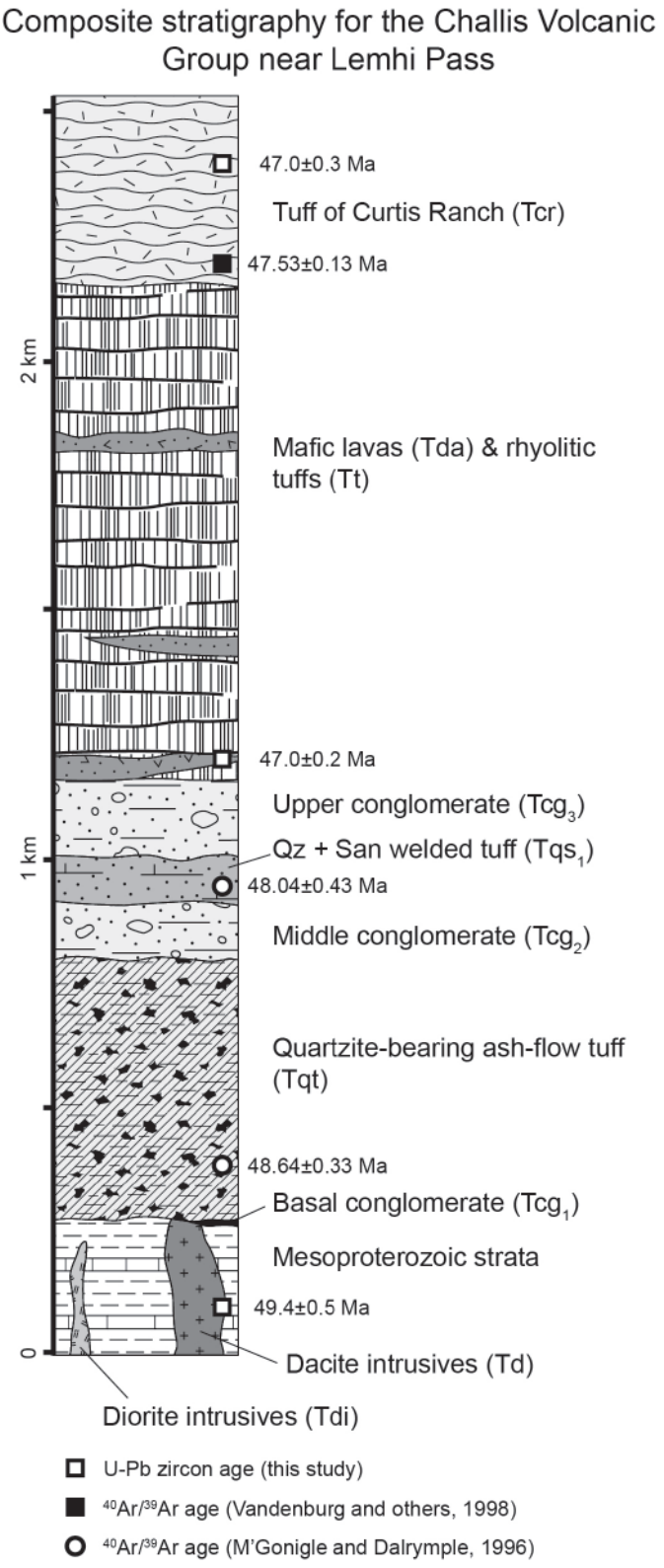

Figure 6. Stratigraphic column showing the Challis Volcanic Group and overlying sedimentary rocks in the Lemhi Pass area.

STOP 3—9.1 mi
Sedimentary deposits of Agency Creek

(44.9777°N, 113.5056°W).

Park on the left before a left bend if there is enough room (44.978°N, 113.506°W), otherwise drive another 0.1 mile and park in an open area at Flume Creek and walk back.

Clast-supported pebble to boulder conglomerate (fig. 7). Rounded to subrounded pebbles, cobbles, and some small boulders of Mesoproterozoic quartzite and siltite predominate, but clasts of Challis volcanics also are present. A single small boulder of coarse-grained Mesoproterozoic biotite granite, similar to boulders in Tcg3, is present northeast of the mouth of Flume Creek. This unit is equivalent to Blankenau's (1999) middle conglomerate of the sedimentary rocks of Tendoy (Flume Creek facies of Tcg3 unit) and portions of the conglomerate of Flume Creek of Staatz (1972, 1979).

Figure 7. Conglomerate in sedimentary deposits of Agency Creek. Location is across Agency Creek from Stop 3; view is looking northward into the creek.

STOP 4—10.1 mi
Quartzite-bearing ash-flow tuff

(44.9733°N, 113.4852°W).

Outcrop is on corner. Some parking is available beyond the corner (wide spot at cattle guard). Parking also available on shoulders between here and next stop.

Exposure here is a distinctive Challis tuff that contains abundant angular lithic fragments of dark-gray to black quartzite, less abundant quartz and plagioclase, and minor sanidine. Equivalent to Tcq unit of VanDenburg (1997) and Tqt unit of Blankenau (1999), who obtained a $^{40}Ar/^{39}Ar$ age of 49.51 ± 0.14 Ma for a sample collected along Withington Creek, about 30 km (18 mi) to the west–northwest in the Sal Mountain quadrangle. M'Gonigle and Dalrymple (1996) reported a $^{40}Ar/^{39}Ar$ weighted mean age of 48.64 ± 0.12 Ma from a sample collected near Lemhi Pass. Estimated to be as thick as 520 m (1,700 ft) in the area south of Lemhi Pass (Staatz, 1972), but thins to the south and is absent in the southeast part of the map (fig. 8).

11.1 mi The road crosses the Lemhi Pass fault from the hanging wall to the footwall rocks. (44.980°N, 113.471°W).

STOP 5—11.9 mi
Lemhi Group at Horseshoe Bend. Parking best on NW outside bend

(44.984°N, 113.4607°W)

We are now on the footwall of the Lemhi Pass fault. Because of correlation uncertainties, this Mesoproterozoic unit was given the informal name "quartzite of Horseshoe Bend Creek" by Lewis and others (2017) but boldly named "Gunsight Formation?" by Burmester and others (2018a). However, the Gunsight Formation was defined in the Lemhi Range (Ruppel, 1975) as underlying the coarser-grained Swauger Formation and overlying a unit with less quartzite, now named the Yellow Lake Formation. We think this unit is below the Swauger Formation but have been unable to find an underlying finer-grained unit in the Beaverhead Mountains, so we now refer to this as Lemhi Group. It consists of feldspathic quartzite, siltite, and argillite. Surprised? Characteristically, quartzite beds as thick as 1 m are flat laminated and grade to siltite and argillite tops. Here the grading from light quartzite to dark siltite and argillite gives the rock a candy-striped appearance (fig. 9). Where these rocks are more deformed, this gradation is emphasized by cleavage curving to be more parallel to bedding in the finer-grained tops. Less common but widespread in this unit are hummocky and trough cross stratification, climbing ripple

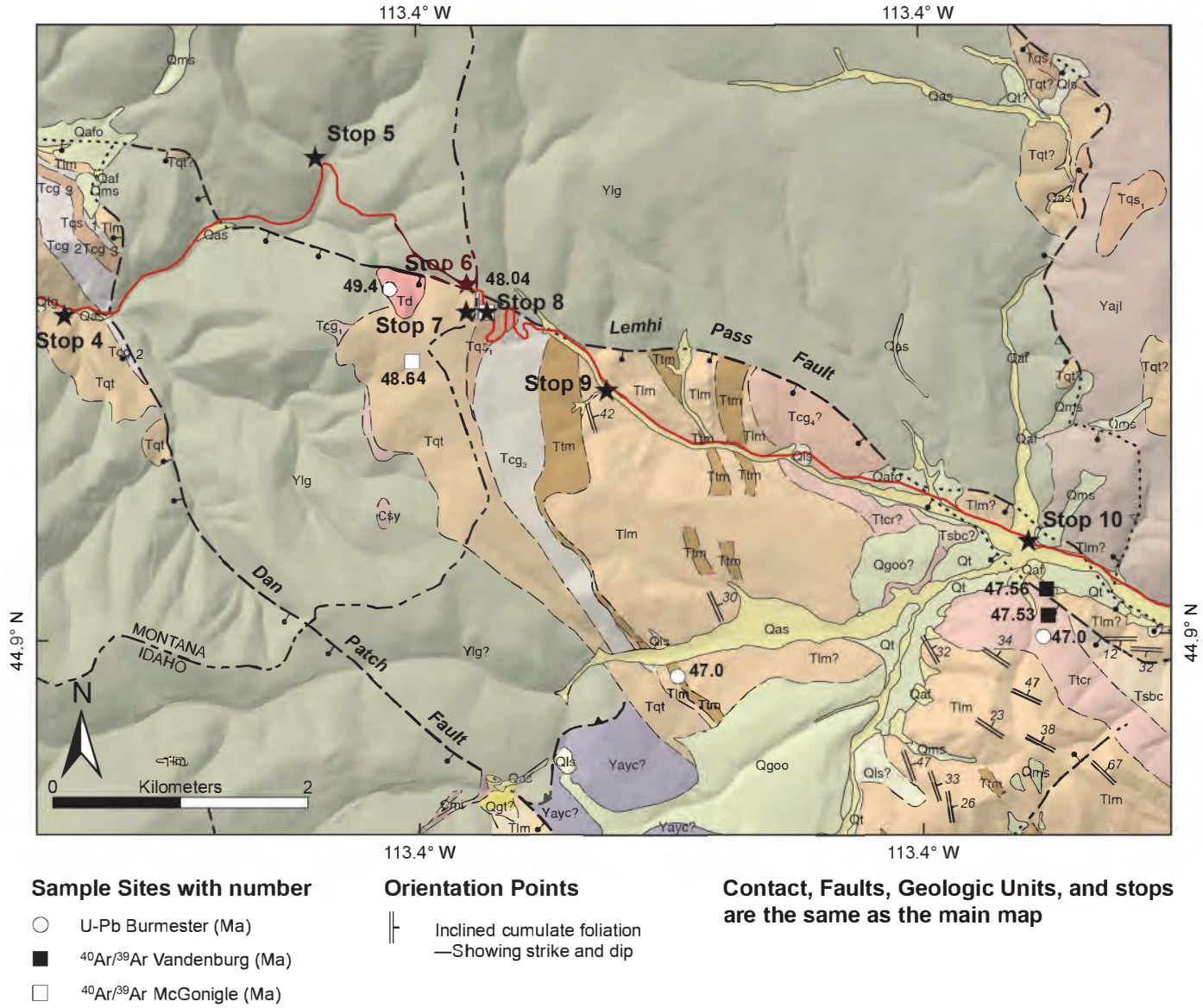

Figure 8. Simplified geologic map showing field trip stops 4–10. See figure 3 for legend. Map data derived from Burmester and others (2018a,b) and unpublished mapping by the authors.

Figure 9. View northwest of Lemhi Group quartzite at Horseshoe Bend Creek.

or ripple drift cross laminations, loads into argillite tops of underlying beds, and soft-sediment deformation. Loads and soft sediment deformation are abundant on the ridge about 0.2 mi north of Lemhi Pass. Platy parting with muscovite surfaces are rare. Some intervals contain decimeter- to meter-thick beds of white, very fine- to fine-grained feldspathic quartzite. Some of the thicker beds have bedding defined by dark millimeter-scale laminations. A stained quartzite sample from here contained 40 percent plagioclase and no potassium feldspar. Potassium feldspar is similarly lacking in about half of the samples from Kitty Creek quadrangle to the north (Lewis and others, 2009), and constitutes less than a third of the feldspar in the other half.

STOP 6—12.1 mi
Lemhi Pass

(44.9746°N, 113.4450°W)

Beware, last stretch of road is steep and rough. Proceed into Montana 0.1 mi and stop on left near the rest stop facility.

The Lemhi Pass fault strikes east–southeast to west–northwest across Lemhi Pass. It juxtaposes Mesoproterozoic rocks on the north against Challis volcanosedimentary rocks to the south. VanDenburg (1997), VanDenburg and others (1998), and Blankenau (1999) interpreted the structure as a 22° to 24° south-dipping detachment fault that likely formed at a higher angle before rotating to its present dip during the latest phase of extensional faulting. Eocene volcanic and volcaniclastic deposits are interpreted to have accumulated in a half-graben formed by the Lemhi Pass fault, and therefore the fault's minimum heave is roughly equivalent to the stratigraphic thickness of the Challis group in this area, estimated as 1 km (VanDenburg and others, 1998). Gillerman (2008) speculated that the fault might have a prolonged history, however, and that Tertiary extension reactivated older structures including Neoproterozoic faults that contributed to localization of REE mineralization in this district, and possibly Cretaceous thrust faults.

Walk or drive from Lemhi Pass SE along road toward Sacagawea picnic area. First exposures along the road are light-colored Challis tuff.

Stop 7—(walk from Stop 6)
Quartz-sanidine tuff

(44.973°N, 113.443°W)

Eocene quartz–sanidine welded tuff of the Challis Volcanic Group. Unit contains sparse, euhedral to subhedral crystals of sanidine and quartz. Our estimate of maximum thickness is 60–90 m (200–300 ft). Equivalent to Tqs1 of Blankenau (1999). Locally mapped as vitric tuff of Lemhi Pass by Staatz (1972, 1979). M'Gonigle and Dalrymple (1996) reported a $^{40}Ar/^{39}Ar$ weighted mean age of 47.95 ± 0.12 Ma for this unit near Lemhi Pass.

Hike up the hill from Stop 7, or south from Lemhi Pass to Stop 8.

Stop 8—(walk from Stop 7)
Mesoproterozoic boulders

(44.973°N, 113.445°W)

Lag deposits of cobbles and boulders from an Eocene conglomerate. Most are quartzite, but the unit includes distinctive cobbles and boulders of megacrystic coarse-grained Mesoproterozoic biotite granite (fig. 10) that were likely derived from exposures now 40 km (25 mi) to the northwest (Burmester and others, 2016b). Rare garnet amphibolite cobbles have also been observed north of Agency Creek. Because of the general east dip of the Challis strata, these lag deposits are west of the actual surface exposures of the unit. Equivalent to the granite clast conglomerate (Tcg2) of Blankenau (1999) but mapped higher in the stratigraphic section in the area north of Agency Creek. Blankenau (1999), Janecke and others (2000), and Chetel and others (2011) postulated that an Eocene paleoriver, which flowed southeast before the Salmon Basin formed, transported the granite clasts across the Beaverhead Range at Lemhi Pass. The conglomerate is as thick as 150 m (500 ft)

Figure 10. Small boulder of Mesoproterozoic granite south of Lemhi Pass that formed as a lag deposit. Weathered from Eocene conglomerate unit sourced northwest of Salmon (Janecke and others, 2000).

but thins southward and is absent in the southern part of the Lemhi Pass quadrangle.

Alternate side trip to see a fine-grained syenite plug (44.959°N, 113.453°W).

Drive or walk south along the Continental Divide Trail about 1.4 mi from Lemhi Pass and stop before the trees. Follow the track to the WNW 0.3 to 0.4 mi through trees to exploration pits. The magnetite-rich rock there has been dated at 529.1 ± 4.5 Ma, or earliest Cambrian (Gillerman and others, 2008, 2010).

STOP 9—13.9 mi
Tilted mafic-to-intermediate lava flows of the Challis Volcanic Group

(44.9673°N, 113.4312°W)

Look for parking along a dirt track that doubles back on the right or goes through a fence on the left.

A thick section of eastward-tilted lava flows and interbedded tuff preserved in the hanging wall of the Lemhi Pass Fault can be viewed from the road while driving southeast from Stop 8 to Stop 9 (fig. 11). These rocks should look familiar—we visited correlative lava flows on the west side of Lemhi Pass earlier in the trip (Stop 2). The lava flows exhibit a similar mineralogy consisting of pyroxene and olivine with some plagioclase and xenocrystic quartz. Autobreccias are common throughout the section. Intercalated tuff intervals are generally recessive and contain a wide range of crystal, lithic, and vitric fragments. Tuffs lower in the sequence commonly contain conspicuous biotite phenocrysts. An intercalated quartzite-bearing tuff intercalated with mafic flows north of Trail Creek yielded a U-Pb zircon age of 47.0 ± 0.2 Ma (Burmester and others, 2018a).

The lava flows and surrounding geology can be viewed by hiking an optional ~1 mi loop north of the road, traversing eastward across strike of the tilted volcanic sequence. This route crosses private property, so be sure to gain permission from the landowner to access this area.

STOP 10—16.2 mi
Tuff of Curtis Ranch

(44.957°N, 113.389°W)

The tuff of Curtis Ranch overlies the intertonguing tuff and mafic lava section, marking the stratigraphic top of the CVG in this area (fig. 12). Outcrops of tuff are typically white to greenish white, poorly to densely welded, and contain conspicuous biotite along with broken phenocrysts of plagioclase and quartz in an ash matrix with glass shards. Pumice is abundant to rare and typically concentrated at the top of the unit. Sandstone is present locally at the base of the unit. The tuff of Curtis Ranch yielded a U-Pb zircon age of 47.0 ± 0.3 Ma (Burmester and others, 2018a). Equivalent to Tcr unit of VanDenburg (1997) with a reported $^{40}Ar/^{39}Ar$ age of 47.53 ± 0.06 Ma (VanDenburg and others, 1998). Staatz (1972) reported a thickness of 120 to 370 m (400 to 1,200 ft).

Figure 11. Field photograph showing eastward tilted mafic lavas in the hanging wall of Lemhi Pass fault. Bar and ball represent apparent dip of lava flows.

Figure 12. Field photograph showing the tuff of Curtis Ranch resting on mafic lava flows. Bar and ball represent apparent dip of the volcanic sequence.

The tuff of Curtis Ranch can be viewed from the road at this location. With permission from the landowner, subdued outcrops of tuff can be reached by an optional ~1 mi (roundtrip) hike south, crossing Frying Pan Creek. This route also crosses private property so be sure to gain permission from the landowner to access the geology.

END OF TRIP

ACKNOWLEDGMENTS

Rich Gaschnig kindly reviewed the manuscript.

REFERENCES

Blankenau, J.J., 1999, Cenozoic structural and stratigraphic evolution of the southeastern Salmon basin, east-central Idaho: Logan, Utah, Utah State University, M.S. thesis, 143 p., 3 plates.

Breitsprecher, K., Thorkelson, D.J., Groome, W.G., and Dostal, J., 2003, Geochemical confirmation of the Kula-Farallon slab window beneath the Pacific northwest in Eocene time: Geology, v. 31, p. 351–354.

Burmester, R.F., Lonn, J.D., Lewis, R.S., and McFaddan, M.D., 2016a, Stratigraphy of the Lemhi subbasin of the Belt Supergroup, *in* MacLean, J.S., and Sears, J.W., eds., Belt Basin: Window to Mesoproterozoic Earth: Geological Society of America Special Paper 522, p. 121–137.

Burmester, R.F., Lewis, R.S., Othberg, K.L., Stanford, L.R., Lonn, J.D., and McFaddan, M.D., 2016b, Geologic map of the western part of the Salmon 30' x 60' minute quadrangle, Idaho and Montana: Idaho Geological Survey Geologic Map 52, scale 1:75,000.

Burmester, R.F., Mosolf, J., Stanford, L.R., Lewis, R.S., Othberg, K.L., and Lonn, J.D., 2018a, Geologic map of the Lemhi Pass quadrangle, Lemhi County, Idaho, and Beaverhead County, Montana: Montana Bureau of Mines and Geology Open-File Report 701, 1 sheet, scale 1:24,000.

Burmester, R.F., Othberg, K.L., Stanford, L.R., Lewis, R.S., and Lonn, J.D., 2018b, Geologic map of the Agency Creek quadrangle, Lemhi County, Idaho: Idaho Geologic Survey DWM-182, 1 sheet, scale 1:24,000.

Case, J.C., Arneson, C.S., and Hallberg, L.L., 2013, Surficial geologic map of Wyoming: Wyoming State Geological Survey: Geologic Map WSGS-1998-HSDM-1a, scale 1:500,000.

Chetel, L.M., Janecke, S.U., Carroll, A.R., Beard, B.L., Johnson, C.M., and Singer, B.S., 2011, Paleogeographic reconstruction of the Eocene Idaho River: Geological Society of America Bulletin, v. 123, no 1/2, p. 71–88.

Constenius, K.N., 1996, Late Paleogene extensional collapse of the Cordilleran foreland fold and thrust belt: Geological Society of America Bulletin, v. 108, p. 20–39.

Dudas, F.O., 1991, Geochemistry of igneous rocks from the Crazy Mountains, Montana, and tectonic models for the Montana alkalic province: Journal of Geophysical Research, v. 96, p. 13261–13277.

Feeley, T.C., 2003, Origin and tectonic implications of across-strike geochemical variations in the Eocene Absaroka Volcanic Province, United States: Journal of Geology, v. 111, no. 3, p. 329–346.

Foster, D.A., Doughty, P.T., Kalakay, T.J., Fanning, C.M., Coyner, S., Grice, W.C., and Vogl, J.J., 2007, Kinematics and timing of exhumation of Eocene metamorphic core complexes along the Lewis and Clark fault zone, northern Rocky Mountains, USA, *in* Till, A., Roeske, S., Sample, J., and Foster, D.A., eds., Exhumation along major continental strike-slip systems: Geological Society of America Special Paper 434, p. 205–229.

Fisher, F.S., McIntyre, D.H., and Johnson, K.M., 1992, Geologic map of the Challis quadrangle, Idaho: U.S. Geological Survey Miscellaneous Investigations Series Map I-1819, scale 1:250,000.

Gaschnig, R.M., Vervoort, J.D., Lewis, R.S., and McClelland, W.C., 2010, Migrating magmatism in the northern US Cordillera: *in situ* U-Pb geochronology of the Idaho batholith: Contributions to Mineralogy and Petrology, v. 159, p. 863–883.

Gillerman, V.S., 2008, Geochronology of iron oxide-copper-thorium-REE mineralization in Proterozoic rocks at Lemhi Pass, Idaho, and a comparison to copper-cobalt ores, Blackbird Mining District, Idaho: Final Technical Report to U.S. Geological Survey, December, 149 p., MRERP Award #06HQGR0170.

Gillerman, V.S., Fanning, C.M., Link, P.K., Layer, P., and Burmester, R.F., 2008, Newly discovered intrusives at the Lemhi Pass thorium-REE-iron oxide district, Idaho: Cambrian syenite and mystery ultramafics: Signatures of a buried alkaline complex or two systems?: Geological Society of America Abstracts with Programs, v. 40, no. 1, p. 51.

Gillerman, V.S., Schmitz, M.D., Jercinovic, M.J., and Reed, R., 2010, Cambrian and Mississippian magmatism associated with neodymium-enriched rare earth and thorium mineralization, Lemhi Pass district, Idaho: Geological Society of America Abstracts with Programs, v. 42, no. 5, p. 334.

Gillerman, V.S., 2011, Rare earth elements and other critical metals in Idaho: Idaho Geological Survey GeoNote 44, 4 p.

Gillerman, V.S., Schmitz, M.D., and Jercinovic, M.J., 2013, REE-Th Deposits of the Lemhi Pass Region, Northern Rocky Mountains–Paleozoic magmas and hydrothermal activity along a continental margin: Geological Society of America Abstracts with Programs, v. 45, no. 5, p. 41.

Humphreys, E.D., 1995, Post-Laramide removal of the Farallon slab, western United States: Geology, v. 23, p. 987–990.

Janecke, S.U., Hammond, B.F., Snee, L.W., and Geissman, J.W., 1997, Rapid extension in an Eocene volcanic arc: Structure and paleogeography of an intra-arc half graben in central Idaho: Geological Society of America Bulletin, v. 109, p. 253–267.

Janecke, S.U., VanDenburg, C.J., Blankenau, J.J., and M'Gonigle, J.W., 2000, Long-distance longitudinal transport of gravel across the Cordilleran thrust belt of Montana and Idaho: Geology, v. 28, no. 5, p. 439-442.

Kiilsgaard, T.H., Fisher, F.S., and Bennett, E.H., 1986, The trans-Challis fault system and associated precious metal deposits, Idaho: Economic Geology and the Bulletin of the Society of Economic Geologists, v. 81, p. 721–724.

Kiilsgaard, T.H., Lewis, R.S., and Bennett, E.H., 2000, Plutonic and hypabyssal rocks of the Hailey 1° × 2° quadrangle, Idaho: U.S. Geological Survey Bulletin 2064-U, 18 p.

Lewis, R.S., Burmester, R.F., Stanford, L.R., Lonn, J.D., McFaddan, M.D., and Othberg, K.L., 2009, Geologic map of the Kitty Creek quadrangle, Lemhi County, Idaho and Beaverhead County, Montana: Idaho Geological Survey Digital Web Map 112 and Montana Bureau of Mines and Geology Open-File Report 582, scale 1:24,000.

Lewis R.S., Link, P.K., Stanford, L.R., and Long, S.P., 2012, Geologic map of Idaho: Idaho Geological Survey Geologic Map 9, scale 1:500,000.

Lewis, R.S., Gillerman, V.S., Burmester, R.F., Mosolf, J., and Lonn, J.D., 2017, Road log to the geology and mineralization of the Agency Creek and Lemhi Pass areas, Idaho and Montana: Northwest Geology, v. 46, 2017, p. 119–132.

Lonn, J.D, Burmester, R.F., and Lewis, R.S., this volume,The Mesoproterozoic Belt–Lemhi connection, western Montana and east-central Idaho.

Massey, N.W.D., MacIntyre, D.G., Desjardins, P.J. and Cooney, R.T., 2005: Digital map of British Columbia: Whole Province, B.C. Ministry of Energy and Mines, GeoFile 2005-1, scale 1:250,000.

M'Gonigle, J.W., and Dalrymple, G.B., 1996, $^{40}Ar/^{39}Ar$ ages of some Challis Volcanic Group rocks and the initiation of Tertiary sedimentary basins in southwestern Montana: U.S. Geological Survey Bulletin 2132, 17 p.

McIntyre, D.H., Ekren, E.B., and Hardyman, R.F., 1982, Stratigraphic and structural framework of the Challis volcanics in the eastern half of the Challis 1° × 2° quadrangle, *in* Breckenridge, R.M., and Bonnichsen, B., eds., Cenozoic geology of Idaho: Idaho Bureau of Mines and Geology Bulletin 26, p. 3–22.

Meen, J.K., and Eggler, D.H., 1987, Petrology and geochemistry of the Cretaceous Independence volcanic suite, Absaroka Mountains: Clues to the composition of the Archean sub-Montanan mantle: Geological Society of American Bulletin, v. 98, p. 238–247.

Morris, G.A., Larson, P.B., and Hooper, P.R., 2000, "Subduction style" magmatism in a nonsubduction setting: The Colville igneous complex, northeast Washington State, USA: Journal of Petrology, v. 41, p. 43–67.

Moye, F.J., Hackett, W.R., Blakley, J.D., and Snider, L.G., 1988, Regional geologic setting and volcanic stratigraphy of the Challis volcanic field, central Idaho, *in* Link, P.K., and Hackett, W.R., eds., Guidebook to the Geology of Central and Southern Idaho: Idaho Geological Survey Bulletin 27, p. 87–97.

Norman, M.C., and Mertzman, S.A., 1991, Petrogenesis of Challis volcanics from central and southwestern Idaho: Trace element and Pb isotopic evidence: Journal of Geophysical Research: v., 96, p. 13279–13293.

Rodgers, D.W., and Janecke, S.U., 1992, Tertiary paleogeologic maps of the western Idaho-Wyoming-Montana thrust belt, *in* Link, P.K., Kuntz, M.A., and Platt, L.B., eds., Regional geology of eastern Idaho and western Wyoming: Geological Society of America Memoir 179, p. 83–94.

Ruppel, E.T., 1975, Precambrian Y sedimentary rocks in east-central Idaho: U.S. Geological Survey Bulletin 889-A, 23 p.

Schuster, J.E., 2005, Geologic map of Washington State: Washington Division of Geology and Earth Resources Geologic Map GM-53, scale 1:500,000.

Snider, L.G., 1995, Stratigraphic framework, geochemistry, geochronology and eruptive styles of Eocene volcanic rocks in the White Knob Mountains area, southeastern Challis volcanic field, central Idaho: Pocatello, Idaho, Idaho State University, M.S. thesis, 212 p.

Staatz, M.H., 1972, Geology and description of the thorium-bearing veins, Lemhi Pass quadrangle, Idaho and Montana: U.S. Geological Survey Bulletin 1351, 94 p., 2 plates.

Staatz, M.H., Shaw, V.E., and Wahlberg, J.S., 1972, Occurrence and distribution of rare earths in the Lemhi Pass thorium veins, Idaho and Montana: Economic Geology, v. 67, p. 72–82.

Staatz, M.H., 1979, Geology and mineral resources of the Lemhi Pass thorium district, Idaho and Montana: U.S. Geological Survey Professional Paper 1049-A, 90 p.

Stroup, C.N., Link, P.K., Janecke, S.U., Fanning, C.M., Yaxley, G.M., and Beranek, L.P., 2008, Eocene to Oligocene provenance and drainage in extensional basins of southwest Montana and east-central Idaho: Evidence from detrital zircon populations in the Renova Formation and equivalent strata, *in* Spencer, J.E., and Titley, S.R., eds., Ores and Orogenesis: Circum-Pacific tectonics, geologic evolution, and ore deposits: Arizona Geological Society Digest, v. 22, p. 529–546.

VanDenburg, C.J., 1997, Cenozoic tectonic and paleogeographic evolution of the Horse Prairie half graben, southwest Montana: Logan, Utah, Utah State University, M.S. thesis, 152 p., 2 plates.

VanDenburg, C.J., Janecke, S.U., and McIntosh, W.C., 1998, Three-dimensional strain produced by >50 my of episodic extension, Horse Prairie basin area, SW Montana, U.S.A.: Journal of Structural Geology, v. 20, no. 12, p. 1747–1767.

Vuke, S.M., Porter, K.W., Lonn, J.D., and Lopez, D.A., 2007, Geologic map of Montana: Montana Bureau of Mines and Geology Geologic Map 62, 73 p., 2 sheets, scale 1:500,000.

Walker, G.W., and MacLeod, N.S., 1991, Geologic map of Oregon: U.S. Geological Survey, 2 sheets, scale 1:500,000.

NEOPROTEROZOIC AND CAMBRIAN STRATA OF THE LOCALLY MINERALIZED BAYHORSE SUCCESSION ON THE WESTERN SIDE OF THE LEMHI ARCH IN EAST-CENTRAL IDAHO

Daniel T. Brennan,[1] Paul K. Link,[2] David M. Pearson,[2] Jacob Milton,[2] Kurt E. Sundell,[2] and Kyle Mangum[2]

[1]Montana Bureau of Mines and Geology, Butte, Montana
[2]Department of Geosciences, Idaho State University, Pocatello, Idaho

INTRODUCTION

This 3-day field trip focuses on the Neoproterozoic to early Paleozoic stratigraphy and tectonic history of central Idaho. Collectively, these rocks constitute a regional record of a relatively complex segment of the western Laurentian rift margin associated with the breakup of supercontinent Rodinia. The first 2 days of field trip stops include locations along a ~3-km-thick Neoproterozoic to Ordovician stratigraphic section (the Bayhorse succession) that likely contains several disconformities and is locally mineralized, near the mining ghost town of Bayhorse in the Salmon River Mountains. The third day includes stops along South Creek in the southern Lemhi Range, approximately 130 km to the east/southeast of Bayhorse. Our field investigations, provenance data, and regional correlations demonstrate the importance of the Lemhi arch, which is an intermittently positive topographic rift feature within the east-central Idaho segment of the Cordilleran margin. It is generally marked by Middle Ordovician strata unconformably overlying Mesoproterozoic Lemhi Group strata of the Belt Supergroup. At South Creek, a much thinner, ~0.5-km-thick section of mostly lower Cambrian rocks of the Wilbert and Tyler Peak Formations are bounded by angular unconformities above Mesoproterozoic upper Belt Supergroup equivalents and below Ordovician strata of the Summerhouse Formation. Thus, the rocks at South Creek record significantly less subsidence in this region associated with the Lemhi arch.

Collectively, the rocks near Bayhorse and South Creek constitute a comparably complete transect of the Neoproterozoic to early Paleozoic Laurentian margin between better preserved strata in southeastern Idaho and northeastern Washington. However, in both southeastern Idaho and northeastern Washington, Cambrian strata exhibit similar, traceable facies, over long distances perpendicular to the rift margin, indicating a low-relief early Paleozoic margin in these regions. The stops along this field trip in central Idaho will demonstrate the heterogeneity in thickness and preservation of Neoproterozoic to Cambrian strata perpendicular to the rift margin in the central Idaho segment. This heterogeneity likely indicates the higher Neoproterozoic topographic relief and more structurally complex Lemhi arch of central Idaho.

GEOLOGIC SETTING

Scattered along the western (or Cordilleran) margin of Laurentia from Baja, Mexico to the Yukon, Canada, outcrops of Neoproterozoic to lower Paleozoic (Windermere Supergroup correlative) strata that have succeeded in skirting obliteration from younger Cordilleran tectonism document prolonged rifting and eventual passive margin sedimentation associated with the breakup of supercontinent Rodinia. These rocks reflect the Neoproterozoic (ca. 780–540 Ma) rift-related removal of landmasses, of debated identities but probably including Australia and East Antarctica, from their locations adjacent to western Laurentia.

Early geologists in central Idaho (e.g., Sloss, 1964; Ruppel, 1986), identified a widespread Middle Ordovician-on-Mesoproterozoic "Lemhi arch" unconformity in east-central Idaho (fig. 1) and incorrectly assigned an Ordovician—rather than Neoproterozoic and Cambrian—age to quartzite and shale near Bayhorse in central Idaho (Ross, 1937). These observations led workers to conclude that Neoproterozoic and Cambrian strata recording the breakup of Rodinia are absent in this segment of the rift margin.

However, recent work has shown that Neoproterozoic and Cambrian rocks are indeed present within central Idaho, just of limited exposure and overprinted by younger Cordilleran tectonism (Lund and others, 2003, 2010; Link and others, 2017; Isakson, 2017; Brennan and others, 2020a,b). This field trip will provide an overview of the ~3.5 km of Neoproterozoic to Ordovician stratigraphy near Bayhorse, Idaho (the Bayhorse succession; Brennan and others, 2020a,b; Krohe and others, 2020) and the much thinner, yet at least partially correlative ~0.5 km of Neoproterozoic to Ordovician stratigraphy near South Creek, Idaho. Collectively this eastward-thinning succession is associated with erosion or stratigraphic onlap onto the western edge of the Lemhi arch (fig. 1).

At Bayhorse, the Neoproterozoic strata are locally mineralized. Silver, lead, copper, and zinc ore occurs in mineralized shear zones or as replacement lenses, notably within the Neoproterozoic Bayhorse Dolomite and Ramshorn Slate units. Granitic intrusive rocks of the Idaho Batholith, and possibly the Challis magmatic suite, are associated with many of the deposits. The largest and best developed historic mine in the Bayhorse Mining district, the Ramshorn

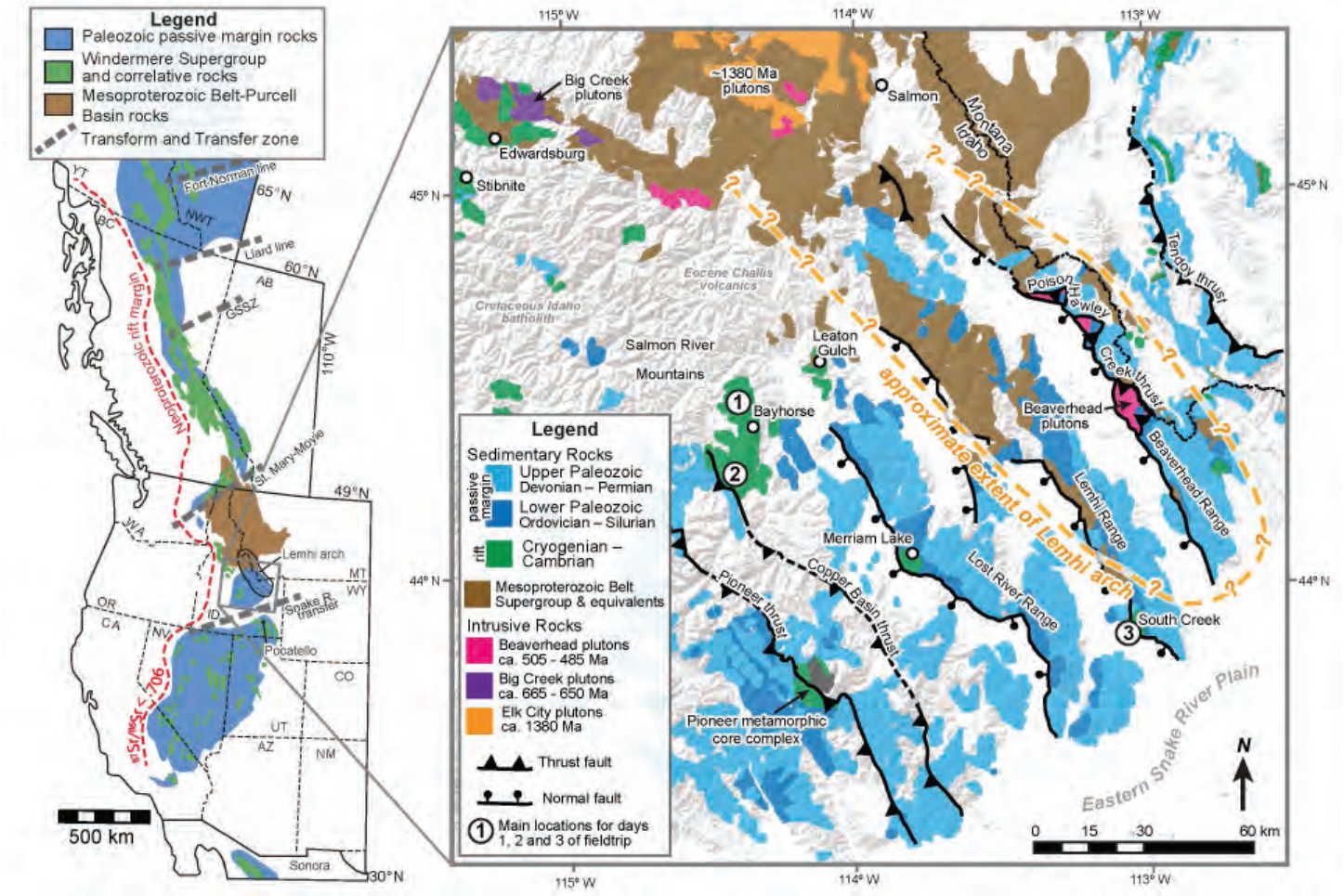

Figure 1. Regional map of the U.S. and Canadian Cordillera showing exposure belts for Mesoproterozoic Belt–Purcell Supergroup rocks, Neoproterozoic Windermere Supergroup (and correlative) rocks, Paleozoic passive-margin sedimentary rocks, the approximate extent of the Lemhi arch, and transform–transfer zones that were interpreted to separate the miogeoclinal segments of Lund (2008). Inset map shows the present-day outcrop map of Mesoproterozoic to Paleozoic rocks of the northern segment of the U.S. Cordillera, including the main field locations for days 1, 2, and 3 of this field trip. $^{87}Sr/^{86}Sr$ <0.706 line approximates the western edge of Laurentia. Abbreviations: GSSZ, Great Slave shear zone; AZ, Arizona; CA, California; CO, Colorado; ID, Idaho; MT, Montana; NM, New Mexico; NV, Nevada; OR, Oregon; UT, Utah; WA, Washington; WY, Wyoming; BC, British Columbia; AB, Alberta; NWT, Northwest Territories; YT, Yukon Territory. Figure from Brennan and others (2023).

Mine, between 1902 and 1970 produced 152 oz of gold, 2,400,000 oz of silver, 1,065,000 lbs of copper, 5,980,000 lbs of lead and 37,000 lbs of zinc (Mitchell, 1999) worth in excess of $65 million in 2023 commodity prices. Today, Bayhorse is a ghost town turned into an Idaho State Park. In addition to the geology, several stops will also “dig into” the mining history of this interesting time in the not-so-distant past.

FIELD TRIP LOG

Days 1 and 2: Bayhorse Stratigraphy

Days 1 and 2 of this field trip will explore Neoproterozoic to Ordovician strata exposed in the northwest-trending Bayhorse anticline west of Challis, Idaho (fig. 2). The field trip mileage log starts at the intersection of Highway 93 and Garden Creek Road in Challis, Idaho. While on Highway 93, turn west onto Main Street (USFS Road 070). At the first road intersection after turning off Highway 93 (Main and 13th Street), pull over and reset your trip odometer. Continue west on Main Street (USFS Road 070), then at 2.4 mi (3.9 km) keep right as the road crosses Garden Creek. The bluffs on either side of the road consist of dacitic rocks of the Eocene Challis Volcanic Group. At 5.0 mi (8.0 km), you will reach a fork in the road with USFS Road 070 (Yankee Fork Road) on the right leading to Stop 1 and the left fork, USFS Road 069 (Garden Creek Road), leading to Stops 2, 3 and 4. Turn right and continue onto USFS Road 070, at 6.0 mi (9.7 km) on your trip (1.0 mi after the intersection with USFS Road 069); there is a left turn onto an unnamed Forest Service road, where you will continue approximately 0.2 mi (320 m) to Stop 1 (fig. 3).

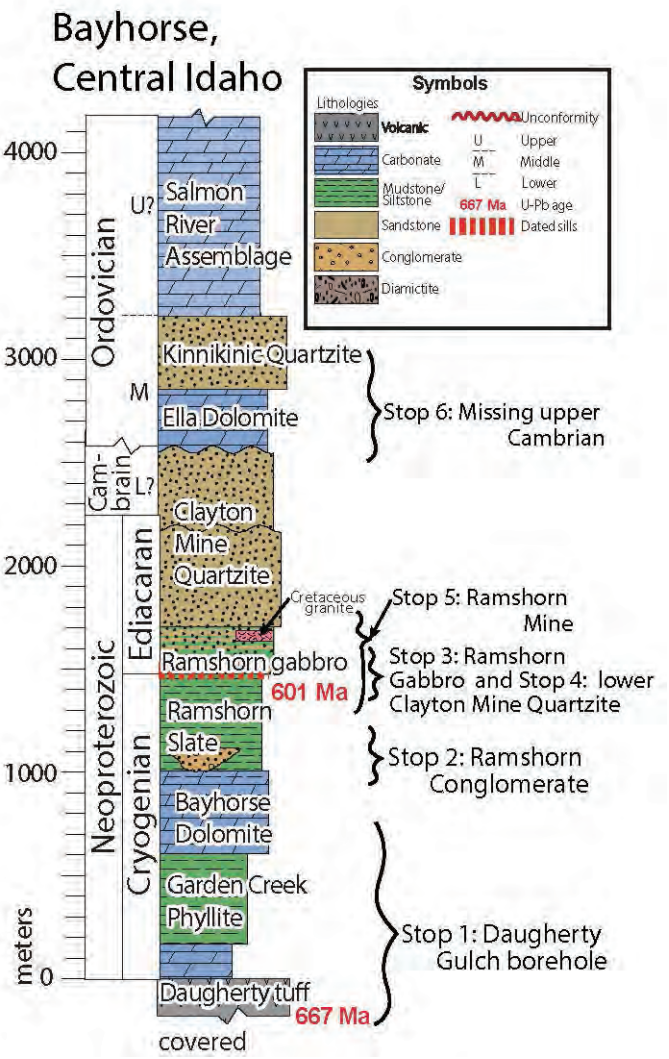

Figure 2. Stratigraphic column of the Bayhorse area stratigraphy (adapted from Brennan and others, 2020a) and the stratigraphic interval of each stop for days 1 and 2 of the field trip.

STOP 1

Daugherty Gulch Borehole

(44.48583°N, -114.33167°W)

Stop 1 involves locating a borehole that was critical in constraining the Bayhorse stratigraphy as Neoproterozoic in age, and observing the minor faulting in the Bayhorse Dolomite that crops out adjacent to the borehole. The unnamed spur of USFS Road 070 will take you up to the outcrop, and the ground surrounding the outcrop is generally flat and easily hikeable. After locating the Daugherty Gulch borehole (fig. 3), have a look at the adjacent outcrops of Bayhorse Dolomite. You may observe some minor faulting with slickensides recording strike-slip and normal sense of shear. Fluorite (also called fluorspar, CaF_2), with its cubic crystal habit, is observable on some fault and fracture surfaces. Approximately 300 m (984 ft) northwest of the Daugherty Gulch borehole, the Chalspar No. 1 mining claim covers exposures of Bayhorse Dolomite, which was actively mined from 1952 to 1954 (?) and produced 475 tons of metallurgical grade (88% CaF_2) and 245 tons of milling grade (55% CaF_2) fluorspar (Anderson, 1954), with a 2023 commodity value of around $200,000. Fluorspar is a USGS critical mineral resource, with fluorine being an essential element in a number of industries including aluminum production, steelmaking, gasoline refining, glass manufacturing, and the production of enamels, insulating foams, refrigerants, and uranium for nuclear power. The United States is the world's second-highest consumer of fluorine products, but from 1996 to 2012 mined no fluorspar domestically. China and Mexico are the world's leading producers of fluorspar (Hayes and others, 2017).

In 1987, a 1,143 m (3,749 ft) vertical exploration borehole by Shama Minerals was drilled into the eastern limb of the Bayhorse anticline near Daugherty Gulch and intersected a lithic tuff not exposed elsewhere within the Bayhorse region (Jacob, 1990). Strata within the drillhole dip approximately 15° to 30° ESE. The drillhole intersected 3.4 m (11 ft) of overburden, 149 m (488 ft) of Bayhorse Dolomite, 874 m (2866 ft) of Garden Creek Phyllite, 60 m (196 ft) of basal dolomite of Bayhorse Creek (the stratigraphically lowest exposed unit within the Bayhorse Anticline), and 58 m (189 ft) of lithic tuff (hereby referred to as the Daugherty Gulch tuff) in which the hole was terminated (Jacob, 1990). Estimated true thicknesses for the units are: Bayhorse Dolomite, 144 m (471 ft); Garden Creek Phyllite, 757 m (2,482 ft); basal dolomite of Bayhorse Creek, 52 m (170 ft); and Daugherty Gulch tuff, 50 m (164 ft). See figure 4.

Lund and others (2010) conducted further study of the Daugherty Gulch drill hole, with a particular focus on the lowest ~50-m-thick tuffaceous unit. They described this lowest unit as containing two types of diamictite showing lower-greenschist facies metamorphism. The lower approximately 55 m (180 ft) of the borehole is characterized by the lower diamictite and contains an unsorted clay to sand matrix composed primarily of quartz, lithic fragments and altered sericitic and carbonaceous material interpreted to have originated as feldspar or mafic minerals in a tuffaceous matrix. Clasts make up ~50% of this lower diamictite, are as large as 25 cm in diameter, and composed dominantly of rhyolite with lesser quartzite and metasandstone, and minor carbonaceous phyllite and dolostone, and a few plutonic clasts. The sources of the volcanic and plutonic clasts are unknown, but Lund and others (2010) suggested that the clastic sedimentary clasts could have been sourced from nearby Mesoproterozoic Lemhi Group strata of the Gunsight and Swauger Formations.

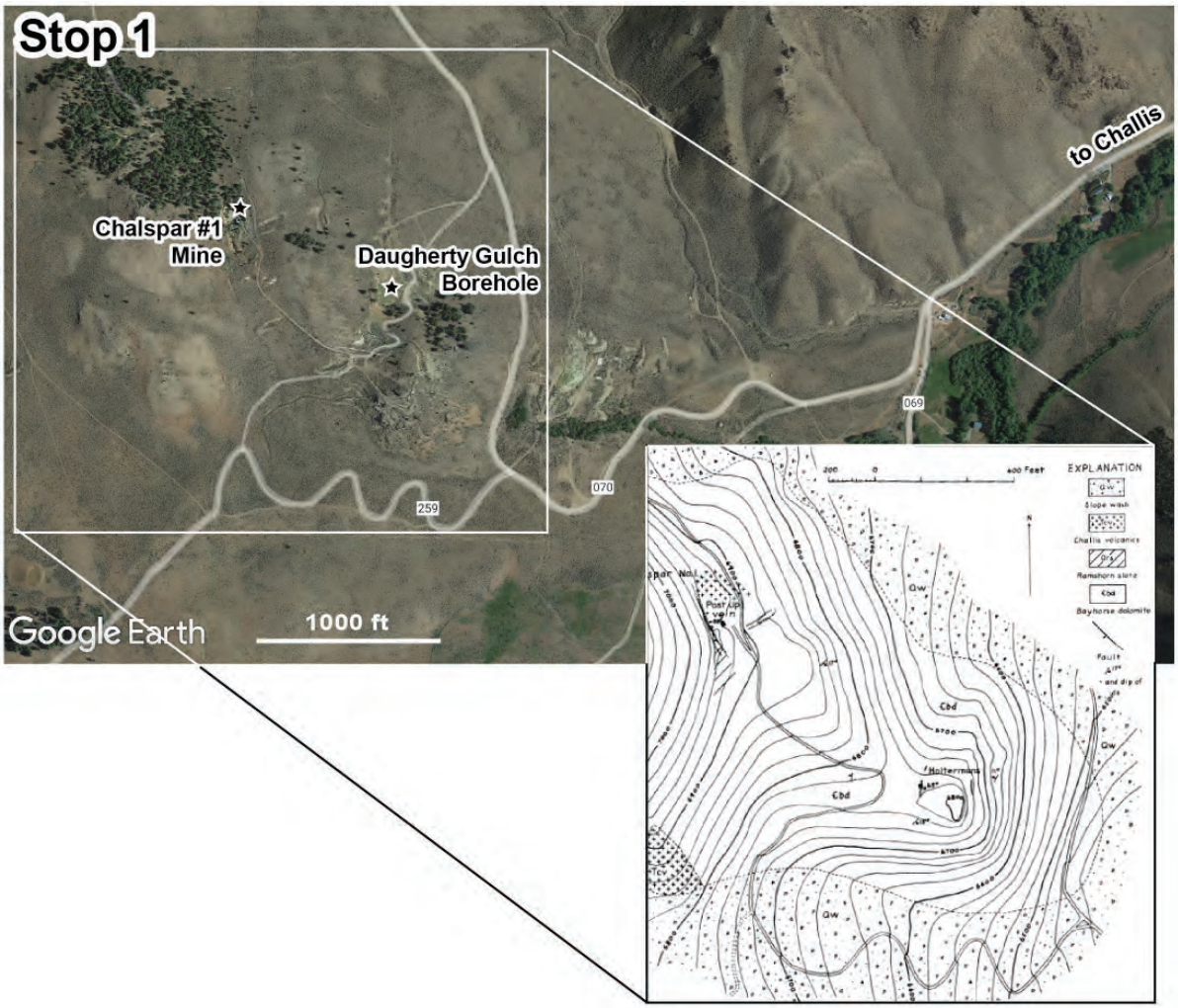

Figure 3. Aerial imagery and simplified geologic map (Anderson, 1954) of the Daugherty Gulch Borehole region for field trip Stop 1.

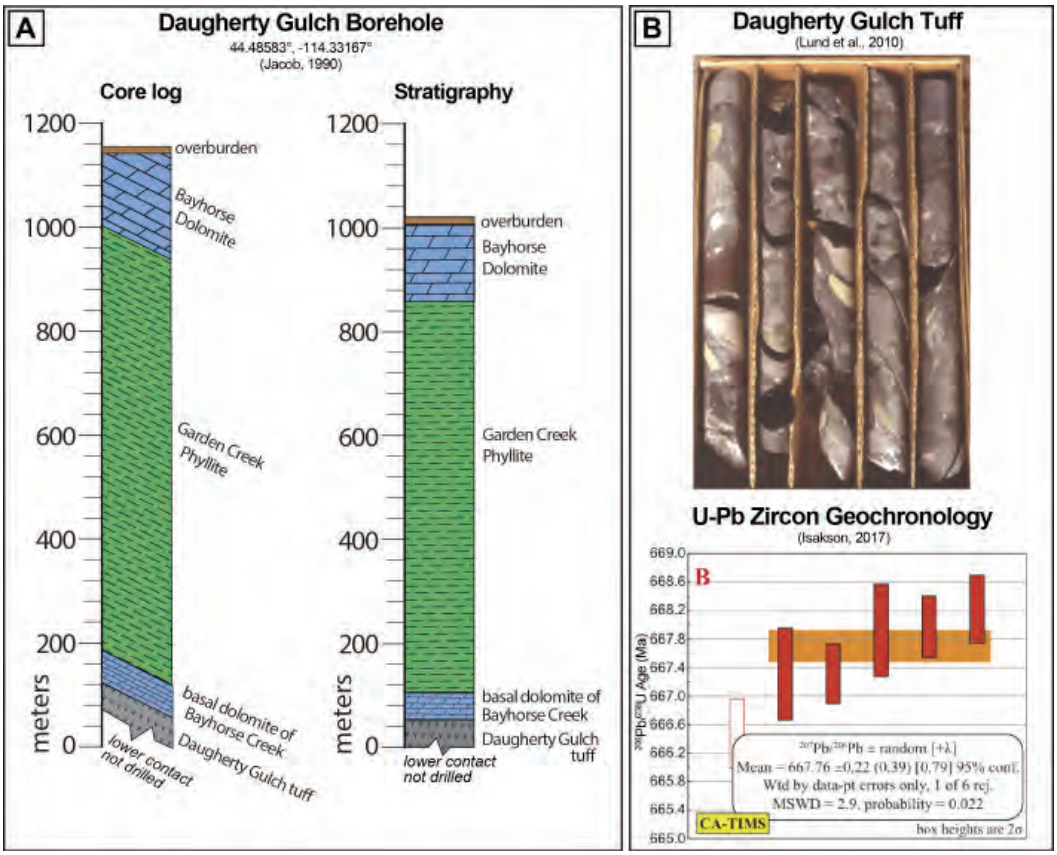

Figure 4. (A) The stratigraphic results of the Daugherty Gulch borehole (modified from Jacob, 1990). (B) The sampled tuffaceous interval from the Daugherty Gulch core (Lund and others, 2010) and U/Pb geochronology results from Isakson (2017).

For ~3 m (10 ft) above this lower diamictite, the borehole encountered a light-greenish, chloritic, unsorted siltite to metasandstone with grit to pebble-sized clasts composed primarily of quartzite and metasandstone. Notably, volcanic clasts that dominate the lower diamictite are rare in this upper interval.

Lund and others (2010) dated zircon grains from the tuffaceous matrix of the diamictite at 1140 m depth in the core, approximately ~1.5 m (5 ft) above the bottom of the hole, and ~55 m (180 ft) below the top of the diamictite unit. U/Pb dating using sensitive high-resolution ion microprobe (SHRIMP) isotopic data from 15 zircon grains gave a 664 ± 6 Ma age (all uncertainties given at 2σ), which Lund and others (2010) interpreted as the time of extrusion of the tuff. Isakson (2017) conducted further U/Pb geochronologic study of the Daugherty Gulch tuff/diamictite utilizing the same zircon separate as Lund and others (2010). Isakson (2017) first conducted laser ablation inductively coupled mass spectroscopy (LA-ICPMS) of 138 grains, with 71 grains returning dates between ca. 1839 and 1010 Ma, and 32 (of 66, ≤10% discordant) <1000 Ma dates returning a weighted mean age of 664 ± 6 Ma (equivalent to Lund and others' 2010 age). Isakson (2017) further refined this age using chemical abrasion thermal ionization mass spectroscopy (CA-TIMS) of the youngest zircon grains, which yielded an equivalent U/Pb age of 667.8 ± 0.2 Ma (fig. 4). However, due to the presence of older, likely detrital zircon grains within the Daugherty Gulch tuff, Isakson (2017) cautioned that this age could represent a maximum depositional age, not a primary volcanic age.

Lund and others (2010) speculated—in part based on the discrepancy between the ca. 667 Ma Daugherty Gulch Tuff age and the alleged Cambrian to Early Ordovician age of the overlying Bayhorse stratigraphy intersected within the borehole (Hobbs and Hays, 1990; Jacob, 1990)—that the rocks intersected within the borehole are part of a section not exposed within east-central Idaho. However, our mapping (Brennan and others, 2020a) identified several small faults in the outcrops adjacent to the borehole but found no evidence of significant "terrane bounding" faults, suggesting that the borehole did intersect a relatively intact stratigraphic section. Thus, we interpret that the strata exposed in the Bayhorse anticline directly adjacent to the borehole do indeed overlie the ca. 667 Ma Tuff of Daugherty Gulch. This revised interpretation thus has important consequences for redesignation of the age of these strata.

Once you are done with these outcrops, return to your vehicles and navigate back to the intersection of USFS roads 070 and 069. Here, turn right and continue southwest on USFS Road 070 (Garden Creek Road). At approximately 10.5 mi (16.9 km), just after you have passed steeply dipping beds of Bayhorse Dolomite, you will encounter the intersection of USFS Road 070 (Garden Creek Road), and a steeper road (USFS Road 052) spur that leads to the south. There is space for several vehicles to park here. Stop 2 will include a relatively short (~0.5 mi, ~0.8 km) but uneven and steep hike to excellent outcrops of the Ramshorn conglomerate.

STOP 2

Ramshorn Conglomerate

(44.4589°N, -114.3271°W)

In part, early and incorrect correlation of the Ramshorn Slate to the generally lithologically similar Ordovician graptolite-bearing Phi Kappa Formation that crops out approximately 20 mi (~32 km) to the south in the Pioneer Mountains (Ross, 1937) contributed to the assignment of a mostly Ordovician age to the Bayhorse stratigraphic section (e.g., Hobbs and Hays, 1990). However, the "basal conglomerate" within the Ramshorn Slate, notably exposed at this stop along Garden Creek, indicates a distinct lithologic difference between the exposed stratigraphy within the Bayhorse section and otherwise generally fine-grained Ordovician strata in Idaho.

This basal "Ramshorn conglomerate" flanks both sides of the Bayhorse anticline for a distance of nearly 4 mi (6.5 km), is locally more than 150 m thick (500 ft), and interfingers with fine sandstone and siltstone that are part of the lower main Ramshorn Slate lithology (figs. 2, 4; Hobbs and Hays, 1990). Interestingly, the Ramshorn conglomerate is composed almost exclusively of moderately well-rounded pebbles of vein or microcrystalline quartz (not quartzite or sandstone), generally less than 8 cm (~3 in) in diameter, with an unknown source terrane. The abundance of these quartz pebbles is enigmatic but may suggest extensive chemical weathering of the source terrane. Where the conglomerate interfingers with the coarse sandstone facies of the lower Ramshorn Slate, the detrital zircon grains within the coarse sandstone show major age-populations at ca. 1174, 1391, 1768, and 2711 Ma (fig. 5) that are commonly associated with eastern/southeastern Laurentian sources (e.g., Rainbird and others, 1997; Matthews and others, 2018; Brennan and others, 2021a).

At the Stop #2 outcrop, you can observe several notable features of the interfingering facies of the lower Ramshorn Slate and Ramshorn conglomerate (fig. 6). These include: (A) the predominantly quartz pebble conglomerate, flute casts (B and C), and enigmatic

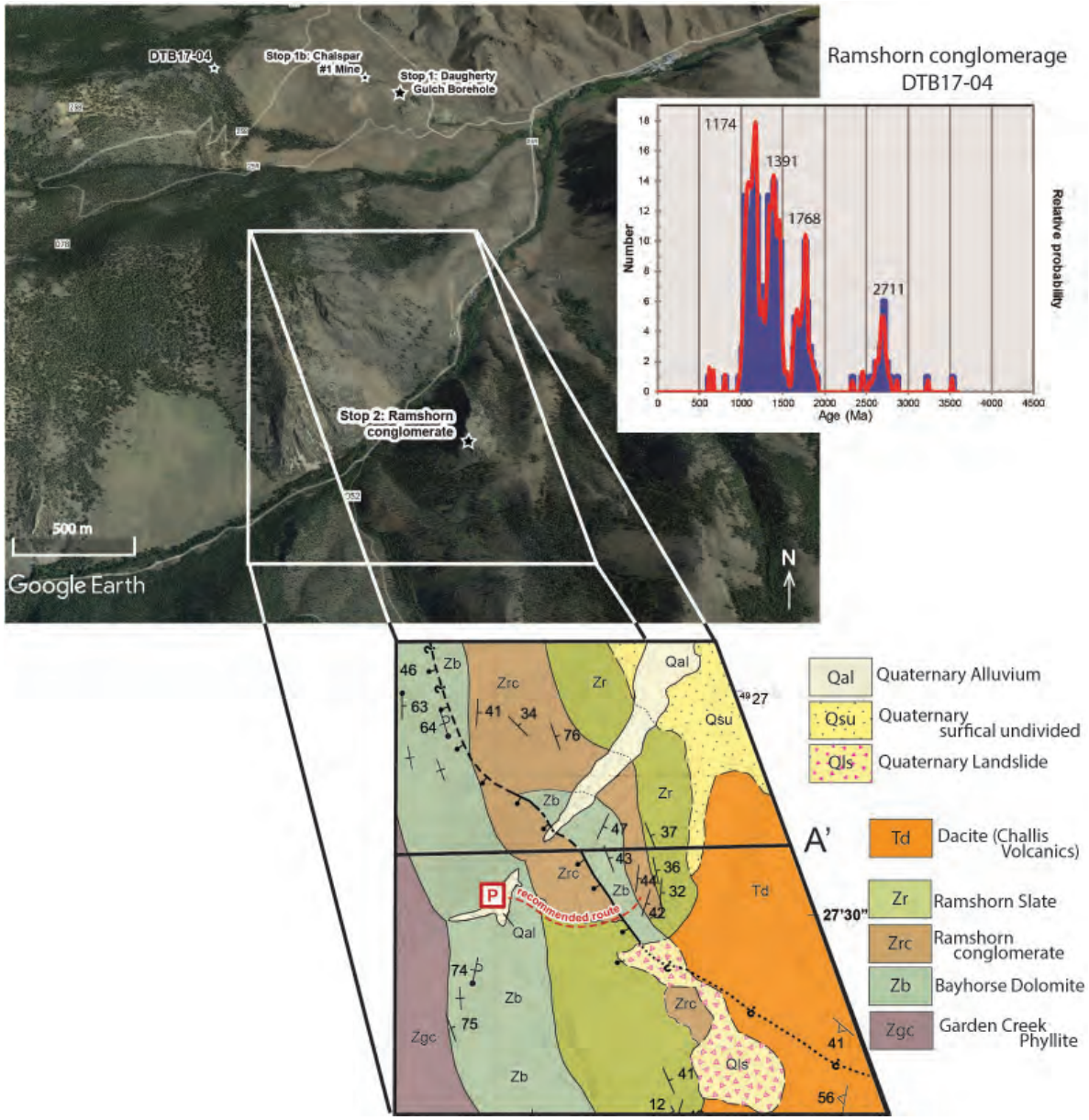

Figure 5. Aerial imagery and geologic map (Brennan and others, 2020a) of fieldtrip Stop 2, The Ramshorn Slate/conglomerate outcrop. The dashed redline indicates the approximate hiking traverse. In the upper right are the detrital zircon U/Pb results for the Ramshorn conglomerate (sample DTB17-04, Brennan, 2018) near where it interfingers with the Ramshorn Slate, along strike from Stop 2.

"wrinkle structures" that are likely parallel load and fold structures perhaps suggesting seismically driven soft-sediment deformation (J. Hagadorn, 2018 personal commun.), and centimeter-scale graded beds (not pictured). Although relatively rare, large angular ~30 cm (1 ft) clasts can be found in the conglomerate facies. Collectively, the coarse clast size and evidence of turbidity currents (scours, flute casts, graded beds, etc.) could reflect deposition proximal to a normal-fault escarpment, perhaps related to the Lemhi arch. Several interesting questions, such as the ones previously mentioned, regarding these units could be investigated by more detailed stratigraphic, paleoenvironmental, and provenance study. At the conclusion of exploring this outcrop, return to the vehicles and continue to Stop 3.

Continuing to the west, Garden Creek Road (USFS 069) runs essentially perpendicular to the fold trace of the Bayhorse anticline. At about 10.8 mi (17.4 km), the road crosses a cattle guard, and the relatively open hillslope on your right (north) is the recessive-weathering Garden Creek Phyllite, the stratigraphically lowest unit exposed along Garden Creek, in the core of the anticline. At about 11.5 mi (18.5 km), you will see the west-dipping resistant ridge of Bayhorse Dolomite and you are now again driving stratigraphically upsection in generally west-dipping strata. From ~11.5 mi until the next stop at mi ~13.8 (22.2 km), you are driving primarily upsection through folded Ramshorn Slate. Stop 3 is near the contact of the Ramshorn Slate and overlying Clayton Mine Quartzite, which is intruded by ca. 601 Ma gabbroic sills.

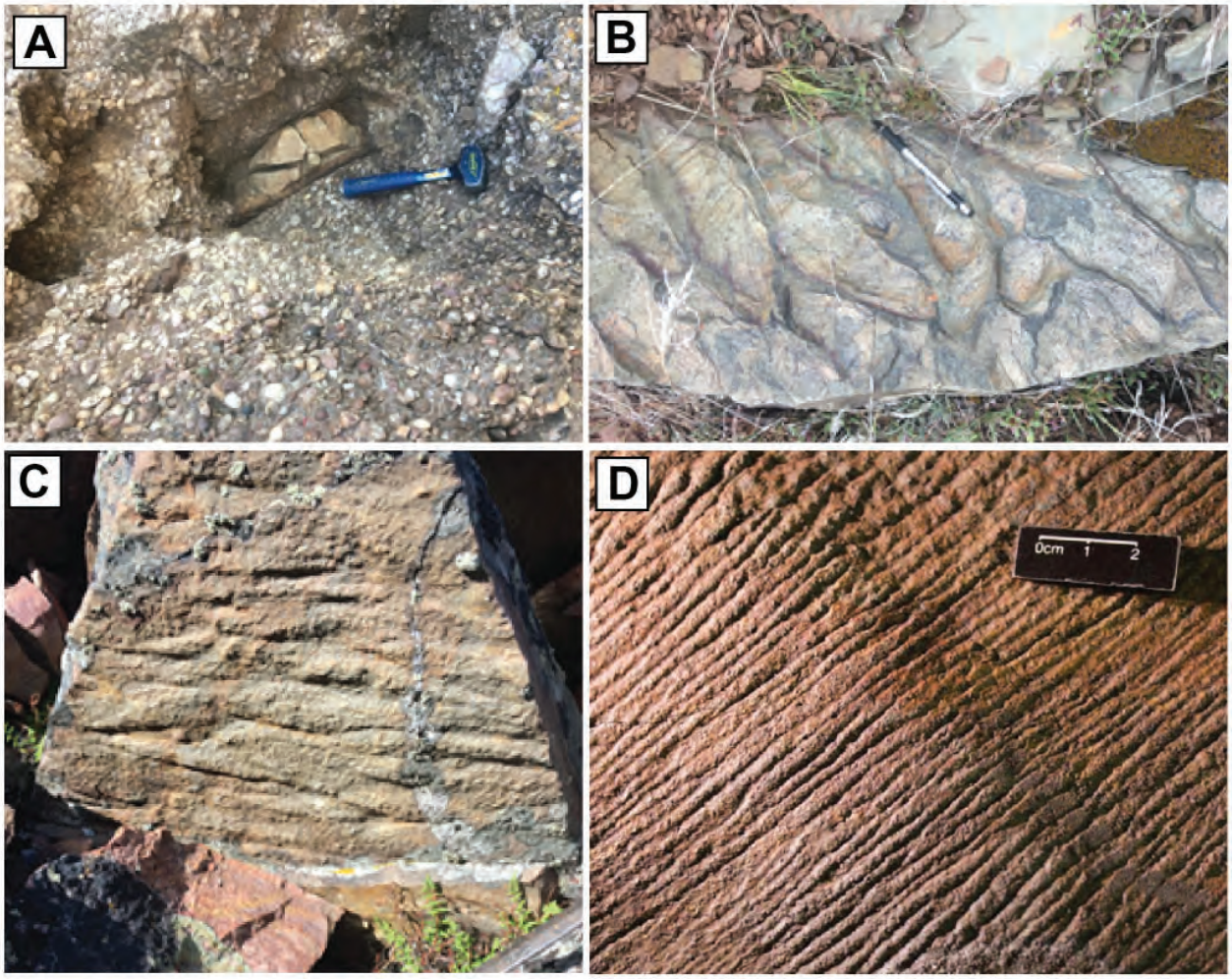

Figure 6. Characteristic lithologies of the interfingering Ramshorn Slate and Conglomerate facies viewed at Stop 2, including (A) Ramshorn conglomerate; (B) flute casts where Ramshorn Slate overlies Ramshorn Conglomerate just east of Keystone Gulch; (C) probable load casts; and (D) enigmatic "wrinkle" structures found in talus near the Ramshorn Slate/Conglomerate contact. Photos from Brennan (2018).

STOP 3

Ramshorn Gabbro

(44.4429°N, -114.3910°W)

Stop 3 is at a relatively inconspicuous outcrop of gabbro along USFS Road 069, near the Bruno Cabin ruins, just before the switchback (fig.7). Though the low-lying outcrops of this gabbro are not particularly interesting, they yielded impressive geochronology results. Please note that the actual outcrop sampled and analyzed for geochronology is approximately 0.6 mi (1 km) up the ridge to the north of stop 3 (at 44.4526°N, -114.3899°W). This particular gabbro body was sampled due to its slightly larger and coarser nature. However, for ease of access, having a look at the correlative gabbro intrusion adjacent to USFS Road 069 will suffice. This gabbro is medium- to coarse-grained, containing a primary mineral assemblage of calcic plagioclase, clinopyroxene, and magnetite that has been variably altered to primarily chlorite, amphibolite, albite, titanite (sphene) and small amounts of secondary quartz (Hobbs and others, 1991).

As discussed, previous mappers (e.g. Hobbs and Hays, 1990; Hobbs and others, 1991) interpreted the Cambrian Clayton Mine Quartzite to overlie the "Ordovician" Ramshorn Slate, and thus mapped a (usually thrust) faulted contact everywhere the Clayton Mine Quartzite overlay the Ramshorn Slate. In several locations, these hypothesized thrust faults were intruded by these undated gabbro sills. The age of the gabbro was inferred to be Jurassic, on the basis of a fission track date from an immediately adjacent quartzite (R.A. Zimmerman, written commun., 1983, in Hobbs and others, 1991). Our mapping (Brennan and others, 2020a; Krohe and others, 2020) further indicated that the gabbro only intruded the lower Paleozoic or older strata of the Bayhorse Anticline, usually in a relatively consistent stratigraphic horizon near the Ramshorn Slate and Clayton Mine Quartzite contact, and also was folded with the strata. Given that Jurassic magmatism is very rare in central Idaho, we speculated that perhaps the gabbro was older than the poorly constrained Jurassic (?) age proposed by Hobbs and others (1991).

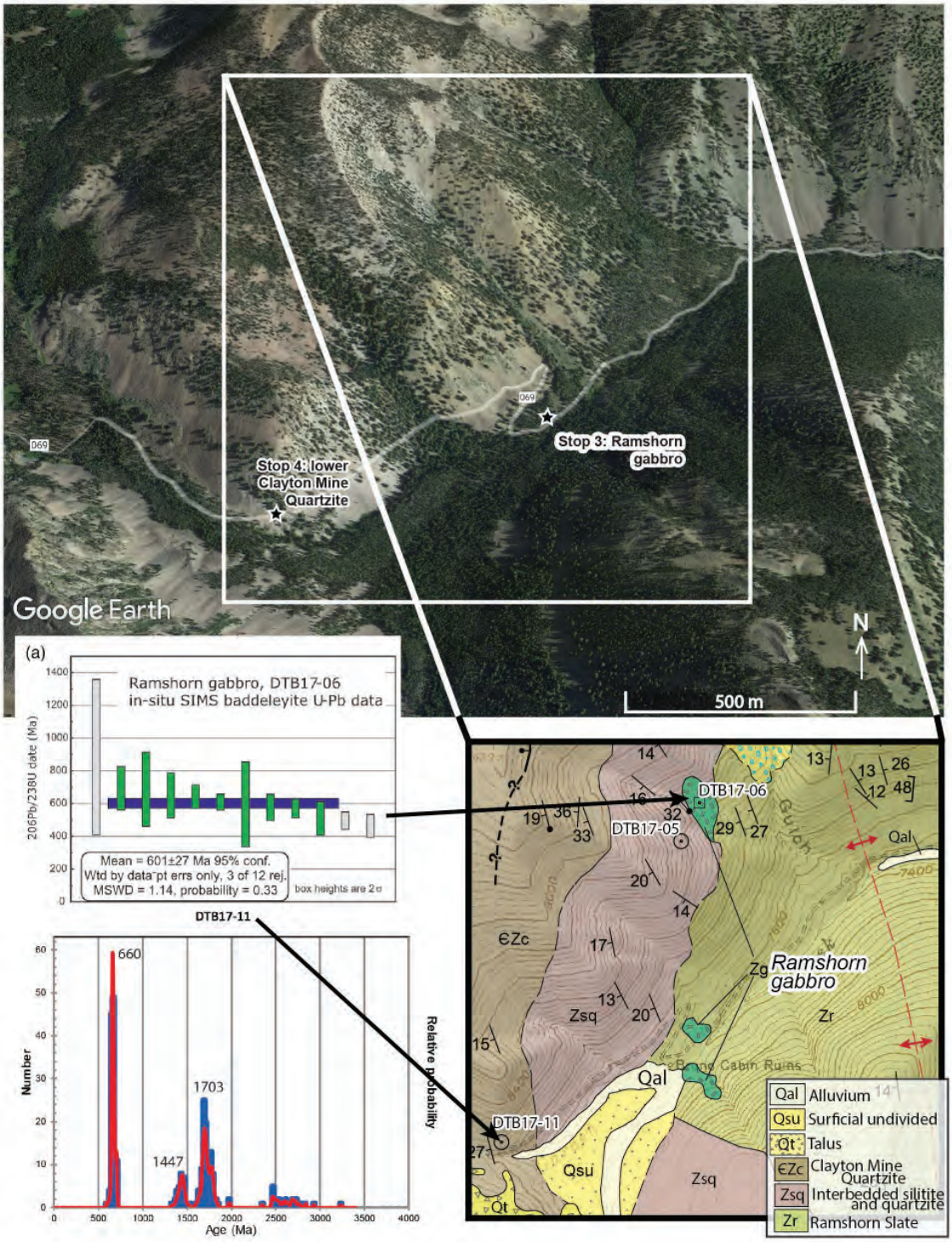

Figure 7. Aerial imagery and geologic map (Brennan and others, 2020a) of fieldtrip Stops 3 and 4. The geochronology plots show the weighted mean age (601 ± 27 Ma) for the Ramshorn gabbro and detrital zircon age-spectra for the lower Clayton Mine Quartzite (Brennan and others, 2020b).

Due to the silica-poor nature of this gabbro, several kilograms of crushed rock yielded no zircon ($ZrSiO_4$) separate. However, in thin-section, micro (generally <5 um) baddeleyite (ZrO_2) was present. Due to the small size, these baddeleyite grains were targeted with secondary ionization mass spectrometry (SIMS) by K.R. Chamberlain and yielded an age of 601 ± 27 Ma (95% confidence interval, MSWD = 1.1), interpreted as the timing of gabbro crystallization (fig. 7).

STOP 4

Lower Clayton Mine Contact

(44.4405°N, -114.4003°W)

From this point on, the road becomes rougher and 4 x 4 or high-clearance vehicles are recommended. Continue west approximately another 0.8 mi (1.3 km), past the two switchbacks, to the gradational contact between the Ramshorn Slate and Clayton Mine Quartzite (fig.

7). Just past the cattle guard there is space to park, but the best exposures of the gradational contact are on the ridge southeast of the cattle guard.

Here, at Stop 4, you will observe mixed lithologies consisting of quartzite and siltstone, with crossbedding and individual beds separated by green, micaceous shaley partings representative of the gradational contact between the Ramshorn Slate and Clayton Mine Quartzite. Sample DTB17-11 was collected just above this gradational contact near its top and yielded much different detrital zircon age-components than the underlying Ramshorn Slate/conglomerate (fig. 7). Sample DTB19-11 yielded no ca. 1000–1300 Ma grains associated with the Grenville province, and notably contained a large proponent of ca. 660 Ma grains. The remaining older age components at ca. 1447 and 1703 are similar to those that characterize Belt Supergroup strata. These ages suggest that the lower Clayton Mine Quartzite records a local provenance from the ca. 666–650 Ma Big Creek plutons that intrude Apple Creek Formation (or equivalents) of the Belt Supergroup (fig. 8) approximately 100 km to the north/northwest (see fig. 1). Consequently, there appears be a relationship between the mafic magmatism recorded in the Ramshorn gabbro, apparent shoreline regression recorded by the coarsening upwards contact between the Ramshorn Slate and Clayton Mine Quartzite, and rift-flank incision/exhumation recorded by the proximal provenance signature.

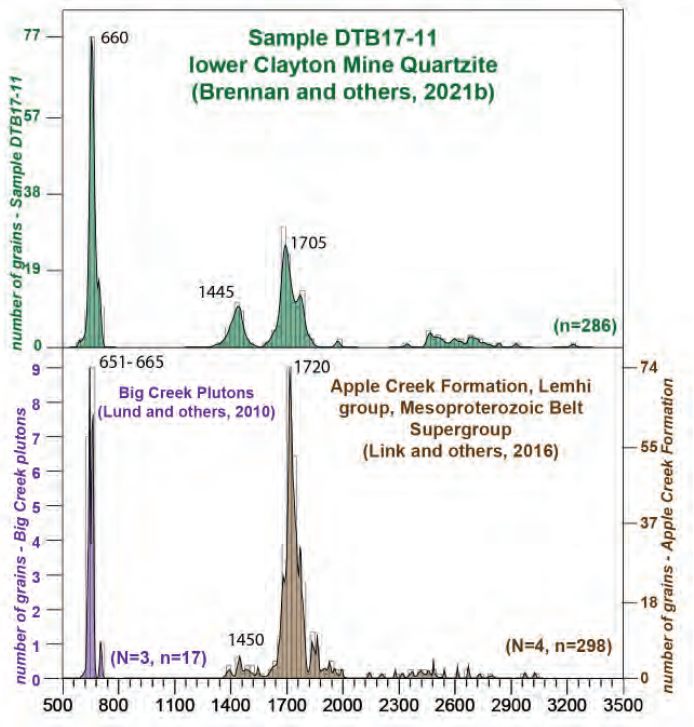

Figure 8. Top plot: Detrital zircon ages for the lower Clayton Mine Quartzite (sample DTB17-11) with the unique ca. 660 Ma age component. Bottom plot: Igneous U/Pb zircon ages for the ca. 660 Ma Big Creek plutons (Lund and others, 2010) and Belt Supergroup strata the plutons intruded (Link and others, 2016). N= no. of samples, n= no. of grains.

Drive to Bayhorse Creek.

The remaining stops today (time permitting) will be along Bayhorse Creek with overnight camping at Bayhorse campground. Stopping for fuel in Challis may be pertinent as refueling opportunities over the next 2 days (~210 mi, 338 km, of total travel) are limited. Please navigate the 11.4 miles (18.3 km; odometer at ~26.1 total mi, 42 total km) back to Challis, at the intersection of Main Street and Highway 93 turn south (right); 2.3 mi (3.7 km) south of Challis (28.4 total mi, 45.7 km), turn west (right) onto Highway 75. Continue on Highway 75, tracing the Salmon River, another 8.1 mi (13 km, 36.5 total mi, 58.7 total km) and turn right (north) onto Bayhorse Road. There is a large sign approximately 100 m (328 ft) before the turn, indicating 4 mito the Historic Bayhorse Ghost Town, and 8 mi to Bayhorse Lake campground. Continue across the truss bridge to the north side of the Salmon River. Once on the north side of the river, Bayhorse Creek Road veers to the right (north) around a private residence. Take the first left turn past this residence, about 150 m (500 ft) from the end of the bridge.

For the first 2.4 mi (total odometer 36.5 to 40.7 mi, 58.7 to 65.5 km) of the drive up Bayhorse Creek Road, the relatively low relief hills on either side of the road are Eocene Challis mudflow, silicic tuff, and sedimentary and extrusive volcanic rocks. At 40.7 mi (65.5 km) on the odometer, you will enter the main canyon, the rocks on either side are Bayhorse Dolomite. Note how these exposures are thicker than the steeply dipping Bayhorse Dolomite beds observed along Garden Creek (e.g., Stop 2). This apparent variable thickness and localized brecciation observed in the upper Bayhorse Dolomite led Hobbs and others (1990) to propose an unconformity between the Bayhorse Dolomite and overlying Ramshorn Slate. At approximately 41.6 mi (~70 km), you will reach the Bayhorse Ghost Town State Park.

STOP 5
Bayhorse Ghost Town

(44.3976°N, -114.3129°W)

Time permitting, the final stop of the day will include exploring Bayhorse Ghost Town. More time tomorrow morning will be spent on this topic. A lone prospector travelling through the Salmon River Mountains in 1864 with two bay-colored horses found mineralization along a creek soon to be named for his equine companions. Mining at Bayhorse gained stability in 1880 with the construction of a 30-ton smelter, and in the next couple years the town of Bayhorse peaked with a population of about 300, boasting a complex of sub-

stantial, permanent buildings—mostly saloons (Wells, 1983). Like many central Idaho mines during this period, the remoteness of the Bayhorse mines hindered their economic feasibility, and by 1888, Bayhorse's last full year of operation, the mining time of Bayhorse was in decline. At the time, the Bayhorse mining district's total production amounted to ~$6.9 million in silver, ~$2.7 million in lead, and $650,000 in copper. The Ramshorn Mine accounted for roughly a quarter of this production (Wells, 1983). In 2023 dollars, the total Bayhorse district's production of ~$10.25 million in 1890 dollars is equivalent to roughly $337 million. For those interested in further information about the mining history at Bayhorse, please review pages 103 to 106 in Wells (1983).

An excellent, free campground (Bayhorse campground) with pit toilet facilities is available at the end of the Bayhorse Creek Road, approximately 5.2 mi (8.4 km) above (west) of Bayhorse Ghost Town. While unpaved, the road is well maintained, and when dry should be navigable by non 4 x 4 vehicles.

Spend night at Bayhorse Lake Campground (44.4105°N, -114.3987W°).

Day 2

Day 2 of this field trip will include a stop related to the Cretaceous intrusions hosted within the Bayhorse Dolomite and Ramshorn Slate, and responsible for the mineralization in the Bayhorse region. A second stop will look at the upper Clayton Mine Quartzite and overlying Middle Ordovician rocks of the Ella Dolomite and Kinnikinic Quartzite along the Salmon River, near Clayton approximately 10 mi (~16 km) south/southwest of Bayhorse. The day will conclude with an ~3-hour drive to South Creek in the southern Lemhi Range, where the third and final day will explore a correlative, yet less complete, section of Neoproterozoic to Ordovician rocks near South Creek.

Assuming the night was spent at Bayhorse Campground, please reset your trip odometer at the intersection of USFS roads 383 and 051 (the triple intersection that leads east to Bayhorse campground, northwest to Bayhorse Lake, and south to Bayhorse Ghost Town and eventually back to highway 95).

STOP 6
Juliette stock (44.4116°N, -114.3725°W)
and Ramshorn Mine (44.4104°N, -114.3623°W)

Stop 6 (fig. 9) explores the Cretaceous intrusions associated with the mineralization and largest producing mines of the Bayhorse district. After resetting your trip odometer at the intersection of USFS road 383 and 051 (the triple intersection described above) that leads east to Bayhorse campground, northwest to Bayhorse Lake, and south to Bayhorse Ghost Town and eventually back to highway 95, please turn east (back towards highway 95) and continue approximately 1.7 mi (2.7 km) until you reach the four-way junction. At this junction, USFS Road 382 turns west (left) to Little Bayhorse Lake, a hard right keeps you on USFS Road 051 (the main road that will take you back to Bayhorse Ghost Town and eventually to Highway 95); we will be taking the jeep road (USFS Road 381) straight ahead/slight right. Due to the narrowness of this road, limited space for turnarounds, and for a better view of the rocks, we recommend most vehicles park here near the intersection and walk the ~1.5 mi (2.4 km), ~100 m (330 ft) elevation gain along USFS Road 381. A higher clearance vehicle could drive this route if some participants prefer that option.

Approximately ~360 m (~1,200 ft) up USFS Road 381, a small satellite pluton of the Juliette stock intruded the Ramshorn Slate along the north side of the road. The main body of the Juliette stock is ~0.6 mi² (~1.5 km²) in area and exposed approximately ~0.6 mi (1 km) to the south (fig. 9). The intrusion is primarily granodiorite and quartz monzonite, with a contact aureole containing metamorphic biotite, sericite, chlorite, and in close proximity to the larger intrusions, andalusite and cordierite. At this small satellite intrusion, a contact aureole of metamorphic biotite, sericite, and chlorite is present but andalusite may be absent. Krohe (2016) reported a U/Pb zircon age of 96.9 ± 0.9 Ma (MSWD = 0.28) and zircon εHf = -6 to -8 for the Juliette stock. Approximately 12 mi (~19 km) to the west, near the Thompson Creek molybdenite mine, Montoya (2019) reports the same U/Pb zircon age of 96.9 ± 0.8 Ma for a small pluton that intrudes the Pioneer thrust, which refines an earlier K-Ar age of ca. 87 Ma (Marvin and others, 1973). These overlapping ages suggest that ca. 97 Ma magmatism may have been a regional, magmatic and mineralization event within the Bayhorse district. Although bulk rock chemistry is not available for the Juliette stock, it is likely part of the early metaluminous suite of the Idaho Batholith, which are characterized by mixed crust-mantle isotopic signatures (fig. 10; Gaschnig and others, 2010).

At approximately 0.7 mi (1.1 km) up USFS Road 381, the road will end near the ruins of the Ramshorn Mine, the greatest producing mine of the Bayhorse district. The remnants of a tramway, which opened on September 1, 1883 to transport Ramshorn ore down to wagons that carried the ore down the Bayhorse smelter, are still present (Wells, 1983). The higher elevation ruins visible above the Ramshorn Mine are the Skylark Mine,

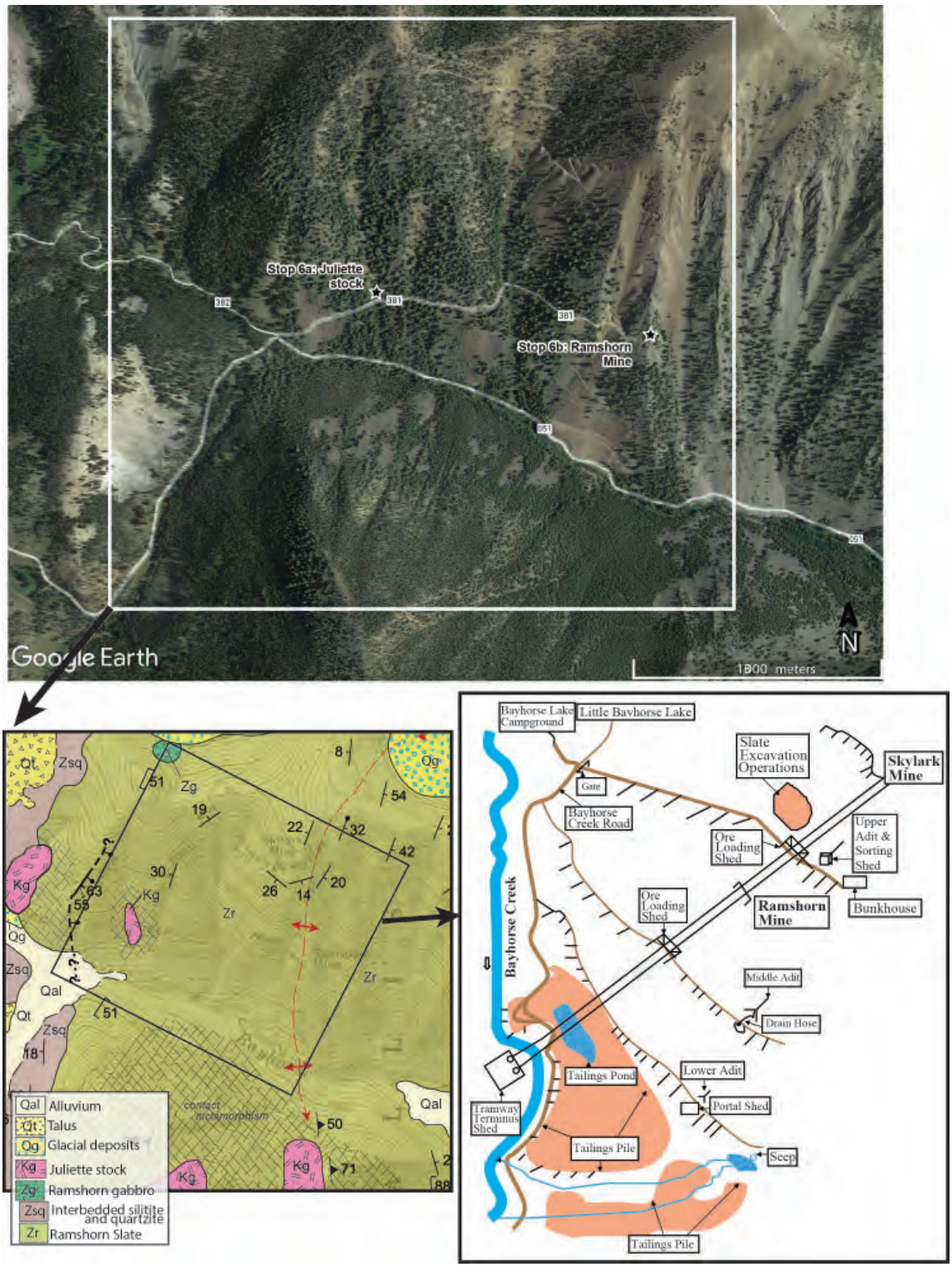

Figure 9. Aerial imagery and geologic map (Brennan and others, 2020a) of field trip Stops 6a and 6b. The map on the lower right is a simplified representation of the existing workings of the Ramshorn and Skylark mines (from Idaho Department of Environmental Quality 2003 Ramshorn Mine Preliminary Assessment).

which shared owners and tramway use with the Ramshorn. The Ramshorn Mine consists of 17 tunnels and 10 intermediate levels totaling about 6.5 mi (10.5 km) in length of mine workings. The main mineral targeted was tetrahedrite [$(Cu,Fe,Zn,Ag)_{12}Sb_4S_{13}$] in veins that varied from ~6 in to 6 ft thick. Other minerals include argentiferous galena [(Pb,Ag)S], sphalerite [(Zn, Fe)S], pyrite [FeS_2], arsenopyrite [AsFeS] and chalcopyrite [$AsFeS_2$], while siderite is the primary gangue mineral [$FeCO_3$] (Ross, 1937). Both the Ramshorn and Skylark Mines are located along an anticline within the Ramshorn Slate, consistent with Ross' (1937) assertion that "concentration of the ore solutions in areas of tension during deformation appears to be afforded by

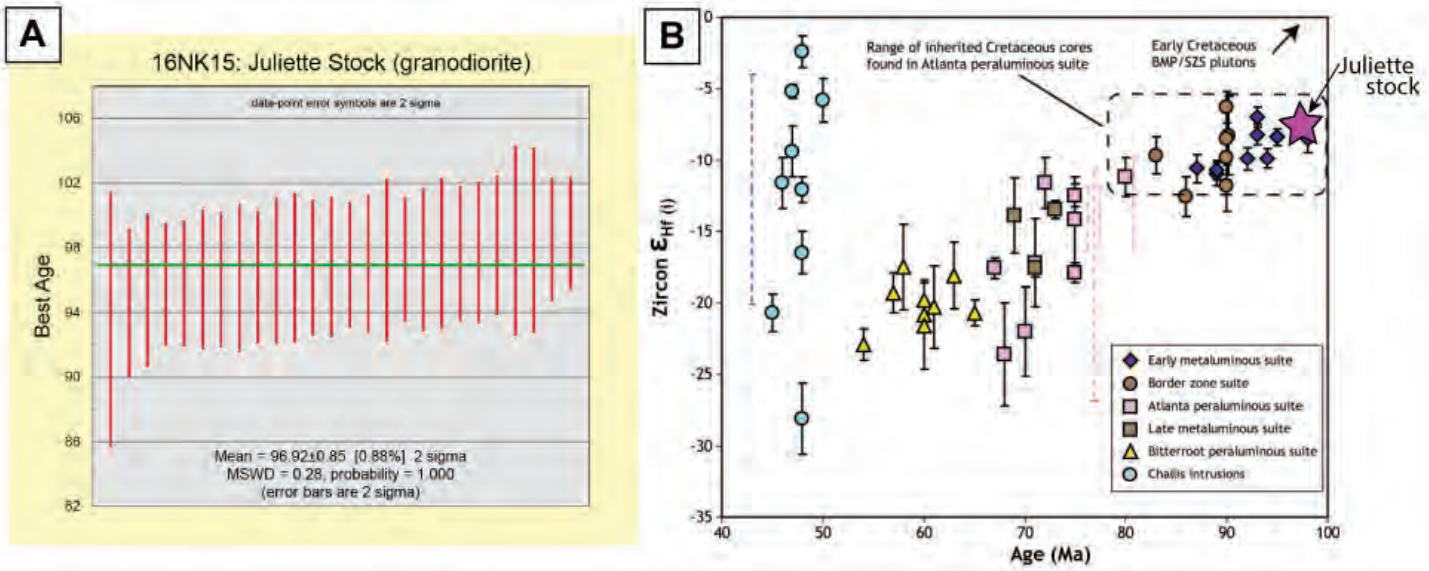

Figure 10. (A) U/Pb geochronology results for the Juliette stock indicating a 96.92 ± 0.85 Ma crystallization age (Krohe, 2016). (B) U/Pb-Lu/Hf results for the Juliette stock compared to the other magmatic suites of the Idaho Batholith and Challis intrusive rocks (Gaschnig and others, 2010).

the ore shoots in the Ramshorn Mine". Building ruins present at the end of USFS Road 381 include an ore loading shed, upper adit and sorting shed, and miner's bunkhouse (fig. 9; Idaho Department of Environmental Quality, 2003).

The Ramshorn Mine was listed by the EPA to the CERCLIS (Comprehensive Environmental Response, Compensation, and Liability Information System) in 2003. High levels of arsenic and lead were found in soil, sediment, and water samples taken around the Ramshorn tailing pile and adjacent Bayhorse Creek. As a result, the EPA completed in-place capping and regrading of the remaining tailings pile during the summer of 2011. Subsequent study found that generation of acidic surface or groundwater near the Ramshorn mine was minimal, likely due to the limited presence of pyrite (FeS_2) and/or neutralization by dolomitic bedrock (likely Bayhorse Dolomite). Iron (Fe) was the only contaminant found at relatively high concentrations and loads, and this metal appears to be removed from Bayhorse Creek by ferrihydrite ($Fe^{3+}_{10}O_{14}(OH)$) precipitation posing a limited environmental risk (Lachmar and others, 2019).

After exploring the Ramshorn Mine, walk back down USFS Road 381 and return to the vehicles parked at the junction of USFS roads 382 and 051. Continue east, back down USFS Road 051, past Bayhorse Ghost Town and to Highway 75. At the junction of Highway 75 and USFS Road 051, your odometer should read ~8.6 mi (13.8 km); turn right (south/southeast) onto Highway 75 and continue towards the town of Clayton. About 2 mi past Clayton, at a total odometer reading of ~24.1 mi (~38.8 km), stop at a small pulloff on the right (north side) of Highway 95 with room for 3–4 vehicles. There is space to park on the side of the road just before the bridge across the Salmon River. You are now near the southern extent of the Bayhorse anticline, and the final stop for the Bayhorse stratigraphy. Please exercise caution, as vehicles often drive fast on this relatively narrow portion of the highway.

STOP 7
Kinnikinic Quartzite and missing Cambrian strata

(44.2610°N, -114.4379°W)

At Stop 7 there is a relatively intact section of steeply west-dipping strata. All the strata at this stop were originally defined by Ross (1937) as the Kinnikinic Quartzite, a designation that he applied to over 1,070 m (~3,500 ft) of extensive exposures of mostly quarzitic rocks along the lower reaches of Kinnikinic Creek; he noted that revision of this designation was to be expected in the future. Later, Hobbs and others (1968) conducted a detailed study of these strata, which resulted in the subdivision of Ross' (1937) original Kinnikinic Quartzite into six formations. Krohe and others (2020) mapped three of these formations, which we will observe at this stop. The steeply west-dipping beds near the bridge are Middle Ordovician Kinnikinic Quartzite, stratigraphically below the Kinnikinic Quartzite is the Ella Dolomite, and stratigraphically below that is the uppermost Clayton Mine Quartzite (fig. 11). We recommend observing these units by traversing east, back along highway 75, in a downsection direction.

The Ella Dolomite is predominantly a sequence of medium- to thick-bedded dolostone, most of which contains some silt and fine sand in thin laminae.

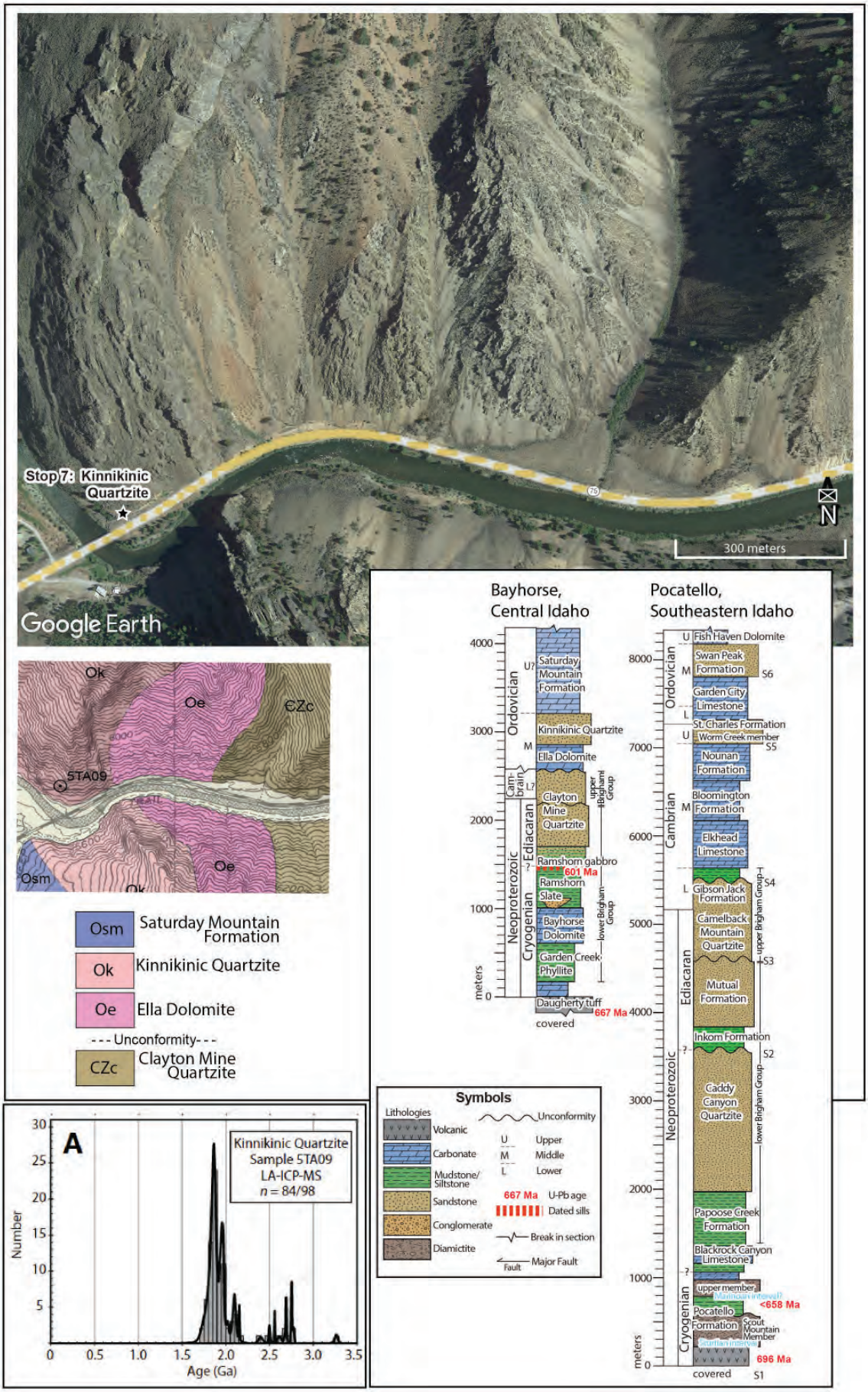

Figure 11. Aerial imagery and geologic map (Krohe and others, 2020) of field trip Stop 7. The geochronology plots show the detrital zircon age spectra for the Middle Ordovician Kinnikinic Quartzite (Beranek and others, 2016). The stratigraphic columns are adapted from Brennan and others (2023) and demonstrate notable absence of thick Cambrian carbonates at Bayhorse in central Idaho, compared to southeastern Idaho.

Fossils recovered from these Ella Dolomite exposures along Highway 75 contain brachiopods and conodonts of Middle Ordovician age (Hobbs and others, 1968). These fossil constraints provide the Middle Ordovician depositional age for the Ella Dolomite, and the conformably overlying Kinnikinic Quartzite. The Kinnikinic Quartzite is an exceptionally pure, medium-grained quartz arenite (Hobbs and others, 1968) that records a detrital zircon signature indicative of sourcing from the Peace River arch, a long-lived positive topographic feature in northwestern Alberta and northeastern British Columbia, as well as additional sources including recycling of underlying Mesoproterozoic Belt Supergroup and provinces further east such as the Wyoming and Trans-Hudson (Baar, 2009; Beranek and others, 2016). Together, the Ella Dolomite and Kinnikinic Quartzite represent a deepening, or transgressive, sequence associated with the onset of the Laurentian-wide Tippecanoe Sequence (Sloss, 1963).

One of the puzzles of the Bayhorse region is that the middle Ordovician Ella Dolomite and Kinnikinic Quartzite (deposited around ca. 470–450 Ma) overlie the ~1 km (0.6 mi) thick Clayton Mine Quartzite, which, as we observed in Stop 3, was intruded near the base by the ~601 Ma Ramshorn gabbro, and thus is at least partially Neoproterozoic in age. Consequently, the nearly ~2 km (~1.2 mi) thick carbonate and finer-grained strata that represent the majority of the upper Cambrian and lower Ordovician epochs in southeastern Idaho (fig. 11) are absent in central Idaho. Brennan and others (2020b) suggested that the absence of this strata in central Idaho indicates significant-in-time duration, yet difficult-to-recognize in the field, unconformities (paraconformities, or low angle disconformities) within the upper Clayton Mine Quartzite and its contact with the overlying Ella Dolomite and Kinnikinic Quartzite. This interpretation seems to be supported by the absence of any ca. 500 Ma detrital zircon grains in the upper Clayton Mine Quartzite that characterize upper Cambrian and lower Ordovician strata in southeastern Idaho and southwestern Montana, and represent exhumation of the Beaverhead plutons within the Lemhi arch uplift (Link and others, 2017). On the third and final day of this field trip, exploration of the Neoproterozoic to Ordovician South Creek strata will reveal much more obvious unconformities, some angular, within the stratigraphic section that likely correlate to these difficult-to-recognize gaps in the Neoproterozoic to lower Paleozoic stratigraphic record near Bayhorse.

This stop concludes the review of the Bayhorse region and the remainder of the day will include an ~114 mi (183 km) drive, with a couple stops of geologic interest along the way, to arrive in camp at Summit Creek Recreation Area, approximately 75 mi (120 km) to the southeast. A significant portion of this drive (~56 mi) is on gravel roads, but they are generally well-maintained and should be accessible to non-4 x 4 passenger vehicles. The third and final day of this fieldtrip will be spent hiking along a traverse to observe the South Creek Meso- and Neoproterozoic to lower Paleozoic stratigraphic section, which is generally less complete yet correlative to the rocks just observed near Bayhorse (Milton, 2020; Brennan and others, 2023).

Drive to Summit Creek Recreation Site (44.2743°N, -113.4561°W).

Please cross the Highway 75 bridge, pull off into the turnoff on the right (Salmon River Drive), turn around, and head back the ~2 mi (3.2 km) east to Clayton. In Clayton (population 7) there is a park with some picnic tables, a restaurant (Clayton Silver Bar), and a small museum that was once the Idaho Mining and Smelting Company Store. We will stop in Clayton for lunch and visit the museum if interested. Please reset your trip odometers at the Clayton Silver Bar (intersection of Highway 75 and Ford Street) and continue east on Highway 75. The turn by turn directions from Clayton are as follows.

Head east on Highway 75, at 4.2 mi (~6.8 km, opposite a BLM campground) turn right (southeast) onto E. Fork Road. Continue another 4.1 mi (6.6 km) on E. Fork Road. At total odometer reading 8.3 mi (13.4 km), take a slight left (east) onto Spar Canyon Road. Note, this is ~0.2 mi (~330 m) past the first bridge you will take across the East Fork of the Salmon River. Continue 27.4 mi (44 km; total odometer reading 35.7 mi, 57.5 km) to Highway 93. This is a shortcut to see some more interesting geology; alternatively one could have skipped turns 1 and 2, and continued east on Highway 75 until its intersection with Highway 93. Optional stops along Spar Canyon road include:

At odometer reading 9.6 mi (15.4 km), the ridge to your left (north) is composed mostly of Silurian and perhaps some Ordovician rocks of the Laketown Dolomite and Roberts Mountain Formation. Just stratigraphically below these units, but poorly exposed, is the Ordovician graptolite-bearing shale and argillite of the Phi Kappa Formation, which was the unit incorrectly originally correlated to the Ramshorn Slate (e.g.. Dover and others, 1980).

At odometer reading 19.3 mi (~31 km), the ridge on either side of the road is again mostly Silurian and likely some Devonian rocks faulted against Challis volcanic rocks. At odometer reading 30.6 mi (~49 km), the ridge on either side of the road is Silurian strata thrusted over

Devonian strata. At total odometer reading 35.7 mi (57.5 km), Spar Canyon Road intersects Highway 93. Turn right (south) onto Highway 93 and continue 13.0 mi (21 km; total odometer 48.7 mi reading, 78.4 km), where you will turn left (northeast) onto Doublespring Pass Road (USFS Road 116). Approximately 100 m (330 ft) before the turn are historical markers for Borah Peak [the highest point in Idaho at 3,860 m (12,662 ft)] and the 1983 Borah Peak magnitude 6.9 earthquake.

The Borah Peak Earthquake interpretive site, 2.5 mi (4.0 km) up Doublespring Pass Road, has interesting geological information signs and restrooms. Past the Borah Peak Earthquake interpretive site, continue east through the Lost River Range on Doublespring Pass Road for another 18.7 mi (30 km; total odometer reading 56.9 mi, 91.6 km), where you will take a slight right as Doublespring Pass Road joins with Hatch Lane and Custer Road for a couple of miles. Continue southeast on Doublespring Pass Road/Custer Road to total odometer reading 74.3 mi (119.6 km). Here (44.2743°N, -113.4561°W) there is a toilet and primitive camping at the Summit Creek Recreation site, where we will spend the night. Another 0.5 mi (~0.9 km) down the road (south), Barney warm springs (reported water temperature consistently ~85° F) provides a nice soak with some small tropical fish for company.

Day 3: South Creek Stratigraphic Section

The third and final day of this field trip consists of a steep stratigraphic traverse hike along South Creek in the southern Lemhi Range, and primarily covers the recent thesis research of Idaho State University MS student Jacob Milton (Milton, 2020). At South Creek, Wilbert Formation (McCandless, 1982) overlies Mesoproterozoic Lemhi Group strata (Mangum and others, 2022) in a low-angular (~15–35°) unconformity. The Wilbert Formation is in turn overlain by the Tyler Peak Formation, which is overlain by the Summerhouse Formation (fig. 12). These units are at least partially correlative to the Clayton Mine Quartzite and Ella Dolomite near Bayhorse (Milton, 2020; Brennan and others, 2023).

If starting at Summit Creek Recreation site (44.2743°N, -113.4561°W), please reset your odometer and continue south along Summit Creek Road/Little Lost River

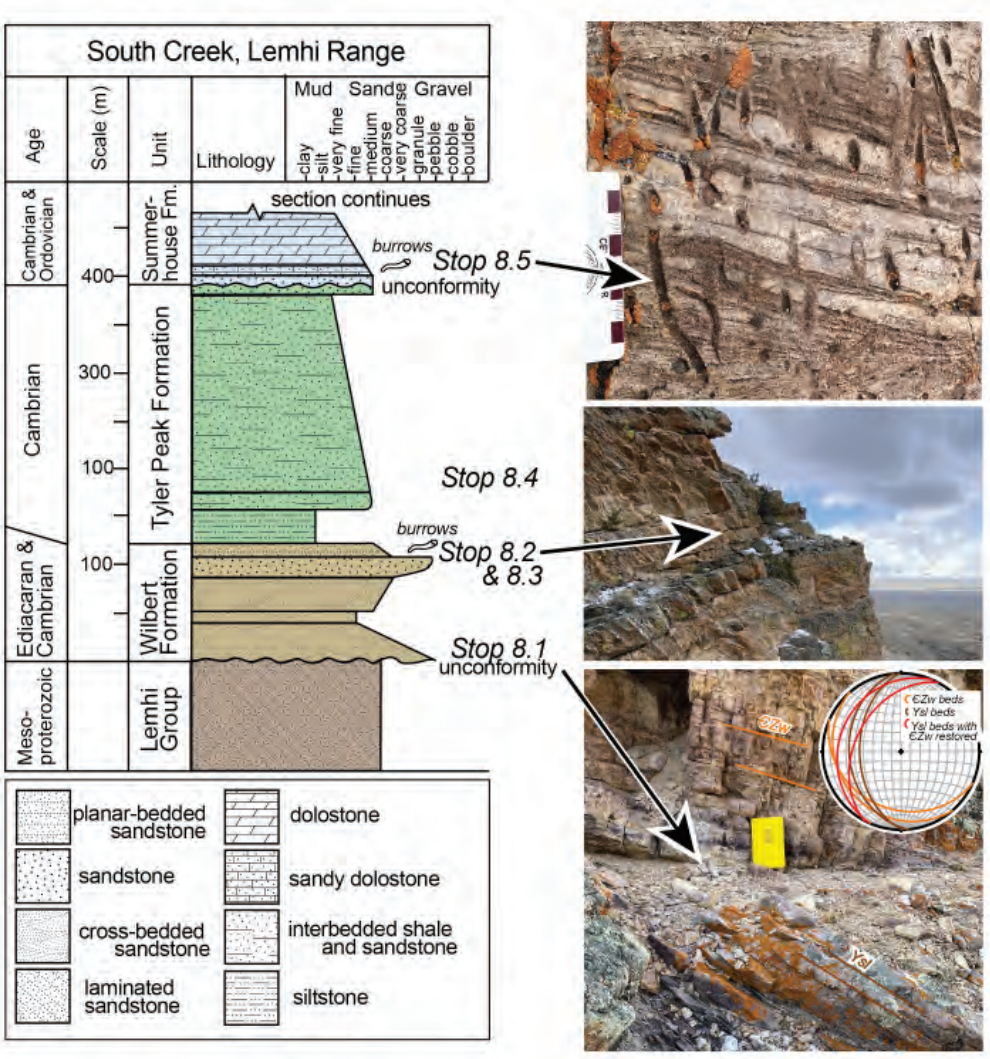

Figure 12. The Mesoproterozoic to Ordovician stratigraphy at South Creek, Idaho (adapted from Milton, 2020). The stratigraphic interval of stops along the hiking traverse shown in figure 14 are indicated along with representative field photos of the lithologies. The stereogram along with Stop 8.1 indicates the shallowing (~20–30°) southwest-dipping Wilbert Formation beds (in orange) above the unconformity, with more steeply (~35–45°) west-dipping probable Lemhi Group strata (in brown) beneath. The red great circles indicate the orientation of the Lemhi Group strata beneath the unconformity with the overlying Wilbert Formation beds restored to horizontal. The restored dip of the Lemhi Group strata indicates northwest tilting of ~20 to 40° during the Neoproterozoic within this region of the Lemhi arch. This orientation is interesting as in the northern extent of the Lemhi range (approximately 125 km or ~78 mi to the north of South Creek near the Poison Creek thrust) Lemhi Group strata dip ~10–20° to the northeast when unconformably overlying Middle Ordovician strata are restored to horizontal (Hanson and Pearson, 2017; Burmester and others, 2020). The detrital zircon age spectra for the Lemhi Group strata at this location is shown in figure 13.

Highway; after 34.6 mi (55.7 km) turn left (east) onto South Creek Road. At total odometer reading 36.6 mi (58.9 km) turn left off South Creek Road (2 mi up South Creek Road) onto the unnamed jeep trail (a spur of USFS Trail 4342); higher clearance vehicles are recommended. Continue on this road for another ~1.9 mi (~3 km; total odometer reading 38.5 mi, 62 km) around a cattle pasture where there is a parking space (43.9152°N, -113.0388°W), horse hitching post, and less traveled spur of the road trending off to the north. Past here, the right (east) spur of the road will drop down into the South Creek drainage as USFS trail 4342, which may be passable by ATV but is too narrow for trucks. Thus, a walking field traverse will start from this location. The traverse will be approximately ~4.5 mi (7.2 km) round trip, with about 540 m (~2,100 ft) of elevation gain, so it is a fairly rigorous hike but the only way to access the stratigraphy.

STOP 8

South Creek Stratigraphic Traverse

(43.9152°N, -113.0388°W)

Here, we will be walking an ~450-m-thick (~1,475 ft) stratigraphic section that consists of the Swauger, Wilbert, Tyler Peak, and Summerhouse Formations (McCandless, 1982; Skipp and others, 2009; Mangum and others, 2022). The traverse will cross an ~125-m (410 ft) section of Wilbert Formation that consists of coarse-grained, poorly sorted, cross-bedded quartz arenite that locally contains Skolithos trace fossils and Olenellus trilobite body fossils. McCandless (1982) designated this the Wilbert Formation type locality and noted that it overlies tilted and poorly dated quartzite tentatively correlated to the Mesoproterozoic Swauger Formation (Ruppel and others, 1975), of which on our traverse a small outcrop is visible at stop 8.1. Detrital zircon U/Pb geochronology supports this correlation (fig. 13). The contact was described as an angular unconformity in excess of 15° that sometimes contains up to 7.5 m (24.6 ft) of local relief. The Tyler Peak Formation is ~275 m (902 ft) thick and consists of medium- to coarse-grained, poorly sorted quartz arenite interbedded with green siltstone and shale. The Tyler Peak Formation overlies the Wilbert Formation in an abrupt but apparently conformable contact. The Summerhouse Formation unconformably overlies the Tyler Peak Formation in a clear unconformity that thins the Tyler Peak Formation to the north (McCandless, 1982). In this location the Summerhouse Formation consists of a basal thick-bedded quartz arenite overlain by carbonate-cemented arenites and carbonate. Farther north in the Lemhi Range, the Summerhouse Formation is conformably overlain by Ordovician Kinnikinic Quartzite (Ruppel and others, 1975; McCandless, 1982).

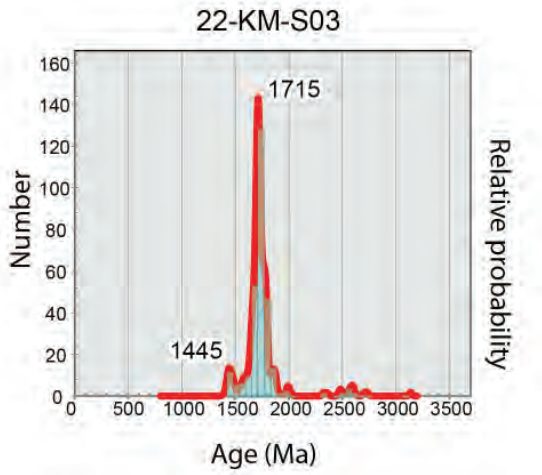

Figure 13. Detrital zircon U/Pb probability density plot from the probable Lemhi Group strata sampled below the sub-Wilbert unconformity at South Creek, Idaho (Mangum and others, 2022).

Important stops along the traverse:

Stop 8-1: 43.9152°N, -113.0388°W, Angular unconformity with Neoproterozoic–Cambrian Wilbert Formation overlying Mesoproterozoic strata of the Lemhi Group (figs. 10, 12). You can save a few hundred meters of walking by driving a bit closer to this outcrop along the path indicated in red on figure 14. The lowest exposed rocks were assigned to the Mesoproterozoic Swauger Formation of the upper Belt Supergroup (Skipp and others, 2009), and their detrital zircons were studied by Mangum and others (2022, fig. 13). Within these strata beneath the unconformity, Mangum and others (2022) report detrital zircon age peaks of ca. 1445 and 1715 Ma, consistent with the Swauger Formation of the Lemhi Group (Link and others, 2016).

Stop 8-2 (43.9179°N, -113.0255°W) and **Stop 8-3** (43.9157°N, -113.0261°W): Neoproterozoic–Cambrian Wilbert Formation with rare burrows/bioturbation (figs. 10, 12). Sample 01JM18 (Milton, 2020) was collected near stop 8-3 and contains a single ca. 519 Ma grain, with a scattering of ca. 1000–1100 Ma grains, along with older ca. 1375, 1445, and 1785 age peaks (fig. 15).

Stop 8-4 (43.9147°N, -113.0202°W): Cambrian Tyler Peak Formation. Sample 02JM18 was collected near stop 8-4 and contains detrital zircon age peaks at ca. 1450 and 1780 with a scattering of older Neoarchean ages (Milton, 2020).

Stop 8-5 (43.9191°N, -113.0133°W): Cambrian to Ordovician Summerhouse Formation with abundant Skolithos/vertical burrows (figs. 10, 12). Sample 05JM18 was collected near this location and contains several ca. 500–510 Ma detrital zircon grains with older age peaks at 1440 and 1720, with a couple of ca. 2480 Ma grains (Milton, 2020).

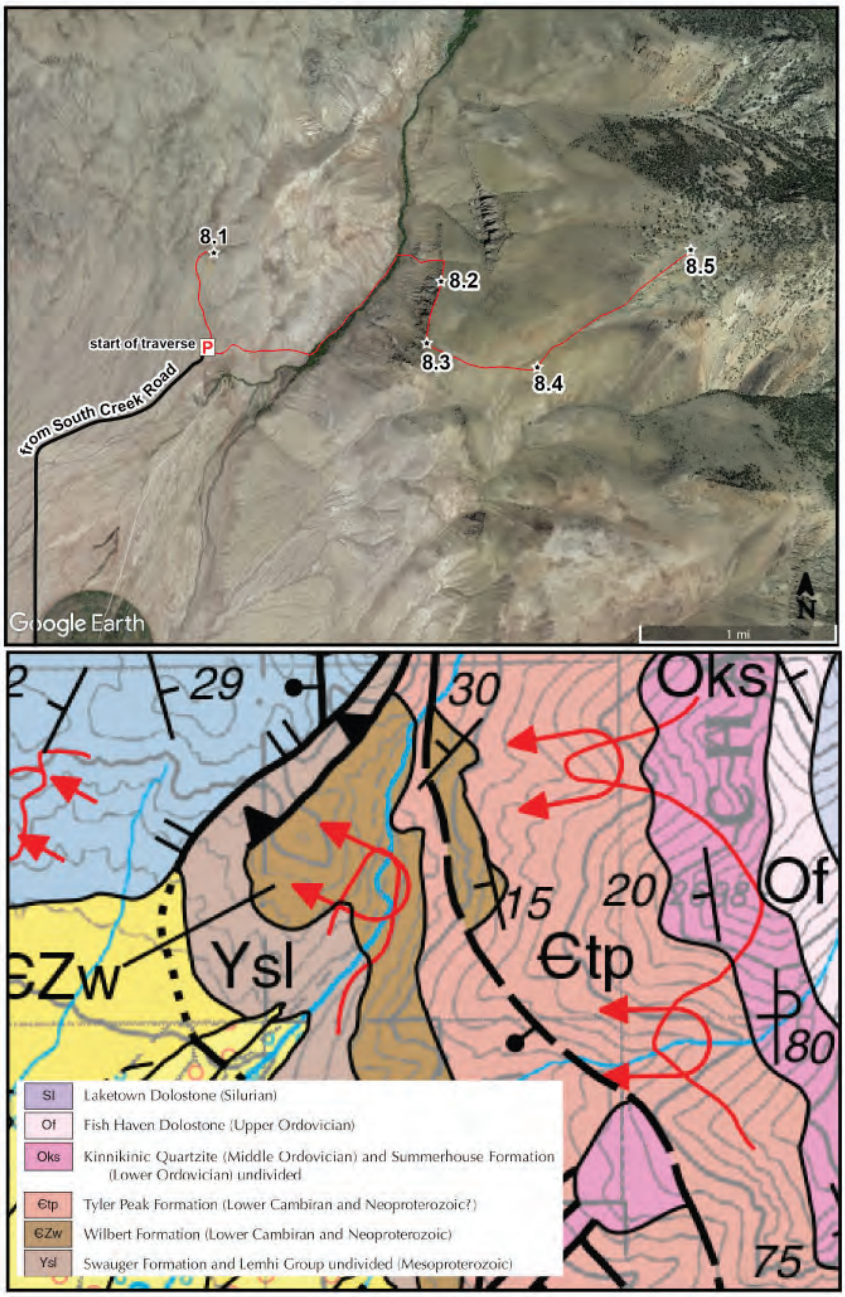

Figure 14. Aerial imagery and geologic map (modified from Skipp and others, 2009) of field trip Stop 8. The black line on the imagery indicates the unnamed access road and the red is generalized hiking traverse route with stops indicated. Unit abbreviations include Ysl, Mesoproterozoic Swauger Formation; CZw, Neoproterozoic to Cambrian Wilbert Formation; Ctp, Cambrian Tyler Peak Formation; Oks, Ordovician Summerhouse Formation and Kinnikinic Quartzite; Ofs, Ordovician Fish Haven Dolostone; Dj, Devonian Jefferson Formation.

LINKING SOUTH CREEK WITH BAYHORSE

On the basis of stratigraphic position, fossil constraints and detrital zircon age patterns, Milton (2020) correlated the Neoproterozoic–Ordovician stratigraphy at South Creek to coeval stratigraphy at Bayhorse. On the basis of Skolithos trace fossils in the Wilbert Formation and conformably overlying Tyler Peak Formation exposed at South Creek, the higher stratigraphic interval of the Wilbert Formation is Cambrian in age, and likely at least partially correlative to the upper Clayton Mine Quartzite at Bayhorse. Given that the upper Wilbert Formation overlies Mesoproterozoic Belt Supergroup rocks in an angular unconformity at South Creek, this relationship requires tilting and exhumation within the Lemhi arch during Neoproterozoic time. This tilting and exhumation recorded at South Creek could be correlative to the exhumation event inferred from the locally derived ca. 660 Ma detrital zircon population found in the lower Clayton Mine Quartzite (refer to Stop 4 of this trip).

On the basis of stratigraphic position, fossil constraints and detrital zircon age-components (notably the ca. 500 Ma grains), the Summerhouse Formation is probably an eastern correlative to the Ella Dolomite exposed at Bayhorse and/or perhaps even falls within the upper Cambrian to lower Ordovician stratigraphic interval not recognized in the Bayhorse stratigraphy (refer to Stop 6 of this trip). Interestingly, the ca. 500 Ma detrital grains within the Summerhouse Formation record exhumation of the Beaverhead plutons, and thus a second and younger, Late Cambrian to Early Ordovician, interval of exhumation within the Lemhi arch (see Link and others, 2017).

Thus, it is likely that the Neoproterozoic strata exposed at Bayhorse were once more extensive throughout central Idaho, and represent a rare preservation of Neoproterozoic strata that was mostly eroded, and/or only partially deposited across the east-central Idaho Lemhi arch, which is likely the uplifted rift-flank of a graben or half-graben. The spatial correlation of the Lemhi arch with the Lemhi subbasin of the Belt Supergroup has previously been noted (e.g., Hansen and Pearson, 2016; Link and others 2017; see fig. 1), and suggests that Mesoproterozoic modification of the central Idaho lithosphere made it more resistant to Neoproterozoic rift-related thinning and subsidence. Other tectonostratigraphic investigations in northeastern Washington State and southeastern British Columbia have noted that the St. Mary–Moyie fault system (see fig. 1), also a Mesoproterozoic syn-Belt Supergroup depositional structure (e.g., Sears, 2007), appears to have undergone several periods of reactivation, including controlling Neoproterozoic rift-structure and subsidence (e.g., Lund, 2008; Brennan and others, 2021b), and Cretaceous shortening style and magnitude (e.g., Price and Sears, 2000; Fuentes and others, 2012). Consequently, for understanding most post-Mesoproterozoic geologic phenomenon in the Belt Basin region, it appears that a good grasp of Beltian geology is a prerequisite.

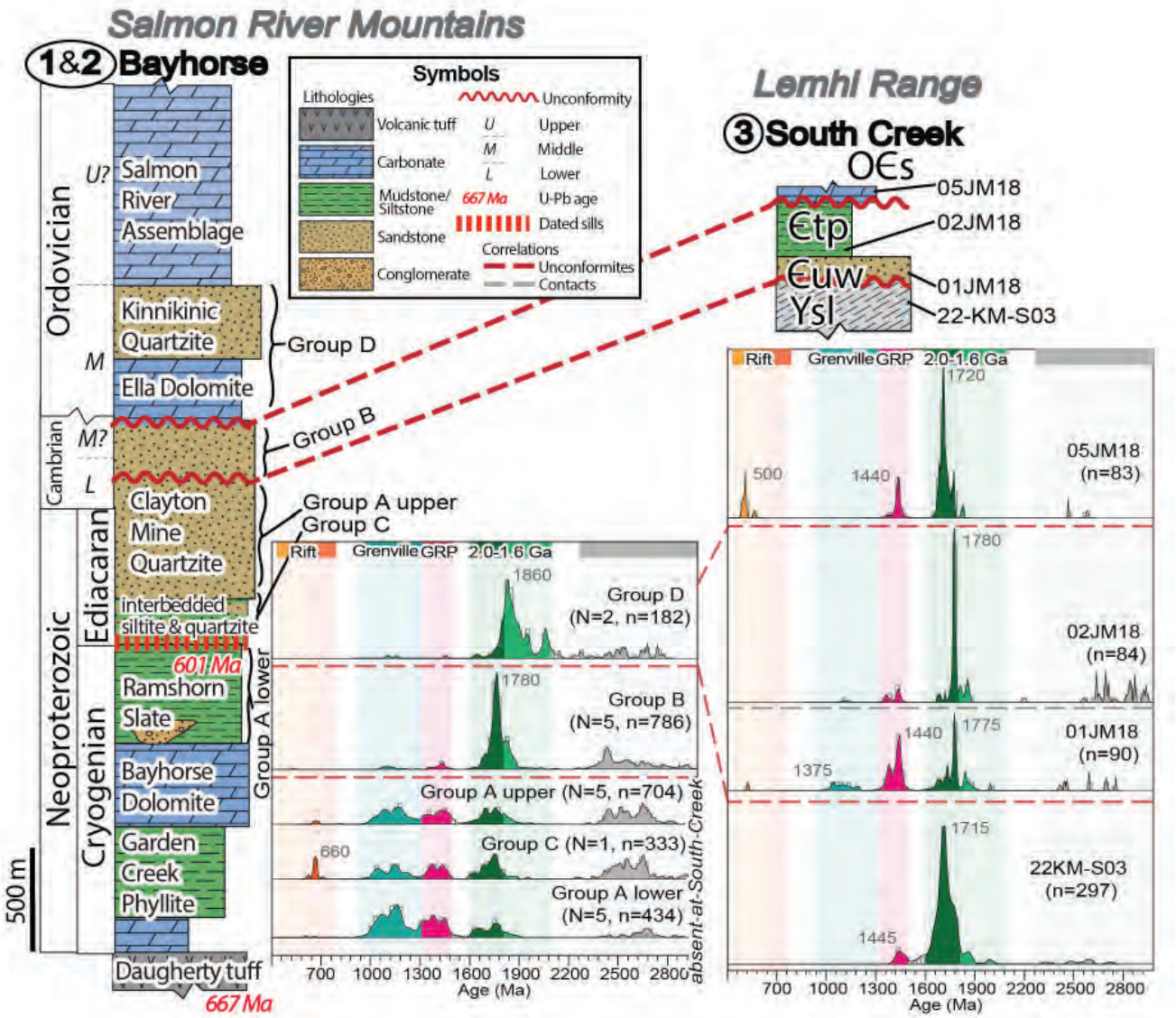

Figure 15. Central Idaho stratigraphic sections and detrital zircon results linking the more complete Bayhorse stratigraphy to the much thinner section at South Creek (adapted from Brennan and others, 2023).

REFERENCES

Anderson, A, 1954, A preliminary report on the fluorspar mineralization near Challis, Custer County, Idaho: Idaho Bureau of Mines and Geology Pamphlet 101, 13 p.

Baar, E.E., 2009, Determining the regional-scale detrital zircon provenance of the middle-late Ordovician Kinnikinic (Eureka) quartzite, east-central Idaho, U.S.: Pullman, Wash., Washington State University, M.S. thesis., 134 p.

Beranek, L.P., Link, P.K., and Fanning, C.M., 2016, Detrital zircon record of mid-Paleozoic convergent margin activity in the northern U.S. Rocky Mountains: Implications for the Antler orogeny and early evolution of the North American Cordillera: Lithosphere, no. 8, v. 5, p. 533–550.

Brennan, D.T., 2018, Geologic mapping and detrital zircon provenance of the Bayhorse anticline, central Idaho: Revised Neoproterozoic and lower Paleozoic stratigraphy: Pocatello, Idaho, Idaho State University, M.S. thesis. 155 p., 1 plate.

Brennan, D.T., Pearson, D.M., Link, P.K., and Chamberlain, K.R., 2020a, Geologic map of the Bayhorse anticline, Custer County, Idaho: Idaho Geological Survey Technical Report T-20-01, 1:24,000 scale.

Brennan, D.T., Pearson, D.M., Link, P.K., and Chamberlain, K.R., 2020b, Neoproterozoic Windermere Supergroup near Bayhorse, Idaho: Late-stage Rodinian rifting was deflected west around the Belt basin: Tectonics, v. 39, no. 8, 27 p.

Brennan, D.T., Mitchell, R.N., Spencer, C.J., Murphy, J.B., and Li, Z., 2021a, A tectonic model for the Transcontinental Arch: Progressive migration of a Laurentian drainage divide during the Neoproterozoic–Cambrian Sauk Transgression: Terra Nova, v. 33, no. 4, p. 430–440.

Brennan, D.T., Li, Z., Rankenburg, K., Evans, N., Link, P.K., Nordsvan, A.R., Kirkland, C. L., Mahoney, J.B., Johnson, T., and McDonald, B.J., 2021b, Recalibrating Rodinian rifting in the northwestern United States: Geology, v. 49, no. 6, p. 617–622.

Brennan, D.T., Pearson, D.M., Link, P.K., and Milton, J., 2023, Neoproterozoic to early Paleozoic tectono-stratigraphic framework for central Idaho: Windermere Supergroup in the northern sector of the U.S. Cordillera, *in* Whitmeyer and

others, eds., Laurentia: Turning points in the evolution of a continent: Geological Society of America Memoir 220, p. 457–486, doi:https://doi.org/10.1130/2022.1220(23)

Burmester, R.F., Lonn, J.D., and Lewis, R.S., 2020, Further speculation on Belt stratigraphy and structure around Salmon, Idaho: Alternative interpretations and tests: Northwest Geology, v. 49, p. 19–34.

Dover, J.H., Berry, W.B.M., and Ross, R.J., 1980, Ordovician and Silurian Phi Kappa and Trail Creek Formations, Pioneer Mountains, Central Idaho stratigraphic and structural revisions, and new data on gaptolite faunas: U.S. Geological Survey Professional Paper 1090, 54 p.

Fuentes, F., DeCelles, P.G., and Constenius, K.N., 2012, Regional structure and kinematic history of the Cordilleran fold-thrust belt in northwestern Montana, USA: Geosphere, v. 8, no. 5, p. 1104–1128.

Gaschnig, R.M., Vervoort, J.D., Lewis, R.S., and McClelland, W.C., 2010, Migrating magmatism in the northern US Cordillera: *In situ* U-Pb geochronology of the Idaho batholith: Contributions to Mineralogy and Petrology, v. 159, no. 6, p. 863–883.

Hansen, C.M., and Pearson, D.M., 2016, Geologic map of the Poison Creek thrust fault and vicinity, Lemhi County, Idaho: Idaho Geological Survey Technical Report T-16-1, scale 1:24,000.

Hayes, T.S., Miller, M.M., Orris, G.J., and Piatak, N.M., 2017, Fluorine, chap. G, *in* Schulz, K.J., DeYoung, J.H., Jr., Seal, R.R. II, and Bradley, D.C., eds., Critical mineral resources of the United States—Economic and environmental geology and prospects for future supply: U.S. Geological Survey Professional Paper 1802, p. G1–G80, doi: http://doi.org/10.3133/pp1802G.

Hobbs, S.W., Hays, W.H., and Ross, R.J., 1968, The Kinnikinic Quartzite of central Idaho—Redefinition and subdivision: U.S. Geological Survey Bulletin 1254, 22 p.

Hobbs, S.W., and Hays, W.H., 1990, Ordovician and older rocks of the Bayhorse area, Custer County, Idaho: U.S. Geological Survey Bulletin 1891, 40 p.

Hobbs, S W., Hays, W.H., and McIntyre, D.H., 1991, Geologic map of the Bayhorse area, central Custer County, Idaho: U.S. Geological Survey Miscellaneous Investigations Series Map I-1882, scale 1:62,500, 14 p.

Idaho Department of Environmental Quality, 2003, Ramshorn Mine preliminary assessment report, Custer County, Idaho: Submitted to United States Department of Environmental Quality, January 30th, 2004.

Isakson, V.H., 2017, Geochronology of the tectonic, stratigraphic, and magmatic evolution of Neoproterozoic to early Paleozoic, North American Cordillera and Cryogenian glaciation: Boise, Idaho, Boise State University, Ph.D. dissertation, 657 p.

Jacob, T., 1990, Late Proterozoic(?) tuff near Challis, Idaho, *in* Moye, F.J., ed., Geology and ore deposits of the trans-Challis fault system/Great Falls tectonic zone: Guidebook of the Fifteenth Annual Tobacco Root Geological Society Field Conference, Northwest Geology, v. 19, p. 97–106.

Krohe, N., 2016, Structural framework and detrital zircon provenance of the southern portion of the Clayton quadrangle, Custer County, Idaho: Pocatello, Idaho, Idaho State University, M.S. thesis, 107 p.

Krohe, N., Brennan, D.T., Link, P.K., Pearson, D.M., and Armstrong, T., 2020, Geologic map of the southern portion of the Clayton quadrangle, Custer County, Idaho: Idaho Geological Survey Technical Report T-20-02, 1:24,000 scale.

Lachmar, T.E., McDonough, H.L., Burk, N.I., Kolesar, P.T., and Doucette, W.J., 2019, Effect of ore mineralogy and bedrock lithology on metal loading rates and acid-mine drainage: Bayhorse Creek, Idaho and the North Fork of the American Fork River, Utah: Mine Water and the Environment, no. 38, p. 3–15.

Link, P.K., Steel, T.D., Stewart, E.S., Sherwin, J.A., Hess, L.R., and McDonald, C., 2016, Detrital zircons in the Mesoproterozoic upper Belt Supergroup in the Pioneer, Beaverhead, and Lemhi Ranges, Montana and Idaho: The Big White arc: Geological Society of America Special Paper 522, no. 7, p. 39–44.

Link, P.K., Todt, M.K., Pearson, D.M., and Thomas, R.C., 2017, 500–490 Ma detrital zircons in Upper Cambrian Worm Creek and correlative sandstones, Idaho, Montana, and Wyoming: Magmatism and tectonism within the passive margin: Lithosphere, no. 9, v. 6, p. 910–926.

Lund, K., 2008, Geometry of the Neoproterozoic and Paleozoic rift margin of western Laurentia: Implications for mineral deposit settings: Geosphere, no. 4, v. 2, p. 429–444.

Lund, K., Aleinikoff, J.N., Evans, K.V., and Fanning, C.M., 2003, SHRIMP U-Pb geochronology of Neoproterozoic Windermere Supergroup, central Idaho: Implications for rifting of western Laurentia and synchroneity of Sturtian glacial deposits: Geological Society of America Bulletin, no. 115, v. 3, p. 349–372.

Lund, K., Aleinikoff, J.N., Evans, K.V., duBray, E.A., Dewitt, E.H., and Unruh, D.M., 2010, SHRIMP U-Pb dating of recurrent Cryogenian and Late Cambrian–Early Ordovician alkalic magmatism in central Idaho: Implications for Rodinian rift tectonics: Geological Society of America Bulletin, no. 112, v. 3–4, p. 430–453.

Mangum, K, Sundell, K.E., Anderson, R.B, Pearson D.M., Link, P.K., and Lever, J., 2022, Detrital zircon data support a Neoproterozoic phase of tilting within the Lemhi Arch in east-central Idaho: Geological Society of America Abstracts with Programs: v. 54, no. 5, doi: 10.1130/abs/2022AM-383161

Marvin, R.F., Tschanz, C.M., Mehnert, H.H., and Mangum, K., 1973, Late Cretaceous age of molybdenite mineralization in Custer County Idaho: Isochron/West: Bulletin of Isotopic Geochronology, v. 7, p. 1.

Matthews, W., Guest, B., and Madronich, L., 2018, Latest Neoproterozoic to Cambrian detrital zircon facies of western Laurentia: Geosphere, no. 14, v. 1, p. 243–264.

McCandless, D.O., 1982, A re-evaluation of Cambrian through Middle Ordovician stratigraphy of the Southern Lemhi

Range: State College, Penn., Pennsylvania State University, M.S. thesis, 160 p.

Milton, J., 2020, Geologic mapping, stratigraphy, and detrital zircon geochronology of the southeastern Borah Peak horst, Custer County, Idaho: Age reassignment and correlation of Neoproterozoic to lower Paleozoic strata: Pocatello, Idaho, Idaho State University, M.S. thesis, 115 p.

Mitchell, V., 1999, History of the mines at Bayhorse: Idaho Geological Survey Staff Report 99-8, 40 p.

Montoya, L.M., 2019, Investigation of structural style within the Sevier fold-thrust belt along the southwestern boundary of the Lemhi arch, central Idaho: Pocatello, Idaho State University, M.S thesis, 80 p.

Price, R.A., and Sears, J.W., 2000, A preliminary palinspastic map of the Mesoproterozoic Belt/Purcell Supergroup, Canada and U.S.A: Implications for the tectonic setting and structural evolution of the Purcell anticlinorium and the Sullivan deposit, *in* Lydon and others, eds., The geological environment of the Sullivan deposit, British Columbia: Geological Association of Canada Mineral Deposits Division Special Publication no. 1, p. 61-81.

Rainbird, R.H., McNicoll, V.J., Theriault, R.J., Heaman, L.M., Abbott, J.G., Long, D.G.F., and Thorkelson, D.J., 1997, Pan-continental river system draining Grenville orogen recorded by U-Pb and Sm-Nd geochronology of Neoproterozoic quartz arenites and mudrocks, northwestern Canada: The Journal of Geology, v. 105, no. 1, 17 p.

Ross, C.P., 1937, Geology and ore deposits of the Bayhorse region, Custer County, Idaho: U.S. Geological Survey Bulletin, v. 877, 161 p.

Ruppel, E.T., Ross, R.J., and Schleicher, D., 1975, Precambrian and Lower Ordovician rocks in east-central Idaho: U.S. Geologic Survey Professional Paper 889, p. 1–34.

Ruppel, E.T., 1986, The Lemhi Arch: A Late Proterozoic and Early Paleozoic landmass in Central Idaho: American Association of Petroleum Geologists Memoir, v. 41, p. 119–130.

Sears, J.W., 2007, Belt-Purcell basin: Keystone of the Rocky Mountain fold-and-thrust belt, United States and Canada, *in* Whence the mountains? Inquiries into the evolution of orogenic systems: A volume in honor of Raymond A. Price: Geological Society of America Special Paper 433, p. 147–166.

Skipp, B., Snider, L.G., Janecke, S.U., and Kuntz, M.A., 2009, Geologic map of the Arco 30 x 60 minute quadrangle, South-Central Idaho: Idaho Geological Survey Geology Map 47, scale 1:100,000.

Sloss, L.L., 1963, Sequences in the cratonic interior of North America: Geological Society of America Bulletin, no. 74, v. 2, p. 93–114.

Sloss, L.L., 1964, Lemhi Arch, A Mid-Paleozoic positive element in South-Central Idaho: Geological Society of America Bulletin, v. 66, p. 365–368.

Wells, M.W., 1983, Gold camps and silver cities: Nineteenth century mining in central and southern Idaho: Idaho Geological Survey Bulletin B-22.

NORTHWEST GEOLOGY

The Journal of The Tobacco Root Geological Society

Requirements for Contributions

TEXT FORMAT: Word Doc (not docm), or plain text (TXT or RTF)
IMAGE FORMAT: jpg (for photos), tif, pdf, png, or ai-do not embed in Word
FINAL DEADLINE FOR RECEIPT BY EDITORS: JUNE 1 (may be earlier; check website)

Generally, follow USGS style for writing. See COMPLETE REQUIREMENTS at trgs.org. YOU MUST READ AND FOLLOW.

Text should be submitted to the Editor(s) in MS Word-compatible (DOC) format (plain TXT or RTF is fine). **Please DO NOT provide formatting.** Do not assign page numbers, do not double space, do not use columns or backgrounds, **do not indent** anything. Do not include large tables in text—make a separate file for tables: Excel, Word, or pdf. Especially, **PLEASE do not include images within Word documents or PowerPoint—**they are not usable. IMAGES PROVIDED AS WORD DOCUMENTS WILL BE RETURNED.

Photographs and other images should be submitted as JPG, PDF, PNG, or TIF files, **separate** from text. Dimensions should be so that the full size of the image is approximately as it will be displayed—that is, if it will be 3 inches wide when printed, it should be 3 inches wide when displayed on the computer monitor, or larger. We appreciate images being as high-resolution as possible.

We can accept many different types of high-resolution images. If necessary, we can scan hard-copy drawings or photos for you. Figure captions should be submitted as a separate text file, or part of the text file.

Road Logs **must** be accompanied by (at a minimum) a location map of stops; ideally, a geologic map with stops should be included. Such maps should be provided separately from the text.

Please use the following bibliographic format. Note especially capitalization and use and position of commas and colons. For journals, do not abbreviate except for U.S. in "U.S. Geological Survey."

Sears, J.W., and Hendrix, M., 2004, Lewis and Clark Line and the rotational origin of the Alberta and Helena Salients, North American Cordillera, *in* Sussman, A., and Weill, A., eds., Orogenic Curvature: Geological Society of America Special Paper 383, p. 173-186.

Tikoff, B., and Teyssier, C., 1992, Crustal-scale, en-echelon P-shear tensional bridges: A possible solution to the batholithic room problem: Geology, v. 20, p. 927-930.

Topics: In general, papers published in Northwest Geology do NOT need to be directly related to a particular TRGS Field Conference.

Abstracts: In general, we prefer to NOT publish stand-alone abstracts. Exceptions may be made, but we encourage you to create a short paper (which can be thought of as an expanded abstract) including at least one informative map, cross section, or image.

The Tobacco Root Geological Society, Inc.
P.O. Box 118
Butte, Montana 59703
http://trgs.org